frontiers | Research Topics

Extracellular vesicles in cardiovascular diseases

Edited by
Junjie Yang, Zhen-Ao Zhao, Zhongjian Cheng, Phuong-Uyen Dinh, Ke Huang and Zhenhua Li

Published in
Frontiers in Cardiovascular Medicine

ISSN 1664-8714
ISBN 978-2-8325-2417-6
DOI 10.3389/978-2-8325-2417-6

About Frontiers

Frontiers is more than just an open access publisher of scholarly articles: it is a pioneering approach to the world of academia, radically improving the way scholarly research is managed. The grand vision of Frontiers is a world where all people have an equal opportunity to seek, share and generate knowledge. Frontiers provides immediate and permanent online open access to all its publications, but this alone is not enough to realize our grand goals.

Frontiers journal series

The Frontiers journal series is a multi-tier and interdisciplinary set of open-access, online journals, promising a paradigm shift from the current review, selection and dissemination processes in academic publishing. All Frontiers journals are driven by researchers for researchers; therefore, they constitute a service to the scholarly community. At the same time, the *Frontiers journal series* operates on a revolutionary invention, the tiered publishing system, initially addressing specific communities of scholars, and gradually climbing up to broader public understanding, thus serving the interests of the lay society, too.

Dedication to quality

Each Frontiers article is a landmark of the highest quality, thanks to genuinely collaborative interactions between authors and review editors, who include some of the world's best academicians. Research must be certified by peers before entering a stream of knowledge that may eventually reach the public - and shape society; therefore, Frontiers only applies the most rigorous and unbiased reviews. Frontiers revolutionizes research publishing by freely delivering the most outstanding research, evaluated with no bias from both the academic and social point of view. By applying the most advanced information technologies, Frontiers is catapulting scholarly publishing into a new generation.

What are Frontiers Research Topics?

Frontiers Research Topics are very popular trademarks of the *Frontiers journals series*: they are collections of at least ten articles, all centered on a particular subject. With their unique mix of varied contributions from Original Research to Review Articles, Frontiers Research Topics unify the most influential researchers, the latest key findings and historical advances in a hot research area.

Find out more on how to host your own Frontiers Research Topic or contribute to one as an author by contacting the Frontiers editorial office: frontiersin.org/about/contact

Extracellular vesicles in cardiovascular diseases

Topic editors

Junjie Yang — University of Maryland, United States
Zhen-Ao Zhao — Hebei North University, China
Zhongjian Cheng — Temple University, United States
Phuong-Uyen Dinh — North Carolina State University, United States
Ke Huang — North Carolina State University, United States
Zhenhua Li — Southern Medical University, China

Citation

Yang, J., Zhao, Z.-A., Cheng, Z., Dinh, P.-U., Huang, K., Li, Z., eds. (2023). *Extracellular vesicles in cardiovascular diseases*. Lausanne: Frontiers Media SA. doi: 10.3389/978-2-8325-2417-6

Table of contents

frontiers in Cardiovascular Medicine

REVIEW
published: 13 April 2021
doi: 10.3389/fcvm.2021.672600

Circular RNAs and Cardiovascular Regeneration

*Ling Tang, Pengsheng Li, Michelle Jang and Wuqiang Zhu**

Department of Cardiovascular Diseases, Physiology and Biomedical Engineering, Center of Regenerative Medicine, Mayo Clinic, Scottsdale, AZ, United States

circular RNAs (circRNAs) are a type of non-coding RNAs that are widely present in eukaryotic cells. They have the characteristics of stable structure, high abundance, and cell or tissue specific expression. circRNAs are single-stranded RNAs that are covalently back spliced to form closed circular loops. They may participate in gene expression and regulation through a variety of action modes. circRNAs can encode proteins or function by acting as miRNA sponges for protein translation. Since 2016, a growing number of research studies have shown that circRNAs play important role in the pathogenesis of cardiovascular disease. With the construction of circRNA database, the differential expression of circRNAs in the heart tissue samples from different species and the gradual elucidation of its mode of action in disease may become an ideal diagnosis biomarker and an effective therapeutic target. What can be expected surely has a broader application prospect. In this review, we summarize recent publications on circRNA biogenesis, expression profiles, functions, and the most recent studies of circRNAs in the field of cardiovascular diseases with special emphasis on cardiac regeneration.

Keywords: circular RNA, cardiovascular disease, pathogenesis, cardiomyocyte, regeneration

OPEN ACCESS

Edited by:
Junjie Yang,
University of Alabama at Birmingham, United States

Reviewed by:
Jiacheng Sun,
University of Alabama at Birmingham, United States
Shiyue Xu,
The First Affiliated Hospital of Sun Yat-sen University, China

****Correspondence:***
Wuqiang Zhu
zhu.wuqiang@mayo.edu

Specialty section:
This article was submitted to Cardiovascular Biologics and Regenerative Medicine, a section of the journal Frontiers in Cardiovascular Medicine

Received: *26 February 2021*
Accepted: *22 March 2021*
Published: *13 April 2021*

Citation:
Tang L, Li P, Jang M and Zhu W (2021) Circular RNAs and Cardiovascular Regeneration. Front. Cardiovasc. Med. 8:672600. doi: 10.3389/fcvm.2021.672600

INTRODUCTION

Circular RNAs (circRNAs) are single-stranded RNAs that, unlike linear RNA, form a covalently closed continuous loop without 5′ end caps or 3′ Poly (A) tails. The concept of "circular RNA" was introduced by Sanger et al. when the team found that viroids are single-stranded covalently closed circRNA molecules (1). The cytoplasmic localization of circular RNA in eukaryotic cells was discovered by Hsu et al. through the electron microscope in 1979 (2). These pilot studies established the foundation of this research field.

Transcription of circRNAs had been a mystery for many years. The circular transcription of the Sry gene was discovered in mice in the early 1990s (3). In 2012, Salzman et al. (4) discovered that circRNA is a transformed transcript produced by reverse splicing of mRNA precursor and found that it is abundantly present in different types of human cells. As the field advances rapidly, a large number of circRNAs were discovered with the utilization of high-throughput sequencing technology, and their biological functions were intensively investigated. In 2016, Hansen et al. (5) found that circular RNA can act as a sponge of microRNA (miRNA) to regulate the growth and development of cells. This study shed new light on the circRNA field. Most recently, Li et al. developed a quickly screening and discovering tool for functional circular RNAs based on the CRISPR-Cas13d system, and discovered a set of functionalities that are important for cell growth and embryonic development (6). This technology provided a new research tool to the circRNA field.

Cardiovascular diseases (CVDs) are the leading cause of mortality worldwide. Several lines of evidence showed that circRNAs play important roles in regulating cardiovascular function. Jakobi et al. were the first group to provide a comprehensive catalog of RNase R-resistant circRNA species for the adult murine heart and explored the circRNA landscape of heart tissue (7). Over the next years, studies had reported that circRNAs are involved in the regulation of the physiology and pathology of the cardiovascular system. In particular, it is noted that circRNAs are involved in the pathogenesis of CVDs, such as myocardial infarction (MI) (8–14), heart failure (15, 16) and coronary artery disease (CAD) (17–23). Some circRNAs served as potential biomarkers for the diagnosis of CVDs (24–26). These findings suggest that circRNAs may be the new target molecules for the diagnosis and treatment of CVDs. In this review, we summarize circRNA classification, biogenesis, properties, functions, and some new research progress in the field of CVDs.

CLASSIFICATION OF CIRCRNA

circRNAs can be divided into three types according to the different sources of the sequences: ecRNAs (exonic circRNAs) which are derived from single or multiple exons (4, 27), ciRNAs (circular intronic RNAs) which are derived from introns (28), EIciRNAs (exon-intron circRNAs) which are composed of exons and introns (29) and tricRNAs (tRNA intronic circRNAs) which are formed by splicing tRNA introns (30).

BIOGENESIS OF CIRCRNA

There are four primary models for the formation of circRNA loops from pre-mRNAs (**Figure 1**), namely lariat-driven circularization (exon skipping), intron-pairing driven circularization (direct back-splicing), circular intronic RNAs, and RNA-binding protein (RBP)-driven circularization.

Lariat-driven circularization (exon skipping) is formed by connecting the splice site of 30 nucleotides upstream of the exon to the site of 50 nucleotides downstream (**Figure 1A**). This connection leads to exon-skipping and the formation of an RNA lariat consisting of several exons and introns. The introns are then removed to generate circRNAs (27, 31).

Intron-pairing driven circularization (direct back-splicing) is formed when pre-mRNA flanking introns contain inverted complementary sequences (**Figure 1B**). The complementary pairing on both sides of the intron can lead to alternative cyclization and then a generation of various circRNAs, including ecircRNAs and EIciRNAs (27, 32). Furthermore, longer introns can be found in the flanking sequences of circRNAs, and reverse complementary sequences in longer introns can aid the formation of circRNAs (29, 33).

Circular intronic RNAs are produced by eukaryotic spliceosome-mediated splicing (**Figure 1C**). The lariat intron generated from the splicing reaction evades normal debranching and degradation, and the 3′ "tail" downstream from the branchpoint is trimmed leading to the formation of a stable circRNA. Conserved motifs at both ends, including the 7-nt GU-rich element near the 5′ splice site and the 11-nt C-rich element near the branch point site, are combined to prevent introns form circular branches, which promote the formation of loop structures (28, 34).

Reverse complementary sequences, such as Alu repeats, are located in upstream and downstream introns. RBP-driven circularization is formed when certain transactivator RNA binding proteins that bind to each flanking intron trigger the splicing of the donor and acceptor sites close enough to form circRNA (**Figure 1D**) (32, 34–38).

FUNCTION OF CIRCRNA

Despite the rapid growth in the field, the biological functions of circRNAs in eukaryotic cells have not been fully understood. circRNAs share some common characters. First, circRNAs are widely distributed and abundantly expressed in a diverse of cells. circRNAs can be found in a large amount in the cytoplasm of eukaryotic cells derived from animals and plants (27, 39). In humans, more than 30,000 circRNAs have been discovered and are still increasing year by year (40, 41). Second, circRNAs are stable. Due to the covalently closed structure, circRNA is resistant to degradation by ribonuclease (RNase) or exonuclease and is more stable than linear RNA (42). The expression of circRNA differs according to time, tissues, or species (39, 43). circRNA profiles change at different stages of cardiac differentiation or during cardiogenic differentiation of induced pluripotent stem cells (44, 45). Moreover, circRNAs are evolutionarily conserved (43, 46). In 2016, Werfel et al. (47) reported high homology of 1288 circRNAs across humans, mice, and rats. However, many studies have also illustrated that circRNAs are species-specific (48, 49). circRNAs show different expression profiles between normal and diseased tissues (45, 47, 50). Increasing evidence suggests some circRNAs are derived from genomic loci associated with human diseases, and contribute to transcriptional, post-transcriptional, and translational regulations (51). To summarize, there are four main modes for circRNA function (**Figure 2**).

1) circRNAs can act as competitive endogenous RNAs (ceRNAs) to regulate gene expression by microRNAs (miRNAs) sponge effects (**Figure 2A**). miRNAs are important post-transcriptional regulators of gene expression that act by direct base pairing to target sites within untranslated regions of messenger RNAs (mRNAs) (52, 53). circRNAs contain miRNA response elements (MREs) that promote the binding between circRNAs and miRNAs. This binding can decrease the level of functional miRNAs and increase the expression of miRNA targets (53, 54). It has been reported that circRNAs regulate cell function by acting as miRNA sponges. For example, circFOXK2 promotes cell growth, migration, invasion, and apoptosis by binding to multiple sites and functioning as a sponge for miR-942 (55). Similarly, circRNA_100876 regulates the progression of triple-negative breast cancer by functioning as a sponge for miR-136 (56). Other circRNAs, such as circSLC26A4, circRNA_0000253, and circRNA_ANKIB1 can also function

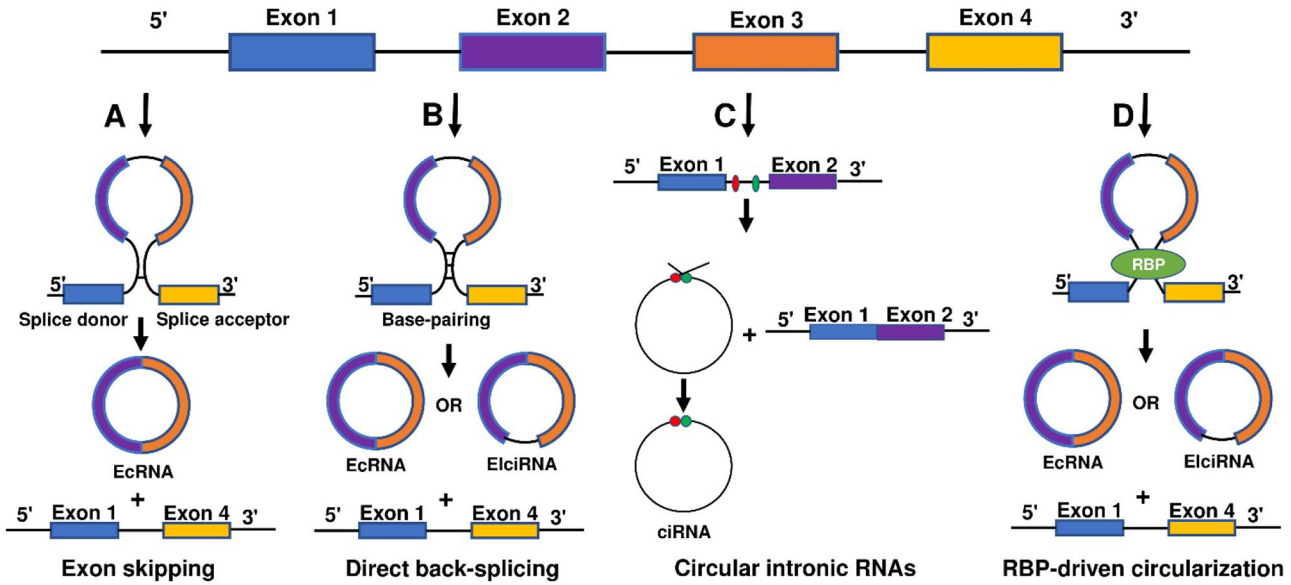

FIGURE 1 | Biogenesis of circ RNAs. There are four main models for the formation of circRNA loops from pre-mRNAs including **(A)** lariat-driven circularization (exon skipping), **(B)** intron-pairing driven circularization (direct back-splicing), **(C)** circular intronic RNAs, and **(D)** RNA-binding protein (RBP)-driven circularization.

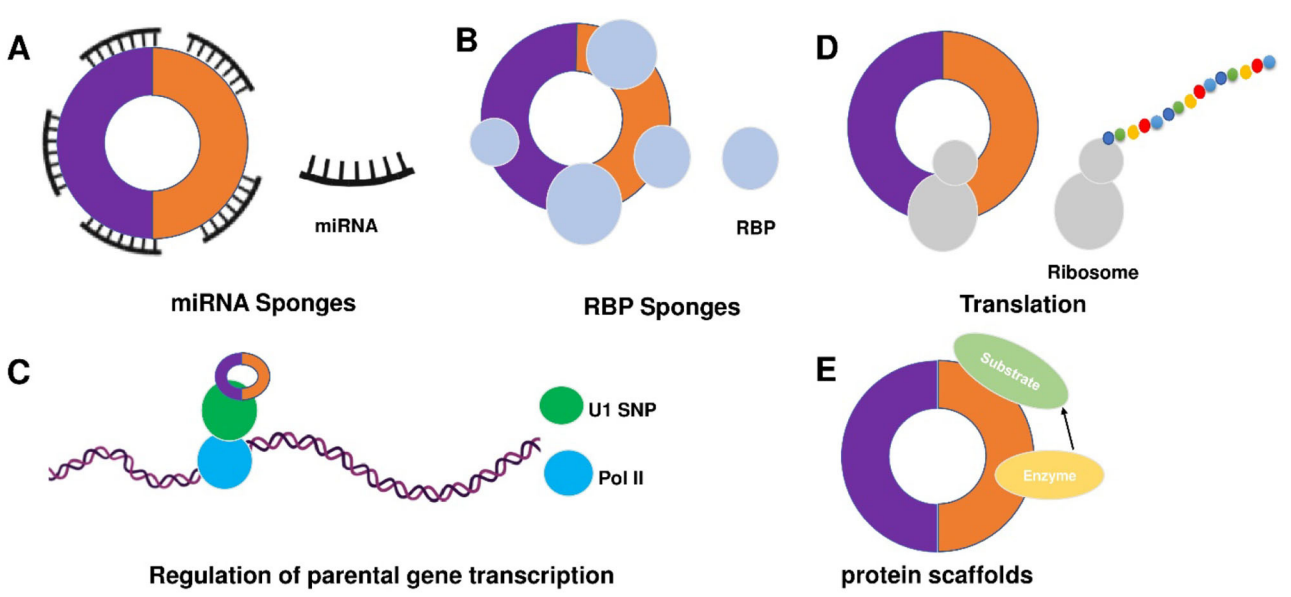

FIGURE 2 | Mechanisms of circRNA functions. There are five main action mechanisms of circRNAs, including **(A)** circRNAs can act as miRNAs sponge, **(B)** circRNAs can function as RBP sponges, **(C)** circRNAs mediated regulation of the transcription of parental genes, **(D)** circRNAs can be translated into proteins via some modification, and **(E)** circRNAs can act as dynamic scaffolding molecules that modulate protein-protein interactions.

as the sponge of miR-1287-5p (57), miRNA-141-5p (58), and miR-195a-5p (59), respectively. circALMS1_6 may participate in the regulation of cardiac remodeling by functioning as a sponge for miR-133 (60).

2) circRNAs can function as RBP sponges and RBPs can also participate in back-splicing (**Figure 2B**) (61–66). RBPs are a group of proteins involved in gene transcription and translation. circRNAs can interact with RBP and inhibit their activities (66–68). circMbl absorbs MBL proteins and regulates the subsequent physiological processes (32). circPABPN1 can bind to HuR to suppress the translation of PABPN1 mRNA (69). circANRIL competitively recruits PES1 to inhibit ribosome biogenesis (70). circFoxo3 interacts with different RBPs to participate in the processes of cardiomyocyte senescence and cell cycle progression

(71). circAmotl1 can protect cardiomyocytes and promote cell proliferation and wound healing by binding to PDK1, AKT1, and STAT3 (72, 73). The studies confirm the involvement of circRNAs in post-transcriptional regulation by chelating RBP. In 2020, Okholm et al. (74) conducted an extensive screen of circRNA-RBP interactions and analyzed circRNA-RBP interactions using a large set of eCLIP data with binding sites of 150 RBPs in the ENCODE cell lines HepG2 and K562 with deep-sequenced total RNA samples. Through this study, they confirmed the interactions between circCDYL and RBPs in bladder cancer cells.

3) circRNAs mediated regulation of the transcription of parental genes (**Figure 2C**). For example, circβ-catenin can produce a novel 370-amino acid β-catenin isoform using the start codon as the linear β-catenin mRNA transcript and terminates translation at a new stop codon created by circularization (75). ci-ankrd52 is a circular intronic RNA that is abundant in the nucleus and has little enrichment at microRNA target sites. ci-ankrd52 can bind to the transcription sites and acts as a positive regulator of Pol II transcription (28). For the circRNAs that interact with RNA polymerase II, exons are typically circularized with introns which are 'retained' between exons. These circRNAs are termed exon-intron circRNAs or EIciRNAs. They are mainly localized in the nucleus and interact with U1 snRNP to promote transcription of their parental genes (29).

4) circRNAs can be translated into proteins via some modification (**Figure 2D**). **As we know, the translation is performed by ribosomes and involves initiation, elongation, termination and ribosome recycling.** Base-modification N6-methyladenosine (m6A) is a common form of base modification in RNAs. It can promote efficient initiation of protein translation from circRNAs in human cells. Legnini et al. revealed that m6A-driven translation of circRNAs is widespread with hundreds of endogenous circRNAs carrying the translation potential (76). circ-ZNF609 is an example of a protein-coding circRNA in eukaryotes. It is related to heavy polysomes and can be translated into a protein in a splicing-dependent and cap-independent manner (77). circRNAs play biological functions through the formation of complexes with proteins; otherwise, a novel protein circFAM188B-103aa encoded by circFAM188B that promotes the proliferation but inhibits the differentiation of chicken SMSCs was identified (78). Moreover, artificial (79) and endogenous circRNAs containing an internal ribosome entry site (IRES) that directly recruits ribosomes (80) can also be translated into protein. Additionally, circRNA with an infinite ORF has hundred-fold higher productivity than linear transcript by rolling circle amplification in an IRES-independent manner (81).

5) circRNAs may bind, store, sort, and sequester proteins to particular subcellular locations, can and act as dynamic scaffolding molecules that modulate protein-protein interactions (**Figure 2E**). circRNAs can bind to RNAs and can also bind, store, sort or sequester selected proteins such as RBPs to modulate their activity or localization (82). RNA-binding protein 3 (RBM3) dynamically adjusts the proliferation of hepatocellular carcinoma cells by regulating the production of SCD-circRNA2 encoded by the 3′-UTR of the stearoyl-CoA desaturase (SCD) gene (83). Recent studies have shown that RBP quaking could also modify the formation of circRNA through forming RNA-protein complexes (RPCs) (36). In addition to interacting with RBPs, circRNAs can function as protein sponges by adsorbing one or more proteins in binding sites, thereby acting as protein scaffolding by the mediating interaction between proteins. For example, CircFOXO3 could mediate the formation of circFOXO3-p21-CDK2 ternary complex and then serve as scaffolding, affecting the cell cycle progression of cancer (84).

SEQUENCING OF CIRCRNA

RNA-seq emerges as a powerful research tool to study the expression and function of non-coding RNAs including circRNAs (85). The technology of circRNA-seq generally includes library construction, computer sequencing, data analysis and processing, and function prediction (86). Either full transcriptome or circRNA profiling may be used to sequence circRNAs. The full transcriptome profiling is aimed to explore the expression patterns of both coding and non-coding RNA. This approach is suitable for the study of the biological function of circRNA. The circRNA profiling is focused on enriched circRNAs and this approach is appropriate to discover unknown circRNAs. Technically, the main difference between the two approaches is the construction of the sequencing library. The circRNA sequencing library not only requires the removal of most rRNA and poly (A), but also requires the use of ribonuclease RNase R to remove the interference of linear RNA. It has been reported that the abundance of circRNAs decreases after de-linear RNA because some circRNAs are sensitive to RNase R mediated digestion (87, 88). It is worthy to note that the alternative splicing of circRNA requires distinguishing the source of sense and antisense chains in the sequencing results. Therefore, constructing a chain-specific library is ideal as it may improve the accuracy of circRNA sequencing (87). Thus far, more than 100,000 unique human circRNAs have been discovered (89, 90).

After obtaining the circRNA sequencing data, the prediction and identification of circRNAs were carried out based on the identification software such as find circ, CIRCexplorer2, and CIRI (91–93). Real-time fluorescence quantitative PCR (quantitative real-time PCR, qRT-PCR), Northern blot hybridization (Northern blot), *in situ* hybridization (*In situ* hybridization, ISH), RPAD (RNase R treatment, polyadenylation, and poly (A) + RNA Depletion) and other techniques are used to validate the data of circRNA sequencing (94–97).

Microarray chip is another efficient tool for circRNA analysis, and it is commonly used in clinics for disease diagnosis. Compared to RNA-seq, microarray chip analysis is different in the following aspects: (2) microarray analysis of circRNA requires a known reference sequence, while RNA-seq can be utilized to analyze unknown circRNAs; (3) microarray chip analysis can be used to quantify circRNA expression when comparing with RNA-seq (98); and (4) microarray chip analysis can efficiently detect reverse splice site sequences and obtain a larger number of circRNAs than RNA-seq (99). However, some limitations of microarray chip analysis include: (2) high total RNA input is required during sample pretreatment; and

(3) unlike full transcriptome sequencing, microarray chip does not give the linear RNA data (100). If the reference sequence is unknown, many studies usually use RNA-seq to determine the full transcriptional sequence, then analyze the circRNAs by microarray.

CIRCRNA AND CVDs

With the development of deep sequencing technology, we can now understand the types and differential expression of circRNAs and their associated miRNAs in cardiovascular tissues (101–103). Many circRNAs have been reported to be associated with CVDs and their expression pattern are different between healthy and diseased human hearts (15, 19, 104, 105). Quantitative proteomics may be used to discover the regulatory networks of circRNAs in cardiovascular tissues (106). Here, we summarized recent publications on the roles of circRNAs in the development and treatment of CVDs (**Table 1**).

1) Cardiac hypertrophy. Cardiac hypertrophy is the heart's response to a variety of extrinsic and intrinsic stimuli that impose increased biomechanical stress and can be caused by various cardiovascular diseases. circRNA wwp1 exerts inhibitory roles of cardiac hypertrophy via down-regulation of ANF and miR-23a in isoproterenol hydrochloride-induced cardiac hypertrophy (107). A circRNA HRCR functions as an endogenous miR-223 sponge to sequester and inhibit miR-223 activity, resulting in an increase of ARC expression and protection of the heart from pathological hypertrophy and heart failure (108). Modulation of circRNAs levels may provide a promising therapeutic target for the treatment of cardiac hypertrophy.

2) Cardiac fibrosis. Activation and phenotypical transition of cardiac fibroblasts contribute to cardiac fibrosis. It was reported that circ_BMP2K enhances the regulatory effects of miR-455-3p on its target gene SUMO1 which leads to the inhibition of TGF-β1 or Ang II to induce the activation of cardiac fibroblasts (109). circRNA_010567, circRNA_000203, and circHIPK3 were upregulated in Angiotensin-II (Ang-II)-induced activation of cardiac fibroblasts (111, 112, 114). circNFIB was downregulated in TGF-β induced activation of primary adult cardiac fibroblasts (113). Some studies showed that targeting circRNAs improve myocardial ischemic and reperfusion injuries by attenuating myocardial fibrosis. For example, circ_LAS1L is down-regulated in patients with acute myocardial infarction and regulates cardiac fibroblast activation, growth, and migration by inhibiting miR-125b/SFRP5 pathway (12). circPAN3 knockdown attenuated autophagy-mediated cardiac fibrosis after myocardial infarction via miR-221/FoxO3/ATG7 axis (110). The roles of circRNAs in cardiac fibrosis has been summarized in a recent review article (54).

3) Cardiomyocyte apoptosis. It was reported that some circRNAs may be involved in injury-induced cardiomyocyte apoptosis. For example, circRNA ITCH mediates H_2O_2-induced myocardial cell apoptosis by upregulating miR-17-5p via wnt/β-catenin signaling pathway (115). circSAMD4A aggravates hypoxia/reoxygenation (H/R)-induced cardiomyocyte apoptosis and inflammatory response by sponging miR-138-5p (116). MicroRNA-31-5p acts as a negative regulator of circPAN3 by directly suppressing QKI in doxorubicin-induced apoptosis of cardiomyocytes (117). circPAN3 also ameliorates myocardial ischemia and reperfusion injury by regulating miR-421/Pink1 axis-mediated suppression of autophagy (118). HECTD1 overexpression increases cell viability and decreases cell apoptosis and migration, and circDLPAG4/HECTD1 mediates ischemia/reperfusion injury in endothelial cells via ER stress (119). Down-regulation of circFndc3b was observed in mice with myocardial infarction, and overexpression of circFndc3b increases angiogenic activity and reduces cell apoptosis in cardiac endothelial cells and cardiomyocytes which led to improved left ventricular functions (8). Other studies showed that miR-133 was regulated by circMAT2B. CircMAT2B knockdown attenuates oxygen-glucose deprivation-induced injury through up-regulating miR-133 in H9c2 cells (120). circNFIX can serve as a pro-apoptosis factor in cardiomyocytes (121). The expression of circ ACAP2 is induced by myocardial infarction which leads to increased cardiomyocyte apoptosis by sponging miR-29 (109). Salidroside inhibits apoptosis and autophagy of cardiomyocytes by regulation of circular RNA hsa_circ_0000064 in cardiac ischemia-reperfusion injury (122). These data suggest that circRNAs may be the new targets for designing cardioprotective treatments against cardiomyocyte death.

4) Coronary heart disease. circRNAs are involved in the pathogenesis of atherosclerosis and coronary heart disease. It has been reported that suppression of circDHCR24 alleviates aortic smooth muscle cell proliferation and migration by targeting miR-149-5p/MMP9 axis in human aortic vascular smooth muscle cells after PDGF-BB treatment (20). Recent studies showed that the expression level of circZNF609 in peripheral blood leukocytes of patients with coronary artery disease was significantly decreased, and circZNF609 regulates the release of inflammatory cytokines such as IL-6, IL-10, and TNF-α by serving as sponges to different miRNAs that control the expression of these cytokines (19). circMAP3K5 was downregulated in patients with coronary heart disease and acted as a microRNA-22-3p sponge to promote resolution of intimal hyperplasia via TET2-mediated smooth muscle cell differentiation (23). circRNA-100338 may induce angiogenesis after myocardial ischemia-reperfusion injury by sponging miR-200a-3p in human coronary endothelial cells (17). The level of hsa_circ_0001445 in plasma was associated with the severity of coronary atherosclerosis. *In vitro*, hsa_circ_0001445 was downregulated in extracellular vesicles secreted by human coronary smooth muscle cells upon exposure to atherogenic conditions (22). The 3 circRNAs (hsa_circ_0016868, hsa_circ_0001364, hsa_circ_0006731) have been verified by the coronary artery segments Sanger sequencing obtained from an 81-year-old male patient with the sudden death of myocardial infarction (18). In addition, a recent study on the differential expression of circRNAs in plasma samples from patients with coronary heart disease identified 9 circRNAs that promote the expression of transient receptor potential cation channel subfamily M member 3 by inhibiting hsa-miR-130a-3p (21). These data demonstrate that circRNAs play important roles in the pathogenesis of coronary heart disease and may serve as diagnostic or therapeutic targets for coronary heart disease.

TABLE 1 | Circular RNAs in cardiovascular disease and regeneration.

CVD type	CircRNAs	Source	Action mechanism	Regulation	References
Cardiac Hypertrophy	circRNA wwp1	Mouse myocardial tissue	Sponge miR-23a	Down	(107).
	circRNA HRCR	Mouse heart tissue	Sponge miR-223	Down	(108).
Myocardial Fibrosis	circ_LAS1L	Human cardiac fibroblasts	Sponge miR-125b	Down	(12)
	circ_BMP2K	Cardiac fibroblast	Sponge miR-455-3p	Down	(109)
	circPAN3	Rat myocardial tissue	Sponge miR-221	Up	(110)
	circ ACAP2	Rat cardiomyocytes cell lines	Sponge miR-29	Up	(109).
	circRNA_010567	Mouse cardiac fibroblasts	Sponge miR-141	Up	(111)
	circRNA_000203	Mouse cardiac fibroblasts	Sponge miR-26b-5p	Up	(112)
	circNFIB	Mouse heart tissue	Sponge miR-433	Down	(113)
	circHIPK3	Mouse cardiac fibroblasts	Sponge miR-29b-3p	UP	(114)
Cardiomyocyte	circ-ITCH	Rat cardiomyocytes cell lines	Sponge miR-17-5p	Down	(115)
Apoptosis	circSAMD4A	Rat cardiomyocytes cell lines	Sponge miR-138-5p	Up	(116)
	circPAN3	Rat myocardial tissue / Rat cardiomyocytes cell lines	Sponge miR-31-5p	Down	(117)
		Rat myocardial tissue / Rat Mouse myocardial tissue	Sponge miR-421	Down	(118)
	circDLGAP4	Human endothelial cell lines	Sponge miR-143	Down	(119)
	circFndc3b	Mouse myocardial tissue	Sponge RBP FUS	Up	(8)
	circMAT2B	Rat cardiomyocytes cell lines	Sponge miR-134	Up	(120)
	circNFIX	Rat cardiomyocytes cell lines	Unknown	Down	(121)
	circ ACAP2	Rat cardiomyocytes cell lines	Sponge miR-29	Up	(109)
	hsa_circ_0000064	Rat myocardial tissue	Unknown	Up	(122)
Coronary Heart Disease	circDHCR24	Human aortic vascular smooth muscle cell	Sponge miR-149	Up	(20)
	circZNF609	Human peripheral blood	Unknow	Down	(19)
	circMAP3K5	Human coronary artery smooth muscle cells	Sponge miR-22-3p	Down	(23)
	circRNA-100338	Human endothelial cell lines	Sponge miRNA-200a-3p	Down	(17)
	hsa_circ_0089378	Plasma	Sponge hsa-miR-130a-3p	Up	(21)
	hsa_circ_0083357				
	hsa_circ_0082824				
	hsa_circ_0068942				
	hsa_circ_0057576				
	hsa_circ_0054537				
	hsa_circ_0051172				
	hsa_circ_0032970				
	hsa_circ_0006323				
Heart Failure	hsa_circ_0005565	Human heart tissue	Unknown	Up	(16)
	hsa_circ_0097435	Human peripheral blood	Sponge Hsa_miR_609 Sponge Hsa_miR_1294 Sponge Hsa_miR_6799_5P Sponge Hsa_miR_5000_5P Sponge Hsa_miR_96_5P	Up	(15)
Myocardial Regeneration	circTLK1	Mouse myocardial tissue	Sponge miR-214	Up	(11)
	circRNA CDR1as	Pig myocardial tissue	Sponge miR-7	Up	(10)
	circ003593	Cardiomyocytes cell lines	Unknown	Up	(13)
	circ-0001273	Human umbilical cord mesenchymal stem cells (UMSCs)	Unknown	Down	(9)
	circCDYL	Mouse myocardial tissue	Sponge miR-4793-5p	Down	(14)
	circFASTKD1	Human endothelial cell lines	Sponge miR-106a	Down	(123)
	hsa_circ_0007623	Human endothelial cell lines	Sponge miR-297	Up	(124)
	circHipk3	Mouse heart tissue	Sponge miR-133a	Up	(104)
	circRNA_0001379	Mouse myocardial tissue	Sponge miR-17-5p	Up	(103)

5) Heart failure. Despite the detailed roles of circRNAs in the progression of human heart failure remains elusive, recent high-throughput sequencing studies identified many circRNAs with changed expression in patients with heart failure. The top highly expressed EAT circRNAs corresponded to genes involved in cell proliferation and inflammatory responses. A recent study on circRNA expression profile in epicardial adipose tissue in patients with heart failure showed that EAT circRNAs may contribute to the pathogenesis of metabolic disorders (16). Another study showed that the upregulation of Hsa_circ_0097435 contributes to the pathogenesis of heart failure via sponging multiple microRNAs (15).

6) Cardiac regeneration and repair. Recent studies indicated that modulating circRNA activity may have great therapeutic potential for myocardial regeneration and repair. Up- or down-regulation of circRNAs and miRNAs and circRNA-miRNA coexpression had been shown to change the expression of the genes associated with myocardial ischemia and reperfusion injuries (101, 103). It has been reported that circRNAs can regulate inflammatory factors to improve myocardial ischemia and reperfusion injury. The circTLK1 exacerbates myocardial ischemia and reperfusion injury via targeting miR-214/RIPK1 through TNF signaling pathway (11). circ003593 has also been shown to confer cardioprotection through NLRP3 inflammasome myocardial infarct rats (13). circRNA CDR1as was identified in pig hearts. Elevated circRNA CDR1as in the infarction region of the pig heart is negatively associated with infarct size and positively associated with improved heart function (10). circ-0001273 can remarkably inhibit myocardial cell apoptosis and promote repair in myocardial infarction hearts (9). circCDYL was downregulated in myocardial tissues and hypoxia myocardial cells after acute myocardial infarction. circCDYL overexpression and downregulation can promote and inhibit the proliferation of cardiomyocytes *in vitro*, respectively. Additionally, circCDYL can promote the proliferation of cardiomyocytes through the miR-4793-5p/APP pathway (14). The downregulation of circFASTKD1 induces angiogenesis and improves cardiac function and repair after myocardial infarction (123). Hsa_circ_0007623 can bind to miR-297 and acts as a sponge of microRNA-297 which promotes cardiac repair after acute myocardial ischemia and protects cardiac function (124). circHipk3 was overexpressed in the fetal or neonatal heart of mice and functioned to promote the proliferation of cardiomyocyte and endothelial cells which leads to angiogenesis. Further study showed that circHipk3 regulates cardiac regeneration in mice post myocardial infarction by interacting with Notch1 and miR-133a (104). These findings highlight the physiological role of circRNAs in cardiac repair and indicate that modulation of circRNA may represent a potential strategy to promote cardiac function and remodeling after myocardial injuries.

FUTURE PERSPECTIVES

The studies we discussed in the paper highlight the significance of circRNAs in the pathogenesis of CVDs. circRNAs are stable and abundantly present in the circulatory system which enables them to serve as biomarkers for the diagnosis and treatment of CVDs; however, there are some critical issues to be addressed. Firstly, there is no reliable methodology for the detection of circRNAs. In terms of circRNA detection, newer, simpler, and more reliable methods will be expected to appear. This will provide convenience for us to study circRNAs, facilitate the faster output of research results, and obtain more target circRNAs with diagnostic and therapeutic significance. Secondly, some circRNA biomarkers come from small samples and populations. This makes us question the reliability and representativeness of the research results. Thirdly, the mechanism underlying circRNA functions in the cardiovascular system remain largely elusive. For the function and mechanism studies, the current research methods are limited and difficult to operate. New research protocols need to be further explored. Rapid development can be achieved only by breaking through the technological bottleneck in the field of circRNA research. Lastly, there is a lack of efficient approaches for modulating circRNA expression in the cardiovascular system. It is supposed to be that in the future there will be new and more diverse methods in modulating the overexpression and inhibition of circRNAs. This will promote the development of the mechanism underlying circRNA functions. Then the research results can be quickly used for clinical diagnosis and treatment in the field of vascular diseases.

AUTHOR CONTRIBUTIONS

All authors listed have made a substantial, direct and intellectual contribution to the work, and approved it for publication.

FUNDING

This work is supported by NIH R01 grant HL142627 and American Heart Association Grant 20TPA35490001.

REFERENCES

1. Sanger HL, Riesner D, and Gross HJ, Kleinschmidt AK. Viroids are single-stranded covalently closed circular RNA molecules existing as highly base-paired rod-like structures. *Proc Natl Acad Sci USA*. (1976) 73:3852–6. doi: 10.1073/pnas.73.11.3852
2. Hsu MT, Coca-Prados M. Electron microscopic evidence for the circular form of RNA in the cytoplasm of eukaryotic cells. *Nature*. (1979) 280:339–40. doi: 10.1038/280339a0
3. Capel B, Nicolis AS, Hacker S, Walter M, Koopman P, Goodfellow P. Lovell-Badge R. Cell-Circular transcripts of the testis-determining gene Sry in adult mouse testis. *Cell*. (1993) 73:1019–30. doi: 10.1016/0092-8674(93)90279-Y
4. Salzman J, Gawad C, Wang PL, Lacayo N, Brown PO. Circular RNAs are the predominant transcript isoform from hundreds of human genes in diverse cell types. *PLoS One*. (2012) 7:e30733. doi: 10.1371/journal.pone.0030733
5. Hansen TB, Veno MT, Damgaard CK, Kjems J. Comparison of circular RNA prediction tools. *Nucleic Acids Res*. (2016) 44:e58. doi: 10.1093/nar/gkv1458
6. Li S, Li X, Xue W, Zhang L, Yang LZ, Cao SM, et al. Screening for functional circular RNAs using the CRISPR-Cas13 system. *Nat Methods*. (2021) 18:51–59. doi: 10.1038/s41592-020-01011-4
7. Jakobi T, Czaja-Hasse LF, Reinhardt R, Dieterich C. Profiling and validation of the circular RNA repertoire in adult murine hearts. *Gen Prot Bioinform*. (2016) 14:216–23. doi: 10.1016/j.gpb.2016.02.003

8. Garikipati VNS, Verma SK, Cheng Z, Liang D, Truongcao MM, Cimini M, et al. Circular RNA CircFndc3b modulates cardiac repair after myocardial infarction via FUS/VEGF-A axis. *Nat Commun.* (2019) 10:4317. doi: 10.1038/s41467-019-11777-7
9. Lei D, Wang Y, Zhang L, Wang Z. Circ_0010729 regulates hypoxia-induced cardiomyocyte injuries by activating TRAF5 via sponging miR-27a-3p. *Life Sci.* (2020) 262:118511. doi: 10.1016/j.lfs.2020.118511
10. Mester-Tonczar J, Winkler J, Einzinger P, Hasimbegovic E, Kastner N, Lukovic D, et al. Association between circular RNA CDR1as and post-infarction cardiac function in pig ischemic heart failure: influence of the anti-fibrotic natural compounds bufalin and lycorine. *Biomolecules.* (2020) 10:1180. doi: 10.3390/biom10081180
11. Song YF, Zhao L, Wang BC, Sun JJ, Hu JL, Zhu XL, et al. The circular RNA TLK1 exacerbates myocardial ischemia/reperfusion injury via targeting miR-214/RIPK1 through TNF signaling pathway. *Free Radic Biol Med.* (2020) 155:69–80. doi: 10.1016/j.freeradbiomed.2020.05.013
12. Sun LY, Zhao JC, Ge XM, Zhang H, Wang CM, Bie ZD. Circ_LAS1L regulates cardiac fibroblast activation, growth, and migration through miR-125b/SFRP5 pathway. *Cell Biochem Funct.* (2020) 38:443–50. doi: 10.1002/cbf.3486
13. Xiao Y, Oumarou DB, Wang S, Liu Y. Circular RNA involved in the protective effect of *Malva sylvestris* L. on myocardial ischemic/re-perfused *Injury Front Pharmacol.* (2020) 11:520486. doi: 10.3389/fphar.2020.520486
14. Zhang M, Wang Z, Cheng Q, Wang Z, Lv X, Wang Z, et al. Circular RNA (circRNA) CDYL induces myocardial regeneration by ceRNA amyocardial infarction. *Med Sci Monit.* (2020) 26:e923188. doi: 10.12659/MSM.923188
15. Han J, Zhang L, Hu L, Yu H, Xu F, Yang B, et al. Circular RNA-expression profiling reveals a potential role of Hsa_circ_0097435 in heart failure via sponging multiple MicroRNAs. *Front Genet.* (2020) 11:212. doi: 10.3389/fgene.2020.00212
16. Zheng ML, Du XP, Zhao L, Yang XC. Expression profile of circular RNAs in epicardial adipose tissue in heart failure. *Chin Med J.* (2020) 133:2565–72. doi: 10.1097/CM9.0000000000001056
17. Chang H, Wu ZB, Zhang L. Circ-100338 induces angiogenesis after myocardial ischemia-reperfusion injury by sponging miR-200a-3p. *Eur Rev Med Pharmacol Sci.* (2020) 24:6323–32.doi: 10.26355/eurrev_202006_21530
18. Hou C, Gu L, Guo Y, Zhou Y, Hua L, Chen J, et al. Association between circular RNA expression content and severity of coronary atherosclerosis in human coronary artery. *J Clin Lab Anal.* (2020) 34:e23552. doi: 10.1002/jcla.23552
19. Liang B, Li M, Deng Q, Wang C, Rong J, He S, et al. CircRNA ZNF609 in peripheral blood leukocytes acts as a protective factor and a potential biomarker for coronary artery disease. *Ann Transl Med.* (2020) 8:741. doi: 10.21037/atm-19-4728
20. Peng W, Li T, Pi S, Huang L, Liu Y. Suppression of circular RNA circDHCR24 alleviates aortic smooth muscle cell proliferation and migration by targeting miR-149-5p/MMP9 axis. *Biochem Biophys Res Commun.* (2020) 529:753–9. doi: 10.1016/j.bbrc.2020.06.067
21. Pan RY, Liu P, Zhou HT, Sun WX, Song J, Shu J, et al. Circular RNAs promote TRPM3 expression by inhibiting hsa-miR-130a-3p in coronary artery disease patients. *Oncotarget.* (2020) 8:60280–90. doi: 10.18632/oncotarget.19941
22. Vilades D, Martinez-Camblor P, Ferrero-Gregori A, Bar C, Lu D, Xiao K, et al. Plasma circular RNA hsa_circ_0001445 and coronary artery disease: performance as a biomarker. *FASEB J.* (2020) 34:4403–14. doi: 10.1096/fj.201902507R
23. Zeng Z, Xia L, Fan S, Zheng J, Qin J, Fan X, et al. Circular RNA CircMAP3K5 acts as a MicroRNA-22-3p sponge to promote resolution of intimal hyperplasia via TET2-mediated smooth muscle cell differentiation. *Circulation.* (2021) 143:354–71. doi: 10.1161/CIRCULATIONAHA.120.049715
24. Vausort M, Salgado-Somoza A, Zhang L, Leszek P, Scholz M, Teren A, et al. Myocardial infarction-associated circular RNA predicting left ventricular dysfunction. *J Am Coll Cardiol.* (2016) 68:1247–8. doi: 10.1016/j.jacc.2016.06.040
25. Zhao Z, Li X, Gao C, Jian D, Hao P, Rao L, et al. Peripheral blood circular RNA hsa_circ_0124644 can be used as a diagnostic biomarker of coronary artery disease. *Sci Rep.* (2017) 7:39918. doi: 10.1038/srep39918
26. Zhang J, Xu Y, Xu S, Liu Y, Yu L, Li Z, et al. Plasma circular RNAs, Hsa_circRNA_025016, predict postoperative atrial fibrillation after isolated off-pump coronary artery bypass grafting. *J Am Heart Assoc.* (2018) 7:6642. doi: 10.1161/JAHA.117.006642
27. Jeck WR, Sorrentino JA, Wang K, Slevin MK, Burd CE, Liu J, et al. Circular RNAs are abundant, conserved, and associated with ALU repeats. *RNA.* (2013) 19:141–157. doi: 10.1261/rna.035667.112
28. Zhang Y, Zhang XO, Chen T, Xiang JF, Yin QF, Xing YH, et al. Circular intronic long noncoding RNAs. *Mol Cell.* (2013) 51:792–806. doi: 10.1016/j.molcel.2013.08.017
29. Li Z, Huang C, Bao C, Chen L, Lin M, Wang X, et al. Exon-intron circular RNAs regulate transcription in the nucleus. *Nat Struct Mol Biol.* (2015) 22:256–64. doi: 10.1038/nsmb.2959
30. Schmidt CA, Matera AG. tRNA introns: presence, processing, and purpose. *Wiley Interdiscip Rev RNA.* (2020) 11:e1583. doi: 10.1002/wrna.1583
31. Zhang XO, Wang HB, Zhang Y, Lu X, Chen LL, Yang L. Complementary sequence-mediated exon circularization. *Cell.* (2014) 159:134–47. doi: 10.1016/j.cell.2014.09.001
32. Ashwal-Fluss R, Meyer M, Pamudurti NR, Ivanov A, Bartok O, Hanan M, et al. circRNA biogenesis competes with pre-mRNA splicing. *Mol Cell.* (2014) 56:55–66. doi: 10.1016/j.molcel.2014.08.019
33. Petkovic S, Muller S. RNA circularization strategies *in vivo* and *in vitro*. *Nucleic Acids Res.* (2015) 43:2454–65. doi: 10.1093/nar/gkv045
34. Shi Y, He R, Yang Y, He Y, Shao K, Zhan L, et al. Circular RNAs: Novel biomarkers for cervical, ovarian and endometrial cancer. *Oncol Rep.* (2020) 44:1787–98. doi: 10.3892/or.2020.7780
35. Bachmayr-Heyda A, Reiner AT, Auer K, Sukhbaatar N, Aust S, Bachleitner-Hofmann T, et al. Correlation of circular RNA abundance with proliferation–exemplified with colorectal and ovarian cancer, idiopathic lung fibrosis, and normal human tissues. *Sci Rep.* (2015) 5:8057. doi: 10.1038/srep08057
36. Conn SJ, Pillman KA, Toubia J, Conn VM, Salmanidis M, Phillips CA, et al. The RNA binding protein quaking regulates formation of circRNAs. *Cell.* (2015) 160:1125–1134. doi: 10.1016/j.cell.2015.02.014
37. Kramer MC, Liang D, Tatomer DC, Gold B, March ZM, Cherry S, et al. Combinatorial control of Drosophila circular RNA expression by intronic repeats, hnRNPs, SR proteins. *Genes Dev.* (2015) 29:2168–82. doi: 10.1101/gad.270421.115
38. Li X, Liu CX, Xue W, Zhang Y, Jiang S, Yin QF, et al. Coordinated circRNA biogenesis and function with NF90/NF110 in viral infection. *Mol Cell.* (2017) 67:214–27 e217. doi: 10.1016/j.molcel.2017.05.023
39. Salzman J, Chen RE, Olsen MN, Wang PL, Brown PO. Cell-type specific features of circular RNA expression. *PLoS Genet.* (2013) 9:e1003777. doi: 10.1371/annotation/f782282b-eefa-4c8d-985c-b1484e845855
40. Xu T, Wu J, Han P, Zhao Z, Song X. Circular RNA expression profiles and features in human tissues: a study using RNA-seq data. *BMC Genomics.* (2017) 18:680. doi: 10.1186/s12864-017-4029-3
41. Zeng X, Lin W, Guo M, Zou Q. A comprehensive overview and evaluation of circular RNA detection tools. *PLoS Comput Biol.* (2017) 13:e1005420. doi: 10.1371/journal.pcbi.1005420
42. Li XF, Lytton J. A circularized sodium-calcium exchanger exon 2 transcript. *J Biol Chem.* (1999) 274:8153–60. doi: 10.1074/jbc.274.12.8153
43. Memczak S, Jens M, Elefsinioti A, Torti F, Krueger J, Rybak A, et al. Circular RNAs are a large class of animal RNAs with regulatory potency. *Nature.* (2013) 495:333–8. doi: 10.1038/nature11928
44. Li Y, Zhang J, Huo C, Ding N, Li J, Xiao J, et al. Dynamic Organization of lncRNA and circular RNA regulators collectively controlled cardiac differentiation in humans. *EBioMedicine.* (2017) 24:137–46. doi: 10.1016/j.ebiom.2017.09.015
45. Siede D, Rapti K, Gorska AA, Katus HA, Altmuller J, Boeckel JN, et al. Identification of circular RNAs with host gene-independent expression in human model systems for cardiac differentiation and disease. *J Mol Cell Cardiol.* (2017) 109:48–56. doi: 10.1016/j.yjmcc.2017.06.015
46. Guo JU, Agarwal V, Guo H, Bartel DP. Expanded identification and characterization of mammalian circular RNAs. *Genome Biol.* (2014) 15:409. doi: 10.1186/s13059-014-0409-z
47. Werfel S, Nothjunge S, Schwarzmayr T, Strom TM, Meitinger T, Engelhardt S. Characterization of circular RNAs in human, mouse and rat hearts. *J Mol Cell Cardiol.* (2016) 98:103–7. doi: 10.1016/j.yjmcc.2016.07.007

48. Aufiero S, Reckman YJ, Pinto YM, Creemers EE. Circular RNAs open a new chapter in cardiovascular biology. *Nat Rev Cardiol.* (2019) 16:503–14. doi: 10.1038/s41569-019-0185-2
49. Lim TB, Lavenniah A, Foo RS. Circles in the heart and cardiovascular system. *Cardiovasc Res.* (2020) 116:269–78. doi: 10.1093/cvr/cvz227
50. Gupta SK, Garg A, Bar C, Chatterjee S, Foinquinos A, Milting H, et al. Quaking inhibits doxorubicin-mediated cardiotoxicity through regulation of cardiac circular RNA expression. *Circ Res.* (2018) 122:246–54. doi,: 10.1161/C.I.R.C.R.E.S.A.H.A.117.311335
51. Dong R, Zhang XO, Zhang Y, Ma XK, Chen LL, Yang L. CircRNA-derived pseudogenes. *Cell Res.* (2016) 26:747–50. doi: 10.1038/cr.2016.42
52. Bartel DP. MicroRNAs: target recognition and regulatory functions. *Cell.* (2009) 136:215–33. doi: 10.1016/j.cell.2009.01.002
53. Hansen TB, Jensen TI, Clausen BH, Bramsen JB, Finsen B, Damgaard CK, et al. Natural RNA circles function as efficient microRNA sponges. *Nature.* (2013) 495:384–8. doi: 10.1038/nature11993
54. Zhang L, Zhang Y, Wang Y, Zhao Y, Ding H, Li P. Circular RNAs: functions and clinical significance in cardiovascular disease. *Front Cell Dev Biol.* (2020) 8:584051. doi: 10.3389/fcell.2020.584051
55. Wong CH, Lou UK, Li Y, Chan SL, Tong JH, To KF, et al. CircFOXK2 promotes growth and metastasis of pancreatic ductal adenocarcinoma by complexing with RNA-binding proteins and sponging MiR-942. *Cancer Res.* (2020) 80:2138–49. doi: 10.1158/0008-5472.CAN-19-3268
56. Yu X, Xiao W, Song H, Jin Y, Xu J, Liu X. CircRNA_100876 sponges miR-136 to promote proliferation and metastasis of gastric cancer by upregulating MIEN1 expression. *Gene.* (2020) 748:144678. doi: 10.1016/j.gene.2020.144678
57. Ji F, Du R, Chen T, Zhang M, Zhu Y, Luo X, et al. Circular RNA circSLC26A4 accelerates cervical cancer progression via miR-1287-5p/HOXA7 axis. *Mol Ther Nucleic Acids.* (2020) 19:413–20. doi: 10.1016/j.omtn.2019.11.032
58. Song J, Chen ZH, Zheng CJ, Song KH, Xu GY, Xu S, et al. Exosome-Transported circRNA_0000253 competitively adsorbs MicroRNA-141-5p and increases IDD. *Mol Ther Nucleic Acids.* (2020) 21:1087–99. doi: 10.1016/j.omtn.2020.07.039
59. Li C, Mu J, Shi Y, Xin H. LncRNA CCDC26 interacts with CELF2 protein to enhance myeloid leukemia cell proliferation and invasion via the circRNA_ANKIB1/miR-195-5p/PRR11 axis. *Cell Transplant.* (2021) 30: 80. doi: 10.1177/0963689720986080
60. Dong K, He X, Su H, Fulton DJR, Zhou J. Genomic analysis of circular RNAs in heart. *BMC Med Genomics.* (2020) 13:167. doi: 10.1186/s12920-020-00817-7
61. Pan X, Shen HB. RNA-protein binding motifs mining with a new hybrid deep learning based cross-domain knowledge integration approach. *BMC Bioinform.* (2017) 18:136. doi: 10.1186/s12859-017-1561-8
62. Pan X, Rijnbeek P, Yan J, Shen HB. Prediction of RNA-protein sequence and structure binding preferences using deep convolutional and recurrent neural networks. *BMC Gen.* (2018) 19:511. doi: 10.1186/s12864-018-4889-1
63. Pan X, Shen HB. Predicting RNA-protein binding sites and motifs through combining local and global deep convolutional neural networks. *Bioinformatics.* (2018) 34:3427–36. doi: 10.1093/bioinformatics/bty364
64. Wang Z, Lei X, Wu FX. Identifying cancer-specific circRNA-RBP binding sites based on deep learning. *Molecules.* (2019) 24:35. doi: 10.3390/molecules24224035
65. Bhuyan R, Bagchi A. Prediction of the differentially expressed circRNAs to decipher their roles in the onset of human colorectal cancers. *Gene.* (2020) 762:145035. doi: 10.1016/j.gene.2020.145035
66. Wawrzyniak O, Zarebska Z, Kuczynski K, Gotz-Wieckowska A, Rolle K. Protein-related circular RNAs in human pathologies. *Cells.* (2020) 9:1841. doi: 10.3390/cells9081841
67. Tang Q, Hann SS. Biological roles and mechanisms of circular RNA in human cancers. *Onco Targets Ther.* (2020) 13:2067–92. doi: 10.2147/OTT.S233672
68. Zang J, Lu D, Xu A. The interaction of circRNAs and RNA binding proteins: An important part of circRNA maintenance and function. *J Neurosci Res.* (2020) 98:87–97. doi: 10.1002/jnr.24356
69. Abdelmohsen K, Panda AC, Munk R, Grammatikakis I, Dudekula DB, De S, et al. Identification of HuR target circular RNAs uncovers suppression of PABPN1 translation by CircPABPN1. *RNA Biol.* (2017) 14:361–9. doi: 10.1080/15476286.2017.1279788
70. Holdt LM, Stahringer A, Sass K, Pichler G, Kulak NA, Wilfert W, et al. Circular non-coding RNA ANRIL modulates ribosomal RNA maturation and atherosclerosis in humans. *Nat Commun.* (2016) 7:12429. doi: 10.1038/ncomms12429
71. Du WW, Yang W, Chen Y, Wu ZK, Foster FS, Yang Z, et al. Foxo3 circular RNA promotes cardiac senescence by modulating multiple factors associated with stress and senescence responses. *Eur Heart J.* (2017) 38:1402–12. doi: 10.1093/eurheartj/ehw001
72. Yang ZG, Awan FM, Du WW, Zeng Y, Lyu J, Wu, et al.upta S, et al. The circular RNA interacts with STAT3, increasing its nuclear translocation and wound repair by modulating Dnmt3a and miR-17 function. *Mol Ther.* (2017) 25:2062–74. doi: 10.1016/j.ymthe.2017.05.022
73. Zeng Y, Du WW, Wu Y, Yang Z, Awan FM, Li X, et al. A circular RNA binds to and activates AKT phosphorylation and nuclear localization reducing apoptosis and enhancing cardiac repair. *Theranostics.* (2017) 7:3842–55. doi: 10.7150/thno.19764
74. Okholm TLH, Sathe S, Park SS, Kamstrup AB, Rasmussen AM, Shankar A, et al. Transcriptome-wide profiles of circular RNA and RNA-binding protein interactions reveal effects on circular RNA biogenesis and cancer pathway expression. *Genome Med.* (2020) 12:112. doi: 10.1186/s13073-020-00812-8
75. Kalyana-Sundaram S, Kumar-Sinha C, Shankar S, Robinson DR, Wu YM, Cao X, et al. Expressed pseudogenes in the transcriptional landscape of human cancers. *Cell.* (2012) 149:1622–34. doi: 10.1016/j.cell.2012.04.041
76. Yang Y, Fan X, Mao M, Song X, Wu P, Zhang Y, et al. Extensive translation of circular RNAs driven by N(6)-methyladenosine. *Cell Res.* (2017) 27:626–41. doi: 10.1038/cr.2017.31
77. Legnini I, Di Timoteo G, Rossi F, Morlando M, Briganti F, Sthandier O, et al. Circ-ZNF609 is a circular RNA that can be translated and functions in myogenesis. *Mol Cell.* (2017) 66:22–37 e29. doi: 10.1016/j.molcel.2017.02.017
78. Yin H, Shen X, Zhao J, Cao X, He H, Han S, et al. Circular RNA circfam188b encodes a protein that regulates proliferation and differentiation of chicken skeletal muscle satellite cells. *Front Cell Dev Biol.* (2020) 8:522588. doi: 10.3389/fcell.2020.522588
79. Cy C, Sarnow P. Initiation of protein synthesis by the eukaryotic translational apparatus on circular RNAs. *Science.* (1995) 268:415–7. doi: 10.1126/science.7536344
80. Macejak GD, Sarnow P. Internal initiation of translation mediated by the 5′ leader of a cellular mRNA. *Nature.* (1991) 353:90–4. doi: 10.1038/353090a0
81. Abe N, Hiroshima M, Maruyama H, Nakashima Y, Nakano Y, Matsuda A, et al. Rolling circle amplification in a prokaryotic translation system using small circular RNA. *Angew Chem Int Ed Engl.* (2013) 52:7004–8. doi: 10.1002/anie.201302044
82. Hentze MW, Preiss T. Circular RNAs: splicing's enigma variations. *EMBO J.* (2013) 32:923–5. doi: 10.1038/emboj.2013.53
83. Dong W, Dai ZH, Liu FC, Guo XG, Ge CM, Ding J, et al. The RNA-binding protein RBM3 promotes cell proliferation in hepatocellular carcinoma by regulating circular RNA SCD-circRNA 2 production. *EBioMed.* (2019) 45:155–67. doi: 10.1016/j.ebiom.2019.06.030
84. Du WW, Yang W, Liu E, Yang Z, Dhaliwal P, Yang BB. Foxo3 circular RNA retards cell cycle progression via forming ternary complexes with p21 and CDK2. *Nucleic Acids Res.* (2016) 44:2846–58. doi: 10.1093/nar/gkw027
85. Van Dijk EL, Auger H, Jaszczyszyn Y, Thermes C. Ten years of next-generation sequencing technology. *Trends Genet.* (2014) 30:418–26. doi: 10.1016/j.tig.2014.07.001
86. Wang J, Ren Q, Hua L, Chen J, Zhang J, Bai H, et al. Comprehensive analysis of differentially expressed mRNA, lncRNA and circRNA and their ceRNA networks in the longissimus dorsi muscle of two different pig breeds. *Int J Mol Sci.* (2019) 20:1107. doi: 10.3390/ijms20051107
87. Zhang XO, Dong R, Zhang Y, Zhang JL, Luo Z, Zhang J, et al. Diverse alternative back-splicing and alternative splicing landscape of circular RNAs. *Genome Res.* (2016) 26:1277–87. doi: 10.1101/gr.202895.115
88. Dahl M, Daugaard I, Andersen MS, Hansen TB, Gronbaek K, Kjems J, et al. Enzyme-free digital counting of endogenous circular RNA molecules in B-cell malignancies. *Lab Invest.* (2018) 98:1657–69. doi: 10.1038/s41374-018-0108-6
89. Glazar P, Papavasileiou P, Rajewsky N. circBase: a database for circular RNAs. *RNA.* (2014) 20:1666–70. doi: 10.1261/rna.043687.113

90. Vo JN, Cieslik M, Zhang Y, Shukla S, Xiao L, Zhang Y, et al. The landscape of circular RNA in cancer. *Cell.* (2019) 176:869–81 e813. doi: 10.1016/j.cell.2018.12.021
91. Sekar S, Cuyugan L, Adkins J, Geiger P, Liang WS. Circular RNA expression and regulatory network prediction in posterior cingulate astrocytes in elderly subjects. *BMC Genomics.* (2018) 19:340. doi: 10.1186/s12864-018-4670-5
92. Sekar S, Geiger P, Cuyugan L, Boyle A, Serrano G, Beach TG, et al. Identification of circular RNAs using RNA sequencing. *J Vis Exp*. (2019). doi: 10.3791/59981
93. Zhang QL, Ji XY, Li HW, Guo J, Wang F, Deng XY, et al. Identification of circular RNAs and their altered expression under poly(I:C) challenge in key antiviral immune pathways in amphioxus. *Fish Shellfish Immunol.* (2019) 86:1053–7. doi: 10.1016/j.fsi.2018.12.061
94. Panda AC, De S, Grammatikakis I, Munk R, Yang X, Piao Y, et al. High-purity circular RNA isolation method (RPAD) reveals vast collection of intronic circRNAs. *Nucleic Acids Res.* (2017) 45:e116. doi: 10.1093/nar/gkx297
95. Chuang TJ, Chen YJ, Chen CY, Mai TL, Wang YD, Yeh CS, et al. Integrative transcriptome sequencing reveals extensive alternative trans-splicing and cis-backsplicing in human cells. *Nucleic Acids Res.* (2018) 46:3671–91. doi: 10.1093/nar/gky032
96. Yang Y, Gao X, Zhang M, Yan S, Sun C, Xiao F, et al. Novel role of FBXW7 circular RNA in repressing glioma tumorigenesis. *J Natl Cancer Inst.* (2018) 110:166. doi: 10.1093/jnci/djx166
97. Wang L, Long H, Zheng Q, Bo X, Xiao X, Li B. Circular RNA circRHOT1 promotes hepatocellular carcinoma progression by initiation of NR2F6 expression. *Mol Cancer.* (2019) 18:119. doi: 10.1186/s12943-019-1046-7
98. Labaj PP, Leparc GG, Linggi BE, Markillie LM, Wiley HS, Kreil DP. Characterization and improvement of RNA-Seq precision in quantitative transcript expression profiling. *Bioinformatics.* (2011) 27:i383–91. doi: 10.1093/bioinformatics/btr247
99. Li S, Teng S, Xu J, Su G, Zhang Y, Zhao J, et al. Microarray is an efficient tool for circRNA profiling. *Brief Bioinform.* (2019) 20:1420–33. doi: 10.1093/bib/bby006
100. López-Jiménez E, Ana R., Andrés-León E. RNA sequencing and prediction tools for circular RNAs analysis. *Adv Exp Med Biol*. (2018) 1087:17–33. doi: 10.1007/978-981-13-1426-1_2
101. Lin F, Yang Y, Guo Q, Xie M, Sun S, Wang X, et al. Analysis of the molecular mechanism of acute coronary syndrome based on circRNA-miRNA network regulation. *Evid Based Complement Alternat Med.* (2020) 2020:1584052. doi: 10.1155/2020/1584052
102. Liu T, Zhang G, Wang Y, Rao M, Zhang Y, Guo A, et al. Identification of Circular RNA-MicroRNA-Messenger RNA regulatory network in atrial fibrillation by integrated analysis. *Biomed Res Int.* (2020) 2020:8037273. doi: 10.1155/2020/8037273
103. Sun Z, Yu T, Jiao Y, He D, Wu J, Duan W, et al. Expression profiles and ontology analysis of circular RNAs in a mouse model of myocardial ischemia/reperfusion injury. *Biomed Res Int.* (2020) 2020:2346369. doi: 10.1155/2020/2346369
104. Si X, Zheng H, Wei G, Li M, Li W, Wang H, et al. circRNA Hipk3 induces cardiac regeneration after myocardial infarction in mice by binding to Notch1 and miR-133a. *Mol Ther Nucleic Acids.* (2020) 21:636–55. doi: 10.1016/j.omtn.2020.06.024
105. Sun JY, Shi Y, Cai XY, Liu J. Potential diagnostic and therapeutic value of circular RNAs in cardiovascular diseases. *Cell Signal.* (2020) 71:109604. doi: 10.1016/j.cellsig.2020.109604
106. Chen JX, Hua L, Zhao CH, Jia QW, Zhang J, Yuan JX, et al. Quantitative proteomics reveals the regulatory networks of circular RNA BTBD7_hsa_circ_0000563 in human coronary artery. *J Clin Lab Anal.* (2020) 34:e23495. doi: 10.1002/jcla.23495
107. Ming-Hui Yang HW, Sheng-Na, H.an, Xin, J.ia, Si, et al.hang, Fei-Fei, D.ai, Meng-Jiao, Z.hou, Zhongnan, et al. Circular RNA expression in isoproterenol hydrochloride-induced cardiac hypertrophy. *Aging.* (2020) 12:2530–44. doi: 10.18632/aging.102761
108. Wang K, Long B, Liu F, Wang JX, Liu CY, Zhao B, et al. A circular RNA protects the heart from pathological hypertrophy and heart failure by targeting miR-223. *Eur Heart J.* (2016) 37:2602–11. doi: 10.1093/eurheartj/ehv713
109. Liu X, Wang M, Li Q, Liu W, Jiang H. *CircRNA ACAP2 Induces Myocardial Apoptosis After Myocardial Infarction by Sponging miR-29*. Minerva Medica. (2020).
110. Li F, Long TY, Bi SS, Sheikh SA, Zhang CL. circPAN3 exerts a profibrotic role via sponging miR-221 through FoxO3/ATG7-activated autophagy in a rat model of myocardial infarction. *Life Sci.* (2020) 257:118015. doi: 10.1016/j.lfs.2020.118015
111. Zhou B, Yu JW. A novel identified circular RNA. circRNA_010567, promotes myocardial fibrosis via suppressing miR-141 by targeting TGF-beta1. *Biochem Biophys Res Commun.* (2017) 487:769–75. doi: 10.1016/j.bbrc.2017.04.044
112. Tang CM, Zhang M, Huang L, Hu ZQ, Zhu JN, Xiao Z, et al. CircRNA_000203 enhances the expression of fibrosis-associated genes by derepressing targets of miR-26b-5p, Col1a2 and CTGF, in cardiac fibroblasts. *Sci Rep.* (2017) 7:40342. doi: 10.1038/srep40342
113. Zhu Y, Pan W, Yang T, Meng X, Jiang Z, Tao L, et al. Upregulation of circular RNA CircNFIB attenuates cardiac fibrosis by sponging miR-433. *Front Genet.* (2019) 10:564. doi: 10.3389/fgene.2019.00564
114. Ni H, Li W, Zhuge Y, Xu S, Wang Y, Chen Y, et al. Inhibition of circHIPK3 prevents angiotensin II-induced cardiac fibrosis by sponging miR-29b-3p. *Int J Cardiol.* (2019) 292:188–96. doi: 10.1016/j.ijcard.2019.04.006
115. Zhang N, Wang X. Circular RNA ITCH mediates H2O2-induced myocardial cell apoptosis by targeting miR-17-5p via wnt/beta-catenin signalling pathway. *Int J Exp Pathol.* (2020) 102:22–31. doi: 10.1111/iep.12367
116. Hu X, Ma R, Cao J, Du X, Cai X, Fan Y. CircSAMD4A aggravates H/R-induced cardiomyocyte apoptosis and inflammatory response by sponging miR-138-5p. *J Cell Mol Med.* (2020). doi: 10.1111/jcmm.16093
117. Ji X, Ding W, Xu T, Zheng X, Zhang J, Liu M, et al. MicroRNA-31-5p attenuates doxorubicin-induced cardiotoxicity via quaking and circular RNA Pan3. *J Mol Cell Cardiol.* (2020) 140:56–67. doi: 10.1016/j.yjmcc.2020.02.009
118. Zhang CL, Long TY, Bi SS, Sheikh SA, Li F. CircPAN3 ameliorates myocardial ischaemia/reperfusion injury by targeting miR-421/Pink1 axis-mediated autophagy suppression. *Lab Invest.* (2021) 101:89–103. doi: 10.1038/s41374-020-00483-4
119. Chen L, Luo W, Zhang W, Chu H, Wang J, Dai X, et al. circDLPAG4/HECTD1 mediates ischaemia/reperfusion injury in endothelial cells via ER stress. *RNA Biol.* (2020) 17:240–53. doi: 10.1080/15476286.2019.1676114
120. Zhu Y, Zou C, Jia Y, Zhang H, Ma X, Zhang J. Knockdown of circular RNA circMAT2B reduces oxygen-glucose deprivation-induced inflammatory injury in H9c2 cells through up-regulating miR-133. *Cell Cycle.* (2020) 19:2622–30. doi: 10.1080/15384101.2020.1814025
121. Cui X, Dong Y, Li M, Wang X, Jiang M, Yang W, et al. A circular RNA from NFIX facilitates oxidative stress-induced H9c2 cells apoptosis. *In Vitro Cell Dev Biol Anim.* (2020) 56:715–22. doi: 10.1007/s11626-020-00476-z
122. Jin P, Li LH, Shi Y, Hu NB. Salidroside inhibits apoptosis and autophagy of cardiomyocyte by regulation of circular RNA hsa_circ_0000064 in cardiac ischemia-reperfusion injury. *Gene.* (2021) 767:145075. doi: 10.1016/j.gene.2020.145075
123. Gao WQ, Hu XM, Zhang Q, Yang L, Lv XZ, Chen S, et al. (2021). Downregulation of circFASTKD1 ameliorates myocardial infarction by promoting angiogenesis. *Aging.* 13:3588–604. doi: 10.18632/aging.202305
124. Zhang Q, Sun W, Han J, Cheng S, Yu P, Shen L, et al. The circular RNA hsa_circ_0007623 acts as a sponge of microRNA-297 and promotes cardiac repair. *Biochem Biophys Res Commun.* (2020) 523:993–1000. doi: 10.1016/j.bbrc.2019.12.116

Conflict of Interest: The authors declare that the research was conducted in the absence of any commercial or financial relationships that could be construed as a potential conflict of interest.

frontiers in Cardiovascular Medicine

REVIEW
published: 31 May 2021
doi: 10.3389/fcvm.2021.691548

Therapeutic Exosomes in Prognosis and Developments of Coronary Artery Disease

Ai-Qun Chen[1], Xiao-Fei Gao[1,2], Zhi-Mei Wang[1], Feng Wang[1], Shuai Luo[1], Yue Gu[1], Jun-Jie Zhang[1,2] and Shao-Liang Chen[1,2]**

[1] Department of Cardiology, Nanjing First Hospital, Nanjing Medical University, Nanjing, China, [2] Department of Cardiology, Nanjing Heart Centre, Nanjing, China

Exosomes, with an diameter of 30∼150 nm, could be released from almost all types of cells, which contain diverse effective constituent, such as RNAs, proteins, lipids, and so on. In recent years, exosomes have been verified to play an important role in mechanism, diagnosis, treatment, and prognosis of cardiovascular disease, especially coronary artery disease (CAD). Moreover, it has also been shown that exosomes derived from different cell types have various biological functions based on the cell stimulation and microenvironment. However, therapeutic exosomes are currently far away from clinical translation, despite it is full of hope. In this review, we summarize an update of the recent studies and systematic knowledge of therapeutic exosomes in atherosclerosis, myocardial infarction, and in-stent restenosis, which might provide a novel insight into the treatment of CAD and promote the potential clinical application of therapeutic exosomes.

Keywords: exosomes, CAD, atherosclerosis, myocardial infarction, drug delivery

OPEN ACCESS

Edited by:
Junjie Yang,
University of Alabama at Birmingham, United States

Reviewed by:
Chaoshan Han,
University of Alabama at Birmingham, United States
Na Xu,
Heart Institute, Cincinnati Children's Hospital Medical Center, United States

****Correspondence:***
Jun-Jie Zhang
jameszll@163.com
Shao-Liang Chen
chmengx@126.com

Specialty section:
This article was submitted to Cardiovascular Biologics and Regenerative Medicine, a section of the journal Frontiers in Cardiovascular Medicine

Received: *06 April 2021*
Accepted: *11 May 2021*
Published: *31 May 2021*

Citation:
Chen A-Q, Gao X-F, Wang Z-M, Wang F, Luo S, Gu Y, Zhang J-J and Chen S-L (2021) Therapeutic Exosomes in Prognosis and Developments of Coronary Artery Disease. Front. Cardiovasc. Med. 8:691548. doi: 10.3389/fcvm.2021.691548

INTRODUCTION

Coronary artery disease (CAD) still remains a high-prevalence, high-risk, and high-fatality cardiovascular disease worldwide. In spite of the profound development of device and agents in CAD treatment, the prognosis of CAD, especially acute myocardial infarction, is far from being satisfactory (1, 2). Recently, exosome emerges as a novel, full of hope, and potential alternative to cell-based therapies of CAD due to its cardioprotective properties (3).

Exosomes, with diameter of 30∼150 nm and density of 1.13∼1.19 g/ml, are the smallest extracellular vesicles (EVs) (4), with a bilayer membrane structure released by almost all types of cells (5, 6). The biogenesis of exosomes triggers from membrane proteins being endocytosed via inward budding of the cell membrane, which are then transferred to early endosomes (EEs). Afterwards, the EEs mature into multivesicle bodies (MVBs), filled with numerous intraluminal vesicles (ILVs) (7, 8), which incorporate proteins, lipids, and genetic material during invagination (9). Finally, MVBs can fuse with cell membrane and release ILVs to the extracellular space (10), as we call them exosomes, or result in degradation via fusing with lysosomes (**Figure 1**) (11).

However, therapeutic exosomes are currently far away from clinical application, in spite of so many outstanding qualities of exosomes. In this review, we will summarize an update of the recent findings and systematic knowledge of therapeutic exosomes in CAD, which might provide a novel insight into the treatment of CAD and promote the potential clinical translation of therapeutic exosomes.

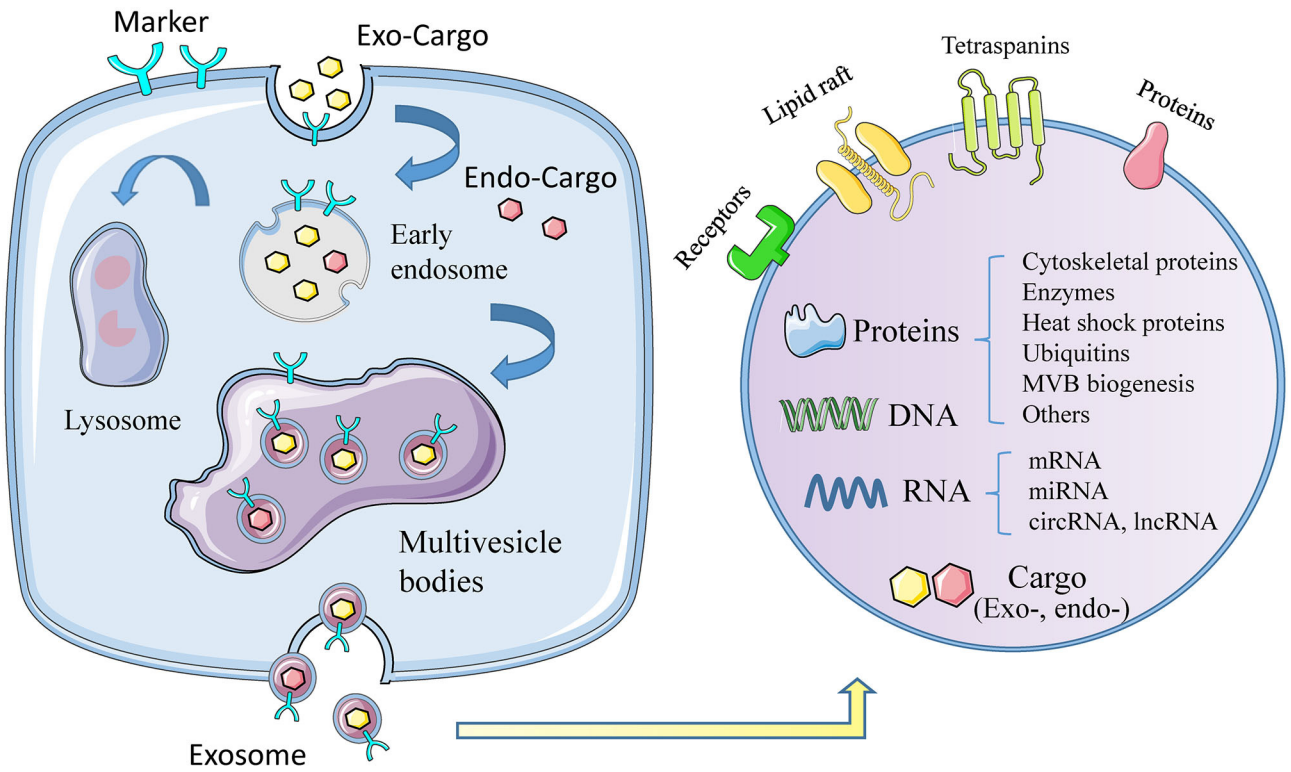

FIGURE 1 | The biogenesis, formation, and content of exosomes. The formation of exosomes begins with invagination of the plasma membrane, and then forms early exosomes, which form multiple vesicles after fusion, and finally release the exosomes out of the cell. During the formation of exosomes, it will actively or passively carry exogenous or endogenous cargoes. The picture on the right shows the membrane structure of exosomes, the contents of exosomes, including proteins, DNA, RNA, and others.

EXOSOMES AND CAD

According to the progress of CAD, the relationships between exosomes and CAD are summarized into three parts: exosomes in the prevention of atherosclerosis, exosomes in the diagnosis and treatment of myocardial infarction, and exosomes in the development of in-stent restenosis (**Table 1**).

Therapeutic Exosomes in Atherosclerosis

A basic progress in the development of atherosclerosis is monocytes/macrophages accumulation into the vessel wall to produce pro-inflammatory cytokines (32). It has been reported that molecularly engineered M2 macrophage-derived exosomes (Further electroporated with hexyl 5-aminolevulinate hydrochloride) alleviated inflammation by promoting the release of anti-inflammatory cytokines (33). Paeonol could restrict atherosclerosis by obviously increasing miR-223 expression in exosomes from monocytes and inhibiting STAT3 pathway (34). Exosomes laden with heat shock protein 27 (HSP27) significantly stimulated NF-κB activation and IL-10 release, suggesting that exosomes could act as a vector in anti-inflammatory therapy (35). Mitochondria constituted a major subset of extracellular vesicles released by LPS-activated monocytes *in vitro*, which were associated with type I IFN and TNF signaling (36). Exosomes from nicotine-stimulated macrophages could promote atherosclerosis through facilitating VSMC migration and proliferation by targeting miR-21-3p/*PTEN* (37). Moreover, helicobacter pylori-infected gastric epithelial cells-derived exosomes accelerated macrophage foam cell formation and promoted atherosclerosis by CagA (38). Insulin resistance adipocyte-derived exosomes (IRADEs) has been reported to aggravate the plaque burden, whereas its effect could be attenuated by silencing sonic hedgehog in IRADEs (12). Besides, Jiang et al. (13) also reported that steatotic hepatocyte-derived EVs promoted endothelial inflammation by miR-1 delivery, KLF4 suppression and the NF-κB pathway activation. And in this instance, exosome therapy might be the reduction of negative contents in exosomes such as miR-1 instead of increasing therapeutic exosomes.

Therapeutic Exosomes in Myocardial Infarction

Myocardial infarction, which often results in poor clinical outcomes, still remains the lack of effective treatment, especially for those without culprit vessel revascularization (14). Therefore, current clinical treatments are mostly based on easinesss of symptoms rather than repairing infarcted cardiomyocyte (15).

TABLE 1 | Relationship between exosomes and CAD.

Disease	Exosomal cargo	Parent cells	Recipient cells	Target	Biological/clinical relevance	Reference
AS	miR-223	THP-1 monocyte	HUVEC	STAT-3 pathway	Anti-inflammation	(12)
	HSP27	THP-1 monocyte	–	NF-κB, IL-10	Anti-inflammation	(13)
	Mitochondria	Monocyte	Endothelial cell	IFN, TNF	Anti-inflammation	(14)
	miR-1	Hepatocyte	Endothelial cell	KLF4, NF-κB	Anti-inflammation	(15)
	miR-21-3p	MACROPHAGE	VSMC	PTEN	Promote VSMC proliferation and degradation	(16)
	–	Gastric epithelial cell	Macrophage	CagA	Promote foam cell formation	(17)
	Sonic hedgehog	Adipocyte	HUVECs, MAECs	TGF-α, IL-1β, IL-6	Reduce plaque vulnerability	(18)
MI	miR-342-5p	Endothelials	CMs	Caspase9, Jnk2, Akt	Anti-apoptsis/proliferation	(19)
	miR-21	HEK293T cell	CMs, HUVECs	PDCD4	Anti-apoptosis	(20)
	miR-125b-5p	MSC	CMs	p53, BAK1	Anti-apoptosis	(21)
	miR-210	EPC	Endothelial cell	Mitochondria	Anti-apoptosis/promote angiogenic function	(22)
	miR-24	Serum	H9c2 cell	Bim	Mediate Remote ischemic preconditioning	(23)
	miR-93-5p	Adipose stromal cell	CMs	Atg7, TLR4	Inhibit autophagy, anti-inflammatory	(24)
	lncR	–	Fibroblast, CMs	Neat1	Anti-fibrosis	(25)
	miR-24	MSC	CD8+T	Bim	Anti-fibrosis	(26)
	miR-130-3p	Adipocyte	CMs	AMPKα1/α2, Birc6, and Ucp3	Anti-apoptosis (diabetic)	
	Cytotoxic substance	Serum	HL-1 CMs	Compliment C4, ApoE, Apo C-IV	Anti-apoptosis (diabetic)	(27)
	ILK	Progenitor	CMs	NF-κB	Enhance myocardial repair	(28)
ISR	miR-222	M1-macrophages	VSMC	CDKN1B/CDKN1C	Promote VSMC proliferation and degradation	(29)
	miR-125b	MSC	VSMC	Myosin-1E	Promote VSMC proliferation and degradation	(30)
	miR-21-5p	EPC	HUVEC	THBS1	Promote repair of endothelial cells	(31)

AS, atherosclerosis; MI, myocardial infraction; ISR, in stent restenosis; MSC, mesenchymal stem cell; EPC, endothelial progenitor cell; CM, cardiomyocyte; VSMC, vascular smooth muscle cell; HUVEC, human umbilical vein endothelial cell.

Exosomes reveal significant anti-apoptosis of cardiomyocyte after myocardial infarction. Exercise-derived exosomal miR-342-5p inhibited cardiomyocyte apoptosis by targeting *Caspase9* and *Jnk2* after left anterior descending artery occlusion (16). EVs overexpressing miR-21 could dramatically reduce PDCD4 expression and alleviate myocardial apoptosis (15). Hypoxia-conditioned bone marrow-mesenchymal stem cells (MSCs)-derived exosomes (Hypo-Exo) could also protect cardiomyocytes from apoptosis by enrichment of miR-125b-5p and suppressing the expression of genes *p53* and *BAK1* (17). In addition, miR-210 in endothelial progenitor cell-derived exosomes (EPC-EXs) possessed antiapoptotic functions onto hypoxia/reoxygenation-injured human endothelial cells (18). Remote ischemic preconditioning-induced exosomes (RIPC-Exo) also could transfer miR-24 into myocardium to inhibit apoptosis (39).

Exosomes also provide cardioprotection by activating cell survival signals, inhibiting inflammatory factors, delaying ventricular remodeling, and reducing myocardial fibrosis after the occurrence of myocardial infarction. Exercise-derived exosome (Ex-exo) could carry miR-342-5p to promote Akt phosphorylation by targeting gene *Ppmlf* (16). MiR-93-5p in adipose stromal cell-derived exosomes (ADSC-Exo) inhibited inflammatory response and prevented myocardial infarction by targeting *Atg7* and *TLR4* (20). Kenneweg et al. (19) had reported that fibroblasts absorbed lncR-EVs and promoted myocardial fibrosis by targeting *Neat1*. Moreover, exosomal miR-24, derived from allogenic human umbilical MSC, could inhibit cardiac fibrosis (21).

Patients suffering from myocardial infarction often have a history of diabetes. Gan et al. (22) had demonstrated that the enrichment of miR-130b-3p from dysfunctional adipocyte exacerbated myocardial infarction and cardiomyocyte apoptosis. Serum-exosomes from normoglycemic rats could alleviate the death of hypoxia/reoxygenation-induced *HL-1* cell, however, which disappears in type-2 diabetes rat model (23).

Exosomes also can serve as an adjuvant therapy. Integrin Linked Kinase (ILK) acted as a target kinase by which progenitor cell-derived exosomes attenuated myocardial injury (24). Cheng et al. (25) have reported that miRNA in EVs contributed to early detection of CAD by means of point-of care applications.

Therapeutic Exosomes in In-stent Restenosis

Percutaneous coronary intervention has become a very important treatment strategy for CAD, but in-stent restenosis is blamed for the main cause of stent failure in patients with CAD (26, 40). Several previous studies have shown that the risk of in-stent restenosis in CAD patients undergoing coronary stent implantation during 1 year follow-up was ∼5–10% (27). The underlying mechanisms of in-stent restenosis are quite complex, and at least exosomes play a crucial role in the development of in-stent restenosis. For example, miR-222 from M1 macrophages (M1M)-derived exosomes promoted vascular smooth muscle

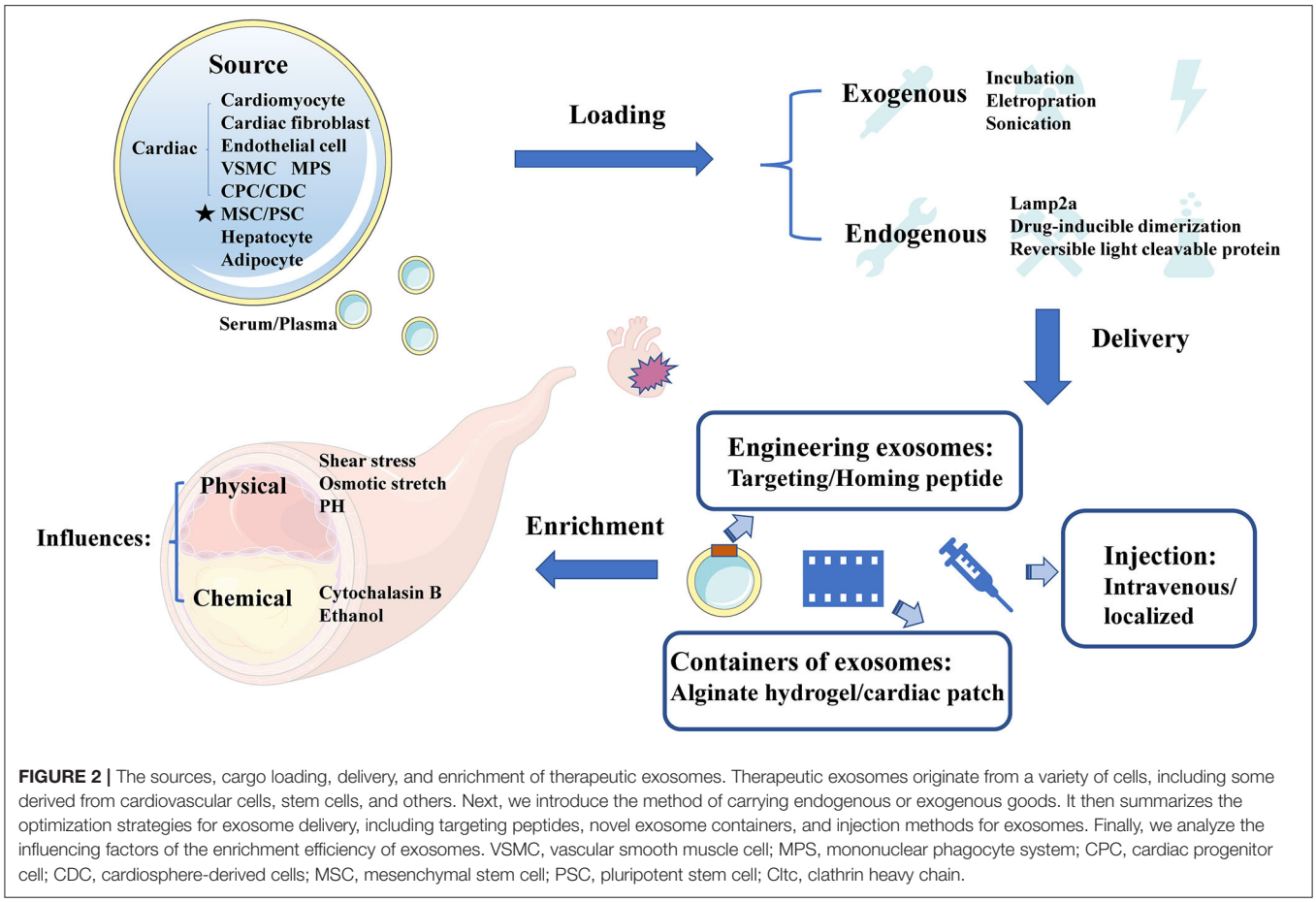

FIGURE 2 | The sources, cargo loading, delivery, and enrichment of therapeutic exosomes. Therapeutic exosomes originate from a variety of cells, including some derived from cardiovascular cells, stem cells, and others. Next, we introduce the method of carrying endogenous or exogenous goods. It then summarizes the optimization strategies for exosome delivery, including targeting peptides, novel exosome containers, and injection methods for exosomes. Finally, we analyze the influencing factors of the enrichment efficiency of exosomes. VSMC, vascular smooth muscle cell; MPS, mononuclear phagocyte system; CPC, cardiac progenitor cell; CDC, cardiosphere-derived cells; MSC, mesenchymal stem cell; PSC, pluripotent stem cell; Cltc, clathrin heavy chain.

cells (VSMCs) proliferation and migration, which resulted in restenosis (41). Wang et al. (42) reported that MSC-Exo enriched miR-125b and inhibited the proliferation and migration of VSMC by targeting myosin 1E. Moreover, EPC-Exo also were involved in the prevention of restenosis through delivering miR-21-5p and inhibiting *THBS1* expression (43). Recently, exosome-eluting stents have been proven to reduce intimal hyperplasia and accelerate re-endothelialization in the ischemic injury rat model.

OPTIMIZED TREATMENT STRATEGY

Exosomes appear superiority and irreplaceable biological functions, and the clinical application of therapeutic exosomes is full of hope. In the first place, exosomes can avoid phagocytosis and bypass the engulfment by lysosomes (44) to exhibit a longer circulation half-life due to the protection of phospholipid bilayer membrane (28). Secondly, phospholipid bilayer of exosomes is also beneficial to the fusion with membrane of recipient cells (29). Thirdly, exosomes derived from animals or patients have the high homolog and low immune response to avoid exosomes degradation (30). Finally, exosomal regulation of "Homing" effect has been reported to target the cell type where exosomes were produced (31), which can provide a shortcut for exosomes delivery. In need of optimized treatment strategy, we summarized the latest research involved of sources, cargo loading, delivery and enrichment of therapeutic exosomes (**Figure 2**).

Source of Therapeutic Exosomes

It has been reported that the sources of CAD related therapeutic exosomes were commonly cardiovascular-derived endothelial cells, smooth muscle cells, macrophages and cardiac fibroblasts (45). In recent years, several studies have highlighted the value of MSC-Exo therapy in cardiac protection (46, 47), and MSC could secret the highest amount of exosomes (48). Moreover, other studies found that circulating-Exo, adipocyte-EVs (12), hepatocyte-EVs (13), accompanied with different degrees of heterogeneity, all existed therapeutically effect upon CAD.

Loading Therapeutic Cargo in Exosomes

Although many therapeutic cargoes are inherent in parent cells previously, some therapeutic cargoes could only be loaded into exosomes by artificial means. Normally, cargoes could be loaded through fusion with liposomes, adsorption of molecules to the surface of exosomes and the insertion of lipids (49). It has been reported that a few procedures, such as incubation, electroporation (33), sonication (50), and so on (51), could promote cargo loading. When choosing the loading method of

cargoes, we should consider the loading efficiency (52), and whether this loading method will change the physical and chemical characteristics of exosomes (53). Besides, membrane protein Lamp2a could increase the loading of miRNA into EVs (54). Moreover, drug-inducible dimerization (55), reversible light cleavable protein (56), and several advanced means of engineering exosomes also contribute to the loading of endogenous cargoes.

Delivery Method

Normally, therapeutic exosomes were injected intravenously and act on the cardiovascular diseases through the circulatory system as an essential treatment. However, most of these exosomes are taken up by liver or spleen (57). Loading homing peptides has become a popular way to optimize delivery of exosomes (58). In cardiovascular field, several homing peptides in connection with atherosclerosis (59, 60), and ischemia/reperfusion–injured cardiomyocytes (61) have been identified and applied in therapeutic regimen. For example, Wang et al. (62) have demonstrated that engineered exosomes fused with ischemic myocardium-targeting peptide (IMTP) increasingly accumulated in ischemic heart area. Furthermore, it has been reported that exosomes conjugated with cardiac homing peptide (CHP) has higher retention in infarcted heart (63).

Besides, Song et al. (15) have reported that localized injection of EVs attenuated the apoptosis of cardiomyocytes and endothelial cells in a preclinical myocardial infarction (MI) animal model. To reduce losses during transportation, Lv et al. (64) have reported that sEVs, incorporated in alginate hydrogel, act as a new regimen of therapy. An off-the-shelf therapeutic cardiac patch, composed of extracellular matrix and cardiac stromal cells (CSC), has been confirmed in the model of MI (65). The examples above demonstrate the superiority of local delivery of exosomes and improve the retention rate of exosomes.

Enrichment Efficiency

The enrichment efficiency of exosomes is affected by physical and chemical stimuli. The physical stimulation of exosomes mainly includes shear stress, osmotic stretch, PH and others (66). More importantly, the change of blood flow shear force, as the initiating factor of coronary artery disease, has also become a difficult problem for exosome delivery. Here, we focus on the shear stress in vessel where exosomes were regulated. While shear stress remain within 1–70 dynes/cm^2 in normal blood vessels, severely narrowed blood vessels can produce over 1,000 dynes/cm^2 (67). High shear stress, occurring in atherosclerotic arteries, could accelerate the release of circulating-EVs gradually (68). The mechanisms of shear stress on EVs secretion relate to the response of membrane tension (69). Besides, calcium could enhance exosomes secretion from a microenvironment perspective (70), whereas arterial hypertension was also associated with the increase of shear stress from a macro perspective (71). Evidence proved that exercise training could increase EVs release under high shear stress, and decrease the risk of thrombosis correspond to stenotic arteries (72). Exosomes could also be affected by chemical trigger, including cytochalasin B and ethanol (46).

CONCLUSION AND FUTURE PERSPECTIVE

In recent years, the therapeutic effect of exosomes on heart diseases has been gradually discovered. We have summarized the progress in studying exosomes as drug delivery vehicles. Before entering the clinical transformation, a perfect therapeutic concept of exosomes is essential (3), and pioneering in the field of exosomes is tumor-related studies. We can draw on tumor-related studies to optimize treatment regimens. Certainly, CAD-targeted treatment options also need to take notice of the cardiovascular lineage specificity.

Exosomes, as natural drug delivery vehicles, have excellent biocompatibility and targeting properties. We have discovered the potential of exosomes in the treatment of CAD based on existing research. However, exosomes still face huge resistance in clinical transformation. Moreover, we hope that the optimization of therapeutic exosomes is getting better and enter the clinical application stage as soon as possible.

AUTHOR CONTRIBUTIONS

A-QC and X-FG wrote the manuscript. Z-MW and FW prepared the figures. SL and YG prepared the table. J-JZ and S-LC provided the idea and revised the manuscript. All authors have agreed to the published version of the manuscript.

FUNDING

This study was funded by the National Natural Science Foundation of China (NSFC 81970307), and was jointly supported by Six Talent Peaks Project of Jiangsu Province (2019-WSN-156), Social Development Project of Jiangsu Province (BE2019615, BE2019616), Jiangsu Commission of Health (H2019077), and Nanjing Health Youth Talent Training project (QRX17017).

REFERENCES

1. Sousa-Uva M, Neumann FJ, Ahlsson A, Alfonso F, Banning AP, Benedetto U, et al. 2018 ESC/EACTS Guidelines on myocardial revascularization. *Eur J Cardio Thorac Surg.* (2019) 55:4–90. doi: 10.1093/ejcts/ezy289
2. Benjamin EJ, Muntner P, Alonso A, Bittencourt MS, Callaway CW, Carson AP, et al. Heart disease and stroke statistics-2019 update: a report from the American Heart Association. *Circulation.* (2019) 139:e56–e528. doi: 10.1161/CIR.0000000000000659
3. Nazari-Shafti TZ, Stamm C, Falk V, Emmert MY. Exosomes for cardioprotection: are we ready for clinical translation? *Eur Heart J.* (2019). 40:953–6. doi: 10.1093/eurheartj/ehz106
4. Shao H, Im H, Castro CM, Breakefield X, Weissleder R, Lee H. New technologies for analysis of extracellular vesicles. *Chem Rev.* (2018) 118:1917–50. doi: 10.1021/acs.chemrev.7b00534

5. Théry C, Zitvogel L, Amigorena S. Exosomes: composition, biogenesis and function. *Nat Rev Immunol.* (2002) 2:569–79. doi: 10.1038/nri855
6. Kalluri R, LeBleu VS. The biology, function, and biomedical applications of exosomes. *Science.* (2020) 367:eaau6977. doi: 10.1126/science.aau6977
7. Février B, Raposo G. Exosomes: endosomal-derived vesicles shipping extracellular messages. *Curr Opin Cell Biol.* (2004) 16:415–21. doi: 10.1016/j.ceb.2004.06.003
8. Merchant ML, Rood IM, Deegens JKJ, Klein JB. Isolation and characterization of urinary extracellular vesicles: implications for biomarker discovery. *Nat Rev Nephrol.* (2017) 13:731–49. doi: 10.1038/nrneph.2017.148
9. van Niel G, D'Angelo G, Raposo G. Shedding light on the cell biology of extracellular vesicles. *Nat Rev Mol Cell Biol.* (2018) 19:213–28. doi: 10.1038/nrm.2017.125
10. Lo Cicero A, Stahl PD, Raposo G. Extracellular vesicles shuffling intercellular messages: for good or for bad. *Curr Opin Cell Biol.* (2015). 35:69–77. doi: 10.1016/j.ceb.2015.04.013
11. Raiborg C, Stenmark H. The ESCRT machinery in endosomal sorting of ubiquitylated membrane proteins. *Nature.* (2009) 458:445–52. doi: 10.1038/nature07961
12. Wang F, Chen FF, Shang YY, Li Y, Wang ZH, Han L, et al. Insulin resistance adipocyte-derived exosomes aggravate atherosclerosis by increasing vasa vasorum angiogenesis in diabetic ApoE(-/-) mice. *Int J Cardiol.* (2018) 265:181–7. doi: 10.1016/j.ijcard.2018.04.028
13. Jiang F, Chen Q, Wang W, Ling Y, Yan Y, Xia P. Hepatocyte-derived extracellular vesicles promote endothelial inflammation and atherogenesis via microRNA-1. *J Hepatol.* (2020) 72:156–66. doi: 10.1016/j.jhep.2019.09.014
14. Rao SV, Kaul P, Newby LK, Lincoff AM, Hochman J, Harrington RA, et al. Poverty, process of care, and outcome in acute coronary syndromes. *J Am Coll Cardiol.* (2003) 41:1948–54. doi: 10.1016/S0735-1097(03)00402-9
15. Song Y, Zhang C, Zhang J, Jiao Z, Dong N, Wang G, et al. Localized injection of miRNA-21-enriched extracellular vesicles effectively restores cardiac function after myocardial infarction. *Theranostics.* (2019) 9:2346–60. doi: 10.7150/thno.29945
16. Hou Z, Qin X, Hu Y, Zhang X, Li G, Wu J, et al. Longterm exercise-derived exosomal miR-342-5p: a novel exerkine for cardioprotection. *Circ Res.* (2019) 124:1386–400. doi: 10.1161/CIRCRESAHA.118.314635
17. Zhu LP, Tian T, Wang JY, He JN, Chen T, Pan M, et al. Hypoxia-elicited mesenchymal stem cell-derived exosomes facilitates cardiac repair through miR-125b-mediated prevention of cell death in myocardial infarction. *Theranostics.* (2018) 8:6163–77. doi: 10.7150/thno.28021
18. Ma X, Wang J, Li J, Ma C, Chen S, Lei W, et al. Loading MiR-210 in endothelial progenitor cells derived exosomes boosts their beneficial effects on hypoxia/reoxygeneation-injured human endothelial cells via protecting mitochondrial function. *Cell Physiol Biochem.* (2018) 46:664–75. doi: 10.1159/000488635
19. Kenneweg F, Bang C, Xiao K, Boulanger CM, Loyer X, Mazlan S, et al. Long noncoding RNA-enriched vesicles secreted by hypoxic cardiomyocytes drive cardiac fibrosis. *Mol Ther Nucleic Acids.* (2019) 18:363–74. doi: 10.1016/j.omtn.2019.09.003
20. Liu J, Jiang M, Deng S, Lu J, Huang H, Zhang Y, et al. miR-93-5p-containing exosomes treatment attenuates acute myocardial infarction-induced myocardial damage. *Mol Ther Nucleic Acids.* (2018) 11:103–15. doi: 10.1016/j.omtn.2018.01.010
21. Shao L, Zhang Y, Pan X, Liu B, Liang C, Zhang Y, et al. Knockout of β-2 microglobulin enhances cardiac repair by modulating exosome imprinting and inhibiting stem cell-induced immune rejection. *Cell Mol Life Sci.* (2020) 77:937–52. doi: 10.1007/s00018-019-03220-3
22. Gan L, Xie D, Liu J, Lau WB, Christopher TA, Lopez B, et al. Small extracellular microvesicles mediated pathological communications between dysfunctional adipocytes and cardiomyocytes as a novel mechanisms exacerbating ischemia/reperfusion injury in diabetic mice. *Circulation.* (2020) 141:968–83. doi: 10.1161/CIRCULATIONAHA.119.042640
23. Wider J, Undyala VVR, Whittaker P, Woods J, Chen X, Przyklenk K. Remote ischemic preconditioning fails to reduce infarct size in the Zucker fatty rat model of type-2 diabetes: role of defective humoral communication. *Basic Res Cardiol.* (2018) 113:16. doi: 10.1007/s00395-018-0674-1
24. Yue Y, Wang C, Benedict C, Huang G, Truongcao M, Roy R, et al. Interleukin-10 deficiency alters endothelial progenitor cell-derived exosome reparative effect on myocardial repair via integrin-linked kinase enrichment. *Circ Res.* (2020) 126:315–29. doi: 10.1161/CIRCRESAHA.119.315829
25. Cheng HL, Fu CY, Kuo WC, Chen YW, Chen YS, Lee YM, et al. Detecting miRNA biomarkers from extracellular vesicles for cardiovascular disease with a microfluidic system. *Lab Chip.* (2018) 18:2917–25. doi: 10.1039/C8LC00386F
26. Zhang J, Gao X, Kan J, Ge Z, Han L, Lu S, et al. Intravascular ultrasound versus angiography-guided drug-eluting stent implantation: the ULTIMATE trial. *J Am Coll Cardiol.* (2018) 72:3126–37. doi: 10.1016/j.jacc.2018.09.013
27. Gao XF, Kan J, Zhang YJ, Zhang JJ, Tian NL, Ye F, et al. Comparison of one-year clinical outcomes between intravascular ultrasound-guided versus angiography-guided implantation of drug-eluting stents for left main lesions: a single-center analysis of a 1, 016-patient cohort. *Patient Prefer Adherence.* (2014) 8:1299–309. doi: 10.2147/PPA.S65768
28. Saunderson SC, Dunn AC, Crocker PR, McLellan AD. CD169 mediates the capture of exosomes in spleen and lymph node. *Blood.* (2014) 123:208–16. doi: 10.1182/blood-2013-03-489732
29. Mathivanan S, Ji H, Simpson RJ. Exosomes: extracellular organelles important in intercellular communication. *J Proteomics.* (2010) 73:1907–20. doi: 10.1016/j.jprot.2010.06.006
30. Ha D, Yang N, Nadithe V. Exosomes as therapeutic drug carriers and delivery vehicles across biological membranes: current perspectives and future challenges. *Acta Pharm Sin B.* (2016) 6:287–96. doi: 10.1016/j.apsb.2016.02.001
31. Park EJ, Prajuabjinda O, Soe ZY, Darkwah S, Appiah MG, Kawamoto E, et al. Exosomal regulation of lymphocyte homing to the gut. *Blood Adv.* (2019) 3:1–11. doi: 10.1182/bloodadvances.2018024877
32. Libby P, Okamoto Y, Rocha VZ, Folco E. Inflammation in atherosclerosis: transition from theory to practice. *Circ J.* (2010) 74:213–20. doi: 10.1253/circj.CJ-09-0706
33. Wu G, Zhang J, Zhao Q, Zhuang W, Ding J, Zhang C, et al. Molecularly engineered macrophage-derived exosomes with inflammation tropism and intrinsic heme biosynthesis for atherosclerosis treatment. *Angew Chem Int Ed Engl.* (2020) 59:4068–74. doi: 10.1002/anie.201913700
34. Liu Y, Li C, Wu H, Xie X, Sun Y, Dai M. Paeonol attenuated inflammatory response of endothelial cells via stimulating monocytes-derived exosomal microRNA-223. *Front Pharmacol.* (2018) 9:1105. doi: 10.3389/fphar.2018.01105
35. Shi C, Ulke-Lemée A, Deng J, Batulan Z, O'Brien ER. Characterization of heat shock protein 27 in extracellular vesicles: a potential anti-inflammatory therapy. *FASEB J.* (2019) 33:1617–30. doi: 10.1096/fj.201800987R
36. Puhm F, Afonyushkin T, Resch U, Obermayer G, Rohde M, Penz T, et al. Mitochondria are a subset of extracellular vesicles released by activated monocytes and induce type I IFN and TNF responses in endothelial cells. *Circ Res.* (2019) 125:43–52. doi: 10.1161/CIRCRESAHA.118.314601
37. Zhu J, Liu B, Wang Z, Wang D, Ni H, Zhang L, et al. Exosomes from nicotine-stimulated macrophages accelerate atherosclerosis through miR-21-3p/PTEN-mediated VSMC migration and proliferation. *Theranostics.* (2019) 9:6901–19. doi: 10.7150/thno.37357
38. Yang S, Xia YP, Luo XY, Chen SL, Li BW, Ye ZM, et al. Exosomal CagA derived from *Helicobacter pylori*-infected gastric epithelial cells induces macrophage foam cell formation and promotes atherosclerosis. *J Mol Cell Cardiol.* (2019) 135:40–51. doi: 10.1016/j.yjmcc.2019.07.011
39. Minghua W, Zhijian G, Chahua H, Qiang L, Minxuan X, Luqiao W, et al. Plasma exosomes induced by remote ischaemic preconditioning attenuate myocardial ischaemia/reperfusion injury by transferring miR-24. *Cell Death Dis.* (2018) 9:320. doi: 10.1038/s41419-018-0274-x
40. Gao XF, Lu S, Ge Z, Zuo GF, Wang ZM, Wang F, et al. Relationship between high platelet reactivity on clopidogrel and long-term clinical outcomes after drug-eluting stents implantation (PAINT-DES): a prospective, propensity score-matched cohort study. *BMC Cardiovasc Disord.* (2018) 18:103. doi: 10.1186/s12872-018-0841-1
41. Wang Z, Zhu H, Shi H, Zhao H, Gao R, Weng X, et al. Exosomes derived from M1 macrophages aggravate neointimal hyperplasia following carotid artery injuries in mice through miR-222/CDKN1B/CDKN1C pathway. *Cell Death Dis.* (2019) 10:422. doi: 10.1038/s41419-019-1667-1

42. Wang D, Gao B, Yue J, Liu F, Liu Y, Fu W, et al. Exosomes from mesenchymal stem cells expressing miR-125b inhibit neointimal hyperplasia via myosin IE. *J Cell Mol Med.* (2019) 23:1528–40. doi: 10.1111/jcmm.14060
43. Hu H, Wang B, Jiang C, Li R, Zhao J. Endothelial progenitor cell-derived exosomes facilitate vascular endothelial cell repair through shuttling miR-21-5p to modulate Thrombospondin-1 expression. *Clin Sci (Lond).* (2019) 133:1629–44. doi: 10.1042/CS20190188
44. Bunggulawa EJ, Wang W, Yin T, Wang N, Durkan C, Wang Y, et al. Recent advancements in the use of exosomes as drug delivery systems. *J Nanobiotechnol.* (2018) 16:81. doi: 10.1186/s12951-018-0403-9
45. Chistiakov DA, Orekhov AN, Bobryshev YV. Cardiac extracellular vesicles in normal and infarcted heart. *Int J Mol Sci.* (2016) 17:63. doi: 10.3390/ijms17010063
46. Piffoux M, Nicolás-Boluda A, Mulens-Arias V, Richard S, Rahmi G, Gazeau F, et al. Extracellular vesicles for personalized medicine: The input of physically triggered production, loading and theranostic properties. *Adv Drug Deliv Rev.* (2019) 138:247–58. doi: 10.1016/j.addr.2018.12.009
47. Caplan AI, Dennis JE. Mesenchymal stem cells as trophic mediators. *J Cell Biochem.* (2006) 98:1076–84. doi: 10.1002/jcb.20886
48. Yeo RW, Lai RC, Zhang B, Tan SS, Yin Y, Teh BJ, et al. Mesenchymal stem cell: an efficient mass producer of exosomes for drug delivery. *Adv Drug Deliv Rev.* (2013) 65:336–41. doi: 10.1016/j.addr.2012.07.001
49. Richter M, Vader P, Fuhrmann G. Approaches to surface engineering of extracellular vesicles. *Adv Drug Deliv Rev.* (2021) 173:416–26. doi: 10.1016/j.addr.2021.03.020
50. Kim MS, Haney MJ, Zhao Y, Mahajan V, Deygen I, Klyachko NL, et al. Development of exosome-encapsulated paclitaxel to overcome MDR in cancer cells. *Nanomed Nanotechnol Biol Med.* (2016) 12:655–64. doi: 10.1016/j.nano.2015.10.012
51. Haney MJ, Klyachko NL, Zhao Y, Gupta R, Plotnikova EG, He Z, et al. Exosomes as drug delivery vehicles for Parkinson's disease therapy. *J Control Release.* (2015) 207:18–30. doi: 10.1016/j.jconrel.2015.03.033
52. Elsharkasy OM, Nordin JZ, Hagey DW, de Jong OG, Schiffelers RM, Andaloussi SE, et al. Extracellular vesicles as drug delivery systems: Why and how? *Adv Drug Deliv Rev.* (2020) 159:332–43. doi: 10.1016/j.addr.2020.04.004
53. Kooijmans SAA, Stremersch S, Braeckmans K, de Smedt SC, Hendrix A, Wood MJA, et al. Electroporation-induced siRNA precipitation obscures the efficiency of siRNA loading into extracellular vesicles. *J Control Release.* (2013) 172:229–38. doi: 10.1016/j.jconrel.2013.08.014
54. Sutaria DS, Jiang J, Elgamal OA, Pomeroy SM, Badawi M, Zhu X, et al. Low active loading of cargo into engineered extracellular vesicles results in inefficient miRNA mimic delivery. *J Extracell Vesicles.* (2017) 6:1333882. doi: 10.1080/20013078.2017.1333882
55. Banaszynski LA, Liu CW, Wandless TJ. Characterization of the FKBP.rapamycin.FRB ternary complex. *J Am Chem Soc.* (2005) 127:4715–21. doi: 10.1021/ja043277y
56. Yim N, Ryu SW, Choi K, Lee KR, Lee S, Choi H, et al. Exosome engineering for efficient intracellular delivery of soluble proteins using optically reversible protein-protein interaction module. *Nat Commun.* (2016) 7:12277. doi: 10.1038/ncomms12277
57. Armstrong JPK, Stevens MM. Strategic design of extracellular vesicle drug delivery systems. *Adv Drug Deliv Rev.* (2018) 130:12–6. doi: 10.1016/j.addr.2018.06.017
58. Shen B, Wu N, Yang JM, Gould SJ. Protein targeting to exosomes/microvesicles by plasma membrane anchors. *J Biol Chem.* (2011) 286:14383–95. doi: 10.1074/jbc.M110.208660
59. Hong HY, Lee HY, Kwak W, Yoo J, Na MH, So IS, et al. Phage display selection of peptides that home toatherosclerotic plaques: IL-4 receptor as a candidate target in atherosclerosis. *J Cell Mol Med.* (2008) 12:2003–14. doi: 10.1111/j.1582-4934.2008.00189.x
60. Lee GY, Kim JH, Oh GT, Lee BH, Kwon IC, Kim IS. Molecular targeting of atherosclerotic plaques by a stabilin-2-specific peptide ligand. *J Control Release.* (2011) 155:211–7. doi: 10.1016/j.jconrel.2011.07.010
61. Won YW, McGinn AN, Lee M, Bull DA, Kim SW. Targeted gene delivery to ischemic myocardium by homing peptide-guided polymeric carrier. *Mol Pharm.* (2013) 10:378–85. doi: 10.1021/mp300500y
62. Wang X, Chen Y, Zhao Z, Meng Q, Yu Y, Sun J, et al. Engineered exosomes with ischemic myocardium-targeting peptide for targeted therapy in myocardial infarction. *J Am Heart Assoc.* (2018) 7:e008737. doi: 10.1161/JAHA.118.008737
63. Vandergriff A, Huang K, Shen D, Hu S, Hensley MT, Caranasos TG, et al. Targeting regenerative exosomes to myocardial infarction using cardiac homing peptide. *Theranostics.* (2018) 8:1869–78. doi: 10.7150/thno.20524
64. Lv K, Li Q, Zhang L, Wang Y, Zhong Z, Zhao J, et al. Incorporation of small extracellular vesicles in sodium alginate hydrogel as a novel therapeutic strategy for myocardial infarction. *Theranostics.* (2019) 9:7403–16. doi: 10.7150/thno.32637
65. Huang K, Ozpinar EW, Su T, Tang J, Shen D, Qiao L, et al. An off-the-shelf artificial cardiac patch improves cardiac repair after myocardial infarction in rats and pigs. *Sci Transl Med.* (2020) 12:eaat9683. doi: 10.1126/scitranslmed.aat9683
66. Liu H, Liu S, Qiu X, Yang X, Bao L, Pu F, et al. Donor MSCs release apoptotic bodies to improve myocardial infarction via autophagy regulation in recipient cells. *Autophagy.* (2020) 16:2140–55. doi: 10.1080/15548627.2020.1717128
67. Korin N, Gounis MJ, Wakhloo AK, Ingber DE. Targeted drug delivery to flow-obstructed blood vessels using mechanically activated nanotherapeutics. *JAMA Neurol.* (2015) 72:119–22. doi: 10.1001/jamaneurol.2014.2886
68. Miyazaki Y, Nomura S, Miyake T, Kagawa H, Kitada C, Taniguchi H, et al. High shear stress can initiate both platelet aggregation and shedding of procoagulant containing microparticles. *Blood.* (1996) 88:3456–64. doi: 10.1182/blood.V88.9.3456.bloodjournal8893456
69. Staykova M, Holmes DP, Read C, Stone HA. Mechanics of surface area regulation in cells examined with confined lipid membranes. *Proc Natl Acad Sci U S A.* (2011) 108:9084–8. doi: 10.1073/pnas.1102358108
70. Savina A, Fader CM, Damiani MT, Colombo MI. Rab11 promotes docking and fusion of multivesicular bodies in a calcium-dependent manner. *Traffic (Copenhagen, Denmark).* (2005) 6:131–43. doi: 10.1111/j.1600-0854.2004.00257.x
71. Gatzoulis MA, Alonso-Gonzalez R, Beghetti M. Pulmonary arterial hypertension in paediatric and adult patients with congenital heart disease. *Eur Respir Rev.* (2009) 18:154–61. doi: 10.1183/09059180.00003309
72. Chen YW, Chen YC, Wang JS. Absolute hypoxic exercise training enhances *in vitro* thrombin generation by increasing procoagulant platelet-derived microparticles under high shear stress in sedentary men. *Clin Sci (Lond).* (2013) 124:639–49. doi: 10.1042/CS20120540

Conflict of Interest: The authors declare that the research was conducted in the absence of any commercial or financial relationships that could be construed as a potential conflict of interest.

frontiers in Cardiovascular Medicine

ORIGINAL RESEARCH
published: 06 July 2021
doi: 10.3389/fcvm.2021.692540

Lacidipine Ameliorates the Endothelial Senescence and Inflammatory Injury Through CXCR7/P38/C/EBP-β Signaling Pathway

Xing Liu[2†], Zhuoshan Huang[2†], Yuanyuan Zhang[2], Xing Shui[2], Fanmao Liu[1], Zhen Wu[2] and Shiyue Xu[1,3,4*]*

[1] Department of Hypertension and Vascular Disease, The First Affiliated Hospital, Sun Yat-sen University, Guangzhou, China, [2] Department of Cardiology, The Third Affiliated Hospital, Sun Yat-sen University, Guangzhou, China, [3] National-Guangdong Joint Engineering Laboratory for Diagnosis and Treatment of Vascular Diseases, Guangzhou, China, [4] National Health Commission Key Laboratory of Assisted Circulation, Sun Yat-sen University, Guangzhou, China

OPEN ACCESS

Edited by:
Junjie Yang,
University of Alabama at Birmingham,
United States

Reviewed by:
Lianbo Shao,
The First Affiliated Hospital of Soochow University, China
Maria Cimini,
Temple University, United States

***Correspondence:**
Zhen Wu
wuzh@mail.sysu.edu.cn
Shiyue Xu
xushy25@mail.sysu.edu.cn

[†]These authors have contributed equally to this work and share first authorship

Specialty section:
This article was submitted to Cardiovascular Biologics and Regenerative Medicine, a section of the journal Frontiers in Cardiovascular Medicine

Received: 08 April 2021
Accepted: 31 May 2021
Published: 06 July 2021

Citation:
Liu X, Huang Z, Zhang Y, Shui X, Liu F, Wu Z and Xu S (2021) Lacidipine Ameliorates the Endothelial Senescence and Inflammatory Injury Through CXCR7/P38/C/EBP-β Signaling Pathway. Front. Cardiovasc. Med. 8:692540. doi: 10.3389/fcvm.2021.692540

Background: Lacidipine, a third-generation calcium channel blocker, exerts beneficial effects on the endothelium of hypertensive patients in addition to blood pressure lowering. However, the detailed mechanism underlying Lacidipine-related endothelial protection is still elusive.

Methods: Sixteen spontaneous hypertensive rats (SHRs) were randomly divided into two groups: Lacidipine-treated SHR group and saline-treated control group. Tail systolic blood pressure was monitored for four consecutive weeks. Endothelial cells (ECs) were pretreated with Lacidipine prior to being stimulated with H_2O_2, bleomycin, or Lipopolysaccharides (LPS) *in vitro*. Then, cell activity, migration, and senescence were measured by Cell Counting Kit-8 assay, transwell assay, and β-galactosidase staining, respectively. The fluorescent probe 2′, 7′-dichlorofluorescein diacetate (DCFH-DA) was used to assess the intracellular reactive oxygen species (ROS). Related protein expression was detected by Western blotting and immunofluorescence.

Results: Our data showed that Lacidipine treatment lowered the blood pressure of SHRs accompanied by the elevation of CXCR7 expression and suppression of P38 and CCAAT/enhancer-binding protein beta (C/EBP-β) compared with the control group. *In vitro* experiments further demonstrated that Lacidipine increased the cell viability and function of ECs under oxidative stress, cell senescence, and inflammatory activation *via* the CXCR7/P38/signaling pathway.

Conclusions: Our results suggested that Lacidipine plays a protective role in EC senescence, oxidative stress, and inflammatory injury through the regulation of CXCR7/P38/C/EBP-β signaling pathway.

Keywords: lacidipine, oxidative stress, senescence, inflammation, CXCR7

INTRODUCTION

Hypertension is recognized as a leading risk factor for cardiovascular diseases due to its effects on vascular injury (1). Moreover, endothelial dysfunction is considered to be the initial step of hypertension-related vascular injury (2, 3). Emerging evidence suggests that oxidative stress, inflammation activation, and cell senescence play crucial roles in the pathogenesis of hypertension-related endothelial dysfunction (4–7). Hence, it is important to decipher the detailed mechanisms underlying hypertension-related endothelial cell (EC) injury and dysfunction in order to improve the prognosis of hypertensive patients.

Studies showed that CXC chemokine receptor 7 (CXCR7) plays a key role in the modulation of cellular oxidative damage and senescence (8). Suppression of CXCR7 partially reduces the *in vitro* functions and *in vivo* re-endothelialization capacity of endothelial progenitor cells (EPCs) from hypertensive patients (9). Moreover, the CXCR7/p38 axis has been reported to be highly involved in the protection against high glucose-induced EPC dysfunction (10). In addition to oxidative stress, inflammatory injury usually occurs in the pathogenesis of hypertension (11) of which CCAAT/enhancer-binding protein beta (C/EBP-β) is a critical regulator (12). However, whether CXCR7/P38/C/EBP-β participated in the regulation of endothelial senescence and inflammatory injury remains to be uncovered. Lacidipine, a third-generation calcium channel blocker, has been demonstrated to be effective for preventing endothelial dysfunction in salt-loaded stroke-prone hypertensive rats (13) and restoring endothelial-dependent vasodilation in hypertensive patients (14). In addition to calcium channel-modulated vasodilation, Lacidipine displays an antioxidant activity greater than other dihydropyridine calcium antagonists (15) and exerts an anti-inflammatory effect in carrageenan model in intact rats (16). Our previous study demonstrated that Lacidipine improved the endothelial repair capacity of EPCs from patients with essential hypertension (17). Thus, we hypothesized that Lacidipine may attenuate endothelial senescence and inflammatory injury by modulating the CXCR7/P38/C/EBP-β pathway.

To validate our hypothesis, the *in vivo* effects of Lacidipine on CXCR7/P38/C/EBP-β were assessed by using spontaneous hypertensive rats (SHRs). Then, the detailed mechanisms by which Lacidipine affected oxidative damage, cell senescence, and inflammatory activation *via* the CXCR7/P38/C/EBP-β pathway in ECs were further investigated *in vitro*.

MATERIALS AND METHODS

Experimental Animals

A total of 16 SHRs were obtained from the Vital River Laboratory Animal Technology Co., Ltd. (Beijing, China) and housed in room temperature (∼25°C) on 12 h day/12 h night cycles, which had free access to standard chow diet and water. For the experimental requirement, all SHRs were randomly assigned into two groups, including Lacidipine-treated group ($n = 8$, rats were intragastrically treated with Lacidipine at a dose of 3 mg/kg/d for 4 weeks) and control group ($n = 8$, rats were intragastrically treated with physiologic saline for 4 weeks). Systolic blood pressure (SBP) was measured with a non-invasive computerized tail-cuff method and obtained by averaging 10 measurements. Meanwhile, their body weights were measured each week. After 4 weeks, all rats were sacrificed under isoflurane (2%) anesthesia. Aortic tissues were acquired for further analysis. All animal experimental protocols complied with institutional guidelines and were reviewed and approved by the Animal Care and Use Committee of the Ethics Committee of the First Affiliated Hospital of Sun Yat-sen University (Guangzhou, China).

EC Culture and Treatment

Human aortic endothelial cells (HAECs; Cambrex, Walkersville, MD, USA) from passage three to eight were cultured in Endothelial Growth Medium 2 (EGM-2; Lonza, Allendale, NJ, USA) with 20% fetal bovine serum (FBS; Hyclone, South Logan, UT, USA) in a 5% CO_2 incubator at 37°C. To simulate oxidative damage and senescence, ECs were stimulated with H_2O_2 (100 μM for 1 h) and bleomycin (50 μg/ml for 3 h), respectively, following Lacidipine pretreatment (100 nM for 12 h). C/EBP-β expression vector pcDNA3.0-C/EBP-β and small interfering RNA-CXCR7 (si-CXCR7: 5′-ATCAAATGACCTTGGATACTG-3′) were synthesized by RiboBio Co., Ltd. (Guangzhou, China) and transfected into ECs through a lipofectamine 2000 kit (Invitrogen, Carlsbad, CA, USA).

CCK-8 Assay

Cell viability was assessed by performing the Cell Counting Kit-8 (CCK-8) assay. In brief, the cells in each group were made into a cell suspension and seeded into 96-well plates at a density of 3,000 cells per well. Afterwards, the cells in each well were incubated with 10 μl of CCK-8 solution at 37°C for 2 h. The absorbance at a wavelength of 450 nm was measured using a microplate reader.

β-Galactosidase Staining

ECs were harvested and washed after treatment. Then, the cells were fixed with 2% formaldehyde and subsequently stained with a Senescence β-Galactosidase Staining Kit (CST, Boston, MA, USA). Level of senescence was quantified by visual examination of dark blue stained cells with an inverted microscope (Nikon, Japan) at 200× magnification.

ROS-Level Measurement

Intracellular reactive oxygen species (ROS) was determined with the non-fluorescent probe 2′,7′-dichlorofluorescein diacetate (DCFH-DA; Beyotime Institute of Biotechnology, China) according to the manufacturer's instructions. Briefly, the cells at a density of 1×10^5 cells per well were plated into six-well plates and incubated with 20 μM DCFH-DA for 30 min at 37°C. ROS generation was analyzed by flow cytometric analysis.

Detection of NADPH Activity

The cells from different groups were harvested and applied into NADPH oxidase activity analysis following the instructions provided by Beyotime Institute of Biotechnology (Shanghai, China). The NADPH activity was expressed as μmol/min/mg.

EC Migration *in vitro*

Transwell assay was performed to analyze cell migration. In brief, approximately 200 μl of serum-free medium containing 2×10^4 ECs was seeded into the upper chamber (8 μm pore size; Corning, NY, USA), whereas 500 μl of medium containing 10% serum was added to the lower chamber. After 24 h of incubation at 37°C, the cells that migrated into the lower chamber were fixed with 4% paraformaldehyde for 15 min, stained with 1% crystal violet (#C0775; Sigma-Aldrich, Milwaukee, WI, USA) for 30 min, and counted by independent investigators.

Immunofluorescence

Briefly, the cells were cultured on coverslips, washed with cold phosphate-buffered saline (PBS), and fixed for 30 min with 95% ethanol. After permeabilization in 0.5% Triton X-100, the cells were incubated with primary antibodies against CXCR7 (1:500; Abcam, Cambridge, MA, USA), followed by incubation with secondary antibody Alexa Fluor 488 goat anti-rabbit (Cwbiotech, Beijing, China). Next, the cells were washed three times in the dark for 1 h and counterstained with DAPI (Solarbio, Beijing, China). The fluorescent signal was analyzed under a fluorescence microscope (Nikon, Japan).

Apoptosis Analysis

The cells from different groups were harvested, seeded onto six-well plates, and cultured overnight. On the next day, the cells were incubated with Annexin V-FITC/PI Apoptosis Kit (#KA3805; Abnova, Shanghai, China) according to the manufacturer's instructions. Apoptotic cells were examined using flow cytometry (BD Biosciences, San Jose, CA, USA) and confirmed to be a positive Annexin V-FITC signal.

Western Blot

RIPA lysis buffer (Beyotime Institute of Biotechnology, Haimen, China) was used to extract all protein samples from tissues or cells according to the manufacturer's instructions. After quantitation by BCA assay, an equal amount of protein sample was separated on SDS-PAGE and then transferred onto PVDF membranes. Afterwards, the membranes were incubated with primary antibodies against CXCR7, NOX1, NOX2, C/EBP-β, P38, p-P38, VCAM1, Endoglin, MCP-1, IL-6, NLRP3, caspase-1 (all Abcam), and GAPDH overnight at 4°C. Then, the membranes were incubated with HRP-conjugated secondary antibodies for 2 h at room temperature, and protein bands were detected with ECL reagents (#131023-60-4; BOC Sciences, Shirley, NY, USA) with GAPDH as the internal control.

Statistical Analysis

All quantitative data were expressed as mean ± standard deviation (SD) of at least three independent experiments. Statistical analysis was performed with GraphPad Prism software 6.0. Student's *t*-test was used to analyze differences between two groups, whereas one-way analysis of variance followed by Tukey's *post-hoc* test was utilized to compare differences among multiple groups. All values with $p < 0.05$ indicated a significant difference.

RESULTS

Lacidipine Attenuates Hypertension and Regulates CXCR7/P38/C/EBP-β Expression *in vivo*

Our previous study showed that Lacidipine treatment improved the endothelial repair capacity of EPCs from hypertensive patients. To further explore the molecular mechanism underlying the protective role of Lacidipine against hypertension, SHRs were treated with or without Lacidipine for 4 weeks. Our data showed that Lacidipine treatment significantly reduced the blood pressure in SHRs (**Figure 1A**) but did not significantly affect the weight of SHRs (**Figure 1B**). The expression of CXCR7 was significantly elevated in the aortic tissues isolated from SHRs after Lacidipine treatment. On the contrary, P38 expression and its phosphorylation, as well as the protein expression of C/EBP-β and NADPH oxidases (NOX1 and NOX2), were suppressed in the Lacidipine group compared with the control group (**Figures 1C,D**). Furthermore, Lacidipine reduced the level of malondialdehyde (MDA) in serum, whereas it significantly increased the levels of superoxide dismutase (SOD) and glutathione (GSH) (**Figure 1E**).

Lacidipine Enhances the *in vitro* Function of ECs Under Oxidative Stress

To further explore the effect of Lacidipine on the oxidative damage in ECs, cultured ECs were treated with Lacidipine, followed by H_2O_2 stimulation (ROS induction). Our results showed that H_2O_2 stimulation significantly impaired cell viability (**Figure 2A**) and migration (**Figure 2D**) *in vitro* that were notably ameliorated by Lacidipine treatment. Moreover, Lacidipine treatment significantly suppressed the mitochondrial ROS production (**Figure 2B**), NADPH activity (**Figure 2C**), and MDA level induced by H_2O_2 in ECs. In contrast, the levels of SOD and GSH were significantly higher in the H_2O_2 + Lacidipine group than in the H_2O_2 group (**Figure 2E**). These results suggested that Lacidipine treatment attenuated the oxidative damage induced by H_2O_2 in ECs.

Lacidipine Ameliorates the Senescence of ECs Induced by Bleomycin

To determine the role of Lacidipine in the modulation of EC senescence, cultured ECs were treated with Lacidipine, followed by bleomycin stimulation. β-Galactosidase staining showed that Lacidipine treatment partially attenuated the senescence of ECs induced by bleomycin stimulation (**Figure 3A**). This result was further confirmed by Western blot analysis of cell senescence markers P16 and P21 (**Figure 3E**). Furthermore, the protein level of CXCR7 was decreased by bleomycin stimulation, and Lacidipine treatment markedly restored the reduction of CXCR7 expression (**Figures 3B,C**). In addition, the levels of P38, p-P38, and inflammatory factors (VCAM1, Endoglin, MCP-1, and IL-6) were increased in bleomycin-stimulated ECs that were significantly inhibited by Lacidipine (**Figures 3C–E**).

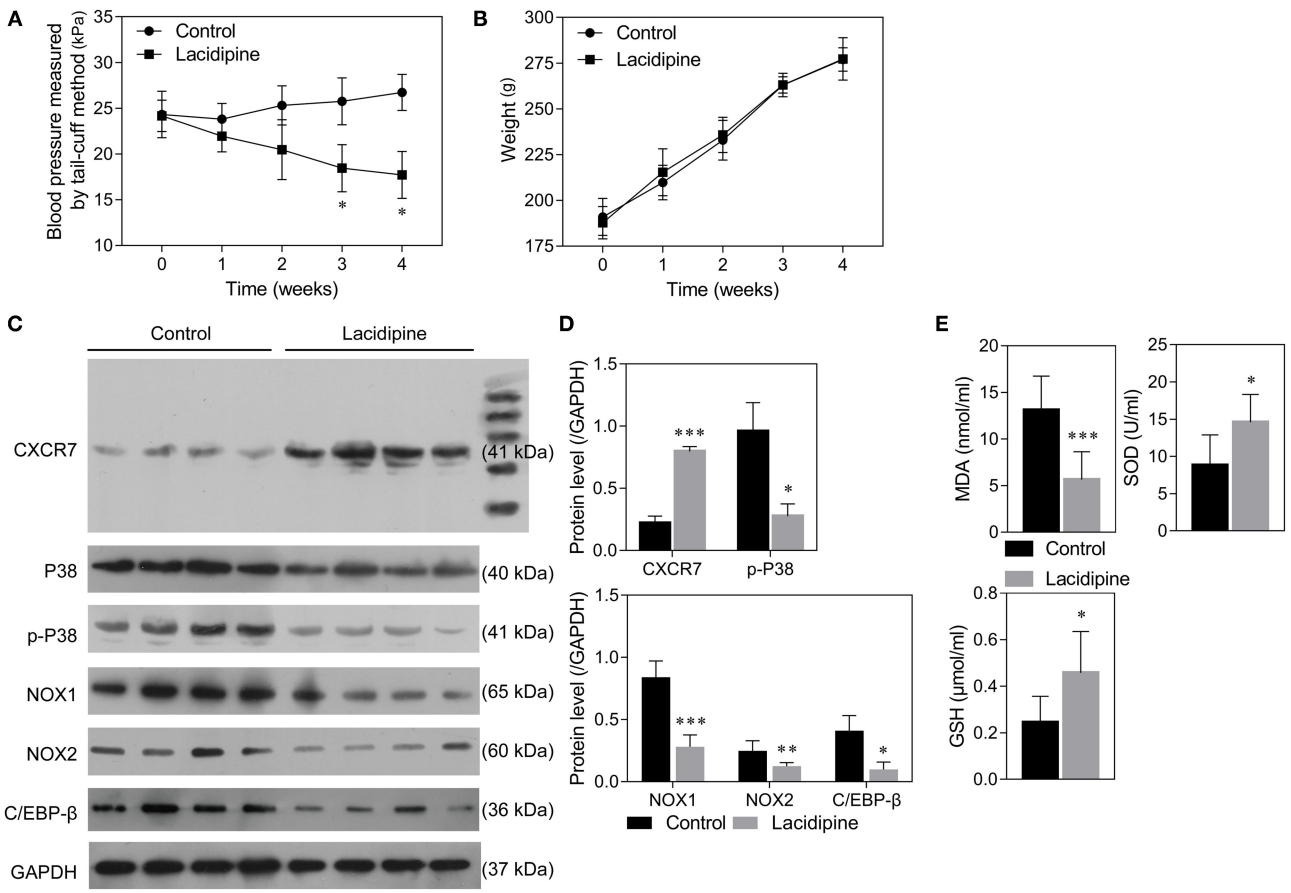

FIGURE 1 | Lacidipine attenuated arterial hypertension and regulated CXCR7/P38/C/EBP-β expression *in vivo*. Blood pressure of spontaneously hypertensive rats (SHRs) treated with and without Lacidipine was measured by the tail-cuff method **(A)**. (Data are mean ± SD, $n = 8$ in each group). The weight of SHRs in the control and Lacidipine groups **(B)**. Western blot was performed to analyze the protein expression of CXCR7, P38, p-P38, C/EBP-β, NOX1, and NOX2 in the aortic tissues from the control and Lacidipine groups **(C,D)**. The levels of MDA, SOD, and GSH in serum were measured by ELISA assays **(E)**. ($^{*}p < 0.05$, $^{**}p < 0.01$, $^{***}p < 0.001$, compared with the control group).

Lacidipine Protects ECs Against Cell Senescence Through the CXCR7 Pathway

To investigate whether the CXCR7 signaling pathway was the key regulator of Lacidipine-related endothelial protection, we specifically knocked down CXCR7 or overexpressed P38 in ECs *in vitro*, respectively. Our results showed that the cell viability (**Figure 4A**) and migration capacity (**Figure 4C**) were significantly impaired in the si-CXCR7 + bleomycin + Lacidipine and bleomycin + Lacidipine + P38 groups. The cells in senescence (**Figures 4B,F**) in the si-CXCR7 + bleomycin + Lacidipine and bleomycin + Lacidipine + P38 groups were remarkably increased compared with those in the bleomycin + Lacidipine group. Moreover, CXCR7 knockdown or P38 overexpression significantly increased the level of P38 and P38 phosphorylation and promoted the expression of VCAM1, Endoglin, MCP-1, and IL-6 (**Figures 4D–F**). These results indicated that CXCR7/P38 plays an important role in Lacidipine-related endothelial protection.

CXCR7/P38/C/EBP-β Mediates the Anti-inflammation Effects of Lacidipine on ECs

Considering the important role of C/EBP-β in inflammation, we further examined whether C/EBP-β participated in the CXCR7/P38-mediated anti-inflammatory effects of Lacidipine on ECs. Our results showed that the expression level of C/EBP-β was increased in ECs treated with bleomycin. Lacidipine treatment partly inhibited the increase of C/EBP-β induced by bleomycin in ECs, and CXCR7 knockdown or P38 overexpression in ECs abolished the effect of Lacidipine on C/EBP-β (**Figures 5A,B**). Furthermore, ECs were stimulated with Lipopolysaccharides (LPS) after Lacidipine treatment. As shown in **Figure 5C**, Lacidipine treatment notably improved the impaired cell viability induced by LPS in ECs. LPS-induced cell apoptosis in ECs was significantly reduced by Lacidipine treatment (**Figure 5D**). Western blot analysis further manifested that the upregulation of C/EBP-β, NLRP3, and caspase-1 induced by LPS was all markedly

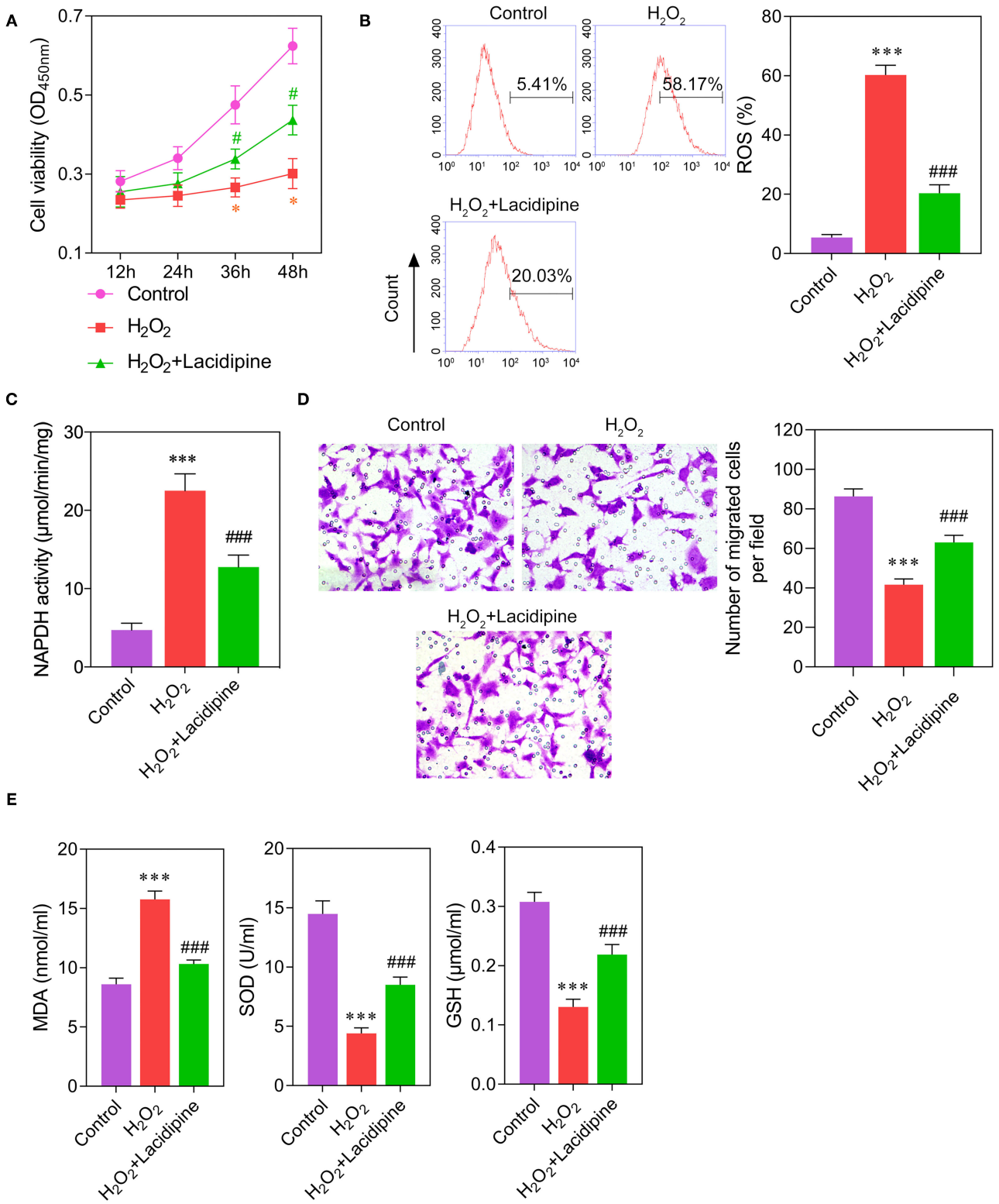

FIGURE 2 | Effects of Lacidipine on the *in vitro* function of ECs under oxidative stress. Cultured ECs were treated with Lacidipine, followed by H_2O_2 stimulation (ROS induction). Cell viability was determined using CCK-8 assay **(A)**. ROS generation was assessed by flow cytometry with 2′,7′-dichlorofluorescein diacetate **(B)**. NADPH activity was measured in different groups **(C)**. Transwell assay was applied to analyze cell migration ability **(D)**. The levels of MDA, SOD, and GSH in culture supernatant were detected by ELISA assays **(E)**. (Data are mean ± SD of three independent experiments. $^{*}p < 0.05$, $^{***}p < 0.001$, compared with the control group; $\#p < 0.05$, $\#\#\#p < 0.001$, compared with the H_2O_2 group).

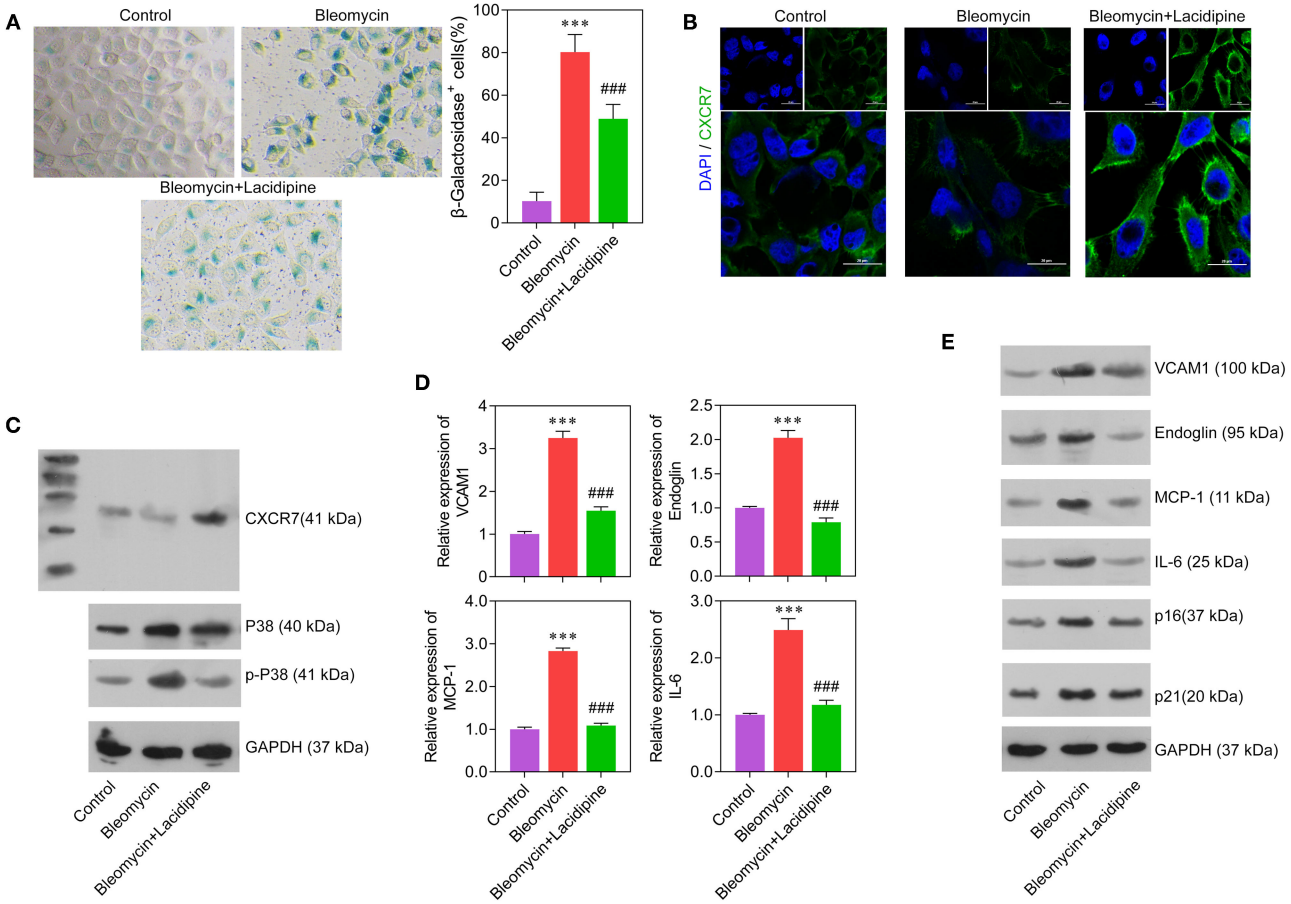

FIGURE 3 | Lacidipine inhibited endothelial senescence and promoted CXCR7 expression. Cultured ECs were treated with Lacidipine, followed by bleomycin stimulation (senescence induction). Cell senescence was determined through β-galactosidase staining **(A)**. Immunofluorescence assay was applied to determine the protein expression of CXCR7 **(B)**. Western blot was performed to analyze the protein expression of CXCR7, P38, and p-P38 **(C)**. qPCR **(D)** and Western blot were performed to analyze the levels of VCAM1, Endoglin, MCP-1, IL-6, P16, and P21 **(E)**. (Data are mean ± SD of three independent experiments. ***$p < 0.001$, compared with the control group; ###$p < 0.001$, compared with the bleomycin group).

reduced by Lacidipine treatment (**Figure 5E**). We also performed gain-of-function assays in ECs from the LPS + Lacidipine group by C/EBP-β overexpression. As expected, C/EBP-β overexpression abrogated the protective effects of Lacidipine on cell viability (**Figure 5F**) and apoptosis (**Figure 5G**) in ECs stimulated with LPS. In addition, C/EBP-β overexpression led to the upregulation of NLRP3 and caspase-1 in the LPS + Lacidipine group (**Figure 5H**). These results demonstrated that Lacidipine suppressed the inflammatory activation and apoptosis in ECs through CXCR7/P38/C/EBP-β.

DISCUSSION

In this study, we demonstrated that Lacidipine protects ECs against oxidative stress, inflammatory activation, and cell senescence through the CXCR7/P38/C/EBP-β signaling pathway. Arterial hypertension is associated with increased levels of ROS that are important contributors to hypertension-related endothelial dysfunction and senescence (18–21). ROS explosion caused by the disorder of mitochondrial metabolism has been considered as the main cause of cell senescence (22). The increase in ROS leads to the increase in intracellular (DNA) damage and ultimately can result in the onset of apoptosis or the induction of cellular senescence in ECs (23). In our study, we found that Lacidipine effectively suppressed the ROS production, NADPH activity, and expression of NOX1/NOX2 in ECs. Under H_2O_2-induced oxidative stress, we observed decreased cell viability and migration capacities in ECs that can be restored by Lacidipine treatment. Studies from other groups also reported that Lacidipine displays antioxidant activity, which is effective for preventing endothelial dysfunction (13, 15). By using bleomycin to induce EC senescence *in vitro*, we found that Lacidipine-pretreated ECs were also partially resistant to cell senescence. Taken together, our study demonstrated that Lacidipine exerts additional beneficial effects on hypertension-related endothelial injury by attenuating EC oxidative damage and cell senescence.

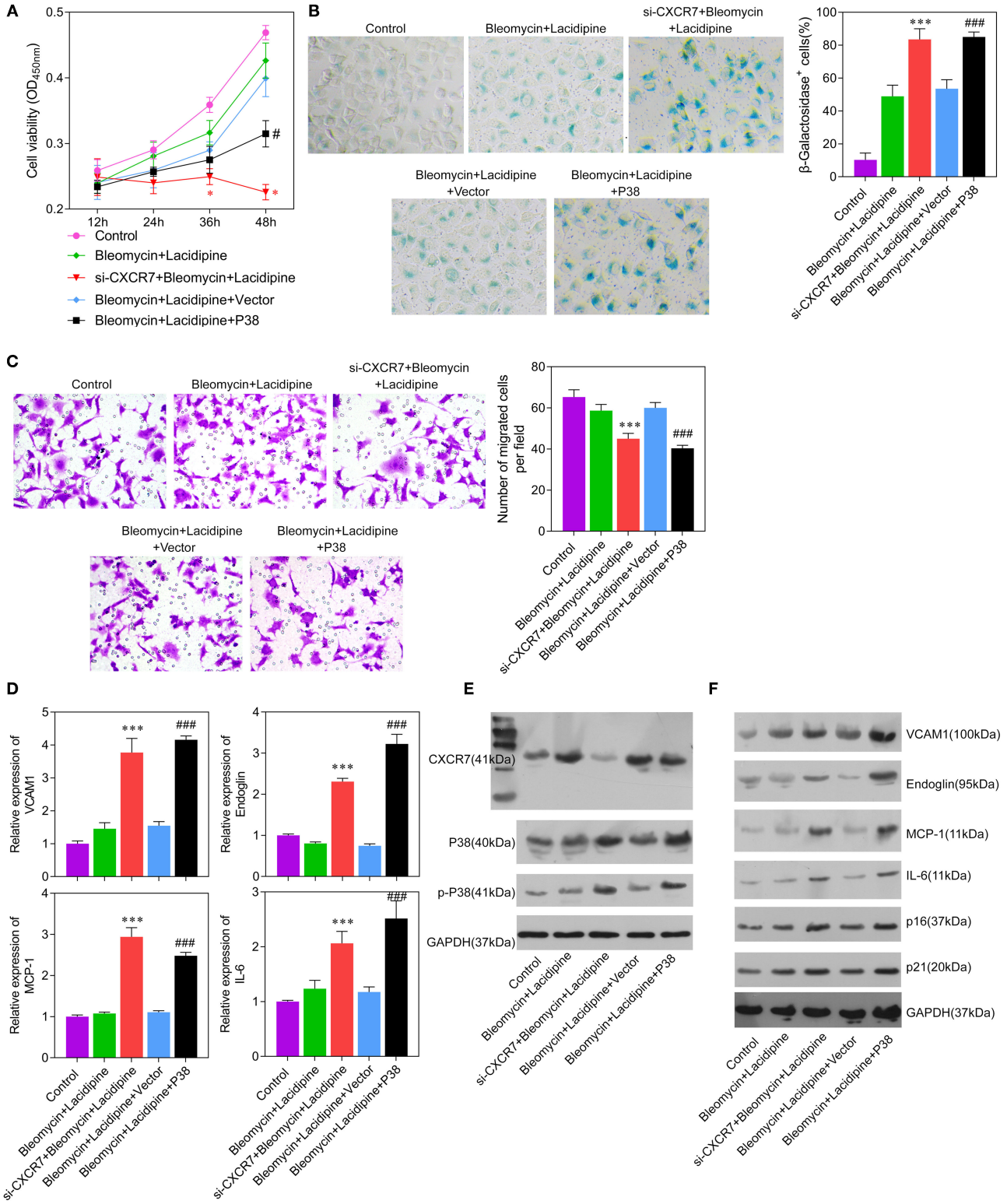

FIGURE 4 | CXCR7 knockdown reversed the effects of Lacidipine on the *in vitro* function of ECs under senescence. ECs from the bleomycin + Lacidipine group were transfected with si-CXCR7 or overexpressed P38, respectively. Cell viability was determined using CCK-8 assay **(A)**. Cell senescence was determined through β-galactosidase staining **(B)**. Transwell assay was applied to analyze cell migration ability **(C)**. qPCR was performed to analyze the mRNA levels of VCAM1, Endoglin, MCP-1, and IL-6 **(D)**. Western blot was performed to analyze the protein levels of CXCR7, P38, p-P38, VCAM1, Endoglin, MCP-1, IL-6, P16, and P21 **(E,F)**. (Data are mean ± SD of three independent experiments. *$p < 0.05$, ***$p < 0.001$, compared with the bleomycin + Lacidipine group; #$p < 0.05$, ###$p < 0.001$, compared with the bleomycin + Lacidipine + Vector group).

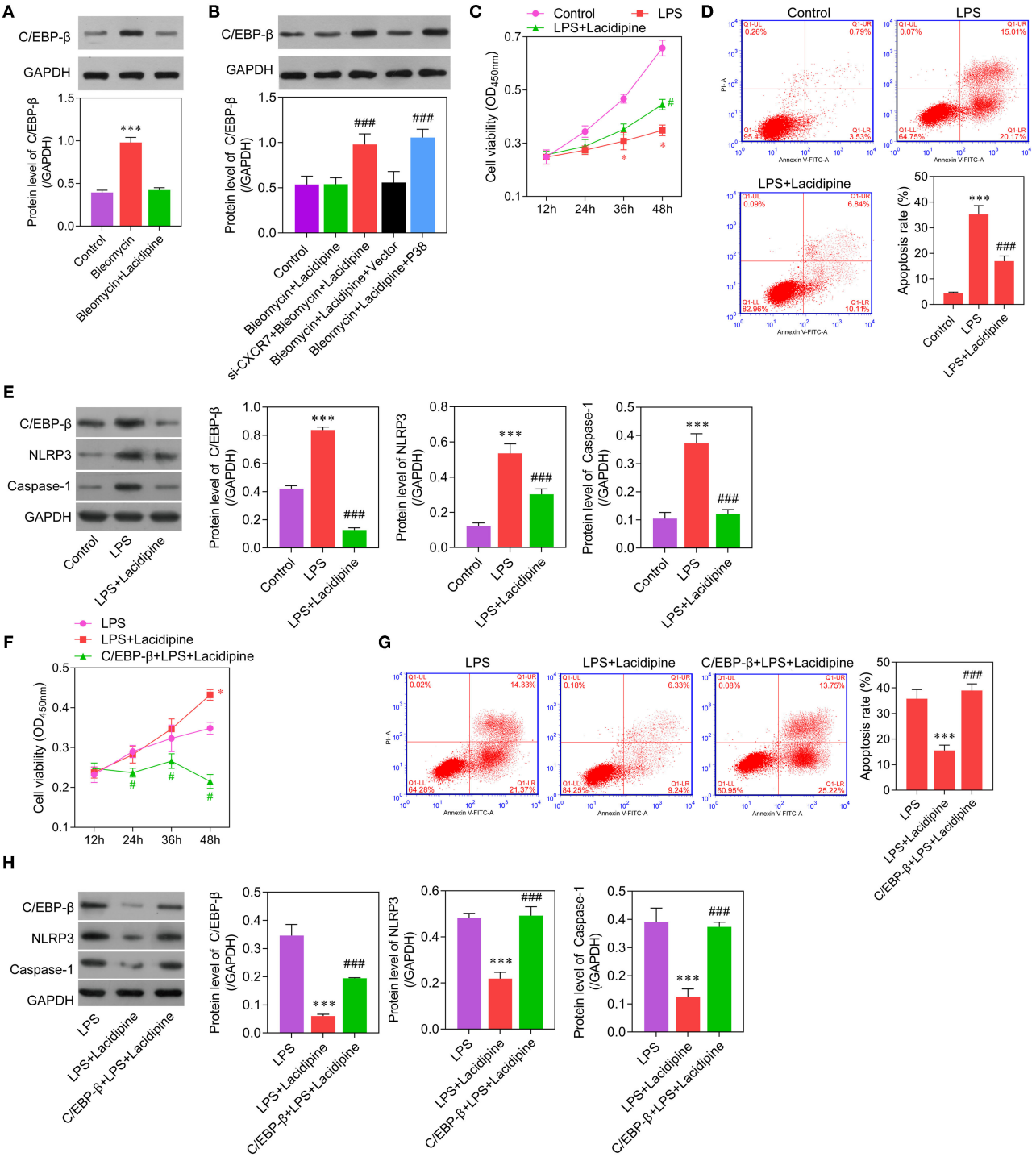

FIGURE 5 | C/EBP-β was involved in Lacidipine-mediated anti-inflammation and anti-apoptosis effects on ECs. Cultured ECs were treated with Lacidipine, followed by bleomycin stimulation. Western blot was performed to analyze the level of C/EBP-β **(A,B)**. (***$p < 0.001$, compared with the bleomycin + Lacidipine group; ###$p < 0.001$, compared with the bleomycin + Lacidipine + Vector group). To further study the inflammatory activation, ECs were treated with Lacidipine, followed by LPS stimulation. Cell viability was determined using CCK-8 assay in ECs from the control, LPS, and LPS + Lacidipine groups **(C)**. Apoptotic cells were determined by flow cytometry in ECs from the control, LPS, and LPS + Lacidipine groups **(D)**. The protein expression of C/EBP-β, NLRP3, and caspase-1 was detected by Western blot in ECs from the control, LPS, and LPS + Lacidipine groups **(E)**. (Data are mean ± SD of three independent experiments. *$p < 0.05$, ***$p < 0.001$, compared with the control group; #$p < 0.05$, ###$p < 0.001$, compared with the LPS group). Cell viability was determined using CCK-8 assay in ECs from the LPS, LPS + Lacidipine, and C/EBP-β + LPS + Lacidipine groups **(F)**. Apoptotic cells were determined by flow cytometry in ECs from the LPS, LPS + Lacidipine, and C/EBP-β + LPS + Lacidipine groups **(G)**. The protein expression of C/EBP-β, NLRP3, and caspase-1 was detected by Western blot in ECs from the LPS, LPS + Lacidipine, and C/EBP-β + LPS + Lacidipine groups **(H)**. (Data are mean ± SD of three independent experiments. *$p < 0.05$, ***$p < 0.001$, compared with the LPS group; #$p < 0.05$, ###$p < 0.001$, compared with the LPS + Lacidipine group).

To further decipher the molecular mechanisms underlying Lacidipine-related protective effects, we specifically knocked down the expression of CXCR7 in ECs using si-RNA transfection. We observed that CXCR7 deficiency abolished the protective effects of Lacidipine on the function of ECs *in vitro* under the stimulation of bleomycin. As we know, CXCR7 is essential for the regulation of cellular biological functions (24). In some cancer cells, CXCR7 was involved in the resistance to apoptosis (25, 26). Yu et al. found that CXCR7 enhances ovarian cancer cell invasion through the P38 MAPK pathway (27). More importantly, CXCR7 plays a critical role in the regulation of EPC growth and survival (28). In the present study, we demonstrated that CXCR7 attenuated the oxidative injury and cell senescence in ECs through the inhibition of P38 phosphorylation. Moreover, the overexpression of P38 can inhibit Lacidipine-related beneficial effects on ECs. These findings suggest that the CXCR7/P38 axis is essential for Lacidipine-related EC protection.

Given the important role of P38 in the regulation of inflammation (29), we further explored the effect of the CXCR7/P38/C/EBP-β pathway on the inflammatory activation in ECs. We found that the inhibition of CXCR7 or overexpression of P38 led to the increase of C/EBP-β level. In addition, Lacidipine could effectively suppress LPS-induced inflammation and apoptosis by downregulating C/EBP-β expression in ECs. Studies showed that C/EBP-β is crucial for the inflammation and apoptosis associated with the pathogenesis of aging (11, 12). According to the report by Jain et al. (30), the C/EBP family of transcription factors may be involved in essential hypertension. Considering the association between inflammation and EC senescence, our results indicate that the CXCR7/P38/C/EBP-β pathway was involved in Lacidipine-related protection against endothelial inflammatory injury and apoptosis.

In summary, to the best of our knowledge, the present study demonstrates for the first time that Lacidipine attenuated endothelial oxidative injury, inflammatory activation, and senescence associated with hypertension by regulating the CXCR7/P38/C/EBP-β pathway. Our findings provide a new insight for the molecular mechanisms underlying Lacidipine-mediated EC protection that might be helpful for developing novel therapeutic strategies for hypertension-related vascular disease.

DATA AVAILABILITY STATEMENT

The original contributions presented in the study are included in the article/supplementary materials, further inquiries can be directed to the corresponding author/s.

ETHICS STATEMENT

The animal study was reviewed and approved by the First Affiliated Hospital of Sun Yat-sen University.

AUTHOR CONTRIBUTIONS

XL, ZH, ZW, and SX contributed to the design, data collecting, and manuscripts preparation of this study. YZ and XS contributed to the *in vitro* and molecular study. FL contributed to the animal experiment. All authors contributed to the article and approved the submitted version.

FUNDING

This study was supported by the National Natural Science Foundation of China (82000466).

REFERENCES

1. Thomas F, Rudnichi A, Bacri AM, Bean K, Guize L, Benetos A. Cardiovascular mortality in hypertensive men according to presence of associated risk factors. *Hypertension.* (2001) 37:1256-61. doi: 10.1161/01.HYP.37.5.1256
2. Taddei S, Virdis A, Mattei P, Ghiadoni L, Gennari A, Fasolo CB, et al. Aging and endothelial function in normotensive subjects and patients with essential hypertension. *Circulation.* (1995) 91:1981-7. doi: 10.1161/01.CIR.91.7.1981
3. Wang JM, Su C, Wang Y, Huang YJ, Yang Z, Chen L, et al. Elevated circulating endothelial microparticles and brachial-ankle pulse wave velocity in well-controlled hypertensive patients. *J Hum Hypertens.* (2009) 23:307-15. doi: 10.1038/jhh.2008.137
4. Landmesser U, Dikalov S, Price SR, McCann L, Fukai T, Holland SM, et al. Oxidation of tetrahydrobiopterin leads to uncoupling of endothelial cell nitric oxide synthase in hypertension. *J Clin Invest.* (2003) 111:1201-9. doi: 10.1172/JCI200314172
5. Liu Y, Yin HL, Li C, Jiang F, Zhang SJ, Zhang XR, et al. Sinapine thiocyanate ameliorates vascular endothelial dysfunction in hypertension by inhibiting activation of the NLRP3 inflammasome. *Front Pharmacol.* (2020) 11:620159. doi: 10.3389/fphar.2020.620159
6. Bai B, Yang Y, Wang Q, Li M, Tian C, Liu Y, et al. NLRP3 inflammasome in endothelial dysfunction. *Cell Death Dis.* (2020) 11:776. doi: 10.1038/s41419-020-02985-x
7. Higashi Y, Kihara Y, Noma K. Endothelial dysfunction and hypertension in aging. *Hypertens Res.* (2012) 35:1039-47. doi: 10.1038/hr.2012.138
8. Zhao Y, Tan Y, Xi S, Li Y, Li C, Cui J, et al. A novel mechanism by which SDF-1β protects cardiac cells from palmitate-induced endoplasmic reticulum stress and apoptosis via CXCR7 and AMPK/p38 MAPK-mediated interleukin-6 generation. *Diabetes.* (2013) 62:2545-58. doi: 10.2337/db12-1233
9. Zhang XY, Su C, Cao Z, Xu SY, Tao J. CXCR7 upregulation is required for early endothelial progenitor cell-mediated endothelial repair in patients with hypertension. *Hypertension.* (2014) 63:383-9. doi: 10.1161/HYPERTENSIONAHA.113.02273
10. Yang Y, Zhou Y, Wang Y, Wei X, Ma A. Exendin-4 reverses high glucose-induced endothelial progenitor cell dysfunction *via* SDF-1β/CXCR7–AMPK/p38-MAPK/IL-6 axis. *Acta Diabetologica.* (2020) 57:1315-26. doi: 10.1007/s00592-020-01551-3
11. Park JH, Ahn JH, Lee TK, Park CW, Kim B, Lee JC, et al. Laminarin pretreatment provides neuroprotection against forebrain ischemia/reperfusion injury by reducing oxidative stress and neuroinflammation in aged gerbils. *Mar Drugs.* (2020) 18:213. doi: 10.3390/md18040213
12. Park BH, Kook S, Lee S, Jeong JH, Brufsky A, Lee BC. An isoform of C/EBPbeta, LIP, regulates expression of the chemokine receptor CXCR4 and modulates breast cancer cell migration. *J Biol Chem.* (2013) 288:28656-67. doi: 10.1074/jbc.M113.509505
13. Krenek P, Salomone S, Kyselovic J, Wibo M, Morel N, Godfraind T. Lacidipine prevents endothelial dysfunction in salt-loaded stroke-prone hypertensive rats. *Hypertension.* (2001) 37:1124-8. doi: 10.1161/01.HYP.37.4.1124

14. Taddei S, Virdis A, Ghiadoni L, Uleri S, Magagna A, Salvetti A. Lacidipine restores endothelium-dependent vasodilation in essential hypertensive patients. *Hypertension.* (1997) 30:1606-12. doi: 10.1161/01.HYP.30.6.1606
15. McCormack PL, Wagstaff AJ. Lacidipine: a review of its use in the management of hypertension. *Drugs.* (2003) 63:2327-56. doi: 10.2165/00003495-200363210-00008
16. Suleyman H, Halici Z, Hacimuftuoglu A, Gocer F. Role of adrenal gland hormones in antiinflammatory effect of calcium channel blockers. *Pharmacol Rep.* (2006) 58:692-9.
17. Liu X, Zhang GX, Zhang XY, Xia WH, Yang Z, Su C, et al. Lacidipine improves endothelial repair capacity of endothelial progenitor cells from patients with essential hypertension. *Int J Cardiol.* (2013) 168:3317-26. doi: 10.1016/j.ijcard.2013.04.041
18. Chakraborty S, Liu L, Fitzsimmons L, Porwollik S, Kim JS, Desai P, et al. Glycolytic reprograming in *Salmonella* counters NOX2-mediated dissipation of DeltapH. *Nat Commun.* (2020) 11:1783. doi: 10.1038/s41467-020-15604-2
19. Rao KNS, Shen X, Pardue S, Krzywanski DM. Nicotinamide nucleotide transhydrogenase (NNT) regulates mitochondrial ROS and endothelial dysfunction in response to angiotensin II. *Redox Biol.* (2020) 36:101650. doi: 10.1016/j.redox.2020.101650
20. Regina C, Panatta E, Candi E, Melino G, Amelio I, Balistreri CR, et al. Vascular ageing and endothelial cell senescence: molecular mechanisms of physiology and diseases. *Mech Ageing Dev.* (2016) 159:14-21. doi: 10.1016/j.mad.2016.05.003
21. Wind S, Beuerlein K, Armitage ME, Taye A, Kumar AH, Janowitz D, et al. Oxidative stress and endothelial dysfunction in aortas of aged spontaneously hypertensive rats by NOX1/2 is reversed by NADPH oxidase inhibition. *Hypertension.* (2010) 56:490-7. doi: 10.1161/HYPERTENSIONAHA.109.149187
22. Stefanatos R, Sanz A. The role of mitochondrial ROS in the aging brain. *FEBS Lett.* (2018) 592:743-58. doi: 10.1002/1873-3468.12902
23. Oeseburg H, de Boer RA, Buikema H, van der Harst P, van Gilst WH, Sillje HH. Glucagon-like peptide 1 prevents reactive oxygen species-induced endothelial cell senescence through the activation of protein kinase A. *Arterioscler Thromb Vasc Biol.* (2010) 30:1407-14. doi: 10.1161/ATVBAHA.110.206425
24. Dai X, Tan Y, Cai S, Xiong X, Wang L, Ye Q, et al. The role of CXCR7 on the adhesion, proliferation and angiogenesis of endothelial progenitor cells. *J Cell Mol Med.* (2011) 15:1299-309. doi: 10.1111/j.1582-4934.2011.01301.x
25. Hattermann K, Held-Feindt J, Lucius R, Muerkoster SS, Penfold MET, Schall TJ, et al. The chemokine receptor CXCR7 is highly expressed in human glioma cells and mediates antiapoptotic effects. *Cancer Res.* (2010) 70:3299-308. doi: 10.1158/0008-5472.CAN-09-3642
26. Wang J, Shiozawa Y, Wang J, Wang Y, Jung Y, Pienta KJ, et al. The role of CXCR7\/RDC1 as a chemokine receptor for CXCL12\/SDF-1 in prostate cancer. *J Biol Chem.* (2008) 283:4283-94. doi: 10.1074/jbc.M707465200
27. Yu Y, Li H, Xue B, Jiang X, Huang K, Ge J, et al. SDF-1/CXCR7 axis enhances ovarian cancer cell invasion by MMP-9 expression through p38 MAPK pathway. *DNA Cell Biol.* (2014) 33:543-9. doi: 10.1089/dna.2013.2289
28. Sierro F, Biben C, Martinez-Munoz L, Mellado M, Ransohoff RM, Li M, et al. Disrupted cardiac development but normal hematopoiesis in mice deficient in the second CXCL12\/SDF-1 receptor, CXCR7. *Proc Natl Acad Sci.* (2007) 104:14759-64. doi: 10.1073/pnas.0702229104
29. Canovas B, Nebreda AR. Diversity and versatility of p38 kinase signalling in health and disease. *Nat Rev Mol Cell Biol.* (2021). 22:346-66. doi: 10.1038/s41580-020-00322-w
30. Jain S, Li Y, Patil S, Kumar A. A single-nucleotide polymorphism in human angiotensinogen gene is associated with essential hypertension and affects glucocorticoid induced promoter activity. *J Mol Med.* (2005) 83:121-31. doi: 10.1007/s00109-004-0621-5

Conflict of Interest: The authors declare that the research was conducted in the absence of any commercial or financial relationships that could be construed as a potential conflict of interest.

frontiers in Cardiovascular Medicine

REVIEW
published: 08 July 2021
doi: 10.3389/fcvm.2021.709169

New Developments in Exosomal lncRNAs in Cardiovascular Diseases

*Zhu Yuan and Weiqiang Huang**

Department of Geriatric Cardiology, Guangxi Key Laboratory Base of Precision Medicine in Cardio-Cerebrovascular Diseases Control and Prevention, Guangxi Clinical Research Center for Cardio-Cerebrovascular Diseases, The First Affiliated Hospital of Guangxi Medical University, Nanning, China

Long non-coding RNAs (lncRNAs) are non-coding RNAs with lengths >200 nt and are involved in the occurrence and development of cardiovascular diseases (CVDs). Exosomes are secreted and produced by various cell types. Exosome contents include various ncRNAs, proteins and lipids. Exosomes are also important mediators of intercellular communication. The proportion of lncRNAs in exosomes is low, but increasing evidence suggests that exosomal lncRNAs play important roles in CVDs. We focused on research progress in exosomal lncRNAs in atherosclerosis, myocardial infarction, myocardial ischemia-reperfusion injury, cardiac angiogenesis, cardiac aging, rheumatic heart disease, and chronic kidney disease combined with CVD. The potential diagnostic and therapeutic effects of exosomal lncRNAs in CVDs are summarized based on preclinical studies involving animal and cell models and circulating exosomes in clinical patients. Finally, the challenges and possible prospects of exosomes and exosomal lncRNAs in clinical applications related to CVD are discussed.

Keywords: exosomal lncRNA, cardiovascular disease, atherosclerosis, myocardial infarction, cardiac angiogenesis

OPEN ACCESS

Edited by:
Zhen-Ao Zhao,
Hebei North University, China

Reviewed by:
You Yu,
Soochow University, China
Juan Feng,
Peking University Health Science Center, China

***Correspondence:**
Weiqiang Huang
hwq2388@sina.com

Specialty section:
This article was submitted to Cardiovascular Biologics and Regenerative Medicine, a section of the journal Frontiers in Cardiovascular Medicine

Received: *13 May 2021*
Accepted: *21 June 2021*
Published: *08 July 2021*

Citation:
Yuan Z and Huang W (2021) New Developments in Exosomal lncRNAs in Cardiovascular Diseases. Front. Cardiovasc. Med. 8:709169. doi: 10.3389/fcvm.2021.709169

INTRODUCTION

Cardiovascular disease (CVD) is currently one of the main causes of death worldwide (1), and atherosclerosis and coronary heart disease are still representative challenges in CVD. In addition, the advent of an aging society has increased the cardiovascular burden, and the high incidence of rheumatic heart disease in developing countries and various concomitant cardiovascular diseases lead to final heart failure and other problems. The mainstream treatments, such as drugs, interventions, and surgery, cannot meet the needs of CVD patients with limited causes. In the case of myocardial infarction, emergency PCI or thrombolytic therapy can save the life of the patient but cannot block the adverse progression of the ischemic myocardium. For cancer patients, chemotherapeutic interventions can easily lead to premature heart failure (2). Therefore, exploring the molecular mechanisms underlying CVD and developing new treatments are critical for reducing CVD mortality.

LncRNAs are non-coding RNAs with lengths >200 nt. These factors were once considered noise in the genome. With the development of high-throughput sequencing, the continuous identification of functional lncRNAs has changed the view of junk RNA (3, 4). LncRNAs are found in various cells and circulation and play key roles in cardiovascular development and CVDs, and lncRNAs are expected to become targets for the treatment of CVDs (5). LncRNAs are transcribed through various regulatory methods, and their interaction with microRNAs (miRNAs) has become a hot spot for studying the functional mechanism of lncRNAs (6).

Exosomes are natural nanoscale cellular vesicles. The exosome surface is rich with specific marker proteins. After binding target cells, exosomes mainly introduce nucleic acids, proteins, and lipids through fusion with the plasma membrane and endocytosis. This content is delivered to the target cell for molecular regulation, representing an important mode of cell-to-cell communication (7). Although the level of lncRNAs in exosomes is low, their role cannot be ignored. In recent years, many studies investigating exosomal lncRNAs provided new insight into crosstalk in the tumor microenvironment (8, 9), and research in the field of CVDs has begun to emerge. This review focuses on the relationship between exosomal lncRNAs and CVD, including the production of exosomal lncRNAs and their mechanism in CVD. Current studies have shown that lncRNAs derived from exosomes are mainly involved in post-transcriptional regulation by sponge adsorption of miRNAs. We hope that this review can provide a basis for their future clinical application through current research investigating exosomes and exosomal lncRNAs in CVD.

LNCRNA CLASSIFICATION AND FUNCTION

Similar to mRNAs, most lncRNAs are transcribed by RNA polymerase II (Pol II), capped at the 5′ end (m7G), tailed at the 3′ end (polyadenylation) and spliced, but lncRNAs lack an open reading frame and do not encode proteins for translation (10). According to the positional relationship between lncRNAs and protein-coding genes, lncRNAs can be divided into (1) sense lncRNAs that overlap with protein-coding genes; (2) antisense lncRNAs that are opposite to protein-coding genes; (3) lncRNAs from introns of protein-coding genes; (4) intergenic lncRNAs located between protein-coding genes; (5) lncRNAs derived from enhancers of protein-coding genes; (6) divergent lncRNAs transcribed from bidirectional promoters; and (7) circular RNAs (circRNAs) formed by the reverse splicing of protein-coding genes (11, 12). LncRNAs are located in the nucleus and cytoplasm and participate in the regulation of gene transcription through cis-acting or trans-acting mechanisms (10, 13–15). Before transcription, lncRNAs can bind proteins or RNAs for chromatin modification. For example, *LNCPRESS1* interacts with *SIRT6* to prevent the chromatin localization of *SIRT6*, maintain histone H3K56 and H3K9 acetylation, and activate transcription (10, 15, 16). During transcription, lncRNAs can mediate gene silencing by interfering with the recruitment of transcription factors and Pol II to prevent transcription (10, 15). For example, the transcription of the lncRNA *AIRN* can interfere with the recruitment of Pol ll and inhibit the transcription of *LGF2R* (17). LncRNAs can also form an R-loop triplet structure with DNA to complete the recruitment of transcriptional cofactors to the promoter, regulate chromatin accessibility, and promote transcription through lncRNAs transcribed by enhancers (10, 15). LncRNAs participate in regulation after transcription and translation. For example, lncRNAs bind miRNAs through a ceRNA mechanism that regulates target gene expression and interact with proteins to form lncRNA-protein complexes to regulate mRNA splicing and translation (10, 15).

EXOSOME BIOLOGY

Extracellular vesicles can be secreted by various cell types and are detected in body fluids. According to their biological mechanism and size, these vesicles are classified as exosomes, microcapsules, and apoptotic bodies. Exosomes are 30–150 nm in size; the plasma membrane initially invaginates to form early endosomes, and the endocytic membrane invades again to form late endosomes and multivesicular bodies (MVBs) (18). Studies have shown that there are two mechanisms underlying the formation of intraluminal vesicles (ILVs) in MVBs as follows: an ESCRT-dependent pathway and an ESCRT-independent pathway. The ESCRT complex includes ESCRT-0, ESCRT-I, ESCRT-II, ESCRT-III and the auxiliary proteins Alix and Vps4 (18, 19). ESCRT-0 recognizes ubiquitinated proteins outside the endosomal membrane. The complete recruitment of ESCRT-I and ESCRT-II occurs under the stimulation of phosphatidylinositol 3-phosphate (PIP3), hepatocyte growth factor-regulated tyrosine kinase substrate (HRS), ubiquitination of the cytosolic tails of endocytic proteins, or curved membrane topology. ESCRT-I binds the ubiquitinated cargo to the endosomal membrane and cooperates with ESCRT-II to open the endoluminal membrane for germination. ESCRT-III participates in the membrane rupture of the ILV neck under the recruitment of Alix, binds TSG101 and participates in the formation of the ESCRT-I complex. Under the action of a deubiquitinating enzyme, the ubiquitin mark is removed from the carrier protein to complete the sorting process. ESCRT-III is decomposed and recycled by the AAA-ATPase suppressor of potassium transport growth defect-1 (SKD1) for the next round of cargo recruitment (18–20). Studies have shown that ILVs can be formed in the absence of the ESCRT complex, indicating that the biological behavior of MVBs can be independent of the ESCRT pathway (21). For example, the lipid raft microdomains formed by ceramide and tetraspanin microdomains formed by CD63 trigger the transport of ILVs to MVBs (19, 20). Usually, MVBs are degraded by fusion with lysosomes after ISG-mediated modification of the TSG101 protein or are fused with the plasma membrane under the coordinated control of the cytoskeleton (microtubules and actin), soluble NSF attachment protein receptor (SNARE), and Rab GTPase to release exosomes (19) (**Figure 1**). A layer-by-layer analysis of the biological behavior of exosomes suggests that exosomes have great potential as a new type of biomarker for prediction and diagnosis in the field of cancer (22). Regarding CVD, exosomes have been reported to have potential application in the diagnosis and treatment of adriamycin-induced cardiotoxicity (23). In addition, Ghafarian et al. discussed the basic science and clinical application of exosomes in CVD (24).

EXOSOMAL LNCRNA SORTING AND MECHANISM OF ACTION

The mechanism by which lncRNAs are sorted into exosomes is still unclear. However, RNA-binding proteins (RBPs), including the hnRNP family [hnRNPA2B1 (25, 26), hnRNPG (27),

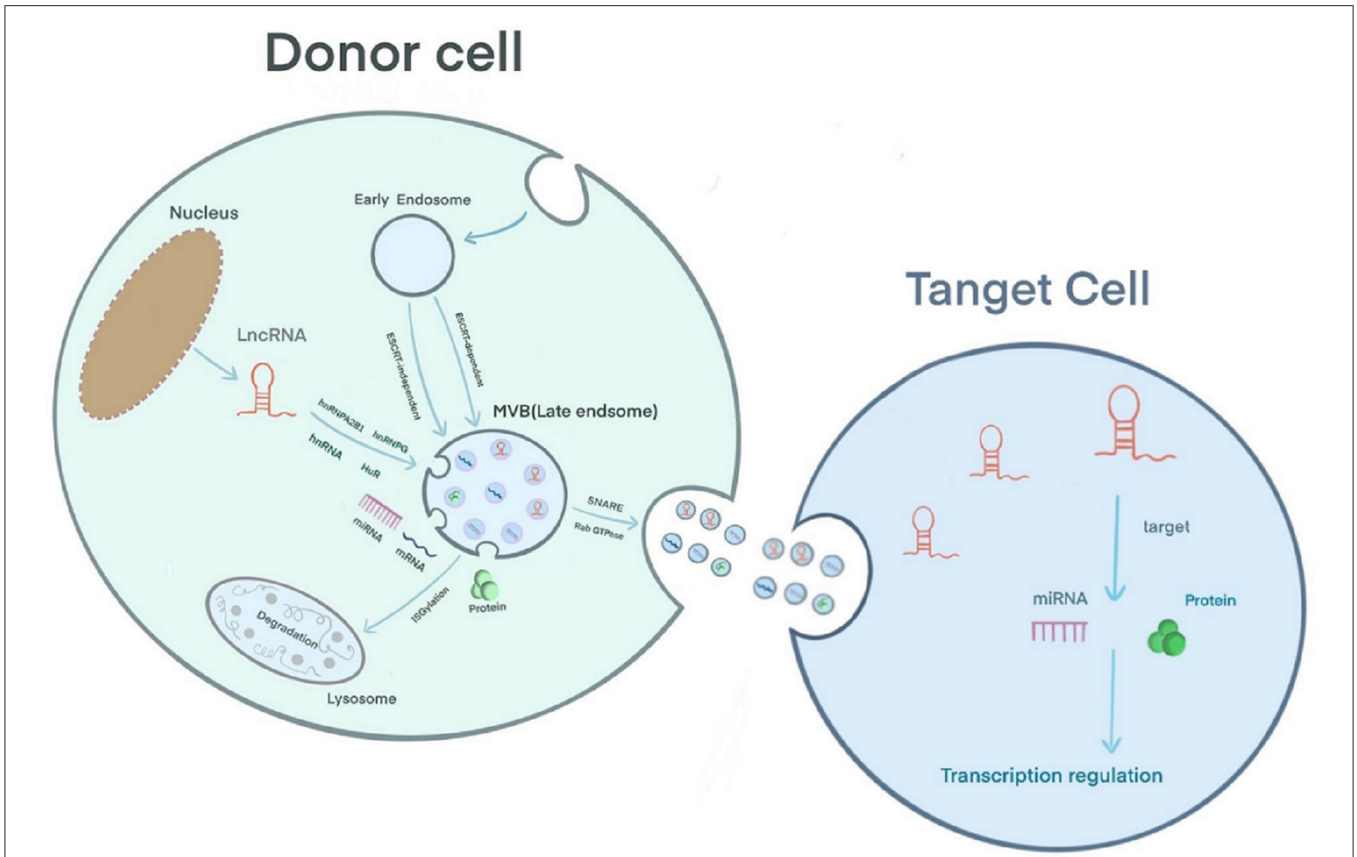

FIGURE 1 | Exosome biology and the sorting and action mechanism of exosomal lncRNA.

hnRNPK (28)] and human antigen R (HuR) (29), have been confirmed to participate in the sorting of lncRNAs into exosomes (30). Furthermore, in sunitinib-resistant kidney cancer cells, hnRNPA2B1 has been shown to bind the 5′ end of *LNCARSR,* and knocking down the level of hnRNPA2B1 or mutating the binding site of hnRNPA2B1 reduces the level of *LNCARSR* in exosomes, suggesting that hnRNPA2B1 specifically facilitates *LNCARSR* loading into exosomes (31) (**Figure 1**). Previously, Zheng et al. introduced the mechanism of action of exosomal miRNAs, i.e., exosomal miRNAs affect the progression of CVD by binding target genes and mediating target mRNA silencing (32). The difference is that exosomal lncRNAs can be used for disease regulation through epigenetic modification. Furthermore, exosomal lncRNAs often act as sponges of endogenous miRNAs, mediating the expression of their target genes or activating related signaling pathways to produce biological effects. For example, Zang et al. found that the combination of the lncRNAs *UFC1* and *EZH2* resulted in H3K27 trimethylation and *PTEN* expression inhibition, which ultimately promoted the progression of non-small cell lung cancer (33). Zhuo et al. found that the exosomal lncRNA *FAM138B* derived from cancer cells can alleviate the progression of hepatocellular carcinoma by sponging *MIR-765* (34).

EXOSOMAL LNCRNA IN CARDIOVASCULAR DISEASE

In recent years, research investigating exosomal lncRNAs has become a trend. Especially in the field of cancer, several studies have shown that exosomal lncRNAs may become new biomarkers of and targets for cancer progression and treatment (35). In addition, similar studies investigated exosomal lncRNAs in various systemic diseases. For example, exosomal lncRNAs are expected to become a therapeutic target for lung diseases (36). In the field of CVD, Wang et al. found that the release of the exo-circRNA *HIPK3* from hypoxic cultured cardiomyocytes protects against cardiac microvascular endothelial oxidative damage by targeting the *MIR29A*/*IGF-1* pathway and promotes the proliferation and migration of cardiac endothelial cells through the *MIR29a*/*VEGF* axis (37, 38). Ni et al. discussed the relationship between exocrine-derived non-coding RNAs (lncRNAs and miRNAs) in endothelial cells and vascular smooth muscle cells and their mechanism in vascular senescence (39). Recently, Cheng et al. found *in vitro* that the exo-lncRNA *ZEB1-AS1* secreted by human umbilical vein endothelial cells induced by oxidized low-density lipoprotein (ox-LDL) enhances the damage caused by the *MIR-590-5P*/*ETS1* axis to human umbilical vein endothelial cells through the TGF-β/Smad pathway (40).

TABLE 1 | Progress of exosomal lncRNA in preclinical study of CVD.

LncRNA	Donor cell	Target cell	Pathway	Type of CVD	Function	References
RNCR3	HUVEC	VSMC	miR-185-5P/KLF2	AS	Promote the proliferation of ECs and VCMCs; inhibition of ECs apoptosis	(41)
MALAT1	HUVEC	iDC	NRF2	AS	Promote the maturation of DCs; promote the accumulation of oxidative stress	(42)
	HUVEC	THP-1	-	AS	Promote the polarization of M2 macrophages	(43)
	hCVPC	Cardiomyocyte; HUVEC	MiR-497	AMI	Inhibit cardiomyocyte apoptosis; promote angiogenesis of ECs	(44)
	Cardiomyocyte		miR-92a/KLF2/CD31	AMI	Reduce the area of myocardial infarction;Improve cardiac function; promote angiogenesis after myocardial infarction	(45)
	UMSC	H9C2	NF-κB/TNF-α	Cardiac aging	Delay cardiac aging	(46)
	AD-MSC	Cardiomyocyte	miR-92a-3p/ATG4a	Cardiac aging	Improve cardiac mitochondrial metabolism ;delay the senescence of cardiac myocytes	(47)
GAS5	THP-1	HUVEC	-	AS	Promote apoptosis of vascular endothelial cells	(48)
SNHG9	ADSC	HUVEC	TRADD/ NF-κB	AS	Inhibit the release of inflammatory factors ;inhibition of endothelial cell apoptosis	(49)
LINC01005	HUVEC	VSMC	miR-128-3P/KLF4	AS	Promote phenotypic transformation, proliferation and migration of vascular smooth muscle	(50)
NEAT1	ADMSC	HiPSC-derived cardiomyocytes	miR-142-3p/ FOXO1	MI	Anti-oxidative stress ;inhibit cardiomyocyte apoptosis	(51)
	BM-MSC	Cardiomyocyte	miR-221-3p/Sirt2	Cardiac aging	Anti-aging of cardiomyocytes	(52)
AK139128	cardiomyocyte	CF	-	MI	Inhibit the proliferation of cardiac fibroblasts and promote apoptosis	(53)
KLF3-AS1	hMSC	H9c2	miR-138-5p/ Sirt1	MI	Inhibit the release of inflammatory factors; attenuate pyroptosis of cardiomyocytes	(54)
ENSRNOT00000039868	PMN	Cardiomyocyte	PDGFD/AKT	MIRI	Anti-oxidative stress of cardiomyocytes;inhibit cardiomyocyte apoptosis;reduce I/R injury	(55)
UCA1	hUCMSC	CMEC	miR-143/Bcl-2/Beclin1	MIRI	Inhibition of cardiomyocyte autophagy;inhibition of myocardial apoptosis;reduce H/R injury	(56)
	hMSC	H9C2	miR-873-5p/XIAP	MI	Inhibit cardiomyocyte apoptosis;improve cardiac function	(57)
LINC00174	EC	cardiomyocyte	SRSF1/ P53/ myocardin/AKT/AMPK	MIRI	Inhibition of autophagy and apoptosis of cardiomyocytes	(58)
H19	MSC	H9C2; HUVEC	miR-675-3p/miR-675-5p/VEGF/ICAM-1	MI	Promote angiogenesis of ECs ;inhibit cardiomyocyte apoptosis ;inhibit myocardial fibrosis; improve cardiac function	(59)
ZFAS1	human cardiomyocyte	CF	miR-4711-5p/WNT/β	Myocardial fibrosis	induce myocardial fibrosis	(60)

Current studies have shown that exosomal lncRNAs participate in the dynamic evolution of underlying cardiovascular diseases through various pathways, involving all aspects of their pathophysiology and potential treatment. For example, lncRNAs participate in the initial development of atherosclerosis, the occurrence of acute myocardial infarction (AMI) and ischemia-reperfusion injury, cardiac angiogenesis, repair and protection against cardiac aging (**Table 1** and **Figure 2**). The differential changes in lncRNAs in patient plasma exosomes make them potential

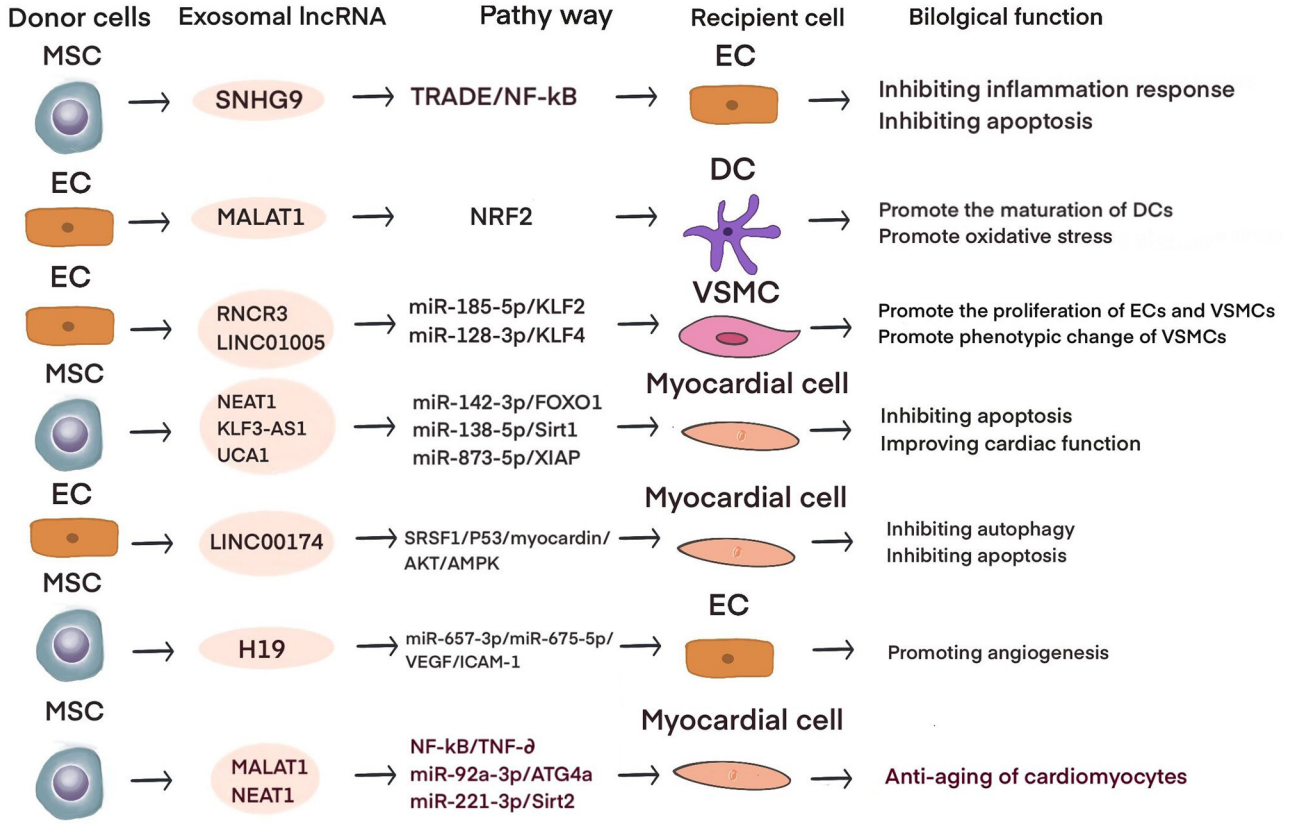

FIGURE 2 | The role of exosomal lncRNA in preclinical studies of cardiovascular diseases.

TABLE 2 | The role of serum exosomal lncRNA in cardiovascular disease.

Exosomal lncRNA	Expression	Disease	Function	References
HIF1a-AS1	Up	AS	Diagnostic	(61)
NEAT1	Up	STEMI	Diagnostic	(62)
ENST00000556899.1; ENST00000575985.1	Up	AMI	Prognostic	(63)
UCA1	Up	AMI	Diagnostic	(57)
SOCS2-AS1	Down	CAD	Diagnostic	(64)
RP13-820C6.2 RP11-339B21.15 G004800 XLOC_010028	Down	RHD	Diagnostic; Therapeutic	(65)
XLOC_004201	Up			

biomarkers for the diagnosis and treatment of CVDs (**Table 2** and **Figure 3**).

ATHEROSCLEROSIS

Atherosclerosis (AS) is the most common type of CVD and the root cause of myocardial infarction. The main risk factors are aging, hyperlipidemia, obesity, hypertension, and smoking. Endothelial injury is considered the first step in the development of atherosclerosis. Subsequently, after inflammatory cell infiltration, vascular smooth muscle cells (VSMCs) proliferate and activate, exacerbating plaque formation. Therefore, targeting endothelial dysfunction, inflammatory cells and the phenotypic transition of VSMCs are critical for the study of the development and treatment of atherosclerosis. For example, exo-*MIR143*/*MIR145* secreted by endothelial cells expressing *KLF2* can communicate with smooth muscle cells, increase the expression of dedifferentiation-related genes, and reduce atherosclerosis in ApoE-/- mice (66). Macrophage-derived exo-*MIR99A*/*MIR146B*/*MIR378A* targets NF-κB/TNF-α signaling to inhibit inflammation, promote macrophage M2 polarization, and reduce the area of atherosclerotic necrosis (67).

Obesity is a risk factor for atherosclerosis; obesity promotes endothelial cell (EC) dysfunction, accelerates endothelial cell apoptosis and the release of inflammation, and promotes the development of atherosclerosis (68, 69). Exosomal lncRNAs are involved in endothelial dysfunction. For example, lncRNA *SNHG9* overexpression in adipose stem cell-derived exosomes can inhibit endothelial cell apoptosis, inhibit NF-κB signaling, and reduce inflammation. *TRADD*, which is the target gene of *SNHG9*, is negatively associated with *SNHG9* and inversely regulates the protective effects of *SNHG9* to inhibit EC disorders (49).

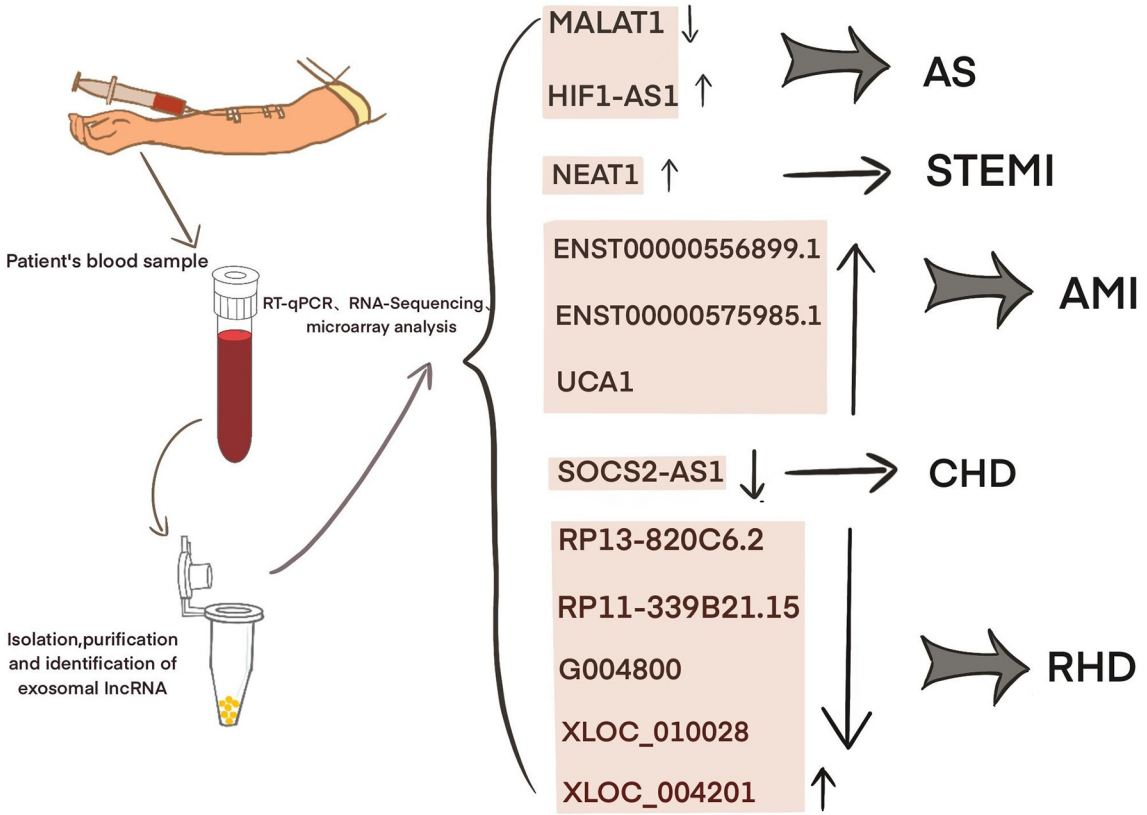

FIGURE 3 | Exosomal lncRNA in the serum of CVD patients as potential biomarkers.

M2 macrophages can fight the progression of atherosclerosis (67). Exosomal lncRNAs mediate communication between ECs and immune cells. For example, Huang et al. found that the expression level of the lncRNA *MALAT1* was significantly increased in exosomes secreted by ox-LDL-stimulated human umbilical vein endothelial cells (HUVECs) and that coculture with these exosomes increased THP-1 cell expression of *MALAT1* and promoted the polarization of M2 macrophages (43). A study by Chen et al. showed that the expression of the lncRNA *GAS5* in exosomes derived from THP-1 cells under ox-LDL stimulation was significantly upregulated. Exosomes secreted by ox-LDL-stimulated THP-1 cells with *GAS5* knockout were cocultured with HUVECs, and PHK67-labeled exosomes were internalized by HUVECs and significantly reduced HUVEC apoptosis. In contrast, exosomes secreted by ox-LDL-stimulated *GAS5*-overexpressing THP-1 cells could accelerate HUVEC apoptosis (48). Hong et al. found that the expression of *MALAT1* was significantly reduced in the serum of patients with atherosclerosis and exosomes derived from ox-LDL-stimulated HUVECs. Exosomes derived from ox-LDL-stimulated HUVECs overexpressing *MALAT1* are taken up by dendritic cells (DCs) and can inhibit DC maturation, activate NRF2 signaling, and inhibit reactive oxygen species (ROS) accumulation in DCs. Silencing *MALAT1* results in the opposite effects. Similarly, in a mouse model of atherosclerosis, ox-LDL-stimulated exosomes exacerbated atherosclerosis in mice. This finding shows that the expression of *MALAT1* is decreased in vascular endothelial cell-derived exosomes induced by ox-LDL, inhibits NRF2 signaling, leads to ROS accumulation and DC maturation, and accelerates the development of atherosclerosis (42).

Exosomal lncRNAs mediate the interaction between endothelial cells and VSMCs. For example, Shan et al. found that apoE-/- mice expressed increased levels of the lncRNA *RNCR3* during the atherosclerotic stage, and RNA fluorescence *in situ* hybridization revealed RNCR3 localization in endothelial cells and arterial smooth muscle cells. After knocking out *RNCR3 in vivo*, the endothelial cell coverage and smooth muscle proliferation were significantly reduced. *In vitro* cell experiments showed that after knocking out *RNCR3*, HUVEC proliferation slowed, and apoptosis accelerated. After coculturing HUVEC-derived exosomes (HUVEC-exos) with VSMCs, VSMC proliferation and migration were inhibited. Biological analyses and luciferase assays show that HUVEC-exo-*RNCR3* targets the *MIR-185-5P*/*KLF2* axis to promote the proliferation of ECs and VSMCs and plays a protective role in the development of atherosclerosis (41). Zhang found that coculturing ox-LDL-stimulated HUVECs-exo-*LINC01005* with VSMCs significantly downregulated the smooth muscle cell contraction markers α-SMA and SM22a and upregulated the

VSMC proliferation marker OPN, indicating that HUVECs-exo-*LINC01005* promoted phenotypic changes in VSMCs. The database and luciferase reporter assay show that HUVECs-exo-*LNC01005* mediates phenotypic changes in endothelial cells and VSMC proliferation through the *MIR-128-3P*/*KLF4* axis (50). It is suggested that the communication of exosomal lncRNAs among ECs, VSMCs and immune cells is mainly involved in the progression of atherosclerosis by targeting miRNAs or directly regulating the expression of genes.

The differences in the expression of exosomal lncRNAs in peripheral circulation in patients with atherosclerosis may represent a potential biomarker for the diagnosis of atherosclerosis. For example, Song et al. found significantly low expression of exosomal *SNHG9* in the plasma of obese patients and revealed that this level was associated with endothelial dysfunction (49). Hong et al. found that a low expression of exosomal *MALAT1* in the serum of patients with atherosclerosis led to DC maturation and promoted the progression of atherosclerosis (42). Wang et al. examined 65 blood samples from atherosclerosis patients and 68 blood samples from healthy volunteers and found that the blood exosomal concentration and exo-lncRNA *HIF1A-AS1* expression in the atherosclerosis patients were significantly higher than those in the healthy group. A receiver operating characteristic (ROC) curve analysis showed that the areas under the curve of the plasma exosomes and exo-*HIF1A-AS1* were 0.856 and 0.823, respectively. This finding indicates that plasma exo-*HIF1A-AS1* may be a potential biomarker for the diagnosis of atherosclerosis (61). It is suggested that the differential expression of serum exosomal lncRNAs in patients with atherosclerosis may play an auxiliary role in diagnosis.

MYOCARDIAL INFARCTION

Myocardial infarction is caused by coronary artery stenosis or occlusion, and the myocardium is in a state of ischemia and hypoxia. Apoptosis and fibrosis of ischemic and hypoxic cardiomyocytes lead to ventricular remodeling, which, in turn, causes arrhythmia and heart failure. Since the 21st century, the performance of cell therapy in the treatment of myocardial regeneration has been unsatisfactory. The paracrine mechanism that plays a major role in cell therapy has given high hopes regarding the use of exosomes characterized by non-cellular therapy (70–74). For example, in a mouse model of myocardial infarction, exosomes derived from mouse embryonic stem cells promote survival and proliferation in cardiac progenitor cells by delivering miR-294 (75). Intramuscular injection of exosomes derived from cardiosphere-derived cells can reduce acute and chronic myocardial infarction injury in pigs, reduce the area of myocardial infarction, reduce the area of scars, and combat cardiac remodeling (76).

In addition to exosomal miRNAs, mesenchymal stem cell (MSC)-derived exosomal lncRNAs also play important roles in myocardial infarction. For example, Che et al. found that the exosomal lncRNA *NEAT1* secreted by migration inhibitory factor (MIF)-induced human adipose mesenchymal stem cells (ADMSCs) inhibits H2O2-induced cardiomyocyte apoptosis. The database and dual luciferase gene reports show that the $ADMSC^{MIF}$-derived exosomal *NEAT1* reduces H2O2-induced oxidative stress in cardiomyocytes and reduces cardiomyocyte apoptosis through the *MIR-142-3p*/*FOXO1* axis (51). Mao et al. detected the lncRNA *KLF3-AS1* in exosomes secreted by human MSCs (hMSCs). Injection of hMSC-exos in a rat myocardial infarction model significantly reduced the expression of the proinflammatory factors IL-1β and IL-18 in cardiomyocytes and the expression of NLRP3, Asc, and Caspase-1, indicating that hMSC-exos induced cardiomyocyte pyrolysis. In an *in vitro* hypoxic cardiomyocyte model, the protective effect of hMSC-exos was consistent with that observed in the *in vivo* experiments. Database and dual luciferase gene reporter experiments showed that the hMSC-exo-*KLF3-AS1*/*MIR-138-5p*/*SIRT1* axis mediates protection in hypoxic cardiomyocytes (54). Sun et al. performed cell and animal experiments and showed that the exosomal lncRNA *UCA1* secreted by hypoxia-induced human bone marrow MSCs (BMSCs) sponges *MIR-873-5p*, regulates *XIAP*, and enhances AMPK phosphorylation in cardiomyocytes. This lncRNA also increases the expression of antiapoptotic proteins, such as p53, bax, and cleaved caspase-3, and inhibits the expression of the apoptotic protein bcl-2 (57).

Studies have shown that exosomal lncRNAs mediate communication between cardiomyocytes and cardiac fibroblasts (CFs) in the context of myocardial infarction. For example, Wang et al. found that coculturing hypoxic cardiomyocyte-derived exosomes and CFs significantly inhibited CF proliferation, migration and invasion and promoted apoptosis. An RNA-seq analysis revealed the differential expression of the lncRNA AK139128. *In vivo* experiments showed that exo-AK139128 exacerbated CF apoptosis in rats with myocardial infarction. Western blot analyses showed that the expression of the apoptotic protein bcl-2 increased, while the expression of the antiapoptotic protein bax decreased. This finding shows that exosomal AK139128 secreted by hypoxic cardiomyocytes promotes CF apoptosis (53). The above studies show that in addition to exosomal lncRNAs derived from mesenchymal stem cells, which are expected to become therapeutic targets for the treatment of infarcted myocardium, exosomal lncRNAs between cardiac cells also have potential therapeutic significance and research value.

Recent studies have shown that significant differences exist in plasma exosomal lncRNAs in patients with myocardial infarction, suggesting that these factors may have an auxiliary diagnostic effect. For example, Chen et al. found that the serum expression of exosomal *NEAT1* and *MMP9* in patients with ST-segment elevation myocardial infarction (STEMI) was significantly higher than that in patients with unstable angina and non-myocardial infarction, while the level of *MIR204* was relatively lower. Spearman tested the correlation among the three factors and found that *NEAT1* was positively correlated with the *MMP9* levels, but *NEAT1* was not significantly correlated with *MIR204*, *MIR204*, or *MMP9*. A logistic regression analysis revealed that *NEAT1*, *MIR204*, and *MMP9* are independent predictors of STEMI (62). Zheng et al. found that ENST00000556899.1 and ENST00000575985.1 were

significantly upregulated in circulating exosomes from AMI patients and control patients. An ROC analysis showed that ENST00000556899.1 and ENST00000575985.1 have areas under the myocardial infarction curve of 0.661 and 0.751, respectively, and are positively correlated with inflammatory biomarkers, myocardial infarction prognostic indicators, and myocardial injury markers (63). Sun et al. showed that the plasma expression of the exosomal lncRNA *UCA1* in patients with myocardial infarction was increased. An ROC analysis showed that human plasma exosomal *UCA1* may be a non-invasive biomarker for the diagnosis of AMI (57). Liang et al. enrolled 227 subjects and divided them into a coronary heart disease group, an early coronary heart disease group, and a normal coronary artery control group. Gene chip detection and RT-PCR showed that the exo-lncRNA *SOCS2-AS1* was significantly downregulated in the coronary heart disease group. A Pearson correlation analysis showed that the plasma exo-*SOCS2-AS1* levels were negatively correlated with the LPA and PLT levels. Univariate and multivariate logistic regression analyses showed that the plasma exosomal SOCS2-AS1 levels were an independent protective factor for coronary heart disease (64). These data suggest that exosomal lncRNAs may play an auxiliary role in the prediction and diagnosis of patients with myocardial infarction.

MYOCARDIAL ISCHEMIA-REPERFUSION INJURY

Myocardial ischemia-reperfusion injury (MIRI) refers to the pathological process during which the ischemic myocardium returns to normal perfusion after a coronary artery is partially or completely occluded, which, in turn, exacerbates myocardial injury. In clinical practice, MIRI is common in patients with myocardial infarction after emergency percutaneous coronary intervention (PCI) or thrombolytic therapy (77). The potential molecular mechanisms involved include oxidative stress, intracellular calcium ion overload, rapid recovery of PH, opening of the mitochondrial permeability transition pore (MPTP), the inflammatory response, and late myocardial reperfusion injury (77, 78). In recent years, treatments for MIRI have included ischemic preconditioning (IPC), ischemic post-processing (IPost), remote ischemic conditioning (IPC), the use of drugs to prevent myocardial reperfusion injury, therapeutic hyperbaric oxygen (HBO) and hypothermia (77–79). Recent studies have shown that the cardioprotective effect of IPC is mediated by exosomes (80). For example, exosomes derived from rat fibroblasts can protect cardiomyocytes after ischemia by targeting *MIR-423-3p*/*RAP2C* to reduce MIRI (81).

Similarly, exosomal *UCA1* derived from hMSCs was discovered by Sun et al. to exert myocardial protection after myocardial infarction (57). Diao et al. found that exosomes derived from human umbilical cord blood MSCs (hUCMSCs) could inhibit hypoxia/reoxygenation (H/R)-induced cardiac microvascular endothelial cell (CMEC) apoptosis in Sprague-Dawley rats. In addition, hUCMSC-exos can inhibit macrophage autophagy under hypoxia. In an *in vivo* IR rat model, injection of hUCMSC-exos improved the ultrastructure of rat CMECs, inhibited apoptosis, and reduced the vascular endothelial injury markers TM and vWF. An RT-qPCR analysis verified that hUCMSC-exos were enriched with *UCA1*. In addition, dual luciferase reporter and RNA pull-down experiments showed that hUCMSC-exo-*UCA1* inhibited autophagy and apoptosis in H/R-injured rat CMECs by regulating the *miR143*/*BCL-2*/*BECLIN1* axis (56).

Recent studies have shown that exosomal lncRNAs are involved in the communication between polymorphonuclear cells (PMNs) and IR cardiomyocytes. For example, Zhai et al. used an H/R cardiomyocyte model and showed that PMN-exos stimulated by the calcium sensitive receptor (CaSR) activator cinacalcet were taken up by cardiomyocytes, increased the expression of p-AKT and Bcl-xL, reduced the production of NOX2 and ROS, and reduced cardiomyocyte apoptosis, while the AKT inhibitor HY15186 could reverse these effects. A high-throughput sequencing analysis of CaSR-PMN-exos found differential expression of the lncRNA ENSRNOT00000039868 (lncRNA 39868) and predicted PDGFD as the target protein of lncRNA 39868. siRNA-mediated silencing of the lncRNA 39868 significantly reduced PDGFD mRNA expression. *In vivo* experiments showed that after intravenous injection of CaSR-PMN-exos via the tail vein in rats, the area of myocardial infarction and MDA secretion were significantly reduced, the SOD levels were increased, and cardiac function was improved. These results suggest that CaSR-PMN-exosomal lncRNA 39868 upregulates the protein PDGFD, regulates these effects through the AKT pathway, and reduces MIRI (55).

Exosomal lncRNAs derived from endothelial cells have protective effects on IR cardiomyocytes. For example, Su et al. measured the expression of exosomal *LINC00174* derived from vascular endothelial cells. After coculturing H/R cardiomyocytes with exo-*LINC00174* *in vitro*, *P53* was inhibited, and P53-induced autophagy enhancement and cardiomyocyte apoptosis were inhibited. In contrast, the expression of *SRSF1* was increased. RNA pull-down experiments and RIP verified the binding of *LINC00174* to *SRSF1*. In I/R mice, AKT/AMPK phosphorylation was increased, indicating that myocardial autophagy was activated, but *P53* knockout inhibited autophagy activation and cardiomyocyte apoptosis. A dual luciferase reporter assay confirmed that *MYOCARDIN* was the binding site of *P53*. Vascular endothelial cell exo-*LNC00174* bound *SRSF1* to inhibit *P53* expression, *MYOCARDIN* transcription, AKT/AMPK activation, and ultimately autophagy activation and apoptosis in I/R cardiomyocytes (58). These results suggest that the mechanism of cardiomyocyte protection mediated by exosomal lncRNAs in myocardial ischemia-reperfusion injury involves crosstalk among mesenchymal stem cells, polymorphonuclear cells and endothelial cells. The study of exosomal lncRNAs in myocardial ischemia-reperfusion still needs more exploration.

CARDIAC ANGIOGENESIS

Currently, revascularization treatment for AMI or ischemic cardiomyopathy mainly involves PCI, coronary artery bypass

grafting and thrombolysis to restore the myocardial blood supply and save the dying myocardium. However, MIRI follows, and for patients who cannot undergo surgery, there is an urgent need for a new alternative therapy. In addition to cell therapy to rescue and restore cardiomyocytes, increasing research suggests that promoting the survival of cardiac endothelial cells, treating cardiac angiogenesis, and mediating the recanalization of cardiac collaterals have great therapeutic potential for the treatment of myocardial infarction. Examples include angiogenesis gene therapy (82), proangiogenic stem cell therapy (83), angiogenic ncRNA therapy (84), and exosome- and exosome-derived proangiogenic ncRNA therapy (85–88). For example, a study by Ma et al. showed that exosomes derived from murine BMSCs can deliver *MIR132*, induce tube formation in HUVECs *in vitro*, and promote angiogenesis in the ischemic area of the infarcted heart in mice (89).

Exosomal lncRNAs derived from stem cells can promote endothelial cell proliferation and angiogenesis after myocardial infarction. For example, Q. Wu et al. found that hypoxia-induced cardiovascular progenitor cells derived from human pluripotent stem cell (hCVPC)-EVs could improve heart function in mice with myocardial infarction, and immunohistochemistry studies showed that *CD31* and α-SMA expression increased. Similarly, *in vitro* experiments showed that hCVPC-EVs can reduce the damage induced by oxygen glucose deprivation (OGD) to cardiomyocytes and promote endothelial cell migration and tube formation. RNA sequencing and RT-qPCR analyses showed that the expression of *MALAT1* in hypoxic hCVPC-EVs was significantly increased, and knocking down the expression of *MALAT1* inhibited angiogenesis. Database and dual luciferase gene reporter assays suggest that *MALAT1* targets *MIR497* (44). After culturing atorvastatin-treated (ATV)-MSC-exos with HUVECs *in vitro*, Huang et al. showed that HUVECs treated with ATV-MSC-exos had enhanced tube-forming abilities. When cocultured with H9C2 cardiomyocytes stimulated with hypoxia and serum deprivation (H/SD), HUVEC-exos increased the survival rates of cardiomyocytes under H/SD conditions and inhibited myocardial fibrosis. In addition, rats with myocardial infarction were injected with ATV-MSC-exos, resulting in improved heart function, inhibited cardiomyocyte apoptosis, reduced inflammatory cell infiltration, and increased blood vessel density. The sequencing of ATV-MSC-exos demonstrated that the lncRNA *H19* was highly expressed, and the protective effect of ATV-MSC-exos on cardiomyocytes and the promotion of endothelial cell angiogenesis were eliminated after *H19* knockout. Furthermore, *MIR-675-3p*, *MIR-675-5p*, *VEGF*, and *ICAM1* were positively expressed with *H19*. These results suggest that atorvastatin increases the secretion of *H19* exosomes by rat mesenchymal cells, activates *VEGF* and *ICAM1* by regulating the expression of *MIR−675-3p* and *MIR−675-5p*, and promotes angiogenesis in the endothelium after myocardial infarction (59).

Studies have shown that HBO can promote the expression of angiogenic exosomal lncRNAs and mediate angiogenesis after myocardial infarction. For example, Shyu et al. found that HBO-induced cardiomyocyte exosomes increased the expression of *MALAT1*, decreased the expression of *MIR92A*, increased the expression of *KLF2* and *CD31*, reduced the area of myocardial infarction and inhibited heart remodeling. A luciferase activity assay verified that the target gene of *MIR92A* was *KLF2*. In an *in vitro* rat cardiomyocyte hypoxia model, an HBO intervention promoted the expression of exosomal *MALAT1* more than hypoxia stimulation. HBO induces the enrichment of exo-*MALAT1* derived from cardiomyocytes, regulates the expression of *CD31* and *KLF2* through the MIR92A/KLF2 axis, and promotes cardiac angiogenesis after myocardial infarction (45). The metastasis of angiogenic lncRNAs in exosomes is of great significance for ischemic diseases. There have been many reports in the field of cancer. We look forward to more studies concerning angiogenesis in exosomal lncRNAs. It is believed that exosomal lncRNAs could be a new target for the treatment of ischemic cardiomyopathy.

CARDIAC AGING

Cellular aging is an irreversible factor in the occurrence and development of CVD. Aging leads to excessive oxidative stress, chronic low-grade inflammation, telomere shortening, autophagy, and mitochondrial dysfunction (90–92). Aging also mediates communication between cardiomyocytes and endothelial cells, fibroblasts, and immune cells (93) and promotes vascular wall endothelial damage, atherosclerosis, myocardial fibrosis, coronary heart disease, and heart failure (94, 95). Currently, the strategies applied to delay cardiac aging include repairing mitochondrial dysfunction (96), targeting cardiac stem cell senescence and senescence-associated secretory phenotype changes (97), inducing autophagy (90), and hydrogen sulfide-mediated regulation of senescence signals (98). It has been reported that extracellular vesicles mediate cell senescence (99). Recently, Lei et al. found that the transfer of proliferating cell nuclear antigen from MSC-EVs derived from neonatal umbilical cords could reverse aging in adult BMSCs. In mice, UCMSC-EVs could delay the aging phenotype in aging mice and reduce degeneration in bones and kidneys (100).

Recent studies have shown that stem cell exosomal lncRNAs can combat myocardial aging. For example, Zhu et al. injected hUCMSC-exo-*MALAT1* into the tail veins of aging mice and found that the UCMSC-exos reversed the adverse effects of aging on cardiac function, increased the mRNA expression of the cardiac antiaging marker *TERT*, reduced the mRNA expression of the cardiac aging marker *P21* and the inflammatory factor *TNF-α*, and reduced the protein expression of p-p65 in cardiac tissue, but these antiaging effects were reversed by siMALAT1. Culturing UCMSC-exo-*MALAT1* with senescent cardiomyocytes reduced the activity of *NF-κB* and the expression levels of p-p65 and *TNF-α*, but silencing MALAT1 blocked these effects. These studies suggest that UCMSC-exos can fight cardiac aging through the *MALAT1*/*NF-κB*/*TNF-α* axis (46). Similarly, Xia showed that adipose MSC (ADMSC)-derived exosomes were enriched with *MALAT1* under hypoxic conditions. Hypoxic MSC-exos were cultured with cardiomyocytes and inhibited doxorubicin (Dox)-induced cardiomyocyte senescence. In addition, hypoxic MSCs-exos can improve myocardial cell metabolism disorders.

Database and luciferase reporter assays show that hypoxia-induced ADMSCs-exo-*MALAT1* can improve mitochondrial dysfunction in cardiomyocytes after Dox treatment by targeting *MIR-92a-3p*/*ATG4A* and combating cardiac aging (47). In addition, Zhuang et al. found that the lncRNA *NEAT1* was significantly enriched in exosomes derived from BMSCs treated with MIF. $MSCs^{MIF}$-exos can resist Dox-induced myocardial aging in mice and improve heart function. In cell experiments, $MSCs^{MIF}$-exos could also resist Dox-induced senescence in cardiomyocytes by reducing the number of cells in the G0/G1 phase, reducing the expression of the senescence genes *P27* and *P16*, reducing the percentage of SA-β-gal-positive cells, and increasing the telomere length and activity. Database and luciferase reporter assays show that $MSCs^{MIF}$-exos regulate the *MIR−221-3p*/*SIRT2* axis by transporting *NEAT1* to protect against Dox-induced cardiomyocyte senescence (52). We agree that stem cells are regarded as a breakthrough point against cell senescence, and the results of exosomal lncRNAs derived from stem cells against cardiomyocyte senescence are encouraging. Furthermore, exosomal lncRNAs provide a new perspective for the treatment of cell senescence and cell metabolic damage.

OTHER CARDIOVASCULAR DISEASES

Wang et al. found exosomal lncRNA crosstalk in chronic kidney disease (CKD) and CVD. The authors showed an increased expression of the lncRNA *ZFAS1* in the hearts of CKD mice, transfected ZFAS1 into human cardiomyocytes (HCMs) and collected exosomes, and found that *ZFAS1* was significantly enriched in HCM-derived exosomes. Injection of HCM-exos into mice significantly reduced their heart function and induced myocardial fibrosis. Similarly, HCM-exos activated the WNT/β-catenin signaling pathway in mouse cardiomyocytes after intervention *in vitro*. Silencing *ZFAS1* can inhibit fibrosis in human CFs (HCFs). Biological database and luciferase assays show that *ZFAS1* is transferred to HCFs through exosomes secreted by HCMs and induces myocardial fibrosis through the *MIR−4711-5p*/WNT/β signaling pathway (60). The communication of exosomal lncRNAs between CKD and CVD provides a reference for the study of the relationship between other systemic diseases and CVD.

Luo et al. found 105 significantly upregulated lncRNAs, 126 significantly downregulated lncRNAs, 77 significantly upregulated mRNAs, and 102 significantly downregulated mRNAs in plasma exosomes from five patients with rheumatic mitral stenosis. GO and KEGG analyses of the differentially expressed lncRNA-related genes showed that these cells are involved in magnesium homeostasis, ERBB signaling, RAS signaling, and inflammation. The KEGG pathway analysis of the upregulated mRNAs showed that they are associated with pathways associated with hypertrophic cardiomyopathy and dilated cardiomyopathy. In addition, the analysis of differentially expressed lncRNA subgroups indicated that five pairs of lncRNAs and their accessory-related genes were coexpressed simultaneously; the four downregulated pairs were RP13-820C6.2/*EP400*, RP11-339B21.15/*CERCAM*, G004800/*ZBTB7B*, XLOC_010028/*PDE3A*, and the one downregulated pair was XLOC_004201/*STOX2*. This finding highlights the potential diagnostic and therapeutic role of exosomal lncRNAs in rheumatic heart disease (65).

OUTLOOK AND SUMMARY

Current research concerning exosomes and exosomal lncRNAs is still in its infancy. First, the current methods used for the separation and purification of exosomes are different, and the production capacity is low, which is far from the standard of clinical application. It is of practical significance to upgrade the technology used for the separation and purification of exosomes. For example, Chen et al. optimized the yield and purity of exosomes by using an ultrafast separation system (EXODUS), which was innovated by ultrafiltration (101). We suggest that the separation and purification of exosomes should achieve a high a standard as possible.

Second, the organ targeting of exosomes needs to be examined. Local injection into a target organ may have improved therapeutic effects. However, intravenous injection results in unsatisfactory retention rates of exosomes in the target organ. We agree that the targeting of organs can be increased by surface modification of engineered exosomes, but the low immunogenicity and non-tumorigenicity of exosomes should be retained (102). In addition, heterogeneity is a difficult problem in the study of exosomes (103). The biological and functional mechanisms of serum exosomal lncRNAs from different CVD patients and exosomal lncRNAs secreted by different cells are different. Therefore, we suggest that the separation and purification of exosomes should be carried out under uniform and appropriate standards to the greatest extent possible. Therefore, we should search for traces of exosomes and exosomal lncRNAs in serum or tissues from more CVD patients and perform functional analyses. Furthermore, the exploration of the interaction between cells from different sources and target cells of exosomal lncRNAs should be more groundbreaking. Finally, deciphering the specific molecular mechanism of lncRNA selection and modification in exosomes may introduce new perspectives.

In addition, the relationship between lncRNAs and exosomes is intriguing. In general, exosomes act as carriers of lncRNAs to achieve cell-to-cell transfer and regulation. However, Yang et al. found that increasing the level of the lncRNA *HOTAIR* can promote the secretion of hepatocellular carcinoma exosomes (104). Similarly, Xing et al. found that the lncRNA *HAND2-AS1* can inhibit the level of exo-*MIR-106a-5p* secreted by MSCs (105). In the field of CVD, research by Li showed that the overexpression of the lncRNA *NRON* can significantly inhibit the expression of exo-*MIR23A* secreted by atrial myocytes, promote the polarization of M2 macrophages, and reduce atrial fibrosis (106). The above studies show that lncRNAs, exosomes and lncRNAs and miRNAs in exosomes are closely related and complex. Therefore, we believe that in the CVD field, more attention and action are still needed in the study of the

interaction mechanism among exosomes and exosomal lncRNAs and miRNAs.

The application and innovation of engineered exosomes may compensate for the disadvantage of exosomes produced by natural cells. Gene-enriched exosomes can be obtained through physical and chemical approaches, such as electroporation, ultrasound, and liposome-mediated membrane fusion (107). The surface modification of engineered exosomes allows exosomes to target tissues or organs and can be used to monitor the pharmacokinetics of exosomes in the body in real time to produce ideal biological effects (102). Therefore, using the advantages of engineered exosomes can provide reveries for the therapeutic effects of exosomal lncRNAs in the clinical application of real CVD patients. Of course, these applications can only be applied after solving the heterogeneity of exosomal lncRNAs and satisfying their basic conditions as drug carriers. In addition, proteomic and lipidomic studies of exosomes are potential hotspots in the study of CVD. For example, Takov et al. conducted a proteomic analysis of EVs derived from MSCs and found that migration-promoting mediators, such as PTX3, BGN, and RTN4, mediate angiogenesis after myocardial infarction (108). In summary, we believe that exosomes and exosomal lncRNAs may play an important role in the diagnosis and treatment of CVD in the future.

AUTHOR CONTRIBUTIONS

ZY wrote the manuscript, figure legends, and created the figures and tables. WH revised the manuscript. All authors contributed to the article and approved the submitted version.

FUNDING

The present study was funded by the National Natural Science Foundation of China (Grant No. 81960056).

ACKNOWLEDGMENTS

The authors thank all of the individuals who participated in the investigations.

REFERENCES

1. Roth GA, Mensah GA, Johnson CO, Addolorato G, Ammirati E, Baddour LM, et al. Global burden of cardiovascular diseases and risk factors, 1990-2019: update from the GBD 2019 study. *J Am Coll Cardiol.* (2020) 76:2982–3021. doi: 10.1016/j.jacc.2020.11.010
2. Wu Q, Bai B, Tian C, Li D, Yu H, Song B, et al. The molecular mechanisms of cardiotoxicity induced by HER2, VEGF, and tyrosine kinase inhibitors: an updated review. *Cardiovasc Drugs Therapy.* (2021). doi: 10.1007/s10557-021-07181-3. [Epub ahead of print].
3. Lee H, Zhang Z, Krause HM. Long noncoding RNAs and repetitive elements: junk or intimate evolutionary partners? *Trends Genet.* (2019) 35:892–902. doi: 10.1016/j.tig.2019.09.006
4. Palazzo AF, Koonin EV. Functional long non-coding RNAs evolve from junk transcripts. *Cell.* (2020) 183:1151–61. doi: 10.1016/j.cell.2020.09.047
5. Zhang C, Han B, Xu T, Li D. The biological function and potential mechanism of long non-coding RNAs in cardiovascular disease. *J Cell Mol Med.* (2020) 24:12900–9. doi: 10.1111/jcmm.15968
6. Lou W, Ding B, Fu P. Pseudogene-derived lncRNAs and their miRNA sponging mechanism in human cancer. *Front Cell Dev Biol.* (2020) 8:85. doi: 10.3389/fcell.2020.00085
7. Raposo G, Stoorvogel W. Extracellular vesicles: exosomes, microvesicles, and friends. *J Cell Biol.* (2013) 200:373–83. doi: 10.1083/jcb.201211138
8. Zhou R, Chen KK, Zhang J, Xiao B, Huang Z, Ju C, et al. The decade of exosomal long RNA species: an emerging cancer antagonist. *Mol Cancer.* (2018) 17:75. doi: 10.1186/s12943-018-0823-z
9. Zhang WL, Liu Y, Jiang J, Tang YJ, Tang YL, Liang XH. Extracellular vesicle long non-coding RNA-mediated crosstalk in the tumor microenvironment: tiny molecules, huge roles. *Cancer Sci.* (2020) 111:2726–35. doi: 10.1111/cas.14494
10. Statello L, Guo CJ, Chen LL, Huarte M. Gene regulation by long non-coding RNAs and its biological functions. *Nat Rev Mol Cell Biol.* (2021) 22:96–118. doi: 10.1038/s41580-020-00315-9
11. Chen LL. Linking long noncoding RNA localization and function. *Trends Biochem Sci.* (2016) 41:761–72. doi: 10.1016/j.tibs.2016.07.003
12. Xu ZM, Huang F, Huang WQ. Angiogenic lncRNAs: a potential therapeutic target for ischaemic heart disease. *Life Sci.* (2018) 211:157–71. doi: 10.1016/j.lfs.2018.09.022
13. Quinn JJ, Chang HY. Unique features of long non-coding RNA biogenesis and function. *Nat Rev Genet.* (2016) 17:47–62. doi: 10.1038/nrg.2015.10
14. Kopp F, Mendell JT. Functional classification and experimental dissection of long noncoding RNAs. *Cell.* (2018) 172:393–407. doi: 10.1016/j.cell.2018.01.011
15. Yao RW, Wang Y, Chen LL. Cellular functions of long noncoding RNAs. *Nat Cell Biol.* (2019) 21:542–51. doi: 10.1038/s41556-019-0311-8
16. Jain AK, Xi Y, McCarthy R, Allton K, Akdemir KC, Patel LR, et al. LncPRESS1 Is a p53-regulated LncRNA that safeguards pluripotency by disrupting SIRT6-mediated de-acetylation of histone H3K56. *Mol Cell.* (2016) 64:967–81. doi: 10.1016/j.molcel.2016.10.039
17. Latos PA, Pauler FM, Koerner MV, Senergin HB, Hudson QJ, Stocsits RR, et al. Airn transcriptional overlap, but not its lncRNA products, induces imprinted Igf2r silencing. *Science.* (2012) 338:1469–72. doi: 10.1126/science.1228110
18. Abels ER, Breakefield XO. Introduction to extracellular vesicles: biogenesis, RNA Cargo selection, content, release, and uptake. *Cell Mol Neurobiol.* (2016) 36:301–12. doi: 10.1007/s10571-016-0366-z
19. Teng F, Fussenegger M. Shedding light on extracellular vesicle biogenesis and bioengineering. *Adv Sci.* (2020) 8:2003505. doi: 10.1002/advs.202003505
20. D'Souza-Schorey C, Schorey JS. Regulation and mechanisms of extracellular vesicle biogenesis and secretion. *Essays Biochem.* (2018) 62:125–33. doi: 10.1042/EBC20170078
21. Stuffers S, Sem Wegner C, Stenmark H, Brech A. Multivesicular endosome biogenesis in the absence of ESCRTs. *Traffic.* (2009) 10:925–37. doi: 10.1111/j.1600-0854.2009.00920.x
22. Xu R, Rai A, Chen M, Suwakulsiri W, Greening DW, Simpson RJ. Extracellular vesicles in cancer - implications for future improvements in cancer care. *Nat Rev Clin Oncol.* (2018) 15:617–38. doi: 10.1038/s41571-018-0036-9
23. Tian C, Yang Y, Bai B, Wang S, Liu M, Sun RC, et al. Potential of exosomes as diagnostic biomarkers and therapeutic carriers for doxorubicin-induced cardiotoxicity. *Int J Biol Sci.* (2021) 17:1328–38. doi: 10.7150/ijbs.58786
24. Ghafarian F, Pashirzad M, Khazaei M, Rezayi M, Hassanian SM, Ferns GA, et al. The clinical impact of exosomes in cardiovascular disorders: from basic science to clinical application. *J Cell Physiol.* (2019) 234:12226–36. doi: 10.1002/jcp.27964
25. Lei Y, Guo W, Chen B, Chen L, Gong J, Li W. Tumor-released lncRNA H19 promotes gefitinib resistance via packaging into exosomes in non-small cell lung cancer. *Oncol Rep.* (2018) 40:3438–46. doi: 10.3892/or.2018.6762
26. Han M, Gu Y, Lu P, Li J, Cao H, Li X, et al. Exosome-mediated lncRNA AFAP1-AS1 promotes trastuzumab resistance through binding

with AUF1 and activating ERBB2 translation. *Mol Cancer.* (2020) 19:26. doi: 10.1186/s12943-020-1145-5
27. Ahadi A, Brennan S, Kennedy PJ, Hutvagner G, Tran N. Long non-coding RNAs harboring miRNA seed regions are enriched in prostate cancer exosomes. *Sci Rep.* (2016) 6:24922. doi: 10.1038/srep24922
28. Gao T, Liu X, He B, Nie Z, Zhu C, Zhang P, et al. Exosomal lncRNA 91H is associated with poor development in colorectal cancer by modifying HNRNPK expression. *Cancer Cell Int.* (2018) 18:11. doi: 10.1186/s12935-018-0506-2
29. Deng X, Ruan H, Zhang X, Xu X, Zhu Y, Peng H, et al. Long noncoding RNA CCAL transferred from fibroblasts by exosomes promotes chemoresistance of colorectal cancer cells. *Int J Cancer.* (2020) 146:1700–16. doi: 10.1002/ijc.32608
30. Fabbiano F, Corsi J, Gurrieri E, Trevisan C, Notarangelo M, D'Agostino VG. RNA packaging into extracellular vesicles: an orchestra of RNA-binding proteins? *J Extracell Vesicles.* (2020) 10:e12043. doi: 10.1002/jev2.12043
31. Qu L, Ding J, Chen C, Wu ZJ, Liu B, Gao Y, et al. Exosome-transmitted lncARSR promotes sunitinib resistance in renal cancer by acting as a competing endogenous RNA. *Cancer Cell.* (2016) 29:653–68. doi: 10.1016/j.ccell.2016.03.004
32. Zheng D, Huo M, Li B, Wang W, Piao H, Wang Y, et al. The role of exosomes and exosomal microRNA in cardiovascular disease. *Front Cell Dev Biol.* (2020) 8:616161. doi: 10.3389/fcell.2020.616161
33. Zang X, Gu J, Zhang J, Shi H, Hou S, Xu X, et al. Exosome-transmitted lncRNA UFC1 promotes non-small-cell lung cancer progression by EZH2-mediated epigenetic silencing of PTEN expression. *Cell Death Dis.* (2020) 11:215. doi: 10.1038/s41419-020-2409-0
34. Zhuo C, Yi T, Pu J, Cen X, Zhou Y, Feng S, et al. Exosomal linc-FAM138B from cancer cells alleviates hepatocellular carcinoma progression via regulating miR-765. *Aging.* (2020) 12:26236–47. doi: 10.18632/aging.202430
35. Xie Y, Dang W, Zhang S, Yue W, Yang L, Zhai X, et al. The role of exosomal noncoding RNAs in cancer. *Mol Cancer.* (2019) 18:37. doi: 10.1186/s12943-019-0984-4
36. Li Y, Yin Z, Fan J, Zhang S, Yang W. The roles of exosomal miRNAs and lncRNAs in lung diseases. *Signal Transduct Target Therapy.* (2019) 4:47. doi: 10.1038/s41392-019-0080-7
37. Wang Y, Zhao R, Shen C, Liu W, Yuan J, Li C, et al. Exosomal CircHIPK3 released from hypoxia-induced cardiomyocytes regulates cardiac angiogenesis after myocardial infarction. *Oxidat Med Cell Longevity.* (2020) 2020:8418407. doi: 10.1155/2020/8418407
38. Wang Y, Zhao R, Liu W, Wang Z, Rong J, Long X, et al. Exosomal circHIPK3 released from hypoxia-pretreated cardiomyocytes regulates oxidative damage in cardiac microvascular endothelial cells via the miR-29a/IGF-1 pathway. *Oxid Med Cell Longev.* (2019) 2019:7954657. doi: 10.1155/2019/7954657
39. Ni YQ, Lin X, Zhan JK, Liu YS. Roles and functions of exosomal non-coding RNAs in vascular aging. *Aging Dis.* (2020) 11:164–78. doi: 10.14336/AD.2019.0402
40. Chen D, Wang K, Zheng Y, Wang G, Jiang M. Exosomes-mediated LncRNA ZEB1-as1 facilitates cell injuries by mir-590-5p/ETS1 axis through the TGF-β/smad pathway in oxidized low-density lipoprotein-induced human umbilical vein endothelial cells. *J Cardiovasc Pharmacol.* (2021) 77:480–90. doi: 10.1097/FJC.0000000000000974
41. Shan K, Jiang Q, Wang XQ, Wang YN, Yang H, Yao MD, et al. Role of long non-coding RNA-RNCR3 in atherosclerosis-related vascular dysfunction. *Cell Death Dis.* (2016) 7:e2248. doi: 10.1038/cddis.2016.145
42. Li H, Zhu X, Hu L, Li Q, Ma J, Yan J. Loss of exosomal MALAT1 from ox-LDL-treated vascular endothelial cells induces maturation of dendritic cells in atherosclerosis development. *Cell Cycle (Georgetown, Tex).* (2019) 18:2255–67. doi: 10.1080/15384101.2019.1642068
43. Huang C, Han J, Wu Y, Li S, Wang Q, Lin W, et al. Exosomal MALAT1 derived from oxidized low-density lipoprotein-treated endothelial cells promotes M2 macrophage polarization. *Mol Med Rep.* (2018) 18:509–15. doi: 10.3892/mmr.2018.8982
44. Wu Q, Wang J, Tan WLW, Jiang Y, Wang S, Li Q, et al. Extracellular vesicles from human embryonic stem cell-derived cardiovascular progenitor cells promote cardiac infarct healing through reducing cardiomyocyte death and promoting angiogenesis. *Cell Death Dis.* (2020) 11:354. doi: 10.1038/s41419-020-2508-y
45. Shyu KG, Wang BW, Fang WJ, Pan CM, Lin CM. Hyperbaric oxygen-induced long non-coding RNA MALAT1 exosomes suppress MicroRNA-92a expression in a rat model of acute myocardial infarction. *J Cell Mol Med.* (2020) 24:12945–54. doi: 10.1111/jcmm.15889
46. Zhu B, Zhang L, Liang C, Liu B, Pan X, Wang Y, et al. Stem cell-derived exosomes prevent aging-induced cardiac dysfunction through a novel exosome/lncRNA MALAT1/NF-κB/TNF-α signaling pathway. *Oxid Med Cell Longev.* (2019) 2019:9739258. doi: 10.1155/2019/9739258
47. Xia W, Chen H, Xie C, Hou M. Long-noncoding RNA MALAT1 sponges microRNA-92a-3p to inhibit doxorubicin-induced cardiac senescence by targeting ATG4a. *Aging.* (2020) 12:8241–60. doi: 10.18632/aging.103136
48. Chen L, Yang W, Guo Y, Chen W, Zheng P, Zeng J, et al. Exosomal lncRNA GAS5 regulates the apoptosis of macrophages and vascular endothelial cells in atherosclerosis. *PLoS ONE.* (2017) 12:e0185406. doi: 10.1371/journal.pone.0185406
49. Song Y, Li H, Ren X, Li H, Feng C. SNHG9, delivered by adipocyte-derived exosomes, alleviates inflammation and apoptosis of endothelial cells through suppressing TRADD expression. *Eur J Pharmacol.* (2020) 872:172977. doi: 10.1016/j.ejphar.2020.172977
50. Zhang Z, Yi D, Zhou J, Zheng Y, Gao Z, Hu X, et al. Exosomal LINC01005 derived from oxidized low-density lipoprotein-treated endothelial cells regulates vascular smooth muscle cell phenotypic switch. *BioFactors.* (2020) 46:743–53. doi: 10.1002/biof.1665
51. Chen H, Xia W, Hou M. LncRNA-NEAT1 from the competing endogenous RNA network promotes cardioprotective efficacy of mesenchymal stem cell-derived exosomes induced by macrophage migration inhibitory factor via the miR-142-3p/FOXO1 signaling pathway. *Stem Cell Res Ther.* (2020) 11:31. doi: 10.1186/s13287-020-1556-7
52. Zhuang L, Xia W, Chen D, Ye Y, Hu T, Li S, et al. Exosomal LncRNA-NEAT1 derived from MIF-treated mesenchymal stem cells protected against doxorubicin-induced cardiac senescence through sponging miR-221-3p. *J Nanobiotechnol.* (2020) 18:157. doi: 10.1186/s12951-020-00716-0
53. Wang L, Zhang J. Exosomal lncRNA AK139128 derived from hypoxic cardiomyocytes promotes apoptosis and inhibits cell proliferation in cardiac fibroblasts. *Int J Nanomedicine.* (2020) 15:3363–76. doi: 10.2147/IJN.S240660
54. Mao Q, Liang XL, Zhang CL, Pang YH, Lu YX. LncRNA KLF3-AS1 in human mesenchymal stem cell-derived exosomes ameliorates pyroptosis of cardiomyocytes and myocardial infarction through miR-138-5p/Sirt1 axis. *Stem Cell Res Ther.* (2019) 10:393. doi: 10.1186/s13287-019-1522-4
55. Zhai TY, Cui BH, Zhou Y, Xu XY, Zou L, Lin X, et al. Exosomes released from CaSR-stimulated PMNs reduce ischaemia/reperfusion injury. *Oxid Med Cell Longev.* (2021) 2021:3010548. doi: 10.1155/2021/3010548
56. Diao L, Zhang Q. Transfer of lncRNA UCA1 by hUCMSCs-derived exosomes protects against hypoxia/reoxygenation injury through impairing miR-143-targeted degradation of Bcl-2. *Aging.* (2021) 13:202520. doi: 10.18632/aging.202520
57. Sun L, Zhu W, Zhao P, Wang Q, Fan B, Zhu Y, et al. Long noncoding RNA UCA1 from hypoxia-conditioned hMSC-derived exosomes: a novel molecular target for cardioprotection through miR-873-5p/XIAP axis. *Cell Death Dis.* (2020) 11:696. doi: 10.1038/s41419-020-02783-5
58. Su Q, Lv XW, Xu YL, Cai RP, Dai RX, Yang XH, et al. Exosomal LINC00174 derived from vascular endothelial cells attenuates myocardial I/R injury via p53-mediated autophagy and apoptosis. *Mol Ther Nucl Acids.* (2021) 23:1304–22. doi: 10.1016/j.omtn.2021.02.005
59. Huang P, Wang L, Li Q, Tian X, Xu J, Xu J, et al. Atorvastatin enhances the therapeutic efficacy of mesenchymal stem cells-derived exosomes in acute myocardial infarction via up-regulating long non-coding RNA H19. *Cardiovasc Res.* (2020) 116:353–67. doi: 10.1093/cvr/cvz139
60. Wang Y, Cao X, Yan L, Zheng Y, Yu J, Sun F, et al. Exosome-derived long non-coding RNA ZFAS1 controls cardiac fibrosis in chronic kidney disease. *Aging.* (2021) 13:202599. doi: 10.18632/aging.202599
61. Wang Y, Liang J, Xu J, Wang X, Zhang X, Wang W, et al. Circulating exosomes and exosomal lncRNA HIF1A-AS1 in atherosclerosis. *Int J Clin Exp Pathol.* (2017) 10:8383–8.

62. Chen Z, Yan Y, Wu J, Qi C, Liu J, Wang J. Expression level and diagnostic value of exosomal NEAT1/miR-204/MMP-9 in acute ST-segment elevation myocardial infarction. *IUBMB Life.* (2020) 72:2499–507. doi: 10.1002/iub.2376
63. Zheng ML, Liu XY, Han RJ, Yuan W, Sun K, Zhong JC, et al. Circulating exosomal long non-coding RNAs in patients with acute myocardial infarction. *J Cell Mol Med.* (2020) 24:9388–96. doi: 10.1111/jcmm.15589
64. Liang C, Zhang L, Lian X, Zhu T, Zhang Y, Gu N. Circulating exosomal SOCS2-AS1 acts as a novel biomarker in predicting the diagnosis of coronary artery disease. *Biomed Res Int.* (2020) 2020:9182091. doi: 10.1155/2020/9182091
65. Luo Y, Huang L, Luo W, Ye S, Hu Q. Genomic analysis of lncRNA and mRNA profiles in circulating exosomes of patients with rheumatic heart disease. *Biol Open.* (2019) 8:bio045633. doi: 10.1242/bio.045633
66. Hergenreider E, Heydt S, Tréguer K, Boettger T, Horrevoets AJ, Zeiher AM, et al. Atheroprotective communication between endothelial cells and smooth muscle cells through miRNAs. *Nat Cell Biol.* (2012) 14:249–56. doi: 10.1038/ncb2441
67. Bouchareychas L, Duong P, Covarrubias S, Alsop E, Phu TA, Chung A, et al. Macrophage exosomes resolve atherosclerosis by regulating hematopoiesis and inflammation via MicroRNA Cargo. *Cell Rep.* (2020) 32:107881. doi: 10.1016/j.celrep.2020.107881
68. Neeland IJ, Ross R, Després JP, Matsuzawa Y, Yamashita S, Shai I, et al. Visceral and ectopic fat, atherosclerosis, and cardiometabolic disease: a position statement. *Lancet Diabet Endocrinol.* (2019) 7:715–25. doi: 10.1016/S2213-8587(19)30084-1
69. Rocha VZ, Libby P. Obesity, inflammation, and atherosclerosis. *Nat Rev Cardiol.* (2009) 6:399–409. doi: 10.1038/nrcardio.2009.55
70. Huang K, Hu S, Cheng K. A new era of cardiac cell therapy: opportunities and challenges. *Adv Healthc Mater.* (2019) 8:e1801011. doi: 10.1002/adhm.201801011
71. Li Z, Hu S, Cheng K. Chemical engineering of cell therapy for heart diseases. *Acc Chem Res.* (2019) 52:1687–96. doi: 10.1021/acs.accounts.9b00137
72. Spannbauer A, Mester-Tonczar J, Traxler D, Kastner N, Zlabinger K, Hašimbegović E, et al. Large animal models of cell-free cardiac regeneration. *Biomolecules.* (2020) 10:1392. doi: 10.3390/biom10101392
73. Tan SJO, Floriano JF, Nicastro L, Emanueli C, Catapano F. Novel applications of mesenchymal stem cell-derived exosomes for myocardial infarction therapeutics. *Biomolecules.* (2020) 10:707. doi: 10.3390/biom10050707
74. Saludas L, Oliveira CC, Roncal C, Ruiz-Villalba A, Prósper F, Garbayo E, et al. Extracellular vesicle-based therapeutics for heart repair. *Nanomaterials (Basel, Switzerland).* (2021) 11:570. doi: 10.3390/nano11030570
75. Khan M, Nickoloff E, Abramova T, Johnson J, Verma SK, Krishnamurthy P, et al. Embryonic stem cell-derived exosomes promote endogenous repair mechanisms and enhance cardiac function following myocardial infarction. *Circ Res.* (2015) 117:52–64. doi: 10.1161/CIRCRESAHA.117.305990
76. Gallet R, Dawkins J, Valle J, Simsolo E, de Couto G, Middleton R, et al. Exosomes secreted by cardiosphere-derived cells reduce scarring, attenuate adverse remodelling, and improve function in acute and chronic porcine myocardial infarction. *Eur Heart J.* (2017) 38:201–11. doi: 10.1093/eurheartj/ehw240
77. Fröhlich GM, Meier P, White SK, Yellon DM, Hausenloy DJ. Myocardial reperfusion injury: looking beyond primary PCI. *Eur Heart J.* (2013) 34:1714–22. doi: 10.1093/eurheartj/eht090
78. Hausenloy DJ, Yellon DM. Ischaemic conditioning and reperfusion injury. *Nat Rev Cardiol.* (2016) 13:193–209. doi: 10.1038/nrcardio.2016.5
79. Hausenloy DJ, Yellon DM. Myocardial ischemia-reperfusion injury: a neglected therapeutic target. *J Clin Investigat.* (2013) 123:92–100. doi: 10.1172/JCI62874
80. Røsand Ø, Høydal MA. Cardiac exosomes in ischemic heart disease- a narrative review. *Diagnostics (Basel, Switzerland).* (2021) 11:269. doi: 10.3390/diagnostics11020269
81. Luo H, Li X, Li T, Zhao L, He J, Zha L, et al. microRNA-423-3p exosomes derived from cardiac fibroblasts mediates the cardioprotective effects of ischaemic post-conditioning. *Cardiovasc Res.* (2019) 115:1189–204. doi: 10.1093/cvr/cvy231
82. Ylä-Herttuala S, Bridges C, Katz MG, Korpisalo P. Angiogenic gene therapy in cardiovascular diseases: dream or vision? *Eur Heart J.* (2017) 38:1365–71. doi: 10.1093/eurheartj/ehw547
83. Wang Z, Su X, Ashraf M, Kim IM, Weintraub NL, Jiang M, et al. Regenerative therapy for cardiomyopathies. *J Cardiovasc Transl Res.* (2018) 11:357–65. doi: 10.1007/s12265-018-9807-z
84. Yu B, Wang S. Angio-LncRs: LncRNAs that regulate angiogenesis and vascular disease. *Theranostics.* (2018) 8:3654–75. doi: 10.7150/thno.26024
85. Johnson T, Zhao L, Manuel G, Taylor H, Liu D. Approaches to therapeutic angiogenesis for ischemic heart disease. *J Mol Med.* (2019) 97:141–51. doi: 10.1007/s00109-018-1729-3
86. Kesidou D, da Costa Martins PA, de Windt LJ, Brittan M, Beqqali A, Baker AH. Extracellular vesicle miRNAs in the promotion of cardiac neovascularisation. *Front Physiol.* (2020) 11:579892. doi: 10.3389/fphys.2020.579892
87. Witman N, Zhou C, Grote Beverborg N, Sahara M, Chien KR. Cardiac progenitors and paracrine mediators in cardiogenesis and heart regeneration. *Semin Cell Dev Biol.* (2020) 100:29–51. doi: 10.1016/j.semcdb.2019.10.011
88. Moghiman T, Barghchi B, Esmaeili SA, Shabestari MM, Tabaee SS, Momtazi-Borojeni AA. Therapeutic angiogenesis with exosomal microRNAs: an effectual approach for the treatment of myocardial ischemia. *Heart Failure Rev.* (2020) 26:205–13. doi: 10.1007/s10741-020-10001-9
89. Ma T, Chen Y, Chen Y, Meng Q, Sun J, Shao L, et al. MicroRNA-132, delivered by mesenchymal stem cell-derived exosomes, promote angiogenesis in myocardial infarction. *Stem Cells Int.* (2018) 2018:3290372. doi: 10.1155/2018/3290372
90. Miyamoto S. Autophagy and cardiac aging. *Cell Death Differ.* (2019) 26:653–64. doi: 10.1038/s41418-019-0286-9
91. Liang WJ, Gustafsson Å B. The aging heart: mitophagy at the center of rejuvenation. *Front Cardiovasc Med.* (2020) 7:18. doi: 10.3389/fcvm.2020.00018
92. Quan Y, Xin Y, Tian G, Zhou J, Liu X. Mitochondrial ROS-modulated mtDNA: a potential target for cardiac aging. *Oxidat Med Cell Longev.* (2020) 2020:9423593. doi: 10.1155/2020/9423593
93. Tang X, Li PH, Chen HZ. Cardiomyocyte senescence and cellular communications within myocardial microenvironments. *Front Endocrinol.* (2020) 11:280. doi: 10.3389/fendo.2020.00280
94. Triposkiadis F, Xanthopoulos A, Butler J. Cardiovascular aging and heart failure: JACC review topic of the week. *J Am Coll Cardiol.* (2019) 74:804–13. doi: 10.1016/j.jacc.2019.06.053
95. Dong M, Yang Z, Fang H, Xiang J, Xu C, Zhou Y, et al. Aging attenuates cardiac contractility and affects therapeutic consequences for myocardial infarction. *Aging Dis.* (2020) 11:365–76. doi: 10.14336/AD.2019.0522
96. Yeh CH, Chou YJ, Kao CH, Tsai TF. Mitochondria and calcium homeostasis: Cisd2 as a big player in cardiac ageing. *Int J Mol Sci.* (2020) 21:9238. doi: 10.3390/ijms21239238
97. Cianflone E, Torella M, Biamonte F, De Angelis A, Urbanek K, Costanzo FS, et al. Targeting cardiac stem cell senescence to treat cardiac aging and disease. *Cells.* (2020) 9:1558. doi: 10.3390/cells9061558
98. Testai L, Citi V, Martelli A, Brogi S, Calderone V. Role of hydrogen sulfide in cardiovascular ageing. *Pharmacol Res.* (2020) 160:105125. doi: 10.1016/j.phrs.2020.105125
99. Urbanelli L, Buratta S, Sagini K, Tancini B, Emiliani C. Extracellular vesicles as new players in cellular senescence. *Int J Mol Sci.* (2016) 17:1408. doi: 10.3390/ijms17091408
100. Lei Q, Gao F, Liu T, Ren W, Chen L, Cao Y, et al. Extracellular vesicles deposit PCNA to rejuvenate aged bone marrow-derived mesenchymal stem cells and slow age-related degeneration. *Sci Transl Med.* (2021) 13:aaz8697. doi: 10.1126/scitranslmed.aaz8697
101. Chen Y, Zhu Q, Cheng L, Wang Y, Li M, Yang Q, et al. Exosome detection via the ultrafast-isolation system: EXODUS. *Nat Methods.* (2021) 18:212–8. doi: 10.1038/s41592-020-01034-x
102. Peng H, Ji W, Zhao R, Yang J, Lu Z, Li Y, et al. Exosome: a significant nano-scale drug delivery carrier. *J Mater Chem B.* (2020) 8:7591–608. doi: 10.1039/D0TB01499K

103. Zhang Y, Bi J, Huang J, Tang Y, Du S, Li P. Exosome: a review of its classification, isolation techniques, storage, diagnostic and targeted therapy applications. *Int J Nanomed.* (2020) 15:6917–34. doi: 10.2147/IJN.S264498
104. Yang L, Peng X, Li Y, Zhang X, Ma Y, Wu C, et al. Long non-coding RNA HOTAIR promotes exosome secretion by regulating RAB35 and SNAP23 in hepatocellular carcinoma. *Mol Cancer.* (2019) 18:78. doi: 10.1186/s12943-019-0990-6
105. Xing L, Tang X, Wu K, Huang X, Yi Y, Huan J. LncRNA HAND2-AS1 suppressed the growth of triple negative breast cancer via reducing secretion of MSCs derived exosomal miR-106a-5p. *Aging.* (2020) 13:424–36. doi: 10.18632/aging.202148
106. Li J, Zhang Q, Jiao H. LncRNA NRON promotes M2 macrophage polarization and alleviates atrial fibrosis through suppressing exosomal miR-23a derived from atrial myocytes. *J Formos Med Assoc.* (2020) 120:1512–9. doi: 10.1016/j.jfma.2020.11.004
107. Wu P, Zhang B, Ocansey DKW, Xu W, Qian H. Extracellular vesicles: a bright star of nanomedicine. *Biomaterials.* (2021) 269:120467. doi: 10.1016/j.biomaterials.2020.120467
108. Takov K, He Z, Johnston HE, Timms JF, Guillot PV, Yellon DM, et al. Small extracellular vesicles secreted from human amniotic fluid mesenchymal stromal cells possess cardioprotective and promigratory potential. *Basic Res Cardiol.* (2020) 115:26. doi: 10.1007/s00395-020-0785-3

Conflict of Interest: The authors declare that the research was conducted in the absence of any commercial or financial relationships that could be construed as a potential conflict of interest.

frontiers in Cardiovascular Medicine

REVIEW
published: 28 July 2021
doi: 10.3389/fcvm.2021.712828

The Role of Exosomes and Their Cargos in the Mechanism, Diagnosis, and Treatment of Atrial Fibrillation

Shengyuan Huang[1], Yating Deng[2], Jiaqi Xu[3], Jiachen Liu[2], Liming Liu[1] and Chengming Fan[1]**

[1] Department of Cardiovascular Surgery, The Second Xiangya Hospital, Central South University, Changsha, China, [2] Xiangya Medical College of Central South University, Changsha, China, [3] Department of Spine Surgery and Orthopaedics, Xiangya Hospital, Central South University, Changsha, China

Atrial fibrillation (AF) is the most common persistent arrhythmia, but the mechanism of AF has not been fully elucidated, and existing approaches to diagnosis and treatment face limitations. Recently, exosomes have attracted considerable interest in AF research due to their high stability, specificity and cell-targeting ability. The aim of this review is to summarize recent literature, analyze the advantages and limitations of exosomes, and to provide new ideas for their use in understanding the mechanism and improving the diagnosis and treatment of AF.

Keywords: non-coding RNA, exosomes, atrial fibrillation, biomarkers, mechanism, treatment

OPEN ACCESS

Edited by:
Junjie Yang,
University of Alabama at Birmingham, United States

Reviewed by:
Teng Ma,
Tongji University, China
Wei Lei,
Soochow University, China
Jiacheng Sun,
University of Alabama at Birmingham, United States

***Correspondence:**
Liming Liu
liulimingjia@csu.edu.cn
Chengming Fan
fanchengming@csu.edu.cn

Specialty section:
This article was submitted to Cardiovascular Biologics and Regenerative Medicine, a section of the journal Frontiers in Cardiovascular Medicine

Received: *21 May 2021*
Accepted: *07 July 2021*
Published: *28 July 2021*

Citation:
Huang S, Deng Y, Xu J, Liu J, Liu L and Fan C (2021) The Role of Exosomes and Their Cargos in the Mechanism, Diagnosis, and Treatment of Atrial Fibrillation. Front. Cardiovasc. Med. 8:712828. doi: 10.3389/fcvm.2021.712828

INTRODUCTION

Atrial fibrillation (AF) is the most common persistent arrhythmia. In the United States, 2.3 million people have AF, and this number is expected to increase to 5.6 million by 2050 (1). AF greatly increases the risk of stroke, with a more than five-fold excess of stroke in subjects with AF (2), and contemporary studies have shown that 20–30% of patients with ischemic stroke had been diagnosed with AF (3). AF is also one of the main causes of heart failure, sudden death, and other cardiovascular diseases (3). After adjusting for preexisting cardiovascular conditions, AF increases all-cause mortality by a factor of two (4).

AF is widespread and harmful, but current diagnostic methods are not very efficient. Twelve lead electrocardiography is currently the gold standard for diagnosis, but due to its short recording time window, paroxysmal atrial fibrillation goes undetected in many patients (5). To address this limitation, ambulatory electrocardiographic recording devices were developed (6), but they are uncomfortable for patients during recording, and even the extended recording time may be insufficient (5). Therefore, it would be helpful to develop alternative convenient and efficient diagnostic tools.

Currently, scholars believe that AF occurs when atrial tissue undergoes structural and/or electrophysiological remodeling, which can promote formation and propagation of abnormal electrical pulses (7). Atrial abnormalities can occur *via* several mechanisms, such as renin angiotensin aldosterone system (RAAS) activation, cardiac fibrosis, decreased action duration potential, and others (8). The variety of mechanisms and pathways involved in atrial fibrillation contribute to its mechanism not yet being fully understood.

As the understanding of AF has improved, many treatments have emerged, including antiarrhythmic drugs (AADs), biologicals, catheter ablation, and the COX-maze procedure (9). However, most currently available treatments have major limitations. For example, AADs can

cause malignant ventricular arrhythmia and lung and hepatic damage. Catheter ablation requires a long operation, while the result is not ideal (rhythm control is achieved in only 57–80% of cases), and long-term complications often result (9, 10). Although the COX-maze procedure yields a higher rate of postoperative freedom from AF (90% after 1 year), it is mainly suitable for symptomatic patients undergoing other cardiac surgical procedures (11). Therefore, further research on treatments for atrial fibrillation is warranted.

As mentioned above, AF is associated with a high risk of stroke, and the mechanism, diagnosis and treatment of AF require further study. Currently, exosomes and non-coding RNAs (ncRNAs) are areas of active cardiovascular research. What new perspectives and ideas will exosomes and ncRNAs bring to AF? We review recent research on ncRNAs and exosomes in AF, and provide suggestions for further research and clinical applications.

A BRIEF INTRODUCTION OF EXOSOMES AND THEIR CARGOS

Exosomes

Exosomes are extracellular vesicles that originate from endosomes and have diameters ranging from 40 to 160 nm. At the time of their discovery, exosomes were regarded as a kind of "cell junk." Researchers believed that the role of exosomes was mainly to remove excess components in cells to maintain cell homeostasis (12). It later became clear that they have a role in intercellular communication and disease progression (13). Researchers believe that exosomes might constitute an ideal treatment because they can target specific cells and regulate complex pathways. In addition, exosomes have been detected in various body fluids (14), indicating that they have the potential to become biomarkers of multiple diseases.

The formation of exosomes begins with invagination of the plasma membrane. This process produces early sorting endosomes (ESEs). After cargos are transferred to and from other membranous structures, ESEs become late sorting endosomes (LSEs), whose secondary invagination forms intraluminal vesicles (ILVs). After processing and modification, ILVs become exosomes that carry a variety of cargos, including proteins, amino acids, lipids, DNA, RNA, and metabolites (15). LSEs transform into multivesicular bodies (MVBs) that dock on the plasma membrane and release the enclosed exosomes to the extracellular space (**Figure 1A**).

Research on cargos has concentrated on RNA, and here we focus on ncRNAs.

Non-coding RNAs in Exosomes

Non-coding RNAs (ncRNAs) are RNA molecules that are not translated, but rather participate in post-transcriptional regulation of microRNAs (miRNAs), piwi-interacting RNAs, long non-coding RNAs (lncRNAs), circular RNAs (circRNAs), and endogenous small interfering RNAs, among others. Due to their extensive and complex regulatory effects, ncRNAs are involved in a variety of diseases, and have gradually become key molecules for diagnosis and treatment (16).

MicroRNAs

MicroRNAs are members of a family of small ncRNAs with a length of 18–23 bases, which are highly conserved among species (17). Although miRNAs do not code for proteins, they play important roles in inhibiting or promoting mRNA degradation to regulate gene expression (18). The occurrence and maturation of miRNAs are regulated by a variety of cellular factors, and their biosynthesis involves transcription and cleavage of primary miRNAs (pri-miRNAs) by the microprocessor complex to form precursor miRNAs (pre-miRNAs) (19). Pre-miRNAs are then transported into the cytoplasm and further processed by DICER or co-factors, including the trans-activation response RNA-binding protein (TRBP) or the protein activator of protein kinase R (PACT) (20). Mature miRNAs in the cytoplasm are then transported to the RNA-induced silencing complex (RISC), which can bind to the Argonaute (AGO) protein and ultimately guide the complex to the target mRNA (21) (**Figure 1B**). According to the principle of base complementarity, miRNAs directly regulate the stability of mRNA to affect cell behavior.

Circular RNAs

Circular RNAs are a unique class of ncRNAs. In contrast to linear RNAs, circRNAs have a closed ring structure without a 5′-end cap and 3′-end polyadenosine tail structure (22). This structure promotes cyclization of exons and/or introns to each other, potentially protecting them from degradation and providing a half-life of about 48 h (23). The circRNA sequences are highly conserved and have distinctive histological and temporal characteristics (24), participating in the regulation of transcriptional and post-transcriptional gene expression (25). CircRNAs can act as miRNA sponges, thereby reducing the inhibitory effect of miRNA and increasing expression of specific target genes (26) (**Figure 1C**).

Long Non-coding RNAs

Long non-coding RNAs are a kind of ncRNA with a length of more than 200 base pairs. Unlike mRNA (**Figure 1D**), many lncRNAs are processed incompletely and retained in the nucleus (27), while others are spliced efficiently and transported to the cytoplasm. In the cytoplasm, lncRNAs can interact with different types of RBPs and ribosomes. In addition, lncRNAs are usually sorted into mitochondria or other organelles, including exosomes (**Figure 1E**). The lncRNAs function primarily in three ways. First, they can bind transcription factors and the promoter region of target genes, which upregulates their transcription. Second, they can act like miRNA to downregulate mRNA. Third, they can target other post-transcriptional regulators such as miRNAs. The lncRNAs can act as miRNA sponges to affect mRNA levels and thus regulate gene expression (28). A more detailed description can be found in the article by Statello et al. (27). In addition to transcriptional or post-transcriptional regulation, lncRNAs also have roles in epigenetics, cellular stability, etc.

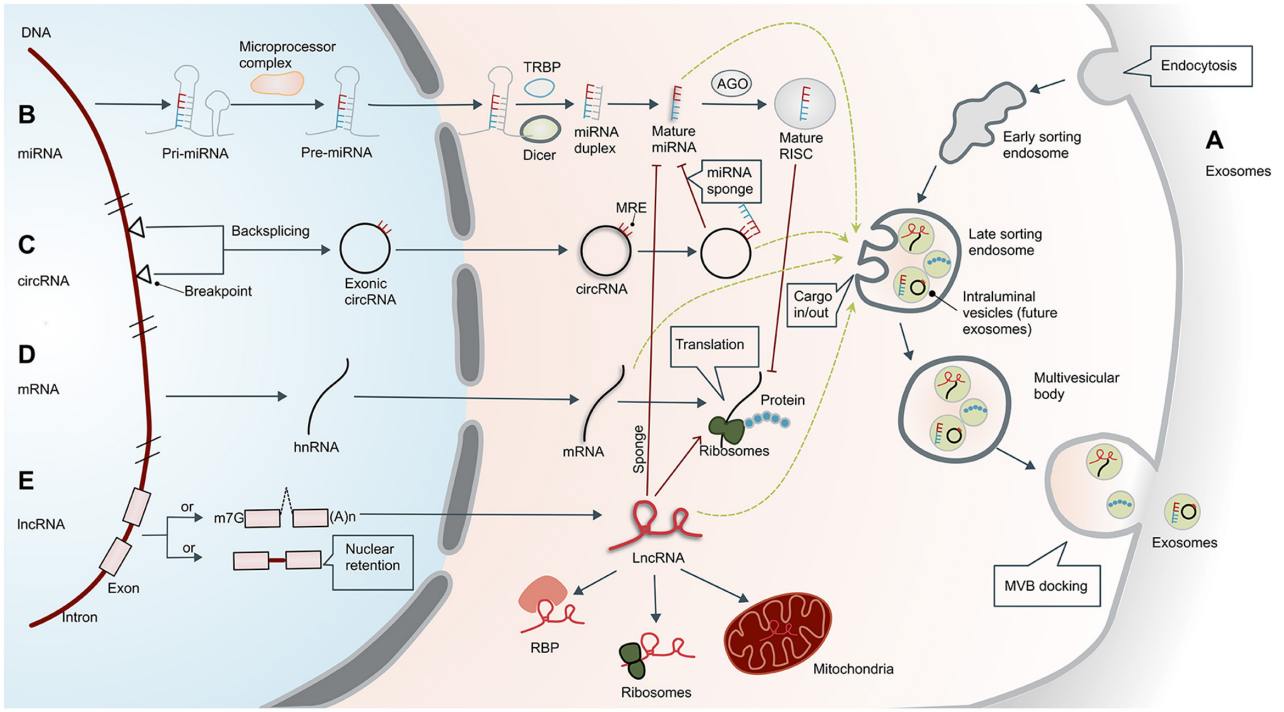

FIGURE 1 | Biogenesis of exosomes and non-coding RNAs. **(A)** Biogenesis of exosomes. Formation of exosomes begins with invagination of the plasma membrane. This process produces early sorting endosomes (ESEs) with cargos of what had been extracellular material. After cargos are transferred to and from other membranous structures, ESEs become late sorting endosomes (LSEs), whose secondary invagination forms intraluminal vesicles (ILVs—the future exosomes) that give rise to multivesicular bodies (MVBs). Finally, MVBs are transferred to and dock on the plasma membrane, resulting in release of the exosomes. The exosomes usually contain mRNA, proteins, and non-coding RNAs (ncRNAs), including microRNAs (miRNAs), circular RNAs (circRNAs), and long non-coding RNAs (lncRNAs). **(B)** Biogenesis and functional mechanism of microRNAs. Primary miRNAs (pri-miRNAs) are transcribed and cleaved by the microprocessor complex to form precursor miRNAs (pre-miRNAs). Pre-miRNAs are then transported into the cytoplasm and further processed by DICER or co-factors, including the trans-activation response RNA-binding protein (TRBP). Mature miRNAs in the cytoplasm are transported to the RNA-induced silencing complex (RISC), which can bind to the Argonaute (AGO) protein and ultimately guide the complex to the target mRNA. **(C)** Biogenesis of circular RNAs. Exonic circRNAs are formed by backsplicing the transcription products between two breakpoints on DNA. CircRNAs have a closed ring structure without a 5′-end cap and a 3′-end polyadenosine tail structure. In the cytoplasm, circRNAs can act as ceRNAs by sponging miRNAs with miRNA response elements (MREs), thereby reducing the inhibitory effect of the miRNAs. **(D)** Biogenesis of mRNAs. Translation of mRNA is the key regulatory target of ncRNA, which is separate from the regulatory effect of lncRNAs and miRNAs. The mRNAs can also enter exosomes. **(E)** Biogenesis of long non-coding RNAs. Unlike mRNA, many lncRNAs are processed incompletely and remain in the nucleus, while others are spliced efficiently and transported to the cytoplasm. In the cytoplasm, lncRNAs can interact with different types of RNA-binding proteins (RBPs) and ribosomes. In addition, lncRNAs are usually sorted into mitochondria or other organelles, including exosomes. They perform post-transcriptional functions by promoting/suppressing mRNA stability or sponging miRNA as competing endogenous RNAs (ceRNAs). m7G, 7-methyl guanosine 5′ cap; (A)n, poly(A) 3′ tail.

CLINICAL POTENTIAL OF EXOSOMES AND THEIR CARGOS

The Potential of Exosomes

Researchers have extensively studied the role of exosomes in cardiovascular disease. Zeng et al. revealed that increased circulating levels of the exosomal lncRNAs ENST00000556899.1 and ENST00000575985.1 can be a potential biomarker for acute myocardial infarction (29). The study by Zhu et al. (30) showed that exosomes can also release the lncRNA MALAT1, which prevents aging-induced cardiac dysfunction by inhibiting the NF-κB/TNF-α signaling pathway. Zhou et al. (31) reviewed the role of circulating exosomes, and nine types of exosomal MiRNAs were suggested to be useful for the diagnosis and prognosis of heart failure.

The Potential of MicroRNAs

Currently, only a small number of miRNAs have been identified. Analysis of miRNA sites in the genome showed that miRNAs play an important role in several physiological processes, including blood cell differentiation, homeobox gene regulation, neuronal polarity, insulin secretion, brain morphogenesis, and cardiogenesis (32, 33). Recent studies have identified ∼50 miRNAs associated with essential hypertension, and more than 30 miRNAs associated with heart failure and myocardial infarction, many of which might serve as useful biomarkers (34–36). Some miRNAs, such as miR-29b, miR-323-5p, miR-455, and miR466, regulate expression of matrix metalloproteinase-9 in diabetic heart tissue and promote proliferation of endothelial cells (ECs) and formation of capillary-like structures, which could protect oxygen-damaged cardiomyocytes (37). Ong et al. (38)

found that miR-27b-3p could target Wnt3A to regulate Wnt/β-catenin signaling in experiments using a rat model, thereby attenuating atrial fibrosis. These studies suggest that miRNA may play an important role in AF.

The Potential of Circular RNAs

Recent studies have indicated that circRNAs are widely involved in cardiovascular disease. Huang et al. (39) showed that the absence of the Super-Enhancer-Regulated circRNA Nfix in a mouse model of myocardial ischemia promotes regeneration and repair of myocardial cells. Li et al. (40) showed that circRNA_000203 enhances Gata4 gene expression by down-regulating miR-26b-5p and miR-140-3p, thereby exacerbating cardiac hypertrophy. Other studies have also shown that circRNAs also play an important regulatory role in myocardial fibrosis and vascular regeneration (41, 42).

The Potential of Long Non-coding RNAs

Long non-coding RNAs are widely involved in cardiovascular disease. Studies have shown that inhibition of AK088388 can increase the level of miR-30a and reduce the levels of mRNA and protein of the autophagy markers Beclin-1 and LC3-II, thus significantly reducing autophagy and cardiomyocyte damage (43). Fan et al. used microarray analysis to evaluate the variability of lncRNA in mouse aortic endothelial cells carrying vulnerable plaques, and found that the expression pattern of lncRNA UC.98 was closely related to the vulnerability of atherosclerotic plaques (44). Tao et al. found that expression of miR-21 can be down-regulated when expression of growth specific blocking factor 5 (GAS5) lncRNA is elevated, and miR-21, which promotes the progression of cardiac fibrosis, is overexpressed in cardiac fibrotic tissue and activated cardiac fibroblasts (45).

The Advantages of Exosomes and Their Cargos for Clinical Use

The use ncRNAs, such as miRNAs, in clinical practice may encounter several problems. First, in the search for biomarkers for diagnosing AF, there have been inconsistencies between different studies (**Table 1**). An explanation for these inconsistencies may be that the RNAs in the circulating blood come from different tissues or cells, and other components in the blood may also affect the results. In addition, expression of miRNA is related to the heterogeneity of the population of patients with AF (50). Second, as a treatment method, miRNAs also have problems with delivery efficiency and off-target effects. Because they can target a variety of organs and tissues, miRNA mimics used for treatment may not be accurately delivered to the intended tissues (51). Thus, delivery efficiency is relatively low and may cause side effects.

However, loading ncRNA into exosomes provides several advantages for diagnosis and treatment:

(1) Abnormal cells and diseased tissues tend to produce more exosomes because of changes in cytoplasmic physiology (52). So exosomes are often from abnormal tissues, better reflecting the disease state.
(2) Compared with ncRNAs in biological fluids, the contents of exosomes are more stable and therefore more useful as clinical biomarkers.
(3) The ncRNAs in exosomes are naturally enriched, facilitating detection.
(4) Exosomes are a natural mechanism of cellular communication and molecular transportation, and deliver materials with high efficiency. This feature makes them very attractive for pharmaceutical applications.
(5) Their biophysical properties make it easy to extract exosomes and manipulate their protein and RNA cargoes (53).
(6) Exosomes are composed of multiple components, which means that they have greater potential to perform complex functions, such as modifying protein or lipid components to reduce adverse reactions (15) (**Figure 2**).

All these characteristics make exosomes more effective than free ncRNAs in the diagnosis and treatment of AF.

DIAGNOSTIC AND THERAPEUTIC ROLE OF EXOSOMES IN ATRIAL FIBRILLATION

Exosomes in the Diagnosis of Atrial Fibrillation

Since 2019, there have been attempts to identify links between exosomes and AF that might improve its diagnosis and prognosis, and most studies have focused on miRNAs in exosomes. Wang et al. compared differences in circulating exosomes between AF patients and control groups, and analyzed three differentially expressed miRNA components, miR-483-5p, miR-142-5p, miR-223-3p, and miR-223-5p. Among them, miR-483-5p was independently related to AF, revealing that exosomes have great potential for diagnosing AF (54). The studies of Wei et al. and Liu et al. are similar. The former study showed that expression of miR-92b-3p, miR-1306-5p and miR-let-7b-3p are different in patients with AF compared to those with normal sinus rhythm (55), while the latter identified miR-382-3p as a differentially expressed miRNA (56). The study of Mun et al. attempted to identify specific biomarkers for persistent AF. They identified four kinds of miRNA in exosomes (miRNA-103a,−107,−320d,−486, and let-7b) found in patients with persistent AF but not in those with paroxysmal AF or in control patients (50).

There have also been studies trying to use other components in exosomes for diagnosis of AF, such as mitochondrial DNA (mtDNA) and protein. Soltész et al. searched for differentially expressed mtDNA in exosomes of AF patients. However, in addition to finding that mtDNA levels were different in exosomes, peripheral blood and cell-free plasma, there was no obvious difference between AF patients and healthy controls, indicating that mtDNA is not suitable for use as a biomarker for AF (57). Ni et al. believed that the protein in exosomes had not been fully studied, so they analyzed the difference in protein content in exosomes between AF patients and controls. Their results showed that the difference between the proteins in exosomes of AF patients and the control group was mainly reflected in protein folding, which caused the protein content of

TABLE 1 | miRNAs as biomarkers for the diagnosis of AF patients.

miRNAs	Tissue	Changes in AF	Characteristics	References
miRNA-150	Plasma	Reduced	OR 1.96, 95% CI 1.5–3.57, P < 0.001	Liu et al. (46)
miRNA-29b	Plasma/Atrial	Reduced	Plasma concentrations were decreased by 53.8% in patients with AF (P = 0.007); tissue-expression was decreased by 54%	Dawson et al. (47)
miR-328	Plasma	Increased	OR 1.21, 59%CI 1.09–1.33, P < 0.001	McManus et al. (48)
miR-99a-5p,−192-5p,−214-3p, and−342-5p	Plasma	Increased	The area under the curves (AUCs) were 0.67, 0.73, 0.78, and 0.79, and the Youden's indices were 0.38, 0.44, 0.50, and 0.50, respectively.	Natsume et al. (49)

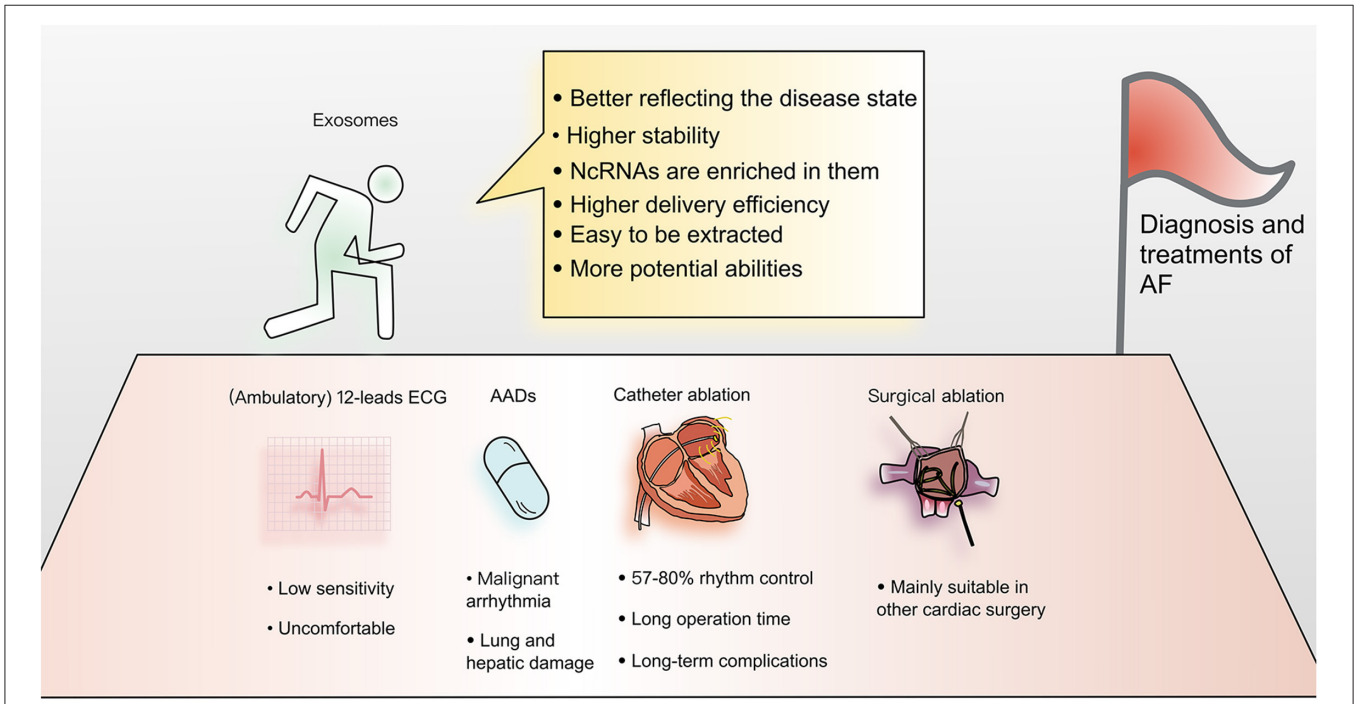

FIGURE 2 | Advantages of applying exosomes to the diagnosis and treatment of atrial fibrillation. Current diagnosis and treatment methods for AF have many limitations. Exosomes have become a focus of cardiovascular research. Due to their many advantages, exosomes are thought to have the potential to overcome current limitations and provide new methods for understanding the mechanism and improving the diagnosis and treatment of AF.

exosomes from AF patients to be less due to protein misfolding or unfolding (58).

Exosomes in the Pathogenic Mechanism of Atrial Fibrillation

Many studies have clarified the mechanism by which exosomes are involved in the development of AF. Recently, Shaihov-Teper et al. discovered that epicardial fat (eFat) could facilitate AF, and extracellular vesicles were one of the important mechanisms. They extracted and cultured eFat from patients with AF, then collected extracellular vesicles in the culture medium, and found that these vesicles had proinflammatory, profibrotic, and proarrhythmic effects, which ultimately promoted the formation of AF (59). Similarly, the study by Li et al. tried to reveal the mechanism by which myofibroblasts (MFBs) promote the progression of AF. They found that exosomes secreted by MFBs can act on cardiomyocytes (CMs) and cause the latter to down-regulate the expression of the L-type calcium channel Cav1.2, which is a typical AF-associated ionic remodeling marker. Further studies have shown the miR-21-3p in exosomes may be the inhibitory molecule responsible for this down-regulation (60). In addition, it has been observed that the lncRNA NRON (ncRNA repressor of the nuclear factor of activated T cells) can promote polarization of M2 macrophages to reduce atrial fibrosis, and a study by Li et al. showed that exosomes are involved in this process. The exosomes secreted by CMs stimulated by NRON can promote polarization of M2 macrophages and reduce expression of fibrosis markers in cardiac fibroblasts (61).

Exosomes in the Treatment of Atrial Fibrillation

Although there has been no research on the application of exosomes to the treatment of AF patients, there have been studies

that demonstrated a role for exosomes in the treatment of AF in mice. The miR-320d in cardiomyocytes with AF is down-regulated, which leads to increased apoptosis and decreased cell viability. Liu et al. tried to use exosomes from adipose tissue-derived mesenchymal stem cells to deliver miR-320d mimics to cardiomyocytes, and showed that the above process was reversed. These results support exosomes as an effective drug delivery system (62).

NON-CODING RNAs IN ATRIAL FIBRILLATION

To the best of our knowledge, there are currently only 10 articles that directly relate exosomes with AF (discussed in the previous section). Although many ncRNAs have been successfully used to better study the mechanism and aid in the diagnosis and treatment of AF, they were not reported in exosomes in those studies. Therefore, in order to guide future research, we summarize the ncRNAs that have been studied in the context of AF but not yet reported in exosomes.

MicroRNAs

MicroRNA in the Diagnosis of Atrial Fibrillation

The following miRNAs have been shown to appear in exosomes and contribute to the diagnosis of AF: miR-483-5p, miR-142-5p, miR-223-3p, miR-223-5p, miR-92b-3p, miR-1306-5p and miR-let-7b-3p, miR-382-3p, miRNA-103a,−107,−320d,−486, and let-7b (50, 54–56).

In addition, many circulating miRNAs have been shown to be associated with AF, which may guide future exosome research. McManus et al. showed miR-21 and miR-150 in the plasma of AF patients were lower than those in patients with sinus rhythm. And interestingly, the level was lower in the plasma of patients with paroxysmal AF than in those with persistent AF, which means they can not only be a biomarker for AF, but potentially distinguish AF subtypes (63).

As biomarkers, miRNAs were also found to have the potential to evaluate AF in more complex situations. Zhou et al. (64) showed that miR-21 is related to the prognosis of patients with AF after radio-frequency ablation, helping to guide physicians in choosing whether to perform that procedure. And considering miR-29s along with age and amino-terminal procollagen III peptide (PIIINP) helps to predict whether the patient will develop AF after receiving a coronary artery bypass graft (CABG) (65). Goren et al. demonstrated that the circulating level of miR-150 is reduced in patients with AF and systolic heart failure (66).

A means of distinguishing embolic from thrombotic stroke is provided by identification of miRNAs. As we know, patients with AF have a higher probability of stroke, but whether the stroke was caused by AF or atherosclerosis affects clinical decisions, and distinguishing between the two remains a challenge (67). Chen et al. (68) identified miR-15a-5p, miR-17-5p, miR-19b-3p, and miR-20a-5p as biomarkers useful for making this distinction.

MicroRNAs in the Mechanism of Atrial Fibrillation

The miR-21-3p in exosomes has been shown to be related to the mechanism of AF (60). And many other miRNAs have been reported to be associated with AF. As mentioned above, AF-related myocardial remodeling can be divided into structural remodeling and electrical remodeling. The earliest research connecting miRNA to myocardial fibrosis can be traced back to van Rooij et al. (69) and Thum et al. (70) in 2008. van Rooij et al. (69) demonstrated that up-regulated miR-29 in fibroblasts can reduce expression of collagen, fibrin, and elastin, thereby reducing the level of fibrosis; Thum et al. (70) found that the level of miR-21 in fibroblasts was selectively increased in heart failure, and miR-21 enhanced ERK-MAP kinase activity by inhibiting (Spry1), thereby enhancing myocardial fibrosis. In the following decade, more and more studies focused on atrial fibrosis and miRNA-21 (71–73). In addition, the pro-fibrotic response of canine atria to nicotine was dependent on down-regulation of miR-133 and miR-590 (74); miR-132 can target connective tissue growth factor in cardiac fibroblasts to regulate fibrosis (75).

In addition to structural remodeling, miRNAs have also been shown to be related to electrical remodeling. Zhao et al. (76) found that miR-29 not only participated in myocardial fibrosis, but was also related to decreased $I_{ca,L}$ density by reducing expression of Ca^{2+} channel subunits. Binas et al. also found that miR-221 and miR-222 participate in cardiac electrical remodeling by regulating expression of L-type Ca^{2+} channel subunits and potassium channel subunits (77).

MicroRNAs in the Treatment of Atrial Fibrillation

As mentioned above, miR-320d in exosomes has been shown to decrease apoptosis and increase cell viability in AF, suggesting it could be used for treatment (62).

Some studies have experimented with using miRNA to directly treat AF in animal models. MiR-1 was shown to exacerbate arrhythmia when upregulated in rat hearts, which could be relieved by an antisense inhibitor. Further research revealed that associated mechanisms involve down-regulation of the K^+ channel subunit Kir2.1 and connexin 43 (78). Other studies have also shown that miRNA can be used to prevent and treat AF in rat, mouse, and canine models (79–81). However, current research remains limited to animal experiments. Safety issues such as off-target effects must be resolved before conducting human trials (82).

Circular RNAs

Although no studies have yet shown that circRNA in exosomes contributes to the mechanism or is useful for the diagnosis and treatment of AF, many have shown circRNA may have such potential. We expect to see more research on circRNA in exosomes in the future.

Circular RNAs in the Diagnosis of Atrial Fibrillation

Shangguan et al. first reported the expression profile of circRNAs in atrial tissues of dogs with AF using high-throughput sequencing. Differentially expressed circRNAs were identified and annotated as being involved in "cytoskeleton structure composition and ion channel activity" (83), laying the foundation for research in this field.

CircRNAs are likely to become more stable and reliable biomarkers for the diagnosis of AF since in contrast to linear

RNAs with a 5′ cap and 3′ tail at either end, circRNAs are characterized by a covalent closed loop structure, which may be more stable and conserved (84). In an analysis of human peripheral blood, Ruan et al. (85) identified 5 up-regulated and 11 down-regulated circRNAs and described a molecular regulatory network. Subsequent studies revealed the expression profile and target genes of circRNAs in atrial myocytes of patients with AF. By use of competing endogenous RNA (ceRNA) network analysis, Jiang et al. (86) showed that the circRNAs hsa_circ_0000075 and hsa_circ_0082096 may be involved in the pathogenesis of AF *via* the transforming growth factor (TGF)-beta signaling pathway. Hu et al. (87) identified five circRNAs with significantly large differences (ch9:15474007-15490122, chr16:75445723-75448593, hsa_circ_0007256, chr12:56563313-56563992, and hsa_circ_0003533) and speculated that they are related to inflammation associated with AF. Zhang et al. (88) first reported differences in the expression profiles of circRNAs in the left and right atrial appendages of patients with AF. Liu et al. (89) discovered two key miRNA+circRNA regulatory pathways that may be associated with the mechanisms of AF: hsa-circRNA-100053-hsa-miR-455-5p-TRPV1 and hsa-circRNA-005843-hsa-miR-188-5p-SPON. Wu et al. (90) constructed lncRNA-miRNA-mRNA and circRNA-miRNA-mRNA networks, which enriched the AF molecular network.

The expression profiles of patients with AF and other diseases have also been extensively studied. Zhang et al. (73) showed that plasma Hsa_circRNA_025016 can be used to predict the occurrence of AF after off-pump CABG (91); Hu et al. (92) discussed the expression characteristics of circRNA in patients with rheumatic heart disease and AF. Zhu et al. (93) reported the expression profile of circRNAs related to valvular heart disease and persistent AF.

Circular RNAs in the Mechanism of Atrial Fibrillation

It has been reported that circRNAs are involved in the mechanism of AF progression. Gao et al. suggested that circRNAs play an important role in the progression of AF, and identified hsa_circ_0004104 as promoting cardiac fibrosis by targeting the MAPK and TGF-β pathways, and as such is a potential regulator and biomarker of persistent AF (94). Costa et al. demonstrated that an important feature of the progression of paroxysmal to permanent AF is an increase in the expression of circRNAs that can adsorb specific miRNAs, which reduces expression of these post-transcriptional regulatory factors. The targeted miRNA molecules included hsa-miR-181d-5p, hsa- miR-3180-3p, hsa-miR-6868-3p, and hsa-miR-2277-5p (95).

Long Non-coding RNAs

Among the lncRNAs in exosomes, only the lncRNA NRON has been reported to be involved in AF (61), but many lncRNAs have been extensively studied, and these lncRNAs may become a focus of future research on exosomes. Babapoor-Farrokhran et al. reviewed the role of lncRNAs in AF described in articles published prior to 2020 (96). They concluded that lncRNAs play a variety of roles in the development of AF, including up-regulating or down-regulating atrial structural remodeling, down-regulating electrical remodeling, up-regulating the renin angiotensin system, and reducing abnormalities in calcium handling. However, research in this area is very active and many new studies have emerged since publication of their review.

Long Non-coding RNAs in the Diagnosis of Atrial Fibrillation

Studies have shown that lncRNAs can also be used as a biomarker of AF for diagnostic and prognostic evaluation. Shi et al. demonstrated that expression of lncRNA GAS5 was down-regulated in AF patients, which occurred before enlargement of the left atrium, indicating that it can be used as an early biomarker of AF. In addition, they also showed that patients with reduced expression of GAS5 have a higher probability of AF recurring after radio-frequency catheter ablation (97). To be able to predict the risk of stroke in AF patients, Zeng et al. monitored AF patients and compared the levels of the lncRNA ANRIL (antisense non-coding RNA in the INK4 locus) in the stroke group and a non-stroke group. The results showed that higher lncRNA ANRIL levels often correlate with a greater risk of stroke (98).

Long Non-coding RNAs in the Mechanism of Atrial Fibrillation

lncRNAs participate in cardiac structural remodeling and electrical remodeling. It has been shown that lncRNA HOTAIR, NRON, LICPAR and MIAT can participate in structural remodeling (61, 99–101). For example, consider the lncRNA HOTAIR, where previous studies demonstrated that miR-613 can target GJA1 to regulate the expression of Cx43, and HOTAIR can sponge miR-613. Consequently Dai et al. speculated that HOTAIR could act as a ceRNA to regulate Cx43 expression in AF by sponging miR-613. They collected atrial tissue from patients with valvular heart disease and cultured HL-1, a mouse atrial cell line, and using RT-PCR, western blot and luciferase activity assays, found that the suppressive effect of miR-613 on Cx43 expression was attenuated by HOTAIR. Their study identified a novel HOTAIR/miR-613/Cx43 axis in the regulation of AF, which has the potential to be a therapeutic target (99).

In addition, lncRNA can participate in the electrical remodeling. Du et al. found that expression of the lncRNA TCONS-00106987 was significantly higher in AF rabbit models compared with non-AF rabbit models. Then they infected the rabbits with lentiviruses that mediated over-expression of TCONS-00106987 and found that they were more prone to AF. Further research confirmed that TCONS-00106987 promoted electrical remodeling *via* sponging miR-26 to increase expression of the gene KCNJ2, thereby increasing inward-rectifier K^+ current (102). The lncRNAs and their functional mechanisms summarized in the **Table 2**.

EXOSOME-MIMETIC NANOVESICLES AND ENGINEERED NANOPARTICLES

However, there are still obstacles to the clinical application of exosomes in AF. First, isolation of exosomes with high yield, reproductivity and purity is challenging (103). Second, we also lack efficient methods of loading drugs into the exosomes. Third,

TABLE 2 | The lncRNAs and their functional mechanisms on AF.

Model	LncRNA	Effect of AF	Targets and mechanisms	References
Human/Mice	HOTAIR	Alleviates	Regulates Cx43 remolding by sponging miR-613.	(99)
Mice	NRON	Alleviates	Promotes M2 macrophage polarization and alleviates atrial fibrosis through suppressing exosomal miR-23a.	(61)
Human	LICPAR	Aggravate	Modulates TGF-β/Smad pathway.	(100)
Human/Rat	MIAT	Aggravate	MIAT downregulation alleviates AF and AF-induced myocardial fibrosis through targeting miR-133a-3p.	(101)
Rabbit	TCONS-00106987	Aggravate	Promotes atrial electrical remodeling by sponging miR-26 to regulate KCNJ2.	(102)

although numerous reports have shown that exosomes can be used as biomarkers for AF, the results from different studies are often inconsistent. One explanation may lie in the different conditions of patients in the different studies, and another may be methodological differences in exosome purification (104). The potential solution may be to more precisely define experimental conditions and to combine multiple components as biomarkers in exosomes to manage exosome heterogeneity among patients. To successfully use exosomes for drug delivery, the problem of their low yield must be solved. For this reason, generation of exosome-mimetic vesicles or engineered nanoparticles with a substantially greater yield has attracted recent attention.

Exosome-Mimetic Nanovesicles

Jang et al. (105) developed a method to load chemotherapeutics into bioinspired exosome-mimetic nanovesicles for delivery to tumor tissue. Monocytes or macrophages were forced to pass sequentially through filters of diminishing pore size, which caused the cells to break up and release chemotherapeutics-loaded nanovesicles. Surprisingly, these nanovesicles possessed characteristics of exosomes, such as targeting ability, and they were also shown to have anti-tumor properties. More importantly, this method increased the yield by 100-fold compared with exosomes, suggesting that these bioengineered nanovesicles can effectively deliver chemotherapeutics to treat malignant tumors. Similarly, Yoon et al. (106) generated nanovesicles by slicing living cell membranes with microfabricated 500 nm-thick silicon nitride blades, and successfully delivered exogenous substances to recipient cells. These results suggest that exosome-mimetic nanovesicles can deliver drugs on a large scale.

Engineered Nanoparticles

Recently, engineered nanoparticles, such as fluorescent nanodiamonds, magnetic iron oxide nanoparticles, and silica nanoparticles, have attracted enormous attention due to their great potential for applications in medicine (107–109). Compared with natural vesicles, these artificially synthesized particles are more stable and easier to synthesize *in vitro*. In addition, nanoparticles have many useful characteristics, including optical and electromagnetic properties, lacking in natural vesicles (110). Researchers can also adjust the properties of nanoparticles by changing their size (110). For example, particles smaller than 12 nm can pass through the blood-brain barrier, and they can be endocytosed by cells when <30 nm. Shape and surface charge can alter particle affinity for specific organs and tissues (111). As a result, there is much research interest in the application of engineered nanoparticles to the diagnosis and treatment of disease. For example, multifunctional magnetic iron oxide nanoparticles are applied to magnetic hyperthermia treatment and photothermal therapy of tumors (112). Although there are few studies on the application of nanoparticles to AF, we can envision nanoparticles being used as contrast agents for imaging lesions in the cardiovascular system and as carriers for drug delivery. However, since nanoparticles are artificially synthesized, it will be necessary to carefully explore their toxicity and other potential adverse effects before being used in the clinic (113).

CONCLUSION

Exosomes provide a new perspective on AF. With greater stability, higher enrichment, and most importantly, greater targeting ability than non-specific drugs, exosomes are potentially useful diagnostic biomarkers and delivery vehicles for treating AF. Nevertheless, in order to make them useful in clinical practice, several limitations should be overcome. First, there are few existing studies of exosomes in the context of AF, but there are many studies of ncRNAs. Future research on exosomes should focus on ncRNA molecules that have been associated with AF. Second, we lack effective methods for extracting and purifying exosomes, resulting in low exosome yield. To solve this problem, we need, on the one hand, to optimize existing extraction technology, while on the other hand, to take advantage of artificial drug delivery systems such as exosome-mimetic nanovesicles and engineered nanoparticles. In summary, if we carry out detailed research on exosomes,

conduct larger clinical trials, and increase yields, exosome-based diagnosis and therapy could greatly improve current management of patients with AF.

AUTHOR CONTRIBUTIONS

SH wrote the manuscript. SH, YD, and JX carried out the data collection and/or assembly of data and data analysis. JL and LL carried out data analysis and interpretation, and contributed to manuscript revisions. CF was responsible for conception and design of the study and contributed to manuscript revisions. All authors read and approved the final manuscript.

FUNDING

This work was supported by the National Key Research and Development Program (No. 2018YFC1311204 to LL).

REFERENCES

1. Kannel WB, Benjamin EJ. Current perceptions of the epidemiology of atrial fibrillation. *Cardiol Clin.* (2009) 27:13–24, vii. doi: 10.1016/j.ccl.2008.09.015
2. Wolf PA, Abbott RD, Kannel WB. Atrial fibrillation as an independent risk factor for stroke: the Framingham Study. *Stroke.* (1991) 22:983–8. doi: 10.1161/01.STR.22.8.983
3. Kirchhof P, Benussi S, Kotecha D, Ahlsson A, Atar D, Casadei B, et al. 2016 ESC Guidelines for the management of atrial fibrillation developed in collaboration with EACTS. *Eur Heart J.* (2016) 37:2893–962. doi: 10.15829/1560-4071-2017-7-7-86
4. Benjamin EJ, Wolf PA, D'Agostino RB, Silbershatz H, Kannel WB, Levy D. Impact of atrial fibrillation on the risk of death: the Framingham Heart Study. *Circulation.* (1998) 98:946–52. doi: 10.1161/01.CIR.98.10.946
5. Zungsontiporn N, Link MS. Newer technologies for detection of atrial fibrillation. *Bmj.* (2018) 363:k3946. doi: 10.1136/bmj.k3946
6. Mittal S, Movsowitz C, Steinberg JS. Ambulatory external electrocardiographic monitoring: focus on atrial fibrillation. *J Am Coll Cardiol.* (2011) 58:1741–9. doi: 10.1016/j.jacc.2011.07.026
7. January CT, Wann LS, Alpert JS, Calkins H, Cigarroa JE, Cleveland JC, et al. 2014 AHA/ACC/HRS guideline for the management of patients with atrial fibrillation. *J Am Coll Cardiol.* (2014) 64:E1–E76. doi: 10.1016/j.jacc.2014.03.021
8. Wijesurendra RS, Casadei B. Mechanisms of atrial fibrillation. *Heart.* (2019) 105:1860–7. doi: 10.1136/heartjnl-2018-314267
9. Woods CE, Olgin J. Atrial fibrillation therapy now and in the future: drugs, biologicals, and ablation. *Circ Res.* (2014) 114:1532–46. doi: 10.1161/CIRCRESAHA.114.302362
10. Toeg HD, Al-Atassi T, Lam BK. Atrial fibrillation therapies: lest we forget surgery. *Can J Cardiol.* (2014) 30:590–7. doi: 10.1016/j.cjca.2014.02.001
11. Ruaengsri C, Schill MR, Khiabani AJ, Schuessler RB, Melby SJ, Damiano RJJr. The Cox-maze IV procedure in its second decade: still the gold standard? *Eur J Cardiothorac Surg.* (2018) 53:i19–i25. doi: 10.1093/ejcts/ezx326
12. Mills J, Capece M, Cocucci E, Tessari A, Palmieri D. Cancer-derived extracellular vesicle-associated microRNAs in intercellular communication: one cell's trash is another cell's treasure. *Int J Mol Sci.* (2019) 20:6109. doi: 10.3390/ijms20246109
13. Zhou R, Chen KK, Zhang J, Xiao B, Huang Z, Ju C, et al. The decade of exosomal long RNA species: an emerging cancer antagonist. *Mol Cancer.* (2018) 17:75. doi: 10.1186/s12943-018-0823-z
14. Zhu L, Sun HT, Wang S, Huang SL, Zheng Y, Wang CQ, et al. Isolation and characterization of exosomes for cancer research. *J Hematol Oncol.* (2020) 13:152. doi: 10.1186/s13045-020-00987-y
15. Kalluri R, LeBleu VS. The biology function and biomedical applications of exosomes. *Science.* (2020) 367:eaau6977. doi: 10.1126/science.aau6977
16. Esteller M. Non-coding RNAs in human disease. *Nat Rev Genet.* (2011) 12:861–74. doi: 10.1038/nrg3074
17. Song R, Hu XQ, Zhang L. Mitochondrial MiRNA in cardiovascular function and disease. *Cells.* (2019) 8:1475. doi: 10.3390/cells8121475
18. Barwari T, Joshi A, Mayr M. MicroRNAs in cardiovascular disease. *J Am Coll Cardiol.* (2016) 68:2577–84. doi: 10.1016/j.jacc.2016.09.945
19. Correia de Sousa M, Gjorgjieva M, Dolicka D, Sobolewski C, Foti M. Deciphering miRNAs' action through miRNA editing. *Int J Mol Sci.* (2019) 20:6249. doi: 10.3390/ijms20246249
20. Lee HY, Zhou K, Smith AM, Noland CL, Doudna JA. Differential roles of human Dicer-binding proteins TRBP and PACT in small RNA processing. *Nucleic Acids Res.* (2013) 41:6568–76. doi: 10.1093/nar/gkt361
21. van den Berg A, Mols J, Han J. RISC-target interaction: cleavage and translational suppression. *Biochim Biophys Acta.* (2008) 1779:668–77. doi: 10.1016/j.bbagrm.2008.07.005
22. Wilusz JE, Sharp PA. Molecular biology. A circuitous route to noncoding RNA. *Science.* (2013) 340:440–1. doi: 10.1126/science.1238522
23. Altesha MA, Ni T, Khan A, Liu K, Zheng X. Circular RNA in cardiovascular disease. *J Cell Physiol.* (2019) 234:5588–600. doi: 10.1002/jcp.27384
24. Conn SJ, Pillman KA, Toubia J, Conn VM, Salmanidis M, Phillips CA, et al. The RNA binding protein quaking regulates formation of circRNAs. *Cell.* (2015) 160:1125–34. doi: 10.1016/j.cell.2015.02.014
25. Wang Y, Lu T, Wang Q, Liu J, Jiao W. Circular RNAs: crucial regulators in the human body (Review). *Oncol Rep.* (2018) 40:3119–35. doi: 10.3892/or.2018.6733
26. Tay Y, Rinn J, Pandolfi PP. The multilayered complexity of ceRNA crosstalk and competition. *Nature.* (2014) 505:344–52. doi: 10.1038/nature12986
27. Statello L, Guo CJ, Chen LL, Huarte M. Gene regulation by long non-coding RNAs and its biological functions. *Nat Rev Mol Cell Biol.* (2021) 22:96–118. doi: 10.1038/s41580-020-00315-9
28. Furió-Tarí P, Tarazona S, Gabaldón T, Enright AJ, Conesa A. spongeScan: a web for detecting microRNA binding elements in lncRNA sequences. *Nucleic Acids Res.* (2016) 44:W176–W80. doi: 10.1093/nar/gkw443
29. Zheng ML, Liu XY, Han RJ, Yuan W, Sun K, Zhong JC, et al. Circulating exosomal long non-coding RNAs in patients with acute myocardial infarction. *J Cell Mol Med.* (2020) 24:9388–96. doi: 10.1111/jcmm.15589
30. Zhu B, Zhang L, Liang C, Liu B, Pan X, Wang Y, et al. Stem cell-derived exosomes prevent aging-induced cardiac dysfunction through a novel exosome/lncRNA MALAT1/NF-κB/TNF-α signaling pathway. *Oxid Med Cell Longev.* (2019) 2019:9739258. doi: 10.1155/2019/9739258
31. Zhou R, Wang L, Zhao G, Chen D, Song X, Momtazi-Borojeni AA, et al. Circulating exosomal microRNAs as emerging non-invasive clinical biomarkers in heart failure: mega bio-roles of a nano bio-particle. *IUBMB Life.* (2020) 72:2546–62. doi: 10.1002/iub.2396
32. Iorio MV, Croce CM. MicroRNA dysregulation in cancer: diagnostics, monitoring and therapeutics. A comprehensive review. *EMBO Mol Med.* (2012) 4:143–59. doi: 10.1002/emmm.201100209
33. Wojciechowska A, Braniewska A, Kozar-Kamińska K. MicroRNA in cardiovascular biology and disease. *Adv Clin Exp Med.* (2017) 26:865–74. doi: 10.17219/acem/62915
34. Jusic A, Devaux Y. Noncoding RNAs in hypertension. *Hypertension.* (2019) 74:477–92. doi: 10.1161/HYPERTENSIONAHA.119.13412
35. Li X, Wei Y, Wang Z. microRNA-21 and hypertension. *Hypertens Res.* (2018) 41:649–61. doi: 10.1038/s41440-018-0071-z
36. Poller W, Dimmeler S, Heymans S, Zeller T, Haas J, Karakas M, et al. Non-coding RNAs in cardiovascular diseases: diagnostic and therapeutic perspectives. *Eur Heart J.* (2018) 39:2704–16. doi: 10.1093/eurheartj/ehx165

37. Chaturvedi P, Kalani A, Medina I, Familtseva A, Tyagi SC. Cardiosome mediated regulation of MMP9 in diabetic heart: role of mir29b and mir455 in exercise. *J Cell Mol Med.* (2015) 19:2153–61. doi: 10.1111/jcmm.12589
38. Ong SG, Lee WH, Huang M, Dey D, Kodo K, Sanchez-Freire V, et al. Cross talk of combined gene and cell therapy in ischemic heart disease: role of exosomal microRNA transfer. *Circulation.* (2014) 130:S60–S9. doi: 10.1161/CIRCULATIONAHA.113.007917
39. Huang S, Li X, Zheng H, Si X, Li B, Wei G, et al. Loss of super-enhancer-regulated circRNA Nfix induces cardiac regeneration after myocardial infarction in adult mice. *Circulation.* (2019) 139:2857–76. doi: 10.1161/CIRCULATIONAHA.118.038361
40. Li H, Xu J-D, Fang X-H, Zhu J-N, Yang J, Pan R, et al. Circular RNA circRNA_000203 aggravates cardiac hypertrophy *via* suppressing miR-26b-5p and miR-140-3p binding to Gata4. *Cardiovasc Res.* (2020) 116:1323–34. doi: 10.1093/cvr/cvz215
41. Gu X, Jiang YN, Wang WJ, Zhang J, Shang DS, Sun CB, et al. Comprehensive circRNA expression profile and construction of circRNA-related ceRNA network in cardiac fibrosis. *Biomed Pharmacother.* (2020) 125:109944. doi: 10.1016/j.biopha.2020.109944
42. Liu Y, Yang Y, Wang Z, Fu X, Chu XM, Li Y, et al. Insights into the regulatory role of circRNA in angiogenesis and clinical implications. *Atherosclerosis.* (2020) 298:14–26. doi: 10.1016/j.atherosclerosis.2020.02.017
43. Wang JJ, Bie ZD, Sun CF. Long noncoding RNA AK088388 regulates autophagy through miR-30a to affect cardiomyocyte injury. *J Cell Biochem.* (2019) 120:10155–63. doi: 10.1002/jcb.28300
44. Fan Z, Zhang Y, Xiao D, Ma J, Liu H, Shen L, et al. Long noncoding RNA UC.98 stabilizes atherosclerotic plaques by promoting the proliferation and adhesive capacity in murine aortic endothelial cells. *Acta Biochim Biophys Sin (Shanghai).* (2020) 52:141–9. doi: 10.1093/abbs/gmz155
45. Tao H, Zhang JG, Qin RH, Dai C, Shi P, Yang JJ, et al. LncRNA GAS5 controls cardiac fibroblast activation and fibrosis by targeting miR-21 *via* PTEN/MMP-2 signaling pathway. *Toxicology.* (2017) 386:11–8. doi: 10.1016/j.tox.2017.05.007
46. Liu Z, Zhou C, Liu Y, Wang S, Ye P, Miao X, et al. The expression levels of plasma micoRNAs in atrial fibrillation patients. *PLoS ONE.* (2012) 7:e44906. doi: 10.1371/journal.pone.0044906
47. Dawson K, Wakili R, Ordög B, Clauss S, Chen Y, Iwasaki Y, et al. MicroRNA29: a mechanistic contributor and potential biomarker in atrial fibrillation. *Circulation.* (2013) 127:1466–75. doi: 10.1161/CIRCULATIONAHA.112.001207
48. McManus DD, Lin H, Tanriverdi K, Quercio M, Yin X, Larson MG, et al. Relations between circulating microRNAs and atrial fibrillation: data from the Framingham Offspring Study. *Heart Rhythm.* (2014) 11:663–9. doi: 10.1016/j.hrthm.2014.01.018
49. Natsume Y, Oaku K, Takahashi K, Nakamura W, Oono A, Hamada S, et al. Combined analysis of human and experimental murine samples identified novel circulating MicroRNAs as biomarkers for atrial fibrillation. *Circ J.* (2018) 82:965–73. doi: 10.1253/circj.CJ-17-1194
50. Mun D, Kim H, Kang JY, Park H, Park H, Lee SH, et al. Expression of miRNAs in circulating exosomes derived from patients with persistent atrial fibrillation. *FASEB J.* (2019) 33:5979–89. doi: 10.1096/fj.201801758R
51. Xu X, Zhao Z, Li G. The therapeutic potential of microRNAs in atrial fibrillation. *Mediators Inflamm.* (2020) 2020:3053520. doi: 10.1155/2020/3053520
52. Melo SA, Luecke LB, Kahlert C, Fernandez AF, Gammon ST, Kaye J, et al. Glypican-1 identifies cancer exosomes and detects early pancreatic cancer. *Nature.* (2015) 523:177–82. doi: 10.1038/nature14581
53. El-Andaloussi S, Lee Y, Lakhal-Littleton S, Li J, Seow Y, Gardiner C, et al. Exosome-mediated delivery of siRNA *in vitro* and *in vivo*. *Nat Protoc.* (2012) 7:2112–26. doi: 10.1038/nprot.2012.131
54. Wang S, Min J, Yu Y, Yin L, Wang Q, Shen H, et al. Differentially expressed miRNAs in circulating exosomes between atrial fibrillation and sinus rhythm. *J Thorac Dis.* (2019) 11:4337–48. doi: 10.21037/jtd.2019.09.50
55. Wei Z, Bing Z, Shaohuan Q, Yanran W, Shuo S, Bi T, et al. Expression of miRNAs in plasma exosomes derived from patients with atrial fibrillation. *Clin Cardiol.* (2020) 43:1450–9. doi: 10.1002/clc.23461
56. Liu L, Chen Y, Shu J, Tang CE, Jiang Y, Luo F. Identification of microRNAs enriched in exosomes in human pericardial fluid of patients with atrial fibrillation based on bioinformatic analysis. *J Thorac Dis.* (2020) 12:5617–27. doi: 10.21037/jtd-20-2066
57. Soltész B, Urbancsek R, Pös O, Hajas O, Forgács IN, Szilágyi E, et al. Quantification of peripheral whole blood, cell-free plasma and exosome encapsulated mitochondrial DNA copy numbers in patients with atrial fibrillation. *J Biotechnol.* (2019) 299:66–71. doi: 10.1016/j.jbiotec.2019.04.018
58. Ni H, Pan W, Jin Q, Xie Y, Zhang N, Chen K, et al. Label-free proteomic analysis of serum exosomes from paroxysmal atrial fibrillation patients. *Clin Proteomics.* (2021) 18:1. doi: 10.1186/s12014-020-09304-8
59. Shaihov-Teper O, Ram E, Ballan N, Brzezinski RY, Naftali-Shani N, Masoud R, et al. Extracellular vesicles from epicardial fat facilitate atrial fibrillation. *Circulation.* (2021) 143:2475–93. doi: 10.1161/CIRCULATIONAHA.120.052009
60. Li S, Gao Y, Liu Y, Li J, Yang X, Hu R, et al. Myofibroblast-derived exosomes contribute to development of a susceptible substrate for atrial fibrillation. *Cardiology.* (2020) 145:324–32. doi: 10.1159/000505641
61. Li J, Zhang Q, Jiao H. LncRNA NRON promotes M2 macrophage polarization and alleviates atrial fibrosis through suppressing exosomal miR-23a derived from atrial myocytes. *J Formos Med Assoc.* (2020) 120:1512–9. doi: 10.1016/j.jfma.2020.11.004
62. Liu L, Zhang H, Mao H, Li X, Hu Y. Exosomal miR-320d derived from adipose tissue-derived MSCs inhibits apoptosis in cardiomyocytes with atrial fibrillation (AF). *Artif Cells Nanomed Biotechnol.* (2019) 47:3976–84. doi: 10.1080/21691401.2019.1671432
63. McManus DD, Tanriverdi K, Lin H, Esa N, Kinno M, Mandapati D, et al. Plasma microRNAs are associated with atrial fibrillation and change after catheter ablation (the miRhythm study). *Heart Rhythm.* (2015) 12:3–10. doi: 10.1016/j.hrthm.2014.09.050
64. Zhou Q, Maleck C, von Ungern-Sternberg SNI, Neupane B, Heinzmann D, Marquardt J, et al. Circulating microRNA-21 correlates with left atrial low-voltage areas and is associated with procedure outcome in patients undergoing atrial fibrillation ablation. *Circ Arrhythm Electrophysiol.* (2018) 11:e006242. doi: 10.1161/CIRCEP.118.006242
65. Rizvi F, Mirza M, Olet S, Albrecht M, Edwards S, Emelyanova L, et al. Noninvasive biomarker-based risk stratification for development of new onset atrial fibrillation after coronary artery bypass surgery. *Int J Cardiol.* (2020) 307:55–62. doi: 10.1016/j.ijcard.2019.12.067
66. Goren Y, Meiri E, Hogan C, Mitchell H, Lebanony D, Salman N, et al. Relation of reduced expression of MiR-150 in platelets to atrial fibrillation in patients with chronic systolic heart failure. *Am J Cardiol.* (2014) 113:976–81. doi: 10.1016/j.amjcard.2013.11.060
67. Tuttolomondo A, Pecoraro R, Di Raimondo D, Arnao V, Clemente G, Della Corte V, et al. Stroke subtypes and their possible implication in stroke prevention drug strategies. *Curr Vasc Pharmacol.* (2013) 11:824–37. doi: 10.2174/15701611106140128113705
68. Chen LT, Jiang CY. MicroRNA expression profiles identify biomarker for differentiating the embolic stroke from thrombotic stroke. *Biomed Res Int.* (2018) 2018:4514178. doi: 10.1155/2018/4514178
69. van Rooij E, Sutherland LB, Thatcher JE, DiMaio JM, Naseem RH, Marshall WS, et al. Dysregulation of microRNAs after myocardial infarction reveals a role of miR-29 in cardiac fibrosis. *Proc Natl Acad Sci U S A.* (2008) 105:13027–32. doi: 10.1073/pnas.0805038105
70. Thum T, Gross C, Fiedler J, Fischer T, Kissler S, Bussen M, et al. MicroRNA-21 contributes to myocardial disease by stimulating MAP kinase signalling in fibroblasts. *Nature.* (2008) 456:980–4. doi: 10.1038/nature07511
71. Adam O, Lohfelm B, Thum T, Gupta SK, Puhl SL, Schafers HJ, et al. Role of miR-21 in the pathogenesis of atrial fibrosis. *Basic Res Cardiol.* (2012) 107:278. doi: 10.1007/s00395-012-0278-0
72. Cao W, Shi P, Ge JJ. miR-21 enhances cardiac fibrotic remodeling and fibroblast proliferation *via* CADM1/STAT3 pathway. *BMC Cardiovasc Disord.* (2017) 17:88. doi: 10.1186/s12872-017-0520-7

73. Zhang K, Zhao L, Ma Z, Wang W, Li X, Zhang Y, et al. Doxycycline attenuates atrial remodeling by interfering with microRNA-21 and downstream phosphatase and tensin homolog (PTEN)/phosphoinositide 3-kinase (PI3K) signaling pathway. *Med Sci Monit.* (2018) 24:5580–7. doi: 10.12659/MSM.909800
74. Shan H, Zhang Y, Lu Y, Zhang Y, Pan Z, Cai B, et al. Downregulation of miR-133 and miR-590 contributes to nicotine-induced atrial remodelling in canines. *Cardiovasc Res.* (2009) 83:465–72. doi: 10.1093/cvr/cvp130
75. Qiao G, Xia D, Cheng Z, Zhang G. miR132 in atrial fibrillation directly targets connective tissue growth factor. *Mol Med Rep.* (2017) 16:4143–50. doi: 10.3892/mmr.2017.7045
76. Zhao Y, Yuan Y, Qiu C. Underexpression of CACNA1C caused by overexpression of microRNA-29a underlies the pathogenesis of atrial fibrillation. *Med Sci Monit.* (2016) 22:2175–81. doi: 10.12659/MSM.896191
77. Binas S, Knyrim M, Hupfeld J, Kloeckner U, Rabe S, Mildenberger S, et al. miR-221 and−222 target CACNA1C and KCNJ5 leading to altered cardiac ion channel expression and current density. *Cell Mol Life Sci.* (2020) 77:903–18. doi: 10.1007/s00018-019-03217-y
78. Yang B, Lin H, Xiao J, Lu Y, Luo X, Li B, et al. The muscle-specific microRNA miR-1 regulates cardiac arrhythmogenic potential by targeting GJA1 and KCNJ2. *Nat Med.* (2007) 13:486–91. doi: 10.1038/nm1569
79. Cheng WL, Kao YH, Chao TF, Lin YK, Chen SA, Chen YJ. MicroRNA-133 suppresses ZFHX3-dependent atrial remodelling and arrhythmia. *Acta Physiol (Oxf).* (2019) 227:e13322. doi: 10.1111/apha.13322
80. Li PF, He RH, Shi SB, Li R, Wang QT, Rao GT, et al. Modulation of miR-10a-mediated TGF-beta1/Smads signaling affects atrial fibrillation-induced cardiac fibrosis and cardiac fibroblast proliferation. *Biosci Rep.* (2019) 39:BSR20181931. doi: 10.1042/BSR20181931
81. Zhang Y, Zheng S, Geng Y, Xue J, Wang Z, Xie X, et al. MicroRNA profiling of atrial fibrillation in canines: miR-206 modulates intrinsic cardiac autonomic nerve remodeling by regulating SOD1. *PLoS One.* (2015) 10:e0122674. doi: 10.1371/journal.pone.0122674
82. van Rooij E, Olson EN. MicroRNA therapeutics for cardiovascular disease: opportunities and obstacles. *Nat Rev Drug Discov.* (2012) 11:860–72. doi: 10.1038/nrd3864
83. Shangguan W, Liang X, Shi W, Liu T, Wang M, Li G. Identification and characterization of circular RNAs in rapid atrial pacing dog atrial tissue. *Biochem Biophys Res Commun.* (2018) 506:1–6. doi: 10.1016/j.bbrc.2018.05.082
84. E S, Costa MC, Kurc S, Drozdz A, Cortez-Dias N, Enguita FJ. The circulating non-coding RNA landscape for biomarker research: lessons and prospects from cardiovascular diseases. *Acta Pharmacol Sin.* (2018) 39:1085–99. doi: 10.1038/aps.2018.35
85. Ruan ZB, Wang F, Yu QP, Chen GC, Zhu L. Integrative analysis of the circRNA-miRNA regulatory network in atrial fibrillation. *Sci Rep.* (2020) 10:20451. doi: 10.1038/s41598-020-77485-1
86. Zhang PP, Sun J, Li W. Genome-wide profiling reveals atrial fibrillation-related circular RNAs in atrial appendages. *Gene.* (2020) 728:144286. doi: 10.1016/j.gene.2019.144286
87. Hu X, Chen L, Wu S, Xu K, Jiang W, Qin M, et al. Integrative analysis reveals key circular RNA in atrial fibrillation. *Front Genet.* (2019) 10:108. doi: 10.3389/fgene.2019.00108
88. Zhang Y, Ke X, Liu J, Ma X, Liu Y, Liang D, et al. Characterization of circRNA associated ceRNA networks in patients with nonvalvular persistent atrial fibrillation. *Mol Med Rep.* (2019) 19:638–50. doi: 10.3892/mmr.2018.9695
89. Liu T, Zhang G, Wang Y, Rao M, Zhang Y, Guo A, et al. Identification of circular RNA-microRNA-messenger RNA regulatory network in atrial fibrillation by integrated analysis. *Biomed Res Int.* (2020) 2020:8037273. doi: 10.1155/2020/8037273
90. Wu N, Li J, Chen X, Xiang Y, Wu L, Li C, et al. Identification of long non-coding RNA and circular RNA expression profiles in atrial fibrillation. *Heart Lung Circ.* (2020) 29:e157–67. doi: 10.1016/j.hlc.2019.10.018
91. Zhang J, Xu Y, Xu S, Liu Y, Yu L, Li Z, et al. Plasma circular RNAs, Hsa_circRNA_025016, predict postoperative atrial fibrillation after isolated off-pump coronary artery bypass grafting. *J. Am. Heart Assoc.* (2018) 7:e006642. doi: 10.1161/JAHA.117.006642
92. Hu M, Wei X, Li M, Tao L, Wei L, Zhang M, et al. Circular RNA expression profiles of persistent atrial fibrillation in patients with rheumatic heart disease. *Anatol J Cardiol.* (2019) 21:2–10. doi: 10.14744/AnatolJCardiol.2018.35902
93. Zhu X, Tang X, Chong H, Cao H, Fan F, Pan J, et al. Expression profiles of circular RNA in human atrial fibrillation with valvular heart diseases. *Front Cardiovasc Med.* (2020) 7:597932. doi: 10.3389/fcvm.2020.597932
94. Gao Y, Liu Y, Fu Y, Wang Q, Liu Z, Hu R, et al. The potential regulatory role of hsa_circ_0004104 in the persistency of atrial fibrillation by promoting cardiac fibrosis *via* TGF-β pathway. *BMC Cardiovasc Disord.* (2021) 21:25. doi: 10.1186/s12872-021-01847-4
95. Costa MC, Cortez-Dias N, Gabriel A, de Sousa J, Fiúza M, Gallego J, et al. circRNA-miRNA cross-talk in the transition from paroxysmal to permanent atrial fibrillation. *Int J Cardiol.* (2019) 290:134–7. doi: 10.1016/j.ijcard.2019.04.072
96. Babapoor-Farrokhran S, Gill D, Rasekhi RT. The role of long noncoding RNAs in atrial fibrillation. *Heart Rhythm.* (2020) 17:1043–9. doi: 10.1016/j.hrthm.2020.01.015
97. Shi J, Chen L, Chen S, Wu B, Yang K, Hu X. Circulating long noncoding RNA, GAS5, as a novel biomarker for patients with atrial fibrillation. *J Clin Lab Anal.* (2021) 35:e23572. doi: 10.1002/jcla.23572
98. Zeng W, Jin J. The correlation of serum long non-coding RNA ANRIL with risk factors, functional outcome, and prognosis in atrial fibrillation patients with ischemic stroke. *J Clin Lab Anal.* (2020) 34:e23352. doi: 10.1002/jcla.23352
99. Dai W, Chao X, Li S, Zhou S, Zhong G, Jiang Z. Long noncoding RNA HOTAIR functions as a competitive endogenous RNA to regulate Connexin43 remodeling in atrial fibrillation by sponging microRNA-613. *Cardiovasc Ther.* (2020) 2020:5925342. doi: 10.1155/2020/5925342
100. Wang H, Song T, Zhao Y, Zhao J, Wang X, Fu X. Long non-coding RNA LICPAR regulates atrial fibrosis *via* TGF-β/Smad pathway in atrial fibrillation. *Tissue Cell.* (2020) 67:101440. doi: 10.1016/j.tice.2020.101440
101. Yao L, Zhou B, You L, Hu H, Xie R. LncRNA MIAT/miR-133a-3p axis regulates atrial fibrillation and atrial fibrillation-induced myocardial fibrosis. *Mol Biol Rep.* (2020) 47:2605–17. doi: 10.1007/s11033-020-05347-0
102. Du J, Li Z, Wang X, Li J, Liu D, Wang X, et al. Long noncoding RNA TCONS-00106987 promotes atrial electrical remodelling during atrial fibrillation by sponging miR-26 to regulate KCNJ2. *J Cell Mol Med.* (2020) 24:12777–88. doi: 10.1111/jcmm,.15869
103. Lener T, Gimona M, Aigner L, Borger V, Buzas E, Camussi G, et al. Applying extracellular vesicles based therapeutics in clinical trials - an ISEV position paper. *J Extracell Vesicles.* (2015) 4:30087. doi: 10.3402/jev.v4.30087
104. Taylor DD, Shah S. Methods of isolating extracellular vesicles impact down-stream analyses of their cargoes. *Methods.* (2015) 87:3–10. doi: 10.1016/j.ymeth.2015.02.019
105. Jang SC, Kim OY, Yoon CM, Choi DS, Roh TY, Park J, et al. Bioinspired exosome-mimetic nanovesicles for targeted delivery of chemotherapeutics to malignant tumors. *ACS Nano.* (2013) 7:7698–710. doi: 10.1021/nn402232g
106. Yoon J, Jo W, Jeong D, Kim J, Jeong H, Park J. Generation of nanovesicles with sliced cellular membrane fragments for exogenous material delivery. *Biomaterials.* (2015) 59:12–20. doi: 10.1016/j.biomaterials.2015.04.028
107. Jung HS, Cho KJ, Seol Y, Takagi Y, Dittmore A, Roche PA, et al. Polydopamine encapsulation of fluorescent nanodiamonds for biomedical applications. *Adv Funct Mater.* (2018) 28:1801252. doi: 10.1002/adfm.201801252
108. Vangijzegem T, Stanicki D, Laurent S. Magnetic iron oxide nanoparticles for drug delivery: applications and characteristics. *Expert Opin Drug Deliv.* (2019) 16:69–78. doi: 10.1080/17425247.2019.1554647
109. Wang Y, Zhao Q, Han N, Bai L, Li J, Liu J, et al. Mesoporous silica nanoparticles in drug delivery and biomedical applications. *Nanomedicine.* (2015) 11:313–27. doi: 10.1016/j.nano.2014.09.014
110. Alkilany AM, Murphy CJ. Toxicity and cellular uptake of gold nanoparticles: what we have learned so far? *J Nanopart Res.* (2010) 12:2313–33. doi: 10.1007/s11051-010-9911-8

111. Blanco E, Shen H, Ferrari M. Principles of nanoparticle design for overcoming biological barriers to drug delivery. *Nat Biotechnol.* (2015) 33:941–51. doi: 10.1038/nbt.3330
112. Zhao S, Yu X, Qian Y, Chen W, Shen J. Multifunctional magnetic iron oxide nanoparticles: an advanced platform for cancer theranostics. *Theranostics.* (2020) 10:6278–309. doi: 10.7150/thno.42564
113. Zuo G, Kang SG, Xiu P, Zhao Y, Zhou R. Interactions between proteins and carbon-based nanoparticles: exploring the origin of nanotoxicity at the molecular level. *Small.* (2013) 9:1546–56. doi: 10.1002/smll.201201381

Conflict of Interest: The authors declare that the research was conducted in the absence of any commercial or financial relationships that could be construed as a potential conflict of interest.

Publisher's Note: All claims expressed in this article are solely those of the authors and do not necessarily represent those of their affiliated organizations, or those of the publisher, the editors and the reviewers. Any product that may be evaluated in this article, or claim that may be made by its manufacturer, is not guaranteed or endorsed by the publisher.

frontiers in Cardiovascular Medicine

REVIEW
published: 16 August 2021
doi: 10.3389/fcvm.2021.715258

Cardiac Fibrosis: Cellular Effectors, Molecular Pathways, and Exosomal Roles

Wenyang Jiang[1†], *Yuyan Xiong*[1†], *Xiaosong Li*[1] *and Yuejin Yang*[2*]

[1] State Key Laboratory of Cardiovascular Disease, National Center for Cardiovascular Diseases, Fuwai Hospital, Chinese Academy of Medical Science and Peking Union Medical College, Beijing, China, [2] State Key Laboratory of Cardiovascular Disease, Department of Cardiology, National Center for Cardiovascular Diseases, Fuwai Hospital, Chinese Academy of Medical Science and Peking Union Medical College, Beijing, China

Cardiac fibrosis, a common pathophysiologic process in most heart diseases, refers to an excess of extracellular matrix (ECM) deposition by cardiac fibroblasts (CFs), which can lead to cardiac dysfunction and heart failure subsequently. Not only CFs but also several other cell types including macrophages and endothelial cells participate in the process of cardiac fibrosis *via* different molecular pathways. Exosomes, ranging in 30–150 nm of size, have been confirmed to play an essential role in cellular communications by their bioactive contents, which are currently a hot area to explore pathobiology and therapeutic strategy in multiple pathophysiologic processes including cardiac fibrosis. Cardioprotective factors such as RNAs and proteins packaged in exosomes make them an excellent cell-free system to improve cardiac function without significant immune response. Emerging evidence indicates that targeting selective molecules in cell-derived exosomes could be appealing therapeutic treatments in cardiac fibrosis. In this review, we summarize the current understandings of cellular effectors, molecular pathways, and exosomal roles in cardiac fibrosis.

Keywords: cardiac fibrosis, cellular effectors, mechanisms, exosome, treatment

OPEN ACCESS

Edited by:
Zhen-Ao Zhao,
Hebei North University, China

Reviewed by:
Chaoshan Han,
University of Alabama at Birmingham, United States
Teng Ma,
Tongji University, China

***Correspondence:**
Yuejin Yang
yangyjifw@126.com

[†]These authors have contributed equally to this work

Specialty section:
This article was submitted to Cardiovascular Biologics and Regenerative Medicine, a section of the journal Frontiers in Cardiovascular Medicine

Received: *26 May 2021*
Accepted: *20 July 2021*
Published: *16 August 2021*

Citation:
Jiang W, Xiong Y, Li X and Yang Y (2021) Cardiac Fibrosis: Cellular Effectors, Molecular Pathways, and Exosomal Roles. Front. Cardiovasc. Med. 8:715258. doi: 10.3389/fcvm.2021.715258

INTRODUCTION

Cardiac fibrosis, marked by an excess of extracellular matrix (ECM) deposition by cardiac fibroblasts (CFs), is a common pathophysiologic process in most heart diseases such as myocardial infarction (MI), hypertensive heart disease, and different types of cardiomyopathies (1, 2) and impair the heart physically and electrically. Taking acute MI (AMI) as an example, sudden massive loss of cardiomyocytes triggers an intense inflammation and causes the dead myocardium to be replaced with a collagen-based scar (3), which is critical to prevent cardiac rupture. However, prolonged or excessive fibrotic responses could remarkably lead to excessive ECM deposition, which results in hardening of myocardium, poor tissue compliance, and worsening of cardiac dysfunction. According to the location of cardiac scars and underlying cause (4, 5), cardiac fibrosis can be classified into various forms, among which reactive interstitial fibrosis and replacement fibrosis are the most relevant type of the ischemic adult heart. Being the major cell type in the adult myocardium, CFs perform a critical role in maintaining ECM protein homeostasis. The activation of CFs can lead to the transition into myofibroblasts, which is a critical step in the development of cardiac fibrosis. Besides CFs, there are various types of cells involved in the process of cardiac fibrosis *via* different pathways. It is widely known that cardiac fibrosis can provoke

chamber dilation, cardiomyocyte hypertrophy, and apoptosis and finally result in congestive heart failure (6–8). Therefore, it is essential to discover potential diagnostic or therapeutic targets for cardiac fibrosis.

Exosomes, ranging in 30–150 nm of size, play an essential role in cellular communications by their bioactive contents (9, 10). As a cell-free system, exosomes could lead to improvement in cardiac function without triggering an immune response by including cardioprotective components such as miRNAs and proteins, emerging as an appropriate candidate for cardiac fibrosis treatment. Recent research studies show that inhibiting exosome secretion or targeting specific molecules in CF-derived exosomes could be a promising therapeutic strategy in ischemic heart disease (11, 12). In this review, we demonstrate the current understandings of the cellular effectors, molecular pathways, and exosomal roles in cardiac fibrosis.

CELLULAR EFFECTORS OF CARDIAC FIBROSIS

After a myocardial injury, CFs convert to their activated form (termed as myofibroblasts) by upregulating expression of pro-inflammatory cytokines, which is defined as the key cellular event in cardiac fibrosis. Though activated myofibroblasts have been the primary effector cells in the fibrotic heart by producing ECM proteins directly, macrophages/monocytes, mast cells (MCs), lymphocytes, cardiomyocytes, and vascular cells (**Figure 1**) can also play vital roles in the fibrotic response *via* secretion of a variety of fibrogenic mediators such as matricellular proteins and growth factors.

Abbreviations: ECM, extracellular matrix; CF, cardiac fibroblast; AMI, acute myocardial infarction; EMT, epithelial–mesenchymal transition; MMP, matrix metalloproteinases; DDR2, discoidin domain receptor 2; FSP1, fibroblast-specific protein 1; S100a4, S100 calcium-binding protein A4; Thy1, thymus cell antigen 1; TCF21, the transcription factor 21; PDGFR α, platelet-derived growth factor receptor α; α-SMA, α-smooth muscle actin; ED-A, extradomain A; ROS, reactive oxygen species; MC, mast cells; DAMPs, damage-associated molecular patterns; TNF, tumor necrosis factor; IL, interleukin; MCG, mast cell granule; VEGF, vascular endothelial growth factor; MSC, mesenchymal stem cell; ET, endothelin; EndMT, endothelial to mesenchymal transition; HIF, hypoxia-inducible factor; IP, interferon-γ-inducible protein; TβRII, TGF-β receptor II; IGF, insulin-like growth factor; AT2, angiotensin II type 2 receptor; PAI, plasminogen activator inhibitor; PDGF, platelet-derived growth factor; RAAS, renin–angiotensin–aldosterone system; Ang II, angiotensin II; ACE, angiotensin-converting enzyme; AT 1, angiotensin type 1; AR, adrenergic receptor; CCN2, cellular communication network factor 2; GRK2, G protein-coupled receptor kinase 2; MRTF, myocardin-related transcription factor; TSP-1, thrombospondin 1; STAT, signal transducer and activator of transcription; JAK, Janus kinase; mIL-6R, membrane-bound IL-6R; sIL-6R, soluble IL-6R; RAS, renin–angiotensin system; HIMF, hypoxia-induced mitogenic factor; TN-C, Tenascin-C; EE, early endosome; LE, late endosome; ILV, intraluminal vesicle; MVB, multivesicular body; TSG101, tumor susceptibility gene 101; MHC, major histocompatibility complex; PDCD6IP, programmed cell death 6-interacting protein; HSP, heat shock protein; SORBS2, orbin and SH3 domain-containing protein 2; PDLIM5, PDZ and LIM domain; Nrf2, nuclear factor erythroid 2-related factor 2; FoxO, forkhead transcription factors of the O class; YBX-1, Y box binding protein 1; Smurf1, SMAD-specific E3 ubiquitin protein ligase 1; HDAC4, histone deacetylase 4; MKK6, mitogen-activated protein kinase kinase 6; Dyrk2, dual-specificity tyrosine phosphorylation-regulated kinase 2; PTEN, phosphatase and tensin homolog; Mecp2, methyl CpG binding protein 2; BMP2, bone morphogenetic protein 2; EGR1, early growth response factor 1; HuR, human antigen R; Ang, angiotensin.

Fibroblasts and Myofibroblasts

It is recognized that the transdifferentiation from CFs to myofibroblasts is the core cellular event in cardiac fibrosis. In order to clarify the role of CFs and myofibroblasts in cardiac fibrosis, several markers have been found to identify and distinguish CFs and myofibroblasts (13–37) (**Table 1**). It has been clear that most CFs derived from the epicardium, a protective epithelial layer that entirely covers the four cardiac chambers, undergoing epithelial–mesenchymal transition (EMT) (38, 39). Smaller populations are derived from the endocardium (40, 41) and cardiac neural crest (20) and are mostly found in the interventricular septum and right atrium, respectively (**Figure 2**). However, the origin of the myofibroblasts forming fibrotic lesions in failing hearts has been a source of debate. Most investigations in the last 10 years have revealed that activated myofibroblasts in remodeling and the infarcted hearts are primarily derived from resident CFs (20), and it is well-established that the transformation of CFs to myofibroblasts is a core cellular event involved in fibrotic response under cardiac injury. Cardiac myofibroblasts, a contractile and secretory cell type, not only contribute to the structure of ECM proteins in fibrotic hearts but also play an important role in matrix remodeling regulation through the production of proteases including the matrix metalloproteinases (MMPs) as well as their inhibitors.

So far, few factors that can independently induce CF activation have been identified. Evidence has revealed that, following mechanical stress, fibroblasts change to proto-myofibroblasts (an intermediate cell) (42). Proto-myofibroblasts contain unique cell markers including a splice variant of fibronectin called the fibronectin extradomain A (ED-A) and stress fibers (43). The cytokine TGF-β further stimulates proto-myofibroblasts, causing them to develop into the myofibroblast cell phenotype; thus, it, in turn, leads to heart failure associated with cardiac remodeling. Inflammation, MI, changes in mechanical tension, reactive oxygen species (ROS), age, and other factors can all alter the activation of CFs (**Figure 3**). We will discuss the specific molecular pathways contributing to CF activation in the remodeling heart in section Fibrogenic growth factors.

The Monocytes/Macrophages

According to increasing evidence, macrophages and monocytes have both been confirmed to play vital roles in the regulation of cardiac fibrosis. Macrophages and monocytes in the injured heart appear to be increasingly heterogeneous depending on their different subpopulation (44), and their phenotypic and functional flexibility allow them to perform diverse functions in fibrotic responses, such as serving as a primary source of fibrogenic growth factors and cytokines, producing matricellular proteins, and secreting matrix remodeling proteases (45). Moreover, circulating fibroblast progenitors may be implicated in the progression of cardiac fibrosis as suggested by numerous studies using bone marrow transplantation techniques (46). These hematopoietic progenitors could be monocyte subsets that can differentiate fibroblasts, comparable with the CD14+ "fibrocytes" discovered in humans (47), which imply that macrophages and monocytes in fibrotic hearts could be sources of myofibroblasts.

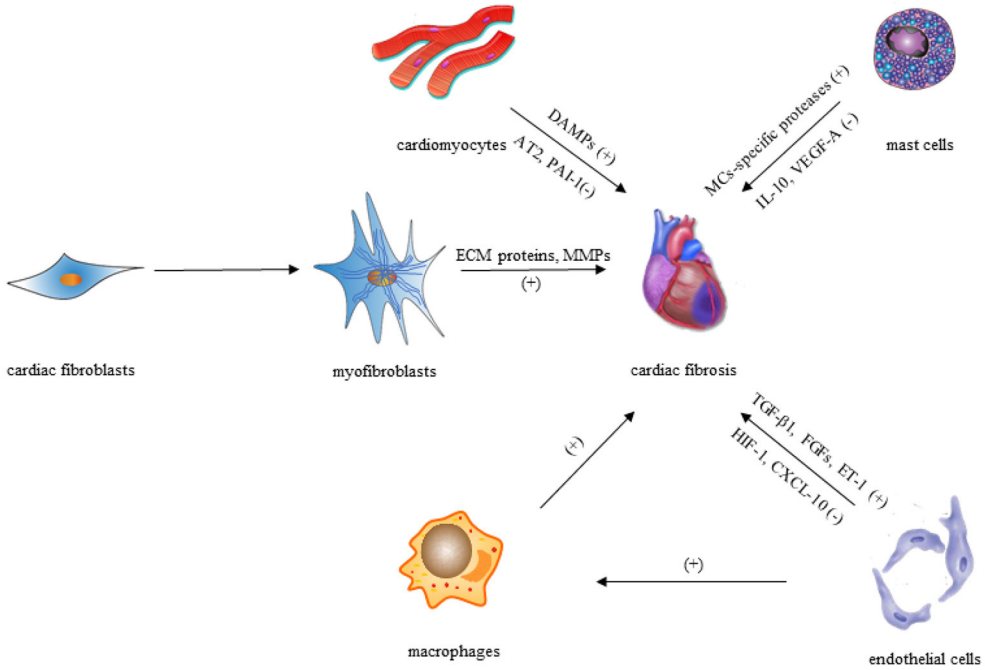

FIGURE 1 | Cellular effectors of cardiac fibrosis.

The Mast Cells

MCs are innate immune cells found almost everywhere of the body, including the heart. Resident MCs in the heart can respond to damage-associated molecular patterns (DAMPs) after injury, thus influencing the development of cardiac remodeling. However, the precise function of MCs in cardiac fibrosis is debatable, as the secretory proteins produced by MCs can be both anti- and profibrotic in nature. MC-specific proteases such as chymase and tryptase released by degranulation could induce TGF-β1 production (48–50), which plays a role in cardiac fibrosis through collagen synthesis, myofibroblast differentiation, and fibroblast stimulation (1, 51). In addition, cytokines like tumor necrosis factor (TNF) (52) and interleukin (IL)-1β (53) stored in MC granule (MCG) can also promote cardiac fibrosis through cardiomyocyte apoptosis during degranulation (54).

MCs, on the other hand, secrete anti-inflammatory mediators including IL-10 (55), which has been shown to inhibit excessive cardiac remodeling by activating STAT3 and suppressing NF-κB (56–58). Besides, MCs can produce vascular endothelial growth factor (VEGF)-A (52, 53), as one of the important anti-fibrotic mediators, which can increase capillary density in damaged tissues and promote proper repair in cardiac fibrosis (59–61). Over the past few years, various studies have been carried out for investigating the functions of MCG in fibrosis. MCG therapy of mesenchymal stem cells (MSCs) *in vitro* reduced TGF-β1-mediated transition of MSCs to myofibroblasts, while *in vivo* delivery of MCGs from rats to the myocardium during AMI lowered fibrosis and enhanced capillary density (62). These findings suggest that MCs have anti-fibrotic properties and could be used as therapeutic targets in cardiac remodeling.

The Endothelial Cells

The prevalence of perivascular fibrosis in the injured heart may indicate that endothelial cells are involved in cardiac fibrosis (63). Under pathophysiologic conditions, endothelial cells may enhance fibrotic responses *via* a variety of mechanisms after the myocardial injury. First, several profibrotic mediators produced by endothelial cells, such as FGFs, TGF-1, and endothelin (ET)-1, may play key roles in the development of cardiac fibrosis (64, 65). Second, endothelial cells may produce pro-inflammatory cytokines and chemokines, contributing to recruitment of lymphocytes and macrophages with fibrogenic actions (66). Third, although low numbers of endothelial-derived fibroblasts were detected in the remodeling myocardium, endothelial cells may undergo endothelial to mesenchymal transition (EndMT), increasing the number of fibroblasts (34).

On the contrary, anti-fibrotic mediators could also be produced by endothelial cells. Endothelial cells have been found to express hypoxia-inducible factor (HIF)-1 for protecting the pressure-overloaded myocardium from fibrosis *via* suppression of TGF-β signaling partially (67). Furthermore, endothelial cells exert inhibitory actions on cardiac fibrosis by producing and secreting interferon-γ-inducible protein (IP)-10/CXCL10, a CXC chemokine that prevents the migration of CFs in the infarcted heart (68).

The Cardiomyocytes

The roles of cardiomyocytes in the process of cardiac fibrosis are two sides of the coin. For one thing, cardiomyocytes may promote interstitial fibrosis through neurohumoral and growth factor-mediated pathways, such as cardiomyocyte-specific

TABLE 1 | Summary of molecular markers used for the identification of cardiac fibroblasts and myofibroblasts.

Biomarker	Location	Function	Expression in cardiac fibroblast	Expression in cardiac myofibroblast	Expression in other cell types	References
Discoidin domain receptor 2 (DDR2)	Cell surface	Collagen-specific receptor tyrosine kinase mediating cell growth, migration, and differentiation	Yes	Yes	Epicardium	(13–18)
Vimentin	Cytoskeletal	Intermediate filaments for motility and cell shape	Yes	Yes	Endothelial cells, macrophages	(19–22)
Fibroblast-specific protein 1 (FSP1)/S100 calcium-binding protein A4 (S100a4)	Cytosolic	Calcium-binding protein for motility and tubulin polymerization	Yes	Unknown	Immune cells	(23, 24)
Thymus cell antigen 1 (Thy1, CD90)	Cell surface	Membrane glycoprotein for cell adhesion	Yes	No	Immune cells, lymphatic endothelial cells and pericytes	(25–27)
The transcription factor 21 (TCF21)	Nucleus	Regulates mesenchymal cell transitions	Yes	Yes	Epicardium	(25, 28, 29)
Platelet-derived growth factor receptor α (PDGFR α)	Cell surface	Tyrosine kinase receptor	Yes	Unknown	Platelets, epicardium	(30)
Collagen 1α1-GFP	Transgene	Targeting collagen I protein-producing cells	Yes	Unknown	Endothelial and vascular smooth muscle cells	(22, 32)
α-Smooth muscle actin (α-SMA)	Cytoskeletal	Intermediate filament-associated protein for cell contraction	No	Yes	Epicardium, smooth muscle cells, pericytes, and cardiomyocytes	(33, 34)
Periostin	Extracellular matrix (ECM)	Cardiac development, remodeling and ECM organization	No	Yes	Epicardium, vascular smooth muscle cells, and valve interstitial cells	(35–37)

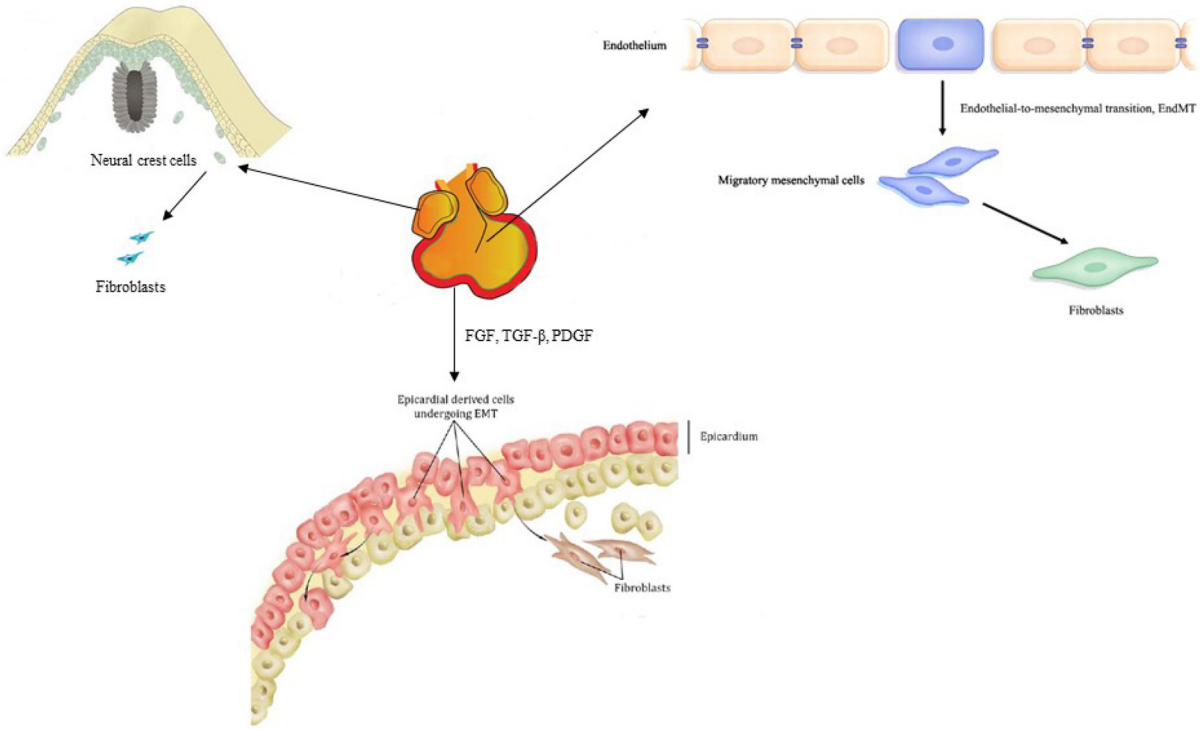

FIGURE 2 | Origin of cardiac fibroblasts.

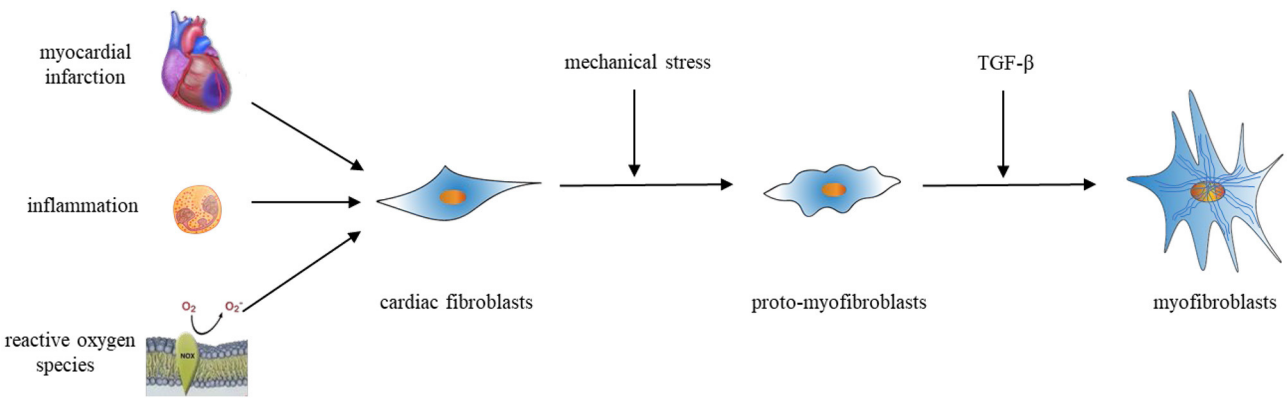

FIGURE 3 | Activation of cardiac fibroblasts.

mineralocorticoid receptor signaling (69), TGF-β receptor II (TβRII) signaling (70), and insulin-like growth factor (IGF)-1 signaling (71). Moreover, necrotic cardiomyocytes trigger an inflammatory response that finally leads to activation of fibroblasts *via* release of DAMPs, which means cardiac fibrosis may occur due to cardiomyocyte death, instead of cardiomyocyte-derived fibrogenic signals (51). For another, cardiomyocyte-specific overexpression of angiotensin II (Ang II) type 2 (AT2) receptor or the plasminogen activator inhibitor (PAI)-1 exerts anti-fibrotic actions *via* the kinin/NO system activation or inhibition of TGF-β synthesis, respectively (72, 73).

MOLECULAR PATHWAYS IN CARDIAC FIBROSIS

The complexity of interconnections and the extensive range of molecular pathways involved in the fibrotic response have restricted our understanding of the mechanism of cardiac fibrosis. High-throughput transcriptomic and genomic techniques have recently been employed to find new molecular signals and pathways linked to the fibrotic response's initiation, regression, and progression (74); and in the development of cardiac fibrosis, various molecular routes have been identified.

Most fibrotic heart diseases, regardless of cause, appear to include the aldosterone/angiotensin axis and fibrogenic growth factors such as platelet-derived growth factor (PDGF) and TGF-β. Moreover, several inflammatory signals (3, 75) such as TNF-α and IL-6 may regulate reparative and ischemic fibrosis by transducing the cascades of intracellular signaling that result in the transcription of ECM genes and translation of matrix remodeling-related proteins. Here, we demonstrate signaling pathways and mediators known to influence process of cardiac fibrosis after myocardial injury, hoping to find novel therapeutic targets or strategies.

Neurohumoral Pathways

The Renin–Angiotensin–Aldosterone System

During the progression of cardiac fibrosis, the renin–angiotensin–aldosterone system (RAAS), of which Ang II appears to be the primary effector, is persistently engaged. In fibrotic hearts, the oligopeptide Ang II, which induces vasoconstriction and high blood pressure, is raised. Angiotensin-converting enzyme (ACE) and renin, which are required for the production of Ang II, are produced by fibroblasts and macrophages invading the damaged heart (76, 77). Both *in vivo* and *in vitro* investigations suggest that Ang II is involved in TGF signaling. TGF-1 expression is induced by Ang II in fibroblasts and cardiomyocytes *via* the Ang II type 1 (AT 1) receptor, which plays a crucial role in profibrotic signaling (78–80); and *in vivo*, TGF-β is necessary for Ang II to induce both cardiac fibrosis and hypertrophy (81, 82). Besides, Ang II is also intimately involved with the inflammatory response, and in CFs, Ang II enhances their collagen-synthetic activity through extracellular signal-regulated kinase by an IL-6-dependent mechanism indeed. Another mechanism underlying the fibrotic capability of Ang II could involve miR-29b. *In vitro*, miR-29b suppression promotes Ang II-induced collagen type I and α-SMA expression, but overexpression of miR-29b inhibits it. It is indeed possible that miR-29b targets a sequence within the TGF-β1 coding area, which explains this observation. On the contrary, AT2 signaling may inhibit AT1-mediated actions, suppressing CF proliferation and matrix synthesis, serving as a negative regulator of Ang II-mediated profibrotic responses.

Aldosterone is also capable of inducing fibrotic responses in the myocardium after cardiac injury, suggested by patients with adrenal adenomas and experimental animal studies. Several potential mechanisms have been involved in the profibrotic activities of aldosterone in the heart. First, aldosterone may have pro-inflammatory effects on vascular cells by increasing the production of cytokines like TNF-α *via* NF-κB activation. Second, aldosterone may induce a fibrogenic phenotype in macrophages *via* the mineralocorticoid receptor. Third, aldosterone may activate cardiomyocyte-derived fibrotic signals, involving regulation of MMP-2/9 activity and the TGF-β-connective tissue growth factor profibrotic pathway. Fourth, aldosterone may exert a direct effect on CFs, stimulating proliferation and increasing collagen synthesis.

GPCR/Adrenergic Signaling

It has been reported that activation of adrenergic signaling *via* β-adrenergic receptor (AR) can induce cardiomyocyte death and subsequent reparative fibrosis, thus leading to cardiac remodeling. Although there are several subtypes of β-AR expressed in the heart, the predominant form of β2-AR seems to be expressed on CFs. Collagen secretion, cell proliferation, migration, and transformation to the myofibroblast phenotype can all be induced by direct activation of β2-AR on CFs, mediated through p38 MAPK signaling partially. In addition, β-AR signaling can also regulate cytokine expression by macrophages and induce growth factor synthesis by cardiomyocytes, which plays an important role in promoting cardiac fibrosis. However, not all types of β-ARs are involved in the profibrotic responses. On the contrary, several studies have proved that, in a model of pressure overload-induced cardiac fibrosis, β3-AR signaling in cardiomyocytes may protect the heart, due to downregulation of the matricellular protein CCN2 by cardiomyocytes.

Adrenergic stimulation causes structural changes in G protein βγ subunits in the damaged myocardium, culminating in activation of G protein-coupled receptor kinase 2 (GRK2). In an experimental model of MI, GRK2 activation in CFs has been shown to have substantial fibrotic effects. Although the specific fibrotic signals activated by GRK2 remain unclear, GRK2 represents a critical target for therapeutic interventions against cardiac fibrosis.

Endothelin-1

The endothelin family of peptides was mostly known for its vasoconstriction capabilities; however, it is now being recognized for its potential role in tissue fibrosis. ET-1, one of the significant endothelin isoforms in humans, is thought to be secreted predominantly by endothelial cells but also can be produced by other cells including fibroblasts, cardiomyocytes, and macrophages. The ETA and ETB receptors, which have been found to perform opposite roles, are two recognized ET-1 receptors in the heart. At first, it was thought that these two receptors were only expressed on endothelial cells; however, the latest evidence suggests (83, 84) that they can also be expressed in other types of cells such as macrophages, cardiomyocytes, and CFs.

Both *in vitro* and *in vivo* studies suggest that ET-1 appears to be a potent fibrogenic mediator. *In vitro*, ET-1 enhances proliferation and collagen production in isolated human CFs *via* ETA receptor; *in vivo*, overexpression of ET-1 in the heart induces myocardial fibrosis associated with biventricular systolic and diastolic dysfunction. In addition to fibroblast-activating characteristics of its own, ET-1 can also act as a downstream of cytokines and neurohumoral mediators such as TGF-β and Ang II, serving as a link between fibrosis and inflammation. For example, the development of cardiac fibrosis in response to Ang II is impaired in mice with vascular endothelial cell-specific ET-1 deficiency, regulated by the myocardin-related transcription factor (MRTF)-A.

Moreover, endothelin antagonists are now approved to treat pulmonary hypertension, and many believe they will also be beneficial in the treatment of heart pathological fibrosis. Bosentan, a non-selective endothelin receptor antagonist routinely used to treat pulmonary hypertension, has also been shown to reduce fibrotic myocardium remodeling in hypertensive and reparative cardiac fibrosis animal models (85).

Despite the failure of several randomized controlled studies exploring the impact of endothelin antagonists in heart failure and coronary artery disease, manipulating ET-1 signaling appears to be promising. More researches are needed to explore whether ET-1 and its receptors may be appropriate clinically viable anti-fibrotic treatment targets.

Fibrogenic Growth Factors

TGF-β

The TGF-β family is a group of pleiotropic and multifunctional peptides activated in experimental models of cardiac fibrosis and fibrotic human hearts markedly (1, 3). TGF-β is found in three isoforms (TGF-β1, TGF-β2, and TGF-β3) in mammals (86), among which TGF-β1 acts as the predominant isoform in the cardiovascular system and expresses ubiquitously. In the injured heart, TGF-β1, which is present in the normal heart as a latent complex, is transformed from the latent form to the active form *via* a variety of mediators. Proteases, including MMP-2, MMP-9, and plasmin, are widely acknowledged to participate in the activation of TGF-β as well as the matricellular protein thrombospondin 1 (TSP-1) (1), which plays an important role in cardiac remodeling. Upon activation, a group of studies have revealed that TGF-β was involved in the pathogenesis of cardiac fibrosis through Smad-mediated pathways where TGF-β binds to the constitutively active TβRII on the cell surface, transphosphorylates the cytoplasmic domain of the type I receptor (TβRI), and then gets connection with the Smads; or through Smad-independent pathways, in which TGF-β/TAK-1 signaling may exert profibrotic actions (1). Meanwhile, negative regulation of TGF-β signaling may be crucial in preventing cardiac fibrosis. A study conducted in a mouse model of pressure overload-induced heart failure has suggested that cleavage and release of a soluble endoglin may inhibit fibrogenic actions of TGF-β (87).

In addition, TGF-β is a critical fibrogenic mediator that may have the potential to affect all cell types involved in cardiac fibrotic response. MCGs are known to contain TGF-β in a large amount, while TGF-β-induced Smad-dependent pathways are activated by MC chymase, which results in fibrogenic effects (88). Besides, profibrotic growth factors including TGF-β can be produced and secreted in significant quantities by macrophages and monocytes. In return, TGF-β-mediated actions of these cell types may also play a paracrine role in fibrotic response. Moreover, endothelial cells may promote fibrotic cardiac remodeling through the expression of profibrotic mediators, such as TGF-β1, FGFs, or ET-1.

What is more, TGF-β-stimulated myofibroblast transdifferentiation is induced by activation of the Smad3 signaling cascade, which promotes α-SMA transcription in fibroblasts (89) and enhances ECM protein synthesis. Furthermore, cardiomyocyte-specific TβRII knockdown significantly reduced fibrosis in the pressure-overloaded heart (70), implying that cardiomyocyte-specific TGF-β signaling is essential in the pathogenesis of fibrotic remodeling.

Platelet-Derived Growth Factor

The PDGF family includes homo- or hetero-dimeric growth factors (such as PDGF-AA, PDGF-BB, PDGF-AB, PDGF-CC, and PDGF-DD) that signal *via* two distinct receptors: PDGFR-α and PDGFR-β (1). *In vivo*, PDGF-A and PDGF-C bind to PDGFRα, while PDGF-B and PDGF-D bind to PDGFRβ in general (90). PDGF-B and PDGF-D are expressed by endothelial cells, whereas PDGFRβ is expressed by vascular mural cells (pericytes and smooth muscle cells). Myocardial cells express both PDGF-A and PDGF-C, while PDGFRα-positive interstitial cells have been found in the myocardium, epicardium, and endocardium (90). With pleiotropic effects of PDGF signaling, all PDGFs have been reported to play a certain role in the development of cardiac fibrosis. Overexpression of PDGF-C (91) and PDGF-D (92) from the α-myosin heavy chain promoter (α-MHC), as well as PDGF-A (both splice variants) and PDGF-B, has been reported to generate cardiac fibrosis and hypertrophy in transgenic mice, though the degree and location of fibrosis vary between the different ligands (90). Besides, a group of studies suggested that PDGF stimulates fibroblast proliferation and differentiation to myofibroblasts *in vitro*, whereas PDGF blockade reduces interstitial fibrosis of the infarcted hearts in rats and suppresses atrial-selective canine fibroblast activation, removing the distinctive atrial–ventricular fibroblast activation differences (93). Moreover, a study implied that PDGF may also act to promote fibrosis by elevating TGF levels, for it can significantly upregulate profibrotic TGF-1 mRNA and accelerate cardiac fibrosis and arteriosclerosis when three of the isoforms, PDGF-A, PDGF-C, or PDGF-D, was introduced into the heart using adenovirus-mediated delivery (94). Similarly, PDGFRα appears to be a strong CF marker, possibly implicated in the production of CFs from epicardium, while PDGFR-β regulates the development of vascular smooth muscle cells from epicardium-derived cells (22, 24). Injection of a neutralizing PDGF receptor-specific antibody was also shown to reduce atrial fibrosis in several studies (95). These findings strongly imply that PDGF and PDGFR could be useful targets for anti-fibrotic treatment in the heart.

Inflammatory Cytokines

Tumor Necrosis Factor-α

TNF-α is a powerful pro-inflammatory cytokine that exerts pleiotropic effects on a variety of cell types and is reported to be crucial in the process of cardiac fibrosis. Transmembrane TNF-α, a precursor of the soluble TNF-α, is expressed on activated lymphocytes and macrophages as well as other cell types, exerting its biological actions by binding to type 1 and 2 TNF receptors (TNF-R1 and TNF-R2) (96), which can play different roles. Studies have shown that TNF-α in deficient mice after non-reperfused MI exacerbates cardiac remodeling, hypertrophy, NF-κB activity, and inflammation as well as border zone fibrosis through TNF-R1, whereas it ameliorates these events through TNF-R2 (97). In addition, an increasing number of studies suggest that cardiac fibrosis is promoted by TNF-α *via* a range of mediators and the interaction with other cell types. Heart failure was accelerated in transgenic mice by cardiac-specific overexpression of TNF-α, which was associated with increased collagen synthesis, deposition, and denaturation, and dramatically elevated MMP-2 and MMP-9 activities (98). Studies have also shown that fibrotic remodeling in the TNF-α overexpressing heart is associated with increased expression

of TGF-βs and the interactions between CFs and MCs (98). Complementally, in models of heart pressure overload induced by Ang II infusion or aortic banding, it is demonstrated that global genetic deletion of TNF-α reduced interstitial and perivascular fibrosis (99).

Interleukin-6

IL-6 is a pleiotropic cytokine that has a wide range of biological functions in hematopoiesis, immunological regulation, inflammation, and cardiac fibrosis. It was first identified as a B-cell differentiation factor (100). Secreted by various types of cells, IL-6 influences a group of cell types and exerts its multiple biological activities through two different signaling pathways: classic signaling and trans-signaling. Both intracellular signaling pathways involve the signal transducer and activator of transcription (STAT) pathway and Janus kinase (JAK) pathway, though they are activated following interaction of signal transducing membrane-bound IL-6R (mIL-6R), soluble IL-6R (sIL-6R), or glycoprotein (gp130) (100, 101). Emerging evidence suggests that IL-6, as a multifunctional cytokine, has a role in cardiac fibrosis. A study using the animal model suggested that elevated production of IL-6 induced by aldosterone could further promote collagen production and cardiac hypertrophy *via* the IL-6 trans-signaling pathway (102). Similarly, increased IL-6 levels and ROS generation in rats could activate the renin–angiotensin system (RAS) and JAK1/2-STAT1/3 signaling pathways, thus ultimately leading to activation of TGF-1β/Smad3 fibrotic pathway (103). Moreover, a study of neonatal rats under hypoxic conditions showed that overexpression of IL-6 was sufficient for inducing myofibroblastic proliferation, differentiation, and fibrosis, probably through improved TGF-β1-mediated MMP-2/MMP-3 signaling (102). Furthermore, IL-6 is a downstream signal of hypoxia-induced mitogenic factor (HIMF), and it plays a key role in cardiomyocyte hypertrophy and cardiac fibrosis *via* the MAPK and CaMKII-STAT3 pathways (104). Directly, by activating CFs to secrete Tenascin-C (TN-C), ET-1, and collagen, IL-6 produced by macrophages can also cause cardiac fibrosis (105). However, different studies on the role of IL-6 in cardiac fibrosis can be conflicting. In models of left ventricular pressure overload, genetic loss of IL-6 reduced cardiac dysfunction and fibrosis, whereas another study utilizing a model of pressure overload caused by transverse aortic constriction found no effect of germline IL-6 loss on ECM protein deposition and cardiac fibrosis (98). Therefore, we conclude that IL-6 and IL-6Rs may act as therapeutic targets of cardiovascular disease in the near future (**Figure 4**).

ROLE OF EXOSOMES IN CARDIAC FIBROSIS

Exosome-mediated intercellular signaling, which can transfer various functional modulators including proteins, lipids, and RNA, plays an increasingly important role in cardiovascular diseases. CFs are major components of the heart, ischemia/hypertrophy activates these fibroblasts, and they are involved in cardiac fibrosis and remodeling (106). Post-cardiac injury, fibroblast-derived miR-21-enriched exosomes can lead to cardiac myocyte hypertrophy and remodeling (11). In addition, miR-155 enriched in macrophage-derived exosomes led to enhanced proliferation and differentiation of resident fibroblasts and further exacerbated inflammation (12). Furthermore, exosomes *via* use of a targeting cardiac homing peptide or encapsulated in functional peptide hydrogels exhibit better ability in improving cardiac function and reducing fibrosis (107, 108). Besides, changes of miRNAs or proteins in exosomes derived from plasma or peripheral blood are considered as novel biomarkers for cardiac fibrosis or cardiac remodeling. Therefore, exosomes could be potential therapeutic treatments in cardiac fibrosis. Thorough knowledge of exosomes and exosome-mediated intercellular communication in cardiac fibrosis will provide better understanding to develop novel strategies for cardiac fibrosis treatments.

Exosomes: Biogenesis, Isolation, and Uptake

In response to different physiological states, exosomes are secreted by various cell types, such as MCs (109), macrophages, CFs, and exogenous MSCs, whose size range from 30 to 150 nm. Initially, transmembrane proteins are endocytosed and trafficked to early endosomes (EEs). EEs then mature into late endosomes (LEs) and generate intraluminal vesicles (ILVs) in the lumen of the organelles. Multivesicular bodies (MVBs), namely, LEs containing these ILVs, can fuse with plasma membrane and release exosomes into the extracellular space or fuse with lysosomes and degrade exosomes (110, 111). Different cell type- and microenvironment-derived exosomes transport distinct proteins, lipids, and nucleic acid cargoes (112, 113). Generally, exosomes are formed with tetraspanin family (CD9, CD63, and CD81) transmembrane proteins, tumor susceptibility gene 101 (TSG101), major histocompatibility complex (MHC) class II molecules, programmed cell death 6-interacting proteins (PDCD6IPs), heat shock proteins (HSPs) (HSP60, HSP70, and HSP90), cytoskeletal proteins (actin and tubulin), annexins (regulate cytoskeletal changes in membranes and membrane fusion), and membrane transport proteins (114).

Different techniques including microfiltration, gel filtration, ultracentrifugation, and commercial exosomes isolation kits are used to isolate exosomes from body fluids, plasma, or cell culture medium (115). Among these, ultracentrifugation is regarded as the gold standard for exosomes isolation and is also the most common method. Exosomes can enter recipient cells *via* distinct mechanisms including lipid membrane fusion, internalization by receptor-mediated endocytosis, receptor-mediated binding, and activation of downstream signaling (116). Total understanding of the biogenesis, isolation, and uptake of exosomes may contribute to find novel strategies for the treatment of cardiac fibrosis.

Exosome Contents for the Treatment of Cardiac Fibrosis

MicroRNAs

MiRNAs, small endogenous oligonucleotides of 21–25 nucleotides, are critical in regulating post-transcriptional

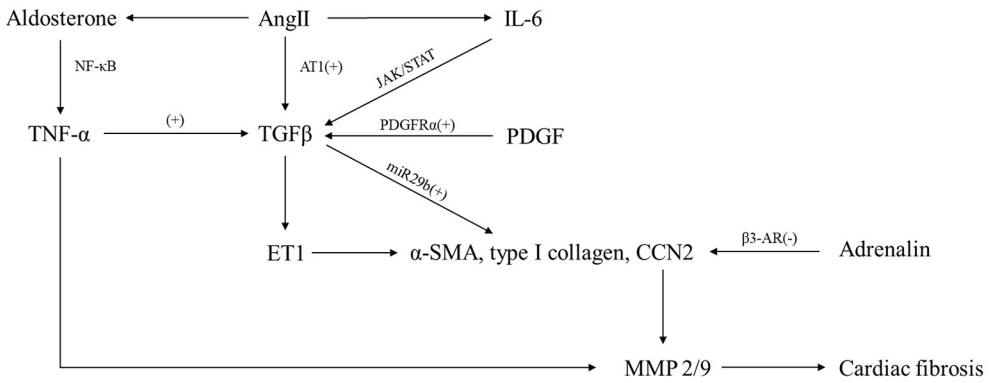

FIGURE 4 | Molecular pathways participated in cardiac fibrosis.

gene. Additionally, exosomes, containing different numerous miRNAs, could contribute to or alleviate a variety of pathologies including cardiac fibrosis. Exosomes, derived from distinct cell types including fibroblasts and exogenous MSCs, with upregulation or downregulation of certain miRNAs, can exhibit better ability in attenuating cardiac fibrosis and improving cardiac function (**Table 2**).

It has been confirmed that miR-21 played an essential role in fibroblast biology and that the levels were selectively increased in the failing heart, which makes it a target in heart failure (146). Bang et al. (11) revealed that miR-21 was enriched in fibroblast-derived exosomes, and the transfer of miR-21 to cardiomyocytes led to cellular hypertrophy. Additionally, Kang et al. demonstrated that miR-21-loaded human peripheral blood derived-exosomes enhanced fibrosis, making it a novel therapeutic target for cardiac fibrosis (137). Another research indicated that miR-27a-, miR-28a-, miR-34a-enriched fibroblast-derived exosomes could regulate cardiomyocyte antioxidant enzymes, thus contributing to cardiac hypertrophy (117). Therefore, exosomes derived from fibroblasts, especially those changing miRNAs contents, are a promising target for cardiac fibrosis.

Furthermore, exosomes derived from cardiomyocytes also exert therapeutic effects in cardiac fibrosis. Exosomes that contain high levels of miR-29b and miR-455 can downregulate MMP-9, thus reducing matrix degradation and mitigating fibrosis and myocyte uncoupling (122). MiR-378 secreted by cardiomyocytes mediated cardiac fibrosis *via* targeting the p38 MAPK-Smad2/3 signaling pathway and then regulating collagen and MMP expression in CFs (123). However, cardiomyocyte-derived miR-217- and miR-208-containing exosomes resulted in cardiac dysfunction and worsened cardiac fibrosis *via* targeting phosphatase and tensin homolog (PTEN) and dual-specificity tyrosine phosphorylation-regulated kinase 2 (Dyrk2) separately (124, 147). Evidence indicated that miR-142-3p-enriched exosomes derived from activated $CD4^+$ T cells contributed to the activation of WNT signaling pathway and CF activation, making it a promising target for treating cardiac fibrosis post-MI (138).

Cell therapy, including different types of stem cells, has been widely considered as a therapeutic approach for the treatment of cardiac fibrosis. Placenta-derived MSCs decreased the expression of TGF-β and reduced fibrosis in cardiac muscles *via* transferring exosomal miR-29c (130). MiR-92a from CDC-derived exosomes can be enriched *via* the activation of β-catenin and contribute to attenuation of cardiac fibrosis and improved cardiac function (131).

Proteins

Functional proteins, as the vital contents of exosomes, also exhibit an ability in regulating cardiac remodeling and cardiac fibrosis. It is generally considered that heat shock response is a cellular intrinsic defense mechanism (148) and that the increased expression of HSPs is beneficial for cells or tissues to fight against stress stimuli and pathological conditions (149). The overexpression of HSP20 in cardiomyocytes contributes to the secretion of exosomes *via* interaction with TSG101 and leads to the elevation of HSP20 in exosomes, which remarkably improved cardiac function and attenuated adverse remodeling (139). However, myocyte-derived HSP90 exerted a profibrotic role through orchestrating the synthesis of IL-6 and activating STAT-3 in fibroblasts, leading to excess collagen secretion and deposition, thus exaggerating cardiac hypertrophy and fibrosis (140). Emerging evidence indicated that proteins of WNT family are involved in the activation of cardiac fibrotic pathologies (150–152). Działo et al. confirmed that WNT3a-rich exosomes could specifically activate WNT/β-catenin signaling pathway and promoted fibrogenesis in post-infarcted hearts, whereas WNT5a-rich exosomes only activated non-canonical WNT pathways and induced production of profibrotic IL-6 (145). Summarizing, exosomes containing WNT proteins can regulate cardiac fibrosis *via* canonical and non-canonical WNT pathways and provide a novel strategy to treat cardiac fibrosis. The upregulated decorin and downregulated periostin in cardiomyocyte-derived exosomes had been confirmed to regulate cardiac fibrosis through targeting Ang II. Additionally, upregulated human antigen R (HuR) in macrophages significantly increased inflammatory and profibrogenic responses in fibroblast and

TABLE 2 | MiRNAs and proteins involved in exosomes for the treatment of cardiac fibrosis.

Name	Level	Derivation	Disease	Target gene/pathway	Effects	References
MiRNAs						
MiR-21-3p	Downregulation	Cardiac fibroblasts	Heart failure (HF)	Orbin and SH3 domain-containing protein 2 (SORBS2) PDZ and LIM domain 5 (PDLIM5)	Cardiac hypertrophy↓	(11)
MiR-27a, MiR-28-3p, MiR-34a	Upregulation	Cardiac fibroblasts	HF	Nuclear factor erythroid 2-related factor 2 (Nrf2)	Oxidative stress↑ Cardiac remodeling↑	(117)
MiR-155	Upregulation	Macrophages	Uremic cardiomyopathy	Forkhead transcription factors of the O class (FoxO3a)	Cardiomyocyte pyroptosis↑ Cardiac hypertrophy and fibrosis↑	(118)
MiR-19a-3p	Upregulation	Endothelial cells	MI	MiR-19a-3p/Thrombospondin 1	Vascularization↑ Myocardial fibrosis↓ Left ventricular ejection fraction↑	(119)
MiR-133	Upregulation	Endothelial cells	Myocardial fibrosis	Y box binding protein 1 (YBX-1)	Angiogenesis↑ mesenchymal-endothelial transition of cardiac fibroblast↑	(120)
MiR-10b-5p	Upregulation	Endothelial cells	MI	SMAD-specific E3 ubiquitin protein ligase 1 (Smurf1) Histone deacetylase 4 (HDAC4)	Cardiac fibroblast activation↓	(121)
MiR-29b, MiR-455	Upregulation	Cardiomyocytes	Diabetes	Matrix metalloproteinase 9 (MMP-9)	Fibrosis and myocyte uncoupling↓	(122)
MiR-378	Upregulation	Cardiomyocytes	Myocardial fibrosis	Mitogen-activated protein kinase kinase 6 (MKK6)/P38 MAPK pathway	Fibrosis↓	(123)
MiR-208a	Upregulation	Cardiomyocytes	Cardiac fibrosis	Dual-specificity tyrosine phosphorylation-regulated kinase 2 (Dyrk2)	Cardiac fibroblast↑ Myofibroblast differentiation↑ Cardiac fibrosis↑	(124)
MiR-19a	Upregulation	Mesenchymal stem cells (MSCs)	MI	Phosphatase and tensin homolog (PTEN)/Akt pathway	Infarct size↓ Fibrosis↓ Cardiac function↑	(125)
MiR-210	Upregulation	MSCs	MI	MiR-210/hypoxia-inducible factor-1 α (HIF-1α)	Fibrosis↓ Angiogenesis↑ Apoptosis↓	(126)
MiR-22	Upregulation	MSCs	MI	Methyl CpG binding protein 2 (Mecp2)	Cardiac fibrosis↓ Anti-apoptosis↑	(127)
MiR-24	Upregulation	Human umbilical MSCs	MI	MiR-24/Bim pathway	Cardiac fibrosis↓ Cardiac function↑	(128)
MiR-26a	Upregulation	Satellite cells	Uremic cardiomyopathy	FBXO32/atrogin-1 TRIM63/MuRF1	Cardiac fibrosis lesions↓	(129)
MiR-29c	Upregulation	Placenta-derived MSCs	Duchenne muscular dystrophy	TGF-β	Fibrosis in the diaphragm and cardiac muscles↓ Inflammation↓ Utrophin↑	(130)
MiR-92a	Upregulation	Cardiosphere-derived cells (CDCs)	MI	Bone morphogenetic protein 2 (BMP2)	Contractility↑ Fibrosis↓	(131)

(Continued)

TABLE 2 | Continued

Name	Level	Derivation	Disease	Target gene/pathway	Effects	References
MiR-126	Upregulation	Adipose-derived stem cells (ADSCs)	MI	–	Cardiac fibrosis↓ Inflammation↓ Apoptosis↓ Angiogenesis↑	(132)
MiR-133a	Upregulation	Cardiac progenitor cells (CPCs)	MI	Bim Bmf bFgf Vegf	Apoptosis↓ Fibrosis↓ Hypertrophy↓	(133)
MiR-146a-5p	Upregulation	CPCs	Doxorubicin/ trastuzumab-induced cardiac toxicity	Traf6 Smad4 Irak1 Nox4 Mpo	Myocardial fibrosis↓ CD68+ inflammatory cell infiltrates↓ Inducible nitric oxide synthase expression↓ Left ventricular dysfunction↓	(134)
MiR-146a	Upregulation	ADSCs	MI	Early growth response factor 1 (EGR1)/TLR4/NFkB	Apoptosis↓ Inflammatory response↓ Fibrosis↓	(135)
MiR-425, MiR-744	Downregulation	Plasma	HF	TGF-β1	Collagen formation↑ Fibrogenesis↑	(136)
MiR-21	Upregulation	Human peripheral blood	MI	Smad7 PTEN MMP-2	Fibrosis↑	(137)
MiR-142-3p	Upregulation	CD4+ T cells	MI	WNT pathway	Cardiac fibrosis↑ Dysfunction↑	(138)
Proteins						
HSP20	Upregulation	Cardiomyocytes	Diabetic cardiomyopathy	Phosphorylated Akt Survivin SOD1	Cell death↓ Cardiac adverse remodeling↓	(139)
HSP90	Downregulation	Cardiomyocytes	Cardiac hypertrophy	STAT3	Collagen synthesis↓	(140)
Decorin Periostin	Upregulation Downregulation	Cardiomyocytes	Cardiac fibrosis	Ang II	Transformation into myofibroblast↓ Fibroblast migration↓	(141)
HSP70	Upregulation	Serum	Aging-related cardiac fibrosis	–	Fibroblast proliferation↓ Myofibroblast differentiation↓	(142)
Lamp2b Ischemic myocardium-targeting peptide CSTSMLKAC (IMTP)	Upregulation	MSCs	MI	–	Inflammation↓ Apoptosis↓ Fibrosis↓ Vasculogenesis↑ Cardiac function↑	(143)
Human antigen R (HuR)	Upregulation	Macrophages	Cardiac fibrosis	Ang II	Inflammatory and profibrogenic responses↑ Cardiac fibrosis↑	(144)
WNT3a WNT5a	Overexpression	Cardiac fibroblasts	Cardiac fibrosis	WNT pathways	Cardiac fibroblast activated↑ Cardiac fibrosis↑	(145)

↑ means the corresponding MiRNA or protein has a positive effect on the process, or could increase the number/area of the subject; ↓ means the corresponding MiRNA or protein has a negative effect on the process, or could decrease the number/area of the subject.

cardiac fibrosis, suggesting that HuR might be targeted to alleviate macrophage dysfunction and pathological fibrosis (144).

Exosomes Act as Biomarkers in Cardiac Fibrosis

Recently, researches have been devoted to using miRNAs or other molecules in serum or plasma as diagnostic or prognostic biomarkers in cardiovascular diseases. Exosomes, as the carrier of those molecular constituents, are highly associated with concurrent physiological or pathological condition. It has been shown that the level of plasma exosomal miR-425 and miR-744 was decreased while the level of miR-21 was increased during the development of heart failure, which makes them novel biomarkers for heart failure and represent the conditions of the CF (136). In addition, surface HSP70 expression in serum exosomes was obviously decreased during senescence in the model of cardiac fibrosis, while HSP70 overexpression attenuated these effects, making it a new biomarker in aging-related cardiac fibrosis (142). Therefore, exosomes may act as a promising diagnostic biomarker in cardiac fibrosis.

CONCLUSION

Cardiac fibrosis, a common pathophysiologic event in most heart disease, can lead to poor tissue compliance, hardening of myocardium, and worsening of cardiac dysfunction. CFs, a major cell type of adult myocardium, play a vital role in the process of cardiac fibrosis. MCs, macrophages/monocytes, endothelial cells, and cardiomyocytes, in addition to CFs, also have a role in the fibrotic response through fibrogenic growth factors, the aldosterone/angiotensin axis, or inflammatory signals. Thus, cardiac fibrosis is a complex process involving multiple cells and regulated by multiple molecular pathways. Based on this, exosomes derived from various cell types are rich in a variety of miRNAs and proteins and could participate in intercellular communication to mediate cardiac fibrosis process, thus providing a novel strategy for the prediction and treatment of cardiac fibrosis.

AUTHOR CONTRIBUTIONS

WJ and YX determined the topic, wrote the initial draft, and revised the manuscript according to the reviewers' comments. XL searched the related literatures and supplemented the content of the manuscript. YY supervised the planning and execution of the research activity. All authors have given approval to the final version of the manuscript, responsible for the accuracy, and authenticity of the article.

FUNDING

This review was supported by grants from the CAMS Innovation Fund for Medical Sciences (CIFMS) (Grant No. 2016-I2M-1-009) and National Natural Science Foundation of China (Grant Nos. 82070307 and 81874461).

REFERENCES

1. Kong P, Christia P, Frangogiannis NG. The pathogenesis of cardiac fibrosis. *Cell Mol Life Sci.* (2014) 71:549–74. doi: 10.1007/s00018-013-1349-6
2. Berk BC, Fujiwara K, Lehoux S. ECM remodeling in hypertensive heart disease. *J Clin Invest.* (2007) 117:568–75. doi: 10.1172/JCI31044
3. Frangogiannis NG. Regulation of the inflammatory response in cardiac repair. *Circ Res.* (2012) 110:159–73. doi: 10.1161/CIRCRESAHA.111.243162
4. Tian J, An X, Niu L. Myocardial fibrosis in congenital and pediatric heart disease. *Exp Ther Med.* (2017) 13:1660–4. doi: 10.3892/etm.2017.4224
5. Ytrehus K, Hulot JS, Perrino C, Schiattarella GG, Madonna R. Perivascular fibrosis and the microvasculature of the heart. Still hidden secrets of pathophysiology? *Vascu Pharmacol.* (2018) 107:78–83. doi: 10.1016/j.vph.2018.04.007
6. Baudino TA, Carver W, Giles W, Borg TK. Cardiac fibroblasts: friend or foe? *Am J Physiol Heart Circul Physiol.* (2006) 291:H1015–26. doi: 10.1152/ajpheart.00023.2006
7. Cleutjens JP, Verluyten MJ, Smiths JF, Daemen MJ. Collagen remodeling after myocardial infarction in the rat heart. *Am J Pathol.* (1995) 147:325–38.
8. Cohn JN, Ferrari R, Sharpe N. Cardiac remodeling–concepts and clinical implications: a consensus paper from an international forum on cardiac remodeling. Behalf of an international forum on cardiac remodeling. *J Am Coll Cardiol.* (2000) 35:569–82. doi: 10.1016/S0735-1097(99)00630-0
9. Corrado C, Raimondo S, Chiesi A, Ciccia F, De Leo G, Alessandro R. Exosomes as intercellular signaling organelles involved in health and disease: basic science and clinical applications. *Int J Mol Sci.* (2013) 14:5338–66. doi: 10.3390/ijms14035338
10. Cerezo-Magaña M, Bång-Rudenstam A, Belting M. The pleiotropic role of proteoglycans in extracellular vesicle mediated communication in the tumor microenvironment. *Semin Cancer Biol.* (2020) 62:99–107. doi: 10.1016/j.semcancer.2019.07.001
11. Bang C, Batkai S, Dangwal S, Gupta SK, Foinquinos A, Holzmann A, et al. Cardiac fibroblast-derived microRNA passenger strand-enriched exosomes mediate cardiomyocyte hypertrophy. *J Clin Invest.* (2014) 124:2136–46. doi: 10.1172/JCI70577
12. Wang C, Zhang C, Liu L, A X, Chen B, Li Y, et al. Macrophage-Derived mir-155-Containing exosomes suppress fibroblast proliferation and promote fibroblast inflammation during cardiac injury. *Mol Ther.* (2017) 25:192–204. doi: 10.1016/j.ymthe.2016.09.001
13. Vogel W, Gish GD, Alves F, Pawson T. The discoidin domain receptor tyrosine kinases are activated by collagen. *Mol Cell.* (1997) 1:13–23. doi: 10.1016/S1097-2765(00)80003-9
14. Souders CA, Bowers SL, Baudino TA. Cardiac fibroblast: the renaissance cell. *Circ Res.* (2009) 105:1164–76. doi: 10.1161/CIRCRESAHA.109.209809
15. Morales MO, Price RL, Goldsmith EC. Expression of discoidin domain receptor 2 (DDR2) in the developing heart. *Microsc Microanal.* (2005) 11:260–7. doi: 10.1017/S1431927605050518
16. Fan D, Takawale A, Lee J, Kassiri Z. Cardiac fibroblasts, fibrosis and extracellular matrix remodeling in heart disease. *Fibrogenesis Tissue Repair.* (2012) 5:15. doi: 10.1186/1755-1536-5-15
17. Goldsmith EC, Hoffman A, Morales MO, Potts JD, Price RL, McFadden A, et al. Organization of fibroblasts in the heart. *Dev Dyn.* (2004) 230:787–94. doi: 10.1002/dvdy.20095
18. Banerjee I, Fuseler JW, Price RL, Borg TK, Baudino TA. Determination of cell types and numbers during cardiac development in the neonatal and adult rat and mouse. *Am J Physiol Heart Circ Physiol.* (2007) 293:H1883–91. doi: 10.1152/ajpheart.00514.2007
19. Lane EB, Hogan BL, Kurkinen M, Garrels JI. Co-expression of vimentin and cytokeratins in parietal endoderm cells of early mouse embryo. *Nature.* (1983) 303:701–4. doi: 10.1038/303701a0

20. Ali SR, Ranjbarvaziri S, Talkhabi M, Zhao P, Subat A, Hojjat A, et al. Developmental heterogeneity of cardiac fibroblasts does not predict pathological proliferation and activation. *Circ Res.* (2014) 115:625–35. doi: 10.1161/CIRCRESAHA.115.303794
21. Franke WW, Schmid E, Osborn M, Weber K. Intermediate-sized filaments of human endothelial cells. *J Cell Biol.* (1979) 81:570–80. doi: 10.1083/jcb.81.3.570
22. Moore-Morris T, Guimarães-Camboa N, Yutzey KE, Pucéat M, Evans SM. Cardiac fibroblasts: from development to heart failure. *J Mol Med.* (2015) 93:823–30. doi: 10.1007/s00109-015-1314-y
23. Strutz F, Okada H, Lo CW, Danoff T, Carone RL, Tomaszewski JE, et al. Identification and characterization of a fibroblast marker: FSP1. *J Cell Biol.* (1995) 130:393–405. doi: 10.1083/jcb.130.2.393
24. Doppler SA, Carvalho C, Lahm H, Deutsch MA, Dreßen M, Puluca N, et al. Cardiac fibroblasts: more than mechanical support. *J Thorac Dis.* (2017) 9 (Suppl 1):S36–51. doi: 10.21037/jtd.2017.03.122
25. Acharya A, Baek ST, Huang G, Eskiocak B, Goetsch S, Sung CY, et al. The bHLH transcription factor Tcf21 is required for lineage-specific EMT of cardiac fibroblast progenitors. *Development.* (2012) 139:2139–49. doi: 10.1242/dev.079970
26. Crisan M, Yap S, Casteilla L, Chen CW, Corselli M, Park TS, et al. A perivascular origin for mesenchymal stem cells in multiple human organs. *Cell Stem Cell.* (2008) 3:301–13. doi: 10.1016/j.stem.2008.07.003
27. Jurisic G, Iolyeva M, Proulx ST, Halin C, Detmar M. Thymus cell antigen 1 (Thy1, CD90) is expressed by lymphatic vessels and mediates cell adhesion to lymphatic endothelium. *Exp Cell Res.* (2010) 316:2982–92. doi: 10.1016/j.yexcr.2010.06.013
28. Braitsch CM, Kanisicak O, van Berlo JH, Molkentin JD, Yutzey KE. Differential expression of embryonic epicardial progenitor markers and localization of cardiac fibrosis in adult ischemic injury and hypertensive heart disease. *J Mol Cell Cardiol.* (2013) 65:108–19. doi: 10.1016/j.yjmcc.2013.10.005
29. Ivey MJ, Tallquist MD. Defining the cardiac fibroblast. *Circ J.* (2016) 80:2269–76. doi: 10.1253/circj.CJ-16-1003
30. Chong JJ, Reinecke H, Iwata M, Torok-Storb B, Stempien-Otero A, Murry CE. Progenitor cells identified by PDGFR-alpha expression in the developing and diseased human heart. *Stem Cells Dev.* (2013) 22:1932–43. doi: 10.1089/scd.2012.0542
31. Cuttler AS, LeClair RJ, Stohn JP, Wang Q, Sorenson CM, Liaw L, et al. Characterization of Pdgfrb-Cre transgenic mice reveals reduction of ROSA26 reporter activity in remodeling arteries. *Genesis.* (2011) 49:673–80. doi: 10.1002/dvg.20769
32. Yata Y, Scanga A, Gillan A, Yang L, Reif S, Breindl M, et al. DNase I-hypersensitive sites enhance alpha1(I) collagen gene expression in hepatic stellate cells. *Hepatology.* (2003) 37:267–76. doi: 10.1053/jhep.2003.50067
33. Porter KE, Turner NA. Cardiac fibroblasts: at the heart of myocardial remodeling. *Pharmacol Ther.* (2009) 123:255–78. doi: 10.1016/j.pharmthera.2009.05.002
34. Zeisberg EM, Tarnavski O, Zeisberg M, Dorfman AL, McMullen JR, Gustafsson E, et al. Endothelial-to-mesenchymal transition contributes to cardiac fibrosis. *Nat Med.* (2007) 13:952–61. doi: 10.1038/nm1613
35. Katsuragi N, Morishita R, Nakamura N, Ochiai T, Taniyama Y, Hasegawa Y, et al. Periostin as a novel factor responsible for ventricular dilation. *Circulation.* (2004) 110:1806–13. doi: 10.1161/01.CIR.0000142607.33398.54
36. Kudo A. Periostin in fibrillogenesis for tissue regeneration: periostin actions inside and outside the cell. *Cell Mol Life Sci.* (2011) 68:3201–7. doi: 10.1007/s00018-011-0784-5
37. Norris RA, Borg TK, Butcher JT, Baudino TA, Banerjee I, Markwald RR. Neonatal and adult cardiovascular pathophysiological remodeling and repair: developmental role of periostin. *Ann N Y Acad Sci.* (2008) 1123:30–40. doi: 10.1196/annals.1420.005
38. Gittenberger-de GA, Vrancken PM, Mentink MM, Gourdie RG, Poelmann RE. Epicardium-derived cells contribute a novel population to the myocardial wall and the atrioventricular cushions. *Circ Res.* (1998) 82:1043–52. doi: 10.1161/01.RES.82.10.1043
39. Muñoz-Chápuli R, Pérez-Pomares JM, Macías D, García-Garrido L, Carmona R, González-Iriarte M. The epicardium as a source of mesenchyme for the developing heart. *Ital J Anat Embryol.* (2001) 10 6(2 Suppl. 1):187–96.
40. Wessels A, van den Hoff MJ, Adamo RF, Phelps AL, Lockhart MM, Sauls K, et al. Epicardially derived fibroblasts preferentially contribute to the parietal leaflets of the atrioventricular valves in the murine heart. *Dev Biol.* (2012) 366:111–24. doi: 10.1016/j.ydbio.2012.04.020
41. Moore-Morris T, Guimarães-Camboa N, Banerjee I, Zambon AC, Kisseleva T, Velayoudon A, et al. Resident fibroblast lineages mediate pressure overload-induced cardiac fibrosis. *J Clin Invest.* (2014) 124:2921–34. doi: 10.1172/JCI74783
42. Baum J, Duffy HS. Fibroblasts and myofibroblasts: what are we talking about? *J Cardiovasc Pharmacol.* (2011) 57:376–9. doi: 10.1097/FJC.0b013e3182116e39
43. Hinz B, Phan SH, Thannickal VJ, Galli A, Bochaton-Piallat ML, Gabbiani G. The myofibroblast: one function, multiple origins. *Am J Pathol.* (2007) 170:1807–16. doi: 10.2353/ajpath.2007.070112
44. Honold L, Nahrendorf M. Resident and monocyte-derived macrophages in cardiovascular disease. *Circ Res.* (2018) 122:113–27. doi: 10.1161/CIRCRESAHA.117.311071
45. Chen B, Frangogiannis NG. Immune cells in repair of the infarcted myocardium. *Microcirculation.* (2017) 24:e12305. doi: 10.1111/micc.12305
46. Szardien S, Nef HM, Troidl C, Willmer M, Voss S, Liebetrau C, et al. Bone marrow-derived cells contribute to cell turnover in aging murine hearts. *Int J Mol Med.* (2012) 30:283–7. doi: 10.3892/ijmm.2012.995
47. Bucala R, Spiegel LA, Chesney J, Hogan M, Cerami A. Circulating fibrocytes define a new leukocyte subpopulation that mediates tissue repair. *Mol Med.* (1994) 1:71–81. doi: 10.1007/BF03403533
48. Saarinen J, Kalkkinen N, Welgus HG, Kovanen PT. Activation of human interstitial procollagenase through direct cleavage of the Leu83-Thr84 bond by mast cell chymase. *J Biol Chem.* (1994) 269:18134–40. doi: 10.1016/S0021-9258(17)32427-4
49. Cho SH, Lee SH, Kato A, Takabayashi T, Kulka M, Shin SC, et al. Cross-talk between human mast cells and bronchial epithelial cells in plasminogen activator inhibitor-1 production *via* transforming growth factor-β1. *Am J Respir Cell Mol Biol.* (2015) 52:88–95. doi: 10.1165/rcmb.2013-0399OC
50. Takai S, Jin D, Sakaguchi M, Katayama S, Muramatsu M, Sakaguchi M, et al. A novel chymase inhibitor, 4-[1-([bis-(4-methyl-phenyl)-methyl]-carbamoyl)3-(2-ethoxy-benzyl)-4-oxo-azetidine-2-yloxy]-benzoic acid (BCEAB), suppressed cardiac fibrosis in cardiomyopathic hamsters. *J Pharmacol Exp Ther.* (2003) 305:17–23. doi: 10.1124/jpet.102.045179
51. Prabhu SD, Frangogiannis NG. The biological basis for cardiac repair after myocardial infarction: from inflammation to fibrosis. *Circ Res.* (2016) 119:91–112. doi: 10.1161/CIRCRESAHA.116.303577
52. Wernersson S, Pejler G. Mast cell secretory granules: armed for battle. *Nat Rev Immunol.* (2014) 14:478–94. doi: 10.1038/nri3690
53. Mukai K, Tsai M, Saito H, Galli SJ. Mast cells as sources of cytokines, chemokines, and growth factors. *Immunol Rev.* (2018) 282:121–50. doi: 10.1111/imr.12634
54. Wang Y, Li Y, Wu Y, Jia L, Wang J, Xie B, et al. 5TNF-α and IL-1β neutralization ameliorates angiotensin II-induced cardiac damage in male mice. *Endocrinology.* (2014) 155:2677–87. doi: 10.1210/en.2013-2065
55. Lin TJ, Befus AD. Differential regulation of mast cell function by IL-10 and stem cell factor. *J Immunol.* (1997) 159:4015–23.
56. Verma SK, Garikipati V, Krishnamurthy P, Schumacher SM, Grisanti LA, Cimini M, et al. Interleukin-10 inhibits bone marrow fibroblast progenitor cell-mediated cardiac fibrosis in pressure-overloaded myocardium. *Circulation.* (2017) 136:940–53. doi: 10.1161/CIRCULATIONAHA.117.027889
57. Verma SK, Krishnamurthy P, Barefield D, Singh N, Gupta R, Lambers E, et al. Interleukin-10 treatment attenuates pressure overload-induced hypertrophic remodeling and improves heart function *via* signal transducers and activators of transcription 3-dependent inhibition of nuclear factor-κB. *Circulation.* (2012) 126:418–29. doi: 10.1161/CIRCULATIONAHA.112.112185
58. Krishnamurthy P, Rajasingh J, Lambers E, Qin G, Losordo DW, Kishore R. IL-10 inhibits inflammation and attenuates left ventricular remodeling after

myocardial infarction *via* activation of STAT3 and suppression of HuR. *Circ Res.* (2009) 104:e9–18. doi: 10.1161/CIRCRESAHA.108.188243
59. Nako H, Kataoka K, Koibuchi N, Dong YF, Toyama K, Yamamoto E, et al. Novel mechanism of angiotensin II-induced cardiac injury in hypertensive rats: the critical role of ASK1 and VEGF. *Hypertens Res.* (2012) 35:194–200. doi: 10.1038/hr.2011.175
60. Tang JM, Luo B, Xiao JH, Lv YX, Li XL, Zhao JH, et al. VEGF-A promotes cardiac stem cell engraftment and myocardial repair in the infarcted heart. *Int J Cardiol.* (2015) 183:221–31. doi: 10.1016/j.ijcard.2015.01.050
61. Yang L, Kwon J, Popov Y, Gajdos GB, Ordog T, Brekken RA, et al. Vascular endothelial growth factor promotes fibrosis resolution and repair in mice. *Gastroenterology.* (2014) 146:1339–50.e1. doi: 10.1053/j.gastro.2014.01.061
62. Nazari M, Ni NC, Lüdke A, Li SH, Guo J, Weisel RD, et al. Mast cells promote proliferation and migration and inhibit differentiation of mesenchymal stem cells through PDGF. *J Mol Cell Cardiol.* (2016) 94:32–42. doi: 10.1016/j.yjmcc.2016.03.007
63. Xia Y, Lee K, Li N, Corbett D, Mendoza L, Frangogiannis NG. Characterization of the inflammatory and fibrotic response in a mouse model of cardiac pressure overload. *Histochem Cell Biol.* (2009) 131:471–81. doi: 10.1007/s00418-008-0541-5
64. Adiarto S, Heiden S, Vignon-Zellweger N, Nakayama K, Yagi K, Yanagisawa M, et al. ET-1 from endothelial cells is required for complete angiotensin II-induced cardiac fibrosis and hypertrophy. *Life Sci.* (2012) 91:651–7. doi: 10.1016/j.lfs.2012.02.006
65. Widyantoro B, Emoto N, Nakayama K, Anggrahini DW, Adiarto S, Iwasa N, et al. Endothelial cell-derived endothelin-1 promotes cardiac fibrosis in diabetic hearts through stimulation of endothelial-to-mesenchymal transition. *Circulation.* (2010) 121:2407–18. doi: 10.1161/CIRCULATIONAHA.110.938217
66. Salvador AM, Nevers T, Velázquez F, Aronovitz M, Wang B, Abadía MA, et al. Intercellular adhesion molecule 1 regulates left ventricular leukocyte infiltration, cardiac remodeling, and function in pressure overload-induced heart failure. *J Am Heart Assoc.* (2016) 5:e003126. doi: 10.1161/JAHA.115.003126
67. Wei H, Bedja D, Koitabashi N, Xing D, Chen J, Fox-Talbot K, et al. Endothelial expression of hypoxia-inducible factor 1 protects the murine heart and aorta from pressure overload by suppression of TGF-β signaling. *Proc Natl Acad Sci USA.* (2012) 109:E841–50. doi: 10.1073/pnas.1202081109
68. Frangogiannis NG, Mendoza LH, Lewallen M, Michael LH, Smith CW, Entman ML. Induction and suppression of interferon-inducible protein 10 in reperfused myocardial infarcts may regulate angiogenesis. *FASEB J.* (2001) 15:1428–30. doi: 10.1096/fj.00-0745fje
69. Rickard AJ, Morgan J, Bienvenu LA, Fletcher EK, Cranston GA, Shen JZ, et al. Cardiomyocyte mineralocorticoid receptors are essential for deoxycorticosterone/salt-mediated inflammation and cardiac fibrosis. *Hypertension.* (2012) 60:1443–50. doi: 10.1161/HYPERTENSIONAHA.112.203158
70. Koitabashi N, Danner T, Zaiman AL, Pinto YM, Rowell J, Mankowski J, et al. Pivotal role of cardiomyocyte TGF-β signaling in the murine pathological response to sustained pressure overload. *J Clin Invest.* (2011) 121:2301–12. doi: 10.1172/JCI44824
71. Ock S, Lee WS, Ahn J, Kim HM, Kang H, Kim HS, et al. Deletion of IGF-1 receptors in cardiomyocytes attenuates cardiac aging in male mice. *Endocrinology.* (2016) 157:336–45. doi: 10.1210/en.2015-1709
72. Kurisu S, Ozono R, Oshima T, Kambe M, Ishida T, Sugino H, et al. Cardiac angiotensin II type 2 receptor activates the kinin/NO system and inhibits fibrosis. *Hypertension.* (2003) 41:99–107. doi: 10.1161/01.HYP.0000050101.90932.14
73. Flevaris P, Khan SS, Eren M, Schuldt A, Shah SJ, Lee DC, et al. Plasminogen activator inhibitor type i controls cardiomyocyte transforming growth factor-β and cardiac fibrosis. *Circulation.* (2017) 136:664–79. doi: 10.1161/CIRCULATIONAHA.117.028145
74. Teufel A, Becker D, Weber SN, Dooley S, Breitkopf-Heinlein K, Maass T, et al. Identification of RARRES1 as a core regulator in liver fibrosis. *J Mol Med.* (2012) 90:1439–47. doi: 10.1007/s00109-012-0919-7
75. Frangogiannis NG. Chemokines in the ischemic myocardium: from inflammation to fibrosis. *Inflamm Res.* (2004) 53:585–95. doi: 10.1007/s00011-004-1298-5
76. Weber KT, Sun Y, Bhattacharya SK, Ahokas RA, Gerling IC. Myofibroblast-mediated mechanisms of pathological remodelling of the heart. *Nat Rev Cardiol.* (2013) 10:15–26. doi: 10.1038/nrcardio.2012.158
77. Hokimoto S, Yasue H, Fujimoto K, Yamamoto H, Nakao K, Kaikita K, et al. Expression of angiotensin-converting enzyme in remaining viable myocytes of human ventricles after myocardial infarction. *Circulation.* (1996) 94:1513–8. doi: 10.1161/01.CIR.94.7.1513
78. Crabos M, Roth M, Hahn AW, Erne P. Characterization of angiotensin II receptors in cultured adult rat cardiac fibroblasts. Coupling to signaling systems and gene expression. *J Clin Invest.* (1994) 93:2372–8. doi: 10.1172/JCI117243
79. Schorb W, Booz GW, Dostal DE, Conrad KM, Chang KC, Baker KM. Angiotensin II is mitogenic in neonatal rat cardiac fibroblasts. *Circ Res.* (1993) 72:1245–54. doi: 10.1161/01.RES.72.6.1245
80. Sadoshima J, Izumo S. Molecular characterization of angiotensin II–induced hypertrophy of cardiac myocytes and hyperplasia of cardiac fibroblasts. Critical role of the AT1 receptor subtype. *Circ Res.* (1993) 73:413–23. doi: 10.1161/01.RES.73.3.413
81. Campbell SE, Katwa LC. Angiotensin II stimulated expression of transforming growth factor-beta1 in cardiac fibroblasts and myofibroblasts. *J Mol Cell Cardiol.* (1997) 29:1947–58. doi: 10.1006/jmcc.1997.0435
82. Schultz JJ, Witt SA, Glascock BJ, Nieman ML, Reiser PJ, Nix SL, et al. TGF-beta1 mediates the hypertrophic cardiomyocyte growth induced by angiotensin II. *J Clin Invest.* (2002) 109:787–96. doi: 10.1172/JCI0214190
83. Chen S, Evans T, Mukherjee K, Karmazyn M, Chakrabarti S. Diabetes-induced myocardial structural changes: role of endothelin-1 and its receptors. *J Mol Cell Cardiol.* (2000) 32:1621–9. doi: 10.1006/jmcc.2000.1197
84. Dashwood MR, Abraham D. Endothelin: from bench to bedside and back. *Pharmacol Res.* (2011) 63:445–7. doi: 10.1016/j.phrs.2011.04.005
85. Singh AD, Amit S, Kumar OS, Rajan M, Mukesh N. Cardioprotective effects of bosentan, a mixed endothelin type A and B receptor antagonist, during myocardial ischaemia and reperfusion in rats. *Basic Clin Pharmacol Toxicol.* (2006) 98:604–10. doi: 10.1111/j.1742-7843.2006.pto_405.x
86. Schiller M, Javelaud D, Mauviel A. TGF-beta-induced SMAD signaling and gene regulation: consequences for extracellular matrix remodeling and wound healing. *J Dermatol Sci.* (2004) 35:83–92. doi: 10.1016/j.jdermsci.2003.12.006
87. Kapur NK, Wilson S, Yunis AA, Qiao X, Mackey E, Paruchuri V, et al. Reduced endoglin activity limits cardiac fibrosis and improves survival in heart failure. *Circulation.* (2012) 125:2728–38. doi: 10.1161/CIRCULATIONAHA.111.080002
88. Zhao XY, Zhao LY, Zheng QS, Su JL, Guan H, Shang FJ, et al. Chymase induces profibrotic response *via* transforming growth factor-beta 1/Smad activation in rat cardiac fibroblasts. *Mol Cell Biochem.* (2008) 310:159–66. doi: 10.1007/s11010-007-9676-2
89. Dobaczewski M, Gonzalez-Quesada C, Frangogiannis NG. The extracellular matrix as a modulator of the inflammatory and reparative response following myocardial infarction. *J Mol Cell Cardiol.* (2010) 48:504–11. doi: 10.1016/j.yjmcc.2009.07.015
90. Gallini R, Lindblom P, Bondjers C, Betsholtz C, Andrae J. PDGF-A and PDGF-B induces cardiac fibrosis in transgenic mice. *Exp Cell Res.* (2016) 349:282–90. doi: 10.1016/j.yexcr.2016.10.022
91. Pontén A, Li X, Thorén P, Aase K, Sjöblom T, Ostman A, et al. Transgenic overexpression of platelet-derived growth factor-C in the mouse heart induces cardiac fibrosis, hypertrophy, and dilated cardiomyopathy. *Am J Pathol.* (2003) 163:673–82. doi: 10.1016/S0002-9440(10)63694-2
92. Pontén A, Folestad EB, Pietras K, Eriksson U. Platelet-derived growth factor D induces cardiac fibrosis and proliferation of vascular smooth muscle cells in heart-specific transgenic mice. *Circ Res.* (2005) 97:1036–45. doi: 10.1161/01.RES.0000190590.31545.d4
93. Chen Y, Surinkaew S, Naud P, Qi XY, Gillis MA, Shi YF, et al. JAK-STAT signalling and the atrial fibrillation promoting fibrotic substrate. *Cardiovasc Res.* (2017) 113:310–20. doi: 10.1093/cvr/cvx004

94. Leask A. Potential therapeutic targets for cardiac fibrosis: TGFbeta, angiotensin, endothelin, CCN2, and PDGF, partners in fibroblast activation. *Circ Res.* (2010) 106:1675–80. doi: 10.1161/CIRCRESAHA.110.217737
95. Liao CH, Akazawa H, Tamagawa M, Ito K, Yasuda N, Kudo Y, et al. Cardiac mast cells cause atrial fibrillation through PDGF-A-mediated fibrosis in pressure-overloaded mouse hearts. *J Clin Invest.* (2010) 120:242–53. doi: 10.1172/JCI39942
96. Horiuchi T, Mitoma H, Harashima S, Tsukamoto H, Shimoda T. Transmembrane TNF-alpha: structure, function and interaction with anti-TNF agents. *Rheumatology.* (2010) 49:1215–28. doi: 10.1093/rheumatology/keq031
97. Hamid T, Gu Y, Ortines RV, Bhattacharya C, Wang G, Xuan YT, et al. Divergent tumor necrosis factor receptor-related remodeling responses in heart failure: role of nuclear factor-kappaB and inflammatory activation. *Circulation.* (2009) 119:1386–97. doi: 10.1161/CIRCULATIONAHA.108.802918
98. Frangogiannis NG. Cardiac fibrosis: cell biological mechanisms, molecular pathways and therapeutic opportunities. *Mol Aspects Med.* (2019) 65:70–99. doi: 10.1016/j.mam.2018.07.001
99. Valiente-Alandi I, Potter SJ, Salvador AM, Schafer AE, Schips T, Carrillo-Salinas F, et al. Inhibiting fibronectin attenuates fibrosis and improves cardiac function in a model of heart failure. *Circulation.* (2018) 138:1236–52. doi: 10.1161/CIRCULATIONAHA.118.034609
100. Mihara M, Hashizume M, Yoshida H, Suzuki M, Shiina M. IL-6/IL-6 receptor system and its role in physiological and pathological conditions. *Clin Sci.* (2012) 122:143–59. doi: 10.1042/CS20110340
101. Choy EH, De Benedetti F, Takeuchi T, Hashizume M, John MR, Kishimoto T. Translating IL-6 biology into effective treatments. *Nat Rev Rheumatol.* (2020) 16:335–45. doi: 10.1038/s41584-020-0419-z
102. Chou CH, Hung CS, Liao CW, Wei LH, Chen CW, Shun CT, et al. IL-6 trans-signalling contributes to aldosterone-induced cardiac fibrosis. *Cardiovasc Res.* (2018) 114:690–702. doi: 10.1093/cvr/cvy013
103. Eid RA, Alkhateeb MA, El-Kott AF, Eleawa SM, Zaki M, Alaboodi SA, et al. A high-fat diet rich in corn oil induces cardiac fibrosis in rats by activating JAK2/STAT3 and subsequent activation of ANG II/TGF-1β/Smad3 pathway: the role of ROS and IL-6 trans-signaling. *J Food Biochem.* (2019) 43:e12952. doi: 10.1111/jfbc.12952
104. Kumar S, Wang G, Zheng N, Cheng W, Ouyang K, Lin H, et al. HIMF (hypoxia-induced mitogenic factor)-IL (Interleukin)-6 signaling mediates cardiomyocyte-fibroblast crosstalk to promote cardiac hypertrophy and fibrosis. *Hypertension.* (2019) 73:1058–70. doi: 10.1161/HYPERTENSIONAHA.118.12267
105. Shimojo N, Hashizume R, Kanayama K, Hara M, Suzuki Y, Nishioka T, et al. Tenascin-C may accelerate cardiac fibrosis by activating macrophages *via* the integrin αVβ3/nuclear factor-κB/interleukin-6 axis. *Hypertension.* (2015) 66:757–66. doi: 10.1161/HYPERTENSIONAHA.115.06004
106. Travers JG, Kamal FA, Robbins J, Yutzey KE, Blaxall BC. Cardiac fibrosis: the fibroblast awakens. *Circ Res.* (2016) 118:1021–40. doi: 10.1161/CIRCRESAHA.115.306565
107. Vandergriff A, Huang K, Shen D, Hu S, Hensley MT, Caranasos TG, et al. Targeting regenerative exosomes to myocardial infarction using cardiac homing peptide. *Theranostics.* (2018) 8:1869–78. doi: 10.7150/thno.20524
108. Han C, Zhou J, Liang C, Liu B, Pan X, Zhang Y, et al. Human umbilical cord mesenchymal stem cell derived exosomes encapsulated in functional peptide hydrogels promote cardiac repair. *Biomater Sci.* (2019) 7:2920–33. doi: 10.1039/C9BM00101H
109. Raposo G, Tenza D, Mecheri S, Peronet R, Bonnerot C, Desaymard C. Accumulation of major histocompatibility complex class II molecules in mast cell secretory granules and their release upon degranulation. *Mol Biol Cell.* (1997) 8:2631–45. doi: 10.1091/mbc.8.12.2631
110. Li N, Rochette L, Wu Y, Rosenblatt-Velin N. New insights into the role of exosomes in the heart after myocardial infarction. *J Cardiovasc Transl Res.* (2019) 12:18–27. doi: 10.1007/s12265-018-9831-z
111. Barile L, Moccetti T, Marbán E, Vassalli G. Roles of exosomes in cardioprotection. *Eur Heart J.* (2017) 38:1372–79. doi: 10.1093/eurheartj/ehw304
112. Hosseini-Beheshti E, Pham S, Adomat H, Li N, Tomlinson GE. Exosomes as biomarker enriched microvesicles: characterization of exosomal proteins derived from a panel of prostate cell lines with distinct AR phenotypes. *Mol Cell Proteomics.* (2012) 11:863–85. doi: 10.1074/mcp.M111.014845
113. Skotland T, Sandvig K, Llorente A. Lipids in exosomes: current knowledge and the way forward. *Prog Lipid Res.* (2017) 66:30–41. doi: 10.1016/j.plipres.2017.03.001
114. Gao XF, Wang ZM, Wang F, Gu Y, Zhang JJ, Chen SL. Exosomes in coronary artery disease. *Int J Biol Sci.* (2019) 15:2461–70. doi: 10.7150/ijbs.36427
115. Konoshenko MY, Lekchnov EA, Vlassov AV, Laktionov PP. Isolation of extracellular vesicles: general methodologies and latest trends. *Biomed Res Int.* (2018) 2018:8545347. doi: 10.1155/2018/8545347
116. Turturici G, Tinnirello R, Sconzo G, Geraci F. Extracellular membrane vesicles as a mechanism of cell-to-cell communication: advantages and disadvantages. *Am J Physiol Cell Physiol.* (2014) 306:C621–33. doi: 10.1152/ajpcell.00228.2013
117. Tian C, Gao L, Zimmerman MC, Zucker IH. Myocardial infarction-induced microRNA-enriched exosomes contribute to cardiac Nrf2 dysregulation in chronic heart failure. *Am J Physiol Heart Circ Physiol.* (2018) 314:H928–39. doi: 10.1152/ajpheart.00602.2017
118. Wang B, Wang ZM, Ji JL, Gan W, Zhang A, Shi HJ, et al. Macrophage-Derived exosomal Mir-155 regulating cardiomyocyte pyroptosis and hypertrophy in uremic cardiomyopathy. *JACC Basic Transl Sci.* (2020) 5:148–66. doi: 10.1016/j.jacbts.2019.10.011
119. Gollmann-Tepeköylü C, Pölzl L, Graber M, Hirsch J, Nägele F, Lobenwein D, et al. miR-19a-3p containing exosomes improve function of ischaemic myocardium upon shock wave therapy. *Cardiovasc Res.* (2020) 116:1226–36. doi: 10.1093/cvr/cvz209
120. Lin F, Zeng Z, Song Y, Li L, Wu Z, Zhang X, et al. YBX-1 mediated sorting of miR-133 into hypoxia/reoxygenation-induced EPC-derived exosomes to increase fibroblast angiogenesis and MEndoT. *Stem Cell Res Ther.* (2019) 10:263. doi: 10.1186/s13287-019-1377-8
121. Liu W, Zhang H, Mai J, Chen Z, Huang T, Wang S, et al. Distinct anti-fibrotic effects of exosomes derived from endothelial colony-forming cells cultured under normoxia and hypoxia. *Med Sci Monit.* (2018) 24:6187–99. doi: 10.12659/MSM.911306
122. Chaturvedi P, Kalani A, Medina I, Familtseva A, Tyagi SC. Cardiosome mediated regulation of MMP9 in diabetic heart: role of mir29b and mir455 in exercise. *J Cell Mol Med.* (2015) 19:2153–61. doi: 10.1111/jcmm.12589
123. Yuan J, Liu H, Gao W, Zhang L, Ye Y, Yuan L, et al. MicroRNA-378 suppresses myocardial fibrosis through a paracrine mechanism at the early stage of cardiac hypertrophy following mechanical stress. *Theranostics.* (2018) 8:2565–82. doi: 10.7150/thno.22878
124. Yang J, Yu X, Xue F, Li Y, Liu W, Zhang S. Exosomes derived from cardiomyocytes promote cardiac fibrosis *via* myocyte-fibroblast cross-talk. *Am J Transl Res.* (2018) 10:4350–66.
125. Yu B, Kim HW, Gong M, Wang J, Millard RW, Wang Y, et al. Exosomes secreted from GATA-4 overexpressing mesenchymal stem cells serve as a reservoir of anti-apoptotic microRNAs for cardioprotection. *Int J Cardiol.* (2015) 182:349–60. doi: 10.1016/j.ijcard.2014.12.043
126. Zhu J, Lu K, Zhang N, Zhao Y, Ma Q, Shen J, et al. Myocardial reparative functions of exosomes from mesenchymal stem cells are enhanced by hypoxia treatment of the cells *via* transferring microRNA-210 in an nSMase2-dependent way. *Artif Cells Nanomed Biotechnol.* (2018) 46:1659–70. doi: 10.1080/21691401.2017.1388249
127. Feng Y, Huang W, Wani M, Yu X, Ashraf M. Ischemic preconditioning potentiates the protective effect of stem cells through secretion of exosomes by targeting Mecp2 *via* miR-22. *PLoS ONE.* (2014) 9:e88685. doi: 10.1371/journal.pone.0088685
128. Shao L, Zhang Y, Pan X, Liu B, Liang C, Zhang Y, et al. Knockout of beta-2 microglobulin enhances cardiac repair by modulating exosome imprinting and inhibiting stem cell-induced immune rejection. *Cell Mol Life Sci.* (2020) 77:937–52. doi: 10.1007/s00018-019-03220-3
129. Wang B, Zhang A, Wang H, Klein JD, Tan L, Wang ZM, et al. miR-26a limits muscle wasting and cardiac fibrosis through exosome-mediated microRNA transfer in chronic kidney disease. *Theranostics.* (2019) 9:1864–77. doi: 10.7150/thno.29579
130. Bier A, Berenstein P, Kronfeld N, Morgoulis D, Ziv-Av A, Goldstein H, et al. Placenta-derived mesenchymal stromal cells and their exosomes exert

therapeutic effects in duchenne muscular dystrophy. *Biomaterials.* (2018) 174:67–78. doi: 10.1016/j.biomaterials.2018.04.055
131. Ibrahim A, Li C, Rogers R, Fournier M, Li L, Vaturi SD, et al. Augmenting canonical Wnt signalling in therapeutically inert cells converts them into therapeutically potent exosome factories. *Nat Biomed Eng.* (2019) 3:695–705. doi: 10.1038/s41551-019-0448-6
132. Luo Q, Guo D, Liu G, Chen G, Hang M, Jin M. Exosomes from MiR-126-Overexpressing adscs are therapeutic in relieving acute myocardial ischaemic injury. *Cell Physiol Biochem.* (2017) 44:2105–16. doi: 10.1159/000485949
133. Izarra A, Moscoso I, Levent E, Cañón S, Cerrada I, Díez-Juan A, et al. miR-133a enhances the protective capacity of cardiac progenitors cells after myocardial infarction. *Stem Cell Rep.* (2014) 3:1029–42. doi: 10.1016/j.stemcr.2014.10.010
134. Milano G, Biemmi V, Lazzarini E, Balbi C, Ciullo A, Bolis S, et al. Intravenous administration of cardiac progenitor cell-derived exosomes protects against doxorubicin/trastuzumab-induced cardiac toxicity. *Cardiovasc Res.* (2020) 116:383–92. doi: 10.1093/cvr/cvz108
135. Pan J, Alimujiang M, Chen Q, Shi H, Luo X. Exosomes derived from miR-146a-modified adipose-derived stem cells attenuate acute myocardial infarction-induced myocardial damage *via* downregulation of early growth response factor 1. *J Cell Biochem.* (2019) 120:4433–43. doi: 10.1002/jcb.27731
136. Wang L, Liu J, Xu B, Liu YL, Liu Z. Reduced exosome miR-425 and miR-744 in the plasma represents the progression of fibrosis and heart failure. *Kaohsiung J Med Sci.* (2018) 34:626–33. doi: 10.1016/j.kjms.2018.05.008
137. Kang JY, Park H, Kim H, Mun D, Park H, Yun N, et al. Human peripheral blood-derived exosomes for microRNA delivery. *Int J Mol Med.* (2019) 43:2319–28. doi: 10.3892/ijmm.2019.4202
138. Cai L, Chao G, Li W, Zhu J, Li F, Qi B, et al. Activated CD4(+) T cells-derived exosomal miR-142-3p boosts post-ischemic ventricular remodeling by activating myofibroblast. *Aging.* (2020) 12:7380–96. doi: 10.18632/aging.103084
139. Wang X, Gu H, Huang W, Peng J, Li Y, Yang L, et al. Hsp20-Mediated activation of exosome biogenesis in cardiomyocytes improves cardiac function and angiogenesis in diabetic mice. *Diabetes.* (2016) 65:3111–28. doi: 10.2337/db15-1563
140. Datta R, Bansal T, Rana S, Datta K, Datta CR, Chawla-Sarkar M, et al. Myocyte-Derived Hsp90 modulates collagen upregulation *via* biphasic activation of STAT-3 in fibroblasts during cardiac hypertrophy. *Mol Cell Biol.* (2017) 37:e00611–16. doi: 10.1128/MCB.00611-16
141. Kuo HF, Hsieh CC, Wang SC, Chang CY, Hung CH, Kuo PL, et al. Simvastatin attenuates cardiac fibrosis *via* regulation of cardiomyocyte-derived exosome secretion. *J Clin Med.* (2019) 8:794. doi: 10.3390/jcm8060794
142. Yang J, Yu XF, Li YY, Xue FT, Zhang S. Decreased HSP70 expression on serum exosomes contributes to cardiac fibrosis during senescence. *Eur Rev Med Pharmacol Sci.* (2019) 23:3993–4001. doi: 10.26355/eurrev_201905_17829
143. Wang X, Chen Y, Zhao Z, Meng Q, Yu Y, Sun J, et al. Engineered exosomes with ischemic myocardium-targeting peptide for targeted therapy in myocardial infarction. *J Am Heart Assoc.* (2018) 7:e008737. doi: 10.1161/JAHA.118.008737
144. Govindappa PK, Patil M, Garikipati V, Verma SK, Saheera S, Narasimhan G, et al. Targeting exosome-associated human antigen R attenuates fibrosis and inflammation in diabetic heart. *FASEB J.* (2020) 34:2238–51. doi: 10.1096/fj.201901995R
145. Działo E, Rudnik M, Koning RI, Czepiel M, Tkacz K, Baj-Krzyworzeka M, et al. WNT3a and WNT5a transported by exosomes activate wnt signaling pathways in human cardiac fibroblasts. *Int J Mol Sci.* (2019) 20:1436. doi: 10.3390/ijms20061436
146. Thum T, Gross C, Fiedler J, Fischer T, Kissler S, Bussen M, et al. MicroRNA-21 contributes to myocardial disease by stimulating MAP kinase signalling in fibroblasts. *Nature.* (2008) 456:980–4. doi: 10.1038/nature07511
147. Nie X, Fan J, Li H, Yin Z, Zhao Y, Dai B, et al. miR-217 promotes cardiac hypertrophy and dysfunction by targeting PTEN. *Mol Ther Nucleic Acids.* (2018) 12:254–66. doi: 10.1016/j.omtn.2018.05.013
148. Richter K, Haslbeck M, Buchner J. The heat shock response: life on the verge of death. *Mol Cell.* (2010) 40:253–66. doi: 10.1016/j.molcel.2010.10.006
149. Fan GC, Kranias EG. Small heat shock protein 20 (HspB6) in cardiac hypertrophy and failure. *J Mol Cell Cardiol.* (2011) 51:574–7. doi: 10.1016/j.yjmcc.2010.09.013
150. Laeremans H, Hackeng TM, van Zandvoort MA, Thijssen VL, Janssen BJ, Ottenheijm HC, et al. Blocking of frizzled signaling with a homologous peptide fragment of wnt3a/wnt5a reduces infarct expansion and prevents the development of heart failure after myocardial infarction. *Circulation.* (2011) 124:1626–35. doi: 10.1161/CIRCULATIONAHA.110.976969
151. Blyszczuk P, Müller-Edenborn B, Valenta T, Osto E, Stellato M, Behnke S, et al. Transforming growth factor-β-dependent Wnt secretion controls myofibroblast formation and myocardial fibrosis progression in experimental autoimmune myocarditis. *Eur Heart J.* (2017) 38:1413–25. doi: 10.1093/eurheartj/ehw116
152. Abraityte A, Vinge LE, Askevold ET, Lekva T, Michelsen AE, Ranheim T, et al. Wnt5a is elevated in heart failure and affects cardiac fibroblast function. *J Mol Med.* (2017) 95:767–77. doi: 10.1007/s00109-017-1529-1

Conflict of Interest: The authors declare that the research was conducted in the absence of any commercial or financial relationships that could be construed as a potential conflict of interest.

Publisher's Note: All claims expressed in this article are solely those of the authors and do not necessarily represent those of their affiliated organizations, or those of the publisher, the editors and the reviewers. Any product that may be evaluated in this article, or claim that may be made by its manufacturer, is not guaranteed or endorsed by the publisher.

frontiers in Cardiovascular Medicine

ORIGINAL RESEARCH
published: 19 August 2021
doi: 10.3389/fcvm.2021.713021

Human Umbilical Cord Mesenchymal Stem Cell Derived Exosomes Delivered Using Silk Fibroin and Sericin Composite Hydrogel Promote Wound Healing

*Chaoshan Han†, Feng Liu†, Yu Zhang†, Wenjie Chen, Wei Luo, Fengzhi Ding, Lin Lu, Chengjie Wu and Yangxin Li**

Department of Cardiovascular Surgery, Institute for Cardiovascular Science, Collaborative Innovation Center of Hematology, First Affiliated Hospital and Medical College of Soochow University, Suzhou, China

OPEN ACCESS

Edited by:
Zhongjian Cheng, Temple University, United States

Reviewed by:
Xiangyang Guo, Emory University, United States
Congwen Yang, Third Military Medical University, China

***Correspondence:**
Yangxin Li
yangxin_li@yahoo.com

†These authors have contributed equally to this work

Specialty section:
This article was submitted to Cardiovascular Biologics and Regenerative Medicine, a section of the journal Frontiers in Cardiovascular Medicine

Received: *21 May 2021*
Accepted: *26 July 2021*
Published: *19 August 2021*

Citation:
Han C, Liu F, Zhang Y, Chen W, Luo W, Ding F, Lu L, Wu C and Li Y (2021) Human Umbilical Cord Mesenchymal Stem Cell Derived Exosomes Delivered Using Silk Fibroin and Sericin Composite Hydrogel Promote Wound Healing. Front. Cardiovasc. Med. 8:713021. doi: 10.3389/fcvm.2021.713021

Recent studies have shown that the hydrogels formed by composite biomaterials are better choice than hydrogels formed by single biomaterial for tissue repair. We explored the feasibility of the composite hydrogel formed by silk fibroin (SF) and silk sericin (SS) in tissue repair for the excellent mechanical properties of SF, and cell adhesion and biocompatible properties of SS. In our study, the SF SS hydrogel was formed by SF and SS protein with separate extraction method (LiBr dissolution for SF and hot alkaline water dissolution for SS), while SF-SS hydrogel was formed by SF and SS protein using simultaneous extraction method (LiBr dissolution for SF and SS protein). The effects of the two composite hydrogels on the release of inflammatory cytokines from macrophages and the wound were analyzed. Moreover, two hydrogels were used to encapsulate and deliver human umbilical cord mesenchymal stem cell derived exosomes (UMSC-Exo). Both SF SS and SF-SS hydrogels promoted wound healing, angiogenesis, and reduced inflammation and TNF-α secretion by macrophages. These beneficial effects were more significant in the experimental group treated by UMSC-Exo encapsulated in SF-SS hydrogel. Our study found that SF-SS hydrogel could be used as an excellent alternative to deliver exosomes for tissue repair.

Keywords: silk fibroin and sericin composite hydrogel, exosome, wound repair, angiogenesis, inflammation

INTRODUCTION

As the biggest organ, skin functions as a barrier to protect the body from pathogen invasion and to prevent fluid loss. However, skin often suffers from injuries caused by burns, diabetes, and ulceration, which cause infections, as well as physical and mental pain of the individual (1). Many ongoing research efforts have been focused on developing methods to promote wound healing. Those method should keep the wound from being infected and allow gas exchange, adsorb excrescent wound exudates and maintain the local moisture of the wound to accelerate the healing (2). Recently, stem cell and exosomes have emerged as promising strategies for skin repair. Exosomes are 30–100 nm extracellular vesicles that can be secreted by almost all cells, and stem cell-derived exosomes have been shown to accelerate the healing of skin wound (3). Exosomes

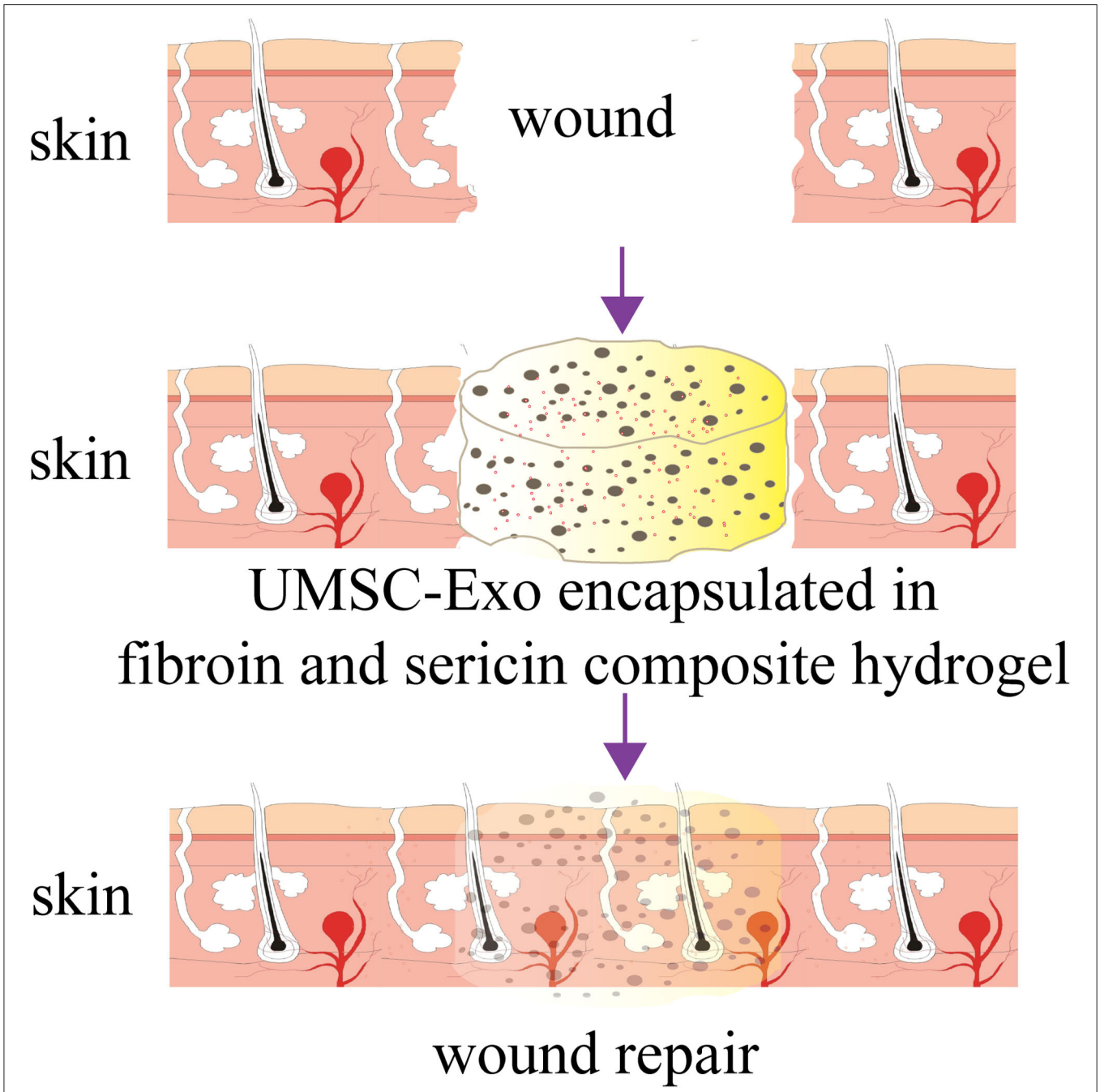

GRAPHICAL ABSTRACT | The composite hydrogel formed by SF and SS did not induces strong immune responses and improved the beneficial effect of the UMSC-Exo by promoting angiogenesis and the wound repair. The composite hydrogel can serve as an excellent media for exosomes delivery and tissue repair.

derived from the human umbilical cord mesenchymal stem cells (UMSC-Exo) have been shown to promote re-epithelialization, enhance collagen maturation and reduce the scar size of skin wound. In addition to UMSC-Exo, exosomes secreted by pluripotent stem cells-derived MSCs, intestinal epithelial cells, oral mucosal epithelial cell, adipose stem cells, induced pluripotent stem cells and platelet (3–8) could also promote skin wound healing. Although these previous studies proved the concept of principal, there are still hurdles that need to be overcome before exosome-based therapy can be used in the clinic. Exosomes have short retention time *in vivo* due to the lack of matrix support. In addition, exosomes often present in solution, which is not able to protect the wound from the pathogenic bacteria, and not absorb excrescent exudates, so exosomes must be delivered together with wound dressing materials to achieve the desired beneficial effects.

Hydrogels have been used as excellent wound dressing (9, 10). Hydrogels can be formed by natural, synthetic or composite materials. Single material-based hydrogel has some drawbacks for the lack of either biological function or good mechanical properties, whereas the composite hydrogel formed by two or more materials can avoid these defects. Silk, an appealing biomaterial that was widely used in medical field, is consisted of 70% silk fibroin (SF), 25% Silk sericin (SS). SF has been used as suture thread and wound dressing for its good biocompatibility and suitable mechanical properties (11–15). The biological properties of SF can be improved when introduce other materials such as chitosan, polyurethane, hyaluronic acid (15–18). Even though SS was originally thought to trigger immune response and was treated as the by-product in traditional silk biomaterial processing (19). Recent studies have shown that SS is biocompatible and has good biological performance. SS shows great hydrophilic and has multiple biological properties, including anti-oxidation, anti-bacterial, and promoting cell adhesion and proliferation (20, 21). However, SS shows poor mechanical properties. It was shown that the Young's moduli of SS hydrogel are much lower than that of most tissues (22). Thus, SS has been mostly used in tissue regeneration and wound repair in combination with other materials (10, 23, 24). It's an interesting find that SF has an opposite characteristic that Young's moduli of SF hydrogel have a higher stiffness than native tissue (25).

Thus, introducing SS into the fibroin hydrogel can adjust the compressive moduli to a more suitable condition for tissue engineering. More importantly, sericin has the beneficial characteristics to promote cell adhesion and growth (26). In addition, the different hydrophilic and hydrophobic nature of sericin and fibroin of the complex hydrogel enables sericin to be exposed to the water, which makes it easier for sericin to interact with surrounding tissue and to exert its beneficial effect.

Thus, in our study, we explored the immunogenicity of the composite hydrogel formed by SF and SS and determined whether the composite hydrogel can deliver UMSC-Exo to repair skin wound.

MATERIALS AND METHODS

Isolation and Identification of Exosomes

The exosomes derived from the human umbilical cord mesenchymal stem cells (UMSCs) were isolated and collected as described previously (27, 28). Briefly, UMSCs (Jiangsu Heze Biotechnology, Heze, Jiangsu, China) were cultured in MEM medium containing 15% FBS and cells of passage 4–6 were digested by 0.125% (w/v) trypsin (Thermo fisher, Waltham, MA, USA) and the cell suspension was transferred to a new 10 cm cell culture dish, until reaching to 70% confluency and was then replaced by MEM medium containing 10% FBS which had been centrifuged at 100,000 g to eliminate bovine-derived exosomes. After 48 h of culture, exosomes were isolated from UMSCs culture supernatants which was centrifuged at 2,000 g for 30 min to remove dead cells and debris, and then centrifuged at 10,000 g for 40 min to remove large extracellular vesicles, then the medium was transferred to a new tube containing 0.5 volumes of Total Exosome Isolation reagent (Life Technology, Grand Island, NY, USA). The mixture was incubated at 4°C overnight and centrifuged at 10,000 g for 1 h at 4°C. The pellets were re-suspended in PBS and stored at −80°C. Protein concentrations of UMSC-Exo were determined using a BCA protein assay kit (Takara, Japan).

The diameter of UMSC-Exo was analyzed by Zetasizer Nano (Malvern Panalytical, Malvern, UK). Exosomes (1 mL) with a concentration of 1 mg/mL were placed in a quartz colorimetric dish for subsequent measurement. Specific protein markers of exosomes were identified by Western blot and flow cytometry as we reported previously (27, 28). Briefly, 40 μg protein extracted from UMSC-Exo or UMSCs protein was separated by SDS-PAGE, transferred to PVDF membranes which were incubated with CD63 (Santa cruz biotechnology, Texas, USA), CD9 (Abcam, Cambridge, MA, USA), Glyceraldehyde 3-phosphate dehydrogenase (GAPDH) (MultiSciences, Hangzhou, China) antibodies, followed by washing and incubation with HRP-linked goat anti-rabbit IgG (MultiSciences, Hangzhou, China) and HRP-linked goat anti-mouse IgG secondary antibodies (MultiSciences, Hangzhou, China). Exosomes were attached to aldehyde/sulfate latex beads (4 μm; Invitrogen, Grand Island, NY, USA) for analysis. The pre-bound exosomes were analyzed by flow cytometry using a fluorescence isothiocyanate-conjugated antibody against CD63 (Abcam, Cambridge, MA, USA), which is a specific marker for exosomes.

Preparation of SF SS Hydrogel

The separate extraction of SF and SS (SF SS) from silkworm (*Dazao* strain) cocoons were performed as described previously. Briefly, 5 g silkworm cocoons were cut into 1 cm^2 pieces and boiled in 1 L 0.02 M Na_2CO_3 solution (Macklin, Shanghai, China) for 30 min with continuous stirring in order to disperse SF and allow SS to be dissolved. SS was obtained by concentration and dialysis of the harvested solution. The SS solution was finally adjusted to 5% w/v with ultrapure water at room temperature. After washing in ultra-pure water to remove the remaining SS protein, the drying SF was extracted as described before (29). Briefly, the SF was dissolved in 9.3 M LiBr (Thermo Scientific, Waltham, MA, USA) and SF solution was load in ordinary dialysis bag (YuanyeBio-Technology, Shanghai, China) with cut-off molecular weight of 3,500 and dialyzed in ultrapure water for 48 h, then centrifuged to remove precipitates. The SF solution was finally adjusted to 5% (w/v) with ultrapure water and stored at 4°C for up to one week. The concentration of SF or SS solution was determined by the measuring dry weight of SF or SS after drying the entire content of the solution. In order to ensure the similar proportion of SF and SS in SF SS and SF-SS hydrogel, we measured the SF and SS in natural silk, the dried weight of SF was 3.71g after removing the SS from 5 g silk, so the content of fibroin was 74.2% (3.71 g ÷ 5 g × 100% = 74.2%). Considering the fact that there is about 3.2% carbohydrates, inorganic matter and pigment dissolved in the SS solution, the content of sericin in silk is 22.6% (100%−74.2%−3.2% = 22.6%). The proportion of SF to SS is about 3:1 in natural silk, which is similar to that of SF-SS hydrogel. The volume ratio of SF solution to SS solution was 3:1, which is consistent with that of the natural silk. The mixed

solution (0.5 ml) was sonicated 3 times for 30 s at 30% ultrasound intensity (S150D, Branson, St. Louis MO, USA), and then the pre-gelling SF SS mixed solution was transferred to the molds with a diameter of 1.2 cm to ensure the hydrogel has a height of 3 mm, and then kept at 37°C for 24 h to form SF SS hydrogel.

Preparation of SF-SS Hydrogel

The simultaneous extraction of SF and SS (SF-SS) from silkworm cocoons were performed using a LiBr dissolution as previously described (30). Briefly, 5 g silkworm cocoons were cut into 1 cm^2 pieces and was dissolved in 9.3 M LiBr to make a 20% (w/v) protein solution and then incubated at 60°C to completely dissolve the SF and SS. After dialysis and concentration, the SF-SS solution was finally adjusted to 5% (w/v) with ultrapure water at room temperature and stored at 4°C for no more than one week. The mixed SF-SS protein solution was sonicated 1 times for 30 s at 30% ultrasound intensity, and then the pre-gelling SF-SS solution was transferred to the suitable molds, and kept at 37°C for 1 h to form the SF-SS hydrogel.

Exosomes Encapsulated Into the SF SS or SF-SS Hydrogel

SF SS hydrogel or SF-SS hydrogel were frozen in −20°C freezer, and then freeze-dried for 48 h in freeze dryer to generate hydrogel sponge. Exosomes derived from UMSCs were isolated and the concentration was measured as described in 2.1. Exosomes concentration would be adjusted to 2 mg/mL and 50 μL exosomes will be dropped into the hydrogel sponge and it will be used for wound repair immediately. The hydrogel sponge lost most of water and it will hold the exosome solution.

Cell Proliferation Assay

The human skin fibroblast cells (BJ cells) were purchased from ATCC (Maryland, USA). The BJ cells were cultured in DMEM to reach 70–80% confluency in 96-well plates and then switched to fresh DMEM. UMSC-Exo (100 or 200 μg), 5 μg freeze-dried SF SS hydrogel, 5 μg SF-SS hydrogel or sterile cotton gauze were added into different wells and then incubated with BJ cells for another 24 h. After removing the residual cotton gauze or the freeze-dried hydrogel, cell viability was determined using the CCK-8 reagent (MesGen Biotech, Shanghai, China) per manufacturer's instruction. In order to observe the cells proliferation directly, a white pipette tip was used to draw a straight line on the monolayer cells to create an open space when the BJ cells were cultured to reach 85–90% confluency in 96-well plates. The cells were washed 3 times with PBS to remove free floating cells formed by scratches. The sterile gauze or the freeze-dried SF SS and SF-SS hydrogel were added into the DMEM medium with 10% FBS and incubated with BJ cells. After 24 h co-culture, the cells were fixed and photographed under a microscope.

Fluorescence and Microstructure of Silk Fibroin and Sericin Mixed Hydrogel

In order to clearly observe the fluorescence characteristics of different hydrogel under a microscope, the thickness of the hydrogel was controlled to 0.5–1 mm. After freeze-drying, the spontaneous fluorescence under different fluorescence channels of an inverted fluorescence microscope is observed directly and recorded.

To reveal the morphology of the SF SS and SF-SS hydrogel, the samples were loaded on top of conductive tapes mounted on SEM sample stubs and sputter-coated with gold for 60 s using gold sputter-coating equipment (Cressington Scientific Instruments, Watford, UK). The samples were examined using a scanning electron microscope (S-4800; Hitachi, Japan) at an accelerating voltage of 3 kV.

Attenuated Total Reflection-Fourier Transform Infrared Spectroscopy (ATR-FTIR) Measurements

A VERTEX 70 FTIR spectrometer (Bruker, Hongkong, China) equipped with a diamond ATR accessory, a deuterated triglycine sulfate detector, and a KBr beam splitter was used for spectral acquisition. The freeze-dried samples were then placed on the diamond ATR crystal. For each sample, three replicate spectra were recorded to ensure the spectral reproducibility and analytical precision. All spectra were recorded in the range of 4,000–600 cm^{-1} using the ATR method with a resolution of 4 cm^{-1} and 32 scans.

Compressive Mechanical Property Testing

The SS and SF mixed solution was sonicated and loaded into the suitable mold to form a cylinder hydrogel with the diameter of 120 mm and the height of 150 mm. After freeze drying, hydrogel were tested by a universal material testing machine at room temperature. In compression test, the loading speed was 5 mm/min. When the sample was compressed to 60% of its original height, the loading was stopped. Each sample was tested three times.

Wound Closure Assay

Before the surgery, the C57BL/6J mice were anesthetized by intraperitoneal injection of sodium pentobarbital (45 mg/kg). After shaving the dorsal hairs and sterilizing the skin, a 10 mm diameter full-thickness wound was created on the upper back. The mice were randomly divided into five groups ($n = 6$/group). Control group: four layers cotton gauze (13 × 13 mm) containing 50 μL PBS were inserted into the skin layer near the skin defect to cover the wound. SF SS or SF-SS Hydrogel group: a freeze-dried hydrogel (13 × 13 mm) containing 50 μL PBS was used to cover the wound as the described in the control group. SF SS Hydrogel-Exosome or SF-SS Hydrogel-Exosome group: a freeze-dried hydrogel containing 100 μg exosomes in 50 μL PBS was used to cover the wound. The restraining bandage (Urgostrapping, URGO) was used to fix the wound and dressings. At 3 and 21 days post-surgery, 3 mice in each group were sacrificed for further analysis. The mice were maintained in a specific pathogen-free animal facility at Soochow University, and fed with sterile food and water. All animal experiments were carried out in accordance with the National Institutes of Health Guide for the Care and Use of Laboratory Animals (NIH Publications No. 8023, revised 1978). The animal protocols were approved by the Laboratory Animal Care and Use Committee of Soochow University.

Immunostaining for CD31 and CD68 Expression

To avoid skin contraction, complete wound specimens and the normal skin tissue within 2–3 mm around the wounds were collected on days 3 and 21 post-operation. The skin tissues were fixed overnight by 4% polyoxymethylene and then dehydrated by 20% sucrose. After embedding in optimal cutting temperature compound and freezing in liquid nitrogen, the specimens were cut into 5-μm sections for immunostaining. After blocking with 5% BSA, skin sections were incubated with a mouse anti-CD31 antibody (Abcam, Cambridge, MA, USA) or anti-CD68 antibody (Abcam), followed by a goat anti-mouse IgG-FITC secondary antibody (Santa Cruz Biotechnology, Texas, USA). The nuclei were stained with DAPI (Sigma-Aldrich, St. Louis, MO USA). Images were analyzed using fluorescent microscopy.

TNF-α Detection by ELISA

The macrophage NR8383 cells (Kang Lang Biological Technology, Shanghai, China) were used to assess the immune response induced by the SF SS or SF-SS hydrogel sponges. 2×10^5 NR8383 cells were seeded into each well of the plate 24-well plate. When the cells reached 75–85% confluency, freeze-dried SF SS, SF-SS hydrogel or cotton gauze were added into culture media and co-culture for 24 h, and then the culture media was harvested and centrifuged at 1,000 rpm for 5 min. TNF-α levels were detected by TNF-α ELISA kit (Abcam).

Blood samples were collected from the animals and the blood samples were placed at 37°C for 1 h and sera were obtained by centrifugation at 5,000 rpm for 5 min. The levels of TNF-α were determined by ELISA kit.

Statistical Analysis

All data with significance of differences were presented as mean ± standard deviation. Statistical analyses and calculation of sample size were performed using Prism 5 software (GraphPad Software, La Jolla, CA, USA). Two-tailed *t*-test was used to determine the significance of differences between two groups. Multiple comparisons were analyzed using ANOVA with post-*hoc* analysis by the Newman-Keuls test.

RESULTS

Isolation, Identification and Function of Exosomes Derived From Human Umbilical Cord Mesenchymal Stem Cells (UMSC-Exo)

In order to obtain pure and well-characterized exosome preparations, we used the commercial ready-to-use precipitation solutions and total exosome isolation reagent to separate exosomes from supernatants of cell culture. Cell debris and large vesicles were removed by centrifugation. The exosomes were characterized by Western blot, and Zetasizer Nano analysis. Western blot showed that GAPDH was highly expressed in the UMSC, whereas exosomes-specific markers CD9 and CD63 were only detected in UMSC-Exo (**Figure 1A**). Flow cytometry results further proved that more than 99% of the exosome-coated beads are CD63 positive (**Figure 1B**). We also found that CD63, which is a universal biomarker of exosomes, has a higher expression in UMSC-Exo. The diameter of exosomes was approximately 47.3 nm determined by Zetasizer Nano (**Figure 1C**), which is consisted with the previous reported value of 30–100nm. In addition, the cell viability of skin fibroblast was significantly enhanced in a dose dependent way when incubated with the exosomes with the concentration of 100 and 200 μg/ml (**Figure 1D**), which is consistent with previous study (31).

Silk Fibroin and Sericin Mixed Hydrogel Increase Skin Fibroblast Cell Viability and Proliferation

SF SS hydrogel was formed by SF and SS protein with separate extraction method (mild LiBr dissolution for SF and high temperature alkaline water method for SS), while SF-SS hydrogel was formed by SF and SS protein using simultaneous extraction method (mild LiBr dissolution for SF and SS protein). When SF SS and SF-SS hydrogel was incubated with the BJ cells, the cell viability was increased significantly (**Figure 2A**). Moreover, the cell doubling time is fast in SF-SS hydrogel with mild extraction method (**Figures 2B,C**), which may be due to the relative mild extraction process for protein in SF-SS hydrogel and more intact bioactive SS can be preserved during extraction process of mild LiBr dissolution method.

Characterization of Silk Fibroin and Sericin Mixed Hydrogel

Hydrogel formed by fibroin and sericin can emit intrinsic fluorescence (**Figure 3A**), which is partly due to 5% tyrosine and 0.25% tryptophan in fibroin, 2.1% tyrosine and 0.9% phenylalanine in sericin (32). SF-SS hydrogel shows a stronger spontaneous fluorescence and a smaller pore diameter compared to SF SS hydrogel (**Figures 3A,B**). The pore size of hydrogel is about 20–100 μm as shown in **Figures 3A,B**, which is much larger than exosomes with a diameter of 30–100 nm. This result suggests that most of exosomes can be diffused into the surrounding environment. The Young's moduli were 1.56 kPa (SF SS hydrogel) and 3.77 kPa (SF-SS hydrogel), which was reflected by straight line slope as shown in **Figure 3C**. Thus, compressive mechanical property revealed that the SS SF hydrogel had a higher stress than the SS-SF hydrogel (**Figure 3C**). The Young's moduli of SF SS hydrogel and SF-SS hydrogel indicated that the complex hydrogels are suitable for the usage on the soft tissue.

FTIR analysis revealed a shift to lower wavelength at the peak of Amide I and Amide II in SF SS hydrogel and SF SS Exo hydrogel compared with the SF solution, and the wavelength became even lower in SF-SS hydrogel and SF-SS Exo hydrogel, suggesting the formation of a more stable β-folding structure (**Figure 3D**). Adding exosome caused only a small shift to lower wavelength in both SF SS hydrogel and SF-SS hydrogel. The significant difference between SF SS hydrogel and SF-SS hydrogel may be attributed to the mild simultaneous protein extraction conditions of SF-SS hydrogel to allow easier formation of hydrogel.

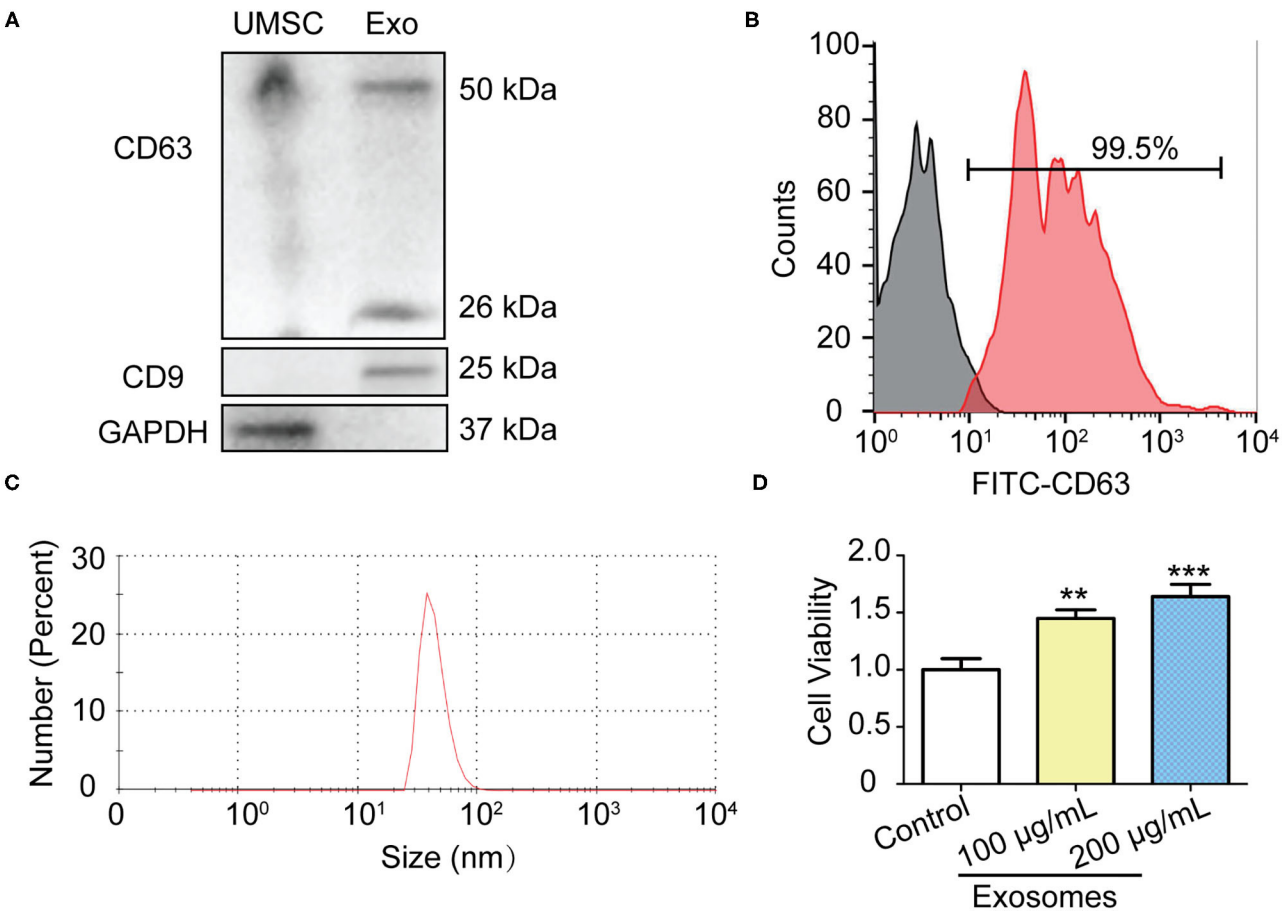

FIGURE 1 | Isolation and identification of UMSC-Exo. **(A)** Western blot analysis of CD9 and CD63 and GAPDH protein expression in UMSC and UMSC-Exo. **(B)** The expression of CD63 in UMSC-Exo was analyzed by flow cytometry. **(C)** Nanoparticle size distribution of UMSC-Exo. **(D)** The BJ cell viability was detected by CCK-8 after treatment with UMSC-Exo. Data is shown as mean ± standard deviation ($n = 3$). $^{**}p < 0.01$, $^{***}p < 0.001$.

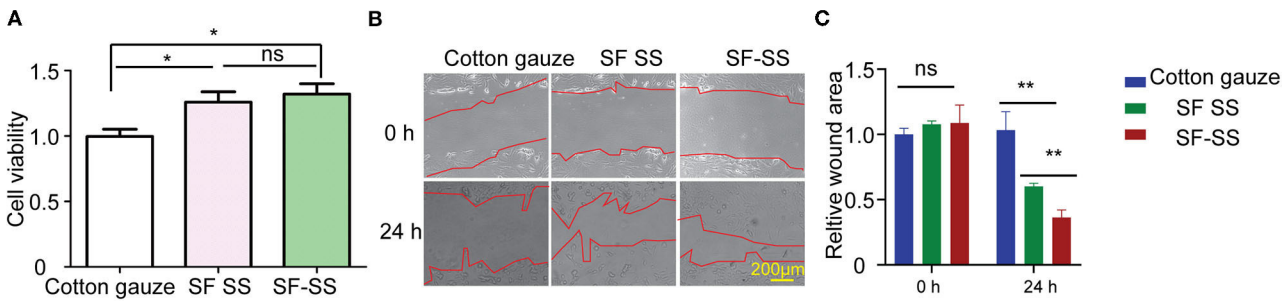

FIGURE 2 | SF SS and SF-SS hydrogel promote BJ cell growth. **(A)** BJ cell viability was detected by CCK-8 after treatment with SF SS and SF-SS hydrogel. **(B)** BJ cell migration after scratch and treatment with SF SS and SF-SS hydrogel was recorded by microscope. **(C)** The quantity of relative wound area in **Figure B** of cell migration by Image J. Data is shown as mean ± standard deviation ($n = 3$). ns, no significant difference, $^{*}p < 0.05$, $^{**}p < 0.01$.

The Effect of Silk Fibroin and Sericin Mixed Hydrogel on Wound Closure

Mice were created a 10 mm diameter full-thickness wound on the upper. After inserting the cotton gauze or hydrogel sponge into the wound, the wound was fixed with restraining bandage and the wound repairment would be observed. Three days after treatment, the two composite hydrogels absorbed most of the wound exudates and maintain the moisture environment, which was favorable to wound healing. However, the gauze induced significant exudates that caused the gauze to stick to the tissue

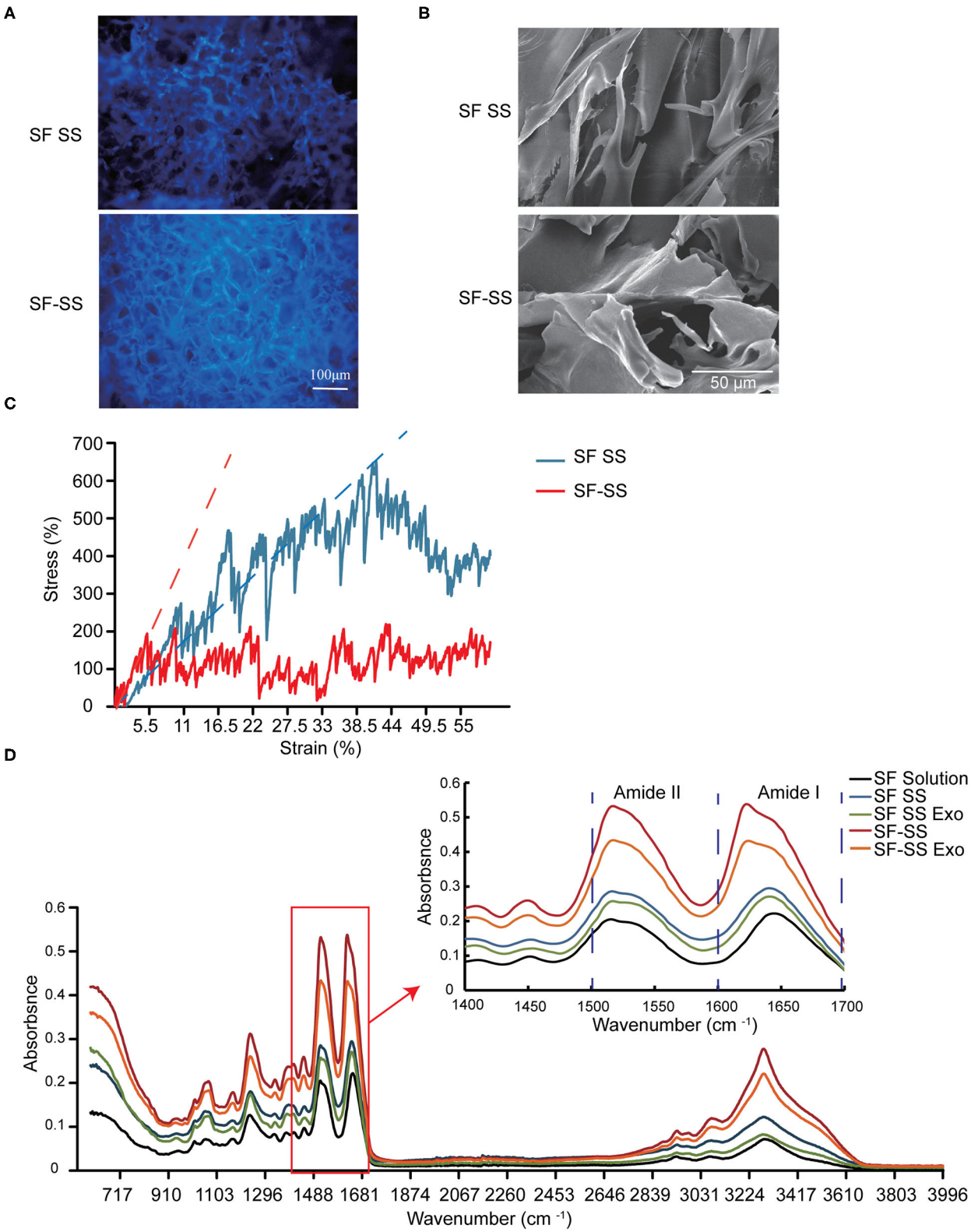

FIGURE 3 | Characterization of SF SS and SF-SS hydrogel. **(A)** Spontaneous fluorescence and microstructure of SF SS and SF-SS hydrogel. **(B)** Microstructure of SF SS and SF-SS hydrogel. **(C)** The stress-strain curve of SF SS and SF-SS hydrogel. **(D)** Fourier transform infrared spectroscopy of SF SS and SF-SS hydrogel.

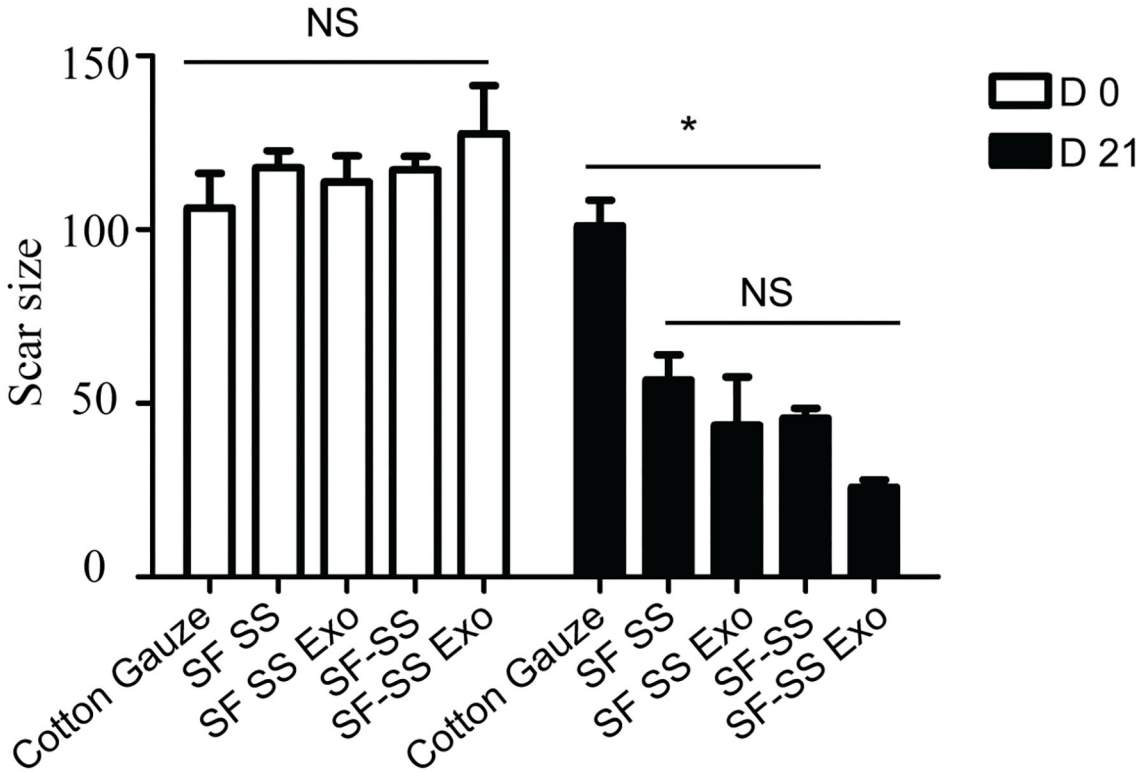

FIGURE 4 | The wound closure ability of SF SS and SF-SS hydrogel. The scar size analysis by Image J. Data is shown as mean ± standard deviation ($n = 3$). ns, no significant difference, $^*p < 0.05$.

and slowed down the healing process. After 21 days treatment, the skin cells can grow on the surface of the composite SF SS and SF-SS hydrogel and the wound was completely healed, whereas the size of the gauze inserted skin wound remains unhealed. In the presence of exosomes, SF SS and SF-SS not only healed the wounds completely but also recovered the hair growth to normal level (**Figure 4**). CD31 staining on skin wound sections was used to assess angiogenesis. Even though density of total vessels in gauze cotton was more than that of other treatment, most of vessels showed a non-mature state in gauze cotton. Thus, we mostly analyzed the vessels diameter in different groups. The blood vessels were longer in the SF SS Exo and SF-SS Exo groups compared with the control, SF SS and SF-SS groups (**Figures 5A,B**). In addition, the scar size in SF-SS group is smaller that of SF SS group (**Figure 4**), and the average diameter of blood vessels is larger than that of SF SS group (**Figure 5B**).

The Inflammatory Response to Silk Fibroin and Sericin Mixed Hydrogel *in vitro* and *in vivo*

To determine whether the hydrogel induces inflammation, the SF SS and SS-SF hydrogel sponges were incubated with macrophages in cell culture for 24 hours or applied to the skin wound of a mice model for 3 days. The cell culture supernatant or serum from the mice was collected to measure the level of TNF-α. Previous studies have suggested that SF and SS can induce inflammation; however, there is no significant difference in the amount of TNF-α released from either the macrophages or mice with injured skin (**Figures 6A,B**). *in vitro*, the amount of TNF-α derived from macrophages induced by the SF SS and SF-SS were similar with that of cotton gauze. *In vivo*, the amount of TNF-α from mice serum of SF SS, SF-SS, SF SS Exo or SF-SS Exo treatment groups was lower than that of the cotton gauze. The difference between the *in vitro* and *in vivo* effect may be due to the presence of various types of macrophages *in vivo*, as well as the different microenvironment of macrophages of *in vivo* and *in vitro*. In addition, CD68 immunofluorescence staining of the injured skin treated by the SF SS and SF-SS hydrogel sponges for 3 days showed similar results to that of the TNF-α (**Figures 7A,B**).

DISCUSSION

In our study, the beneficial effects were more significant in the experimental group treated by exosomes encapsulated in SF-SS hydrogel compared to SF SS. The beneficial effects may be explained by the fact that exosomes could increase the fibroblast cell viability *in vitro* (**Figure 1D**). In addition, Exo encapsulated in SF-SS hydrogels could promote vascular growth (**Figure 4**) and inhibit the inflammatory response (**Figures 7A,B**), suggesting that these hydrogels are promising biomaterials that can be used to enhance wound repair.

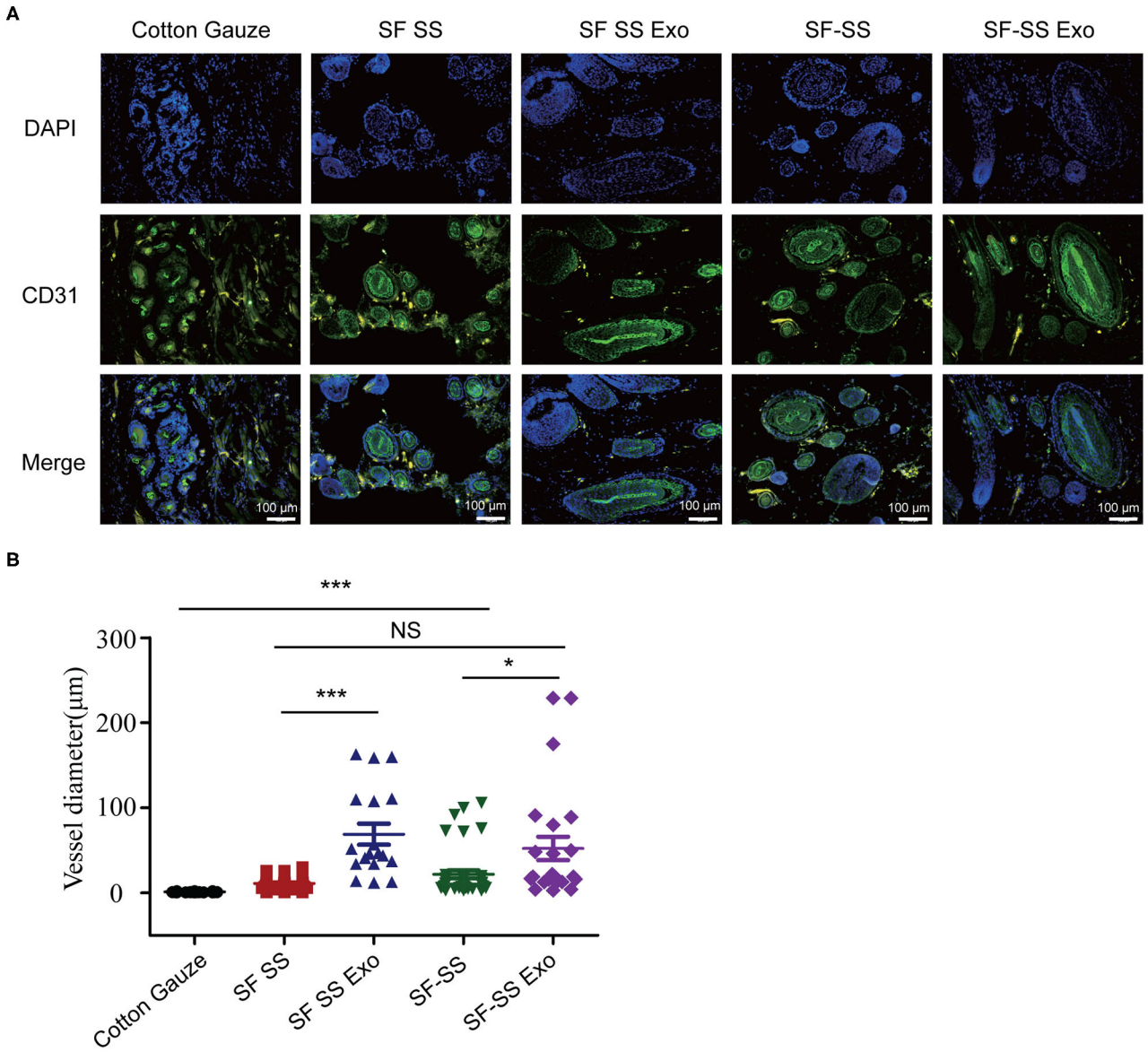

FIGURE 5 | The immunogenicity of SF SS and SF-SS hydrogel sponges. **(A)** Immunofluorescence staining of CD31 in skin wound treated by SF SS and SF-SS hydrogel and UMSC-Exo encapsulated in SF SS and SF-SS hydrogel. SF SS Exo, the Exo was delivered by SF SS composite hydrogel; SF-SS Exo, the Exo was delivered by SF-SS composite hydrogel. **(B)** Quantification of vessel diameter by Image J. Data is shown as mean ± standard deviation ($n = 3$). ns, no significant difference, $^{*}p < 0.01$, $^{***}p < 0.001$.

Exosomes are readily accessible via biological fluids for diagnosis and reflect the disease progression and prognosis, such as in cancer (29), cardiovascular, brain and kidney diseases (33–37). In addition, exosomes involve in regulating multiple biological process, such as reproduction and development, immune response, infection, neurodegeneration, cancer and cardiovascular disease through mediating cell communication (38–40). More importantly, exosomes derived from different kind of cells can treat multiple diseases including ischemic disease (41), cancer (42–44) and inflammatory bowel disease (45). In this study, we also found beneficial function of exosomes derived from UMSC in wound repair.

To improve the retention time of exosomes *in vivo*, we introduced hydrogel formed by SS and SF. It has been found that undegummed native silk can induce a severe immunoglobulin E mediated allergy or inflammation, delaying the wound healing process (46). However, there are some conflicting reports regarding the possible immunogenicity of silk proteins. SS has been considered as the element in the silk that triggers immune responses (47). However, recent studies showed that the immunogenicity of SS is extremely low. Furthermore, SS

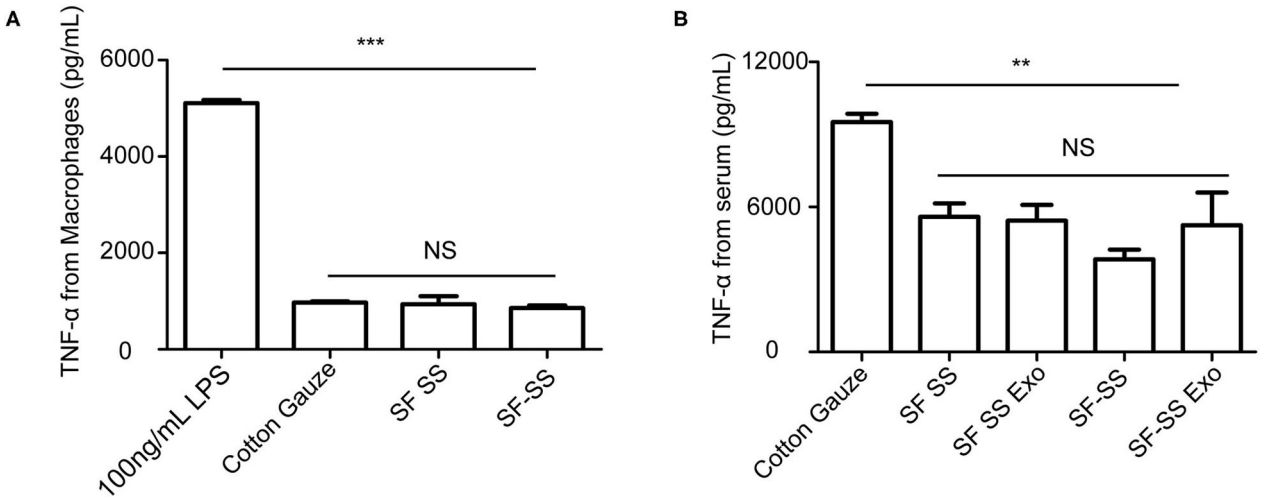

FIGURE 6 | TNF-α released by macrophage or in serum after incubating with SF SS and SF-SS hydrogel sponges. **(A)** TNF-α release from macrophages after incubating with cotton gauze, SF SS and SF-SS hydrogel. **(B)** TNF-α in the serum from mice with different treatments. Data is shown as mean ± standard deviation ($n = 3$). ns, no significant difference, $^{*}p < 0.05$, $^{**}p < 0.01$, $^{***}p < 0.001$.

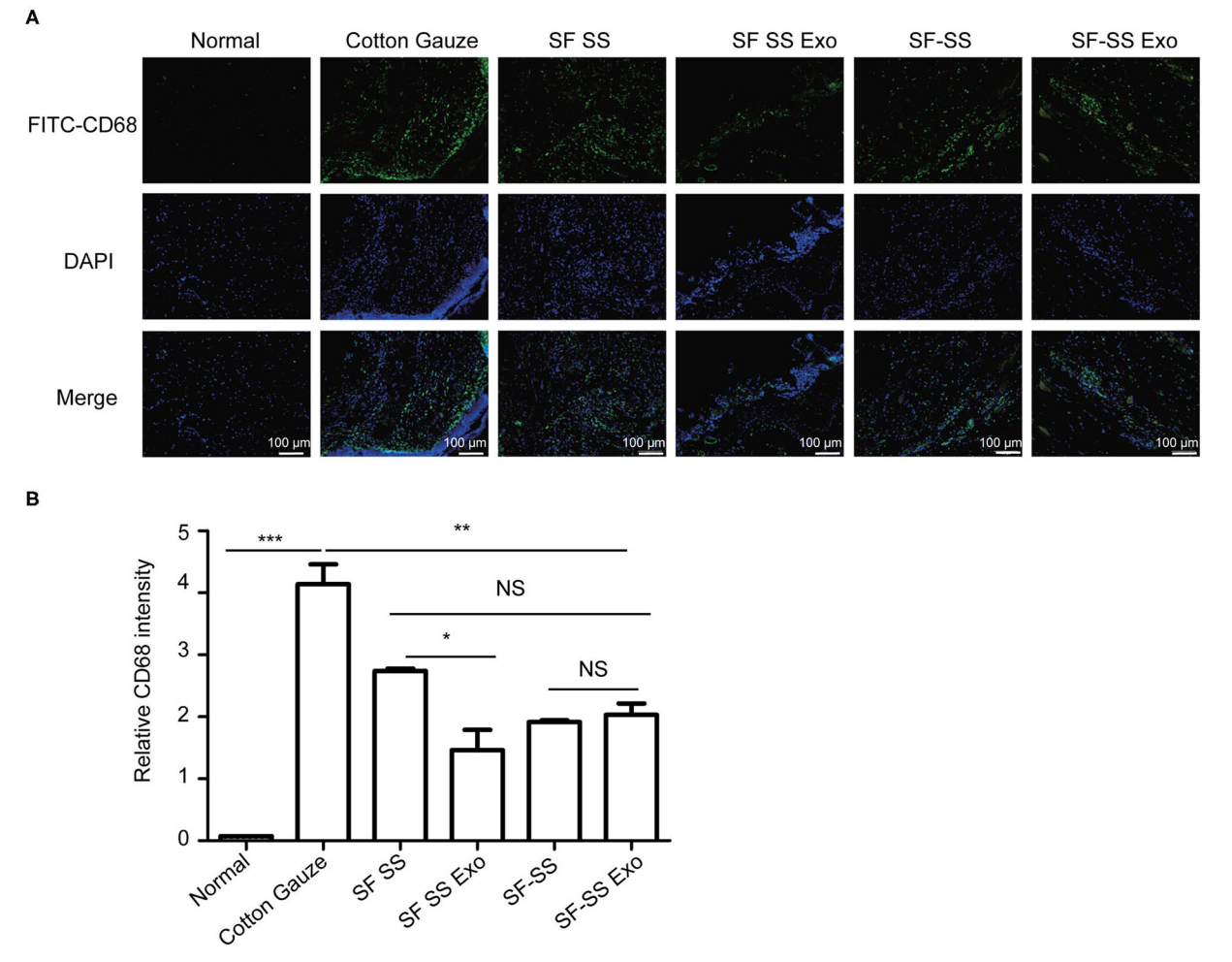

FIGURE 7 | $CD68^{+}$ cells infiltration in wound treated with SF SS and SF-SS hydrogel sponges. **(A)** $CD68^{+}$ inflammatory cell infiltration in skin wound from different treatment groups. **(B)** Quantification of $CD68^{+}$ cells with the FITC fluorescence signal by Image J. Data is shown as mean ± standard deviation ($n = 3$). ns, no significant difference, $^{*}p < 0.05$, $^{**}p < 0.01$, $^{***}p < 0.001$.

promotes the proliferation of vascular endothelial progenitor cells, endothelial cells, and hair follicle stem cells by increasing the transcription of VEGFa (48). Thus, SS has been used to treat myocardial infarction (49), skin wound (50), and bone injury (51–53). During the purification of silk sericin, the majority of small molecule impurities such as waxes, sugars and fats are expected to be removed during dialysis (46, 54), which may indicate that impurities in sericin is the cause for immune response. Another study showed that synergistic effect of crystalline fibroin coated with sericin protein and lipopolysaccharides, trigging significant release of TNF-α from macrophages, which indicates that sericin mediated inflammation activation is dependent on the association with core fibroin fibers (55). Even though there are different views on the source of the immune response, SF and SS hydrogel prepared in our article avoid the potential impurities and natural interaction of sericin and fibroin fibers during the purification and gelling process, which also showed very low immune response.

Previous studies showed that different extraction methods of sericin have different effects on protein integrity, structure and functional properties. Conventional harsh method with high heat and alkali can lead to degradation of sericin into low molecular weights polypeptides, make it difficult to cross-link into hydrogel (23). While gentle LiBr extraction method can produce a relative intact protein profile of sericin and forms a hydrogel that possesses excellent cell-adhesive capability, and promoting proliferation and long-term survival of various types of cells (32, 49). These can explain to a certain extent that SF-SS hydrogel has a short gelling time. SF hydrogel (14, 56) or SS hydrogel (9, 57) have been used to deliver cells and drugs due to the excellent mechanical properties of SF or bioactivity activity of SS. Composite hydrogels such as SF and chitosan hydrogel (58), SF and collagen hydrogel (59), SF and agar hydrogel (60), SF and poly (vinyl alcohol) hydrogel (61), have been used in the past to overcome some of the shortcomings associated with hydrogels formed by single biomaterial. SF and SS have emerged as promising biomaterial for tissue repair because they can be easily acquired and have low immunogenicity (48, 61, 62).

Mechanical properties of extracellular environment (ECM) are intimately related with cell behaviors. Those mechanical signals can be transfer by transmembrane receptors, cytoskeleton or nuclear skeleton, thus regulating the gene expression. Matrix elasticity has been shown to involve in cell survival, proliferation and differentiation (63, 64). Suitable mechanical properties of ECM are critical for the homeostasis of cell or tissue. Exception of bone, most of human tissues are soft, reflected by the value of compressive moduli (Young's moduli) ranging from 1 to 200 kPa (65–67). A better hydrogel should provide similar mechanical properties of certain tissue. As described before, the Young's moduli of SF hydrogel at concentration of 1.5–4% (w/v) ranges from 6.41 ± 0.47 kPa to 63.98 ± 2.42 kPa, which is consistent with a biologically relevant stiffness similar to native vasculature (68). Other studies showed that native silk fibers and fibroin hydrogel at concentrations of 4–15% (w/v) had the value of Young's moduli larger than 400 kPa, which is more suitable for stiff or semi-stiff implants, rather than for regeneration of soft organs (25). The Young's moduli of SS and polyvinyl alcohol hydrogel is only 20 Pa, which is much lower than that of most tissues (22). Thus, introducing SS into the fibroin hydrogel can adjust the compressive moduli to get a complex hydrogel with appropriate mechanical properties for wound repair.

Recent studies show that the hydrogels in encapsulating stem cells shape cell status, improve cells retention time and involve in tissue repair process (69, 70). In addition, recent works demonstrate that the beneficial functions of stem cells in tissue regeneration are largely through paracrine manner, rather than the direct differentiation of the implanted cell (71, 72). During all the secretome, exosomes are regarded as important components to involve in the cell communication and transfer functional molecules for tissue regeneration. We also showed that introducing exosomes derived from UMSCs into SF and SS mixed hydrogel promoted wound repair.

CONCLUSION

In our study, we found that the freeze-dried composite hydrogel formed by SF and SS can be used to enhance wound repair with low immune response. In addition, the beneficial effects of these hydrogel were improved in the presence of UMSC-Exo. In conclusion, SF and SS mixed hydrogel can serve as a good substitute to wound dressing and can be used to deliver exosomes.

DATA AVAILABILITY STATEMENT

The raw data supporting the conclusions of this article will be made available by the authors, without undue reservation.

ETHICS STATEMENT

The animal study was reviewed and approved by Laboratory Animal Care and Use Committee of Soochow University.

AUTHOR CONTRIBUTIONS

YL and CH conceptualized the study, interpreted data, and wrote the manuscript. CH, FL, and YZ performed most of the experiments and statistical analyses. WC, WL, FD, LL, and CW made intellectual contributions in data interpretations. All authors contributed to the article and approved the submitted version.

FUNDING

This work was supported by the National Natural Science Foundation of China (NSFC, No. 91849122 to YL, No. 81870194 to YL), Jiangsu Province Peak of Talent in Six Industries (BU24600117 to YL), National Natural Science Foundation of China (No. 91839101), and Introduction Project of Clinical Medicine Expert Team for Suzhou (No. SZYJTD201704).

REFERENCES

1. Rani S, Ritter T. The exosome - a naturally secreted nanoparticle and its application to wound healing. *Adv Mater.* (2016) 28:5542–52. doi: 10.1002/adma.201504009
2. Tottoli EM, Dorati R, Genta I, Chiesa E, Pisani S, Conti B. Skin wound healing process and new emerging technologies for skin wound care and regeneration. *Pharmaceutics.* (2020) 12:735. doi: 10.3390/pharmaceutics12080735
3. Zhang B, Wang M, Gong A, Zhang X, Wu X, Zhu Y, et al. HucMSC-exosome mediated-wnt4 signaling is required for cutaneous wound healing. *Stem Cells.* (2015) 33:2158–68. doi: 10.1002/stem.1771
4. Leoni G, Neumann PA, Kamaly N, Quiros M, Nishio H, Jones HR, et al. Annexin A1-containing extracellular vesicles and polymeric nanoparticles promote epithelial wound repair. *J Clin Invest.* (2015) 125:1215–27. doi: 10.1172/JCI76693
5. Sjoqvist S, Ishikawa T, Shimura D, Kasai Y, Imafuku A, Bou-Ghannam S, et al. Exosomes derived from clinical-grade oral mucosal epithelial cell sheets promote wound healing. *J Extracell Vesicles.* (2019) 8:1565264. doi: 10.1080/20013078.2019.1565264
6. Zhang W, Bai X, Zhao B, Li Y, Zhang Y, Li Z, et al. Cell-free therapy based on adipose tissue stem cell-derived exosomes promotes wound healing via the PI3K/Akt signaling pathway. *Exp Cell Res.* (2018) 370:333–42. doi: 10.1016/j.yexcr.2018.06.035
7. Kim S, Lee SK, Kim H, Kim TM. Exosomes secreted from induced pluripotent stem cell-derived mesenchymal stem cells accelerate skin cell proliferation. *Int J Mol Sci.* (2018) 19:3119. doi: 10.3390/ijms19103119
8. Xu N, Wang L, Guan J, Tang C, He N, Zhang W, et al. Wound healing effects of a Curcuma zedoaria polysaccharide with platelet-rich plasma exosomes assembled on chitosan/silk hydrogel sponge in a diabetic rat model. *Int J Biol Macromol.* (2018) 117:102–7. doi: 10.1016/j.ijbiomac.2018.05.066
9. Farokhi M, Mottaghitalab F, Fatahi Y, Khademhosseini A, Kaplan DL. Overview of silk fibroin use in wound dressings. *Trends Biotechnol.* (2018) 36:907–22. doi: 10.1016/j.tibtech.2018.04.004
10. Lamboni L, Gauthier M, Yang G, Wang Q. Silk sericin: a versatile material for tissue engineering and drug delivery. *Biotechnol Adv.* (2015) 33:1855–67. doi: 10.1016/j.biotechadv.2015.10.014
11. Chouhan D, Lohe TU, Samudrala PK, Mandal BB. In situ forming injectable silk fibroin hydrogel promotes skin regeneration in full thickness burn wounds. *Adv Healthc Mater.* (2018) 7:31. doi: 10.1002/adhm.201801092
12. Ciocci M, Cacciotti I, Seliktar D, Melino S. Injectable silk fibroin hydrogels functionalized with microspheres as adult stem cells-carrier systems. *Int J Biol Macromol.* (2018) 108:960–71. doi: 10.1016/j.ijbiomac.2017.11.013
13. Fernández-García L, Marí-Buyé N, Barios JA, Madurga R, Elices M, Pérez-Rigueiro J, et al. Safety and tolerability of silk fibroin hydrogels implanted into the mouse brain. *Acta Biomater.* (2016) 45:262–75. doi: 10.1016/j.actbio.2016.09.003
14. Wang X, Ding Z, Wang C, Chen X, Xu H, Lu Q, et al. Bioactive silk hydrogels with tunable mechanical properties. *J Mater Chem B.* (2018) 6:2739–46. doi: 10.1039/C8TB00607E
15. Yan Y, Cheng B, Chen K, Cui W, Qi J, Li X, et al. Enhanced osteogenesis of bone marrow-derived mesenchymal stem cells by a functionalized silk fibroin hydrogel for bone defect repair. *Adv Healthc Mater.* (2019) 8:28. doi: 10.1002/adhm.201801043
16. Hu J, Lu Y, Cai L, Owusu-Ansah KG, Xu G, Han F, et al. Functional compressive mechanics and tissue biocompatibility of an injectable SF/PU hydrogel for nucleus pulposus replacement. *Sci Rep.* (2017) 7:017–02497. doi: 10.1038/s41598-017-02497-3
17. Wu J, Zheng K, Huang X, Liu J, Liu H, Boccaccini AR, et al. Thermally triggered injectable chitosan/silk fibroin/bioactive glass nanoparticle hydrogels for in-situ bone formation in rat calvarial bone defects. *Acta Biomater.* (2019) 91:60–71. doi: 10.1016/j.actbio.2019.04.023
18. Zheng A, Cao L, Liu Y, Wu J, Zeng D, Hu L, et al. Biocompatible silk/calcium silicate/sodium alginate composite scaffolds for bone tissue engineering. *Carbohydr Polym.* (2018) 199:244–55. doi: 10.1016/j.carbpol.2018.06.093
19. Cao TT, Zhang YQ. Processing and characterization of silk sericin from Bombyx mori and its application in biomaterials and biomedicines. *Mater Sci Eng C Mater Biol Appl.* (2016) 61:940–52. doi: 10.1016/j.msec.2015.12.082
20. Ahsan F, Ansari TM, Usmani S, Bagga P. An insight on silk protein sericin: from processing to biomedical application. *Drug Res.* (2018) 68:317–27. doi: 10.1055/s-0043-121464
21. Kamalathevan P, Ooi PS, Loo YL. Silk-based biomaterials in cutaneous wound healing: a systematic review. *Adv Skin Wound Care.* (2018) 31:565–73. doi: 10.1097/01.ASW.0000546233.35130.a9
22. Siritienthong T, Ratanavaraporn J, Aramwit P. Development of ethyl alcohol-precipitated silk sericin/polyvinyl alcohol scaffolds for accelerated healing of full-thickness wounds. *Int J Pharm.* (2012) 439:175–86. doi: 10.1016/j.ijpharm.2012.09.043
23. Kunz RI, Brancalhao RM, Ribeiro LF, Natali MR. Silkworm sericin: properties and biomedical applications. *Biomed Res Int.* (2016) 8175701:14. doi: 10.1155/2016/8175701
24. Napavichayanun S, Ampawong S, Harnsilpong T, Angspatt A, Aramwit P. Inflammatory reaction, clinical efficacy, and safety of bacterial cellulose wound dressing containing silk sericin and polyhexamethylene biguanide for wound treatment. *Arch Dermatol Res.* (2018) 310:795–805. doi: 10.1007/s00403-018-1871-3
25. Leal-Egaña A, Scheibel T. Silk-based materials for biomedical applications. *Biotechnol Appl Biochem.* (2010) 55:155–67. doi: 10.1042/BA20090229
26. Lim KS, Kundu J, Reeves A, Poole-Warren LA, Kundu SC, Martens PJ. The influence of silkworm species on cellular interactions with novel PVA/silk sericin hydrogels. *Macromol Biosci.* (2012) 12:322–32. doi: 10.1002/mabi.201100292
27. Han C, Zhou J, Liang C, Liu B, Pan X, Zhang Y, et al. Human umbilical cord mesenchymal stem cell derived exosomes encapsulated in functional peptide hydrogels promote cardiac repair. *Biomater Sci.* (2019) 15:2920–33. doi: 10.1039/C9BM00101H
28. Han C, Zhou J, Liu B, Liang C, Pan X, Zhang Y, et al. Delivery of miR-675 by stem cell-derived exosomes encapsulated in silk fibroin hydrogel prevents aging-induced vascular dysfunction in mouse hindlimb. *Mater Sci Eng C Mater Biol Appl.* (2019) 99:322–32. doi: 10.1016/j.msec.2019.01.122
29. Casson J, Davies OG, Smith CA, Dalby MJ, Berry CC. Mesenchymal stem cell-derived extracellular vesicles may promote breast cancer cell dormancy. *J Tissue Eng.* (2018) 9:2041731418810093. doi: 10.1177/2041731418810093
30. Rockwood DN, Preda RC, Yucel T, Wang X, Lovett ML, Kaplan DL. Materials fabrication from Bombyx mori silk fibroin. *Nat Protoc.* (2011) 6:1612–31. doi: 10.1038/nprot.2011.379
31. Shao L, Zhang Y, Lan B, Wang J, Zhang Z, Zhang L, et al. MiRNA-sequence indicates that mesenchymal stem cells and exosomes have similar mechanism to enhance cardiac repair. *Biomed Res Int.* (2017) 4150705:22. doi: 10.1155/2017/4150705
32. Wang Z, Zhang Y, Zhang J, Huang L, Liu J, Li Y, et al. Exploring natural silk protein sericin for regenerative medicine: an injectable, photoluminescent, cell-adhesive 3D hydrogel. *Sci Rep.* (2014) 4:7064. doi: 10.1038/srep07064
33. Alvarez-Erviti L, Seow Y, Schapira AH, Gardiner C, Sargent IL, Wood MJ, et al. Lysosomal dysfunction increases exosome-mediated alpha-synuclein release and transmission. *Neurobiol Dis.* (2011) 42:360–7. doi: 10.1016/j.nbd.2011.01.029
34. Cheng M, Yang J, Zhao X, Zhang E, Zeng Q, Yu Y, et al. Circulating myocardial microRNAs from infarcted hearts are carried in exosomes and mobilise bone marrow progenitor cells. *Nat Commun.* (2019) 10:019–08895. doi: 10.1038/s41467-019-08895-7
35. Nilsson J, Skog J, Nordstrand A, Baranov V, Mincheva-Nilsson L, Breakefield XO, et al. Prostate cancer-derived urine exosomes: a novel approach to biomarkers for prostate cancer. *Br J Cancer.* (2009) 100:1603–7. doi: 10.1038/sj.bjc.6605058
36. Rajendran L, Honsho M, Zahn TR, Keller P, Geiger KD, Verkade P, et al. Alzheimer's disease beta-amyloid peptides are released in association with exosomes. *Proc Natl Acad Sci U S A.* (2006) 103:11172–7. doi: 10.1073/pnas.0603838103
37. Zhou H, Pisitkun T, Aponte A, Yuen PS, Hoffert JD, Yasuda H, et al. Exosomal Fetuin-A identified by proteomics: a novel urinary biomarker for detecting acute kidney injury. *Kidney Int.* (2006) 70:1847–57. doi: 10.1038/sj.ki.5001874
38. Kalluri R, LeBleu VS. The biology, function, and biomedical applications of exosomes. *Science.* (2020) 367:6478. doi: 10.1126/science.aau6977

39. Kita S, Maeda N, Shimomura I. Interorgan communication by exosomes, adipose tissue, and adiponectin in metabolic syndrome. *J Clin Invest.* (2019) 129:4041–9. doi: 10.1172/JCI129193
40. Sadri Nahand J, Moghoofei M, Salmaninejad A, Bahmanpour Z, Karimzadeh M, Nasiri M, et al. Pathogenic role of exosomes and microRNAs in HPV-mediated inflammation and cervical cancer: A review. *Int J Cancer.* (2020) 146:305–20. doi: 10.1002/ijc.32688
41. Ong SG, Lee WH, Huang M, Dey D, Kodo K, Sanchez-Freire V, et al. Cross talk of combined gene and cell therapy in ischemic heart disease: role of exosomal microRNA transfer. *Circulation.* (2014) 130:007917. doi: 10.1161/CIRCULATIONAHA.113.007917
42. Bu H, He D, He X, Wang K. Exosomes: isolation, analysis, and applications in cancer detection and therapy. *Chembiochem.* (2019) 20:451–61. doi: 10.1002/cbic.201800470
43. Elsherbini A, Bieberich E. Ceramide and exosomes: a novel target in cancer biology and therapy. *Adv Cancer Res.* (2018) 140:121–54. doi: 10.1016/bs.acr.2018.05.004
44. Melo SA, Luecke LB, Kahlert C, Fernandez AF, Gammon ST, Kaye J, et al. Glypican-1 identifies cancer exosomes and detects early pancreatic cancer. *Nature.* (2015) 523:177–82. doi: 10.1038/nature14581
45. Zhang H, Wang L, Li C, Yu Y, Yi Y, Wang J, et al. Exosome-Induced Regulation in Inflammatory Bowel Disease. *Front Immunol.* (2019) 10:1464. doi: 10.3389/fimmu.2019.01464
46. Zakeri Siavashani A, Mohammadi J, Maniura-Weber K, Senturk B, Nourmohammadi J, Sadeghi B, et al. Silk based scaffolds with immunomodulatory capacity: anti-inflammatory effects of nicotinic acid. *Biomater Sci.* (2019) 8:148–62. doi: 10.1039/C9BM00814D
47. Thurber AE, Omenetto FG, Kaplan DL. *In vivo* bioresponses to silk proteins. *Biomaterials.* (2015) 71:145–57. doi: 10.1016/j.biomaterials.2015.08.039
48. Jiao Z, Song Y, Jin Y, Zhang C, Peng D, Chen Z, et al. *In Vivo* characterizations of the immune properties of sericin: an ancient material with emerging value in biomedical applications. *Macromol Biosci.* (2017) 17:17. doi: 10.1002/mabi.201700229
49. Song Y, Zhang C, Zhang J, Sun N, Huang K, Li H, et al. An injectable silk sericin hydrogel promotes cardiac functional recovery after ischemic myocardial infarction. *Acta Biomater.* (2016) 41:210–23. doi: 10.1016/j.actbio.2016.05.039
50. Qi C, Xu L, Deng Y, Wang G, Wang Z, Wang L. Sericin hydrogels promote skin wound healing with effective regeneration of hair follicles and sebaceous glands after complete loss of epidermis and dermis. *Biomater Sci.* (2018) 6:2859–70. doi: 10.1039/C8BM00934A
51. Griffanti G, Jiang W, Nazhat SN. Bioinspired mineralization of a functionalized injectable dense collagen hydrogel through silk sericin incorporation. *Biomater Sci.* (2019) 7:1064–77. doi: 10.1039/C8BM01060A
52. Yang M, Mandal N, Shuai Y, Zhou G, Min S, Zhu L. Mineralization and biocompatibility of Antheraea pernyi (A. pernyi) silk sericin film for potential bone tissue engineering. *Biomed Mater Eng.* (2014) 24:815–24. doi: 10.3233/BME-130873
53. Zhong Q, Li W, Su X, Li G, Zhou Y, Kundu SC, et al. Degradation pattern of porous CaCO3 and hydroxyapatite microspheres in vitro and in vivo for potential application in bone tissue engineering. *Colloids Surf B Biointerfaces.* (2016) 143:56–63. doi: 10.1016/j.colsurfb.2016.03.020
54. Ak F, Oztoprak Z, Karakutuk I, Okay O. Macroporous silk fibroin cryogels. *Biomacromolecules.* (2013) 14:719–27. doi: 10.1021/bm3018033
55. Panilaitis B, Altman GH, Chen J, Jin HJ, Karageorgiou V, Kaplan DL. Macrophage responses to silk. *Biomaterials.* (2003) 24:3079–85. doi: 10.1016/S0142-9612(03)00158-3
56. Pritchard EM, Kaplan DL. Silk fibroin biomaterials for controlled release drug delivery. *Expert Opin Drug Deliv.* (2011) 8:797–811. doi: 10.1517/17425247.2011.568936
57. Wang Y, Cai R, Tao G, Wang P, Zuo H, Zhao P, et al. A novel AgNPs/Sericin/Agar film with enhanced mechanical property and antibacterial capability. *Molecules.* (2018) 23:1821. doi: 10.3390/molecules23071821
58. Adali T, Kalkan R, Karimizarandi L. The chondrocyte cell proliferation of a chitosan/silk fibroin/egg shell membrane hydrogels. *Int J Biol Macromol.* (2019) 124:541–7. doi: 10.1016/j.ijbiomac.2018.11.226
59. Buitrago JO, Patel KD, El-Fiqi A, Lee JH, Kundu B, Lee HH, et al. Silk fibroin/collagen protein hybrid cell-encapsulating hydrogels with tunable gelation and improved physical and biological properties. *Acta Biomater.* (2018) 69:218–33. doi: 10.1016/j.actbio.2017.12.026
60. Tyeb S, Kumar N, Kumar A, Verma V. Flexible agar-sericin hydrogel film dressing for chronic wounds. *Carbohydr Polym.* (2018) 200:572–82. doi: 10.1016/j.carbpol.2018.08.030
61. Tao H, Kaplan DL, Omenetto FG. Silk materials–a road to sustainable high technology. *Adv Mater.* (2012) 24:2824–37. doi: 10.1002/adma.201104477
62. Zhao Z, Li Y, Xie MB. Silk fibroin-based nanoparticles for drug delivery. *Int J Mol Sci.* (2015) 16:4880–903. doi: 10.3390/ijms16034880
63. Helenius J, Heisenberg CP, Gaub HE, Muller DJ. Single-cell force spectroscopy. *J Cell Sci.* (2008) 121:1785–91. doi: 10.1242/jcs.030999
64. Vogel V. Mechanotransduction involving multimodular proteins: converting force into biochemical signals. *Annu Rev Biophys Biomol Struct.* (2006) 35:459–88. doi: 10.1146/annurev.biophys.35.040405.102013
65. Chang G, Kim HJ, Vunjak-Novakovic G, Kaplan DL, Kandel R. Enhancing annulus fibrosus tissue formation in porous silk scaffolds. *J Biomed Mater Res A.* (2010) 92:43–51. doi: 10.1002/jbm.a.32326
66. Hendriks FM, Brokken D, Oomens CW, Bader DL, Baaijens FP. The relative contributions of different skin layers to the mechanical behavior of human skin *in vivo* using suction experiments. *Med Eng Phys.* (2006) 28:259–66. doi: 10.1016/j.medengphy.2005.07.001
67. Salameh N, Peeters F, Sinkus R, Abarca-Quinones J, Annet L, Ter Beek LC, et al. Hepatic viscoelastic parameters measured with MR elastography: correlations with quantitative analysis of liver fibrosis in the rat. *J Magn Reson Imaging.* (2007) 26:956–62. doi: 10.1002/jmri.21099
68. Floren M, Bonani W, Dharmarajan A, Motta A, Migliaresi C, Tan W. Human mesenchymal stem cells cultured on silk hydrogels with variable stiffness and growth factor differentiate into mature smooth muscle cell phenotype. *Acta Biomater.* (2016) 31:156–66. doi: 10.1016/j.actbio.2015.11.051
69. Chaudhuri O, Gu L, Klumpers D, Darnell M, Bencherif SA, Weaver JC, et al. Hydrogels with tunable stress relaxation regulate stem cell fate and activity. *Nat Mater.* (2016) 15:326–34. doi: 10.1038/nmat4489
70. Lee JH, Kim HW. Emerging properties of hydrogels in tissue engineering. *J Tissue Eng.* (2018) 9:2041731418768285. doi: 10.1177/2041731418768285
71. Alcaraz MJ, Compañ A, Guillén MI. Extracellular vesicles from mesenchymal stem cells as novel treatments for musculoskeletal diseases. *Cells.* (2019) 9:98. doi: 10.3390/cells9010098
72. Andia I, Maffulli N, Burgos-Alonso N. Stromal vascular fraction technologies and clinical applications. *Expert Opin Biol Ther.* (2019) 19:1289–305. doi: 10.1080/14712598.2019.1671970

Conflict of Interest: The authors declare that the research was conducted in the absence of any commercial or financial relationships that could be construed as a potential conflict of interest.

frontiers in Cardiovascular Medicine

REVIEW
published: 26 August 2021
doi: 10.3389/fcvm.2021.738031

Exosomes and Atherogenesis

Bingbing Lin[1†], *Juan Yang*[1†], *Yuwei Song*[1], *Guohui Dang*[1] *and Juan Feng*[1,2*]

[1] Key Laboratory of Molecular Cardiovascular Science, Ministry of Education, Department of Physiology and Pathophysiology, School of Basic Medical Sciences, Peking University, Beijing, China, [2] Department of Integration of Chinese and Western Medicine, School of Basic Medical Sciences, Peking University, Beijing, China

Myocardial infarction and ischemic stroke are the leading causes of mortality worldwide. Atherosclerosis is their common pathological foundation. It is known that atherosclerosis is characterized by endothelial activation/injury, accumulation of inflammatory immune cells and lipid-rich foam cells, followed by the development of atherosclerotic plaque. Either from arterial vessel wall or blood circulation, endothelial cells, smooth muscle cells, macrophages, T-lymphocytes, B-lymphocytes, foam cells, and platelets have been considered to contribute to the pathogenesis of atherosclerosis. Exosomes, as natural nano-carriers and intercellular messengers, play a significant role in modulation of cell-to-cell communication. Under physiological or pathological conditions, exosomes can deliver their cargos including donor cell-specific proteins, lipids, and nucleic acids to target cells, which in turn affect the function of the target cells. In this review, we will describe the pathophysiological significance of various exosomes derived from different cell types associated with atherosclerosis, and the potential applications of exosome in clinical diagnosis and treatment.

Keywords: exosome, vascular injury, inflammation, immunocyte, atherosclerosis

OPEN ACCESS

Edited by:
Zhen-Ao Zhao,
Hebei North University, China

Reviewed by:
Aijuan Qu,
Capital Medical University, China
Jing Wang,
Chinese Academy of Medical Sciences, China

***Correspondence:**
Juan Feng
juanfeng@bjmu.edu.cn

†These authors have contributed equally to this work

Specialty section:
This article was submitted to Cardiovascular Biologics and Regenerative Medicine, a section of the journal Frontiers in Cardiovascular Medicine

Received: *08 July 2021*
Accepted: *04 August 2021*
Published: *26 August 2021*

Citation:
Lin B, Yang J, Song Y, Dang G and Feng J (2021) Exosomes and Atherogenesis. Front. Cardiovasc. Med. 8:738031. doi: 10.3389/fcvm.2021.738031

INTRODUCTION

According to epidemiological investigation, the number of deaths from atherosclerotic cardiovascular disease (ASCVD) in 2016 was about 2.4 million, accounting for 61% of cardiovascular deaths and 25% of total deaths (1). Moreover, ASCVD mortality has increased significantly over the past 30 years. Atherosclerosis, a progressive multifactorial degenerative disease of large and medium arterial walls (2–4), is the root cause of most cardiovascular diseases including coronary artery disease (CAD), ischemic gangrene, abdominal aortic aneurysm, heart failure and ischemic stroke (5). It is known that atherosclerosis is a complex multifactorial disease developed through a series of events involving the cardiovascular system, metabolism, and immune system (6, 7). Increasing evidence suggests that local inflammatory microenvironment consisting of different inflammatory cells is a fundamental pathological characteristic (2, 8–11), in which cells exchange information through different mechanisms and structures, such as secreting bioactive molecules (growth factors, chemokines, peptides, ions, bioactive lipids, and nucleotides), direct cell-cell contact and cell-matrix interaction (12, 13). In the past few years, extracellular vesicles (EVs) derived from various cells have received increasing attention (14). EVs are membranous vesicles abounding in body fluids. There are three types of EVs, including exosomes, microvesicles (MVs) and apoptotic bodies. Among them, exosomes have been paid increasing attention and been considered as a mediator for cellular communication, which can deliver a series of bioactive components to target cells and then modulate their functions (12, 15). This review will focus on the sources of different exosomes and elucidate how they contribute to the pathogenesis of atherosclerosis, eventually provide evidence to suggest their potential clinical applications.

INTRODUCTION OF EXOSOMES

Exosomes used to be considered as "extracellular debris" and received little attention. Now exosomes are generally recognized as a mediator of cell-to-cell communication which are the smallest kind of extracellular vesicles (30–150 nm) with bilayer membrane morphology, and usually in the shape of cup (16).

Exosomes were first described as microvesicles containing 5′-nucleotidase activity released by tumor cell lines (17). In 1983 and 1985, Harding et al. (18) and Pan et al. (19) respectively reported and proved that cultured reticulocytes released exosomes. Using immunoelectron microscope, they saw the dynamic change process of internalized anti-transferrin receptor antibody in the reticulocytes. The released vesicles were separated and purified, and then named after "exosomes". Afterwards, it has been confirmed that apart from reticulocytes, EVs can be secreted from various types of living cells, such as B lymphocytes, macrophages and endothelial cells (14). Moreover, exosomes can be extracted from different body fluids, including blood, ascites, cerebrospinal fluid, saliva, breast milk and urine (16).

To this day, although there is still no standardized method for exosome isolation, many techniques have been established based on the biochemical and physicochemical features of exosomes (20). The exosome separation methods include: ultracentrifugation, ultrafiltration, immunoaffinity capture, charge neutralization-based polymer precipitation, size-exclusion chromatograph, and microfluidic techniques (20). Each one has its unique advantages and disadvantages. Now one of the most common used strategies is ultracentrifugation (21). In recent years, microfluidic techniques are attracting more and more attention for their simplicity, fast-isolating and material-saving features, which may be commonly applied to exosome separation and detection in the future (20).

Exosomes can be formed in two mechanisms: the ESCRT-dependent and ESCRT-independent mechanisms, contribution of which may vary depending on the contents recruited and the type of donor cells (22). According to the current database of the exosome contents, 4,563 proteins, 1,639 mRNAs, 764 miRNAs, and 194 lipids have been identified in exosomes (23). The nucleic acids, proteins and other molecules carried by exosomes give exosomes rich biological information, which is transmitted from donor cells to target cells to play a specific biological effect (24). In addition, exosomes are enriched in membrane markers, such as tetraspanins and endosomal sorting complex required for transport members (25, 26). Furthermore, exosomes can also serve as biomarkers and potential targets for diagnosis and treatment of ASCVD (27, 28).

THE ROLES OF EXOSOMES IN THE OCCURRENCE AND DEVELOPMENT OF ATHEROSCLEROSIS

Atherosclerosis is a multifactorial disease closely associated with endothelial cell damage, vascular inflammation, accumulation of monocytes and macrophages, and thrombosis (29). Exosomes from endothelial cells, smooth muscle cells, macrophages, T-lymphocytes have been considered to contribute to the atherosclerosis-related pathological processes, such as inflammation, vascular injury, calcification, apoptosis, thrombosis, and coagulation (22, 30).

The Roles of Monocytes/Macrophages Exosomes in Atherosclerosis

In the early stages of atherosclerosis, inflammation induces the expression of vascular endothelial cell adhesion molecules and vascular cell chemokines, recruiting circulating monocytes. These monocytes move into the lumen of arteries and then differentiate into macrophages in response to local mediators such as mononuclear colony stimulating factors (10). Monocyte-derived macrophages are recruited, differentiate and proliferate continuously and thus become the main group of cells involved in the formation of atherosclerotic plaques. Monocytes and macrophages can secret abundant exosomes, mainly found in atherosclerotic lesion (6, 31). Exosomes derived from monocytes are key players in inflammation. By interacting with endothelial cells, these exosomes induce expression and activation of adhesion molecules and pro-inflammatory cytokines. Meanwhile, they can also interact with other types of blood vessel cells, including monocytes, fibroblasts and smooth muscle cells and then regulate immune response and vascular inflammation microenvironment (32, 33).

Monocyte Exosomes Promote Vascular Inflammation, Endothelial Cell Apoptosis and Thrombosis

Friedrich et al. isolated exosomes from starved human monocyte cell line (THP-1) and then injected intravenously into ApoE-/- mice fed on a high-fat and high-cholesterol diet. The results showed that monocyte exosomes significantly increased monocyte and T lymphocyte infiltration in mouse vascular wall and enhanced plaque formation. The results of *in vitro* cell culture experiments confirmed that the uptake of monocyte exosomes triggered the production of reactive oxygen species and the release of proinflammatory interleukin-6 in macrophages, as well as macrophage migration regulated by monocyte chemotactic protein 1 (MCP-1). After co-incubation with endothelial cells, monocyte exosomes can also significantly increase the expression of intracellular adhesion molecule-1 (ICAM-1) in monocytes. Therefore, monocyte exosomes may exacerbate vascular inflammation via paracrine during atherosclerosis (34).

During the pathogenesis of atherosclerosis, oxidized lipoprotein (ox-LDL) promotes the adhesion of monocytes to intima by inducing the expression of adhesion molecules of endothelium, thereby promoting the formation and progression of lesions. Chen et al. reported that exosomes secreted by ox-LDL-treated THP-1 cells, were rich in long non-encoding lncRNA GAS5. These exosomes could promote apoptosis of vascular endothelial cells when they transferred to the perinuclear region. In contrast, exosomes released by THP-1 cells knockout of lncRNA GAS5 inhibited endothelial cell apoptosis and expression of P53, Caspase 3, Caspase 7, and Caspase 9 (35). To understand the direct effect of monocyte exosomes on endothelial cells in the NO pathway, Maria et al.

treated THP-1 cells with the apoptotic agent epotoside (VP-16). They discovered that the exosomes secreted by these cells could promote the production of NO in human endothelial cells by inhibiting the expression of caveolin-1 in the pits of endothelial cells. The inhibition of caveolin-1 expression by exosomes could be reversed by inhibiting phosphatidylinositol-3-kinase (PI-3-K) or mitogen-induced extracellular kinase 1/2 (MEK1/2). These results suggest the pleiotropic effect of monocyte microparticles on the function of vascular endothelial cells and dissect the related signaling pathways (36).

Thrombosis of atherosclerotic plaque depends largely on the morphology of the plaque and relative levels of tissue factor (TF) and TF pathway inhibitor (TFPI) (37). Monocyte-derived exosomes are considered potent coagulants for they contain TF that leads to the formation of procoagulant thrombin (38). Manjunath et al. found that exosomes from circulating monocytes carried more TF in lipid-rich carotid atherosclerosis. These exosomes improved the risk of thrombosis by inducing imbalances in TF and TFPI levels in vessels (39).

The Roles of Macrophage Exosomes in Endothelial Cell Migration, Monocyte Infiltration, Foam Cell Aggregation, and Vessel Calcification

During inflammation, endothelial cell migration and leukocyte recruitment are strictly controlled by integrin activation and internalization, which is a critical step in the process of angiogenesis and is closely related to the formation of atherosclerosis (40, 41). In 2014, Lee et al. found that exosomes derived from human macrophages could inhibit the migration of endothelial cells by regulating intracellular integrin $\beta 1$ trafficking. First, the exosomes secreted from macrophages promoted the internalization of integrin $\beta 1$ in primary human umbilical vein endothelial cells (HUVECs). Integrins accumulated in the perinuclear region rather than recycled back to the plasma membrane, leading to the proteolytic degradation of integrin. Second, macrophage-derived exosomes enhanced ubiquitination degradation of HUVECs integrin $\beta 1$. Third, macrophage-derived exosomes inhibited the migration of HUVECs by inhibiting integrin $\beta 1$-regulated collagen-induced mitogen-activated protein kinase/extracellular kinase signaling pathway (42). In addition, ox-LDL-stimulated macrophages might attenuate the growth and tube formation of endothelial cells and exosomes derived from these macrophages might be involved in the process (43).

Monocyte infiltration is closely related to the formation of early lesions in atherosclerosis. Damaged endothelial cells release growth factors to recruit monocytes. Monocytes adhere to the endothelium, and then migrate into the sub-endothelial space, continuously taking up ox-LDL in the intima and convert to foam cells. Tang et al. demonstrated that exosomes released from LPS-treated macrophages increased the expression of adhesion molecules ICAM-1, chemokine ligand CCL-2 and cytokine IL-6 in human vascular endothelial cells, which induced monocyte adhesion and migration (44). In 2017, Osada-Oka et al. found that in addition to ICAM-1, macrophage-derived exosomes could also promote the expression of plasminogen activator inhibitor-1 (PAI-1) and increase monocyte infiltration (45).

Foam cells derived from monocytes and smooth muscle cells accumulate and form fatty streak lesions. Fat streaks are the earliest lesions visible to the naked eye in atherosclerosis and exist through the development of plaques. Studies have shown that the release of galectin-3 (Gal-3) in macrophage- and monocyte- derived exosomes is regulated by the intercellular redox reaction. Gal3 may increase intracellular cholesterol accumulation by regulating macrophage endocytosis of low-density lipoprotein, increasing the formation of foam cells (46). In addition, miR-146a in exosomes derived from cholesterol-loaded macrophages could inhibit the expression of the pro-migratory genes IGF2BP1 and HuR in macrophages *in vitro* and *in vivo* (47). Obstruction of macrophage migration led to further accumulation of foam cells, resulting in the spread of inflammation and instability of atherosclerotic plaques. The fatty streaks are followed by fibrous lesions, which are characterized by the formation of necrotic debris and the presence of VSMCs. Niu et al. established macrophage-derived foam cell models and found that these foam cells released more vesicles than normal macrophages. Proteomic data analysis indicated that foam cell-derived exosomes promoted adhesion and migration of VSMCs by regulating the actin and focal adhesion pathways of the cytoskeleton. Western blot results showed that foam cell-derived vesicles could transport proteins to VSMCs, thereby activating ERK and Akt pathways in VSMCs and promoting adhesion and migration of VSMCs, which might accelerate the development of atherosclerotic plaques (48).

Microcalcification of the thin coronary arteries covering the intimal necrosis of atherosclerotic plaque can lead to plaque rupture, causing acute cardiovascular events (49). Vascular calcification is a ubiquitous phenomenon in atherosclerotic plaque and an inevitable result of atherosclerosis. There are abundant macrophages in the early microcalcification plaques (50). Sophie et al. found that proinflammatory macrophages release pro-calcified exosomes by the phosphatidylserine-membrane adhesion protein 5-S100A9 membrane complex. These exosomes rich in membrane adhesion proteins 5 and S100A9 directly promotes microcalcification (51).

In addition, the study of Yong-Gan Zhang et al. indicated that exosomal miR-146a derived from oxLDL-treated macrophage could promote the overproduction of ROS and NETosis by decreasing SOD2 expression in neutrophils, leading to atherosclerosis deterioration (52). A recent study discovered that Nicotine might induce atherosclerotic lesion progression after administered to $ApoE^{-/-}$ mice. Macrophage-derived exosomes containing miR-21-3p might play a role in the process of plaque progress by increasing VSMC migration and proliferation through its target PTEN (53).

In conclusion, monocyte/macrophage-derived exosomes promote atherosclerosis mainly by inhibition of vascular endothelial cell migration and promotion of endothelial cell apoptosis, monocyte infiltration, inflammation, oxidation and vascular microcalcification.

The Roles of Endothelial Cell Exosomes in Atherosclerosis

Recent studies have shown that endothelial cell-derived exosomes mediated the interactions among endothelial cells, smooth

muscle cells, and macrophages and played an important role in the pathogenesis of atherosclerosis (54). A total of 1,354 proteins and 1,992 mRNA were found in the vesicles released from cultured normal endothelial cells, reflecting the complexity of vesicle transport in endothelial cells (55).

The Roles of Endothelial Cell Exosome in Vessel Homeostasis

The cargo delivered by exosomes can regulate cell survival/death, inflammation and tumor metastasis. Therefore, exosomes are capable of modulating angiogenesis and thus play a role in maintaining vessel homeostasis.

Kruppel-like factor 2 (KLF2) is a shear stress-induced transcription factor with protective effects against atherosclerosis (56). HUVECs could secrete extracellular vesicles rich in miR-143/145 through KLF2-mediated or shear stress-stimulated mechanism. These vesicles could regulate the phenotype of smooth muscle cells and inhibit the dedifferentiation of human aortic smooth muscle cells, which is one of the reasons for its atheroprotective effect in mice (57). Bas et al. showed that miR-214 could control endothelial cell function and angiogenesis, and play a leading role in exosome-mediated signaling between endothelial cells. Endothelial cells released exosomes containing miR-214, which could stimulate angiogenesis by silencing the expression of ataxia telangiectasia mutated in adjacent target cells (58). In addition, IL-3 increased vascular endothelial cell-activated signal transduction and transcriptional activator 5 (pSTAT5)-mediated release of exosomes containing miR-126-3p and pre-miR-126, thereby promoting angiogenesis (59).

Angiogenesis and homeostasis are complex biological processes that are strictly controlled by multiple signaling pathways. Among them, the angiopoietin-Tie2 signaling pathway has received increasing attention in the past decade (60). Angiopoietin-2 (Ang2), involved in the regulation of vascular homeostasis and vascular integrity, is an extracellular protein produced primarily by endothelial cells and the main ligand of the Tie2 receptor (61). Ju et al. demonstrated that Ang2 was secreted by endothelial cells through exosomes, which was regulated positively by the syndecan 4/syntenin signaling pathway and negatively by PI3K/Akt/endothelium-dependent nitric oxide synthase (eNOS) signaling. The vascular defects observed in Akt-/- mice were partly due to the excessive secretion of Ang2 and could be ameliorated by syndecan-4 knockdown that reduced the level of extracellular Ang2. This suggested that three key signaling pathways, including angiopoietin/Tie2, PI3K/Akt/eNOS and syndecan/syntenin, played an important role in blood vessel growth and stabilization (62). Delta-like 4 (Dll4) is a Notch ligand which is expressed in endothelial cells and up-regulated during angiogenesis. As reported, endothelial exosomes incorporated with Dll4 protein could transfer Dll4 to other endothelial cells, resulting in low Notch signaling and injure the vascular integrity (63).

The Roles of Endothelial Cell Exosomes in Vascular Inflammation

High concentrations of ox-LDL and homocysteine (Hcy) are independent risk factors of atherosclerosis and coronary heart disease (64, 65). High level of circulating heat shock protein 70 (HSP70) is also at risk of vascular disease (66). Zhan et al. found that Ox-LDL and Hcy enhanced the release of HSP70-containing exosomes from rat arterial endothelial cells. These extracellular HSP70 cannot directly activate endothelial cells, but can recruit circulating monocytes to adhere to vascular endothelial cells, and thus participating in the pathogenesis of vascular inflammation (54, 67).

Long non-coding RNA-RNCR3 was significantly upregulated in mouse and human aortic atherosclerotic lesions and RNCR3 knockdown could accelerate the development of atherosclerosis and releases of inflammatory factor. Endothelial cell derived-exosomal RNCR3 could exert a remarkable atheroprotective effect *via* mediating the communication between ECs and VSMCs (68). Ten-eleven translocation 2 (TET2), a member of methylcytosine dioxygenase is considered as a key molecular to switch the phenotype of VSMCs. In response to pro-inflammatory stimuli, the CD137 pathway was activated in endothelial cells and the TET2 was reduced in endothelial cell-derived exosomes, which transferred into and then induced VSMC phenotype switch, promoting plaque formation and AS development (69).

Vesicles from TNF-α-induced inflammatory vascular endothelial cells were easily taken up by THP-1 and HUVECs. Compared with the control, the vesicles derived from inflammatory vascular endothelial cells contained intercellular adhesion molecules and chemokines, including ICAM-1, CCL-2, IL-6, IL-8, CXCL-10, CCL-5 and TNF-α. The vesicles could mediate the selective transfer of functional inflammatory mediators to target cells and modulate them to pro- or anti-inflammatory mode. Inflammatory vascular endothelial cell-derived vesicles could increase the expression of pro-inflammatory cytokines IL-6, IL-8 and ICAM-1 in HUVECs. These vesicles also increased the expression of pro-inflammatory ICAM-1 and CCL-4 in THP-1, as well as the expression of pro- and anti-inflammatory CCL-5 and CXCL-10 proteins, thereby inducing the macrophages to exhibit both pro-inflammatory and anti-inflammatory phenotypes. At the functional level, endothelial cell exosomes mediated inflammation and promoted adhesion and migration of THP-1. These evidences suggest that exosomes released by inflammatory endothelial cells are rich in a variety of inflammatory markers, chemokines, and cytokines that establish targeted cross-talk between endothelial cells and monocytes and reprogram them to pro- or anti-inflammatory phenotype (70).

HUVECs released a large quantity of exosomes rich in inflammation-associated miR-155 after ox-LDL stimulation. Later, miR-155 was transferred to THP1 cells by exosomes to promote the polarization of the anti-inflammatory M2 macrophages to pro-inflammatory M1 macrophages. The vesicles expressing KLF2 secreted from endothelial cells inhibited monocyte activation and decreased inflammation. Oil red O staining showed that exosomes secreted by endothelial cell expressing KLF2 significantly reduced atherosclerotic lesions in mice, decreased pro-inflammatory M1 macrophages and increased anti-inflammatory M2 macrophages, which partly resulted from the down-regulation of miR-155 expression (71).

Neutrophil extracellular traps (NETs) play an important role in the pathological process of atherosclerosis. Both exosomes from atherosclerosis patients and ox-LDL treated HUVECs induced NETs release from neutrophils, aggravating atherosclerosis. The highly-expressed miR-505 encapsulated in these exosomes might inhibit Sirtuin 3 (SIRT3) in neutrophils, increasing ROS levels and NET release by neutrophils (72). Metastasis-associated lung adenocarcinoma transcript 1 (MALAT1), a long non-coding RNA has been widely shown to be involved in tumorigenesis, but the role of exosomal MALAT1 in atherosclerosis is likely to be controversial. Gao H et al. came to the conclusion that exosomal MALAT1 derived from ox-LDL-treated HUVECs promoted the formation and release of NETs which might further deteriorated atherosclerosis (73). However, Hongqi L et al. found that the MALAT1 expression in the exosomes derived from ox-LDL treated HUVECs was lower than the exosomes derived from untreated HUVECs. Their further *in vivo* experiments showed the loss of MALAT1 from ox-LDL-VECs-Exos in mouse repressed the nuclear factor erythroid 2-related factor (NRF2) signaling pathway and failed to inhibit dendritic cells maturation, which might be associated with atherosclerosis progression (74). Therefore, the precise roles of exosomal MALAT1 in atherogenesis should be further investigated.

The Roles of Platelet-Derived Exosomes in Atherosclerosis

Platelets are involved in thrombosis. Platelet activation and endothelial damage play an important role in atherosclerosis. A variety of platelet-derived exosomes regulate the progression of atherosclerosis (75, 76).

Various agonist-activated platelets release exosomes from plasma membrane. Orla P. Barry et al. found that activated platelets increased monocyte adhesion to HUVECs in a time- and dose-dependent manner, primarily due to the exosomes secreted by these platelets selectively increasing the expression of the adhesion molecule ICAM-1 and inflammatory cytokines including IL-1β, IL-6, and IL-8 in HUVECs while having no up-regulating effects on the expression of adhesion molecules VCAM-1 and P-/E-selectin (77). Furthermore, in 2003, Kaneider et al. found that thrombin-activated platelet exosomes carried CD40 ligands and triggered dendritic cell maturation through the mechanism of CD40 ligands to modulate inflammatory immune responses (78).

Exosomes secreted by thrombin-activated platelets have protective effects on atherosclerotic endothelial inflammation. The miR-223 was elevated in thrombin-activated platelet exosomes and was transferred into vascular endothelial cells to inhibit phosphorylation of p38, JNK and ERK, then blocked nuclear translocation of p65 of NF-κB, ultimately decreased the high expression of ICAM-1 stimulated by TNF-α (79). MiR-223 in platelet exosomes also regulated apoptosis of vascular endothelial cells and affected the development of atherosclerosis. miR-223 was significantly increased in platelet-derived exosomes stimulated by thrombopoietin or thrombin and in patients with atherosclerosis. Then exosomes introduced miR-223 into HUVECs, which in turn reduced insulin-like growth factor 1 receptors and ultimately promoted apoptosis of HUVECs induced by advanced glycation end products (80). In addition, Yao Y et al. discovered that exosomes derived from platelets of the atherosclerosis models of ApoE-/- mice exhibited high expression level of miR-25-3p which could target Adam 10 and reduce its expression in the ox-LDL-treated coronary vascular endothelial cells (CVECs), leading to the attenuation of CVEC inflammation (81).

Platelet-derived exosomes can also inhibit platelet aggregation *in vitro* and reduce the adhesion of platelets to exposed collagen from damaged blood vessels caused by high shear forces *in vivo*. By decreasing the reactivity of platelets, exosomes inhibit vascular occlusive thrombosis in a model of damaged arterial caused by ferric chloride. In atherosclerosis, exosomes from activated platelets significantly reduce type II scavenger receptor CD36 expression in platelets, thus reducing platelet aggregation. On the other hand, exosomes from activated platelets also inhibit uptake of ox-LDL in macrophages, thereby preventing the formation of foam cells by reducing the expression of type II scavenger receptor CD36 in macrophages, ultimately inhibiting thrombosis in atherosclerosis (82).

In summary, activated platelet-derived exosomes play an important regulatory role in endothelial damage, endothelial cell apoptosis, monocyte adhesion, and dendritic cell maturation during atherosclerosis. At the same time, platelet-derived exosomes inhibit the development of atherosclerosis by inhibiting platelet aggregation and thrombosis. However, the *in vivo* regulatory mechanism still needs further studies.

The Roles of Vascular Smooth Muscle Cell Exosomes in Atherosclerosis

Smooth muscle cells (SMCs) differentiation and endothelial cell damage promote the formation of atherosclerotic plaques (83). Exosomes derived from VSMCs mediate KLF5-induced miR-155 transfer from SMCs to endothelial cells, thereby destroying endothelial tight junctions and barrier integrity, increasing endothelial permeability and promoting atherosclerosis (84). The transfer of miR-155 to endothelial cells leads to the overexpression of miR-155 in endothelial cells, which can inhibit proliferation, migration and re-endothelialization of endothelial cells *in vitro* and *in vivo*, thereby increasing permeability of vascular endothelium (85).

Alexander et al. used calcified cultured human VSMCs as a model of atherosclerotic vascular calcification. Exosomes released by these VSMCs contained high calcium and extracellular matrix proteins. Extracellular high calcium induces expression of sphingomyelin diesterase 3 and release of VSMC-secreted high calcium-contained exosomes *in vitro*. After VSMCs were stimulated by tumor necrosis factor-α and platelet-derived growth factor-BB, exosomes were released and deposited in blood vessels, thereby accelerating the calcification of blood vascular walls (86).

In the diabetic mouse model, exosomes derived from VSMCs containing miR-221/222 were more likely to cause atherosclerosis compared with the non-diabetic mice, and the introduction

of exosomes of diabetic VSMCs into ApoE-/- mice led to deterioration of atherosclerotic lesions (87).

Thrombosis caused by atherosclerotic plaque rupture is the main cause of vascular embolism events including myocardial infarction, unstable angina, and stoke. Exposure to TF upon plaque rupture initiates the extrinsic coagulation pathway. Kapustin et al. found that platelet derived growth factor (PDGF) and tumor necrosis factor-α (TNFα) stimulated release of exosomes from VSMCs (86). This result correlate well with another study which showed that TF is secreted from vesicles (<200 nm) released by VSMCs and this process is regulated by PDGF and TNFα (88). Meanwhile, exosomal PS can bind to coagulation factors. Thus, exosomes released by VSMCs may contribute to vascular thrombosis events (89).

Roles of Other Cell Exosomes in Atherosclerosis

In 2006, Mayerl et al. analyzed 12 human atherosclerotic specimens collected by von Rokitansky's and reported that T cells were involved in the early pathological process of atherosclerosis (90). Subsequent researchers further confirmed that T cells were present in all stages of atherosclerotic plaque, formatting the basis of adaptive immune response in atherosclerosis (91, 92). Although activated $CD4^+$ T lymphocytes infiltrate atherosclerotic plaques, the effects of T-cell exosomes on atherosclerosis-associated cells have not been fully understood. Liudmila et al. isolated exosomes from the supernatant of activated human $CD4^+$ T cells and found that endogenous phosphatidylserine receptors mediated the process of T cell exosomes into monocytes, thereby increasing the appearance of lipid droplets containing cholesterol ester and free cholesterol in cytoplasm of recipient cells (93).

Myeloid derived suppressor cells (MDSC) originate from immature myeloid cells under pathological microenvironment. It has been reported that the inflammatory environment and exogenous stimuli that promoted the differentiation of immature myeloid cells can also facilitate the release of exosomes from MDSCs. Deng Z et al. demonstrated that doxorubicin treatment of mammary carcinoma bearing mice led to the induction of miR-126^+ MDSCs and MDSC miR-$126a^+$ exosomes, which could promote tumor angiogenesis (94). Meanwhile, administration of miR-126-5p could rescue EC proliferation and limit atherosclerosis (95), indicating that MDSC-derived exosomal miR-126a might limit the atherosclerotic lesion formation in the same way (96).

Other types of cells in atherosclerotic plaques, such as dendritic cells, can internalize ox-LDL to become foam cells. They increase in atherosclerotic lesions to mediate adaptive cellular immune inflammation reaction in early stage. Mature dendritic cell-derived exosomes mediated activation of NF-κB pathway via abundant TNF-α on their membrane, which increased endothelial cell inflammation and thereby promoted atherosclerosis (97). A recent study demonstrated that adipose-derived mesenchymal stem cells (ADSCs)-derived exosomes could restrain the expression of miR-324-5p which targeted at PPP1R12B in the lesion model for HUVECs. Their work revealed a possible mechanism in which ADSCs-derived exosomes might protect endothelial cells against atherosclerosis (98).

Vascular adventitial fibroblasts play a key role in vascular wall function and structure regulation. It's reported that miR-155-5p transferred by adventitial fibroblasts-derived exosomes could attenuate VSMC proliferation via suppressing angiotension-converting enzyme, which might be anti-atherosclerotic (99).

Exosomes derived from cardiomyocytes in type 2 diabetic rats exerted an anti-angiogenic function by transferring miR-320 into endothelial cells, suggesting that exosomes could promote atherosclerosis by inducing endothelial dysfunction (100). Recently, Xiong Y et al. found a significant upregulation of miR-20b-5p in circulating exosomes in diabetic patients. This miRNA could suppress endothelial cell angiogenesis by regulating Wnt9b/β-catenin signaling (101). However, the cellular sources of these exosomes need further studies.

POTENTIAL APPLICATION OF EXOSOMES IN THE DIAGNOSIS AND TREATMENT OF ATHEROSCLEROSIS

As a natural carrier, exosomes contain abundant biologically active molecules including proteins, mRNAs, miRNAs and lipids, which are cordoned off and protected from degradation by exosomal membrane. Actually, this property of exosomes makes them a novel promising biomarker for diseases. Furthermore, natural or modified exosomes can also serve as therapeutic tools to modulate target cell dysfunction or deliver drug to cells, altering the phenotype and function of the target cells (102).

As a Biomarker for Disease Detection

Biomarkers have been used for objective measurement and assessment and served as indicators of normal biological function, pathogenic process or pharmacological response to therapeutic interventions (103). Secretion of exosomes increases in response to stress or injury, especially in atherosclerosis patients with vascular injury, inflammation, and prothrombotic state (102). Circulating exosomes have become significant candidates for cardiovascular disease biomarkers. At the same time, the content of exosomes depends largely on the pathological and physiological state of the cells or tissues. The structure of the lipid bilayer keeps the exosome content stable against various enzymes. Therefore, detection of exosomes in plasma may be a novel minimally invasive indicator for early stage of diseases. In addition, extracellular vesicles are similar to their parental cells in many characteristics, such as surface receptors, integrated membrane proteins, cytosolic proteins, mRNAs and miRNAs. Exosomal miRNAs, which may have significantly different circulating levels between healthy subjects and patients with cardiovascular disease, are therefore useful as biomarkers for diagnosis and prognosis.

It's been reported that elevated levels of plasma platelets and/or endothelial extracellular vesicles could be used to predict cardiovascular morbidity and mortality in atherosclerosis patients (104, 105). Kuwabara et al. observed elevated levels of miR-1 and miR-133a in vesicles of patients with myocardial

infarction and unstable angina, which could be used as biomarkers for myocardial cell death and injury (106). In addition, serum miR-34a, miR-192, and miR-194 are elevated in patients with acute myocardial infarction, especially in CD63-positive exosomes, which is associated with a high risk of ischemic heart failure 1 year after myocardial infarction (107). Recently, a study reported a higher expression of miR-30e and miR-92a in exosomes from serum in patients with coronary atherosclerosis compared with healthy subjects. MiR-30e and miR-92a targeted ATP binding cassette (ABC) A1 and downregulated its expression, subsequently regulating cholesterol metabolism. Therefore, the levels of miR-30e and miR-92a in exosomes from serum could be a novel diagnostic biomarker for atherosclerosis (108). In addition, it's reported that specific kind of circulating exosomal miRNAs such as miR-122-5p, miR-27b-3p, and miR-24-3p etc., could be a novel predictor for recurrent ischemic events in intracranial atherosclerosis (109).

Potential Application of Exosomes to the Treatment of Atherosclerosis

As a natural vesicle isolated from tissues or cells, exosomes have biocompatibility, bio-barrier permeability, low toxicity and low immunogenicity, which shows that exosomes have potential therapeutic effects in diseases (24, 110).

Exosomes, delivering miRNAs for repair of damaged tissues caused by atherosclerosis (such as delivery of atheroprotective miRNAs) or anti-miRs (e.g., antisense miRNAs) for clearance of pro-atherosclerotic miRNAs are considered as a promising carrier tool to be used for the treatment of atherosclerosis. The potential miRNAs are mainly miR-126 (endothelium-specific and atheroprotective) and miR-145 (VSMC-specific and atheroprotective) (111).

Exogenous miRNAs, siRNAs, and even drugs can be encapsulated in natural exosomes or engineered exosomes. Mature techniques for encapsulation of therapeutic miRNAs or siRNAs in exosomes can be used through the following methods: (1) donor cells can be co-transfected with two types of plasmids or viruses (112); (2) miRNAs or siRNAs can be directly loaded to purified exosomes through electroporation (113, 114); (3) transient transfection of miRNAs using commercial transfection reagents (115); (4) other loading methods, such as permeabilization by saponin, sonication or extrusion can improve loading efficiency, but still need further verification (116). For example, Wu G et al. discovered that M2 macrophage-derived exosomes electroporated with FDA-approved five-administration hydrochloride exhibited excellent inflammation-tropism and anti-inflammation effects and could be used for AS imaging and therapy (117). Techniques for assembling drugs into exosomes are also evolving. There are currently three different methods for drug loading into exosomes: (1) direct incorporation of small molecule drugs into purified exosomes such as lipophilic small molecules, low molecular weight antioxidants and anticancer agents (113, 118, 119); (2) loading the drug into the donor cell which secretes exosomes thereby loading the drug into the exosomes (116, 120); (3) direct transfection of the drug-encoding DNA into donor cells resulting in drug expression and sorting into exosomes (120). Kalani et al. loaded curcumin into donor mouse brain endothelial cells by direct infiltration. Curcumin-loaded exosomes isolated from endothelial cells penetrated the blood-brain barrier well and could reduce oxidative stress and MMP-9 levels, as well as improve endothelial cell permeability to ultimately reduce dysfunction of endothelial cell induced by hyperhomocysteinemia (121). In general, the characteristics of technology, function and safety for exosomes have not been fully understood. The therapeutic significance of exosomes in atherosclerosis remains to be further studied.

Recently, a study provided a new strategy for the treatment of patients with familial hypercholesterolemia (FH) and managing atherosclerosis. They used low-density lipoprotein receptor (Ldlr)-deficient mice ($Ldlr^{-/-}$ mice) as a model of FH and found that exosomes-mediated Ldlr mRNA delivery could robustly restored Ldlr expression in the $Ldlr^{-/-}$ mouse model. Significantly, serum LDL-cholesterol levels were lowered and the number and size of atherosclerotic plaques were reduced (122). In addition, *in vivo* experiments showed that mesenchymal stem cell-derived exosomes with miR-145 could downregulate JAM-A expression and reduce atherosclerosis plaque size, suggesting the role of exosomes derived from MSCs containing miR-145 in the treatment of atherosclerosis (123). Chrysin could attenuate the expression of miR-92a in exosomes derived from human coronary artery endothelial cell and counteract the inhibitory effect of miR-92a on the expression of KLF2, and play an atheroprotective role (124).

CONCLUSIONS

As a new and effective intercellular communication tool, exosomes have attracted more and more attention in the field of biology, including atherosclerotic cardiovascular diseases. Exosomes envelop various biomolecules according to pathological/physiological conditions and different cellular sources. In most cases, exosomes mainly promote the progression of atherosclerosis. However, there are also studies showing the atheroprotective role of exosomes, indicating the multifuctional property of exosomes in atherosclerosis. To date, there are still many problems to be solved regarding exosomal biology, such as exosome formation, release, internalization and clearance. Besides, the molecular mechanisms of exosome-based intercellular communication associated with atherosclerosis are expected to be elucidated.

As for the clinical application, the assessment of circulating exosomes as a diagnostic and prognostic biomarker for cardiovascular risk has just started. Several technical limitations still exist, such as the lack of gold-standard method for exosome isolation as mentioned earlier and the influence of confounding factors like disease specificity the presence of comorbidities. It needs more research to validate the relationship between disease progression and exosome-associated biomarkers (such as miRNAs carried in exosomes) and figure out the value of exosomes for diagnosis and prognosis. In addition, the precise

cellular origin, package and secretion mechanisms of biomarkers carried by exosomes and their functional roles remain to be studied.

Because exosomes are natural carriers of biologically active molecules, they can be an attractive therapeutic tool. They may act as carriers for drugs or siRNAs to control gene expression and accelerate disease recovery, or to carry excess lipids at the plaque to expel atherosclerotic plaques, thereby slowing the onset and progression of the disease. In addition, although some meaningful findings have been made on the prognosis and treatment of vascular diseases, research on exosome-based treatment methods is still limited, so further basic medical research is needed before applications.

AUTHOR CONTRIBUTIONS

JY wrote the initial version of the manuscript. BL made supplements to the manuscript based on the latest studies. JF revised the manuscript. All authors contributed to the article and approved the submitted version.

FUNDING

This work was supported by the grants from National Natural Science Foundation of China (91939105 and 81770445) and Natural Science Foundation of Beijing, China (M21008).

REFERENCES

1. Zhao D, Liu J, Wang M, Zhang X, Zhou M Epidemiology of cardiovascular disease in china: Current features and implications. *Nat Rev Cardiol.* (2019) 16:203–12. doi: 10.1038/s41569-018-0119-4
2. Galkina E, Ley K Immune and inflammatory mechanisms of atherosclerosis (*). *Annu Rev Immunol.* (2009) 27:165–97. doi: 10.1146/annurev.immunol.021908.132620
3. Freigang S, Ampenberger F, Weiss A, Kanneganti TD, Iwakura Y, Hersberger M, et al. Fatty acid-induced mitochondrial uncoupling elicits inflammasome-independent il-1alpha and sterile vascular inflammation in atherosclerosis. *Nat Immunol.* (2013) 14:1045–53. doi: 10.1038/ni.2704
4. Witztum JL, Lichtman AH The influence of innate and adaptive immune responses on atherosclerosis. *Annu Rev Pathol.* (2014) 9:73–102. doi: 10.1146/annurev-pathol-020712-163936
5. Hansson GK, Robertson AK, Soderberg-Naucler C Inflammation and atherosclerosis. *Annu Rev Pathol.* (2006) 1:297–329. doi: 10.1146/annurev.pathol.1.110304.100100
6. Gistera A, Hansson GK The immunology of atherosclerosis. *Nat Rev Nephrol.* (2017) 13:368–80. doi: 10.1038/nrneph.2017.51
7. Ross R. Atherosclerosis–an inflammatory disease. *N Engl J Med.* (1999) 340:115–26. doi: 10.1056/NEJM199901143400207
8. Tsoref O, Tyomkin D, Amit U, Landa N, Cohen-Rosenboim O, Kain D, et al. E-selectin-targeted copolymer reduces atherosclerotic lesions, adverse cardiac remodeling, and dysfunction. *J Control Release.* (2018) 288:136–47. doi: 10.1016/j.jconrel.2018.08.029
9. Wolak T. Osteopontin - a multi-modal marker and mediator in atherosclerotic vascular disease. *Atherosclerosis.* (2014) 236:327–37. doi: 10.1016/j.atherosclerosis.2014.07.004
10. Libby P, Lichtman AH, Hansson GK Immune effector mechanisms implicated in atherosclerosis: From mice to humans. *Immunity.* (2013) 38:1092–104. doi: 10.1016/j.immuni.2013.06.009
11. Hansson GK, Hermansson A The immune system in atherosclerosis. *Nat Immunol.* (2011) 12:204–12. doi: 10.1038/ni.2001
12. Lee TH, D'Asti E, Magnus N, Al-Nedawi K, Meehan B, Rak J Microvesicles as mediators of intercellular communication in cancer–the emerging science of cellular 'debris'. *Semin Immunopathol.* (2011) 33:455–67. doi: 10.1007/s00281-011-0250-3
13. Sluijter JP, Verhage V, Deddens JC, van den Akker F, Doevendans PA Microvesicles and exosomes for intracardiac communication. *Cardiovasc Res.* (2014) 102:302–11. doi: 10.1093/cvr/cvu022
14. Perrotta I, Aquila S Exosomes in human atherosclerosis: An ultrastructural analysis study. *Ultrastruct Pathol.* (2016) 40:101–6. doi: 10.3109/01913123.2016.1154912
15. Mathieu M, Martin-Jaular L, Lavieu G, Thery C Specificities of secretion and uptake of exosomes and other extracellular vesicles for cell-to-cell communication. *Nat Cell Biol.* (2019) 21:9–17. doi: 10.1038/s41556-018-0250-9
16. Ibrahim A, Marban E Exosomes: Fundamental biology and roles in cardiovascular physiology. *Annu Rev Physiol.* (2016) 78:67–83. doi: 10.1146/annurev-physiol-021115-104929
17. Pan BT, Johnstone RM Fate of the transferrin receptor during maturation of sheep reticulocytes in vitro: Selective externalization of the receptor. *Cell.* (1983) 33:967–78. doi: 10.1016/0092-8674(83)90040-5
18. Harding C, Heuser J, Stahl P Receptor-mediated endocytosis of transferrin and recycling of the transferrin receptor in rat reticulocytes. *J Cell Biol.* (1983) 97:329–39. doi: 10.1083/jcb.97.2.329
19. Pan BT, Teng K, Wu C, Adam M, Johnstone RM Electron microscopic evidence for externalization of the transferrin receptor in vesicular form in sheep reticulocytes. *J Cell Biol.* (1985) 101:942–8. doi: 10.1083/jcb.101.3.942
20. Yang D, Zhang W, Zhang H, Zhang F, Chen L, Ma L, et al. Progress, opportunity, and perspective on exosome isolation - efforts for efficient exosome-based theranostics. *Theranostics.* (2020) 10:3684–707. doi: 10.7150/thno.41580
21. Konoshenko MY, Lekchnov EA, Vlassov AV, Laktionov PP Isolation of extracellular vesicles: General methodologies and latest trends. *Biomed Res Int.* (2018) 2018:8545347. doi: 10.1155/2018/8545347
22. van Niel G, D'Angelo G, Raposo G Shedding light on the cell biology of extracellular vesicles. *Nat Rev Mol Cell Biol.* (2018) 19:213–28. doi: 10.1038/nrm.2017.125
23. Mathivanan S, Fahner CJ, Reid GE, Simpson RJ Exocarta 2012: Database of exosomal proteins, rna and lipids. *Nucleic Acids Res.* (2012) 40:D1241–1244. doi: 10.1093/nar/gkr828
24. Barile L, Vassalli G Exosomes: Therapy delivery tools and biomarkers of diseases. *Pharmacol Ther.* (2017) 174:63–78. doi: 10.1016/j.pharmthera.2017.02.020
25. Colombo M, Raposo G, Thery C Biogenesis, secretion, and intercellular interactions of exosomes and other extracellular vesicles. *Annu Rev Cell Dev Biol.* (2014) 30:255–89. doi: 10.1146/annurev-cellbio-101512-122326
26. Thery C, Zitvogel L, Amigorena S Exosomes: Composition, biogenesis and function. *Nat Rev Immunol.* (2002) 2:569–79. doi: 10.1038/nri855
27. Barile L, Moccetti T, Marban E, Vassalli G Roles of exosomes in cardioprotection. *Eur Heart J.* (2017) 38:1372–9. doi: 10.1093/eurheartj/ehw304
28. Yuan Y, Du W, Liu J, Ma W, Zhang L, Du Z, et al. Stem cell-derived exosome in cardiovascular diseases: Macro roles of micro particles. *Front Pharmacol.* (2018) 9:547. doi: 10.3389/fphar.2018.00547
29. Martin J, Collot-Teixeira S, McGregor L, McGregor JL The dialogue between endothelial cells and monocytes/macrophages in vascular syndromes. *Curr Pharm Des.* (2007) 13:1751–9. doi: 10.2174/138161207780831248
30. Lawson C, Vicencio JM, Yellon DM, Davidson SM Microvesicles and exosomes: New players in metabolic and cardiovascular disease. *J Endocrinol.* (2016) 228:R57–71. doi: 10.1530/JOE-15-0201
31. Hafiane A, Daskalopoulou SS Extracellular vesicles characteristics and emerging roles in atherosclerotic cardiovascular disease. *Metabolism.* (2018) 85:213–22. doi: 10.1016/j.metabol.2018.04.008

32. Halim AT, Ariffin NA, Azlan M Review: The multiple roles of monocytic microparticles. *Inflammation.* (2016) 39:1277–84. doi: 10.1007/s10753-016-0381-8
33. Jansen F, Li Q, Pfeifer A, Werner N Endothelial- and immune cell-derived extracellular vesicles in the regulation of cardiovascular health and disease. *JACC Basic Transl Sci.* (2017) 2:790–807. doi: 10.1016/j.jacbts.2017.08.004
34. Hoyer FF, Giesen MK, Nunes Franca C, Lutjohann D, Nickenig G, Werner N Monocytic microparticles promote atherogenesis by modulating inflammatory cells in mice. *J Cell Mol Med.* (2012) 16:2777–88. doi: 10.1111/j.1582-4934.2012.01595.x
35. Madrigal-Matute J, Fernandez-Garcia CE, Blanco-Colio LM, Burillo E, Fortuno A, Martinez-Pinna R, et al. Thioredoxin-1/peroxiredoxin-1 as sensors of oxidative stress mediated by nadph oxidase activity in atherosclerosis. *Free Radic Biol Med.* (2015) 86:352–61. doi: 10.1016/j.freeradbiomed.2015.06.001
36. Mastronardi ML, Mostefai HA, Soleti R, Agouni A, Martinez MC, Andriantsitohaina R Microparticles from apoptotic monocytes enhance nitrosative stress in human endothelial cells. *Fundam Clin Pharmacol.* (2011) 25:653–60. doi: 10.1111/j.1472-8206.2010.00898.x
37. Fuster V, Moreno PR, Fayad ZA, Corti R, Badimon JJ Atherothrombosis and high-risk plaque: Part i: Evolving concepts. *J Am Coll Cardiol.* (2005) 46:937–54. doi: 10.1016/j.jacc.2005.03.074
38. Aharon A, Tamari T, Brenner B Monocyte-derived microparticles and exosomes induce procoagulant and apoptotic effects on endothelial cells. *Thromb Haemost.* (2008) 100:878–85. doi: 10.1160/TH07-11-0691
39. Basavaraj MG, Sovershaev MA, Egorina EM, Gruber FX, Bogdanov VY, Fallon JT, et al. Circulating monocytes mirror the imbalance in tf and tfpi expression in carotid atherosclerotic plaques with lipid-rich and calcified morphology. *Thromb Res.* (2012) 129:e134–141. doi: 10.1016/j.thromres.2011.11.044
40. Ley K, Laudanna C, Cybulsky MI, Nourshargh S Getting to the site of inflammation: The leukocyte adhesion cascade updated. *Nat Rev Immunol.* (2007) 7:678–89. doi: 10.1038/nri2156
41. Leavesley DI, Schwartz MA, Rosenfeld M, Cheresh DA Integrin beta 1- and beta 3-mediated endothelial cell migration is triggered through distinct signaling mechanisms. *J Cell Biol.* (1993) 121:163–70. doi: 10.1083/jcb.121.1.163
42. Lee HD, Kim YH, Kim DS Exosomes derived from human macrophages suppress endothelial cell migration by controlling integrin trafficking. *Eur J Immunol.* (2014) 44:1156–69. doi: 10.1002/eji.201343660
43. Huang C, Huang Y, Zhou Y, Nie W, Pu X, Xu X, et al. Exosomes derived from oxidized ldl-stimulated macrophages attenuate the growth and tube formation of endothelial cells. *Mol Med Rep.* (2018) 17:4605–10. doi: 10.3892/mmr.2018.8380
44. Tang N, Sun B, Gupta A, Rempel H, Pulliam L Monocyte exosomes induce adhesion molecules and cytokines via activation of nf-kappab in endothelial cells. *FASEB J.* (2016) 30:3097–106. doi: 10.1096/fj.201600368RR
45. Osada-Oka M, Shiota M, Izumi Y, Nishiyama M, Tanaka M, Yamaguchi T, et al. Macrophage-derived exosomes induce inflammatory factors in endothelial cells under hypertensive conditions. *Hypertens Res.* (2017) 40:353–60. doi: 10.1038/hr.2016.163
46. Nachtigal M, Ghaffar A, Mayer EP Galectin-3 gene inactivation reduces atherosclerotic lesions and adventitial inflammation in apoe-deficient mice. *Am J Pathol.* (2008) 172:247–55. doi: 10.2353/ajpath.2008.070348
47. Nguyen MA, Karunakaran D, Geoffrion M, Cheng HS, Tandoc K, Perisic Matic L, et al. Extracellular vesicles secreted by atherogenic macrophages transfer microrna to inhibit cell migration. *Arterioscler Thromb Vasc Biol.* (2018) 38:49–63. doi: 10.1161/ATVBAHA.117.309795
48. Niu C, Wang X, Zhao M, Cai T, Liu P, Li J, et al. Macrophage foam cell-derived extracellular vesicles promote vascular smooth muscle cell migration and adhesion. *J Am Heart Assoc.* (2016) 5:e004099. doi: 10.1161/jaha.116.004099
49. Libby P, Aikawa M Stabilization of atherosclerotic plaques: New mechanisms and clinical targets. *Nat Med.* (2002) 8:1257–62. doi: 10.1038/nm1102-1257
50. Li R, Mittelstein D, Lee J, Fang K, Majumdar R, Tintut Y, et al. A dynamic model of calcific nodule destabilization in response to monocyte- and oxidized lipid-induced matrix metalloproteinases. *Am J Physiol Cell Physiol.* (2012) 302:C658–665. doi: 10.1152/ajpcell.00313.2011
51. New SE, Goettsch C, Aikawa M, Marchini JF, Shibasaki M, Yabusaki K, et al. Macrophage-derived matrix vesicles: An alternative novel mechanism for microcalcification in atherosclerotic plaques. *Circ Res.* (2013) 113:72–7. doi: 10.1161/CIRCRESAHA.113.301036
52. Zhang YG, Song Y, Guo XL, Miao RY, Fu YQ, Miao CF, et al. Exosomes derived from oxldl-stimulated macrophages induce neutrophil extracellular traps to drive atherosclerosis. *Cell Cycle.* (2019) 18:2674–84. doi: 10.1080/15384101.2019.1654797
53. Zhu J, Liu B, Wang Z, Wang D, Ni H, Zhang L, et al. Exosomes from nicotine-stimulated macrophages accelerate atherosclerosis through mir-21-3p/pten-mediated vsmc migration and proliferation. *Theranostics.* (2019) 9:6901–19. doi: 10.7150/thno.37357
54. Danielson KM, Saumya D. Extracellular vesicles in heart disease: excitement for the future? *Exosomes Microvesicles.* (2014) 2:10.5772/58390. doi: 10.5772/58390
55. de Jong OG, Verhaar MC, Chen Y, Vader P, Gremmels H, Posthuma G, et al. Cellular stress conditions are reflected in the protein and RNA content of endothelial cell-derived exosomes. *J Extracell Vesicles.* (2012) 1:18396. doi: 10.3402/jev.v1i0.18396
56. Boon RA, Horrevoets AJ Key transcriptional regulators of the vasoprotective effects of shear stress. *Hamostaseologie.* (2009) 29, 39–40. doi: 10.1055/s-0037-1616937
57. Hergenreider E, Heydt S, Tréguer K, Boettger T, Horrevoets AJ, Zeiher AM, et al. Atheroprotective communication between endothelial cells and smooth muscle cells through mirnas. *Nat Cell Biol.* (2012) 14:249–56. doi: 10.1038/ncb2441
58. van Balkom BW, de Jong OG, Smits M, Brummelman J, den Ouden K, de Bree PM, et al. Endothelial cells require mir-214 to secrete exosomes that suppress senescence and induce angiogenesis in human and mouse endothelial cells. *Blood.* (2013) 121:3997–4006. doi: 10.1182/blood-2013-02-478925
59. Lombardo G, Dentelli P, Togliatto G, Rosso A, Gili M, Gallo S, et al. Activated stat5 trafficking *via* endothelial cell-derived extracellular vesicles controls il-3 pro-angiogenic paracrine action. *Sci Rep.* (2016) 6:25689. doi: 10.1038/srep25689
60. Augustin HG, Koh GY, Thurston G, Alitalo K Control of vascular morphogenesis and homeostasis through the angiopoietin-tie system. *Nat Rev Mol Cell Biol.* (2009) 10:165–77. doi: 10.1038/nrm2639
61. Suri C, Jones PF, Patan S, Bartunkova S, Maisonpierre PC, Davis S, et al. Requisite role of angiopoietin-1, a ligand for the tie2 receptor, during embryonic angiogenesis. *Cell.* (1996) 87:1171–80. doi: 10.1016/S0092-8674(00)81813-9
62. Ju R, Zhuang ZW, Zhang J, Lanahan AA, Kyriakides T, Sessa WC, et al. Angiopoietin-2 secretion by endothelial cell exosomes: Regulation by the phosphatidylinositol 3-kinase (pi3k)/akt/endothelial nitric oxide synthase (enos) and syndecan-4/syntenin pathways. *J Biol Chem.* (2014) 289:510–9. doi: 10.1074/jbc.M113.506899
63. Sheldon H, Heikamp E, Turley H, Dragovic R, Thomas P, Oon CE, et al. New mechanism for notch signaling to endothelium at a distance by delta-like 4 incorporation into exosomes. *Blood.* (2010) 116:2385–94. doi: 10.1182/blood-2009-08-239228
64. Lou Y, Liu S, Zhang C, Zhang G, Li J, Ni M, et al. Enhanced atherosclerosis in tipe2-deficient mice is associated with increased macrophage responses to oxidized low-density lipoprotein. *J Immunol.* (2013) 191:4849–57. doi: 10.4049/jimmunol.1300053
65. Harker LA, Ross R, Slichter SJ, Scott CR Homocystine-induced arteriosclerosis. The role of endothelial cell injury and platelet response in its genesis. *J Clin Invest.* (1976) 58:731–41. doi: 10.1172/JCI108520
66. Zhu J, Quyyumi AA, Wu H, Csako G, Rott D, Zalles-Ganley A, et al. Increased serum levels of heat shock protein 70 are associated with low risk of coronary artery disease. *Arterioscler Thromb Vasc Biol.* (2003) 23:1055–9. doi: 10.1161/01.ATV.0000074899.60898.FD
67. Zhan R, Leng X, Liu X, Wang X, Gong J, Yan L, et al. Heat shock protein 70 is secreted from endothelial cells by a non-classical pathway involving exosomes. *Biochem Biophys Res Commun.* (2009) 387:229–33. doi: 10.1016/j.bbrc.2009.06.095

68. Shan K, Jiang Q, Wang XQ, Wang YN, Yang H, Yao MD, et al. Role of long non-coding rna-rncr3 in atherosclerosis-related vascular dysfunction. *Cell Death Dis.* (2016) 7:e2248. doi: 10.1038/cddis.2016.145
69. Li B, Zang G, Zhong W, Chen R, Zhang Y, Yang P, et al. Activation of cd137 signaling promotes neointimal formation by attenuating tet2 and transferring from endothelial cell-derived exosomes to vascular smooth muscle cells. *Biomed Pharmacother.* (2020) 121:109593. doi: 10.1016/j.biopha.2019.109593
70. Hosseinkhani B, Kuypers S, van den Akker NMS, Molin DGM, Michiels L Extracellular vesicles work as a functional inflammatory mediator between vascular endothelial cells and immune cells. *Front Immunol.* (2018) 9:1789. doi: 10.3389/fimmu.2018.01789
71. He S, Wu C, Xiao J, Li D, Sun Z, Li M Endothelial extracellular vesicles modulate the macrophage phenotype: Potential implications in atherosclerosis. *Scand J Immunol.* (2018) 87:e12648. doi: 10.1111/sji.12648
72. Chen L, Hu L, Li Q, Ma J, Li H Exosome-encapsulated mir-505 from ox-ldl-treated vascular endothelial cells aggravates atherosclerosis by inducing net formation. *Acta Biochim Biophys Sin (Shanghai).* (2019) 51:1233–41. doi: 10.1093/abbs/gmz123
73. Gao H, Wang X, Lin C, An Z, Yu J, Cao H, et al. Exosomal malat1 derived from ox-ldl-treated endothelial cells induce neutrophil extracellular traps to aggravate atherosclerosis. *Biol Chem.* (2020) 401:367–76. doi: 10.1515/hsz-2019-0219
74. Li H, Zhu X, Hu L, Li Q, Ma J, Yan J Loss of exosomal malat1 from ox-ldl-treated vascular endothelial cells induces maturation of dendritic cells in atherosclerosis development. *Cell Cycle.* (2019) 18:2255–67. doi: 10.1080/15384101.2019.1642068
75. Landry P, Plante I, Ouellet DL, Perron MP, Rousseau G, Provost P Existence of a microrna pathway in anucleate platelets. *Nat Struct Mol Biol.* (2009) 16:961–6. doi: 10.1038/nsmb.1651
76. Osteikoetxea X, Nemeth A, Sodar BW, Vukman KV, Buzas EI Extracellular vesicles in cardiovascular disease: Are they jedi or sith? *J Physiol.* (2016) 594:2881–94. doi: 10.1113/JP271336
77. Barry OP, Pratico D, Savani RC, FitzGerald GA Modulation of monocyte-endothelial cell interactions by platelet microparticles. *J Clin Invest.* (1998) 102:136–44. doi: 10.1172/JCI2592
78. Kaneider NC, Kaser A, Tilg H, Ricevuti G, Wiedermann CJ Cd40 ligand-dependent maturation of human monocyte-derived dendritic cells by activated platelets. *Int J Immunopathol Pharmacol.* (2003) 16:225–31. doi: 10.1177/039463200301600307
79. Li J, Tan M, Xiang Q, Zhou Z, Yan H Thrombin-activated platelet-derived exosomes regulate endothelial cell expression of icam-1 *via* microrna-223 during the thrombosis-inflammation response. *Thromb Res.* (2017) 154:96–105. doi: 10.1016/j.thromres.2017.04.016
80. Pan Y, Liang H, Liu H, Li D, Chen X, Li L, et al. Platelet-secreted microrna-223 promotes endothelial cell apoptosis induced by advanced glycation end products via targeting the insulin-like growth factor 1 receptor. *J Immunol.* (2014) 192:437–46. doi: 10.4049/jimmunol.1301790
81. Yao Y, Sun W, Sun Q, Jing B, Liu S, Liu X, et al. Platelet-derived exosomal microrna-25-3p inhibits coronary vascular endothelial cell inflammation through adam10 via the nf-kappab signaling pathway in apoe(-/-) mice. *Front Immunol.* (2019) 10:2205. doi: 10.3389/fimmu.2019.02205
82. Srikanthan S, Li W, Silverstein RL, McIntyre TM Exosome poly-ubiquitin inhibits platelet activation, downregulates cd36 and inhibits pro-atherothombotic cellular functions. *J Thromb Haemost.* (2014) 12:1906–17. doi: 10.1111/jth.12712
83. Libby P, Bornfeldt KE, Tall AR Atherosclerosis: Successes, surprises, and future challenges. *Circ Res.* (2016) 118:531–4. doi: 10.1161/CIRCRESAHA.116.308334
84. Bennett MR, Sinha S, Owens GK Vascular smooth muscle cells in atherosclerosis. *Circ Res.* (2016) 118:692–702. doi: 10.1161/CIRCRESAHA.115.306361
85. Zheng B, Yin WN, Suzuki T, Zhang XH, Zhang Y, Song LL, et al. Exosome-mediated mir-155 transfer from smooth muscle cells to endothelial cells induces endothelial injury and promotes atherosclerosis. *Mol Ther.* (2017) 25:1279–94. doi: 10.1016/j.ymthe.2017.03.031
86. Kapustin AN, Chatrou ML, Drozdov I, Zheng Y, Davidson SM, Soong D, et al. Vascular smooth muscle cell calcification is mediated by regulated exosome secretion. *Circ Res.* (2015) 116:1312–23. doi: 10.1161/CIRCRESAHA.116.305012
87. Su SA, Xie Y, Fu Z, Wang Y, Wang JA, Xiang M Emerging role of exosome-mediated intercellular communication in vascular remodeling. *Oncotarget.* (2017) 8:25700–12. doi: 10.18632/oncotarget.14878
88. Schecter AD, Giesen PL, Taby O, Rosenfield CL, Rossikhina M, Fyfe BS, et al. Tissue factor expression in human arterial smooth muscle cells. Tf is present in three cellular pools after growth factor stimulation. *J Clin Invest.* (1997) 100:2276–85. doi: 10.1172/JCI119765
89. Kapustin AN, Shanahan CM Emerging roles for vascular smooth muscle cell exosomes in calcification and coagulation. *J Physiol.* (2016) 594:2905–14. doi: 10.1113/JP271340
90. Mayerl C, Lukasser M, Sedivy R, Niederegger H, Seiler R, Wick G Atherosclerosis research from past to present–on the track of two pathologists with opposing views, carl von rokitansky and rudolf virchow. *Virchows Arch.* (2006) 449:96–103. doi: 10.1007/s00428-006-0176-7
91. Feng J, Zhang Z, Kong W, Liu B, Xu Q, Wang X Regulatory t cells ameliorate hyperhomocysteinaemia-accelerated atherosclerosis in apoe-/- mice. *Cardiovasc Res.* (2009) 84:155–63. doi: 10.1093/cvr/cvp182
92. Lu S, Deng J, Liu H, Liu B, Yang J, Miao Y, et al. Pkm2-dependent metabolic reprogramming in cd4(+) t cells is crucial for hyperhomocysteinemia-accelerated atherosclerosis. *J Mol Med (Berl).* (2018) 96:585–600. doi: 10.1007/s00109-018-1645-6
93. Zakharova L, Svetlova M, Fomina AF T cell exosomes induce cholesterol accumulation in human monocytes *via* phosphatidylserine receptor. *J Cell Physiol.* (2007) 212:174–81. doi: 10.1002/jcp.21013
94. Deng Z, Rong Y, Teng Y, Zhuang X, Samykutty A, Mu J, et al. Exosomes mir-126a released from mdsc induced by dox treatment promotes lung metastasis. *Oncogene.* (2017) 36:639–51. doi: 10.1038/onc.2016.229
95. Schober A, Nazari-Jahantigh M, Wei Y, Bidzhekov K, Gremse F, Grommes J, et al. Microrna-126-5p promotes endothelial proliferation and limits atherosclerosis by suppressing dlk1. *Nat Med.* (2014) 20:368–76. doi: 10.1038/nm.3487
96. Wu R, Gao W, Yao K, Ge J Roles of exosomes derived from immune cells in cardiovascular diseases. *Front Immunol.* (2019) 10:648. doi: 10.3389/fimmu.2019.00648
97. Gao W, Liu H, Yuan J, Wu C, Huang D, Ma Y, et al. Exosomes derived from mature dendritic cells increase endothelial inflammation and atherosclerosis via membrane tnf-alpha mediated nf-kappab pathway. *J Cell Mol Med.* (2016) 20:2318–27. doi: 10.1111/jcmm.12923
98. Xing X, Li Z, Yang X, Li M, Liu C, Pang Y, et al. Adipose-derived mesenchymal stem cells-derived exosome-mediated microrna-342-5p protects endothelial cells against atherosclerosis. *Aging (Albany NY).* (2020) 12:3880–98. doi: 10.18632/aging.102857
99. Ren XS, Tong Y, Qiu Y, Ye C, Wu N, Xiong XQ, et al. Mir155-5p in adventitial fibroblasts-derived extracellular vesicles inhibits vascular smooth muscle cell proliferation via suppressing angiotensin-converting enzyme expression. *J Extracell Vesicles.* (2020) 9:1698795. doi: 10.1080/20013078.2019.1698795
100. Wang X, Huang W, Liu G, Cai W, Millard RW, Wang Y, et al. Cardiomyocytes mediate anti-angiogenesis in type 2 diabetic rats through the exosomal transfer of mir-320 into endothelial cells. *J Mol Cell Cardiol.* (2014) 74:139–50. doi: 10.1016/j.yjmcc.2014.05.001
101. Xiong Y, Chen L, Yan C, Zhou W, Endo Y, Liu J, et al. Circulating exosomal mir-20b-5p inhibition restores wnt9b signaling and reverses diabetes-associated impaired wound healing. *Small.* (2020) 16:e1904044. doi: 10.1002/smll.201904044
102. Yin M, Loyer X, Boulanger CM Extracellular vesicles as new pharmacological targets to treat atherosclerosis. *Eur J Pharmacol.* (2015) 763:90–103. doi: 10.1016/j.ejphar.2015.06.047
103. Biomarkers Definitions Working Group. Biomarkers and surrogate endpoints: Preferred definitions and conceptual framework. *Clin Pharmacol Ther.* (2001) 69:89–95. doi: 10.1067/mcp.2001.113989
104. Amabile N, Guerin AP, Tedgui A, Boulanger CM, London GM Predictive value of circulating endothelial microparticles for cardiovascular mortality in end-stage renal failure: A pilot study. *Nephrol Dial Transplant.* (2012) 27:1873–80. doi: 10.1093/ndt/gfr573

105. Boulanger CM, Amabile N, Tedgui A Circulating microparticles: A potential prognostic marker for atherosclerotic vascular disease. *Hypertension.* (2006) 48:180–6. doi: 10.1161/01.HYP.0000231507.00962.b5
106. Kuwabara Y, Ono K, Horie T, Nishi H, Nagao K, Kinoshita M, et al. Increased microrna-1 and microrna-133a levels in serum of patients with cardiovascular disease indicate myocardial damage. *Circ Cardiovasc Genet.* (2011) 4:446–54. doi: 10.1161/CIRCGENETICS.110.958975
107. Matsumoto S, Sakata Y, Suna S, Nakatani D, Usami M, Hara M, et al. Circulating p53-responsive microrna are predictive indicators of heart failure after acute myocardial infarction. *Circ Res.* (2013) 113:322–6. doi: 10.1161/CIRCRESAHA.113.301209
108. Wang Z, Zhang J, Zhang S, Yan S, Wang Z, Wang C, et al. Mir-30e and mir-92a are related to atherosclerosis by targeting abca1. *Mol Med Rep.* (2019) 19:3298–304. doi: 10.3892/mmr.2019.9983
109. Jiang H, Toscano JF, Song SS, Schlick KH, Dumitrascu OM, Pan J, et al. Differential expression of circulating exosomal microrna in refractory intracranial atherosclerosis associated with antiangiogenesis. *Sci Rep.* (2019) 9:19429. doi: 10.1038/s41598-019-54542-y
110. Fleury A, Martinez MC, Le Lay S Extracellular vesicles as therapeutic tools in cardiovascular diseases. *Front Immunol.* (2014) 5:370. doi: 10.3389/fimmu.2014.00370
111. Wei Y, Nazari-Jahantigh M, Neth P, Weber C, Schober A Microrna-126,−145, and−155: A therapeutic triad in atherosclerosis? *Arterioscler Thromb Vasc Biol.* (2013) 33:449–54. doi: 10.1161/ATVBAHA.112.300279
112. Xitong D, Xiaorong Z Targeted therapeutic delivery using engineered exosomes and its applications in cardiovascular diseases. *Gene.* (2016) 575:377–84. doi: 10.1016/j.gene.2015.08.067
113. Tian Y, Li S, Song J, Ji T, Zhu M, Anderson GJ, et al. A doxorubicin delivery platform using engineered natural membrane vesicle exosomes for targeted tumor therapy. *Biomaterials.* (2014) 35:2383–90. doi: 10.1016/j.biomaterials.2013.11.083
114. Alvarez-Erviti L, Seow Y, Yin H, Betts C, Lakhal S, Wood MJ Delivery of sirna to the mouse brain by systemic injection of targeted exosomes. *Nat Biotechnol.* (2011) 29:341–5. doi: 10.1038/nbt.1807
115. Ohno S, Takanashi M, Sudo K, Ueda S, Ishikawa A, Matsuyama N, et al. Systemically injected exosomes targeted to egfr deliver antitumor microrna to breast cancer cells. *Mol Ther.* (2013) 21:185–91. doi: 10.1038/mt.2012.180
116. Haney MJ, Klyachko NL, Zhao Y, Gupta R, Plotnikova EG, He Z, et al. Exosomes as drug delivery vehicles for Parkinson's disease therapy. *J Control Release.* (2015) 207:18–30. doi: 10.1016/j.jconrel.2015.03.033
117. Wu G, Zhang J, Zhao Q, Zhuang W, Ding J, Zhang C, et al. Molecularly engineered macrophage-derived exosomes with inflammation tropism and intrinsic heme biosynthesis for atherosclerosis treatment. *Angew Chem Int Ed Engl.* (2019).
118. Zhuang X, Xiang X, Grizzle W, Sun D, Zhang S, Axtell RC, et al. Treatment of brain inflammatory diseases by delivering exosome encapsulated anti-inflammatory drugs from the nasal region to the brain. *Mol Ther.* (2011) 19:1769–79. doi: 10.1038/mt.2011.164
119. Jang SC, Kim OY, Yoon CM, Choi DS, Roh TY, Park J, et al. Bioinspired exosome-mimetic nanovesicles for targeted delivery of chemotherapeutics to malignant tumors. *ACS Nano.* (2013) 7:7698–710. doi: 10.1021/nn402232g
120. Zhao Y, Haney MJ, Gupta R, Bohnsack JP, He Z, Kabanov AV, et al. Gdnf-transfected macrophages produce potent neuroprotective effects in Parkinson's disease mouse model. *PLoS ONE.* (2014) 9:e106867. doi: 10.1371/journal.pone.0106867
121. Kalani A, Kamat PK, Chaturvedi P, Tyagi SC, Tyagi N Curcumin-primed exosomes mitigate endothelial cell dysfunction during hyperhomocysteinemia. *Life Sci.* (2014) 107:1–7. doi: 10.1016/j.lfs.2014.04.018
122. Li Z, Zhao P, Zhang Y, Wang J, Wang C, Liu Y, et al. Exosome-based ldlr gene therapy for familial hypercholesterolemia in a mouse model. *Theranostics.* (2021) 11:2953–65. doi: 10.7150/thno.49874
123. Yang W, Yin R, Zhu X, Yang S, Wang J, Zhou Z, et al. Mesenchymal stem-cell-derived exosomal mir-145 inhibits atherosclerosis by targeting jam-a. *Mol Ther Nucleic Acids.* (2021) 23:119–31. doi: 10.1016/j.omtn.2020.10.037
124. Lin CM, Wang BW, Pan CM, Fang WJ, Chua SK, Cheng WP, et al. Chrysin boosts klf2 expression through suppression of endothelial cell-derived exosomal microrna-92a in the model of atheroprotection. *Eur J Nutr.* (2021). doi: 10.1007/s00394-021-02593-1

Conflict of Interest: The authors declare that the research was conducted in the absence of any commercial or financial relationships that could be construed as a potential conflict of interest.

Publisher's Note: All claims expressed in this article are solely those of the authors and do not necessarily represent those of their affiliated organizations, or those of the publisher, the editors and the reviewers. Any product that may be evaluated in this article, or claim that may be made by its manufacturer, is not guaranteed or endorsed by the publisher.

frontiers in Cardiovascular Medicine

REVIEW
published: 30 September 2021
doi: 10.3389/fcvm.2021.720085

Role of GTPase-Dependent Mitochondrial Dynamins in Heart Diseases

*Jiangen Liu, Xianjing Song, Youyou Yan and Bin Liu**

Department of Cardiology, The Second Hospital of Jilin University, Changchun, China

Heart function maintenance requires a large amount of energy, which is supplied by the mitochondria. In addition to providing energy to cardiomyocytes, mitochondria also play an important role in maintaining cell function and homeostasis. Although adult cardiomyocyte mitochondria appear as independent, low-static organelles, morphological changes have been observed in cardiomyocyte mitochondria under stress or pathological conditions. Indeed, cardiac mitochondrial fission and fusion are involved in the occurrence and development of heart diseases. As mitochondrial fission and fusion are primarily regulated by mitochondrial dynamins in a GTPase-dependent manner, GTPase-dependent mitochondrial fusion (MFN1, MFN2, and OPA1) and fission (DRP1) proteins, which are abundant in the adult heart, can also be regulated in heart diseases. In fact, these dynamic proteins have been shown to play important roles in specific diseases, including ischemia-reperfusion injury, heart failure, and metabolic cardiomyopathy. This article reviews the role of GTPase-dependent mitochondrial fusion and fission protein-mediated mitochondrial dynamics in the occurrence and development of heart diseases.

Keywords: heart disease, DRP1, mfn1, MFN2, OPA1

OPEN ACCESS

Edited by:
Junjie Yang,
University of Maryland, Baltimore, United States

Reviewed by:
Shiyue Xu,
The First Affiliated Hospital of Sun Yat-sen University, China
Junqing An,
Georgia State University, United States

****Correspondence:***
Bin Liu
liubin3333@vip.sina.com

Specialty section:
This article was submitted to Cardiovascular Biologics and Regenerative Medicine, a section of the journal Frontiers in Cardiovascular Medicine

Received: *03 June 2021*
Accepted: *06 September 2021*
Published: *30 September 2021*

Citation:
Liu J, Song X, Yan Y and Liu B (2021) Role of GTPase-Dependent Mitochondrial Dynamins in Heart Diseases. Front. Cardiovasc. Med. 8:720085. doi: 10.3389/fcvm.2021.720085

INTRODUCTION

Over the course of a human lifetime, the heart beats ∼2.5 billion times. The enormous amount of energy required for this cyclic beating process is provided by the mitochondria of myocardial cells. Mitochondria are membrane-bound organelles found in the cytoplasm of almost all eukaryotic cells (cells with clearly defined nuclei), the primary function of which is to generate large quantities of energy in the form of adenosine triphosphate (ATP). Aside from their role in energy production, mitochondria also have a vital role in maintaining cell homeostasis.

Mitochondria are organelles whose morphology and function are interconnected. Through the dynamic balance of fission and fusion, the normal morphology of mitochondria is regulated to meet the energy and metabolic needs of the cell. These dynamic changes in morphology maintain the integrity and distribution of mitochondria, thereby allowing their function to adapt to changing physiological needs (1, 2). Mitochondria are highly abundant and widely distributed throughout the cytoplasm of cardiomyocytes. In fact, more than 40% of the cytoplasmic space of adult cardiac cardiomyocytes is occupied by densely packed mitochondria (3), which are primarily located between the sarcomeres of cardiomyocytes, around the nucleus, and under the serosa (3), allowing them to continuously provide energy for myocardial contraction. Therefore, the morphology of mitochondria is

essential to maintain the health of cardiomyocytes. Cardiac mitochondria can be divided into two types based on their location, namely, subserosa mitochondria and interfiber mitochondria. The cristae morphology of these two mitochondrion types differs; that is, the subserosa mitochondria are flaky, whereas interfiber mitochondria are primarily tubular. However, cristae morphology can change in response to the pathophysiological state of heart disease, suggesting that mitochondrial morphology also has an important role in cardiomyocyte homeostasis (4).

Mitochondrial fission is mediated by dynamin-related protein 1 (DRP1), a GTPase-dependent enzyme that is recruited to the outer mitochondrial membrane through a series of receptor proteins (MFF, FIS1, MID49, and MID50) (5). Together, DRP1 and FIS1 mediate fission and participate in apoptosis activation, necrosis, and autophagy (6), after which DRP1 divides the mitochondria into two in a GTP-dependent manner (See in **Figure 1**). In mammals, mitochondrial fusion is generally regulated by three GTPase-dependent proteins in the dynamin superfamily, namely, mitofusin-1 (MFN1), mitofusin-2 (MFN2), and optic atrophy 1 (OPA1), all of which participate in the processes of energy metabolism, mitochondrial permeability transition, and calcium homeostasis (6, 7). Generally, mitochondrial fusion requires three steps. First, MFN1 or MFN2 reversibly approach the outer mitochondrial membranes. Second, the outer membranes of the two mitochondria fuse *via* MFN1 and MFN2 under GTPase mediation. Third, the inner mitochondrial membranes fuse *via* OPA1 in a GTPase-dependent manner (**Figure 2**).

In most organs, mitochondrial dynamics are highly active, with mitochondria continually undergoing fusion, fission, transportation, and degradation. These dynamic processes are necessary to maintain the normal shape, health, and number of mitochondria, thus, maintaining cellular physiological functioning. Yet, the description of mitochondria in a hyperdynamic state may not be suitable to adult cardiomyocytes, where the mitochondria appear as independent, lowly dynamic organelles. Meanwhile, under stress or pathological conditions, morphological changes have been observed in myocardial mitochondria. Moreover, the delicate balance between fission and fusion is critical to ensure a steady energy supply and cardiomyocyte hemostasis (8). To date, many studies have confirmed that the fusion and fission dynamins of cardiac mitochondria, in particular the GTPase dependent dynamins (DRP1, MFN1, MFN2, OPA1) are associated with the occurrence and development of various heart diseases. As such, this article provides a review of current literature related to the effects of these specific GTPase-dependent dynamins that mediate mitochondrial fusion and fission in myocardial tissue.

ROLE OF GTPase-DEPENDENT DRP1 IN HEART DISEASES

DRP1 Structure and Modification

Along with mitochondrial fusion, fission is essential to maintain normal cell and tissue physiological functions (9, 10). Mitochondrial fission is mediated by the GTPase-dependent dynamin DRP1, which is composed of four fragments: the N-terminal GTPase active fragment, middle fragment, variable fragment, and C-terminal GTPase effector fragment. Before Drp1 participates in the fission of mitochondria, a series of proteins are needed to transport it to the outer mitochondrial membrane. These proteins are called Drp1 Adaptors. The adaptors include fission 1 (Fis1), mitochondrial fission factor (Mff) and mitochondrial dynamics proteins of 49 and 51 kDa (MiD49, MiD51) (5). And MiD49 and MiD51 can act independently of Mff and Fis1 in Drp1 recruitment and suggest that they provide specificity to the division of mitochondria (11). A number of reports have shown that Fis1 is not required for Drp1 recruitment, but Mff is an essential factor for mitochondrial recruitment of Drp1 during mitochondrial fission in mammalian cells (12).

Through the action of various kinases and phosphatases, the C-terminal GTPase effector fragment is reversibly phosphorylated to achieve DRP1 aggregation on the surface of mitochondria (13, 14). This DRP1 aggregation allows for mitochondria reshaping in response to intracellular or extracellular signals. Phosphorylation of the commonly confirmed DRP1 sites, Ser616 and Ser637, represents important regulatory mechanisms following DRP1 translation, whereby Ser616 phosphorylation induces DRP1 activity, while Ser637 phosphorylation reduces DRP1 activity (15). For example, during cell mitosis, CDK1 enhances mitochondrial division through Ser616 phosphorylation (16). Meanwhile, phosphorylation of Ser637 on the DRP1 C-terminal GTPase effector fragment by cAMP-dependent protein kinase, reduces the GTPase activity of DRP1 and inhibits mitochondrial fission (17). In contrast, dephosphorylation of Ser637 mediated by calcium-dependent phosphatase and calcineurin increases DRP1 recruitment from the cytoplasm to the mitochondria (18). Additionally, the sumoylation status of DRP1 can also affect its intracellular localization; that is, when DRP1 is modified by SUMO-1, localization of DRP1 to mitochondria increases (19, 20), while DRP1 modification by SUMO-2/3 inhibits its localization to mitochondria (21) (**Figure 3**).

The Role of DRP1 in Embryogenesis and Heart Development

Endogenous DRP1 plays an important role in mitochondrial quality control and cardiomyocyte survival. For example, *Drp1* knock out in mice leads to embryonic lethality, where the embryos generally die within 9.5–11.5 embryonic days, a phenotype accompanied by elongated mitochondria, decreased cell differentiation, and decreased developmental regulatory apoptosis (22). Moreover, targeted knock out of *Drp1* in murine heart tissue after birth caused dilated cardiomyopathy and death. Meanwhile, the cardiomyocyte mitochondria exhibited internally aggregated ubiquitin proteins accompanied by weakened cell respiration (23–25). The effects associated with DRP1 were also demonstrated with a mutation scan of N-ethyl-N-nitrosourea, in which mice with *Drp1* mutations developed dilated cardiomyopathy related to reduced levels of respiratory

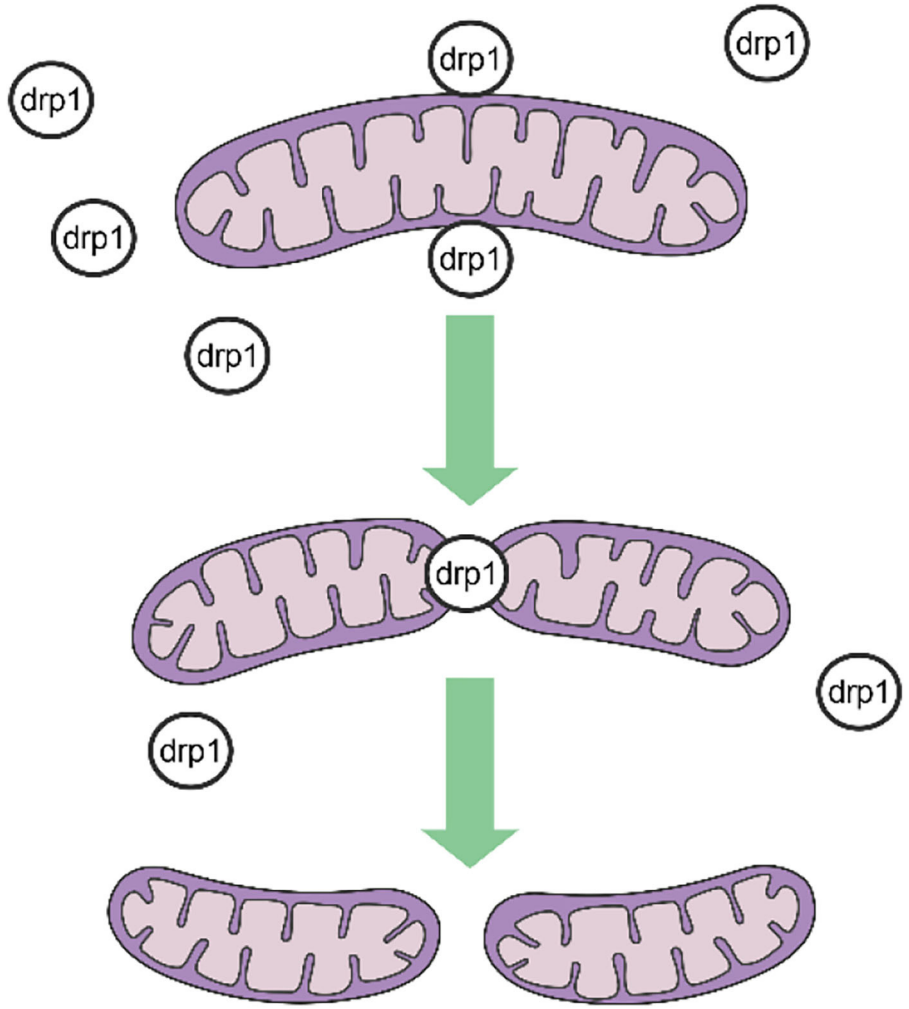

FIGURE 1 | Procedures of mitochondrial fission.

complexes and loss of ATP (26). Additionally, three studies that specifically knocked out *Drp1* in murine cardiac tissues reported that lack of DRP1 led to enlarged mitochondria, while DRP1 loss was fatal during the perinatal period or in the mature heart. Moreover, mitochondrial quality and abundance were found to be related to mitochondrial autophagy (24, 27, 28). The specific deletion of myocardial *Drp1* not only increases the mitochondrial size, but also causes their abundance to progressively decrease (23).

In mice with muscle-specific *Drp1* knockout, all pups died between 7 and 10 days after delivery, however, the death was not accompanied by neonatal defects or weight changes. Meanwhile, the hearts of *Drp1* knockout mice were enlarged 7 days after delivery, accompanied by a thinning of the heart walls, however, the heart weight remained normal. Ultrasonography revealed clear cardiac dysfunction, including an increase in the end-systolic diameter (0.85 mm in the control compared to 1.64 mm in the *Drp1* knockout) and a decrease in the shortening rate of the left ventricular short axis (46.5% in the control compared to 21.4% in the *Drp1* knockout). Furthermore, heart-specific knockout of *Drp1 via* gene recombination after birth caused cardiomyopathy and death in young mice (28). Collectively, these results indicate that DRP1 is necessary for the maintenance of neonatal heart function.

DRP1 clearly plays an important role in embryogenesis and heart development in newborn mice. During these developmental stages, *Drp1* inhibition or knock out causes enlargement and excessive fusion of mitochondria, both of which are lethal to mice. Hence, DRP1 has important roles in different stages of ontogeny. Under normal physiological conditions, inhibiting or silencing *Drp1* reduces mitochondrial fission, increases fusion, and causes loss of heart function and even death. Under pathological conditions, the DRP1 expression becomes increased; its subsequent excessive phosphorylation or acetylation cause apoptosis and autophagy resulting in excessive

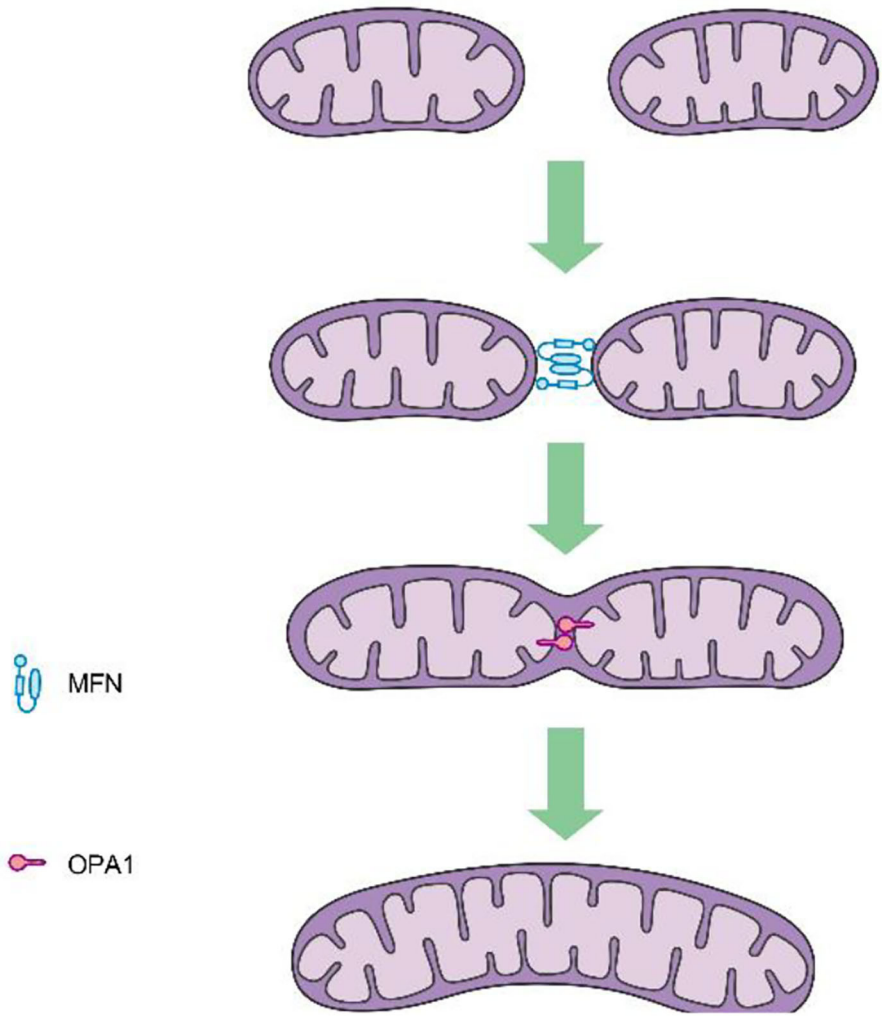

FIGURE 2 | Procedures of mitochondrial fusion.

mitochondrial fission and reduced fusion, thus further inducing cardiac dysfunction.

The Role of DRP1 in Pathological Cardiac Conditions

One study found that within 60 min of ischemia reperfusion, DRP1 expression increased with excessive mitochondrial fission following localization of DRP1 and BAX (apoptosis-related protein) to the mitochondria (29). During this process, MFN1 and MFN2 activity was inhibited, which may have led to induced activation of the mitochondrial permeability transition pore (MPTP) (30), causing subsequent mitochondrial fragmentation and permeation of the outer membrane (31, 32). Increased mitochondrial outer membrane permeability or opening of the MPTP leads to cytochrome C release, thus, further activating the caspase apoptosis pathway (33, 34). In the case of ischemia-reperfusion injury, inhibition of DRP1 activity elicits a protective effect on the heart. Thus, in different stages of the life cycle and development, as well as during physiological and pathological states, the degree of change in DRP1 activity differs, leading to different effects on cardiomyocytes and the heart.

As detailed above, the excessive mitochondrial fission observed within 60 min of reperfusion after transient ischemia, led to mitochondrial dysfunction and a decrease in myocardial contractility. However, P110, an inhibitor of DRP1, can reverse the decrease in myocardial contractility, thereby improving heart function (35). During reperfusion, dephosphorylation of Ser637 on DRP1 induces the transfer of DRP1 to the mitochondrial membrane and enhances mitochondrial fission (36). This dephosphorylation event in ischemia-reperfusion injury can be mediated by calcineurin (36, 37). Thus, because FK506 is an inhibitor of calcineurin, it can inhibit Ser637 dephosphorylation and ultimately preserve cardiac function during ischemia-reperfusion injury (36). In addition, AKT (protein kinase B) can activate DRP1 (38). For instance, in diabetes, the level of SIRT1 (sirtuin 1) in cardiomyocytes

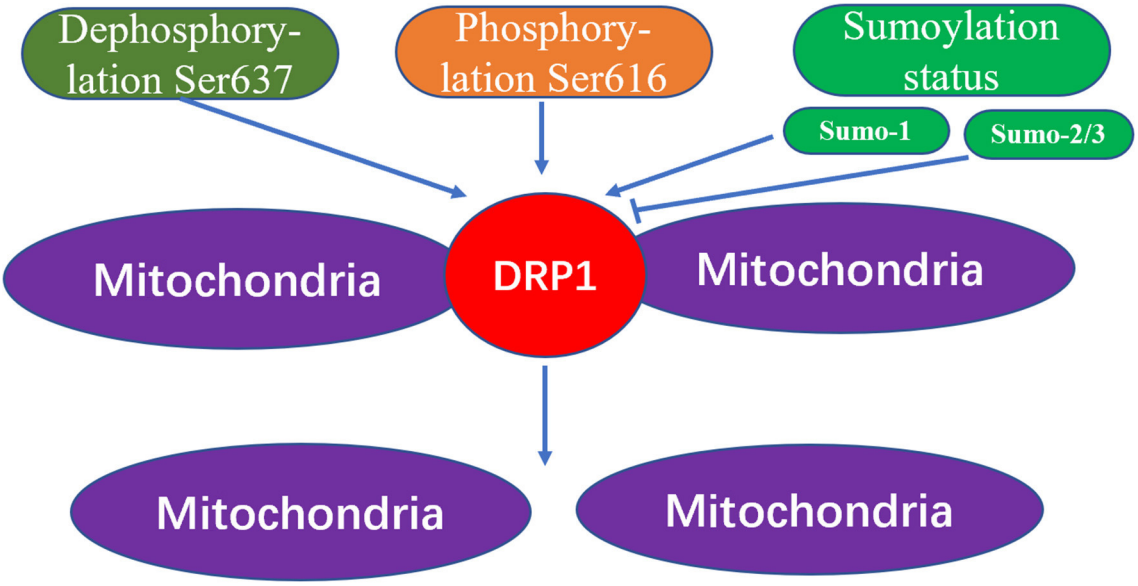

FIGURE 3 | The mechanism of mitochondrial fission caused by Drp1 modification. The increased dephosphorylation of Ser637 on the drp1 protein or the increased phosphorylation of Ser616, and the change of the sumoylation state of DRP1 will effect the activity of DRP1, thereby increasing the fission of mitochondria.

decreases, causing increased phosphorylation of Ser473 on AKT, leading to increased dephosphorylation of Ser637 on DRP1, thereby enhancing DRP1 activity, which subsequently increases mitochondrial fission and aggravates cardiac ischemia-reperfusion injury (39). Meanwhile, mammalian STE20-like kinase 1 (MST1) is upregulated after myocardial infarction and increases mitochondrial fission through the JNK-DRP1 (DJ-1) cell signal transduction pathway, leading to cardiomyocyte fibrosis and aggravating myocardial damage (40). Moreover, DJ-1 activation can alter the sumoylation state of DRP1, thereby inhibiting mitochondrial division, and playing a protective role in ischemia-reperfusion injury. A potential mechanism underlying this process may involve the interaction of DJ-1 with SENP5 to enhance DRP1 sumoylation mediated by SUMO-2/3, which is modified to inhibit mitochondrial division (41).

By inhibiting the DRP1 expression mitochondrial fission is also inhibited, which can alleviate cardiac ischemia-reperfusion injury. At the same time, increased mitochondrial fusion occurs in these DRP1-inhibited cardiomyocytes (36, 42, 43). These studies assessed the effect of mitochondrial fission in cultured cardiomyocytes by RNA interference and *via* expression of the main negative form of DRP1. That is, adenovirus-transfected cells overexpress the negative regulator of DRP1, K38A *in vivo* and *in vitro*, which subsequently protects myocardial cells from the damage associated with ischemia-reperfusion (43). In cardiac ischemia, endogenous levels of the microRNA miR-499 are downregulated, while calcineurin is activated, and Ser637 on DRP1 is dephosphorylated, thus, further increasing mitochondrial fragmentation, and in turn leading to increased apoptosis of cardiomyocytes. Thus, miR-499 overexpression inhibits calcineurin-mediated DRP1 dephosphorylation, thereby reducing cardiomyocyte apoptosis (44). miR-499 can also inhibit DRP1 through the cAMP-PKA cell signal transduction pathway, thereby prolonging the mitochondrial lifespan (17). SIRT3 can further reduce the phosphorylation level of DRP1 by normalizing AMPK cell signal transduction pathways, thus, inhibiting mitochondrial fission and ultimately reducing myocardial damage following myocardial infarction (45). Similarly, treatment of mice with the DRP1 inhibitor Mdivi-1 leads to decreased mitochondrial fission, thus imparting a protective effect against hypoxia and ischemia reperfusion (36, 42). Moreover, *in vitro,* a simulated ischemia-reperfusion model with cultured HL-1 cells pretreated with Mdivi-1 improved cell survival and delayed the opening of MPTP (42). In Mdivi-1 pretreated mice, reperfusion in the occluded artery and the area of myocardial infarction were found to decrease (42). In fact, emergency inhibition of mitochondrial division after acute myocardial infarction can improve long-term cardiac function (35, 36). Meanwhile, in a mouse cardiac arrest model, inhibition of myocardial mitochondria fission improves the survival rate of mice (46). In pressure load-induced heart failure, Mdivi-1 can also improve left ventricular function and reduce myocardial fibrosis (47). Furthermore, as an inhibitor of DRP1, P110 can inhibit the upregulation of the autophagy marker LC3-II whether it is applied before or after cardiac reperfusion, however, it also inhibits the increase in phosphorylation of cleaved caspase 3 and JNK when applied after reperfusion, both of which are associated with cell apoptosis and death (35, 48, 49). Indeed, treatment of the heart with Mdivi-1 and P110 elicited a protective effect against ischemia-reperfusion injury (35, 42, 50), as DRP1 inhibitors

not only maintain mitochondrial morphology but also reduce calcium ions in the cytoplasm, inhibit the opening of MPTP, and inhibit cardiomyocyte apoptosis, thereby reducing myocardial damage. In fact, a recent study showed that injecting Mdivi-1 prior to myocardial infarction in ischemic mice can increase the length of mitochondria in myocardial cells (51). However, other studies that injected Mdivi-1 into the coronary arteries of larger animals, including pigs, as models for cardiac reperfusion after acute myocardial infarction, reported no significant changes in mitochondrial morphology between the blank control and experimental animals. Moreover, a protective cardiac effect was not detected, which may be related to the dose of Mdivi-1, timing of application, method of administration, etc. (52). Further studies are required to resolve these discrepancies in *in vivo* findings; hence, much work is still required before inhibitors of DRP1 can be recommended for the clinical treatment of heart diseases.

Diabetic cardiomyopathy refers to the abnormal structure and function of the heart caused by diabetes after excluding dangerous factors, including hypertension, coronary heart disease, and valvular disease, which may cause cardiac insufficiency. Mitochondrial dysfunction plays an important role in diabetic cardiomyopathy (53). Within minutes, acute hyperglycemia conditions can induce formation of shortened mitochondria mediated by the fission protein DRP1 (54). The acute response depends on the post-translational modification mechanism, which may involve glucose-induced intracellular calcium transients and ERK1/2 activation, causing phosphorylation of Ser616 on DRP1 (55). Specifically, PKCδ, CDK1, and CDK5 phosphorylate Ser616 to increase the fission activity of DLP1 (16, 56, 57). Melatonin regulates the expression of DRP1 through the SIRT1-PGC1α cell signal transduction pathway to reduce mitochondrial fission and ultimately alleviate diabetes-induced cardiac insufficiency (58). The rapid formation of small mitochondria under acute metabolic stress leads to an increase in mitochondrial reactive oxygen species (ROS). When the blood sugar continues to rise, the pathological fragmentation of mitochondria is related to the chronic increase in ROS levels, apoptosis, and necrosis (54, 59).

In the hearts of rats with chronic hypertension and hypertrophy, the level of cardiac DRP1 is reduced (60); however, myocardial DRP1 levels are elevated in the hypertrophic heart induced by neurohormone-norepinephrine (61). Studies have confirmed that mitochondria play an important role in cardiac hypertrophy (26, 62). For example, disorganized and fragmented mitochondria have been shown to cause cardiac hypertrophy (61, 63). Meanwhile, *in vitro,* within the NE (Norepinephrine)-induced cardiomyocyte hypertrophy model, an increase in accumulated DRP1 on the surface of mitochondria, as well as an increase in mitochondrial fragmentation, and a decrease in mitochondrial capacity are observed. However, if adenovirus-transfected cells are used to inhibit the expression of DRP1, mitochondrial fission is reduced, alleviating cardiomyocyte hypertrophy (61). Angiotensin-(1–9) can regulated mitochondria morphology through the AT2R/miR-129-3p/PKA cell signal transduction pathway, thereby inhibiting mitochondria fission and further reducing the occurrence of cardiomyocyte hypertrophy (64). Moreover, leptin can induce cardiac hypertrophy and activate calcineurin (65). The dephosphorylation of Ser637 on DRP1 mediated by calcineurin increases the recruitment of DRP1 from the cytoplasm to the mitochondria (18). It is, therefore, thought that leptin-induced cardiomyocyte hypertrophy is related to enhanced mitochondrial fission. In the cardiac hypertrophy cell model, fission of mitochondria has also been shown to participate in the calcium-dependent calcineurin cell signal transduction pathway (61). Mitochondrial fission is also crucial for the maintenance of heart function. Targeted *Drp1* knock out in the adult mouse heart induced development of cardiomyopathy after 6–13 weeks (27, 28). Moreover, mitochondrial fission was significantly inhibited; however, this failed to inhibit the occurrence of heart failure. Meanwhile, in a murine model of pressure overload, Mdivi-1 reduced myocardial hypertrophy and fibrosis without affecting blood pressure (66). Similarly, in an aortic constriction model in which *Drp1* was specifically knocked out of cardiac tissue cells *via* persistent heterozygous, excessive hypertrophy of cardiomyocytes and decreased heart function were observed. At the same time, it was confirmed that DRP1-dependent mitochondrial autophagy plays a role in resisting pressure load. With this important role, DRP1-dependent mitochondrial autophagy can ensure normal abundance of mitochondria and ultimately, contribute to amelioration of decreased heart function (67). Moreover, during heart failure, IGF-IIR can enhance the phosphorylation of Ser616 of DRP1 through extracellular signal-regulated kinase (ERK), thereby enhancing mitochondrial fission and causing mitochondrial dysfunction (68).

To make a summary of the whole section, DRP1 plays an important role in both the embryonic development period and the development of the newborn heart. DRP1 is elevated in ischemia-reperfusion injury causing excessive mitochondrial fission, thereby, further aggravating ischemia-reperfusion injury. DRP1 also plays an important role in the occurrence and development of heart failure, hence, inhibiting DRP1 can reduce ischemia-reperfusion injury and heart failure (**Table 1**). Specifically, DRP1 can affect mitochondrial morphology and function through phosphorylation, acetylation, sumoylation, and other modifications (**Figure 4**). Thus, DRP1 affects the occurrence and development of heart disease, which may be related to the imbalance of mitochondrial fission and fusion; however, further research is required to understand the specific mechanisms involved.

ROLE OF GTPase-DEPENDENT FUSION PROTEINS IN HEART DISEASES

Mitochondrial fusion is regulated by GTPase-dependent proteins, including MFN1, MFN2, and OPA1. Mitochondrial fusion plays an important role in the maintenance of mitochondrial DNA homeostasis. In cultured cells and skeletal muscle cells lacking mitochondrial fusion factors, mtDNA decreased and mtDNA accumulation mutation increased (69).

TABLE 1 | Drp1 the role of Drp1 in heart development and heart disease.

Diseases	GTP-ase dependent dynamin state	Methods	Effect on the heart	References
Embryogenesis and heart development		Global Knock out in mice	Embryonic lethality	(22)
		Heart specifically knocked out	Dilated cardiomyopathy and death	(28)
Ischemia-Reperfusion	DRP1 activation Increase	Mdivi-1,P110 Drp1 inhibitor	Reverse the decrease in myocardial contractility, thereby improving heart function	(35, 36, 42, 47, 50, 51)
		Inhibit Ser637 dephosphorylation	Preserve cardiac function	(36, 37)
		DRP1 sumoylation mediated by SUMO-2/3	Protect the heart from ischemia-reperfusion injury	(41)
Cardiac hypertrophy	DRP1 activation Increase	Inhibit the expression of DRP1	Alleviate cardiomyocyte hypertrophy	(61, 64)
		Mdivi-1 Drp1 inhibitor	Reduced myocardial hypertrophy and fibrosis	(66)

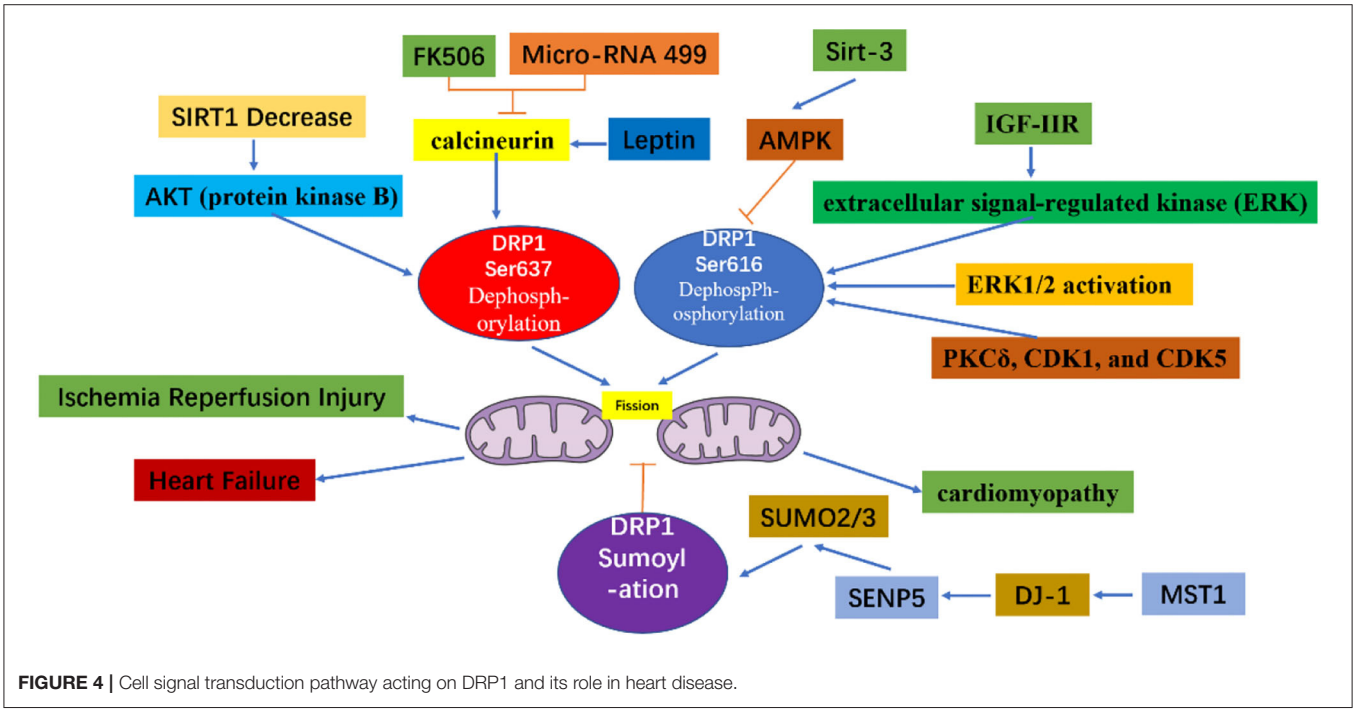

FIGURE 4 | Cell signal transduction pathway acting on DRP1 and its role in heart disease.

Role of GTPase-Dependent Mitofusins in Heart Diseases

Role of Mitofusins (MFN1 and MFN2) in Heart Diseases

Mammalian mitochondrial fusion protein has been identified as a human homolog of the Drosophila fuzzy onion protein (Fzo) (70). MFN1 is composed of 741 amino acids, whereas MFN2 is composed of 757 amino acids. Both are transmembrane GTPases located on the outer mitochondrial membrane, with functional domains that share 63% homology. The conserved domain of mitofusins consists of an amino-terminal GTP binding domain, a coiled-coil domain (heptapeptide repeat HR1), a carboxy-terminal with a two-part transmembrane domain and a second coiled-coil domain (heptapeptide repeat sequence HR2). Both the GTPase and coiled-coil domains are exposed to the cytoplasm. In addition, MFN2 possesses an N-terminal Ras binding domain that does not exist in MFN1, implying that MFN2 has unique functions that are not shared with MFN1 (71). Although both MFN1 and MFN2 support mitochondrial fusion, MFN2 also mediates the coupling of the endoplasmic reticulum and mitochondria (72). Therefore, MFN2 plays a critical role in maintaining intercellular calcium regulation, which is of great significance to the excitation-contraction-metabolic coupling of cardiomyocytes.

Unsurprisingly, MFN2 is highly abundant in the heart compared to other tissues (73).

Cardiac-specific *Mfn1* and *Mfn2* knockout mice exhibit death due to heart failure, respiratory dysfunction, and mitochondrial fragmentation and swelling. In dual *Mfn1* and *Mfn2* cardiac knockout mice, no births were observed with embryos dying on embryonic days 9.5 and 10.5. However, the expression of *Mfn1* or *Mfn2* alone is sufficient for murine survival, thus only the simultaneous absence of both is incompatible with life (74). In single *Mfn1* or *Mfn2* knockout mice, mitochondrial outer membrane fusion and aggregation proceed normally, while double knockout result in loss of fusion induced by mitofusins (75). In 8-week-old mice, when *Mfn1* and *Mfn2* were specifically and simultaneously knocked out in cardiac tissue, the cardiomyocytes showed mitochondrial fragmentation and respiratory dysfunction, rapidly developing into lethal dilated cardiomyopathy (76). Additionally, MFN1 levels have been found to decrease in myocardial hypertrophy (77), while MFN2 levels increase under oxidative stress (78), however, MFN2 levels in the late stage after myocardial infarction and diabetis late stageare significantly reduced (79, 80). A recent study showed that microRNA-20b can downregulate *Mfn2* and promote cytoplasmic Ca^{2+} overload, thus, weakening the buffering capacity of mitochondria and increasing cardiac hypertrophy (81).

In mice with *Mfn1* only knockout, cardiac function, mitochondrial respiratory function, and respiratory function are maintained; however, an increase in spherical mitochondria can still be observed (82, 83). In contrast, cardiac *Mfn2* ablation causes early-dilated cardiomyopathy in mice. Indeed, MFN1 loss is better tolerated than MFN2 loss in cardiomyocytes (30, 84), which may account for why single *Mfn1* knockout elicit minimal effects on heart function. These data imply that when either MFN1 or MFN2 are missing, the other protein may compensate for the lost function, however, this requires further verification.

In ischemia-reperfusion injury, DRP1 and BAX are transferred to mitochondria (29). In this process, the activities of MFN1 and MFN2 are inhibited, resulting in mitochondrial fragmentation and outer membrane permeability (31, 32). MFN inhibition can induce the activation of MTPT (30). When either mitochondrial outer membrane permeability is increased or the mitochondrial permeability transition pore opens, cytochrome C is released, further activating the caspase cell apoptosis pathway (33, 34). In the simulated ischemia-reperfusion injury model, the overexpression of MFN1 or MFN2 in the HL-1 cardiomyocyte cell line reduces cell death (42). Meanwhile, following siRNA silencing of *Mfn2* expression in a rat neonatal cardiomyocyte ischemia-reperfusion injury model, the cell survival rate was significantly decreased (77). Acute knockout of *Mfn1* and *Mfn2* in the heart showed a short-term protective effect against acute myocardial infarction, related to the decreased contact between mitochondria and endoplasmic reticulum, thereby reducing the calcium overload in the mitochondria (76). In response to ischemia-reperfusion injury, mitochondria transport calcium ions from the endoplasmic reticulum to the mitochondria through a calcium ion unidirectional transport pump. Upregulation of calcium ions in the mitochondria can induce the opening of the MPTP, which is a determinant of cardiomyocyte death (85). In ischemia-reperfusion injury, inhibiting calcium overload in mitochondria can reduce myocardial cell death and the myocardial infarction area (86–88). Moreover, MFN2 reportedly has an important role in the connection between mitochondria and the endoplasmic reticulum, ensuring sufficient calcium transfer for the production of bioenergy (72). After its activation, βII protein kinase C can phosphorylate Ser86 on MFN1, effectively inhibiting its GTPase activity and leading to fragmentation and dysfunctional mitochondrial accumulation, which in turn causes deterioration of heart function (89).

Role of OPA1 in Heart Diseases

OPA1 is a GTPase-dependent protein that mediates the fusion of mitochondria, while organizing the morphological regeneration of mitochondrial cristae, and resisting apoptosis for physiological needs (7, 90, 91). Evidencing the important role of OPA1 in the maintenance of mitochondrial morphology, knocking out *Opa1* during embryogenesis is fatal (92). In fact, *Opa1* or *Mfn2* knockout, *via* gene trapping, prevents embryonic stem cells (ESCs) from differentiating into cardiomyocytes (93). Mitochondrial fusion disrupts and increases the entry of capacitive calcium, thereby enhancing Notch1 signaling through calcium-induced calcineurin activation. Meanwhile, inhibition of calcium and calcineurin signals is sufficient to reverse the non-differentiated phenotype of gene-trapped ESCs without affecting mitochondrial morphology. This places mitochondrial dynamics upstream of Notch signaling ESC differentiation in cardiomyocytes, thereby supporting the regulation of mitochondrial dynamics in heart development.

Wai et al. (94) observed morphological changes in the mitochondria of hearts from *Yme1l* knockout mice, finding that the smaller mitochondria aggregated, while their cristae structure was normal. This indicates that mitochondrial dynamics were damaged due to YME1L loss. Furthermore, in cardiomyocytes lacking YME1L, the D form of s-OPA1 disappears, while the C and E forms of s-OPA1 aggregate as a result of OMA1 activation. Fragmentation of the mitochondrial network was also found in fibroblasts with *Yme1l* knocked out *in vitro*, and cell damage caused by s-OPA1 aggravation was also observed. The absence of YME1L in cardiomyocytes activates OMA1, which further increases the processing level of OPA1, increases the fragmentation of mitochondria, and ultimately leads to dilated cardiomyopathy and heart failure. In ischemia-induced heart failure, OPA1 expression decreases, indicating that OPA1 plays an important role in ischemic cardiomyopathy (95). In *Drosophila* and mice, inhibiting *Opa1* expression may cause abnormal mitochondrial morphology and cardiac hypertrophy (96, 97). Therefore, the inhibition of mitochondrial fusion-related proteins can increase mitochondrial fragmentation, which further affects the arrangement of cardiomyocytes and sarcoplasmic reticulum, thus, impacting cardiac function.

The change in OPA1 form represents a key step in mitochondrial cooperative fusion and fission regulation (98, 99). The balance between long and short forms of OPA1 maintains the normal shape of mitochondria: fusion depends on long

OPA1, while short OPA1 is related to mitochondrial fission (100, 101). Cell pressure, mitochondrial dysfunction, or genetic intervention (such as *Yme1l* deletion) can activate OMA1, thereby increasing the conversion of long OPA1 to short OPA1, and increasing the fragmentation of mitochondria (100, 102–104). Thus, GTPase OPA1 located on the inner mitochondrial membrane is a key enzyme that regulates mitochondrial fission-fusion. Mitochondrial protease OMA1 and AAA protease (AAA proteases comprise a conserved family of membrane bound ATP-dependent proteases that ensures the quality control of mitochondrial inner-membrane proteins) YME1L can cleave OPA1 from its long to short form and, while short OPA1 does not play a role in mitochondrial fusion, the aggregation of short OPA1 may cause accelerated fission. In cultured mammalian cells, OMA1 is activated under pressure, which leads to increased mitochondrial fission (94, 105, 106). Sadhana et al. (107) confirmed that SIRT3 can regulate the enzymatic activity of OPA1 through lysine deacetylation. Mitochondrial respiration depends on the acetylation state of the C-terminal K926 and K931 lysine fragments in the GED region of the OPA1 protein. Cardiac stress causes hyperacetylation of OPA1, thereby reducing its GTPase activity, however, SIRT3 can directly bind to OPA1, thereby enhancing mitochondrial function and networking (107). Studies have found that OPA1 is acetylated in the states of cardiac hypertrophy and SIRT3 deficiency. Overexpression of SIRT3 can play a protective role in the process of adriamycin-mediated mitochondrial fragmentation and cell death. These mechanisms are all related to the acetylation status of OPA1. SIRT3 exerts its activity by directly binding to OPA1 on the inner mitochondrial membrane and modifying it by deacetylation. SIRT3 maintains or strengthens the mitochondrial respiratory complex by activating OPA1. SIRT3 can inhibit mitochondria-mediated apoptosis by mediating OPA1. Meanwhile, hyperacetylation reduces the GTPase activity of OPA1, indicating that the decreased activity of OPA1 may partially account for mitochondrial defects in hypertrophy of the heart.

Normal expression of OPA1 is necessary for the maintenance of mitochondrial autophagy. The expression of OPA1 is decreased in infarcted hearts *in vivo* or in cardiomyocytes cultured *in vitro*. Meanwhile, within cardiomyocytes, irisin can activate OPA1-induced mitochondrial autophagy (108). In myocardial ischemia-reperfusion injury, decreased expression of OPA1 leads to increased mitochondrial fragmentation, and thus mitochondrial dysfunction and increased mitochondrial apoptosis, further aggravating ischemia-reperfusion injury (109). The increase or overexpression of OPA1 maintains mitochondrial function and cardiac function during myocardial ischemia and reperfusion (110). In contrast, in H9C2 cells cultured *in vitro*, overexpression of OPA1 leads to mitochondrial lengthening with no detectable reduction in apoptosis under ischemic stimulation (95). OPA1 levels decrease in failing hearts and in late stages after myocardial infarction (80, 95), while increasing in hypertensive hypertrophic hearts and cardiomyocytes treated with insulin (60, 111). MFN1, MFN2, and OPA1 levels showed a consistent decrease in the genetically induced lipid-overloaded heart (112). The stability of OPA1 in cardiomyocytes is regulated by ERK, AMPK, and YAP cell signal transduction pathways (113).

Melatonin can activate OPA1-mediated mitochondrial autophagy and fusion in an AMPK-dependent manner, thereby reducing cardiac ischemia-reperfusion injury (110). Coenzyme Q10 can induce the AMPK-YAP-OPA1 cell signal transduction pathway, thus, improving mitochondrial function and reducing the degree of arteriosclerosis (114). Calenduloside E can reduce cardiac ischemia-reperfusion injury by regulating OPA1-related mitochondrial fusion mediated by AMPK activation (115). In the cardiomyocyte model of ischemia-reperfusion injury, increased expression of OPA1 can reduce the oxidative stress of cells through the Ca^{+2}/calmodulin-dependent protein kinase II (CaMKII signaling) pathway (116).

Studies in murine diabetes models have shown that O-GlcNAc of OPA1 and DLP1 increase mitochondrial fragmentation (117, 118). O-GlcNAc modification of OPA1 can inhibit its function, leading to fragmentation of mitochondria, reduction of mitochondrial membrane potential, and reduction of complex IV activity (118). It is reported that enhanced O-GlcNAc modification of diabetic cardiomyopathy (DCM) is associated with disease progression in type 2 diabetes models, and reversal of this modification can restore cardiac function (119). Studies have shown that the occurrence of heart failure may be related to the fragmentation and dysfunction of mitochondria caused by the short-form aggregation of OPA1. The dysfunction of mitochondrial function causes the energy utilization mode of cardiomyocytes to change from lipid to sugar intake (94), which further causes cardiac function insufficiency (See in **Figure 5**).

The GTPase-dependent mitochondrial fusion proteins MFN1, MFN2, and OPA1 play important roles in maintaining cell homeostasis, cell pressure, calcium regulation, apoptosis, and autophagy. Downregulation or post-translational modification of these fusion proteins have been confirmed as related to a variety of heart diseases (**Table 2**), however, the specific mechanisms through which MFN1, MFN2, and OPA1 function in cardiomyocytes require further research.

DISCUSSION

The morphology of mitochondria in cardiomyocytes is a highly connected network structure that regulates the key functions of mitochondria through the balance of fission and fusion. Under normal physiological conditions, the fission and fusion of mitochondria are balanced to meet the normal physiological cell functions. In response to cellular stress, mitochondrial fragmentation and excessive fusion have been observed in various diseases, including ischemia-reperfusion injury and heart failure. Under normal physiological conditions, mitochondrial dynamin-related proteins maintain the shape and function of mitochondria to meet the organ needs through their own expression and post-translational modifications. However, under pathological conditions, these fission or fusion proteins can cause mitochondria morphological changes and dysfunction. Post-translational modifications of these proteins, such as acetylation and phosphorylation, can cause excessive fusion or fission of

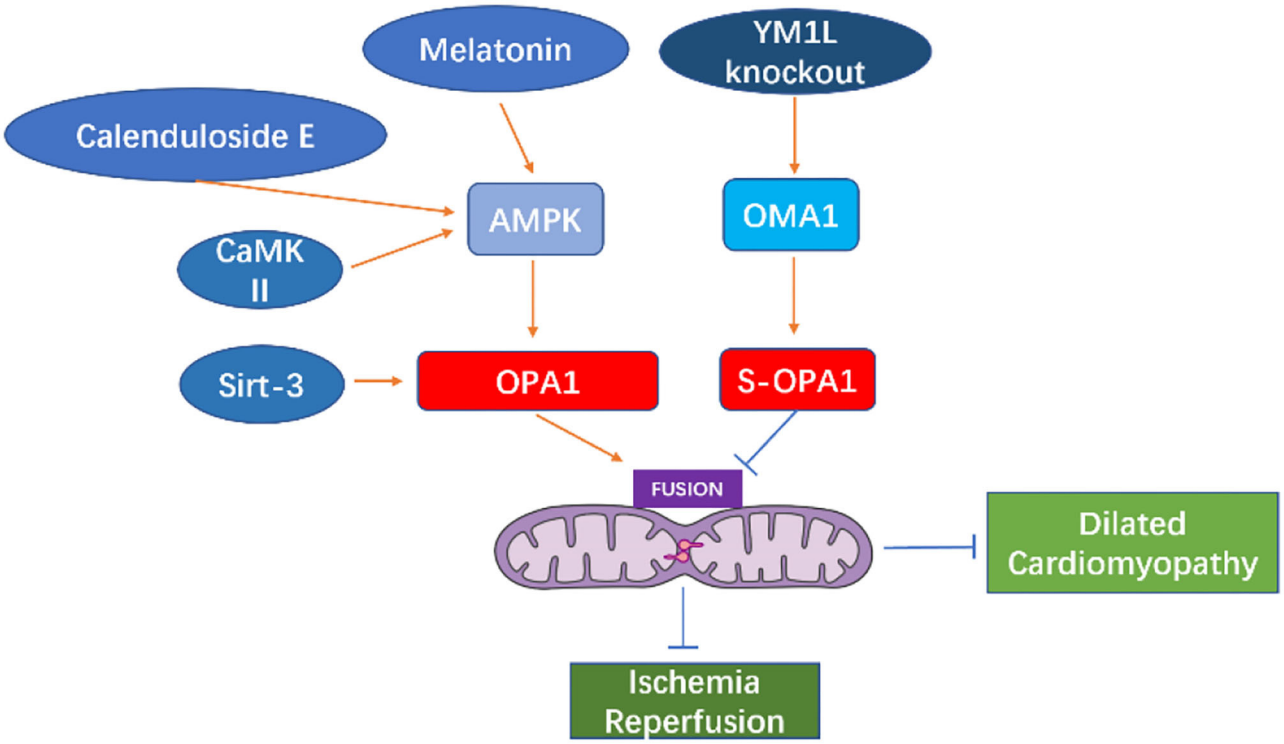

FIGURE 5 | Cell signal transduction pathway acting on OPA1 and its role in heart disease.

TABLE 2 | The role of GTPase-dependent fusion proteins in heart development and heart disease.

Diseases	GTP-ase Dependent dynamin state	Methods	Effect on the heart	References
Embryogenesis and heart development	MFN(MFN1 and MFN2)	Both MFN1 and MFN2 knocked out	Embryonic lethality	(74)
		Mfn1 and Mfn2 specifically and simultaneously knocked out in cardiac tissue	Dilated cardiomyopathy and Death	(76)
	OPA1	Knocking out *Opa1*	FATAL	(92, 93)
Ischemia-Reperfusion	OPA1	OPA1 expression decreases	Ischemic cardiomyopathy	(95)
		Decreased expression of OPA1	Aggravating ischemia-reperfusion injury	(109)
		Increase or overexpression of OPA1	Maintains heart function	(110)
Cardiac hypertrophy	OPA1	Absence of YME1L s-OPA1 aggravation	Dilated cardiomyopathy and heart failure	(94)
		Hyperacetylation reduces the GTPase activity of OPA1	Hypertrophy of the heart	(107)

mitochondria; however, this process can be reversed by inhibiting the related proteins.

Therefore, GTP-ase-dependent mitochondrial dynamic-related proteins may represent target protein for the treatment of heart diseases. However, it remains unclear whether it is more beneficial to inhibit mitochondrial fission or promote its fusion to improve heart disease pathology. For instance, although there is a significant body of evidence suggesting that inhibition of DRP1 activity can inhibit mitochondrial fission, while improving heart function and inhibiting the progression of heart disease, a recent study reported that inhibiting mitochondrial fission by enhancing fusion leads to different cardiac outcomes. Meanwhile, up-regulation of MFN2 in the heart can correct excessive mitochondrial fragmentation compared to down-regulation of DRP1. Additionally, the safest strategies will maintain cardiac mitochondrial function (120).

Maneechote's team used M1 (2 mg/kg) to enhance mitochondrial fusion to interfere with ischemia-reperfusion in rats and found that the application of M1 before ischemia can reduce infarct size and cardiac apoptosis, exerting the greatest cardioprotective effect. This indicates that myocardial ischemia-reperfusion injury can be reduced by increasing mitochondrial fusion (121). Similarly, the mitochondrial fusion enhancing substance M1 can effectively restore mitochondrial balance and improve diabetic cardiomyopathy in an OPA1-dependent manner (122).

Meanwhile, in different animals and different administration methods, the same type of DRP1 inhibition elicited differing effects. For instance, a recent study showed that injection of Mdivi-1 in advance of myocardial infarction can increase the length of mitochondria in myocardial cells and reduce the area of myocardial infarction in ischemic mice (51). However, another study using pigs as a model for cardiac reperfusion after acute myocardial infarction, reported that injection of Mdivi-1 directly into the coronary artery did not impact mitochondrial morphology nor elicit a protective effect on the heart, which may be related to the dose of Mdivi-1, timing of application, method of administration, etc. (52).Therefore, the timing and methods of intervention in mitochondrial dynamics still need further research.

Collectively, the relevant data has indicated that regulating the fission and fusion balance in mitochondria represents an important strategy for maintaining heart health and function. However, prior to clinical applications for the treatment of heart disease, long-term studies are needed to further investigate the effect of inhibiting mitochondrial motility-related proteins, as well as the appropriate timing and doses for administration.

This review demonstrates that the balance of mitochondrial fission and fusion plays a critical role in maintaining cell and heart function. Meanwhile, the imbalance in these processes likely contributes to the pathophysiological process of heart diseases, thereby providing potential new drug targets for heart diseases. Therefore, mitochondrial fission and fusion balance related proteins warrant further research.

AUTHOR CONTRIBUTIONS

BL proposed that mitochondrial-related proteins may play an important role in heart disease based on his previous research and organized the writing of this paper. JL wrote this paper. XS and YY provided guidance, help in the writing process, and the illustrations of the thesis. All authors contributed to the article and approved the submitted version.

FUNDING

This study was supported by grants from the Finance Department Project of Jilin Province (No. 2019SCZT004), Education Department Project of Jilin Province (No. JJKH20190055KJ) and Science and Technology Department Project of Jilin Province (No. 2019090502SF).

REFERENCES

1. Friedman JR, Nunnari J. Mitochondrial form and function. *Nature.* (2014) 505:335–43. doi: 10.1038/nature12985
2. Mishra P, Chan DC. Mitochondrial dynamics and inheritance during cell division, development and disease. *Nat Rev Mol Cell Biol.* (2014) 15:634–46. doi: 10.1038/nrm3877
3. Hom J, Sheu SS. Morphological dynamics of mitochondria–a special emphasis on cardiac muscle cells. *J Mol Cell Cardiol.* (2009) 46:811–20. doi: 10.1016/j.yjmcc.2009.02.023
4. Hoppel CL, Tandler B, Fujioka H, Riva A. Dynamic organization of mitochondria in human heart and in myocardial disease. *Int J Biochem Cell Biol.* (2009) 41:1949–56. doi: 10.1016/j.biocel.2009.05.004
5. Atkins K, Dasgupta A, Chen KH, Mewburn J, Archer SL. The role of Drp1 adaptor proteins MiD49 and MiD51 in mitochondrial fission: implications for human disease. *Clin Sci.* (2016) 130:1861–74. doi: 10.1042/CS20160030
6. Ong SB, Hausenloy DJ. Mitochondrial morphology and cardiovascular disease. *Cardiovasc Res.* (2010) 88:16–29. doi: 10.1093/cvr/cvq237
7. Cipolat S, Martins de Brito O, Dal Zilio B, Scorrano L. OPA1 requires mitofusin 1 to promote mitochondrial fusion. *Proc Natl Acad Sci USA.* (2004) 101:15927–32. doi: 10.1073/pnas.0407043101
8. Li A, Gao M, Jiang W, Qin Y, Gong G. Mitochondrial dynamics in adult cardiomyocytes and heart diseases. *Front Cell Dev Biol.* (2020) 8:584800. doi: 10.3389/fcell.2020.584800
9. Mishra P, Chan DC. Metabolic regulation of mitochondrial dynamics. *J Cell Biol.* (2016) 212:379–87. doi: 10.1083/jcb.201511036
10. Labbe K, Murley A, Nunnari J. Determinants and functions of mitochondrial behavior. *Ann Rev Cell Dev Biol.* (2014) 30:357–91. doi: 10.1146/annurev-cellbio-101011-155756
11. Palmer CS, Elgass KD, Parton RG, Osellame LD, Stojanovski D, Ryan MT. Adaptor proteins MiD49 and MiD51 can act independently of Mff and Fis1 in Drp1 recruitment and are specific for mitochondrial fission. *J Biol Chem.* (2013) 288:27584–93. doi: 10.1074/jbc.M113.479873
12. Otera, Hidenori, Chunxin, Wang, Cleland, Megan, et al. Mff is an essential factor for mitochondrial recruitment of Drp1 during mitochondrial fission in mammalian cells. *J Cell Biol.* (2010) 191:1141–58. doi: 10.1083/jcb.201007152
13. Pitts KR, McNiven MA, Yoon Y. Mitochondria-specific function of the dynamin family protein DLP1 is mediated by its C-terminal domains. *J Biol Chem.* (2004) 279:50286–94. doi: 10.1074/jbc.M405531200
14. Chang CR, Blackstone C. Drp1 phosphorylation and mitochondrial regulation. *EMBO Rep.* (2007) 8:1088–9; author reply 9–90. doi: 10.1038/sj.embor.7401118
15. Nan J, Zhu W, Rahman MS, Liu M, Li D, Su S, et al. Molecular regulation of mitochondrial dynamics in cardiac disease. *Biochim Biophys Acta Mol Cell Res.* (2017) 1864:1260–73. doi: 10.1016/j.bbamcr.2017.03.006
16. Taguchi N, Ishihara N, Jofuku A, Oka T, Mihara K. Mitotic phosphorylation of dynamin-related GTPase Drp1 participates in mitochondrial fission. *J Biol Chem.* (2007) 282:11521–9. doi: 10.1074/jbc.M607279200
17. Chang CR, Blackstone C. Cyclic AMP-dependent protein kinase phosphorylation of Drp1 regulates its GTPase activity and mitochondrial morphology. *J Biol Chem.* (2007) 282:21583–7. doi: 10.1074/jbc.C700083200
18. Cribbs JT, Strack S. Reversible phosphorylation of Drp1 by cyclic AMP-dependent protein kinase and calcineurin regulates mitochondrial fission and cell death. *EMBO Rep.* (2007) 8:939–44. doi: 10.1038/sj.embor.7401062
19. Wasiak S, Zunino R, McBride HM. Bax/Bak promote sumoylation of DRP1 and its stable association with mitochondria during apoptotic cell death. *J Cell Biol.* (2007) 177:439–50. doi: 10.1083/jcb.200610042
20. Figueroa-Romero C, Iniguez-Lluhi JA, Stadler J, Chang CR, Arnoult D, Keller PJ, et al. SUMOylation of the mitochondrial fission protein Drp1 occurs at multiple nonconsensus sites within the B domain and is linked to its activity cycle. *Faseb J.* (2009) 23:3917–27. doi: 10.1096/fj.09-136630
21. Guo C, Hildick KL, Luo J, Dearden L, Wilkinson KA, Henley JM. SENP3-mediated deSUMOylation of dynamin-related protein

1 promotes cell death following ischaemia. *EMBO J.* (2013) 32:1514–28. doi: 10.1038/emboj.2013.65
22. Wakabayashi J, Zhang ZY, Wakabayashi N, Tamura Y, Fukaya M, Kensler TW, et al. The dynamin-related GTPase Drp1 is required for embryonic and brain development in mice. *J Cell Biol.* (2009) 186:805–16. doi: 10.1083/jcb.200903065
23. Song M, Dorn GWJCM. Mitoconfusion: noncanonical functioning of dynamism factors in static mitochondria of the heart. *Cell Metab*. (2015) 21:195–205. doi: 10.1016/j.cmet.2014.12.019
24. Kageyama Y, Hoshijima M, Seo K, Bedja D, Sysa-Shah P, Andrabi SA, et al. Parkin-independent mitophagy requires Drp1 and maintains the integrity of mammalian heart and brain. *EMBO J.* (2014) 33:2798–813. doi: 10.15252/embj.201488658
25. Yoshiyuki I, Akihiro S, Yasuhiro M, Peiyong Z, Sebastiano S, Jessica T, et al. Endogenous Drp1 mediates mitochondrial autophagy and protects the heart against energy stress. *Circul Res.* (2014) 116:264.
26. Ashrafian H, Docherty L, Leo V, Towlson C, Neilan M, Steeples V, et al. A mutation in the mitochondrial fission gene Dnm1l leads to cardiomyopathy. *PLoS Genet.* (2010) 6:e1001000. doi: 10.1371/journal.pgen.1001000
27. Ikeda Y, Shirakabe A, Maejima Y, Zhai P, Sciarretta S, Toli J, et al. Endogenous Drp1 mediates mitochondrial autophagy and protects the heart against energy stress. *Circ Res.* (2015) 116:264–78. doi: 10.1161/CIRCRESAHA.116.303356
28. Song M, Mihara K, Chen Y, Scorrano L, Dorn GW II. Mitochondrial fission and fusion factors reciprocally orchestrate mitophagic culling in mouse hearts and cultured fibroblasts. *Cell Metab*. (2015) 21:273–86. doi: 10.1016/j.cmet.2014.12.011
29. Karbowski, M. Spatial and temporal association of Bax with mitochondrial fission sites, Drp1, and Mfn2 during apoptosis. *J Cell Biol.* (2003) 159:931–8. doi: 10.1083/jcb.200209124
30. Papanicolaou KN, Khairallah RJ, Ngoh GA, Chikando A, Luptak I, O'Shea KM, et al. Mitofusin-2 maintains mitochondrial structure and contributes to stress-induced permeability transition in cardiac myocytes. *Mol Cell Biol.* (2011) 31:1309–28. doi: 10.1128/MCB.00911-10
31. Neuspiel M, Zunino R, Gangaraju S, Rippstein P, McBride H. Activated mitofusin 2 signals mitochondrial fusion, interferes with Bax activation, and reduces susceptibility to radical induced depolarization. *J Biol Chem.* (2005) 280:25060–70. doi: 10.1074/jbc.M501599200
32. Brooks C, Wei Q, Feng L, Dong G, Tao Y, Mei L, et al. Bak regulates mitochondrial morphology and pathology during apoptosis by interacting with mitofusins. *Proc Natl Acad Sci USA.* (2007) 104:11649–54. doi: 10.1073/pnas.0703976104
33. Jason K, Onur K, Brody MJ, Sargent MA, Michael DM, Molkentin JD, et al. Necroptosis interfaces with MOMP and the MPTP in mediating cell death. *PLoS ONE.* (2015) 10:e0130520. doi: 10.1371/journal.pone.0130520
34. Whelan RS, Konstantinidis K, Wei AC, Chen Y, Reyna DE, Jha S, et al. Bax regulates primary necrosis through mitochondrial dynamics. *Proc Natl Acad Sci USA.* (2012) 109:6566–71. doi: 10.1073/pnas.1201608109
35. Disatnik MH, Ferreira JC, Campos JC, Gomes KS, Dourado PM, Qi X, et al. Acute inhibition of excessive mitochondrial fission after myocardial infarction prevents long-term cardiac dysfunction. *J Am Heart Assoc.* (2013) 2:e000461. doi: 10.1161/JAHA.113.000461
36. Sharp WW, Fang YH, Han M, Zhang HJ, Hong Z, Banathy A, et al. Dynamin-related protein 1 (Drp1)-mediated diastolic dysfunction in myocardial ischemia-reperfusion injury: therapeutic benefits of Drp1 inhibition to reduce mitochondrial fission. *FASEB J.* (2014) 28:316–26. doi: 10.1096/fj.12-226225
37. Cereghetti GM, Stangherlin A, Martins de Brito O, Chang CR, Blackstone C, Bernardi P, et al. Dephosphorylation by calcineurin regulates translocation of Drp1 to mitochondria. *Proc Natl Acad Sci USA.* (2008) 105:15803–8. doi: 10.1073/pnas.0808249105
38. Yang YL, Li J, Liu K, Zhang L, Liu Q, Liu BL, et al. Ginsenoside Rg5 increases cardiomyocyte resistance to ischemic injury through regulation of mitochondrial hexokinase-II and dynamin-related protein 1. *Cell Death Dis.* (2017) 8:e2625. doi: 10.1038/cddis.2017.43
39. Tao A, Xu X, Kvietys P, Kao R, Martin C, Rui T. Experimental diabetes mellitus exacerbates ischemia/reperfusion-induced myocardial injury by promoting mitochondrial fission: role of down-regulation of myocardial Sirt1 and subsequent Akt/Drp1 interaction. *Int J Biochem Cell Biol.* (2018) 105:94–103. doi: 10.1016/j.biocel.2018.10.011
40. Wang XS, Song Q. Mst1 regulates post-infarction cardiac injury through the JNK-Drp1-mitochondrial fission pathway. *Cell Mol Biol Lett.* (2018) 23:21. doi: 10.1186/s11658-018-0085-1
41. Shimizu Y, Lambert JP, Nicholson CK, Kim JJ, Wolfson DW, Cho HC, et al. DJ-1 protects the heart against ischemia–reperfusion injury by regulating mitochondrial fission. *J Mol Cell Cardiol.* (2016) 97:56–66. doi: 10.1016/j.yjmcc.2016.04.008
42. Ong SB, Subrayan S, Lim SY, Yellon DM, Davidson SM, Hausenloy DJ. Inhibiting mitochondrial fission protects the heart against ischemia/reperfusion injury. *Circulation.* (2010) 121:2012–22. doi: 10.1161/CIRCULATIONAHA.109.906610
43. Zepeda R, Kuzmicic J, Parra V, Troncoso R, Pennanen C, Riquelme JA, et al. Drp1 loss-of-function reduces cardiomyocyte oxygen dependence protecting the heart from ischemia-reperfusion injury. *J Cardiovasc Pharmacol.* (2014) 63:477–87. doi: 10.1097/FJC.0000000000000071
44. Wang JX, Jiao JQ, Li Q, Long B, Wang K, Liu JP, et al. miR-499 regulates mitochondrial dynamics by targeting calcineurin and dynamin-related protein-1. *Nat Med.* (2011) 17:71–8. doi: 10.1038/nm.2282
45. Jixuan L, Wei Y, Xiaojing Z, Qian J, Jinda W, Huawei Z, et al. Sirt3 attenuates post-infarction cardiac injury *via* inhibiting mitochondrial fission and normalization of AMPK-Drp1 pathways. *Cell Signal.* (2018) 53:1–13. doi: 10.1016/j.cellsig.2018.09.009
46. Sharp WW, Beiser DG, Fang YH, Han M, Piao L, Varughese J, et al. Inhibition of the mitochondrial fission protein dynamin-related protein 1 improves survival in a murine cardiac arrest model. *Crit Care Med.* (2015) 43:e38–47. doi: 10.1097/CCM.0000000000000817
47. Givvimani S, Munjal C, Tyagi N, Sen U, Metreveli N, Tyagi SC. Mitochondrial division/mitophagy inhibitor (Mdivi) ameliorates pressure overload induced heart failure. *PLoS ONE.* (2012) 7:e32388. doi: 10.1371/journal.pone.0032388
48. Kwon SH, Pimentel DR, Remondino A, Sawyer DB, Colucci WS. H2O2 regulates cardiac myocyte phenotype *via* concentration-dependent activation of distinct kinase pathways. *J Mol Cell Cardiol.* (2003) 35:615–21. doi: 10.1016/S0022-2828(03)00084-1
49. El-Mowafy AM, White RE. Resveratrol inhibits MAPK activity and nuclear translocation in coronary artery smooth muscle: reversal of endothelin-1 stimulatory effects. *FEBS Lett.* (1999) 451:63–7. doi: 10.1016/S0014-5793(99)00541-4
50. Ding M, Dong Q, Liu Z, Liu Z, Qu Y, Li X, et al. Inhibition of dynamin-related protein 1 protects against myocardial ischemia–reperfusion injury in diabetic mice. *Cardiovasc Diabetol.* (2017) 16:1–11. doi: 10.1186/s12933-017-0540-8
51. Ra A, Sa B, Csa B, Mm B, Ssn B, Mp C, et al. Pleiotropic effects of mdivi-1 in altering mitochondrial dynamics, respiration, and autophagy in cardiomyocytes. *Redox Biol.* (2020) 36:101660. doi: 10.1016/j.redox.2020.101660
52. Ong SB, Kwek XY, Katwadi K, Hernandez-Resendiz S, Crespo-Avilan GE, Ismail NI, et al. Targeting mitochondrial fission using Mdivi-1 in A clinically relevant large animal model of acute myocardial infarction: a pilot study. *Int J Mol Sci.* (2019) 20:3972. doi: 10.3390/ijms20163972
53. Galloway CA, Yoon Y. Mitochondrial dynamics in diabetic cardiomyopathy. *Antioxid Redox Signal.* (2015) 22:1545–62. doi: 10.1089/ars.2015.6293
54. Yu T, Robotham JL, Yoon Y. Increased production of reactive oxygen species in hyperglycemic conditions requires dynamic change of mitochondrial morphology. *Proc Natl Acad Sci USA.* (2006) 103:2653–8. doi: 10.1073/pnas.0511154103
55. Yu TZ, Jhun BS, Yoon Y. High-glucose stimulation increases reactive oxygen species production through the calcium and mitogen-activated protein kinase-mediated activation of mitochondrial fission. *Antioxid Redox Signal.* (2011) 14:425–37. doi: 10.1089/ars.2010.3284
56. Qi X, Disatnik MH, Shen N, Sobel RA, Mochly-Rosen D. Aberrant mitochondrial fission in neurons induced by protein kinase C{delta} under oxidative stress conditions *in vivo*. *Mol Biol Cell.* (2011) 22:256–65. doi: 10.1091/mbc.E10-06-0551
57. Strack S, Wilson TJ, Cribbs JT. Cyclin-dependent kinases regulate splice-specific targeting of dynamin-related protein 1 to microtubules. *J Cell Biol.* (2013) 201:1037–51. doi: 10.1083/jcb.201210045

58. Ding M, Feng N, Tang D, Feng J, Li Z, Jia M, et al. Melatonin prevents Drp1-mediated mitochondrial fission in diabetic hearts through SIRT1-PGC1α pathway. *J Pineal Res*. (2018) 65:e12491. doi: 10.1111/jpi.12491
59. Yu T, Sheu SS, Robotham JL, Yoon Y. Mitochondrial fission mediates high glucose-induced cell death through elevated production of reactive oxygen species. *Cardiovasc Res.* (2008) 79:341–51. doi: 10.1093/cvr/cvn104
60. Tang Y, Mi C, Liu J, Gao F, Long J. Compromised mitochondrial remodeling in compensatory hypertrophied myocardium of spontaneously hypertensive rat. *Cardiovasc Pathol.* (2014) 23:101–6. doi: 10.1016/j.carpath.2013.11.002
61. Pennanen C, Parra V, López-Crisosto C, Morales PE, del Campo A, Gutierrez T, et al. Mitochondrial fission is required for cardiomyocyte hypertrophy mediated by a Ca2+-calcineurin signaling pathway. *J Cell Sci.* (2014) 127:2659–71. doi: 10.1242/jcs.139394
62. Watanabe T, Saotome M, Nobuhara M, Sakamoto A, Urushida T, Katoh H, et al. Roles of mitochondrial fragmentation and reactive oxygen species in mitochondrial dysfunction and myocardial insulin resistance. *Exp Cell Res.* (2014) 323:314–25. doi: 10.1016/j.yexcr.2014.02.027
63. Molina AJ, Wikstrom JD, Stiles L, Las G, Mohamed H, Elorza A, et al. Mitochondrial networking protects beta-cells from nutrient-induced apoptosis. *Diabetes.* (2009) 58:2303–15. doi: 10.2337/db07-1781
64. Sotomayor-Flores C, Rivera-Mejías P, Vásquez-Trincado C, López-Crisosto C, Lavandero S. Angiotensin-(1–9) prevents cardiomyocyte hypertrophy by controlling mitochondrial dynamics *via* miR-129-3p/PKIA pathway. *Cell Death Different*. (2020) 27:2586–2604. doi: 10.1038/s41418-020-0522-3
65. Jong CJ, Yeung J, Tseung E, Karmazyn M. Leptin-induced cardiomyocyte hypertrophy is associated with enhanced mitochondrial fission. *Mol Cell Biochemy.* (2018) 454:33–44. doi: 10.1007/s11010-018-3450-5
66. Prottoy H, Masao S, Takenori I, Keisuke I, Hideya K, Toshihide I, et al. Mitochondrial fission protein, dynamin-related protein 1, contributes to the promotion of hypertensive cardiac hypertrophy and fibrosis in Dahl-salt sensitive rats. *J Mol Cell Cardiol*. (2018) 121:103–6. doi: 10.1016/j.yjmcc.2018.07.004
67. Shirakabe A, Zhai P, Ikeda Y, Saito T, Maejima Y, Hsu CP, et al. Drp1-dependent mitochondrial autophagy plays a protective role against pressure-overload-induced mitochondrial dysfunction and heart failure. *Circulation*. (2016) 134:e75–6. doi: 10.1161/CIRCULATIONAHA.116.023667
68. Huang CY, Lai CH, Kuo CH, Chiang SF, Pai PY, Lin JY, et al. Inhibition of ERK-Drp1 signaling and mitochondria fragmentation alleviates IGF-IIR-induced mitochondria dysfunction during heart failure. *J Mol Cell Cardiol.* (2018) 122:58–68. doi: 10.1016/j.yjmcc.2018.08.006
69. Chen HC, Vermulst M, Wang YE, Chomyn A, Prolla TA, McCaffery JM, et al. Mitochondrial fusion is required for mtDNA Stability in skeletal muscle and tolerance of mtDNA mutations. *Cell.* (2010) 141:280–9. doi: 10.1016/j.cell.2010.02.026
70. Hales KG, Fuller MT. Developmentally regulated mitochondrial fusion mediated by a conserved, novel, predicted GTPase. *Cell.* (1997) 90:121–9. doi: 10.1016/S0092-8674(00)80319-0
71. Chen KH, Guo X, Ma D, Guo Y, Li Q, Yang D, et al. Dysregulation of HSG triggers vascular proliferative disorders. *Nat Cell Biol.* (2004) 6:872–83. doi: 10.1038/ncb1161
72. de Brito OM, Scorrano L. Mitofusin 2 tethers endoplasmic reticulum to mitochondria. *Nature.* (2008) 456:605–10. doi: 10.1038/nature 07534
73. Santel A, Frank S, Gaume B, Herrler M, Youle RJ, Fuller MT. Mitofusin-1 protein is a generally expressed mediator of mitochondrial fusion in mammalian cells. *J Cell Sci.* (2003) 116(Pt 13):2763–74. doi: 10.1242/jcs.00479
74. Chen Y, Liu YQ, Dorn GW. Mitochondrial fusion is essential for organelle function and cardiac homeostasis. *Circulat Res.* (2011) 109:1327–U36. doi: 10.1161/CIRCRESAHA.111.258723
75. Chen H, Detmer SA, Ewald AJ, Griffin EE, Fraser SE, Chan DC. Mitofusins Mfn1 and Mfn2 coordinately regulate mitochondrial fusion and are essential for embryonic development. *J Cell Biol.* (2003) 160:189–200. doi: 10.1083/jcb.200211046
76. Hall AR, Burke N, Dongworth RK, Kalkhoran SB, Dyson A, Vicencio JM, et al. Hearts deficient in both Mfn1 and Mfn2 are protected against acute myocardial infarction. *Cell Death Dis.* (2016) 7:e2238. doi: 10.1038/cddis.2016.139
77. Fang L, Moore XL, Gao XM, Dart AM, Lim YL, Du XJ. Down-regulation of mitofusin-2 expression in cardiac hypertrophy *in vitro* and *in vivo*. *Life Sci.* (2007) 80:2154–60. doi: 10.1016/j.lfs.2007.04.003
78. Shen T, Zheng M, Cao CM, Chen CL, Tang J, Zhang WR, et al. Mitofusin-2 is a major determinant of oxidative stress-mediated heart muscle cell apoptosis. *J Biol Chemi.* (2007) 282:23354–61. doi: 10.1074/jbc.M702657200
79. Gao Q, Wang XM, Ye HW, Yu Y, Kang PF, Wang HJ, et al. Changes in the expression of cardiac mitofusin-2 in different stages of diabetes in rats. *Mol Med Rep.* (2012) 6:811–4. doi: 10.3892/mmr.2012.1002
80. Javadov S, Rajapurohitam V, Kilić A, Hunter JC, Zeidan A, Faruq NS, et al. Expression of mitochondrial fusion–fission proteins during post-infarction remodeling: the effect of NHE-1 inhibition. *Basic Res Cardiol.* (2011) 106:99–109. doi: 10.1007/s00395-010-0122-3
81. Qiu Y, Cheng R, Liang C, Yao Y, Zhang W, Zhang J, et al. MicroRNA-20b promotes cardiac hypertrophy by the inhibition of mitofusin 2-Mediated Inter-organelle Ca2+ Cross-Talk - ScienceDirect. *Mol Ther Nucleic Acids.* (2020) 19:1343–56. doi: 10.1016/j.omtn.2020.01.017
82. Chen Y, Dorn GW II. PINK1-phosphorylated mitofusin 2 is a Parkin receptor for culling damaged mitochondria. *Science*. (2013) 340:471–5. doi: 10.1126/science.1231031
83. Papanicolaou KN, Ngoh GA, Dabkowski ER, O'Connell KA, Ribeiro RF, Jr., et al. Cardiomyocyte deletion of mitofusin-1 leads to mitochondrial fragmentation and improves tolerance to ROS-induced mitochondrial dysfunction and cell death. *Am J Physiol Heart Circ Physiol.* (2012) 302:H167–79. doi: 10.1152/ajpheart.00833.2011
84. Chen Y, Csordas G, Jowdy C, Schneider TG, Csordas N, Wang W, et al. Mitofusin 2-containing mitochondrial-reticular microdomains direct rapid cardiomyocyte bioenergetic responses *via* interorganelle Ca2+ crosstalk. *Circul Res.* (2012) 111:863–75. doi: 10.1161/CIRCRESAHA.112.266585
85. Ruiz-Meana M, Abellan A, Miro-Casas E, Agullo E, Garcia-Dorado D. Role of sarcoplasmic reticulum in mitochondrial permeability transition and cardiomyocyte death during reperfusion. *Am J Physiol Heart Circ Physiol.* (2009) 297:H1281–9. doi: 10.1152/ajpheart.00435.2009
86. Figueredo VM, Dresdner KP, Jr., Wolney AC, Keller AM. Postischaemic reperfusion injury in the isolated rat heart: effect of ruthenium red. *Cardiovasc Res.* (1991) 25:337–42. doi: 10.1093/cvr/25.4.337
87. Miyamae M, Camacho SA, Weiner MW, Figueredo VM. Attenuation of postischemic reperfusion injury is related to prevention of [Ca2+]m overload in rat hearts. *Am J Physiol.* (1996) 271:H2145–53. doi: 10.1152/ajpheart.1996.271.5.H2145
88. Murata M, Akao M, O'Rourke B, Marban E. Mitochondrial ATP-sensitive potassium channels attenuate matrix Ca(2+) overload during simulated ischemia and reperfusion: possible mechanism of cardioprotection. *Circ Res.* (2001) 89:891–8. doi: 10.1161/hh2201.100205
89. Ferreira JCB, Campos JC, Qvit N, Qi X, Bozi LHM, Bechara LRG, et al. A selective inhibitor of mitofusin 1-βIIPKC association improves heart failure outcome in rats. *Nat Commun.* (2019) 10:329. doi: 10.1038/s41467-018-08276-6
90. Olichon A, Baricault L, Gas N, Guillou E, Valette A, Belenguer P, et al. Loss of OPA1 perturbates the mitochondrial inner membrane structure and integrity, leading to cytochrome c release and apoptosis. *J Biol Chem.* (2003) 278:7743–6. doi: 10.1074/jbc.C200677200
91. Frezza C, Cipolat S, Martins de Brito O, Micaroni M, Beznoussenko GV, Rudka T, et al. OPA1 controls apoptotic cristae remodeling independently from mitochondrial fusion. *Cell.* (2006) 126:177–89. doi: 10.1016/j.cell.2006.06.025
92. Davies VJ, Hollins AJ, Piechota MJ, Yip W, Davies JR, White KE, et al. Opa1 deficiency in a mouse model of autosomal dominant optic atrophy impairs mitochondrial morphology, optic nerve structure and visual function. *Hum Mol Genet.* (2007) 16:1307–18. doi: 10.1093/hmg/ddm079
93. Kasahara A, Cipolat S, Chen Y, Dorn GW II, Scorrano L. Mitochondrial fusion directs cardiomyocyte differentiation *via* calcineurin and Notch signaling. *Science.* (2013) 342:734–7. doi: 10.1126/science.1241359
94. Wai T, Garcia-Prieto J, Baker MJ, Merkwirth C, Benit P, Rustin P, et al. Imbalanced OPA1 processing and mitochondrial fragmentation cause heart failure in mice. *Science.* (2015) 350:aad0116. doi: 10.1126/science.aad0116
95. Chen L, Gong Q, Stice JP, Knowlton AA. Mitochondrial OPA1, apoptosis, and heart failure. *Cardiovasc Res.* (2009) 84:91–9. doi: 10.1093/cvr/cvp181

96. Piquereau J, Caffin F, Novotova M, Prola A, Garnier A, Mateo P, et al. Down-regulation of OPA1 alters mouse mitochondrial morphology, PTP function, and cardiac adaptation to pressure overload. *Cardiovasc Res.* (2012) 94:408–17. doi: 10.1093/cvr/cvs117
97. Le C, Liu T, Tran A, Lu X, Association AAKJJotAH. OPA1 mutation and late-onset cardiomyopathy: mitochondrial dysfunction and mtDNA instability. *J Am Heart Assoc.* (2012) 1:e003012. doi: 10.1161/JAHA.112.003012
98. Quiros PM, Langer T, Lopez-Otin C. New roles for mitochondrial proteases in health, ageing and disease. *Nat Rev Mol Cell Biol.* (2015) 16:345–59. doi: 10.1038/nrm3984
99. Roy M, Reddy PH, Iijima M, Sesaki H. Mitochondrial division and fusion in metabolism. *Curr Opin Cell Biol.* (2015) 33:111–8. doi: 10.1016/j.ceb.2015.02.001
100. Anand R, Wai T, Baker MJ, Kladt N, Schauss AC, Rugarli E, et al. The i-AAA protease YME1L and OMA1 cleave OPA1 to balance mitochondrial fusion and fission. *J Cell Biol.* (2014) 204:919–29. doi: 10.1083/jcb.201308006
101. Ishihara N, Fujita Y, Oka T, Mihara K. Regulation of mitochondrial morphology through proteolytic cleavage of OPA1. *Embo J.* (2006) 25:2966–77. doi: 10.1038/sj.emboj.7601184
102. Baker MJ, Lampe PA, Stojanovski D, Korwitz A, Anand R, Tatsuta T, et al. Stress-induced OMA1 activation and autocatalytic turnover regulate OPA1-dependent mitochondrial dynamics. *EMBO J.* (2014) 33:578–93. doi: 10.1002/embj.201386474
103. Zhang K, Li H, Song Z. Membrane depolarization activates the mitochondrial protease OMA1 By stimulating self-cleavage. *EMBO Rep.* (2014) 15:576–85. doi: 10.1002/embr.201338240
104. Jiang X, Jiang H, Shen Z, Wang X. Activation of mitochondrial protease OMA1 by Bax and Bak promotes cytochrome c release during apoptosis. *Proc Natl Acad Sci USA.* (2014) 111:14782–7. doi: 10.1073/pnas.14172 53111
105. Griparic L, Kanazawa T, van der Bliek AM. Regulation of the mitochondrial dynamin-like protein Opa1 by proteolytic cleavage. *J Cell Biol.* (2007) 178:757–64. doi: 10.1083/jcb.200704112
106. Ehses S, Raschke I, Mancuso G, Bernacchia A, Geimer S, Tondera D, et al. Regulation of OPA1 processing and mitochondrial fusion by m-AAA protease isoenzymes and OMA1. *J Cell Biol.* (2009) 187:1023–36. doi: 10.1083/jcb.200906084
107. Samant SA, Zhang HJ, Hong Z, Pillai VB, Sundaresan NR, Wolfgeher D, et al. SIRT3 deacetylates and activates OPA1 to regulate mitochondrial dynamics during stress. *Mol Cell Biol.* (2014) 34:807–19. doi: 10.1128/MCB.01 483-13
108. Xin T, Lu C. Irisin activates Opa1-induced mitophagy to protect cardiomyocytes against apoptosis following myocardial infarction. *Aging.* (2020) 12:4474–88. doi: 10.18632/aging.102899
109. Wang K, Liu Z, Zhao M, Zhang F, Wang K, Feng N, et al. kappa-opioid receptor activation promotes mitochondrial fusion and enhances myocardial resistance to ischemia and reperfusion injury *via* STAT3-OPA1 pathway. *Europ J Pharmacol.* (2020) 874:172987. doi: 10.1016/j.ejphar.2020. 172987
110. Zhang Y, Wang Y, Xu J, Tian F, Hu S, Chen Y, et al. Melatonin attenuates myocardial ischemia-reperfusion injury *via* improving mitochondrial fusion/mitophagy and activating the AMPK-OPA1 signaling pathways. *J Pineal Res.* (2019) 66:e12542. doi: 10.1111/jpi.12542
111. Parra V, Verdejo HE, Iglewski M, Campo AD, Lavandero SJD. Insulin stimulates mitochondrial fusion and function in cardiomyocytes *via* the Akt-mTOR-NF B-Opa-1 signaling pathway. *Diabetes.* (2014) 63:75. doi: 10.2337/db13-0340
112. Elezaby A, Sverdlov AL, Tu VH, Soni K, Luptak I, Qin F, et al. Mitochondrial remodeling in mice with cardiomyocyte-specific lipid overload. *J Mol Cell Cardiol.* (2015) 79:275–83. doi: 10.1016/j.yjmcc.2014.12.001
113. Xin T, Lv W, Liu D, Jing Y, Hu F. Opa1 reduces hypoxia-induced cardiomyocyte death by improving mitochondrial quality control. *Front Cell Dev Biol.* (2020) 8:853. doi: 10.3389/fcell.2020.00853
114. Xie T, Wang C, Jin Y, Meng Q, Liu Q, Wu J, et al. CoenzymeQ10-induced activation of AMPK-YAP-OPA1 pathway alleviates atherosclerosis by improving mitochondrial function, inhibiting oxidative stress and promoting energy metabolism. *Front Pharmacol.* (2020) 11:1034. doi: 10.3389/fphar.2020.01034
115. Wang M, Wang RY, Zhou JH, Xie XH, Sun GB, Sun XB. Calenduloside E ameliorates myocardial ischemia-reperfusion injury through regulation of AMPK and mitochondrial OPA1. *Oxidative Med Cell Longevity.* (2020) 2020:1–12. doi: 10.1155/2020/2415269
116. Luo H, Song S, Chen Y, Xu M, Zhang W. Inhibitor 1 of protein phosphatase 1 regulates Ca 2+ /calmodulin-dependent protein kinase II to alleviate oxidative stress in hypoxia-reoxygenation injury of cardiomyocytes. *Oxidative Med Cell Longevity.* (2019) 2019:1–19. doi: 10.1155/2019/2193019
117. Gawlowski T, Suarez J, Scott B, Torres-Gonzalez M, Wang H, Schwappacher R, et al. Modulation of dynamin-related protein 1 (DRP1) function by increased O-linked-β-N-acetylglucosamine modification (O-GlcNAc) in cardiac myocytes. *J Biol Chem.* (2012) 287:30024. doi: 10.1074/jbc.M112.390682
118. Makino A, Suarez J, Gawlowski T, Han W, Wang H, Scott BT, et al. Regulation of mitochondrial morphology and function by O-GlcNAcylation in neonatal cardiac myocytes. *Am J Physiol Regul Integr Comp Physiol.* (2011) 300:R1296–302. doi: 10.1152/ajpregu.00437.2010
119. Fricovsky ES, Suarez J, Ihm SH, Scott BT, Suarez-Ramirez JA, Banerjee I, et al. Excess protein O-GlcNAcylation and the progression of diabetic cardiomyopathy. *Am J Physiol Regul Integr Comp Physiol.* (2012) 303:R689–99. doi: 10.1152/ajpregu.00548.2011
120. Qin Y, Li A, Liu B, Jiang W, Gao M, Tian X, et al. Mitochondrial fusion mediated by fusion promotion and fission inhibition directs adult mouse heart function toward a different direction. *FASEB J.* (2020) 34:663–75. doi: 10.1096/fj.201901671R
121. Maneechote C, Palee S, Kerdphoo S, Jaiwongkam T, Chattipakorn S, Chattipakorn N. Balancing mitochondrial dynamics *via* increasing mitochondrial fusion attenuates infarct size and left ventricular dysfunction in rats with cardiac ischemia/reperfusion injury. *Clin Sci.* (2019) 133:497–513. doi: 10.1016/S0735-1097(19)30659-X
122. Ding M, Liu C, Shi R, Yu M, Mi M. Mitochondrial fusion promoter restores mitochondrial dynamics balance and ameliorates diabetic cardiomyopathy in an optic atrophy 1-dependent way. *Acta Physiol.* (2019) 229:e13428. doi: 10.1111/apha.13428

Conflict of Interest: The authors declare that the research was conducted in the absence of any commercial or financial relationships that could be construed as a potential conflict of interest.

frontiers in Cardiovascular Medicine

REVIEW
published: 04 October 2021
doi: 10.3389/fcvm.2021.734562

Latest Advances in Endothelial Progenitor Cell-Derived Extracellular Vesicles Translation to the Clinic

Amankeldi A. Salybekov[1,2,3]*, *Aidyn D. Kunikeyev*[4], *Shuzo Kobayashi*[2,3] and *Takayuki Asahara*[2]*

[1] Division of Regenerative Medicine, Department of Center for Clinical and Translational Science, Shonan Kamakura General Hospital, Kamakura, Japan, [2] Shonan Research Institute of Innovative Medicine, Shonan Kamakura General Hospital, Kamakura, Japan, [3] Kidney Disease and Transplant Center, Shonan Kamakura General Hospital, Kamakura, Japan, [4] Department of Software Engineering, Kazakh National Technical University After K.I. Satpayev, Almaty, Kazakhstan

Almost all nucleated cells secrete extracellular vesicles (EVs) that are heterogeneous spheroid patterned or round shape particles ranging from 30 to 200 nm in size. Recent preclinical and clinical studies have shown that endothelial progenitor cell-derived EVs (EPC-EVs) have a beneficial therapeutic effect in various diseases, including cardiovascular diseases and kidney, and lung disorders. Moreover, some animal studies have shown that EPC-EVs selectively accumulate at the injury site with a specific mechanism of binding along with angiogenic and restorative effects that are superior to those of their ancestors. This review article highlights current advances in the biogenesis, delivery route, and long-term storage methods of EPC-EVs and their favorable effects such as anti-inflammatory, angiogenic, and tissue protection in various diseases. Finally, we review the possibility of therapeutic application of EPC-EVs in the clinic.

Keywords: extracellular vesicles, endothelial progenitor cells, exosomes, miR (microRNA), clinical application of EPC exosomes

OPEN ACCESS

Edited by:
Zhen-Ao Zhao,
Hebei North University, China

Reviewed by:
Jiacheng Sun,
University of Alabama at Birmingham, United States
Maria Cimini,
Temple University, United States

***Correspondence:**
Amankeldi A. Salybekov
a.salybekov@shonankamakura.or.jp
Takayuki Asahara
t_asahara@shonankamakura.or.jp

Specialty section:
This article was submitted to Cardiovascular Biologics and Regenerative Medicine, a section of the journal Frontiers in Cardiovascular Medicine

Received: *01 July 2021*
Accepted: *30 August 2021*
Published: *04 October 2021*

Citation:
Salybekov AA, Kunikeyev AD, Kobayashi S and Asahara T (2021) Latest Advances in Endothelial Progenitor Cell-Derived Extracellular Vesicles Translation to the Clinic. Front. Cardiovasc. Med. 8:734562. doi: 10.3389/fcvm.2021.734562

INTRODUCTION

Endothelial progenitor cells (EPCs) have been widely used to treat cardiovascular ischemic diseases since their discovery in 1997 (1). Initial clinical trials, in parallel with preclinical studies, raised hopes of cures for life-threatening ischemic diseases (2). In subsequent studies, EPC biology was further investigated and it was found that after long-term culture of between 15 and 21 days, cobblestone-shaped colonies emerged, called blood endothelial outgrowth cells (3). The phenotypes of these cells are similar to those of the adult endothelial cells and have a greater proliferative rate (3); Yoder's group (4) found similar cells from umbilical cord blood cells (4). Clinical studies have demonstrated that the origin of EPC is bone marrow, and considering pathological triggers, these cells migrate to damaged tissues and physically contribute to facilitating vasculature (3, 5–7). However, several groups are concerned about the existence of EPCs based on mouse data (8). In addition, the culture of EPCs in diverse systems, different methodologies, and various "misleading terms" has led to confusion in EPC biology and application. To this end, a recent consensus attempted to standardize EPC nomenclature based on cellular phenotypes and biological functions (9). A consensus statement on EPC nomenclature and culture standardization may facilitate progress toward the use of EPC-derived extracellular vesicle (EPC-EV) therapy. Depending on the sequence of appearance in culture, Hur et al. (10) reported two types of EPCs. The first were termed early EPCs or myeloid angiogenic cells that were positive for CD45, CD14, and CD31 markers, and

mainly worked via paracrine mechanisms, such as growth factors and EVs (10, 11). The second cell population, named late-EPC or endothelial colony-forming cells (ECFCs), usually appeared in culture at 2 to 3 weeks after cell culturing, and had similar phenotypes as endothelial cells, and enhanced neovascularization in ischemic tissues (10, 12). Recent studies have demonstrated that ECFCs secrete EVs that are crucial for organ restoration (13–15).

Almost all nucleated cells secrete extracellular vesicles cargo which deliveries nucleic acid and proteins to the recipient cells. The International Society for Extracellular Vesicles consensus recommendation on nomenclature endorses to use "extracellular vesicles" as a generic term for a lipid bilayer particle released from the cell and cannot replicate. Moreover, it has a broader meaning which can cover subtypes like exosomes and microvesicles as well. Depending on the physical size range, EVs divide small (<100 nm), medium (<200 nm), or large (>200 nm), and usually express CD63+, CD81+, Annexin A5, etc., surface markers (16). The small EVs are generated within endosomes as intraluminal vesicles and this complex EVs biogenesis occurs by endosomal sorting complex required for transport (ESCRT) sorting machineries involvement (17). Whereas, medium or large EVs originate by an outward budding at the plasma membrane (**Figure 1**) (18). There are several methods to isolate secreted EVs such as classical differential centrifugation, density gradient centrifugation, size-exclusion chromatography, ultrafiltration, immunocapture, precipitation, and tangential flow filtration, etc. (**Figure 1**) (16). Each EV isolation strategy or its working principle along with their advantages and disadvantages was reviewed previously (19).

A seminal study showed that EPCs secrete microvesicles, and the latter activate an angiogenic program in endothelial cells via horizontal transfer of mRNA (20). Subsequently, preclinical studies showed that EPC-EVs have superior therapeutic effects on various ischemic diseases (**Figure 2**) (21–23). In the last decade, numerous studies on EPC-EVs have shed light on EV biogenesis, uptake, and mechanism of action (24–27). This review highlights recent advances in the biogenesis, biological functions, route of delivery, and long-term storage of EPC-EVs. Finally, we describe potential translation to the clinic and regions of application in the context of various ischemic and inflammatory diseases.

EPCS VS. EPC-EVS

Recently, it has been reported that therapeutic cell transplantation-related effects for cardiovascular diseases are a result of paracrine mechanisms and not from direct cell contribution to damaged organs (28). Regardless of the target delivery technique, the long-term engraftment of cells is limited; hence, the striking short-term improvement in ischemic organ function after cell transplantation is mainly associated with paracrine trophic factors such as EVs (29). It has been shown that early EPC populations are contaminated with hematopoietic cell subsets, such as monocytes (30), and the latter secrete various nanoparticles. In contrast, late EPCs have specific phenotypes and biological functions similar to endothelial cells, and secrete angiomiRs-shuttled EVs, which are a key genetic material for neovascularization of ischemic tissues (14, 31, 32). Dozens of preclinical studies have demonstrated EPC-EV effects that are superior to those of the ancestor (33). EVs possess numerous advantages over cell-based therapies in the context of regenerative medicine in terms of (1) cargo delivery of various favorable miRs responsible for angiogenesis, fibrosis, and cell proliferation; (2) potential for "off the shelf" availability and respective for repetitive transplantation; (3) cell-free biological products that may be utilized as drug carrier systems in the pharmaceutical industry, and finally (4) generally reduced immunogenicity owing to which allogenic transplantation is an additional benefit. The abovementioned benefits are crucial for treating either acute or chronic diseases. The latter listed major advantages of the EVs are linked to less immunogenic than their parental cells because of the lower abundance of transmembrane proteins such as MHC complexes on their surface (34). Unlike live cells, EVs have a long shelf life and may be transported and stored for long periods (see the section on long-term preservation and storage of EVs). In the representative Venn diagram (**Figure 3**) (transcriptome data from previous publication PMID: 28631889), we summarize the similarities and differences between ECFC-derived microRNAs (miRs) and ECFC-EV-derived miRs (35). It can be clearly seen that the majority of parent cell-derived miRs (ECFC-miRs) can be found in ECFC-EV-derived miRs, suggesting a similar transcriptome profile along with the mechanism of action (**Figure 3**). A previous study showed that the therapeutic potential of EPC-EVs is superior in terms of enhancing neovascularization and recovery in a murine hind limb ischemia model (12). The mechanism of activation of the angiogenic program in quiescent endothelial cells is linked by horizontal transfer of genetic materials such as angiomiR, RNA, and proteins (12, 13). Of note, ischemia itself is a trigger for angiogenesis. However, angiogenesis-qualified angiomiRs accelerate not only angiogenesis but also proliferative and anti-apoptotic effects (**Figure 4**). Collectively, well-packed EPC-EVs have a great advantage in preserving ischemic tissue from injury, and future studies are warranted to define the beneficial effects of EPC-EVs.

EPC-EVS IN CARDIOVASCULAR DISEASES

Cardiovascular diseases are the leading cause of mortality and morbidity in the globe (36). It has been shown that therapeutic neoangiogenesis with EPCs is a promising strategy for treating advanced cardiovascular diseases and preventing major adverse events (37). Similar transcriptome profiles of EPC-derived EVs to the EPCs facilitate therapeutic application EPC-EVs in CVD. Yue et al. (38) demonstrated that EPC-derived exosome treatment enhanced left ventricle cardiac function, reduced cell apoptosis, diminished myocardial scar size, and promoted post-myocardial infarction neovascularization. Previous studies have shown that sonic hedgehog modified progenitor cells (CD34+) actively secrete exosome cargo and carry various reparative molecules to cure the ischemic myocardium (39, 40). EPC-EVs regulate cardioprotection by

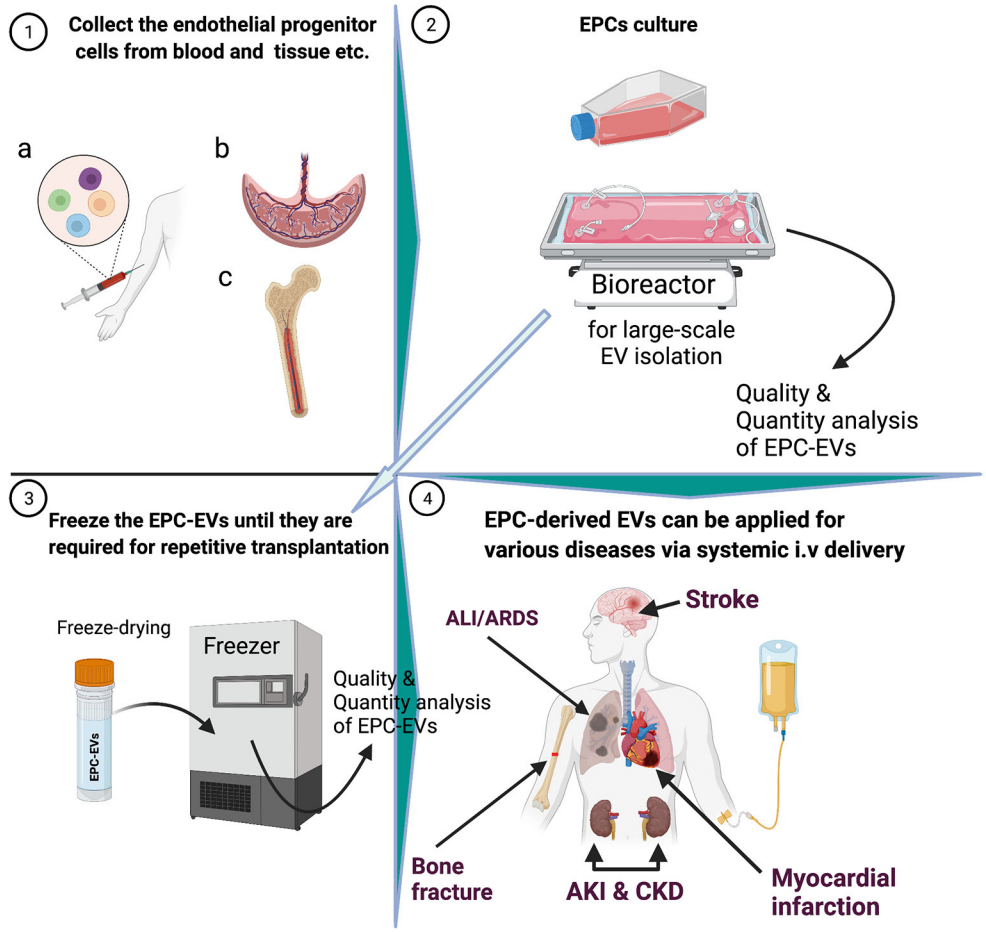

FIGURE 1 | Graphical abstract.

orchestrating cell angiogenesis, migration and adhesion, cell proliferation, and cell differentiation processes (**Figure 5**). Target gene expression analysis of EPC-EV-derived miR revealed that heart regeneration and protection enriched functional gene upregulation (**Figure 5**). Cardioprotective properties of EPC-derived EV is associated with miR-218-5p and miR-363-3p overexpression. The latter facilitated cardiac function via enhanced neoangiogenesis and inhibited myocardial fibrosis (41). Moreover, EPC-EVs treatment promoted mesenchymal-endothelial transition and along with protective effect to myocardial infarcted tissues (42). Recently, Chen et al. (33) showed that using EPC-EVs and encapsulation with a hydrogel could increase biological activity for up to 3 weeks through sustained release. Furthermore, the injected hydrogel system for sustained EPC-EV delivery into the ischemic myocardium augmented hemodynamics via increased vessel density in the peri-infarcted area along with reduction in myocardial scar formation. Interestingly, the regenerative efficacy of hydrogen-encapsulated EPC-EVs is not inferior to that of the parent cells or EPCs (33). Repetitive systemic transplantation of EVs is a simple delivery option. We have recently shown that systemic repetitive transplantation of EVs derived from regeneration-associated cells in a rat model of myocardial IR injury significantly enhanced cardiac functions, such as ejection fraction, and preserved mitral regurgitation. In addition, we could not observe anti-donor immune responses even when EV transplantation was performed in allogeneic settings.

Taken together, EPC-EVs have anti-inflammatory and anti-fibrotic properties and may enhance angiogenesis in the ischemic myocardium.

EPC-EVS IN ACUTE LUNG INJURY AND ACUTE RESPIRATORY DISTRESS SYNDROME (ALI/ARDS) PATHOLOGY

Systematic reviews have demonstrated that the mortality rate in ALI/ARDS is between 36 and 44% and is usually induced by various etiologies such as sepsis, pneumonia, and severe traumas (43). The high mortality rate in ALI/ARDS facilitates various "cell-free" therapeutic EVs, including EPC-EVs. Emerging data shows that EPC-EV administration markedly reduced lipopolysaccharide-induced lung inflammation compared to that in the control groups, indicating a strong anti-inflammatory

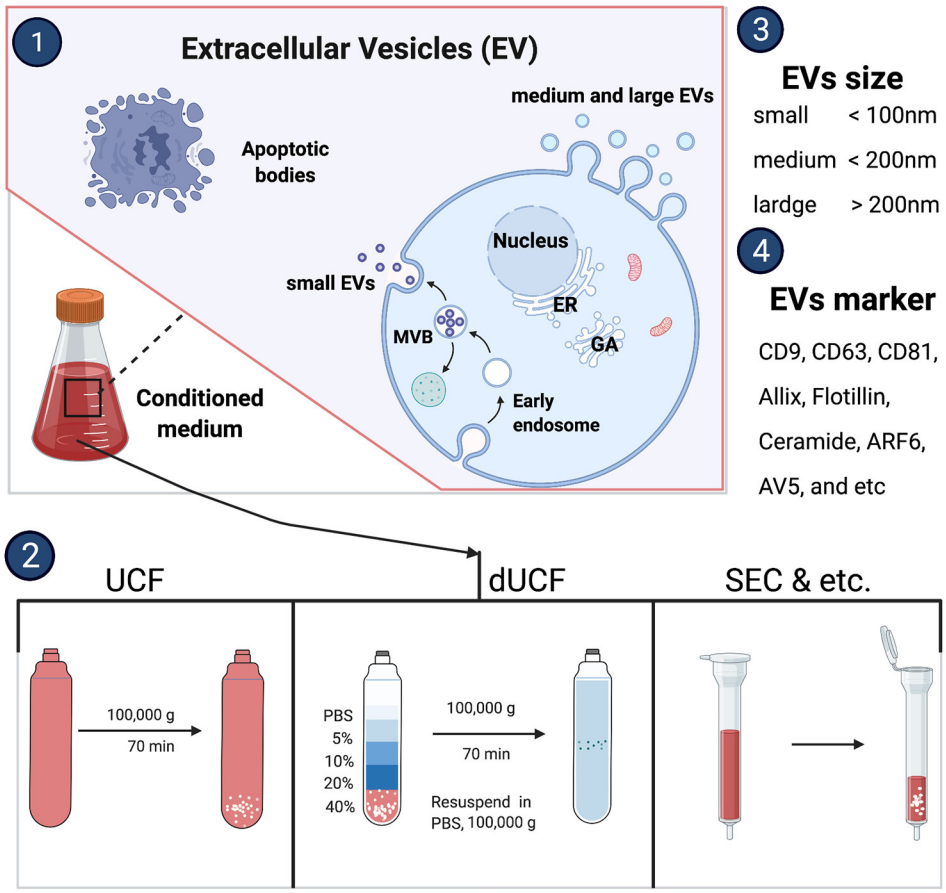

FIGURE 2 | Extracellular vesicles biogenesis and isolation methods. UCF, ultracentrifuge; dUCF, density gradient centrifugation, size-exclusion chromatography.

effect of EVs. Histological examination of the EPC-EV-administered group showed limited alveolar edema and lung neutrophil infiltration, and reduced cytokine/chemokine levels in the bronchoalveolar lavage fluid (44). Mechanistically, EPC-EV contains abundant miRNA-126, and overexpression of miRNA-126-3p can target phosphoinositide-3-kinase regulatory subunit 2, whereas overexpression of miRNA-126-5p inhibits the inflammatory alarmin high mobility group box 1 (HMGB1) and the permeability factor vascular endothelial growth factor (VEGF) α (44). Wu et al. (45) reported different mechanistic insights into EPC exosome-mediated transfer of miR-126 to endothelial cells such as the selective expression of SPRED1 and the enhancement of RAF/ERK signaling pathways that were primarily responsible for restoring the acute-injured lung. In summary, EPC-EVs have a beneficial effect in improving ALI/ARDS outcomes, and further studies are necessary to define optimal and targeted EV delivery methods to the site of injury.

EPC-EVS IN SEPSIS

Sepsis is a systemic inflammation induced mainly by microorganisms, leading to organ dysfunction. Recent studies have highlighted that EPC transplantation has a beneficial effect on animal models of sepsis (46, 47). Mechanistically, various pro-inflammatory cytokines induced by pathogen-associated molecular patterns (PAMPs) and damage-associated molecular patterns (DAMPs) in peripheral blood cause vascular injury and increase permeability (47). Consequently, in response to vascular injury, EPCs mobilize in an SDF1a-dependent manner and directly recruit to the injury site and differentiate into mature endothelial cells (47, 48). Fan et al. (46) demonstrated that EPCs and SDF1a administration synergistically improves survival in septic animals via enhanced miR-126 and miR-125b expression, which is believed to play key roles in the maintenance of endothelial cell function and inflammation. Later, they demonstrated that the protective effect of EPCs on the microvasculature after sepsis occurs via exosome-mediated transfer of miRs such as miR-126-3p and 5p (49). EPC-EVs miR-126-5p and 3p suppressed DAMP-induced *HMGB1* and vascular cell adhesion molecule 1 (VCAM1) levels, whereas inhibition of miR-126-5p and 3p through transfection with miR-126-5p and 3p inhibitors disrupted the beneficial effect of EPC exosomes. Thus, EPC-EVs prevent adverse septic complications via miR-126 delivery (49).

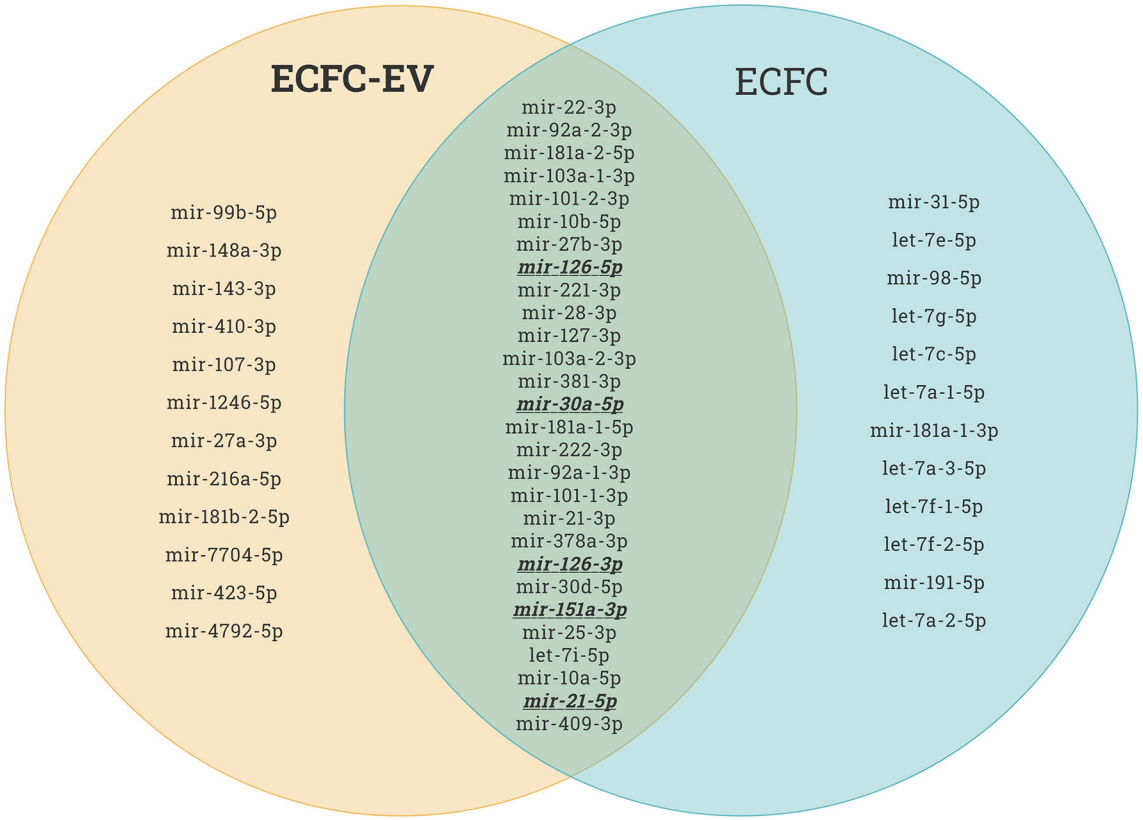

FIGURE 3 | Endothelial colony forming cell (ECFC)-derived microRNAs (miRs) vs. ECFC-extracellular vesicle (EV)-derived miRs. As shown in the Venn diagram, the majority of the top upregulated human miRs of both ECFC-derived and ECFC-EVs-derived miRs comprise similar miRs. This provides evidence that EPCs work via paracrine factors in organ regeneration. This miR sequence data was generated from PMID: 28631889.

EPC-EVS IN ACUTE KIDNEY DISEASES

Ischemia/reperfusion is a major cause of acute kidney injury (AKI) in humans, and is associated with tubular cell necrosis and endothelial cell dysfunction or loss. Growing evidence has shown that the therapeutic potential of EPC-EVs is superior in terms of acute kidney disease. Vinas et al. (15) used ECFC-derived EVs in an acute kidney injury mouse model and showed that miR-486-5p enriched ECFC exosomes significantly reduced ischemia-induced kidney injury. Histologically, exosome treatment decreased the infiltration of neutrophils along with diminished apoptosis and caspase-3 activation. Moreover, administration of exosomes to acute kidney injury-induced animals caused potent protection against kidney injury after 24 h, as evidenced by normalization of plasma creatinine and blood urea nitrogen to the same level as that in the healthy control. Mechanistically, miR-486-5p enriched ECFC exosomes target to reduce the phosphatase and tensin homolog, and stimulate the Akt phosphorylation pathway for ischemic tissue preservation (15). Cantaluppi et al. (13) demonstrated that EPC-EVs carrying miR-126 and miR-296 protect against experimental acute renal IRI, as evidenced by a significant decrease in serum creatinine and blood urea nitrogen levels and improvement in histological signs of microvascular and tubular injury. It is well-known that EPC-EVs exert miR-126 and have strong angiogenic and anti-apoptotic potential (23). In another study, EPC-EV transplantation rescued an experimental model of anti-Thy1.1-induced glomerulonephritis via inhibition of antibody- and complement-mediated injury of mesangial cells (50). In a review article, Sun et al. (51) summarized that stem/progenitor cell-derived EVs, including EPC-EVs, have beneficial effects such as anti-inflammatory, anti-apoptotic, anti-fibrotic, and may also promote renal cancer progression. In summary, EPC-EVs were shown to have a strong renoprotective effect in an acute kidney injury model, and future studies are warranted to extend their application to chronic kidney diseases.

EPC-EVS IN BONE AND CONNECTIVE TISSUE REPAIR

Accumulating evidence demonstrates that EPCs have beneficial effects on bone regeneration by secreting trophic and paracrine factors (52, 53). Pang et al. (54) showed that EPCs modulate the survival, migration, and differentiation potential of osteoclast precursors through the VEGFR-2, CXCR4, Smad2/3, Akt, ERK1, and p38 MAPK pathways (**Figure 6**). Interestingly, target genes of highly expressed EPC-EV miRs yielded several significant bone

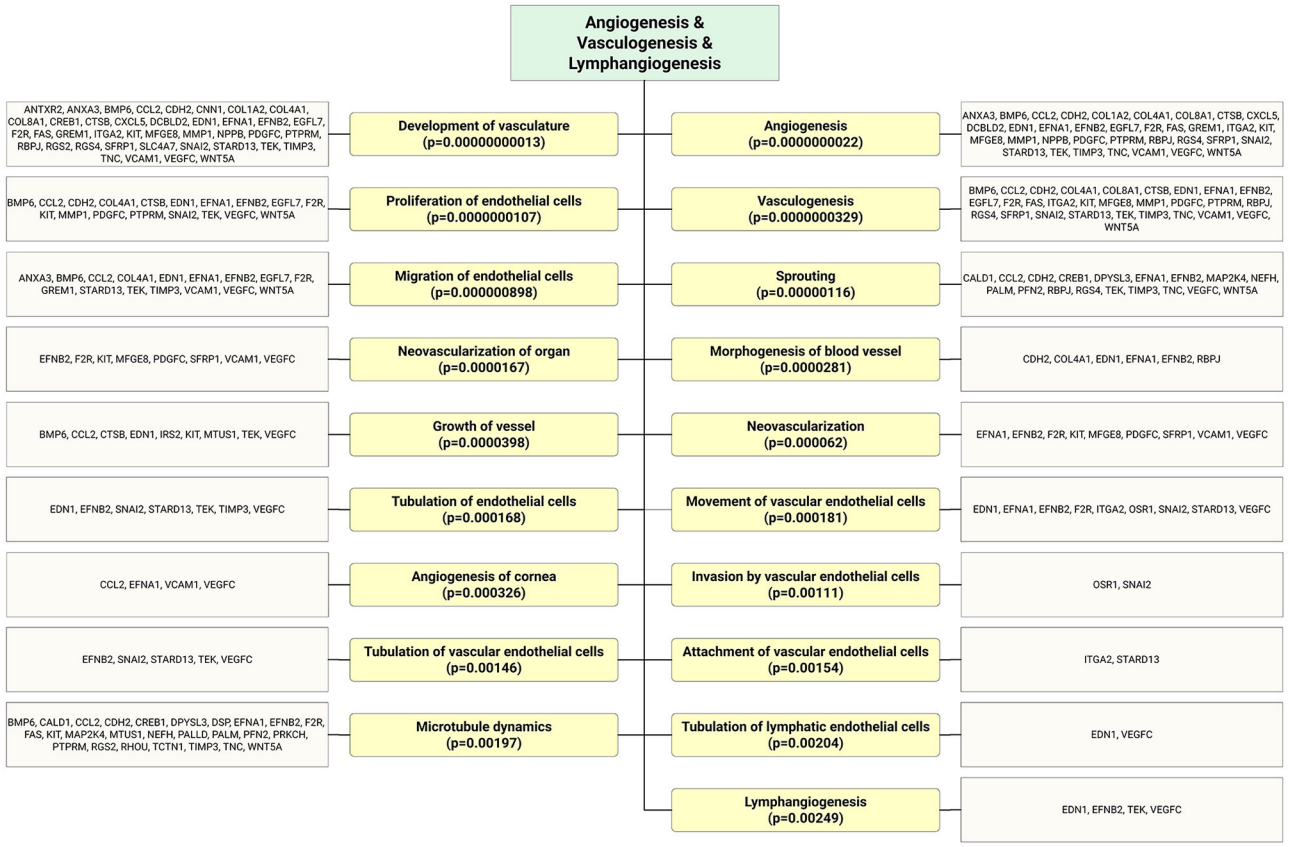

FIGURE 4 | As shown in the flow chart that highly expressed ECFC-EC-derived miRs biological targets were predicted *in silico*. The most significantly enriched functional annotation were Angiogenesis, vasculogenesis, and lymphangiogenesis. This miR sequence data was generated from PMID: 28631889. MicroRNA target genes were predicted using IPA with information from TargetScan, miRecords, and TarBase databases.

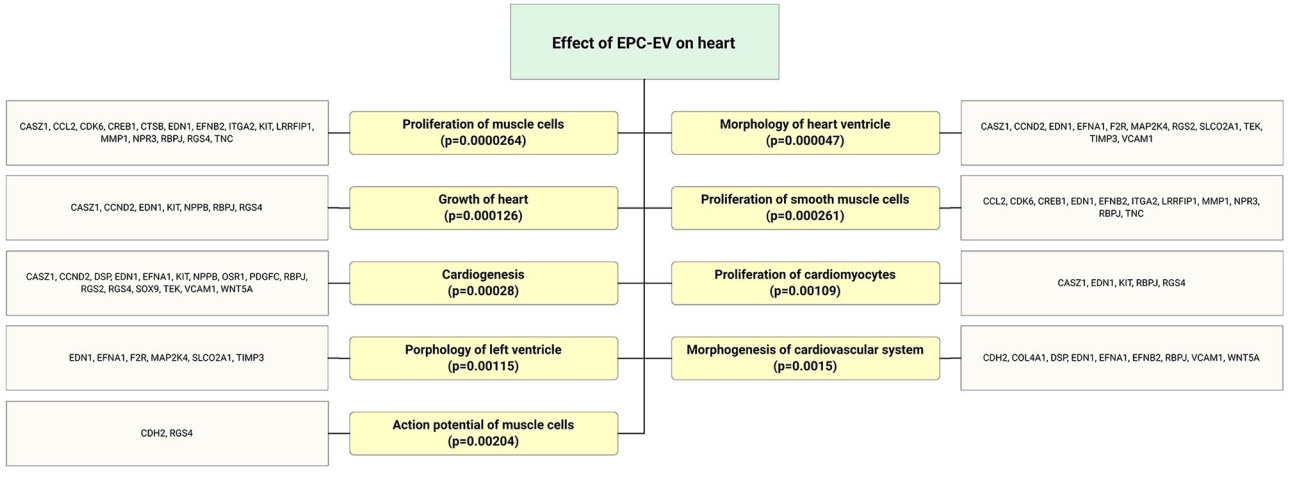

FIGURE 5 | Flow chart depicts highly expressed ECFC-EC-derived miRs biological targets that were predicted *in silico*. The significantly enriched functional annotation was associated with heart tissue repair. This miR sequence data was generated from PMID: 28631889. MicroRNA target genes were predicted using IPA with information from TargetScan, miRecords, and TarBase databases.

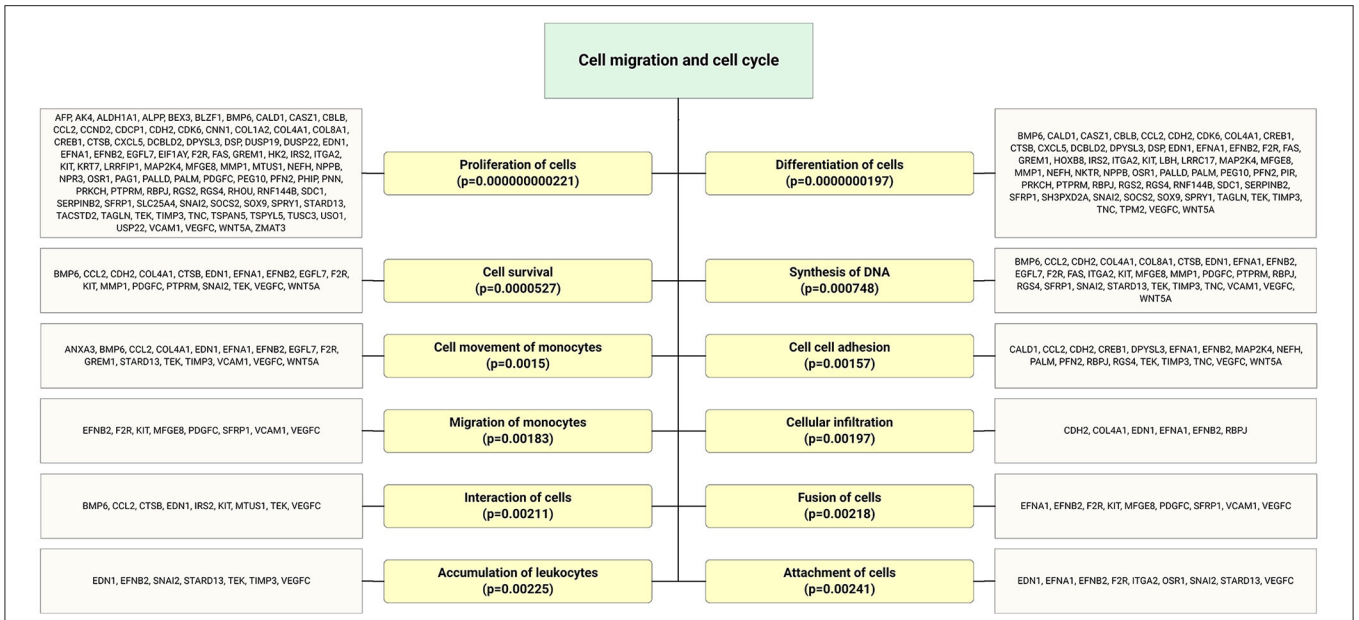

FIGURE 6 | Highly expressed ECFC-EC-derived miRs biological targets were predicted, and the most significantly enriched functional annotations were cell migration and cell cycle. This miR sequence data was generated from PMID: 28631889. MicroRNA target genes were predicted using IPA with information from TargetScan, miRecords, and TarBase databases.

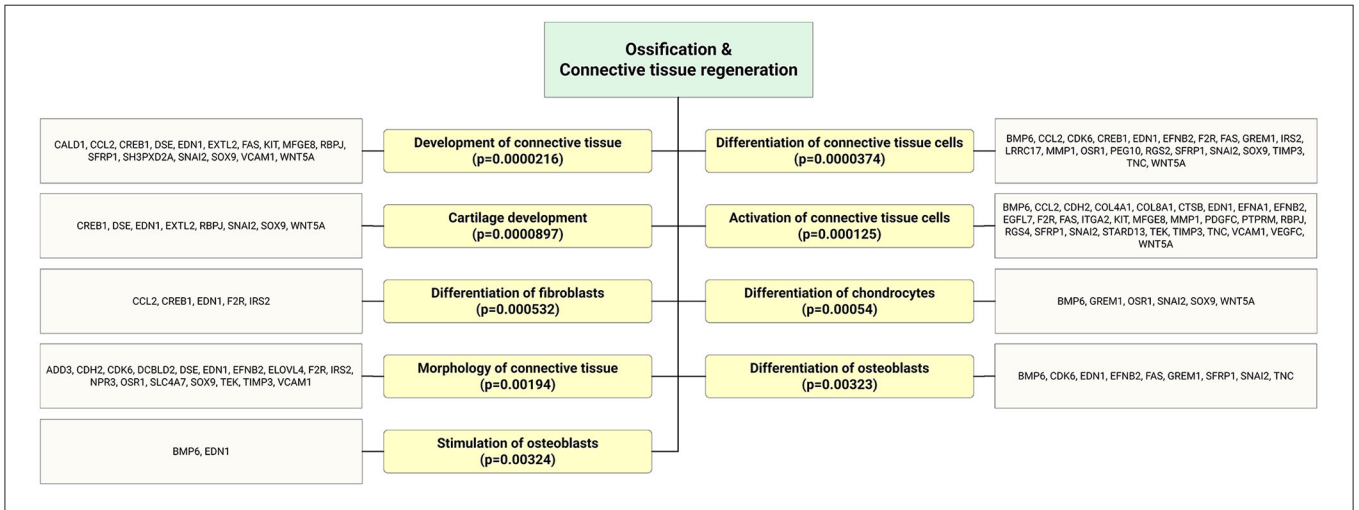

FIGURE 7 | Bioinformatics analysis showed that significantly enriched functional annotation related to bone and connective tissue regeneration. This miR sequence data was generated from PMID: 28631889. MicroRNA target genes were predicted using IPA with information from TargetScan, miRecords, and TarBase databases.

and osteoblast differentiation-enriched functional categories (**Figure 7**). Through *in silico* experiments, Qin et al. (55) showed that EPC-EVs regulate the osteoblastic differentiation of bone marrow-derived mesenchymal stromal cells by inhibiting the expression of osteogenic genes and increasing proliferation. This suggests that EPC-EVs are able to control osteogenesis and have beneficial effects on connective tissue development, such as fibroblasts and chondrocytes (**Figure 7**). A preclinical study showed that EPC-EVs have a strong therapeutic effect on distraction osteogenesis by stimulating angiogenesis and osteogenesis (56). The aforementioned therapeutic advantage of EPC-EVs in bone and connective tissue regeneration expands its application to cure various skeletal muscle diseases.

ANGIOGENIC PROPERTIES OF EPC-EVS

Recent studies have shed light on the biological activity and function of EPC-Ev-derived miRs in various *in vitro* and *in vivo* models. Dellet et al. (35) demonstrated the high expression levels of 15 miRs identified in ECFC and ECFC-derived EVs such as miR-10a/b, miR-21-5p, miR-30a-5p, miR-126-5p, let-7 families, and miR151a-3p (**Figure 3** and **Table 1**). We further investigated

TABLE 1 | EPC-derived angio-miR.

miRs	Mechanism of action	Target diseases	EVs or Exo origin	Ref #
miR-126-3p	*VEGF-A*, *IL-3*, *IL-10*, *IGF-1*, *ANG1*, *ANG2*, and *SPRED1*	Enhanced biological function of EPC from patients with ICM. Knocking down miR-126-3p from EPC abolished their angiogenic activity	EPC-derived EVs	(23, 57)
miR-126-5p	*DLK1*	Prevents atherosclerotic lesion formation via DLK1 suppression	EC	(35, 58)
miR-10b	*VEGF* and *HOX*	Promotes tumor growth via enhanced angiogenesis	Circulating EPC, EC	(35, 59, 60)
let-7b let-7f-2-5p let-7f-1-5p let-7i-5p	Proangiogenic paracrine factors and *IL-10* and *IL-12*	ECFC-derived EVs vastly contain various let-7 miR and modulate ischemia-induced angiogenesis. Tumor-associated macrophages phenotypes were changed upon downregulation	ECFC	(35, 61–64)
miR-486-5p	*PTEN* and Akt pathway	Delivery of ECFC exosomes reduces ischemic kidney injury via transfer of miR-486-5p targeting *PTEN*	ECFC	(15, 35)
miR-296-5p	*HGS, VEGFR2*, *PDGF-b*, and inhibiting *DLL4* and *Notch1*	Augmented primary human brain microvascular endothelial cells angiogenic property	Angiogenic EC	(65)
miR-150	*c-Myb*	MiR-150 significantly promoted the migration and tube formation ability of EPCs *in vitro* and enhanced EPCs' homing, organization, and resolution ability *in vivo*	EPC	(66)

EPC, endothelial progenitor cells; Exo, exosomes; EC, endothelial cells; ECFC, endothelial colony-forming cells; ICM, ischemic cardiomyopathy.

the angiogenic/vasculogenic properties of EPC-EV-derived miRs *in silico*. As shown in **Figure 4**, the EPC-EVs-derived miR targets are expressed on angiogenesis- and vasculogenesis-related genes. The majority of the neovasculogenesis phenomenon is coupled with cardiovascular system development and function (**Figure 4**). Plummder et al. (59) reported that EPC-derived miR-10b and miR-196b overexpression activates VEGF, and the latter enhances breast tumor vasculature. Interestingly, downregulation of miR-10b and miR-196b significantly inhibited tumor angiogenesis in mice, indicating a strong angiogenic potential. miR-126-5p and miR-126-3p overexpression promoted EPC migration and tube-like structure formation in ischemic cardiomyopathy patients *in vitro* (57). Moreover, transplantation of miR-126-3p-overexpressing EPCs into a rat model of MI showed left ventricular hemodynamic functions along with histological improvements (57). Mathiyalagan et al. (23) also demonstrated that silencing miR-126-3p from CD34 cell-derived exosomes abolished their angiogenic activity and beneficial function both *in vitro* and *in vivo*. Furthermore, injection of CD34 cell-derived exosomes increased miR-126-3p levels in mouse ischemic limbs but did not affect the endogenous synthesis of miR-126-3p, indicating a direct transfer of functional miR-126-3p to the ischemic tissue (23).

DELIVERY ROUTES OF EPC-EVS

Systemic Infusion vs. Local Injection

Previous cell therapy trials have reported that the efficacy of cell therapy is limited by poor engraftment of cells or that engrafted cells disappear several months after transplantation, suggesting a paracrine-based effect on the tissues. Depending on the disease state and location, EV transplantation routes may differ. Classical intravenous transplantation of EPC-EVs has been widely used in preclinical and clinical studies (12, 67) (**Table 2**). Several beneficial functions of systemic transplantation are listed, including (i) no requirement for special sophisticated delivery techniques, (ii) the immunomodulatory effect of EPC-EVs, and (iii) option for repetitive transplantation that is advantageous for local delivery. Sometimes, the desired results cannot be obtained after one injection of EVs; consequently, repetitive systemic transplantation via the vein is needed, whereas in several diseases, local transplantation is not allowed for this technique. Recently, Yi et al. (27) reviewed 29 publications on the route of administration in preclinical studies and showed that the intravenous route was selected in ∼80% of exosome injections, and the remaining exosome delivery routes were intraperitoneal, oral, or local. For instance, an ongoing phase one clinical trial (NCT04327635) on safety evaluation of intracoronary infusion of EV in patients with acute myocardial infarction performs within 20 min after stent placement or post-dilation (whichever is last) (**Table 2**). This kind of delivery methodology is widely used in previous/also current cell transplantation trials into stent placement or post-dilation vessels to enhance the treatment of damaged organs. Another completed clinical trial (NCT04134676) primary outcome revealed that stem cell-conditioned media-derived EVs therapeutic potential is promising in terms of chronic ulcer size reduction, edema decrease, and presence of granulation signs (**Table 2**). These

TABLE 2 | Clinical trials on therapeutic applications of extracellular vehicles (EVs).

Study Title	Status	Location	EVs or Exo origin	ClinicalTrials.gov identifier
Antiplatelet therapy effect on extracellular vesicles in acute myocardial infarction (AFFECT EV), Phase 4	Completed	Warsaw, Poland and Amsterdam, Netherland	Extracellular vesicles from endothelial cells, leukocytes, and platelets	NCT02931045
Safety evaluation of intracoronary infusion of extracellular vesicles in patients with AMI, Phase 1	Not yet recruiting	Commercial study of drug called PEP	Unknown	NCT04327635
Safety and efficacy of allogenic mesenchymal stem cells derived exosome on disability of patients with acute ischemic stroke: a randomized, single-blind, placebo-controlled, Phase 1, 2 Trial	Active/recruiting	Tehran, Iran	Allogenic mesenchymal stem cells-derived exosome enriched by miR-124	NCT03384433
Effect of plasma derived exosomes on cutaneous wound healing	Active/recruiting	Kumamoto, Japan	Autologous plasma-derived exosomes	NCT02565264
Therapeutic potential of stem cell conditioned medium on chronic ulcer wounds: pilot study in human, Phase 1	Completed	Banten, Indonesia	Stem cell conditioned media-derived EVs	NCT04134676
Effect of saxagliptin and dapagliflozin on endothelial progenitor cell in patients with type 2 diabetes mellitus	Recruiting	District of Columbia, United States	Exosomes released from kidney podocyte	NCT03660683
Autologous serum-derived EV for venous trophic lesions not responsive to conventional treatments (SER-VES-HEAL)	Recruiting	Turin, Italy	Autologous extracellular vesicles from serum	NCT04652531

macroscopic findings were reported 2 weeks after local delivery of EVs via gel.

In most cases, intravenously transplanted EVs accumulate in the liver, lung, spleen, and kidney (27). For target organ delivery, it has been shown that the local tissue inflammatory environment and activation of receptors and ligands (adhesion molecules) play essential roles in EV uptake. This information is valuable for *in vivo* biodistribution of exosomes and the control of dose and potential side effects.

LOCAL SUSTAINED DELIVERY SYSTEM

To achieve better results, a targeted delivery system with sustained release to damaged organs may be required. Chen et al. (33) demonstrated that the injection of EPC-EVs incorporated with shear-thinning gel into the border zone of myocardial infarction improved the hemodynamic function of the heart. The average steady EPC-EV release from the gel continued for over 21 days. This EV delivery strategy may enhance EV retention by damaged tissue owing to the sustained release and has potential for active use in trophic ulcer treatment.

MECHANISM OF UPTAKE AND ACTION OF EPC-EVS

The mechanism of EV internalization into recipient or acceptor cells is crucial in terms of intercellular communication. Several EV internalization mechanisms have been presented previously in the scientific literature, such as direct uptake followed by fusion, phagocytosis, and macropinocytosis by the recipient cell membrane (25). Indirect EV uptake mechanisms are sophisticated and work through other pathways, such as the clathrin-dependent and clathrin-independent pathways and lipid raft-mediated, caveolin-mediated, and cell surface protein-mediated endocytosis (24, 25, 68). In addition, recent reports revealed that tissue microenvironment pH is a crucial factor for EV uptake and secretion (69); for instance, in a rodent myocardial ischemia injury model, MSC-EVs internalization into ischemic cardiomyocytes was enhanced compared to that in the non-ischemic counterparts, indicating a low pH condition as the likely mechanism (69, 70). Another factor that is common for the preferential accumulation of EPCs and hematopoietic cells in ischemic tissue is the SDF-1/CXCR4 system (71–73). Recently, Viñas et al. (14) showed that CXCR4/SDF-1α interaction plays an essential role in EPC-derived exosome uptake in a mouse acute kidney ischemia-reperfusion injury model. Interestingly, EPC-EVs selectively targeted the ischemic kidney tissues. Hence, transplanted EPC-EVs were detected 30 min to 4 h after reperfusion only within the proximal tubules, glomeruli, and endothelial cells. However, this preferential internalization into the ischemic kidney was interrupted when exosomes were pre-incubated with the CXCR4 inhibitor plerixafor, suggesting CXCR4/SDF-1 α-dependent EPC-EV uptake in ischemic tissues. Taken together, EPC-EVs internalize to the target cells of the CXCR4/SDF-1α system under ischemic conditions, similar to EPCs, although other EPC-EV internalization mechanisms are essential for non-ischemic diseases.

LONG-TERM PRESERVATION AND STORAGE OF EVS

One of the major challenges for the prolonged clinical applicability of EVs is the establishment of proper and

reproducible preservation and storage conditions without compromising their therapeutic potential. Several studies have shown that different methods of storage, chemical compounds, and temperature range optimization are crucial before translation to the clinic (74–76). Recently, Wu et al. (77) evaluated the effect of storage temperature by storing EVs at 4 °C, −20 °C, and −80 °C for up to 28 days and comparing them to fresh EVs. In comparison to fresh EVs, 1 month of storage at 4 °C and −20 °C changed the size distribution, decreased the quantity and content, and affected cellular uptake and biodistribution of EVs; however, storage at −80 °C did not show such effects. The authors concluded that storage at 4 °C or −20 °C is suitable for short-term preservation, whereas −80 °C would be preferable for long-term preservation of EVs for therapeutic applications (77). Jin et al. (78) reported that EVs are stable under the conditions of 4 °C (for 24, 72, and 168 h), at room temperature (for 6, 12, 24, and 48 h), and repeated freeze-thaw (from one to five times).

Moreover, the assessment of DNA content and functionality in EVs was stable in a changing environment over repeated freeze-thaw cycles (78). Freeze-drying or lyophilization seems to be the most reliable method for preserving EVs (76). The common stabilizers used in lyophilization are disaccharides such as glucose, lactose, sucrose, and trehalose. A comparative study of EV storage at 4 °C or −80 °C and freeze-drying showed that lyophilization preserves size and enzyme activity which are indicators of EV stability (79). In summary, for long-term EV storage, preferable conditions are deep freezing, such as at −80 °C or below, whereas 4 °C may be acceptable for short-term use. For advanced EV applications, it is preferable to store EV using lyophilization methods to optimize the biological function and therapeutic potential of EVs.

FUTURE PERSPECTIVES AND CONCLUSION

Intensive research on endothelial progenitor cells and translation to the clinic for various cardiovascular ischemia diseases has increased our understanding of their therapeutic mechanisms (e.g., paracrine mechanism-based action) and biological function (80–82). EPC-EVs may be considered as a primary candidate for use against certain ischemic diseases, owing to their strong angiogenic, anti-fibrosis, and immunomodulatory properties (12, 20, 21, 23, 33, 57, 59, 80, 82–86) and safety in clinical settings (**Table 2**). However, there are hurdles to overcome before EPC-EVs can be applied as therapies such as standardization of classification and nomenclature of EPCs and focusing on the question of which EPCs should be used (9, 87). In addition, depending on the origin, such as tissue-derived or circulating EPCs, EPC-EVs cargo may contain/comprise various genetic materials that could influence the clinical outcome and should be carefully considered before therapy. Another aspect that needs to be addressed is EPC culturing conditions, including the effect of culture media, ischemia preconditioning, and composition of EVs, all of which must be investigated precisely using large animal disease models. The development of optimized and scalable isolation of pure, clinical-grade EPC-EVs for off-the-shelf therapy use will increase their significance. To date, most EV-based studies have used intravenous bolus injection methods, although the choice of the EV delivery route depends on the location of the disease.

Nevertheless, completed and ongoing clinical trials (**Table 2**), as well as numerous preclinical studies (38, 42, 44, 45, 86, 88), indicate that EPC-EV therapy is feasible and that EVs are safe and well-tolerated.

AUTHOR CONTRIBUTIONS

AS and AK contributed to the literature research and data collection, and were involved in the draft of the manuscript. AK contributed to figure generation and bioinformatic analyses. AS, SK, and TA contributed to the coordination and design of the review and writing of the final draft of the manuscript. All authors have read and approved the final manuscript.

FUNDING

This research was supported by JSPS KAKENHI funding (grant no. 20K17163 to AS).

REFERENCES

1. Asahara T, Murohara T, Sullivan A, Silver M, van der Zee R, Li T, et al. Isolation of putative progenitor endothelial cells for angiogenesis. *Science*. (1997) 275:964–6. doi: 10.1126/science.275.5302.964
2. Tateishi-Yuyama E, Matsubara H, Murohara T, Ikeda U, Shintani S, Masaki G. Therapeutic angiogenesis for patients with limb ischaemia by autologous transplantation of bone-marrow cells: a pilot study and a randomised controlled trial. *Lancet*. (2002) 360:427–35. doi: 10.1016/S0140-6736(02)09670-8
3. Lin Y, Weisdorf JD, Solovey A, Hebbel PR. Origins of circulating endothelial cells and endothelial outgrowth from blood. *J Clin Invest*. (2000) 105:71–7. doi: 10.1172/JCI8071
4. Ingram DA, Mead LE, Tanaka H, Meade V, Fenoglio A, Mortell K, et al. Identification of a novel hierarchy of endothelial progenitor cells using human peripheral and umbilical cord blood. *Blood*. (2004) 104:2752–60. doi: 10.1182/blood-2004-04-1396
5. Asahara T, Masuda H, Takahashi T, Kalka C, Pastore C, Silver M, et al. Bone marrow origin of endothelial progenitor cells responsible for postnatal vasculogenesis in physiological and pathological neovascularization. *Circ Res*. (1999) 85:221–8. doi: 10.1161/01.RES.85.3.221
6. Bailey AS, Jiang S, Afentoulis M, Baumann CI, Schroeder AD, Olson SB, et al. Transplanted adult hematopoietic stems cells differentiate into functional endothelial cells. *Blood*. (2004) 103:13–9. doi: 10.1182/blood-2003-05-1684
7. Peters BA, Diaz LA, Polyak K, Meszler L, Romans K, Guinan EC, et al. Contribution of bone marrow-derived endothelial cells to human tumor vasculature. *Nat Med*. (2005) 11:261–2. doi: 10.1038/nm1200
8. Göthert JR, Gustin SE, van Eekelen JM, Schmidt U, Hall MA, Jane SM, et al. Genetically tagging endothelial cells *in vivo*: bone marrow-derived cells do not contribute to tumor endothelium. *Blood*. (2004) 104: 1769–77. doi: 10.1182/blood-2003-11-3952

9. Medina RJ, Barber CL, Sabatier F, Dignat-George F, Melero-Martin JM, Khosrotehrani K, et al. Endothelial progenitors: a consensus statement on nomenclature. *Stem Cells Transl Med*. (2017) 6:1316–20. doi: 10.1002/sctm.16-0360
10. Hur J, Yoon C, Kim H, Choi J, Kang H, Hwang K, et al. Characterization of two types of endothelial progenitor cells and their different contributions to neovasculogenesis. *Arterioscler Thromb Vasc Biol*. (2004) 24: 288–93. doi: 10.1161/01.ATV.0000114236.77009.06
11. O'Neill CL, Guduric-Fuchs J, Chambers SE, O'Doherty M, Bottazzi B, Stitt AW, et al. Endothelial cell-derived pentraxin 3 limits the vasoreparative therapeutic potential of circulating angiogenic cells. *Cardiovasc Res*. (2016) 112:677–88. doi: 10.1093/cvr/cvw209
12. Ranghino A, Cantaluppi V, Grange C, Vitillo L, Fop F, Biancone L, Deregibus MC, et al. Endothelial progenitor cell-derived microvesicles improve neovascularization in a murine model of hindlimb ischemia. *Int J Immunopathol Pharmacol*. (2012) 25:75–85. doi: 10.1177/039463201202500110
13. Cantaluppi V, Gatti S, Medica D, Figliolini F, Bruno S, Deregibus MC, et al. Microvesicles derived from endothelial progenitor cells protect the kidney from ischemia-reperfusion injury by microRNA-dependent reprogramming of resident renal cells. *Kidney Int*. (2012) 82: 412–27. doi: 10.1038/ki.2012.105
14. Viñas JL, Spence M, Gutsol A, Knoll W, Burger D, Zimpelmann J, et al. Receptor-ligand interaction mediates targeting of endothelial colony forming cell-derived exosomes to the kidney after ischemic injury. *Sci Rep*. (2018) 8:1–12. doi: 10.1038/s41598-018-34557-7
15. Viñas JL, Burger D, Zimpelmann J, Haneef R, Knoll W, Campbell P, et al. Transfer of microRNA-486-5p from human endothelial colony forming cell-derived exosomes reduces ischemic kidney injury. *Kidney Int*. (2016) 90:1238–50. doi: 10.1016/j.kint.2016.07.015
16. Théry C, Witwer KW, Aikawa E, Alcaraz MJ, Anderson JD, Andriantsitohaina R, et al. Minimal information for studies of extracellular vesicles 2018 (MISEV2018): a position statement of the International Society for Extracellular Vesicles and update of the MISEV2014 guidelines. *J Extracell Vesicles*. (2018) 7:1535750. doi: 10.1080/20013078.2018.1535750
17. Niel Gv, D'Angelo G, Raposo G. Shedding light on the cell biology of extracellular vesicles. *Nat Rev Mol Cell Biol*. (2018) 19:213–28. doi: 10.1038/nrm.2017.125
18. Raposo G, Stoorvogel W. Extracellular vesicles: exosomes, microvesicles, and friends. *J Cell Biol*. (2013) 200:373–83. doi: 10.1083/jcb.201211138
19. Sahoo S, Adamiak M, Mathiyalagan P, Kenneweg F, Kafert-Kasting S, Thum T. Therapeutic and diagnostic translation of extracellular vesicles in cardiovascular diseases: roadmap to the clinic. *Circulation*. (2021) 143:1426–49. doi: 10.1161/CIRCULATIONAHA.120.049254
20. Deregibus MC, Cantaluppi V, Calogero R, Iacono ML, Tetta C, Biancone L, et al. Endothelial progenitor cell derived microvesicles activate an angiogenic program in endothelial cells by a horizontal transfer of mRNA. *Blood*. (2007) 110:2440–8. doi: 10.1182/blood-2007-03-078709
21. Sahoo S, Klychko E, Thorne T, Misener S, Schultz KM, Millay M, et al. Exosomes from human CD34(+) stem cells mediate their proangiogenic paracrine activity. *Circ Res*. (2011) 109:724–8. doi: 10.1161/CIRCRESAHA.111.253286
22. Bitzer M, Ben-Dov IZ, Thum T. Microparticles and microRNAs of endothelial progenitor cells ameliorate acute kidney injury. *Kidney Int*. (2012) 82:375–7. doi: 10.1038/ki.2012.152
23. Mathiyalagan P, Liang Y, Kim D, Misener S, Thorne T, Kamide CE, et al. Angiogenic mechanisms of human CD34(+) stem cell exosomes in the repair of ischemic hindlimb. *Circ Res*. (2017) 120:1466–76. doi: 10.1161/CIRCRESAHA.116.310557
24. Mathieu M, Martin-Jaular L, Lavieu G, Théry C. Specificities of secretion and uptake of exosomes and other extracellular vesicles for cell-to-cell communication. *Nat Cell Biol*. (2019) 21:9–17. doi: 10.1038/s41556-018-0250-9
25. Mulcahy LA, Pink RC, Carter DR. Routes and mechanisms of extracellular vesicle uptake. *J Extracell Vesicles*. (2014) 3. doi: 10.3402/jev.v3.24641
26. Toribio V, Morales S, López-Martín S, Cardeñes B, Cabañas C, Yáñez-Mó M. Development of a quantitative method to measure EV uptake. *Sci Rep*. (2019) 9:10522. doi: 10.1038/s41598-019-47023-9
27. Yi YW, Lee JH, Kim S, Pack C, Ha DH, Park SR, et al. Advances in Analysis of Biodistribution of Exosomes by Molecular Imaging. *Int J Mol Sci*. (2020) 21:665. doi: 10.3390/ijms21020665
28. Sanganalmath SK, Bolli R. Cell therapy for heart failure: a comprehensive overview of experimental and clinical studies, current challenges, and future directions. *Circ Res*. (2013) 113:810–34. doi: 10.1161/CIRCRESAHA.113.300219
29. Afzal MR, Samanta A, Shah ZI, Jeevanantham V, Abdel-Latif A, Zuba-Surma EK, et al. Adult bone marrow cell therapy for ischemic heart disease: evidence and insights from randomized controlled trials. *Circ Res*. (2015) 117:558–75. doi: 10.1161/CIRCRESAHA.114.304792
30. Medina RJ, O'Neill CL, Sweeney M, Guduric-Fuchs J, Gardiner TA, Simpson DA, et al. Molecular analysis of endothelial progenitor cell (EPC) subtypes reveals two distinct cell populations with different identities. *BMC Med Genomics*. (2010) 3:18. doi: 10.1186/1755-8794-3-18
31. Liu W, Zhang H, Mai J, Chen Z, Huang T, Wang S, et al. Distinct anti-fibrotic effects of exosomes derived from endothelial colony-forming cells cultured under normoxia and hypoxia. *Med Sci Monit*. (2018) 24:6187–99. doi: 10.12659/MSM.911306
32. Minami Y, Nakajima T, Ikutomi M, Morita T, Komuro I, Sata M, et al. Angiogenic potential of early and late outgrowth endothelial progenitor cells is dependent on the time of emergence. *Int J Cardiol*. (2015) 186:305–14. doi: 10.1016/j.ijcard.2015.03.166
33. Chen CW, Wang LL, Zaman S, Gordon J, Arisi MF, Venkataraman CM, et al. Sustained release of endothelial progenitor cell-derived extracellular vesicles from shear-thinning hydrogels improves angiogenesis and promotes function after myocardial infarction. *Cardiovasc Res*. (2018) 114:1029–40. doi: 10.1093/cvr/cvy067
34. Ong S, Wu JC. Exosomes as potential alternatives to stem cell therapy in mediating cardiac regeneration. *Circ Res*. (2015) 117:7–9. doi: 10.1161/CIRCRESAHA.115.306593
35. Dellett M, Brown ED, Guduric-Fuchs J, O'Connor A, Stitt AW, Medina RJ, et al. MicroRNA-containing extracellular vesicles released from endothelial colony-forming cells modulate angiogenesis during ischaemic retinopathy. *J Cell Mol Med*. (2017) 21:3405–19. doi: 10.1111/jcmm.13251
36. Editorial TL. Life, death, and disability in 2016. *Lancet*. (2017) 390:1083. doi: 10.1016/S0140-6736(17)32465-0
37. Liu H, Gong Y, Yu C, Sun Y, Li X, Zhao D, et al. Endothelial progenitor cells in cardiovascular diseases: from biomarker to therapeutic agent. *Regenerat Med Res*. (2013) 1:1–5. doi: 10.1186/2050-490X-1-9
38. Yue Y, Wang C, Benedict C, Huang G, Truongcao M, Roy R, et al. Interleukin-10 deficiency alters endothelial progenitor cell-derived exosome reparative effect on myocardial repair via integrin-linked kinase enrichment. *Circ Res*. (2020) 126:315–29. doi: 10.1161/CIRCRESAHA.119.315829
39. Mackie AR, Klyachko E, Thorne T, Schultz KM, Millay M, Ito A, et al. Sonic hedgehog-modified human CD34+ cells preserve cardiac function after acute myocardial infarction. *Circ Res*. (2012) 122:312–21. doi: 10.1161/CIRCRESAHA.112.266015
40. Salybekov AA, Salybekova AK, Pola R, Asahara T. sonic hedgehog signaling pathway in endothelial progenitor cell biology for vascular medicine. *Int J Mol Sci*. (2018) 19:3040. doi: 10.3390/ijms19103040
41. Ke X, Yang R, Wu F, Wang X, Liang J, Hu X, et al. Exosomal miR-218-5p/miR-363-3p from endothelial progenitor cells ameliorate myocardial infarction by targeting the p53/JMY signaling pathway. *Oxid Med Cell Longevity*. (2021) 2021:5529430. doi: 10.1155/2021/5529430
42. Ke X, Yang D, Liang J, Wang X, Wu S, Wang X, et al. Human endothelial progenitor cell-derived exosomes increase proliferation and angiogenesis in cardiac fibroblasts by promoting the mesenchymal-endothelial transition and reducing high mobility group box 1 protein B1 expression. *DNA Cell Biol*. (2017) 36:1018–28. doi: 10.1089/dna.2017.3836
43. Dushianthan A, Grocott MPW, Postle AD, Cusack R. *Acute Respiratory Distress Syndrome and Acute Lung Injury*. BMJ Publishing Group Limited (2011). doi: 10.1136/pgmj.2011.118398
44. Zhou Y, Li P, Goodwin AJ, Cook JA, Halushka PV, Chang E, et al. Exosomes from endothelial progenitor cells improve outcomes of the lipopolysaccharide-induced acute lung injury. *Crit Care*. (2019) 23:1–12. doi: 10.1186/s13054-019-2339-3

45. Wu X, Liu Z, Hu L, Gu W, Zhu L. Exosomes derived from endothelial progenitor cells ameliorate acute lung injury by transferring miR-126. *Exp Cell Res.* (2018) 370:13–23. doi: 10.1016/j.yexcr.2018.06.003
46. Fan H, Goodwin AJ, Chang E, Zingarelli B, Borg K, Guan S, et al. Endothelial progenitor cells and a stromal cell–derived factor-1α analogue synergistically improve survival in sepsis. *Am J Respir Crit Care Med.* (2014) 189:1509–19. doi: 10.1164/rccm.201312-2163OC
47. Sun R, Huang J, Sun B. Mobilization of endothelial progenitor cells in sepsis. *Inflamm Res.* (2019) 69:1–9. doi: 10.1007/s00011-019-01299-9
48. Cao J, He X, Xu H, Zou Z, Shi X. Autologous transplantation of peripheral blood-derived circulating endothelial progenitor cells attenuates endotoxin-induced acute lung injury in rabbits by direct endothelial repair and indirect immunomodulation. *Anesthesiology*. (2012) 116:1278–87. doi: 10.1097/ALN.0b013e3182567f84
49. Zhou Y, Li P, Goodwin AJ, Cook JA, Halushka PV, Chang E, et al. Exosomes from endothelial progenitor cells improve the outcome of a murine model of sepsis. *Mol Ther.* (2018) 26:1375–84. doi: 10.1016/j.ymthe.2018.02.020
50. Cantaluppi V, Medica D, Mannari C, Stiaccini G, Figliolini F, Dellepiane S, et al. Endothelial progenitor cell-derived extracellular vesicles protect from complement-mediated mesangial injury in experimental anti-Thy1.1 glomerulonephritis. *Nephrol Dialysis Transplant.* (2015) 30:410–22. doi: 10.1093/ndt/gfu364
51. Sun X, Meng H, Wan W, Xie M, Wen C. Application potential of stem/progenitor cell-derived extracellular vesicles in renal diseases. *Stem Cell Res Ther.* (2019) 10. doi: 10.1186/s13287-018-1097-5
52. Bates BD, Godbout C, Ramnaraign DJ, Schemitsch EH, Nauth A. Delayed endothelial progenitor cell therapy promotes bone defect repair in a clinically relevant rat model. *Stem Cells Int.* (2017) 2017:7923826. doi: 10.1155/2017/7923826
53. Cui Y, Fu S, Sun D, Xing J, Hou T, Wu X. EPC-derived exosomes promote osteoclastogenesis through LncRNA-MALAT1. *J Cell Mol Med.* (2019) 23:3843–54. doi: 10.1111/jcmm.14228
54. Pang H, Wu X, Fu S, Luo F, Zhang Z, Hou T, et al. Co-culture with endothelial progenitor cells promotes survival, migration, and differentiation of osteoclast precursors. *Biochem Biophys Res Commun.* (2013) 430:729–34. doi: 10.1016/j.bbrc.2012.11.081
55. Qin Y, Zhang C. Endothelial progenitor cell-derived extracellular vesicle-meditated cell-to-cell communication regulates the proliferation and osteoblastic differentiation of bone mesenchymal stromal cells. *Mol Med Rep.* (2017) 16:7018–24. doi: 10.3892/mmr.2017.7403
56. Jia Y, Zhu Y, Qiu S, Xu J, Chai Y. Exosomes secreted by endothelial progenitor cells accelerate bone regeneration during distraction osteogenesis by stimulating angiogenesis. *Stem Cell Res Ther.* (2019) 10:1–13: doi: 10.1186/s13287-018-1115-7
57. Li H, Liu Q, Wang N, Xu Y, Kang L, Ren Y, et al. Transplantation of endothelial progenitor cells overexpressing miR-126-3p improves heart function in ischemic cardiomyopathy. *Circ J.* (2018) 82:2332–41. doi: 10.1253/circj.CJ-17-1251
58. Schober A, Nazari-Jahantigh M, Wei Y, Bidzhekov K, Gremse F, Grommes J, et al. MicroRNA-126-5p promotes endothelial proliferation and limits atherosclerosis by suppressing Dlk1. *Nat Med.* (2014) 20:368–76. doi: 10.1038/nm.3487
59. Plummer PN, Freeman R, Taft RJ, Vider J, Sax M, Umer BA, et al. MicroRNAs regulate tumor angiogenesis modulated by endothelial progenitor cells. *Cancer Res.* (2013) 73:341–52. doi: 10.1158/0008-5472.CAN-12-0271
60. Hassel D, Cheng P, White MP, Ivey KN, Kroll J, Augustin HG, et al. MicroRNA-10 regulates the angiogenic behavior of zebrafish and human endothelial cells by promoting vascular endothelial growth factor signaling. *Circ Res.* (2012) 111:1421–33. doi: 10.1161/CIRCRESAHA.112.279711
61. Roush S, Slack FJ. The let-7 family of microRNAs. *Trends Cell Biol.* (2008) 18:505–16. doi: 10.1016/j.tcb.2008.07.007
62. Zhao T, Li J, Chen AF. MicroRNA-34a induces endothelial progenitor cell senescence and impedes its angiogenesis via suppressing silent information regulator 1. *Am J Physiol Endocrinol Metab.* (2010) 299:E110–6. doi: 10.1152/ajpendo.00192.2010
63. Landskroner-Eiger S, Moneke I, Sessa WC. miRNAs as modulators of angiogenesis. *Cold Spring Harbor Perspect Med.* (2013) 3:a006643. doi: 10.1101/cshperspect.a006643
64. Wang Z, Xu L, Hu Y, Huang Y, Zhang Y, Zheng X, et al. miRNA let-7b modulates macrophage polarization and enhances tumor-associated macrophages to promote angiogenesis and mobility in prostate cancer. *Sci Rep.* (2016) 6:25602. doi: 10.1038/srep25602
65. Würdinger T, Tannous BA, Saydam O, Skog J, Grau S, Soutschek J, et al. miR-296 regulates growth factor receptor overexpression in angiogenic endothelial cells. *Cancer Cell.* (2008) 14:382–93. doi: 10.1016/j.ccr.2008.10.005
66. Wang W, Li C, Li W, Kong L, Qian A, Hu N, et al. MiR-150 enhances the motility of EPCs *in vitro* and promotes EPCs homing and thrombus resolving *in vivo*. *Thromb Res.* (2014) 133:590–8. doi: 10.1016/j.thromres.2013.12.038
67. Angulski ABB, Capriglione LGA, Barchiki F, Brofman P, Stimamiglio MA, Senegaglia AC, et al. Systemic infusion of expanded CD133 + cells and expanded CD133 + cell-derived EVs for the treatment of ischemic cardiomyopathy in a rat model of AMI. *Stem Cells Int.* (2019) 2019:4802578. doi: 10.1155/2019/4802578
68. Verdera HC, Gitz-Francois JJ, Schiffelers RM, Vader P. Cellular uptake of extracellular vesicles is mediated by clathrin-independent endocytosis and macropinocytosis. *J Controll Release.* (2017) 266:100–8. doi: 10.1016/j.jconrel.2017.09.019
69. Parolini I, Federici C, Raggi C, Lugini L, Palleschi S, De Milito A, et al. Microenvironmental pH is a key factor for exosome traffic in tumor cells. *J Biol Chem.* (2009) 284:34211–22. doi: 10.1074/jbc.M109.041152
70. Lai RC, Yeo RW, Tan KH, Lim SK. Mesenchymal stem cell exosome ameliorates reperfusion injury through proteomic complementation. *Regenerat Med.* (2013) 8:197–209. doi: 10.2217/rme.13.4
71. Ceradini DJ, Kulkarni AR, Callaghan MJ, Tepper OM, Bastidas N, Kleinman ME, et al. Progenitor cell trafficking is regulated by hypoxic gradients through HIF-1 induction of SDF-1. *Nat Med.* (2004) 10:858–64. doi: 10.1038/nm1075
72. van Solingen C, de Boer HC, Bijkerk R, Monge M, van Oeveren-Rietdijk AM, Seghers, et al. MicroRNA-126 modulates endothelial SDF-1 expression and mobilization of Sca-1(+)/Lin(-) progenitor cells in ischaemia. *Cardiovasc Res.* (2011) 92:449–55. doi: 10.1093/cvr/cvr227
73. Yamaguchi J, Kusano KF, Masuo O, Kawamoto A, Silver M, Murasawa S, et al. Stromal cell-derived factor-1 effects on *ex vivo* expanded endothelial progenitor cell recruitment for ischemic neovascularization. *Circulation.* (2003) 107:1322–8. doi: 10.1161/01.CIR.0000055313.77510.22
74. Gandham S, Su X, Wood J, Nocera AL, Alli SC, Milane L, et al. Technologies and standardization in research on extracellular vesicles. *Trends Biotechnol.* (2020) 38:1066–98. doi: 10.1016/j.tibtech.2020.05.012
75. Reiner AT, Witwer KW, van Balkom BWM, de Beer J, Brodie C, Corteling RL, et al. Concise review: developing best-practice models for the therapeutic use of extracellular vesicles. *Stem Cells Transl Med.* (2017) 6:1730–9. doi: 10.1002/sctm.17-0055
76. Kusuma GD, Barabadi M, Tan JL, Morton DAV, Frith JE, Lim R. To Protect and to preserve: novel preservation strategies for extracellular vesicles. *Front Pharmacol.* (2018) 9:1199. doi: 10.3389/fphar.2018.01199
77. Wu J, Li Y, Hu X, Huang S, Xiang D. Preservation of small extracellular vesicles for functional analysis and therapeutic applications: a comparative evaluation of storage conditions. *Drug Delivery.* (2021) 28:162–70. doi: 10.1080/10717544.2020.1869866
78. Jin Y, Chen K, Wang Z, Wang Y, Liu J, Lin L, et al. DNA in serum extracellular vesicles is stable under different storage conditions. *BMC Cancer.* (2016) 16:753. doi: 10.1186/s12885-016-2783-2
79. Frank J, Richter M, de Rossi C, Lehr C, Fuhrmann K, Fuhrmann G. Extracellular vesicles protect glucuronidase model enzymes during freeze-drying. *Sci Rep.* (2018) 8:1–8. doi: 10.1038/s41598-018-30786-y
80. Doyle B, Sorajja P, Hynes B, Kumar AHS, Araoz PA, Stalboerger PG, et al. Progenitor cell therapy in a porcine acute myocardial infarction model induces cardiac hypertrophy, mediated by paracrine secretion of cardiotrophic factors including TGFbeta1. *Stem Cells Dev.* (2008) 17:941–51. doi: 10.1089/scd.2007.0214
81. Di Santo S, Seiler S, Fuchs A, Staudigl J, Widmer HR. The secretome of endothelial progenitor cells promotes brain endothelial cell activity through PI3-kinase and MAP-kinase. *PLoS ONE.* (2014) 9:e95731. doi: 10.1371/journal.pone.0095731

82. Mirotsou M, Jayawardena TM, Schmeckpeper J, Gnecchi M, Dzau VJ. Paracrine mechanisms of stem cell reparative and regenerative actions in the heart. *J Mol Cell Cardiol.* (2011) 50:280–9. doi: 10.1016/j.yjmcc.2010.08.005
83. Bruyndonckx L, Hoymans VY, Frederix G, De Guchtenaere A, Franckx H, Vissers DK, et al. Endothelial progenitor cells and endothelial microparticles are independent predictors of endothelial function. *J Pediatr.* (2014) 165:300–5. doi: 10.1016/j.jpeds.2014.04.015
84. Gu S, Zhang W, Chen J, Ma R, Xiao X, Ma X, et al. EPC-derived microvesicles protect cardiomyocytes from Ang II-induced hypertrophy and apoptosis. *PLoS ONE.* (2014) 9:e85396. doi: 10.1371/journal.pone.0085396
85. Hu H, Wang B, Jiang C, Li R, Zhao J. Endothelial progenitor cell-derived exosomes facilitate vascular endothelial cell repair through shuttling miR-21-5p to modulate Thrombospondin-1 expression. *Clin Sci.* (2019) 133:1629–44. doi: 10.1042/CS20190188
86. Li X, Chen C, Wei L, Li Q, Niu X, Xu Y, et al. Exosomes derived from endothelial progenitor cells attenuate vascular repair and accelerate reendothelialization by enhancing endothelial function. *Cytotherapy.* (2016) 18:253–62. doi: 10.1016/j.jcyt.2015.11.009
87. Coumans FAW, Brisson AR, Buzas EI, Dignat-George F, Drees EEE, El-Andaloussi S, et al. Methodological guidelines to study extracellular vesicles. *Circ Res.* (2017) 120:1632–48. doi: 10.1161/CIRCRESAHA.117.309417
88. Zhang J, Chen C, Hu B, Niu X, Liu X, Zhang G, et al. Exosomes derived from human endothelial progenitor cells accelerate cutaneous wound healing by promoting angiogenesis through Erk1/2 signaling. *Int J Biol Sci.* (2016) 12:1472–87. doi: 10.7150/ijbs.15514

Conflict of Interest: The authors declare that the research was conducted in the absence of any commercial or financial relationships that could be construed as a potential conflict of interest.

Publisher's Note: All claims expressed in this article are solely those of the authors and do not necessarily represent those of their affiliated organizations, or those of the publisher, the editors and the reviewers. Any product that may be evaluated in this article, or claim that may be made by its manufacturer, is not guaranteed or endorsed by the publisher.

frontiers in Cardiovascular Medicine

ORIGINAL RESEARCH
published: 11 October 2021
doi: 10.3389/fcvm.2021.739107

Sustained Release of MiR-217 Inhibitor by Nanoparticles Facilitates MSC-Mediated Attenuation of Neointimal Hyperplasia After Vascular Injury

Hong Yu[1†], Yutao Hua[2†], Yecheng He[3†], Yin Wang[4], Xingjian Hu[4], Si Chen[4], Junwei Liu[4], Junjie Yang[5] and Huadong Li[4*]*

[1] Department of Otorhinolaryngology, Tongji Medical College, Union Hospital, Huazhong University of Science and Technology, Wuhan, China, [2] Department of Medicine, University of Alabama at Birmingham, Birmingham, AL, United States, [3] Department of Clinical Medicine, Suzhou Vocational Health College, Suzhou, China, [4] Department of Cardiovascular Surgery, Tongji Medical College, Union Hospital, Huazhong University of Science and Technology, Wuhan, China, [5] Department of Anesthesiology, University of Maryland School of Medicine, Baltimore, MD, United States

OPEN ACCESS

Edited by:
Zhen-Ao Zhao, Hebei North University, China

Reviewed by:
Lianbo Shao, The First Affiliated Hospital of Soochow University, China
Teng Ma, Tongji University, China

***Correspondence:**
Huadong Li
lihuadong@hust.edu.cn
Junjie Yang
junjie.yang@som.umaryland.edu

[†]These authors have contributed equally to this work and share first authorship

Specialty section:
This article was submitted to Cardiovascular Biologics and Regenerative Medicine, a section of the journal Frontiers in Cardiovascular Medicine

Received: *10 July 2021*
Accepted: *13 September 2021*
Published: *11 October 2021*

Citation:
Yu H, Hua Y, He Y, Wang Y, Hu X, Chen S, Liu J, Yang J and Li H (2021) Sustained Release of MiR-217 Inhibitor by Nanoparticles Facilitates MSC-Mediated Attenuation of Neointimal Hyperplasia After Vascular Injury. Front. Cardiovasc. Med. 8:739107. doi: 10.3389/fcvm.2021.739107

Mesenchymal stem cells (MSCs) have been proven capable of differentiating into endothelial cells (ECs) and increasing vascular density in mouse ischemia models. However, the therapeutic potential of MSCs in neointimal hyperplasia after vascular injury is still not fully understood. In this study, we proposed that sustained release of miR-217 inhibitor encapsulated by nanoparticles in MSCs can enhance the therapeutic effects of MSCs on alleviating neointimal hyperplasia in a standard mouse wire injury model. We intravenously administered MSCs to mice with injured arteries and examined neointimal proliferation, endothelial differentiation and senescence. We demonstrated that MSCs localized to the luminal surface of the injured artery within 24 h after injection and subsequently differentiated into endothelial cells, inhibited neointimal proliferation and migration of vascular smooth muscle cells. Transfection of MSCs with poly lactic-co-glycolic acid nanoparticles (PLGA-NP) encapsulating an miR-217 agomir abolished endothelial differentiation as well as the therapeutic effect of MSCs. On the contrary, silencing of endogenous miR-217 improved the therapeutic efficacy of MSCs. Our study provides a new strategy of augmenting the therapeutic potency of MSCs in treatment of vascular injury.

Keywords: mesenchymal stem cells, atherosclerosis, miR-217, PLGA nanoparticle, vascular injury

INTRODUCTION

Percutaneous transluminal angioplasty (PTA) and hypertension, are characterized by blood vessel wall thickening and stenosis due to endothelium injury, vascular smooth muscle cell (VSMC) proliferation, and extracellular matrix deposition in the blood vessels. Intimal hyperplasia (IH) manifested by thickening of the tunica intima of a blood vessel is closely related to vascular remodeling diseases. IH after vascular injury is the main cause of postoperative stenosis/occlusion after endovascular treatment and has long been the focus of vascular research. Whether a damage of the vascular surface reforms the endothelium depends on the extent and the duration of

the vascular damage (1, 2). Damage to the integrity of vascular endothelial cells (ECs) induces thrombosis and proliferation of VSMCs within the vessels. EC injury induces platelet adhesion, T-lymphocyte, monocyte and macrophage infiltration as well as release of extracellular matrix-degrading enzymes (3, 4). Platelets, ECs and VSMCs generate growth factors, such as platelet derived growth factor (PDGF), fibroblast growth factor (FGF) and epidermal growth factor (EGF), chemotactic substances and mitogens, and stimulate migration of VSMCs to the intima, where the VSMCs and fibroblasts secrete large amounts of extracellular matrix (ECM) at the vascular injury site (5–7). The secreted ECM is continuously deposited at the injury site, resulting in gradual thickening of the intima and eventually stenosis.

Many studies have been performed using different cell types as therapeutics to treat vascular injury-induced IH (8–12). Mesenchymal stem cells (MSCs) have been considered as an effective treatment option for vascular injury owing to their self-renewal and multilineage differentiation capabilities as well as paracrine property (13). Besides, MSCs have important advantages including their easy isolation (from different sources) and preservation without raising any ethical concerns as well as a limited risk of tumorigenesis (14, 15). MSCs can differentiate into ECs and SMCs *in vitro* in the presence of various growth factors (16, 17) and can enhance angiogenesis in a mouse hindlimb ischemia model (18, 19). However, the therapeutic effect of those cells is limited due to their low engraftment rate and their therapeutic potential in neointimal hyperplasia after vascular injury is still not fully understood.

MicroRNAs modulate gene expression on post-transcriptional level and are important regulators of angiogenesis and vascular repair. MiR-217 is one of the microRNAs that play a critical role in regulating angiogenesis. MiR-217 regulates endothelial cell aging through silent information regulator 1 (Sirt-1), which is highly expressed in pluripotent stem cells and plays a vital role in controlling the homeostasis of vascular endothelial cells and angiogenesis (20). However, the half-life of miRNAs is relatively short, and can be quickly degraded by nucleases *in vivo*, thereby limiting its blood stability (19). Promisingly, polylactic acid-glycolic acid (PLGA) is a polymer that has been approved by the U.S. Food and Drug Administration (FDA) for medical applications. A large number of experiments have proved that PLGA-based nanoparticles (NPs) can be used as a delivery system for many therapeutic agents, such as anti-inflammatory drugs, antioxidants, growth factors, antibiotics and therapeutic transgenes (21). In our study, we will use PLGA nanoparticles to encapsulate and control a sustained release of miR-217 inhibitor from MSCs in order to enhance the therapeutic potentials of MSCs in vascular injury of a mouse model.

MATERIALS AND METHODS

Animals

C57BL/6J (8–10 weeks old) mice were purchased from Shanghai Experimental Animal Center (Chinese Academy of Sciences, China). All procedures were performed in accordance with the institutional guidelines and were approved by the Ethics Committee of Wuhan Union Hospital.

Culturing of MSCs

MSCs were isolated from the bone marrow of C57BL/6J mice and cultured in standard medium with 500 mL a-MEM media (Invitrogen), 50 mL FBS, 5 mL Pen/Strep solution (100X), 5 mL L-glutamine (100X) at 37°C in a humidified 5% CO_2 atmosphere. The culture medium was replaced every 3 days to remove non-adherent cells. MSCs were analyzed for the expression of the cell surface markers by a flow cytometry assay.

Identification of Implanted MSCs

GFP-labeled MSCs were transplanted by the tail vein injection. The mice were anesthetized 24 h after cell transplantation and received an ice-cold PBS perfusion. The femoral arteries were immediately harvested and fixed with 4% paraformaldehyde for 10 min. The vessel was split open and put on a slide with the endothelial surface facing upwards and covered with a cover slip following addition of a drop of antifade mounting medium (Beyotime, China). The implanted cells were identified by laser scanning confocal microscope (Leica, Germany).

Differentiation of MSCs Into ECs

EC differentiation was performed as previously described (19). Briefly, MSCs were cultured in the EC medium containing ascorbic acid, heparin, 2% FBS and some growth factors including 50 ng/mL VEGF, 10 ng/mL bFGF, 20 ng/mL IGF and 5 ng/mL EGF (PeproTech, USA). The inducing medium was changed every 2 days. The differentiation process was closely monitored with cell morphology. Immunofluorescence and flow cytometry were performed to confirm the endothelial phenotype after 10 days of culture.

PLGA-Based NPs Preparation

PLGA-NPs were generated by an emulsification-solvent evaporation technique under constant magnetic stirring at room temperature using 1.2 mL of agomir aqueous solution (0.84 mg/mL) added to 3 mL of PLGA solution (2 mg/mL, the molar ratio of PLGA to agomir was 6:1) to achieve spontaneous formation of nanoparticles followed by incubation at room temperature for 30 min. The nanoparticles were collected by centrifugation at 13,000 rpm for 10 min, after which the supernatant was discarded, the nanoparticles were resuspended in distilled water, and the packaging efficiency of nanoparticle-agomir miRNA complexes was determined. In order to fully combine PLGA with agomir (nanoparticles/agomir), 3 uL of agomir (19.95 ug/ul) were first added to the sodium tripolyphosphate (TPP) solution (1.2 mL, 0.84 mg/mL) with or without 3 uL of Lipofectamine 2000 and then the mixture was added dropwise to the PLGA solution (3 mL, 2 mg/mL) under constant stirring at room temperature.

Transfection of MSCs With miRNA or Small Interfering RNA

After 3 days of culture MSCs were re-plated in six-well plates (Corning, USA) at a density of 2.5×10^5 cells/well in the

presence of 100 nM of microRNA or siRNA and incubated overnight. For gene knockdown or overexpression miR-217 agomir or miR-217 antagomir, Sirt-1 siRNA or 100 nM of control siRNA (conR) (Ribobio Co., China) were transfected into MSCs, respectively. All siRNAs and miRNAs were transfected into MSCs with Lipofectamine 2000 (Invitrogen, USA) according to the manufacturer's protocol, and the cells were harvested for further analysis 48 h post transfection.

miRNA Isolation and Quantitative RT-PCR

Total RNA was extracted using a Trizol reagent (Invitrogen, USA) according to the manufacturer's instructions. Reverse transcription was performed by using a SuperScript Reverse Transcriptase (Fermentas, Glen Burnie, MD) and a miR-217 stem loop primer (Sunny Biotechnology Co., China). Real-time PCR quantification of miR-217 was carried out by using SYBR Green PCR master mix (BIO-RAD, CA). All samples were analyzed by a Bio-Rad real-time analyzer (Bio-Rad Laboratories, Hercules, CA). The U6 small nucleolar RNA was used as a housekeeping/small RNA reference gene. The relative gene expression values were obtained after normalization to U6 small nucleolar RNA expression levels.

Surgical Procedures

C57BL/6 male mice (8–10 weeks old) were anesthetized by intraperitoneal injection of ketamine (1.5 mg/kg) and xylazine (0.3 mg/kg). The groin skin on the right side was depilated and sterilized with 75% alcohol. A groin incision was made under a surgical microscope (Yihua, China). The femoral artery was temporarily tightened with a line at the level of the inguinal ligament, and an arteriotomy was made distal to the epigastric branch. A 0.38-mm flexible angioplasty guidewire (COOK, USA) was then inserted under the help of a micro probe (F.S.T, Germany), the line removed, and the wire advanced to the level of the aortic bifurcation and pulled back with 3 passes. After removal of the wire, the arteriotomy site was sutured. After wounding, mice were divided randomly into 6 groups, and underwent intravenous tail injection with PBS containing 2×10^5 MSCs, MSCs transfected with control siRNA (MSC^{CoR}), miR-217 agomir ($MSC^{miR-217}$), miR-217 antagomir ($MSC^{miR-217I}$), Sirt1 siRNA ($MSC^{Sirt1-I}$), respectively. Injured arteries were harvested at 3 weeks with 9 mice in each group.

Western Blot Analysis

Western blot was performed as described previously (22). Antibodies to Sirt-1 (1:1,000, Proteintech, USA), β-actin (1:1,000, Cell Signaling, USA), HRP conjugated Donkey Anti-Rabbit IgG (1:2,000, Jackson ImmunoResearch, USA) were used for the corresponding protein detection. Protein band densities were assessed by using ImageJ 1.45S digital analysis software (National Institute of Health, USA).

Senescence-Associated β-Galactosidase Staining

The MSCs were cultured for 3 days in 500 mL a-MEM media (Invitrogen), 50 mL FBS, 5 mL Pen/Strep solution (100X), 5 mL L-glutamine (100X) at 37°C in a humidified 5% CO_2 atmosphere. Senescence-associated β-galactosidase (SA-β-Gal) staining was performed by using an SA-β-Gal staining kit (BioVision, Milpitas, CA), as described previously (23). Each experiment was repeated 3 times.

Embryoid Body Generation and Culture

The cells (5×10^4 cells/well) were dispensed in embryoid body (EB) medium onto ultra-low attachment 6-well plates (JET BIOFIL, China) and cultured for 72 h. The EB medium included 100 mL DMEM with 2 mM L-glutamine and without ribonucleosides and ribonucleotides (GIBCO, cat. no. 12800-116), 100 mg/mL penicillin and streptomycin, 3.7 g/L NaHCO3 and 15% of FBS.

Immunofluorescence

Fixation of tissues was performed with 4% paraformaldehyde in PBS for 20 min and the vessels were processed for OCT (Tissue-Tek, USA) embedding. Five μm-frozen sections were cut with a cryostat, blocked with donkey serum (BD Pharmingen, USA), and incubated in rabbit anti-mouse CD31 (1:50, Abcam, UK) and mouse anti-mouse GFP (1:50, Santa Cruz, USA) overnight at 4°C. Incubation with Cy3-conjugated donkey anti-rabbit and FITC-conjugated donkey anti-mouse secondary antibodies was carried out for 1 h (1:200, Jackson ImmunoResearch, USA) at 37°C. The slides were then treated with DAPI for 10 min at room temperature. The slides were cover-slipped and imaged with a Leica immunofluorescence microscope.

Immunohistochemistry

Immunocytochemistry was performed according to standard protocols. Slides were pre-incubated with 5% normal donkey serum (Jackson, USA) for 40 min each. The anti-mouse CD31 (1:50, Abcam, USA) antibody was applied at 4°C overnight, followed by the appropriate HRP-conjugated IgG (1:200, Jackson). Sections were counterstained with hematoxylin.

Cell Adhesion Assay

An MSCs adhesion assay with an endothelial monolayer was carried out according to the procedures described previously with some modifications (24). Mouse brain microvascular endothelial cells (bEnd.3) were seeded onto a 96-well plate to form confluent monolayers. Then bEnd.3 cells were preincubated with 10 U/mL of monocyte chemotactic protein 1 (MCP1, R&D systems, USA) for 4 h. Subsequently, 1×10^5 MSCs labeled with PKH26 (Sigma, USA) were added to the endothelial cell monolayer at 37°C for 1 h. Then non-adherent cells were removed by a gentle wash with PBS for three times. Adherent MSCs were fixed, visualized by fluorescence microscopy and counted in five randomly chosen fields-of-view (FOV) for each well. Each experiment was repeated 3 times.

Flow Cytometry

The cells were harvested by 0.05% trypsin treatment for 3 min, then the cells were washed once with FACS buffer (0.5% BSA/PBS) and fixed with 1% PFA at 37°C for 10 min followed by washing 3 times. The CD31-PE (1:100, BD), CD144-FITC (1:100, Bioss, China) antibodies were diluted in FACS buffer and incubated with the cells at 4°C for 30 min. After 3 times washing

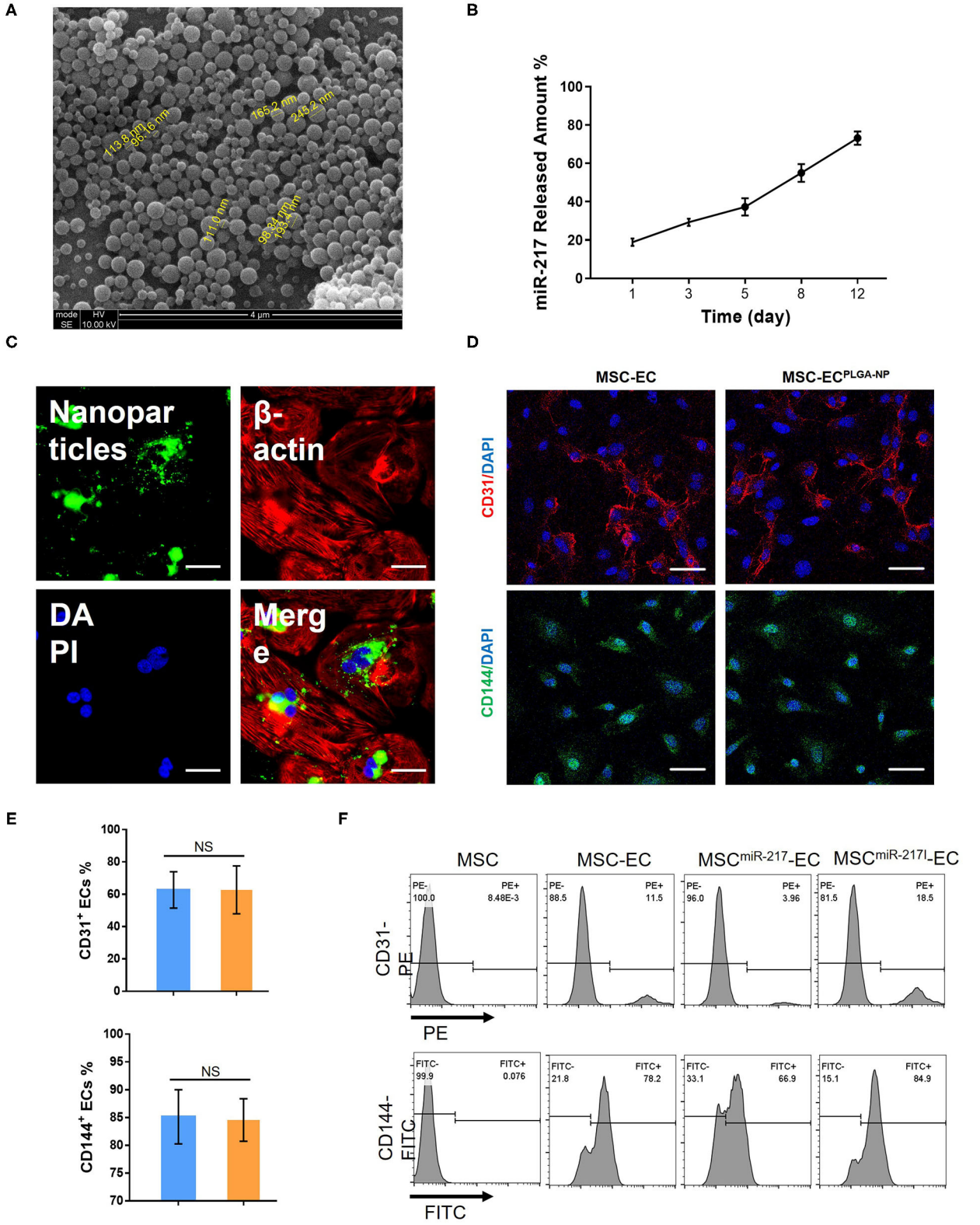

FIGURE 1 | Characterization of PLGA-NP and evaluation of miR-217 effect on endothelial cells (EC) differentiation from MSC. **(A)** PLGA-NP image under a scanning electron microscopy. **(B)** The cumulative amount of miR-217 released from the PLGA-NP was determined *via* qPCR. **(C)** Representative image of MSC after 12 h of

(Continued)

FIGURE 1 | incubation with nanoparticles containing green fluorescence dye FAM-labeled control siRNAs. Scale bars = 50 μm. **(D)** Fluorescent imaging of differentiated endothelial cells (EC) from MSC after transfection with or without PLGA-NP. Scale bars = 50 μm. **(E)** Quantification of $CD31^+$ and $CD144^+$ ECs differentiated from MSC and MSC transfected with NP. **(F)** Flow cytometric analysis of CD31 and CD144 expression on MSC and EC derived from MSC, MSC transfected with agomiR-217 ($MSC^{miR-217}$) or MSC transfected with antagomiR-217 ($MSC^{miR-217I}$).

with FACS buffer, the cells were analyzed on the Cytoflex LX flow cytometer (Beckman, USA).

Analysis of Intracellular ROS Level

Intracellular ROS levels were determined by the fluorescence analysis of cells stained with 5-(and-6)-chloromethyl-2',7'-dichlorodihydrofluorescein diacetate acetyl ester (CM-H_2DCFDA) (Invitrogen). After treatment with PBS of different miRNAs for 48 hr, MSC were incubated with CM-H_2DCFDA for 30 min at 37°C followed by three washes with PBS. Then the cells were fixed with 4% paraformaldehyde for 10 min and all images were captured under the fluorescent microscope, and the fluorescence was quantified by Image J Software (National Institute of Health, USA).

MSC-EC Tube Formation Assay

MSC-EC were firstly transfected with different miRNAs for 48 hr, then tube formation was performed by seeding MSC-EC (2.5×10^4 cells/well) on Matrigel (65 μL/well) into a 96-well plate for 24 h in the incubator. Afterwards, five pictures per well were taken using an Olympus IX83 microscope. The tube length was quantified by Image J Software (NIH).

Statistical Analyses

Data are expressed as mean ± SD. For experiments including multiple comparisons, *P*-values refer to one-way ANOVA followed by Tukey's honestly significant difference (HSD) test. For experiments including only one comparison, *P*-values refer to unpaired 2-tailed Student's *t*-test. $P \leq 0.05$ was considered statistically significant. Analyses were performed using Prism 7 software (GraphPad).

RESULTS

Nanoparticle-Encapsulated MiR-217 Is Slowly Released

PLGA nanoparticles (NP) with a mean diameter of 120 nm (**Figure 1A**) were generated by a double emulsion technique. When 1 mg of nanoparticles loaded with miR-217 agomir was incubated in 1 mL of PBS at 37°C, 20% of the encapsulated miR was released during the first 3 days and 80% was continuously released until day 12 (**Figure 1B**). Green fluorescence dye FAM-labeled control siRNAs were encapsulated into NPs (**Figure 1C** green panel), and a large amount of green fluorescent NPs was taken into MSCs from the culture medium within 12 h (**Figure 1C**).

MiR-217 Can Modulate the Differentiation MSCs Toward ECs

Internalizaiton of empty NPs did not affect the EC differentiation efficiency as shown by the percentages of differentiated $CD31^+$ and $CD144^+$ cells from MSCs (**Figures 1D,E**). However, when miR-217 agomir loaded NPs were internalized by MSCs ($MSC^{miR-217}$), the differentiation efficiency was reduced; on the contrary, miR-217 inhibition ($MSC^{miR-217I}$) improved EC differentiation efficiency (**Figure 1F**).

Intravenously Administered MSCs Home to Femoral Artery Injury Sites

In order to study the therapeutic effect of MSCs on vascular endothelium injury, we first established the standard wire-induced femoral artery injury model using 8–10-weeks-old C57BL/6J mice as previously described (20) (**Figure 2A**). The cell injection time points were determined at 1 h, day 1, day 3, and day 7 after surgery (**Figure 2B**). As shown in **Figure 2C**, the femoral artery of the standard wire-operated C57BL/6J mice showed significant intimal hyperplasia ($n = 3$), as compared to the uninjured femoral artery. To evaluate the therapeutic effects of MSCs on arterial injury, we next injected MSCs (2×10^5 cells) in 200 uL *via* the tail vein. Injecting the same amount of PBS alone served as negative controls. To track the injected MSCs in the recipient mice with femoral artery injury, we used an MSC line stably expressing GFP (GFP-MSCs) and examined the cells using confocal microscopy 24 h after injection. The injured femoral arteries were dissected, and the luminal surfaces were examined. GFP-MSCs were identified on the luminal surface of injured femoral arteries, indicating that MSCs could home to the injury sites (**Figure 2D**). Three weeks after cell injection, mice were sacrificed, and the femoral arteries were harvested for further analysis. We found that only MSCs treated with NPs encapsulating miR-217 antagomir retained in the injured artery and differentiated into ECs (**Figure 2E**).

Intravenously-Administered MSCs Is Sufficient to Exert a Protective Effect on Injured Arteries, Which Is Enhanced by MiR-217 Inhibition

To evaluate the protective effect of MSCs on IH, the tunica neointima-to-tunica media area thickness ratio was examined using Hematoxylin & Eosin (HE) staining across the sections. Compared to the PBS group, injection of MSCs transfected with control siRNA (CoR)-loaded NP (MSC^{CoR}) significantly decreased the neointima-to-media thickness ratio (**Figures 3A,B**), indicating that MSCs successfully inhibited neointimal proliferation in the injured vascular endothelium. MiR-217 overexpression in MSCs abolished the therapeutic effect of the MSCs treatment on IH (**Figure 3B**), whereas MSCs transfected with miR-217 antagomir-loaded NPs ($MSC^{miR-217I}$) significantly improved

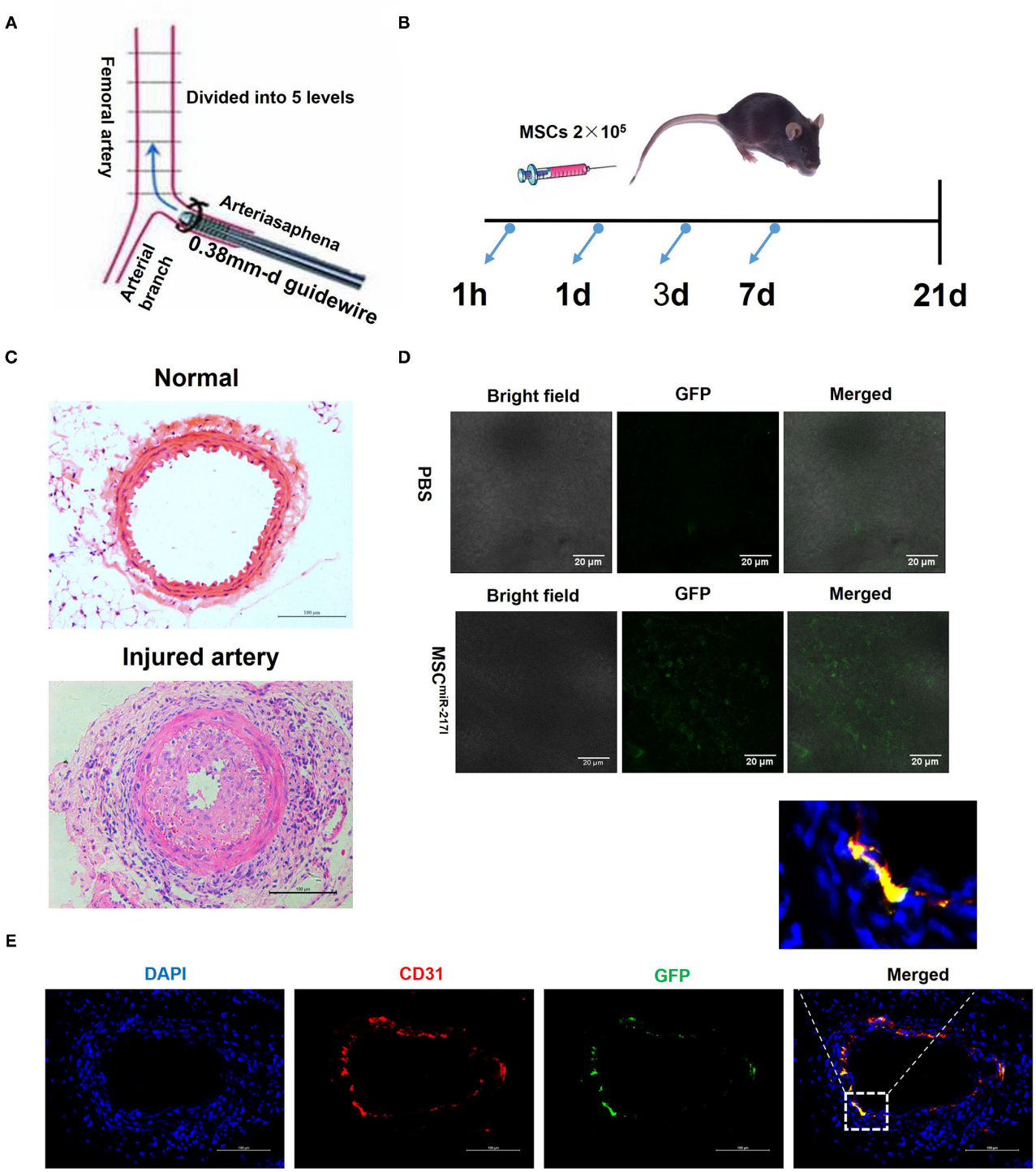

FIGURE 2 | A femoral artery injury model in mice. **(A)** A schematic representation of the surgical procedure. **(B)** A schematic representation about the cell treatment procedure after the femoral artery injury. **(C)** A representative image of uninjured femoral artery and neointima formation 21 days after endothelial cell damage. Scale bars = 100 μm. **(D)** MSCs home to the vascular injury site at 24 h after injection; 2×10^5 GFP-labeled MSCs were intravenously infused directly in the mouse tail vein following the femoral artery injury, and 24 h later the presence of GFP-labeled cells was analyzed by fluorescence microscopy. Representative confocal microscopy images show that the injected MSCs localized exclusively to the site of injury. Scale bars = 20 μm. **(E)** Immunofluorescent analysis revealed differentiation of engrafted GFP-labeled $MSC^{miR-217l}$ into endothelial cells at day 21 after cells injection.

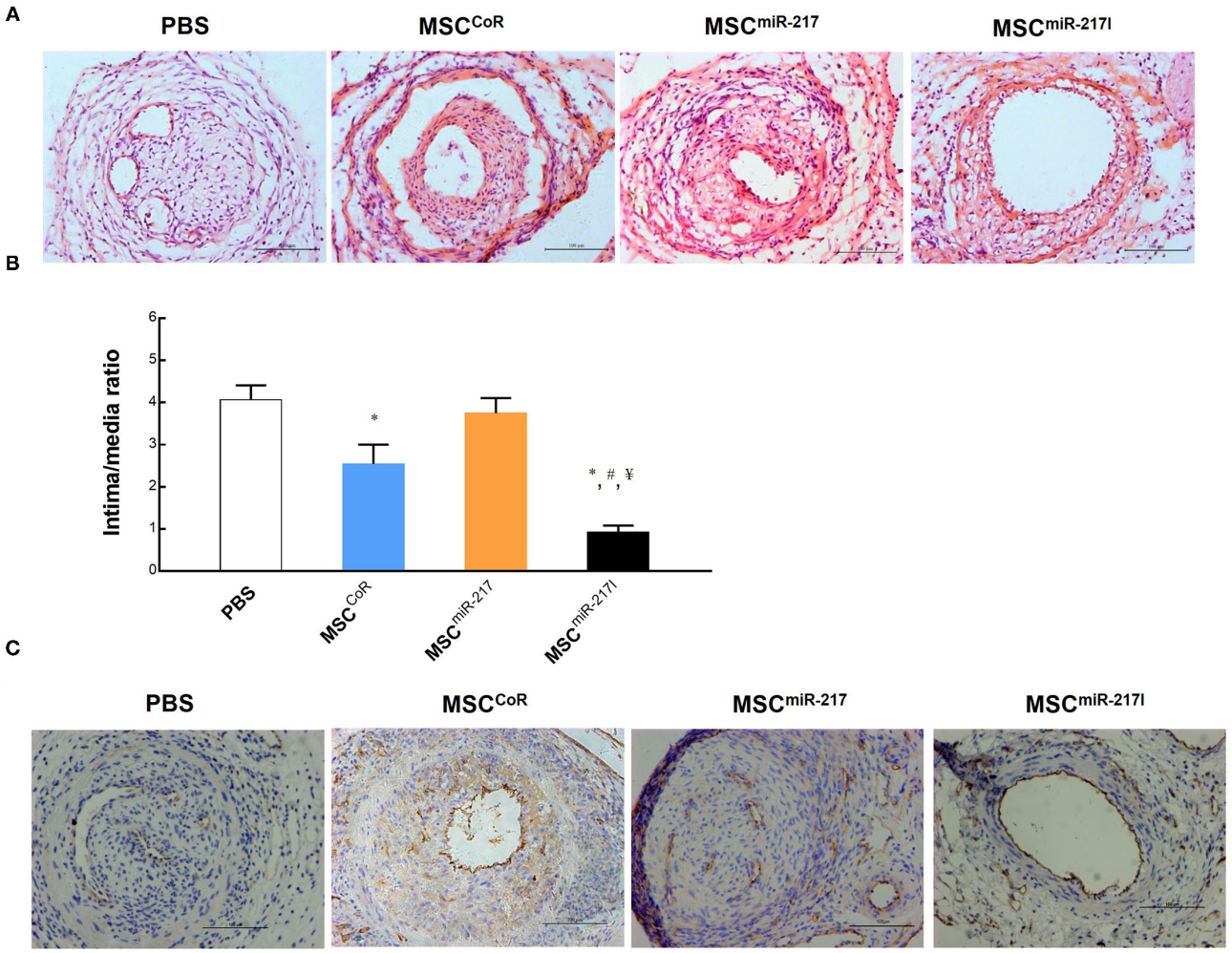

FIGURE 3 | Evaluation of the therapeutic effect of MSC injection on re-endothelialization of the injured vasculature and the role of miRNA-217 in the injured artery repairment process. **(A)** Representative images of injured femoral arteries at 3 weeks after treatment with PBS, MSC^{CoR} (MSCs transfected with control siRNA), $MSC^{miR-217}$, $MSC^{miR-217I}$. Scale bars = 100 μm. **(B)** Analysis of the intima-to-media thickness ratio to reveal the cell treatment effect for neointima formation. $^{*}P < 0.05$ vs. PBS, $^{\#}P < 0.05$ vs. MSC^{CoR}, $^{¥}P < 0.05$ vs. $MSC^{miR-217}$. $n = 9$ each. **(C)** Immunohistochemistry analysis of injured vessels for CD31 endothelial marker expression at day 21 after the surgery and cell treatment.

the therapeutic effect (**Figure 3B**), suggesting that miR-217 negatively regulates MSC-mediated recovery in neointimal hyperplasia. To evaluate efficiency of re-endothelialization of the injured artery, we stained the vessels with an endothelial cell marker CD31. Although each treatment group showed some degree of re-endothelialization, $MSC^{miR-217I}$ treatment group exhibited the greatest number of CD31 positive cells surrounding the luminal surface of the repaired intima (**Figure 3C**).

MiR-217 Inhibits Sirt-1 Expression, Causes EBs Malformation and Senescence in MSCs

Nicotinamide adenosine dinucleotide (NAD)-dependent deacetylase Sirt-1, also known as Sirtuin-1, is a critical factor that promotes angiogenesis and is one of the downstream targets of miR-217 (20). We hypothesized that the adverse effect of miR-217 on the MSC-mediated therapeutic activity on IH could result from downregulation of the Sirt-1 expression in MSCs. Indeed, transfection of miR-217 agomir into MSCs (miR-217 overexpression) significantly inhibited Sirt-1 expression, similar to the effect of Sirt-1 silencing achieved by the siRNA transfection of MSCs (**Figures 4A,B**). These results were consistent with previous reports on the inhibitory effect of miR-217 on Sirt-1 expression in tumor cells, liver cells and endothelial cells (20, 25, 26). In addition, miR-217 overexpression caused malformation of EBs (**Figures 4C,F**), which is an indicator of MSC malfunction and possibly impaired differentiation. Similar to the effect of Sirt-1 siRNA, inhibition of Sirt-1 expression by miR-217 overexpression caused a significant senescence in MSCs (**Figures 4D,G**). Furthermore, miR-217 overexpression could also increase reactive oxygen species (ROS)

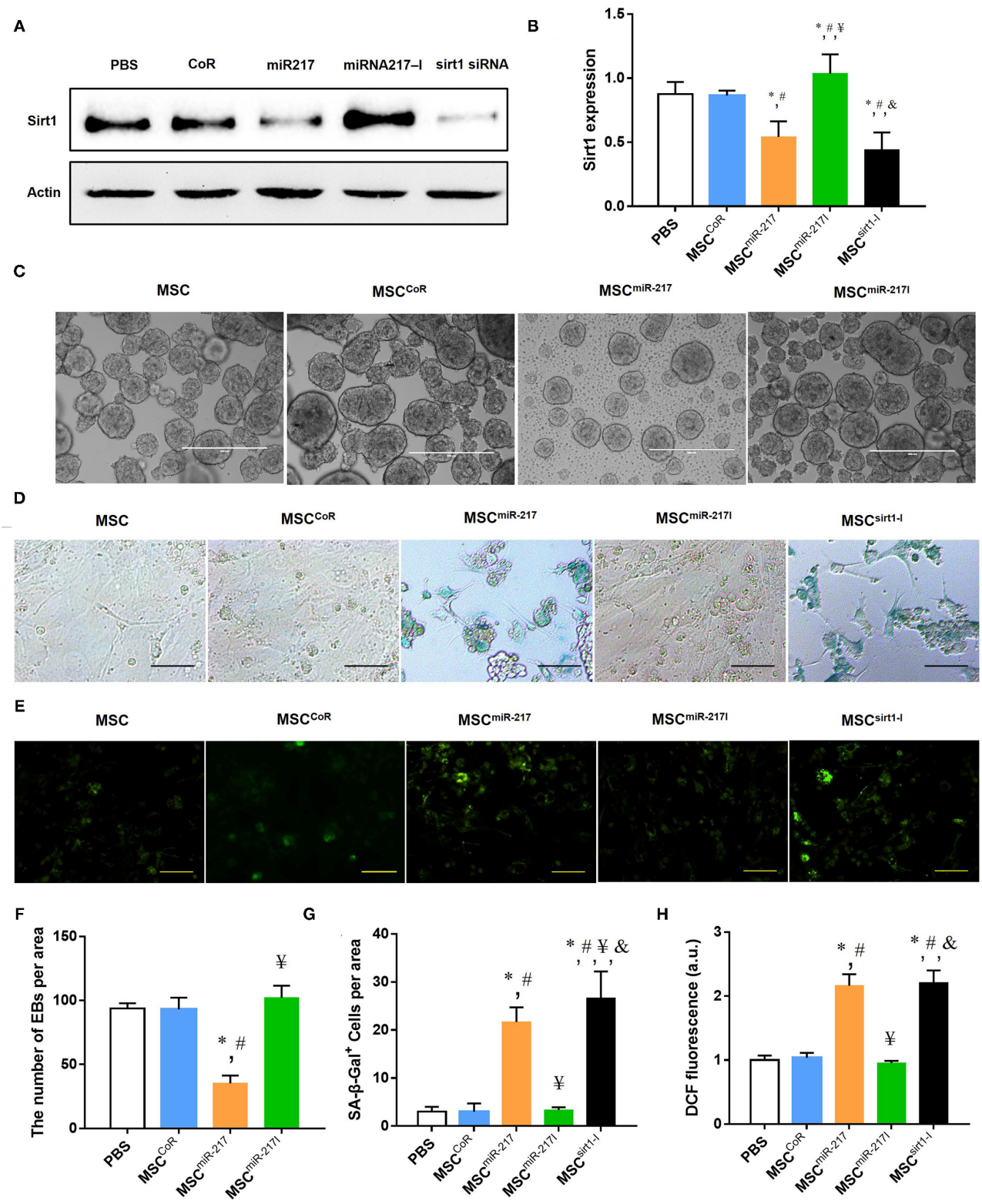

FIGURE 4 | MiR-217 overexpression in MSCs reduces Sirt-1 expression, induces malformation of EBs, increased senescence and ROS activity. **(A)** A comparative analysis of the Sirt-1 expression in intact MSCs and MSC^{CoR}, $MSC^{miR-217}$, $MSC^{miR-217I}$, $MSC^{Sirt1-I}$ by Western blot. **(B)** Protein quantification by band densitometry in gels shown in panel **(A)**, $^{*}P < 0.05$ vs. PBS, $^{\#}P < 0.05$ vs. MSC^{CoR}, $^{¥}P < 0.05$ vs. $MSC^{miR-217}$, $^{\&}P < 0.05$ vs. $MSC^{miR-217I}$, $n = 3$. **(C)** Representative images of

(Continued)

FIGURE 4 | EB formation assay in each group. Scale bars = 500 μm. **(D)** Representative images of β-galactosidase (SA-β-gal) cell staining in each experimental group. Scale bars = 100 μm. **(E)** Fluorescence microscopic images of intracellular ROS production by DCF staining (green) in MSC cells. Scale bars = 100 μm. **(F–H)** Statistical analysis of EB quantification, SA-β-gal positive cells and DCF positive cells. $^{*}P < 0.05$ vs. PBS, $^{\#}P < 0.05$ vs. MSC^{CoR}, $^{¥}P < 0.05$ vs. $MSC^{miR-217}$, $^{\&}P < 0.05$ vs. $MSC^{miR-217I}$, $n = 3$.

expression in MSCs (**Figures 4E,H**). These data suggested that the negative effect of miR-217 on the therapeutic role of MSCs resulted from increased senescence and impaired function of MSCs.

Inhibition of MiR-217 Promotes MSC Adhesion and Re-endothelialization

Previous studies suggested that the adhesion of MSCs to injured endothelial cells is required for MSCs to contribute to angiogenesis (27). We therefore performed a cell adhesion assay to determine if miR-217 inhibition can promote adhesion of MSCs to endothelial cells. As shown in **Figures 5A,C**, the basal adhesion activity did not differ significantly between MSCs and MSC^{CoR}, while the adhesion activities of $MSC^{miR-217I}$ increased dramatically. We next investigated the function of MSCs in a tube formation assay. As shown in **Figures 5B,D**, the tube length of $MSC^{miR-217I}$ group enhanced dramatically, as compared to MSC^{CoR}.

To evaluate the therapeutic effect of MSCs on neointima recovery *in vivo,* we analyzed vascular re-endothelialization at day 21 on the luminal surface of the injured arteries and assessed their integrity. As expected, more $CD31^{+}$ cells were detected in the arterial lumens in cell treatment group as compared to PBS group (**Figure 5E**). However, re-endothelialization was significantly suppressed when applying MSCs with miR-217 overexpression. To track the injected cells, we also detected GFP fluorescence in the luminal surface. We assessed the ratio of GFP/CD31-double positive cells in injuried femoral artery at week 3 after surgery, double positive cells could be found in $MSC^{miR-217I}$ group and could rarely be found in other cell treatment groups (**Figure 5E**). These results indicated that inhibition of miR-217 in MSCs accelerated re-endothelialization.

DISCUSSION

Intimal hyperplasia resulting from vascular injury is the main cause of vascular surgical reconstruction and endovascular treatment, which often leads to postoperative artery stenosis or occlusion. Current clinical approaches to reduce luminal stenosis induced by vascular injury include radiation, drug therapy, cell therapy and other strategies. However, the resulting therapeutic benefits are not satisfactory, while the cell therapy approach is hampered by limited cell sources.

MSCs hold promise for IH therapy owing to their self-renewal, vascular differentiation capabilities and paracrine properties (13) with some advantages lying in the straightforward cell isolation (from different sources) technique and ease of preservation. In addition, utilization of human MSCs raises no ethical concerns and harbors a limited risk of tumor (teratoma) development (14, 15). In this study, we demonstrated that intravenous administration of MSCs results in a significant therapeutic benefit for vascular injury repairment that occurs through re-endothelialization. GFP fluorescence of the transplanted MSCs allowed us to determine that MSCs could home to the vascular luminal surface of the injury site within 24 h, some of which survive for an extended time (3 weeks post MSC treatment). Co-localization of CD31 staining and GFP immunofluorescence indicated that at least some MSCs transdifferentiated into the vascular endothelial cells at the luminal surface of the injury site. Furthermore, the vascular intima-to-media thickness ratio was significantly reduced 3 weeks after MSCs administration. On the other hand, no obvious localization to the injury site was observed for the $MSC^{miR-217}$, suggesting that miR-217 interfered with homing and/or differentiation of MSCs into endothelial lineage. The therapeutic effect of the $MSC^{miR-217}$ was therefore significantly impaired by this inhibition. Our *in vitro* data showed that, miR-217 expression leads to knockdown of Sirt-1 protein expression, and increases senescence, ROS expression and malformation of EBs in the transfected MSCs. MiR-217 expression also inhibited the adhesion of MSCs and tube formation of MSC-ECs. These data suggested that miR-217 downregulates the expression of endogenous Sirt-1 in MSCs thereby hindering their natural process of homing to the vascular injury sites and basal function.

When MSCs were transfected with miR-217 inhibitor-loaded PLGA-NPs, they exhibited higher injury repairing capabilities. $MSC^{miR-217I}$ showed a statistically significant difference in the ability to repair blood vessel damage relative to those of PBS and MSC^{CoR}. Although MSC treatment could reduce intimal hyperplasia and promote re-endothelialization of the injured artery, almost no $CD31^{+}GFP^{+}$ ECs could be located at the luminal surfaces at week 3 after surgery. However, a large number of $CD31^{+}GFP^{+}$ ECs were found in the artery after $MSC^{miR-217I}$ treatment, and the protective effect were significantly improved than the MSC^{CoR}-treated mice, implying that miR-217 might affect MSC differentiation ability and have additional important biological roles in MSCs that warrant further studies.

Our data also suggested that miR-217 downregulates the expression of endogenous Sirt-1, thereby inducing cell aging and diminishing MSC differentiation capability. MiR-217 inhibition mediated by the miR-217 antagomir-loaded PLGA-NPs can significantly improve the efficacy of MSC-mediated IH treatment. In conclusion, our findings demonstrate a profound therapeutic benefit of MSCs on the endothelium recovery post vascular

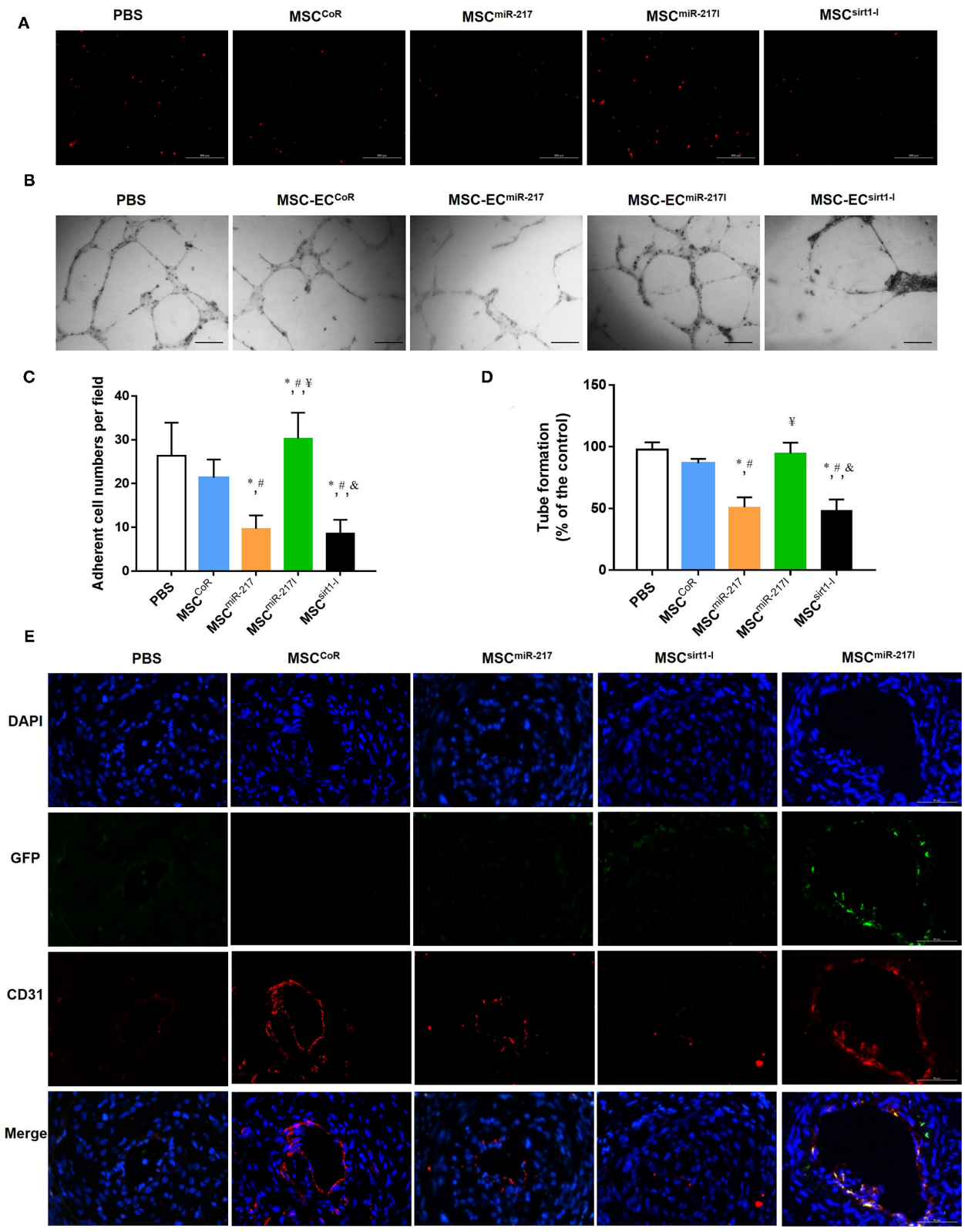

FIGURE 5 | miR-217 inhibition can improve MSC treatment efficiency for IH by increasing the differentiation potential into endothelial cells at the injury site. **(A)** The adhesion properties of MSCs to the endothelial monolayer after treatment with PBS, MSC^{CoR}, $MSC^{miR-217}$, $MSC^{miR-217I}$ or $MSC^{Sirt1-I}$. **(B)** Assessment of MSC-EC

(Continued)

FIGURE 5 | tube formation properties in each treatment group. Scale bars = 200 μm. **(C)** Quantification of the adherent MSCs visualized for each sample in five randomly chosen fields (FOV) of duplicate chambers, $^{*}P < 0.05$ vs. PBS, $^{\#}P < 0.05$ vs. MSC^{CoR}, $^{¥}P < 0.05$ vs. $MSC^{miR-217}$, $^{\&}P < 0.05$ vs. $MSC^{miR-217l}$, $n = 3$. **(D)** Quantification of tube formation experiment. $^{*}P < 0.05$ vs. PBS, $^{\#}P < 0.05$ vs. MSC^{CoR}, $^{¥}P < 0.05$ vs. $MSC^{miR-217}$, $^{\&}P < 0.05$ vs. $MSC^{miR-217l}$, $n = 3$. **(E)** Immunofluorescent analysis revealed differentiation of engrafted GFP-labeled MSCs into endothelial cells. Paraffin sections of wound biopsies in each group were immunostained with anti-CD31 antibody and anti-GFP antibody. Fluorescence images reveal that MSCs expressing GFP (green) were incorporated into the vascular structures of the MSC-treated wounds and expressed CD31 endothelial marker (red). Nuclei were counterstained with DAPI (blue). The merged images evidence that the implanted GFP-labeled MSCs differentiated into $CD31^{+}$ endothelial cells.

injury, which is negatively regulated by miR-217, offering a new potential IH treatment strategy.

DATA AVAILABILITY STATEMENT

The raw data supporting the conclusions of this article will be made available by the authors, without undue reservation.

ETHICS STATEMENT

The animal study was reviewed and approved by the Ethics Committee of Wuhan Union Hospital.

AUTHOR CONTRIBUTIONS

HY, YHu, YHe, and HL contributed to design study. HY, YHu, YHe, JY, and HL analyzed data and prepared the manuscript. HY, YHu, YW, XH, SC, and JL contributed to do the experiments. HY and HL contributed to fund it. All authors contributed to the article and approved the submitted version.

FUNDING

This work was supported by the National Natural Science Foundation of China (81500301 and 81600800).

ACKNOWLEDGMENTS

Thanks for Overseas Research and Study Project of Excellent Young, Middle-aged Teachers and Principals in Colleges and Universities of Jiangsu Province of 2018.

SUPPLEMENTARY MATERIAL

The Supplementary Material for this article can be found online at: https://www.frontiersin.org/articles/10.3389/fcvm.2021.739107/full#supplementary-material

REFERENCES

1. Lindner V, Reidy MA, Fingerle J. Regrowth of arterial endothelium. Denudation with minimal trauma leads to complete endothelial cell regrowth. *Lab Invest.* (1989) 61:556–63.
2. Weidinger FF, McLenachan JM, Cybulsky MI, Gordon JB, Rennke HG, Hollenberg NK, et al. Persistent dysfunction of regenerated endothelium after balloon angioplasty of rabbit iliac artery. *Circulation.* (1990) 81:1667–79. doi: 10.1161/01.CIR.81.5.1667
3. Faxon DP, Coats W, Currier J. Remodeling of the coronary artery after vascular injury. *Prog Cardiovasc Dis.* (1997) 40:129–40. doi: 10.1016/S0033-0620(97)80005-9
4. Mickelson JK, Lakkis NM, Villarreal-Levy G, Hughes BJ, Smith CW. Leukocyte activation with platelet adhesion after coronary angioplasty: a mechanism for recurrent disease? *J Am Coll Cardiol.* (1996) 28:345–53. doi: 10.1016/0735-1097(96)00164-7
5. Abedin M, Tintut Y, Demer LL. Mesenchymal stem cells and the artery wall. *Circ Res.* (2004) 95:671–6. doi: 10.1161/01.RES.0000143421.27684.12
6. Werner N, Junk S, Laufs U, Link A, Walenta K, Bohm M, et al. Intravenous transfusion of endothelial progenitor cells reduces neointima formation after vascular injury. *Circ Res.* (2003) 93:e17–e24. doi: 10.1161/01.RES.0000083812.30141.74
7. Li G, Chen SJ, Oparil S, Chen YF, Thompson JA. Direct in vivo evidence demonstrating neointimal migration of adventitial fibroblasts after balloon injury of rat carotid arteries. *Circulation.* (2000) 101:1362–5. doi: 10.1161/01.CIR.101.12.1362
8. Cho HJ, Kim HS, Lee MM, Kim DH, Yang HJ, Hur J, et al. Mobilized endothelial progenitor cells by granulocyte-macrophage colony-stimulating factor accelerate reendothelialization and reduce vascular inflammation after intravascular radiation. *Circulation.* (2003) 108:2918–25. doi: 10.1161/01.CIR.0000097001.79750.78
9. Rabelink TJ, de Boer HC, de Koning EJ, van Zonneveld AJ. Endothelial progenitor cells: more than an inflammatory response? *Arterioscler Thromb Vasc Biol.* (2004) 24:834–8. doi: 10.1161/01.ATV.0000124891.57581.9f
10. Walter DH, Rittig K, Bahlmann FH, Kirchmair R, Silver M, Murayama T, et al. Statin therapy accelerates reendothelialization: a novel effect involving mobilization and incorporation of bone marrow-derived endothelial progenitor cells. *Circulation.* (2002) 105:3017–24. doi: 10.1161/01.CIR.0000018166.84319.55
11. Gupta PK, Chullikana A, Parakh R, Desai S, Das A, Gottipamula S, et al. A double blind randomized placebo controlled phase I/II study assessing the safety and efficacy of allogeneic bone marrow derived mesenchymal stem cell in critical limb ischemia. *J Transl Med.* (2013) 11:143. doi: 10.1186/1479-5876-11-143
12. Rasmussen JG, Frobert O, Pilgaard L, Kastrup J, Simonsen U, Zachar V, et al. Prolonged hypoxic culture and trypsinization increase the pro-angiogenic potential of human adipose tissue-derived stem cells. *Cytotherapy.* (2011) 13:318–328. doi: 10.3109/14653249.2010.506505
13. Bronckaers A, Hilkens P, Martens W, Gervois P, Ratajczak J, Struys T, et al. Mesenchymal stem/stromal cells as a pharmacological and therapeutic approach to accelerate angiogenesis. *Pharmacol Ther.* (2014) 143:181–96. doi: 10.1016/j.pharmthera.2014.02.013
14. Lu LL, Liu YJ, Yang SG, Zhao QJ, Wang X, Gong W, et al. Isolation and characterization of human umbilical cord mesenchymal stem cells with hematopoiesis-supportive function and other potentials. *Haematologica.* (2006) 91:1017–26.
15. Samsonraj RM, Raghunath M, Nurcombe V, Hui JH, van Wijnen AJ, Cool SM. Concise review: multifaceted characterization of human mesenchymal stem cells for use in regenerative medicine. *Stem Cells Transl Med.* (2017) 6:2173–85. doi: 10.1002/sctm.17-0129
16. Zhang X, Bendeck MP, Simmons CA, Santerre JP. Deriving vascular smooth muscle cells from mesenchymal stromal cells: evolving differentiation

strategies and current understanding of their mechanisms. *Biomaterials.* (2017) 145:9–22. doi: 10.1016/j.biomaterials.2017.08.028
17. Wang C, Li Y, Yang M, Zou Y, Liu H, Liang Z, et al. Efficient differentiation of bone marrow mesenchymal stem cells into endothelial cells in vitro. *Eur J Vasc Endovasc Surg.* (2018) 55:257–65. doi: 10.1016/j.ejvs.2017.10.012
18. Wu Y, Chen L, Scott PG, Tredget EE. Mesenchymal stem cells enhance wound healing through differentiation and angiogenesis. *Stem Cells.* (2007) 25:2648–59. doi: 10.1634/stemcells.2007-0226
19. Yao Z, Liu H, Yang M, Bai Y, Zhang B, Wang C, et al. Bone marrow mesenchymal stem cell-derived endothelial cells increase capillary density and accelerate angiogenesis in mouse hindlimb ischemia model. *Stem Cell Res Ther.* (2020) 11:221. doi: 10.1186/s13287-020-01710-x
20. Menghini R, Casagrande V, Cardellini M, Martelli E, Terrinoni A, Amati F, et al. MicroRNA 217 modulates endothelial cell senescence via silent information regulator 1. *Circulation.* (2009) 120:1524–1532. doi: 10.1161/CIRCULATIONAHA.109.864629
21. Bose RJ, Lee SH, Park H. Lipid-based surface engineering of PLGA nanoparticles for drug and gene delivery applications. *Biomater Res.* (2016) 20:34. doi: 10.1186/s40824-016-0081-3
22. Meng D, Shi X, Jiang BH, Fang J. Insulin-like growth factor-I (IGF-I) induces epidermal growth factor receptor transactivation and cell proliferation through reactive oxygen species. *Free Radic Biol Med.* (2007) 42:1651–60. doi: 10.1016/j.freeradbiomed.2007.01.037
23. Dohi Y, Ikura T, Hoshikawa Y, Katoh Y, Ota K, Nakanome A, et al. Bach1 inhibits oxidative stress-induced cellular senescence by impeding p53 function on chromatin. *Nat Struct Mol Biol.* (2008) 15:1246–54. doi: 10.1038/nsmb.1516
24. Iwai N, Kitajima K, Sakai K, Kimura T, Nakano T. Alteration of cell adhesion and cell cycle properties of ES cells by an inducible dominant interfering Myb mutant. *Oncogene.* (2001) 20:1425–34. doi: 10.1038/sj.onc.1204236
25. Zhang HS, Wu TC, Sang WW, Ruan Z. MiR-217 is involved in Tat-induced HIV-1 long terminal repeat (LTR) transactivation by down-regulation of SIRT1. *Biochim Biophys Acta.* (2012) 1823:1017–23. doi: 10.1016/j.bbamcr.2012.02.014
26. Yin H, Hu M, Zhang R, Shen Z, Flatow L, You M. MicroRNA-217 promotes ethanol-induced fat accumulation in hepatocytes by down-regulating SIRT1. *J Biol Chem.* (2012) 287:9817–26. doi: 10.1074/jbc.M111.333534
27. Shi W, Xin Q, Yuan R, Yuan Y, Cong W, Chen K. Neovascularization: the main mechanism of MSCs in ischemic heart disease therapy. *Front Cardiovasc Med.* (2021) 8:633300. doi: 10.3389/fcvm.2021.633300

Conflict of Interest: The authors declare that the research was conducted in the absence of any commercial or financial relationships that could be construed as a potential conflict of interest.

Publisher's Note: All claims expressed in this article are solely those of the authors and do not necessarily represent those of their affiliated organizations, or those of the publisher, the editors and the reviewers. Any product that may be evaluated in this article, or claim that may be made by its manufacturer, is not guaranteed or endorsed by the publisher.

frontiers in Cardiovascular Medicine

ORIGINAL RESEARCH
published: 14 October 2021
doi: 10.3389/fcvm.2021.763984

Metabolic Profile in Neonatal Pig Hearts

Pengsheng Li[1], *Fan Li*[1,2], *Ling Tang*[1], *Wenjing Zhang*[3,4,5], *Yan Jin*[3], *Haiwei Gu*[3,4,5]* and *Wuqiang Zhu*[1]*

[1] Department of Cardiovascular Diseases, Physiology and Biomedical Engineering, Center for Regenerative Medicine, Mayo Clinic Arizona, Scottsdale, AZ, United States, [2] Laboratory of Regenerative Medicine in Sports Science, School of Physical Education and Sports Science, South China Normal University, Guangzhou, China, [3] College of Health Solutions, Arizona State University, Phoenix, AZ, United States, [4] Department of Environmental Health Sciences, Robert Stempel College of Public Health and Social Work, Florida International University, Miami, FL, United States, [5] Department of Cellular Biology and Pharmacology, Herbert Wertheim College of Medicine, Center for Translational Science, Florida International University, Port St. Lucie, FL, United States

OPEN ACCESS

Edited by:
Junjie Yang,
University of Maryland, Baltimore, United States

Reviewed by:
Jiacheng Sun,
University of Alabama at Birmingham, United States
Shiyue Xu,
The First Affiliated Hospital of Sun Yat-sen University, China

***Correspondence:**
Wuqiang Zhu
zhu.wuqiang@mayo.edu
Haiwei Gu
hgu@fiu.edu

Specialty section:
This article was submitted to Cardiovascular Biologics and Regenerative Medicine, a section of the journal Frontiers in Cardiovascular Medicine

Received: 24 August 2021
Accepted: 22 September 2021
Published: 14 October 2021

Citation:
Li P, Li F, Tang L, Zhang W, Jin Y, Gu H and Zhu W (2021) Metabolic Profile in Neonatal Pig Hearts. Front. Cardiovasc. Med. 8:763984. doi: 10.3389/fcvm.2021.763984

We evaluated the metabolic profile in pig hearts at postnatal day 1, 3, 7, and 28 (P1, P3, P7, and P28, respectively) using a targeted liquid chromatography tandem mass spectrometry assay. Our data showed that there is a clear separation of the detected metabolites in P1 vs. P28 hearts. Active anabolisms of nucleotide and proteins were observed in P1 hearts when cardiomyocytes retain high cell cycle activity. However, the active posttranslational protein modification, metabolic switch from glucose to fatty acids, and the reduced ratio of collagen to total protein were observed in P28 hearts when cardiomyocytes withdraw from cell cycle.

Keywords: neonatal, pig, heart, metabolism, metabolomics

INTRODUCTION

Cardiomyocytes in adult mammals possess very limited regenerative potential as a result of cell cycle exit. Myocardium loss after injuries is typically replaced by fibrotic scar. Several lines of evidence have shown that cardiomyocytes in neonatal mice (1) and pigs (2) retain regenerative capacity. We have recently shown that hearts of postnatal day 1 and day 2 pigs can regenerate lost myocardium in response to injury (2). This regeneration is mediated by proliferation of preexisting cardiomyocytes, which does not occur when cardiomyocytes permanently exit cell cycle. However, mechanisms underlying injury-mounted regenerative response especially in large mammals have not been fully understood.

Cardiomyocytes in postnatal mice undergo hypertrophic growth to adapt to increased blood pressure and volume. The process of cardiomyocyte maturation is associated with a cessation from cell cycle and proliferation activities, along with changes of energy metabolism switching from glycolysis to fatty acid oxidative metabolism to allow more efficient ATP production. Prior research has illustrated metabolic state in developing mouse hearts, and showed that metabolism switch is associated with cell cycle cessation (3, 4). However, metabolic changes and signaling pathways mediating cardiomyocyte maturation and cell cycle withdrawal in postnatal pig hearts have not been reported. Therefore, we performed a targeted metabolomic analysis to evaluate the metabolic profile in pig hearts from postnatal day 1 to day 28.

MATERIALS AND METHODS

Animal Protocol

All animal protocols were approved by the Institutional Animal Care and Use Committee of the Mayo Clinic and were performed in accordance with the National Institutes of Health Guide for the Care and Use of Laboratory Animals. Postnatal day 1 (P1), day 3, (P3), day 7 (P7), and day 28 (P28) pigs (Yorkshire-Landrace Cross background) were obtained from certified vendor S&S Farms.

Tissue Preparation

A small block of heart tissue (∼20 mg) was dissected from apex of each heart ($n = 6$ per age, both male and female were included), and was homogenized in 200 μL MeOH:PBS (4:1, v:v). After adding 800 μL MeOH:PBS, lysates were vortexed for 10 s, and stored at −20°C for 30 min. Samples were sonicated in an ice bath for 30 min, followed by a spin-down at 14,000 rpm for 10 min (4°C). A total of 800 μL supernatant was transferred to a new Eppendorf tube and vacuum dried. The pellets were reconstituted with 150 μL solution containing 40% PBS and 60% acetonitrile prior to mass spectrometry (MS) analysis. A quality control (QC) sample was generated by pooling all the study samples.

Targeted Liquid Chromatography Tandem Mass Spectrometry (LC-MS/MS)

Targeted LC-MS/MS assay was performed as we described before (5). We implemented a pathway-specific LC-MS/MS method that can cover more than 300 metabolites from >35 metabolic pathways. Each sample was injected twice, one injection of 10 μL was for analysis with negative ionization mode and the other injection of 4 μL was used for analysis with positive ionization mode. Both chromatographic separations were performed in hydrophilic interaction chromatography mode on a Waters XBridge BEH Amide column (150 × 2.1 mm, 2.5 μm particle size). The flow rate was set as 0.3 mL/min, auto-sampler temperature was set at 4°C, and the column compartment was kept at 40°C. The mobile phase was composed of Solvents A (10 mM ammonium acetate, 10 mM ammonium hydroxide in a mixed solution containing 95% H_2O and 5% acetonitrile) and Solvents B (10 mM ammonium acetate, 10 mM ammonium hydroxide in a mixed solution containing 5% H_2O and 95% acetonitrile). After the initial isocratic elution for 1 min, the percentage of Solvent B was reduced to 40% ($t = 11$ min), and it was maintained at 40% for 4 min ($t = 15$ min). The mass spectrometer is equipped with an electrospray ionization source. Targeted data acquisition was performed in multiple-reaction-monitoring (MRM) mode. The extracted MRM peaks were integrated using Agilent MassHunter Quantitative Data Analysis.

Western Blot

A small piece (∼100 mg) of left ventricular tissue from each pig heart was isolated. Whole cell lysate was generated using the protocol we reported before (6). Protein concentration was measured with a BCA kit (Thermo Fisher Scientific, cat# 89900). Samples were solubilized in sodium dodecyl sulfate (SDS)-polyacrylamide gel electrophoresis (PAGE) loading buffer for 5 min at 95°C and resolved on 10% SDS–PAGE gels. After the electro-transferred from the gel to nitrocellulose (Amersham) membrane, the equal loading was confirmed by Ponceau S staining (Fisher Scientific, Cat# AAJ6074430). Immunoblotting was performed using antibodies recognizing LDHA (Thermo Fisher Scientific, Cat# PA5-27406), LDHB (Thermo Fisher Scientific, Cat# 14824-1-AP). Signal was visualized by Odyssey CLx Infrared Imaging System (LI-COR Biosciences). Western signal was digitized and quantitated using Image Studio Lite Quantification Software.

Statistical Analysis

All data were log10 transformed, mean-centered, and divided by the square root of standard deviation (SD) for each metabolite (Pareto-scaled) to approximate normal distribution. Data in **Figure 1C** were processed for univariate statistical testing using one-way ANOVA with Fisher's Least Significance Difference Test. Data in **Figures 1E,G,I** were processed for univariate statistical testing using Student's *t*-test in the Metaboanalyst 5.0 package to compare the relative concentrations of metabolites between cohorts. Data in **Figures 2A–C**, **3A–C**, **4B** were presented as box plot showing the minimum, 25th percentile, median, 75th percentile, and maximum. Statistics were analyzed using Graphpad Prism 8.4.3. Differences between these groups were evaluated by one-way ANOVA with Tukey's Honestly Significant Difference Test. $P < 0.05$ was considered statistically significant. Data in **Figure 5C** were presented as Mean ± SEM. Statistics were analyzed using Graphpad Prism 8.4.3. Differences between these groups were evaluated by one-way ANOVA with Tukey's Honestly Significant Difference Test. $P < 0.05$ was considered statistically significant.

RESULTS

Heat map of abundance of metabolites from P1, P3, P7, and P28 samples showed the differently regulated metabolites in these samples (**Figure 1A**, **Table 1**). Principal component analysis (PCA) revealed that metabolomic profile of P28 animals was clearly separated from the P1, P3 and P7 hearts (**Figure 1B**). A total of 79 metabolic features changed significantly ($p < 0.05$) in at least one of the group comparisons (P1 vs. P3, P1 vs. P7, and P1 vs. P28) for analyses with LC-MS/MS (**Figure 1C**). Individual comparison between P1 and P3 hearts didn't reveal a clear separation of metabolomic profiles (**Figure 1D**), and 14 metabolites were identified with differential expression (**Figure 1E**). A comparison between P1 and P7 hearts revealed a clear separation of metabolomic profiles (**Figure 1F**), and 25 metabolites were identified with differential expression (**Figure 1G**). Finally, a comparison between P1 and P28 hearts revealed a clear separation of metabolomic profiles (**Figure 1H**), a total of 135 metabolites were detected and 74 metabolites were identified with differential expression. Of the 74 differentially expressed metabolites, abundance of 40 metabolites were increased, and the abundance of 34 metabolites was decreased (**Figure 1I**).

Nucleotide biosynthesis requires ribose, glycine, aspartate, and glutamine (7). Our data indicated a decreased abundance of

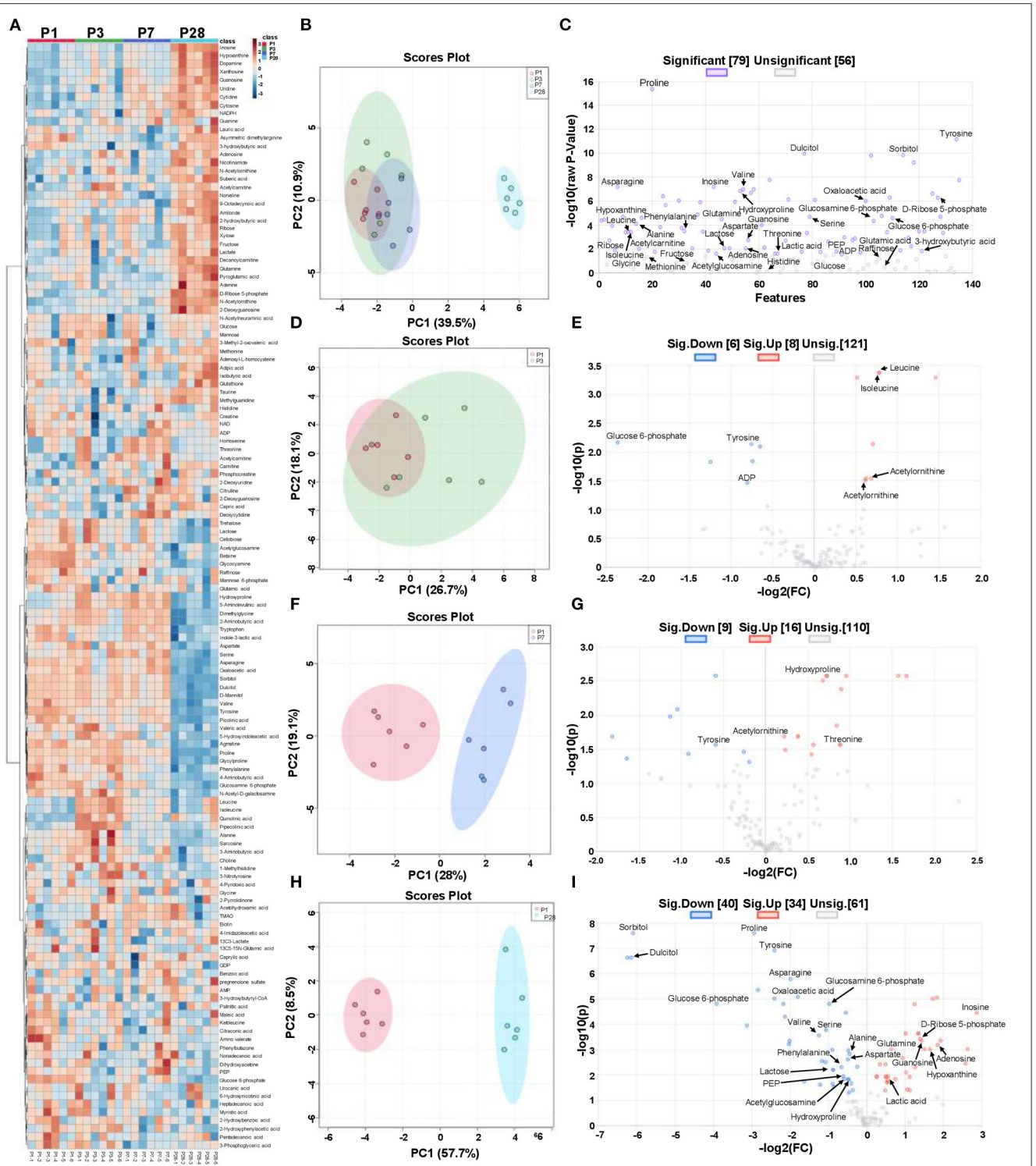

FIGURE 1 | Metabolic state in neonatal pig hearts. Four sets of left ventricular tissue samples were collected on P1, P3, P7, and P28 pigs for LC-MS/MS analysis. **(A)** Heat map of linear mixed effect model estimates for metabolites. **(B)** Principal component analysis (PCA) of metabolites from cardiomyocytes in P1, P3, P7, and P28 hearts. **(C)** Volcano plot of metabolites from P1, P3, P7, and P28 hearts ($p < 0.05$; one-way ANOVA with Fisher's Least Significance Difference Test). The purple and gray dots represented the significant changed and unsignificant changed metabolites. **(D)** PCA of metabolites from cardiomyocytes in P1 and P3 hearts. **(E)** Volcano plot of metabolites from P1 and P3 hearts ($p < 0.05$; Student's *t*-test). **(F)** PCA of metabolites from cardiomyocytes in P1 and P7 hearts. **(G)** Volcano plot of metabolites from P1 and P7 hearts ($p < 0.05$; Student's *t*-test). **(H)** PCA of metabolites from cardiomyocytes in P1 and P28 hearts. **(I)** Volcano plot of metabolites from P1 and P28 hearts ($p < 0.05$, Student's *t*-test). The red, blue, and gray dots represented the up-regulated, down-regulated, and unchanged metabolites, respectively.

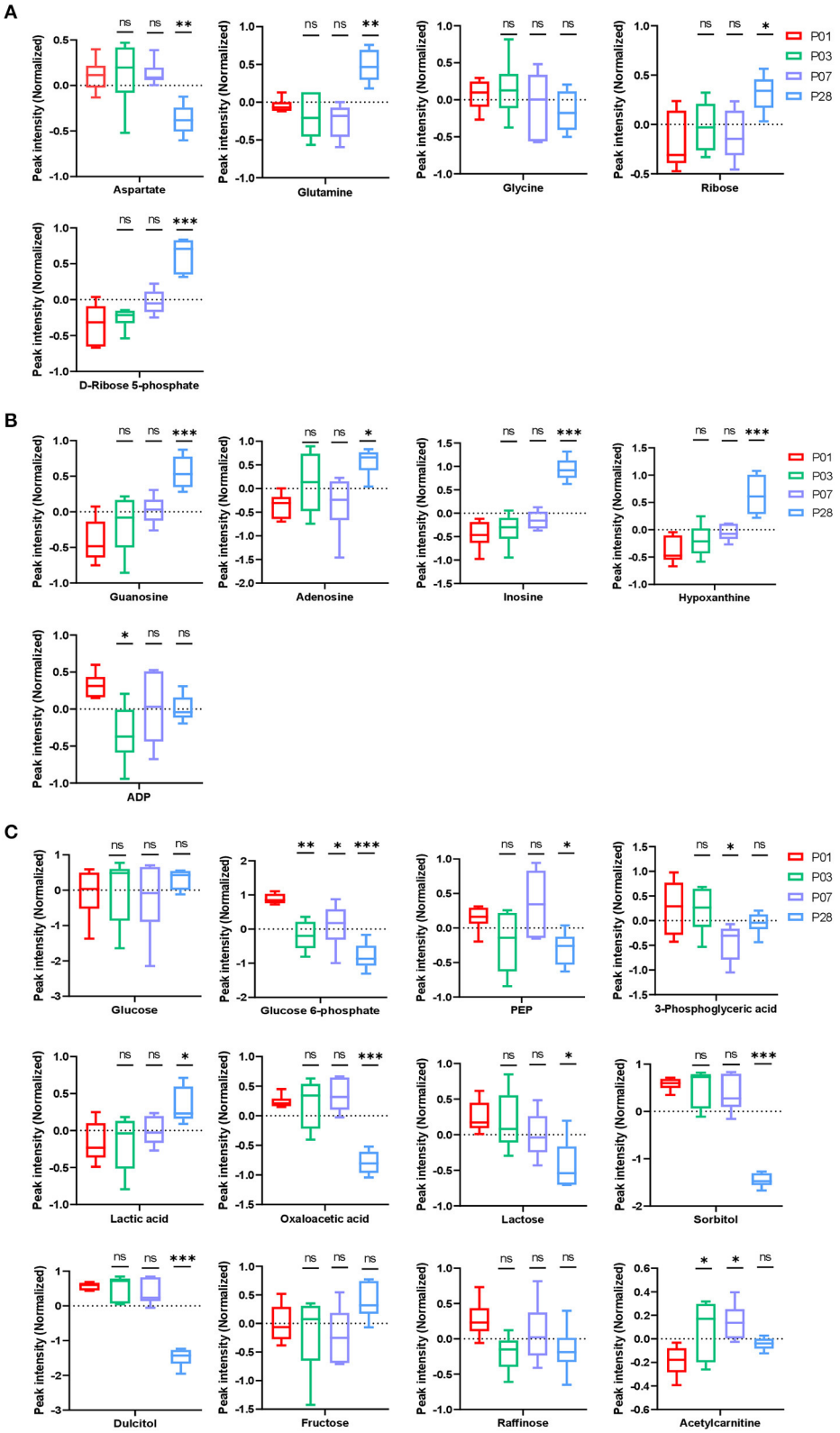

FIGURE 2 | Nucleotide and carbohydrate metabolism in neonatal pig hearts. **(A,B)** Metabolites in the pathway of nucleotide synthesis **(A)** and break down **(B)** in the four sets of heart samples (P1, P3, P7, and P28 hearts). **(C)** Metabolic profile of glucose, other sugars, and fatty acids. $^{*}p < 0.05$, $^{**}p < 0.01$, $^{***}p < 0.001$, one-way ANOVA with Tukey's Honestly Significant Difference Test. $n = 6$ hearts per age.

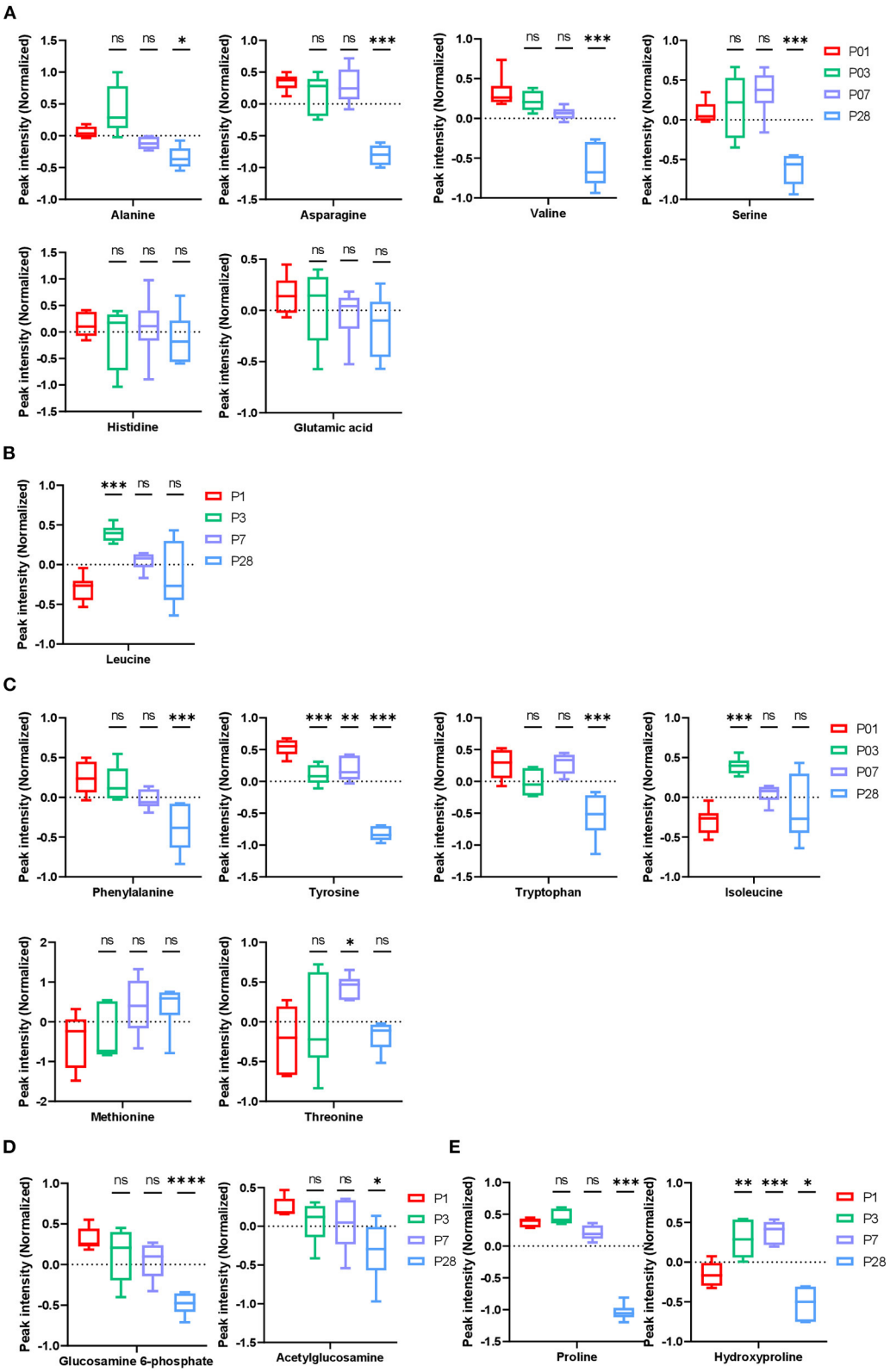

FIGURE 3 | Amino acid and collagen metabolism in neonatal pig hearts. **(A–D)** Metabolic profile of glucogenic amino acids **(A)**, ketogenic amino acids **(B)**, glucogenic/ ketogenic amino acids **(C)**, and glucosamine 6-phosphate **(D)**. **(E)** Metabolites in the collagen synthesis pathway. $^{*}p < 0.05$, $^{**}p < 0.01$, $^{***}p < 0.001$, $^{****}p < 0.0001$, one-way ANOVA with Tukey's Honestly Significant Difference Test. $n = 6$ hearts per age.

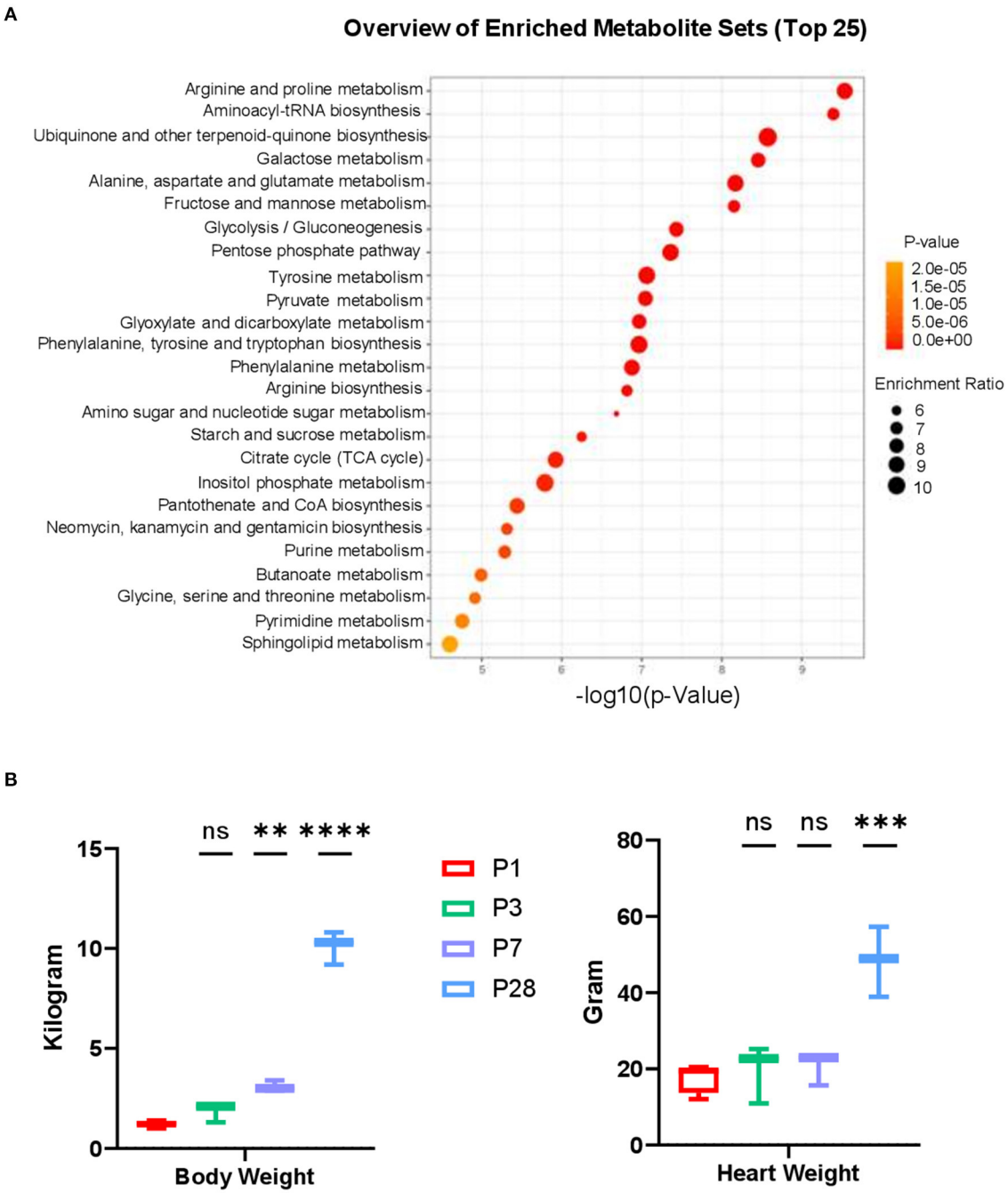

FIGURE 4 | Metabolic pathway analysis and cardiac attributes in neonatal pig hearts. **(A)** Metabolite set enrichment analysis on metabolites in the P1 and P28 hearts. **(B)** Body weight and Heart weight in the P1–P28 animals. $^{**}p < 0.01$, $^{***}p < 0.001$, $^{****}p < 0.0001$, one-way ANOVA with Tukey's Honestly Significant Difference Test. $n = 6$ hearts per age.

glycine and aspartate (**Figure 2A**) and an increased abundance of several intermediate metabolites (guanosine, adenosine, inosine, hypoxanthine, and ADP) in purine degradation pathways (**Figure 2B**) in P28 comparing to P1 hearts. This data is consistent with our previous observation that cardiomyocyte cell cycle is significantly reduced in P28 comparing to P1 hearts. Interestingly, abundance of ribose and ribose-5-phosphate was significantly increased in P28 comparing to P1 hearts (**Figure 2A**). Ribose as its 5-phosphate ester (ribose-5-phosphate) is typically produced from glucose by pentose phosphate pathway. Our data from the pathway analysis of glucose metabolism suggested that, while the intracellular glucose

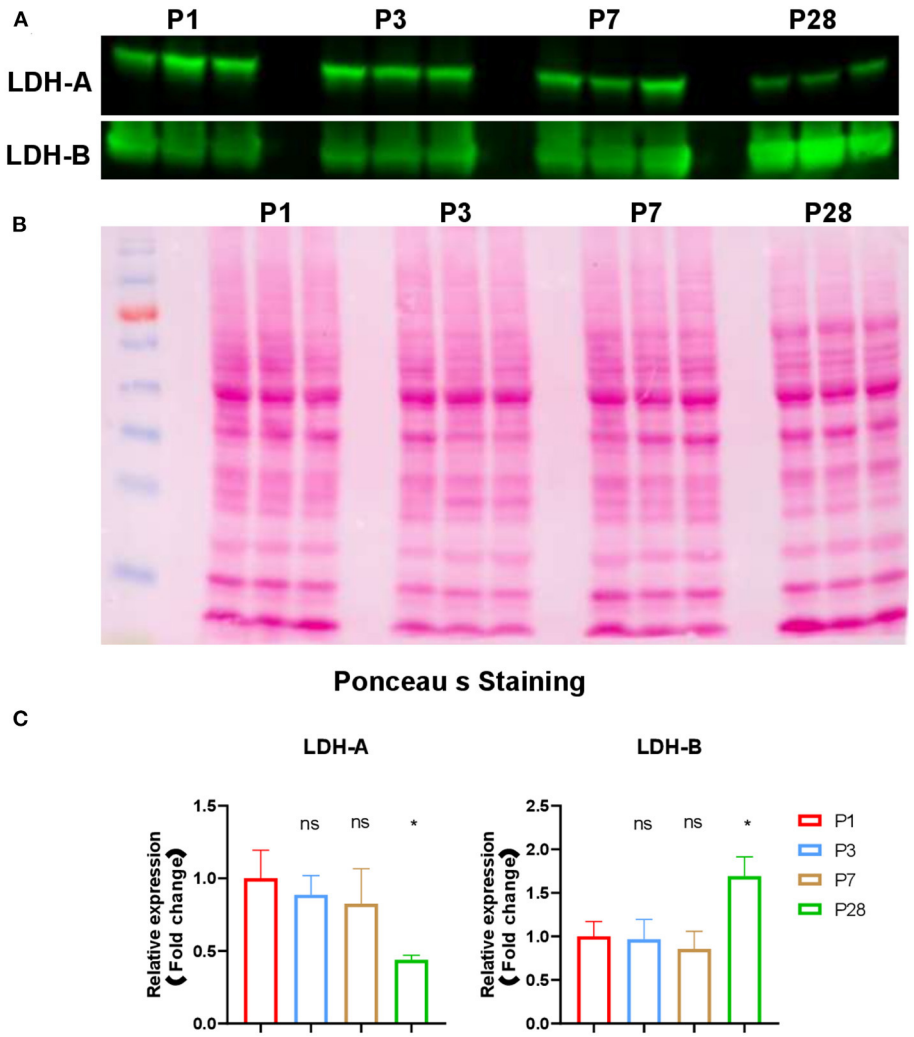

FIGURE 5 | Expression of LDHA and LDHB in neonatal pig hearts. **(A)** Western blot analysis of expression of LDHA and LDHB in in the four sets of heart samples (P1, P3, P7, and P28 hearts, $n = 3$ hearts per age). **(B)** Ponceau S staining of the blot to confirm equal protein loading. **(C)** Quantification of band intensity by western blot via densitometric analysis. *$p < 0.05$; one-way ANOVA with Tukey's Honestly Significant Difference Test.

level remained unchanged among P1, P3, P7, and P28 hearts, abundance of the intermediate metabolites in the pathways of glycolysis [glucose-6-phosphate, Phosphoenolpyruvate (PEP), and 3-phosphoglyceric acid] were decreased in P28 comparing to P1 hearts (**Figure 2C**), which implicates an overall reduced level of glycolysis. The decreased abundance of oxaloacetic acid and increased abundance of lactic acid in P28 hearts suggested that glycolysis rather than glucose oxidation is the main form of glucose metabolism in mature pig hearts (**Figure 2C**). Reduced level of the metabolism of lactose, sorbitol, and dulcitol (galactitol) was also observed, which implicates a reduced availability of the storage form of glucose when pig heart matures. Abundance of fructose remained stable during the postnatal heart development, and abundance of raffinose showed a tendency of reduction though it didn't reach the significant level (**Figure 2C**).

The abundance of glucogenic amino acids (alanine, asparagine, valine, and serine) significantly reduced in P28 comparing to P1 hearts, while no change was found for abundance of glutamic acids and histidine (**Figure 3A**). The biological implication of these changes to heart development is not clear since gluconeogenesis occurs mainly in liver and rarely in heart muscles. Abundance of leucine, a ketogenic amino acid, increased in P3 hearts followed by a tendency of reduction in P7 and P28 hearts (**Figure 3B**), implicating increased keto metabolism in early postnatal pig hearts. Abundance of ketogenic and glucogenic amino acids (phenylalanine, tyrosine, and tryptophan) were constantly reduced from P1 to P28 hearts. Abundance of isoleucine was increased in P3 hearts but gradually decreased in P7 and P28 hearts. In addition, abundance of threonine

TABLE 1 | List of metabolic features changed in the group comparisons.

	F value	*P* value	−Log10(p)	FDR	Fisher's LSD
Proline	254.4	4.31E-16	15.37	5.81E-14	P01–P07; P01–P28; P03–P07; P03–P28; P07–P28
Tyrosine	92.77	6.58E-12	11.18	4.44E-10	P01–P03; P01–P07; P01–P28; P03–P28; P07–P28
Dulcitol	68.41	1.08E-10	9.966	4.16E-09	P01–P28; P03–P28; P07–P28
Sorbitol	66.45	1.41E-10	9.852	4.16E-09	P01–P28; P03–P28; P07–P28
D-Mannitol	65.79	1.54E-10	9.813	4.16E-09	P01–P28; P03–P28; P07–P28
Glycylproline	56.8	5.76E-10	9.24	1.30E-08	P03–P01; P01–P28; P03–P07; P03–P28; P07–P28
Glycocyamine	38.57	1.66E-08	7.779	2.94E-07	P01–P03; P01–P07; P01–P28; P03–P28; P07–P28
Picolinic acid	38.36	1.74E-08	7.758	2.94E-07	P01–P03; P01–P07; P01–P28; P03–P28; P07–P28
Inosine	32.92	6.25E-08	7.204	8.69E-07	P28–P01; P28–P03; P28–P07
Asparagine	32.8	6.44E-08	7.191	8.69E-07	P01–P28; P03–P28; P07–P28
5-Aminolevulinic acid	31.03	1.01E-07	6.994	1.18E-06	P03–P01; P07–P01; P01–P28; P03–P28; P07–P28
Valine	30.91	1.05E-07	6.98	1.18E-06	P01–P07; P01–P28; P03–P28; P07–P28
Hydroxyproline	29.8	1.41E-07	6.852	1.46E-06	P03–P01; P07–P01; P01–P28; P03–P28; P07–P28
Agmatine	28.43	2.06E-07	6.687	1.98E-06	P01–P07; P01–P28; P03–P07; P03–P28; P07–P28
2-Deoxyadenosine	28.04	2.30E-07	6.639	2.07E-06	P28–P01; P28–P03; P28–P07
Cytidine	26.3	3.82E-07	6.418	3.22E-06	P03–P01; P07–P01; P28–P01; P07–P03; P28–P03
Cytosine	25.4	5.03E-07	6.299	3.87E-06	P03–P01; P07–P01; P28–P01; P07–P03; P28–P03; P28–P07
D-Ribose 5-phosphate	25.32	5.16E-07	6.288	3.87E-06	P07–P01; P28–P01; P28–P03; P28–P07
Dimethylglycine	24.24	7.25E-07	6.14	5.15E-06	P01–P28; P03–P28; P07–P28
2-Aminobutyric acid	23.97	7.88E-07	6.104	5.32E-06	P01–P28; P03–P28; P07–P28
Pipecolinic acid	23.51	9.16E-07	6.038	5.89E-06	P03–P01; P03–P07; P03–P28
Oxaloacetic acid	23.32	9.76E-07	6.011	5.99E-06	P01–P28; P03–P28; P07–P28
N-Acetylornithine	22.89	1.13E-06	5.949	6.61E-06	P03–P01; P07–P01; P28–P01; P28–P03; P28–P07
4-Aminobutyric acid	22.62	1.23E-06	5.91	6.92E-06	P01–P07; P01–P28; P03–P07; P03–P28; P07–P28
Norvaline	21.03	2.13E-06	5.671	1.15E-05	P03–P01; P01–P07; P28–P01; P03–P07; P28–P07
Sarcosine	16.38	1.30E-05	4.885	6.76E-05	P03–P01; P01–P28; P03–P07; P03–P28; P07–P28
N-Acetyl-D-galactosamine	15.73	1.73E-05	4.763	8.63E-05	P01–P07; P01–P28; P03–P07; P03–P28; P07–P28
Deoxycytidine	15.41	1.99E-05	4.702	9.12E-05	P07–P01; P07–P03; P28–P03; P07–P28
Hypoxanthine	15.41	1.99E-05	4.701	9.12E-05	P28–P01; P28–P03; P28–P07
Serine	15.37	2.03E-05	4.693	9.12E-05	P01–P28; P03–P28; P07–P28
Dopamine	14.92	2.48E-05	4.605	0.000108	P28–P01; P28–P03; P28–P07
Glucose 6-phosphate	14.81	2.61E-05	4.584	0.00011	P01–P03; P01–P07; P01–P28; P03–P28; P07–P28
Glutamine	14.31	3.28E-05	4.484	0.000134	P28–P01; P28–P03; P28–P07
Quinolinic acid	14.2	3.46E-05	4.461	0.000137	P03–P01; P07–P01; P28–P01; P03–P07; P03–P28
Tryptophan	13.78	4.21E-05	4.376	0.000162	P01–P28; P07–P03; P03–P28; P07–P28
Glucosamine 6-phosphate	13.65	4.49E-05	4.348	0.000168	P01–P28; P03–P28; P07–P28
Alanine	12.55	7.72E-05	4.113	0.000282	P03–P01; P01–P28; P03–P07; P03–P28
Guanosine	12.06	9.95E-05	4.002	0.000353	P07–P01; P28–P01; P28–P03; P28–P07
Betaine	11.81	0.000114	3.945	0.000393	P01–P03; P01–P07; P01–P28
Xanthosine	11.32	0.000147	3.832	0.000497	P07–P01; P28–P01; P28–P03; P28–P07
Uridine	11.03	0.000173	3.763	0.000568	P07–P01; P28–P01; P07–P03; P28–P03
Phenylalanine	9.948	0.000319	3.496	0.001021	P01–P07; P01–P28; P03–P28; P07–P28
9-Octadecynoic acid	9.915	0.000325	3.488	0.001021	P01–P07; P28–P01; P03–P07; P28–P03; P28–P07
5-Hydroxyindoleacetic acid	9.867	0.000334	3.476	0.001026	P01–P28; P03–P28; P07–P28
Asymmetric dimethylarginine	9.779	0.000352	3.453	0.001057	P01–P03; P01–P07; P28–P03; P28–P07
Leucine	9.707	0.000368	3.435	0.001068	P03–P01; P07–P01; P03–P07; P03–P28
Isoleucine	9.688	0.000372	3.43	0.001068	P03–P01; P07–P01; P03–P07; P03–P28
Pyroglutamic acid	9.597	0.000392	3.406	0.001086	P28–P01; P28–P03; P28–P07
Amiloride	9.589	0.000394	3.404	0.001086	P28–P01; P28–P03; P28–P07
Nicotinamide	9.361	0.000452	3.345	0.001198	P28–P01; P28–P03; P28–P07

(Continued)

TABLE 1 | Continued

	F value	*P* value	−Log10(p)	FDR	Fisher's LSD
Suberic acid	9.36	0.000452	3.345	0.001198	P28–P01; P28–P03; P28–P07
Decanoylcarnitine	8.03	0.001046	2.981	0.002715	P28–P01; P28–P03; P28–P07
Adenine	7.858	0.001171	2.931	0.002983	P28–P01; P28–P03; P28–P07
Indole-3-lactic acid	7.697	0.001304	2.885	0.00326	P01–P28; P03–P28; P07–P28
Citrulline	7.227	0.001797	2.746	0.004351	P07–P01; P07–P03; P28–P03; P07–P28
Aspartate	7.22	0.001805	2.744	0.004351	P01–P28; P03–P28; P07–P28
Valeric acid	7.094	0.00197	2.706	0.004666	P01–P28; P03–P28; P07–P28
Methylguanidine	7.054	0.002026	2.693	0.004716	P28–P01; P28–P03; P28–P07
Amino valerate	6.827	0.002379	2.624	0.005443	P01–P03; P01–P07; P01–P28
Adenosyl-L-homocysteine	5.635	0.005752	2.24	0.012942	P07–P01; P07–P03; P28–P03
Taurine	5.285	0.007569	2.121	0.016751	P01–P03; P28–P03
Adenosine	5.119	0.008637	2.064	0.018289	P28–P01; P28–P07
Cellobiose	5.114	0.008676	2.062	0.018289	P01–P28; P03–P28; P07–P28
Lactose	5.113	0.008683	2.061	0.018289	P01–P28; P03–P28; P07–P28
Acetylcholine	5.095	0.008806	2.055	0.018289	P03–P01; P28–P01; P03–P07; P28–P07
Acetylcarnitine	4.993	0.009565	2.019	0.019564	P03–P01; P07–P01
Ribose	4.681	0.012356	1.908	0.024896	P28–P01; P28–P03; P28–P07
2-Hydroxyphenylacetic acid	4.614	0.013069	1.884	0.025945	P01–P28; P03–P07; P03–P28
Xylose	4.525	0.014069	1.852	0.027527	P28–P01; P28–P03; P28–P07
3-hydroxybutyric acid	4.461	0.014851	1.828	0.028641	P01–P03; P01–P07; P28–P03; P28–P07
PEP	4.4	0.015639	1.806	0.029737	P01–P28; P07–P03; P07–P28
Trehalose	4.296	0.01709	1.767	0.03172	P01–P28; P03–P28
Lactate	4.292	0.017152	1.766	0.03172	P28–P01; P28–P03; P28–P07
NADPH	4.265	0.017552	1.756	0.03202	P28–P01; P07–P03; P28–P03
2-Deoxyuridine	4.167	0.019096	1.719	0.034373	P03–P01; P07–P01; P28–P01
Acetylglucosamine	3.881	0.024523	1.61	0.043006	P01–P28; P03–P28
Homoserine	3.866	0.024848	1.605	0.043006	P07–P01; P07–P03; P07–P28
Threonine	3.866	0.024848	1.605	0.043006	P07–P01; P07–P03; P07–P28
ADP	3.725	0.028165	1.55	0.048129	P01–P03

was increased in P7 followed by a reduction in P28 hearts (**Figure 3C**).

The abundance of glucosamine 6-phosphate (GLCN6P) was reduced in P28 hearts comparing to P1 hearts (**Figure 3D**). Fructose 6-phosphate and glutamine are catalyzed by glutamine-fructose 6-phosphate amidotransferase to form GLCN6P, which is then converted to UDP-N-acetylglucosamine (UDP-GlcNAC) through a series of enzyme-driven reactions (8). UDP-GlcNAc is an important posttranslational protein modification on Ser/Thr sites driven by O-GlcNAc transferase (OGT) and this modification has been shown to contribute to cardiomyocyte cell cycle regulation in mouse hearts (9). However, the role of this posttranslational modification (O-glycosylation) in pig hearts has not been reported.

Collagen triple helix is one of the few proteins that contain the amino acid hydroxyproline, therefore, hydroxyproline has been used to estimate total collagen content and concentration in mouse and human tissues (10, 11). It was reported that collagen content increases constantly in developing pig hearts during the first 8 weeks (12). In human hearts, the total amount of collagen increases with age (10). However, the ratio of total collagen to total protein is high after birth and it gradually declines during development, with the total collagen/total protein ratio reaching normal levels around 5 months after birth (10). In the current study, abundance of all metabolites was normalized by total protein content. The abundance of hydroxyproline was high in P1, P3, and P7 hearts comparing to the P28 heart (**Figure 3E**). This data suggests a high ratio of collagen to total protein in the young pig hearts which is consistent with the observations from human hearts.

Functional batch annotation and ontology enrichment analysis identified important representative metabolite ontology categories based on KEGG pathway. The highly enriched metabolites were found in the amino acid and protein metabolism pathways (**Figure 4A**). Along with the increased body weight (**Figure 4B**), the average heart weight of the neonatal pigs was 17.82 ± 1.94 (for P1), 19.63 ± 4.41 (for P3), 20.61 ± 2.44 (for P7), and 48.39 ± 5.32 (for P28) grams, indicating an rapidly increased mass between postnatal day 7 and 28 (**Figure 4B**). We have previously reported that cardiomyocyte cell cycle activity in neonatal pig hearts declines abruptly (i.e., by ∼70%) in the first 7 days after birth. Taken

together, these data implicate a massive hypertrophic growth between P7 and P28 when cardiomyocytes withdrawal from cell cycle. The proliferating cells typically require massive anabolic program to generate biological macromolecules such as proteins and nucleotides. Therefore, the overall reduced abundance of different amino acids in P28 comparing to P1 hearts (**Figures 3A–E**) likely reflects an increased biosynthesis of proteins to accommodate the needs for cell proliferation in P1 hearts, while protein synthesis declines in P28 when proliferation stops.

DISCUSSION

Our data suggested an active anabolism of nucleotide and proteins in the neonatal pig hearts when cardiomyocytes retain some cell cycle activities. Reduced ratio of total collagen to total protein, active posttranslational protein modification, and a metabolic switch from glucose to fatty acids were also observed when cardiomyocytes become mature. To our knowledge, this is the first study to determine metabolic profile in developing pig hearts.

An important finding of current study is the discovery of the transition from carbohydrate to fatty acid metabolism during postnatal heart development (**Figure 2C**). The metabolic switch from glycolysis to phosphorylated oxidation of fatty acids in the postanal hearts has been reported in other mammals (13, 14). The gradually increased abundance of acetylcarnitine in P3 and P7 hearts comparing to P1 hearts likely reflects an increased level of fatty acid β-oxidation when cardiomyocytes become mature. Another interesting finding is that the abundance of several metabolites in extracellular matrix (ECM) remodeling was changed from P1 to P28. For example, a reduced abundance of GLCN6P was observed in P28 hearts compared to P1 hearts (**Figure 3D**). GLCN6P is converted to UDP-GlcNAC through a series of enzyme-driven reactions (8). UDP-GlcNAc is an important substrate for the synthesis of proteoglycans, hyaluronan, glycolipid, et al. (15). We also observed an increased abundance of hydroxyproline in P1, P3, and P7 hearts compared to the P28 heart (**Figure 3E**). Hydroxyproline has been used as a marker for estimating total collagen content and concentration in mouse and human tissues (10, 11). Taken together, our data suggest an active ECM remodeling in the postnatal pig heart.

Despite the reduced abundance of intermediates in glycolysis pathway, the abundance of lactic acid was increased in P28 pig hearts compared to P1 pig hearts (**Figure 2C**). This data are consistent with the observation that lactic acid is gradually increased in postnatal mouse hearts (4). Intracellular lactic acid can be produced from pyruvate during the last step of glycolysis which is a reversible conversion catalyzed by lactate dehydrogenases (LDHs) (16), or be obtained from peripheral circulation by monocarboxylic acid cotransporters (MCTs) (17, 18). LDHs are homo- or hetero-tetramers assembled from two different subunits (M and H), which are encoded by two separate genes, LDHA (M) and LDHB (H), respectively (19). LDH1 is composed of four LDHB subunits and favors the conversion from lactate to pyruvate, and LDH5 is composed of four LDHA subunits and favors the conversion from pyruvate to lactate (20). Expression of LDHA is induced during physiological (e.g., running and swimming) and pathological (e.g., pressure overload induced by thoracic aortic constriction) cardiac hypertrophy (21, 22). We performed western blot experiments to check the expression of LDHs in the postnatal pig hearts. Our data showed that expression of LDHA was decreased and LDHB was increased in P28 hearts comparing to P1, P3, and P7 hearts (**Figures 5A–C**). During cardiac maturation, lactic acid oxidation and glycolysis were reduced, and fatty acid oxidation became the main energy supply (14). However, the ratio of LDH to LDHA continued to rise during the first month after birth in guinea pigs (23), which is consistent with our observations in postnatal pig hearts. Detailed mechanisms underlying the changes of LDHA and LDHB in postnatal hearts were not clear. Considering that glycolysis is reduced in P28 hearts in the current study, we speculate that the increased lactic acid is likely due to increased uptake from peripheral blood.

It is worthy to note that time window for these metabolic switch matches the window that neonatal pig hearts lose their regeneration capacity post injury (2). Recent data showed that simulating the postnatal switch in metabolic substrates from carbohydrates to fatty acids promotes cell cycle arrest in human cardiomyocytes (24). However, it was also reported that stimulation of glycolysis promotes cardiomyocyte proliferation in zebrafish (25). Thus, far, it is not clear if the metabolic switches we observed in postnatal pig hearts contribute to cardiomyocyte cell cycle arrest. Future studies are warranted to explore whether manipulating metabolic pathways enhances myocardial regeneration and repair capacities in neonatal and adult pigs.

The current study has several limitations. First, the whole heart samples were used for this study. Although the mass or volume of cardiomyocytes dominates in the heart, non-myocytes are more abundant than cardiomyocytes. The challenges of cultivating the freshly isolated pig cardiomyocytes precludes the uses of highly purified cardiomyocytes for LC-MS/MS analysis. Second, this is a descriptive study investigating the abundances of different metabolites at different stages of postnatal heart development (P1, P3, P7, and P28) in pigs. The evaluation of activity of certain metabolic pathways was based on the abundances of different metabolites in these pathways. Further studies, e.g., metabolic flux measurements, enzyme activity assays, and uptake of metabolites, are warranted to confirm the data from the metabolomic analysis.

DATA AVAILABILITY STATEMENT

The datasets presented in this study can be found in online repositories (https://data.mendeley.com; DOI: 10.17632).

ETHICS STATEMENT

The animal study was reviewed and approved by Institutional Animal Care and Use Committee of the Mayo Clinic.

AUTHOR CONTRIBUTIONS

PL, FL, LT, WZha, and YJ collected data and performed data analysis. HG and WZhu designed the project and wrote the manuscript. PL and FL revised the manuscript. All authors contributed to the article and approved the submitted version.

FUNDING

This work was supported by NIH grant (R01HL142627) and AHA TPA Award (20TPA35490001) to WZhu.

REFERENCES

1. Porrello ER, Mahmoud AI, Simpson E, Hill JA, Richardson JA, Olson EN, et al. Transient regenerative potential of the neonatal mouse heart. *Science.* (2011) 331:1078–80. doi: 10.1126/science.1200708
2. Zhu W, Zhang E, Zhao M, Chong Z, Fan C, Tang Y, et al. Regenerative potential of neonatal porcine hearts. *Circulation.* (2018) 138:2809–16. doi: 10.1161/CIRCULATIONAHA.118.034886
3. Lopaschuk GD, Jaswal JS. Energy metabolic phenotype of the cardiomyocyte during development, differentiation, postnatal maturation. *J Cardiovasc Pharmacol.* (2010) 56:130–40. doi: 10.1097/FJC.0b013e3181e74a14
4. Talman V, Teppo J, Poho P, Movahedi P, Vaikkinen A, Karhu ST, et al. Molecular atlas of postnatal mouse heart development. *J Am Heart Assoc.* (2018) 7:e010378. doi: 10.1161/JAHA.118.010378
5. Jasbi P, Shi X, Chu P, Elliott N, Hudson H, Jones D, et al. Metabolic profiling of neocortical tissue discriminates Alzheimer's disease from mild cognitive impairment, high pathology controls, normal controls. *J Proteome Res.* (2021) 20:4303–17. doi: 10.1021/acs.jproteome.1c00290
6. Zhu W, Zhao M, Mattapally S, Chen S, Zhang J. CCND2 overexpression enhances the regenerative potency of human induced pluripotent stem cell-derived cardiomyocytes: remuscularization of injured ventricle. *Circ Res.* (2018) 122:88–96. doi: 10.1161/CIRCRESAHA.117.311504
7. Lane AN, Fan TW. Regulation of mammalian nucleotide metabolism and biosynthesis. *Nucleic Acids Res.* (2015) 43:2466–85. doi: 10.1093/nar/gkv047
8. Kolwicz SC Jr, Purohit S, Tian R. Cardiac metabolism and its interactions with contraction, growth, and survival of cardiomyocytes. *Circ Res.* (2013) 113:603–16. doi: 10.1161/CIRCRESAHA.113.302095
9. Magadum A, Singh N, Kurian AA, Sharkar MTK, Chepurko E, Zangi L. Ablation of a single N-Glycosylation site in human FSTL 1 induces cardiomyocyte proliferation and cardiac regeneration. *Mol Ther Nucleic Acids.* (2018) 13:133–43. doi: 10.1016/j.omtn.2018.08.021
10. Marijianowski MM, Van Der Loos CM, Mohrschladt MF, Becker AE. The neonatal heart has a relatively high content of total collagen and type I collagen, a condition that may explain the less compliant state. *J Am Coll Cardiol.* (1994) 23:1204–8. doi: 10.1016/0735-1097(94)90612-2
11. Samuel CS. Determination of collagen content, concentration, and sub-types in kidney tissue. *Methods Mol Biol.* (2009) 466:223–35. doi: 10.1007/978-1-59745-352-3_16
12. Mccormick RJ, Musch TI, Bergman BC, Thomas DP. Regional differences in LV collagen accumulation and mature cross-linking after myocardial infarction in rats. *Am J Physiol.* (1994) 266:H354–9. doi: 10.1152/ajpheart.1994.266.1.H354
13. Lopaschuk GD, Spafford MA, Marsh DR. Glycolysis is predominant source of myocardial ATP production immediately after birth. *Am J Physiol.* (1991) 261:H1698–705. doi: 10.1152/ajpheart.1991.261.6.H1698
14. Makinde AO, Kantor PF, Lopaschuk GD. Maturation of fatty acid and carbohydrate metabolism in the newborn heart. *Mol Cell Biochem.* (1998) 188:49–56. doi: 10.1023/A:1006860104840
15. Tran DH, Wang ZV. Glucose metabolism in cardiac hypertrophy and heart failure. *J Am Heart Assoc.* (2019) 8:e012673. doi: 10.1161/JAHA.119.012673
16. Liu J, Chen G, Liu Z, Liu S, Cai Z, You P, et al. Aberrant FGFR tyrosine kinase signaling enhances the warburg effect by reprogramming LDH isoform expression and activity in prostate cancer. *Cancer Res.* (2018) 78:4459–70. doi: 10.1158/0008-5472.CAN-17-3226
17. Halestrap AP, Wang X, Poole RC, Jackson VN, Price NT. Lactate transport in heart in relation to myocardial ischemia. *Am J Cardiol.* (1997) 80:17A−25A. doi: 10.1016/S0002-9149(97)00454-2
18. Mccullagh KJ, Poole RC, Halestrap AP, Tipton KF, O'brien M, Bonen A. Chronic electrical stimulation increases MCT1 and lactate uptake in red and white skeletal muscle. *Am J Physiol.* (1997) 273:E239–46. doi: 10.1152/ajpendo.1997.273.2.E239
19. Zdralevic M, Marchiq I, De Padua MMC, Parks SK, Pouyssegur J. Metabolic plasiticy in cancers-distinct role of glycolytic enzymes GPI, LDHs or membrane transporters MCTs. *Front Oncol.* (2017) 7:313. doi: 10.3389/fonc.2017.00313
20. Fritz PJ. Rabbit muscle lactate dehydrogenase 5; a regulatory enzyme. *Science.* (1965) 150:364–6. doi: 10.1126/science.150.3694.364
21. York JW, Penney DG, Weeks TA, Stagno PA. Lactate dehydrogenase changes following several cardiac hypertrophic stresses. *J Appl Physiol.* (1976) 40:923–6. doi: 10.1152/jappl.1976.40.6.923
22. Dai C, Li Q, May HI, Li C, Zhang G, Sharma G, et al. Lactate Dehydrogenase A governs cardiac hypertrophic growth in response to hemodynamic stress. *Cell Rep.* (2020) 32:108087. doi: 10.1016/j.celrep.2020.108087
23. Barrie SE, Harris P. Myocardial enzyme activities in guinea pigs during development. *Am J Physiol.* (1977) 233:H707–10. doi: 10.1152/ajpheart.1977.233.6.H707
24. Mills RJ, Titmarsh DM, Koenig X, Parker BL, Ryall JG, Quaife-Ryan GA, et al. Functional screening in human cardiac organoids reveals a metabolic mechanism for cardiomyocyte cell cycle arrest. *Proc Natl Acad Sci USA.* (2017) 114:E8372–81. doi: 10.1073/pnas.1707316114
25. Fukuda R, Marin-Juez R, El-Sammak H, Beisaw A, Ramadass R, Kuenne C, et al. Stimulation of glycolysis promotes cardiomyocyte proliferation after injury in adult zebrafish. *EMBO Rep.* (2020) 21:e49752. doi: 10.15252/embr.201949752

Conflict of Interest: The authors declare that the research was conducted in the absence of any commercial or financial relationships that could be construed as a potential conflict of interest.

Publisher's Note: All claims expressed in this article are solely those of the authors and do not necessarily represent those of their affiliated organizations, or those of the publisher, the editors and the reviewers. Any product that may be evaluated in this article, or claim that may be made by its manufacturer, is not guaranteed or endorsed by the publisher.

frontiers in Cardiovascular Medicine

ORIGINAL RESEARCH
published: 20 October 2021
doi: 10.3389/fcvm.2021.754254

Extracellular Vesicles Derived From Regeneration Associated Cells Preserve Heart Function After Ischemia-Induced Injury

Amankeldi A. Salybekov[1,2,3,4], Ainur Salybekova[4], Yin Sheng[4], Yoshiko Shinozaki[5], Keiko Yokoyama[5], Shuzo Kobayashi[2,3] and Takayuki Asahara[2,4]**

[1] Kidney Disease and Transplant Center, Shonan Kamakura General Hospital, Kamakura, Japan, [2] Shonan Research Institute of Innovative Medicine, Shonan Kamakura General Hospital, Kamakura, Japan, [3] Division of Regenerative Medicine, Department of Center for Clinical and Translational Science, Shonan Kamakura General Hospital, Kamakura, Japan, [4] Department of Advanced Medicine Science, Tokai University School of Medicine, Isehara, Japan, [5] Teaching and Research Support Core Center, Tokai University School of Medicine, Isehara, Japan

OPEN ACCESS

Edited by:
Zhen-Ao Zhao,
Hebei North University, China

Reviewed by:
Jiacheng Sun,
University of Alabama at Birmingham, United States
Jing Mu,
Georgia State University, United States

***Correspondence:**
Amankeldi A. Salybekov
a.salybekov@shonankamakura.or.jp
Takayuki Asahara
t_asahara@shonankamakura.or.jp

Specialty section:
This article was submitted to Cardiovascular Biologics and Regenerative Medicine, a section of the journal Frontiers in Cardiovascular Medicine

Received: 06 August 2021
Accepted: 22 September 2021
Published: 20 October 2021

Citation:
Salybekov AA, Salybekova A, Sheng Y, Shinozaki Y, Yokoyama K, Kobayashi S and Asahara T (2021) Extracellular Vesicles Derived From Regeneration Associated Cells Preserve Heart Function After Ischemia-Induced Injury. Front. Cardiovasc. Med. 8:754254. doi: 10.3389/fcvm.2021.754254

Under vasculogenic conditioning, pro-inflammatory cell subsets of peripheral blood mononuclear cells (PBMCs) shift their phenotype to pro-regenerative cells such as vasculogenic endothelial progenitor cells, M2 macrophages, and regulatory T cells, collectively designated as regeneration-associated cells (RACs). In this study, we evaluated the therapeutic efficacy of RAC-derived extracellular vesicles (RACev) compared to mesenchymal stem cell-derived EVs (MSCev) in the context of myocardial ischemia reperfusion injury (M-IRI). Human PBMCs were cultured with defined growth factors for seven days to harvest RACs. RACev and MSCev were isolated via serial centrifugation and ultracentrifugation. EV quantity and size were characterized by nanoparticle tracking analysis. *In vitro*, RACev markedly enhanced the viability, and proliferation of human umbilical vein endothelial cells in a dose-dependent manner compared to MSCev. Notably, systemic injection of RACev improved cardiac functions at 4 weeks, such as fractional shortening, and protection from mitral regurgitation than the MSCev-treated group. Histologically, the RACev-transplanted group showed less interstitial fibrosis and enhanced capillary densities compared to the MSCev group. These beneficial effects were coupled with significant expression of angiogenesis, anti-fibrosis, anti-inflammatory, and cardiomyogenesis-related miRs in RACev, while modestly in MSCev. *In vivo* bioluminescence analysis showed preferential accumulation of RACev in the IR-injured myocardium, while MSCev accumulation was limited. Immune phenotyping analysis confirmed the immunomodulatory effect of MSCev and RACev. Overall, repetitive systemic transplantation of RACev is superior to MSCev in terms of cardiac function enhancements via crucial angiogenesis, anti-fibrosis, anti-inflammation miR delivery to the ischemic tissue.

Keywords: extracellular vesicles, regeneration-associated cells, myocardial ischemia-reperfusion injury, miR, angiogenesis

INTRODUCTION

Extracellular vesicles (EVs), as messengers, maintain intercellular communication by delivering various types of proteins, lipids, and genetic materials such as DNA, mRNA, and microRNAs (miRs) to recipient cells (1). EVs are highly heterogeneous in terms of their size, origin, morphology, function, and genetic material carried (1). As EV composition/contents are different under physiological and pathological conditions, EVs are widely used as disease biomarkers or treatment agents based on their unique features (2–4).

Preclinical studies have demonstrated that EVs isolated from endothelial progenitor cells (EPCs), cardiac progenitor cells, and mesenchymal stem cells (MSCs) have strong therapeutic potential compared to their parental cells (5–8). In previous study by Lai et al. showed that MSC-derived exosomes or extracellular vesicles (MSCexo/ev) reduced the infarct size in a mouse model of myocardial ischemia/reperfusion injury (M-IRI) (9). MSCev are also known to exert cardioprotective effects by delivering anti-inflammatory and anti-apoptosis miRs and proteins, resulting in preserved cardiac function after ischemic injury (10, 11).

Previously, we have shown that under vasculogenic conditioning, pro-inflammatory cell subsets of peripheral blood mononuclear cells (PBMCs) such as type 1 macrophages (M1Φ), T cells, and EPCs beneficially shifted their phenotype to pro-regenerative cells such as vasculogenic EPCs, M2 macrophages, and regulatory T cells, which are collectively designated as regeneration-associated cells (RACs) (12, 13). Furthermore, systemic transplantation of a small number of RACs ($1 * 10^5$) significantly improved cardiac function by increasing microvascular density (CD31), strong anti-inflammatory action (type 2 macrophage (M2Φ) and regulatory T cells (Treg) infiltration), and initiation of cardiomyogenesis in a rat myocardial infarction model (12).

In this study, we attempted to elucidate the therapeutic efficacy of RAC-derived EVs (RACev) in the context of myocardial ischemia reperfusion injury (M-IRI).

MATERIALS AND METHODS

RAC and MSC Culture

As indicated by the Tokai University School of Medicine Institutional Review Board, human PBMCs were isolated from healthy human volunteers after obtaining written informed consent. Peripheral blood (30–50 mL) was drawn using a heparinized syringe. Briefly, cells were cultured with five growth factor-supplemented culture medium, Stem Line II (Sigma-Aldrich, St. Louis, MO), with 100 ng/mL recombinant human (rh) stem cell factor (SCF), 100 ng/mL Flt-3 ligand (FL3L), 20 ng/mL thrombopoietin (TPO), 50 ng/mL VEGF, and 20 ng/mL interleukin-6 (IL-6) (all from Peprotech, Inc. (Rocky Hill, NJ, USA), and penicillin/streptomycin (100 U/100 μg/mL) (Gibco). PBMCs at a density of $10 * 10^7$ cells were cultured for seven days on a 10-cm dish (Sumitomo Bakelite Co. Tokyo. Japan) in a 37°C incubator with a humidified atmosphere of 5% CO_2, as described earlier (12, 14). Bone marrow-derived MSCs (Lonza, Japan) passage 3–5 were used for all *in vitro* and *in vivo* studies.

Extracellular Vesicles Isolation and Quantification Labeling

Immediately after harvesting RACs and MSCs, the cells were seeded in X-*vivo* 15 (Lonza, for RACs) supplemented with 5% exosome-depleted FBS (Gibco) and in DMEM supplemented with 5% FBS (Gibco, for MSCs) for 48 h. Conditioned culture medium (CCM) was carefully collected, and the cells were removed by centrifugation at 300 × *g* at 4°C for 10 min. Then, larger apoptotic bodies and microvesicles were removed by centrifugation at 2,000 × *g* for 20 min at 12°C, followed by filtration through a 0.2 μm filter (Millipore, Merck) to remove particles larger than 200 nm. The filtered CCM was transferred to new ultracentrifuge tubes (Ultra clear Beckman cat# 344059, rotor type is Ti40SW, Beckman Coulter), which were then sealed and ultracentrifuged at 174 000 × *g* for 110 min at 4°C to pellet the EVs. Then, EVs number and size was measured using nanoparticle tracking analysis with NanoSight NS500® (Malvern Panalytical, UK) according to manufacturer manual. Morphological characteristics of extracellular vesicles was verified common transmission electron microscopy method (JEM-1400, Jeol. Co.Ltd, Japan).

Flow Cytometry Analysis of EVs and Immune Cells

All EV flow cytometry analysis experiments were performed using a 13-color, 3-laser DxFlex Flow Cytometer, equipped with 405 nm, 488 nm, and 638 nm lasers (Beckman Coulter, Brea, CA). For analyzing small EVs, the configuration was modified for violet side scatter (VSSC) detection. Briefly, the 405/10 VSSC filter was moved to the V450 channel in the wavelength-division multiplexing (WDM), and the detector configuration was updated using CytExpert software to assign the VSSC channel within the WDM. Before data acquisition, cleaning was performed using with FlowClean and water passed through a 10 μm filter to reduce the debris and background noise. For EV characterization, fluorophore-conjugated antibodies against CD9 (PE, #312106), CD63 (PE, #353004), Alix (Alexa 594, #634504), and Hsp-70 (Alexa 488, #648003) were used (all from BioLegend) according to the manufacturer's instructions. Latex beads of different sizes (100 nm and 200 nm, Beckman Coulter) were used for comparison with EVs and to adjust the flow cytometry acquisition voltages.

The weight of spleen was evaluated before cell isolation. Peripheral blood and spleen-derived mononuclear cells were isolated by density gradient centrifugation using Lymphocyte Separation Solution (d = 1.077; Nakalai Tesque, Kyoto, Japan), as previously reported (12–14). Isolated PBMC and spleen MNCs incubated with FcR blocking (Miltenyi Biotec, Germany) to reduce non-specific antibody bindings. Briefly, cell surface markers staining was carried out using CD3-FITC (cat#401606), CD4-PE/Cy7 (cat#400126), CD8a-AlexaFlour 647 (cat#400130, CD11b/c-PerCP/Cy5.5 (cat#400258), CD161-PE (cat# 205604) (all antibodies from Biolegend CA, USA) at room temperature

for 20 min, following which cells were washed twice with 2 mmol/L EDTA/0.2% BSA/PBS buffer. The data were acquired on a FACS Verse (BD Biosciences) and analyzed with FlowJo software, version 10.7.

Cell Proliferation and EV Internalization Assays

For the cell proliferation assay, human umbilical vein endothelial cells (HUVECs) (Lonza, Japan) at passage 3–4 were used. Briefly, HUVECs were harvested and incubated with Cytopainter dye (Cat# ab176735) at 37°C for 10–30 min. The working dye solution was removed by two rounds of centrifugation and the labeled cells were seeded with the control group (HUVEC only). After filtration of CCM through a 0.22μm filter (Millipore Merck), 2 μM CM-DiI dye (C7000, Thermo Fisher) was added to the CCM and left in incubator for 30 min prior to ultracentrifugation at 174 000 × g for 110 min at 4 °C. The labeled EVs were enriched at the bottom of the tube and were washed twice by ultracentrifugation in 1X phosphate-buffered saline (PBS) (15). Then, RACev and MSCev added to labeled HUVEC in a dose-dependent manner (EVs-derived from 2.5 or 5 * 10^5 either RACs or MSCs). After 2 days, the cells were isolated and analyzed using flow cytometry (BD Biosciences, FACS Verse).

For the invasion assay, HUVECs were stained with Hoechst (Cat #33342) dye according to the manufacturer's instructions. Finally, pure labeled EVs were mixed with 3 × 10^5 HUVECs and analyzed under a confocal microscope (Zeiss LSM 880, Germany).

Myocardial Ischemia-Reperfusion Injury

All animal experiments were performed in accordance with the Tokai University School of Medicine Animal Care and Use Committee (approval # I-20056) and were based on the Guide for the Care and Use of Laboratory Animals (National Research Council, Japan). Male Lewis rats (6–10 weeks of age) weighing 150–250 g, were purchased from Charles River Laboratories (Yokohama, Japan) through Oriental Yeast Co. Ltd. (Tokyo, Japan). Animals were maintained under standard conditions (20 ± 2°C, relative humidity 50–60%, 12 h/12 h light/dark cycles), and were monitored daily by the Animal Support Center for Medical Research and Education at Tokai University School of Medicine. The animals had *ad libitum* access to water and food.

For the M-IRI model, the animals were anesthetized with 3–4% sevoflurane (Maruishi Pharmaceutical Co., Ltd. Japan), orally intubated, and respired using a rodent ventilator at 15 mL/kg, 65–70 times/min (Harvard Apparatus, USA) (16). After left-sided thoracotomy, myocardial ischemia reperfusion injury was induced by temporary occlusion of the left anterior descending artery for 30 min and subsequent reperfusion. Immediately after thorax closure, animals underwent transplantation of PBS-diluted RACev and MSCev (EVs derived from 5 * 10^5 either RACs or MSCs) via the tail vein using a 24G angiocatheter (Terumo, Japan) as described previously (12). After the completion of each experiment, the animals were sacrificed by an overdose of sevoflurane 5%; after confirming euthanasia, vital organs such as the lung and aorta were harvested.

Echocardiography Assessment

Echocardiography (Aloka Co., Ltd., Tokyo, Japan) with a 3.5-MHz probe was used to determine the left ventricular end-diastolic dimension (LVDD), end-systolic dimension (LVDS), severity of mitral regurgitation (MR), the height of the E-wave and A-wave, and the size of the left atrium and ascending aorta. These measurements were repeated before M-IRI induction (baseline) and then weekly following M-IRI injury for 4 weeks. The severity of mitral regurgitation was defined by the size of the regurgitation flow reaching the left atrial wall (severe, score 3), 2/3 of the left atrium (moderate, score 2), and 1/3 of the left atrium (mild or trace, score 1). Fractional shortening (%FS) was defined as (LVDD-LVDS)/LVDD × 100 (12, 16).

Immunohistochemistry Analysis

The heart was perfused with heparinized PBS (1,000 U/500 mL) and fixed overnight with 4% paraformaldehyde (PFA, #163-20145, Fujifilm. Co. Ltd.), embedded in paraffin, and cut into 3- to 4-mm-thick sections. The sections were stained with picrosirius red (Muto Co., Ltd. Japan) to determine the size of interstitial fibrosis, as described previously (11). The immunohistochemistry data were evaluated from 3 to 5 high-power fields per section in a blinded manner using Image J (version 1.51, National Institutes of Health). The sections were blocked in an avidin and streptavidin complex and incubated with isolectin B4-FITC (1:100) (Invitrogen, CA, USA) to evaluate the infarcted tissue microvascular density (MVD) (12). To discriminate auto-fluorescence, spectral analysis of stained tissue sections was performed using a Carl Zeiss LSM880 meta confocal microscope (Oberkochen, Germany).

EV Tracking

The CCM was stained with DiI, as mentioned above (in section Cell Proliferation and EV Internalization Assays). Briefly, labeled MSCev and RACev, and the control solution (saline) were injected via the tail vein using a 24G angiocatheter (Terumo) immediately after releasing the ligated left anterior descending artery. After 3.5 h of injection, the animals were sacrificed and the heart was excised for further EV tracking analysis as described elsewhere (15, 17). Briefly, in *vivo* imaging system (IVIS) Lumina III (Perkin Elmer, USA) was used to analyze EV entrapment at the site of injury. DiI dye excitation and emission wavelength filters were set at 520 nm and 570 nm, respectively (15). Frozen heart sections of 6 μm thickness were then analyzed under a LSM 880 confocal microscope (Carl Zeiss, Germany).

EV-Derived Total RNA Isolation, Library Preparation, and Sequencing

According to the manufacturer's protocol, CCM-derived small and large RNAs were fractionated using the miRNeasy mini kit (Qiagen, USA) and the RNeasy MinElute Cleanup Kit (Qiagen). Sequencing libraries were constructed according to the manufacturer' s protocols using the QIAseq™ miRNA Library Kit (Cat#331505, Qiagen, Hilden, Germany). Library quality was assessed with an Agilent Bioanalyzer using a High Sensitivity DNA chip (Agilent Technologies, Santa Clara, CA, USA). The pooled libraries were sequenced using NextSeq 500

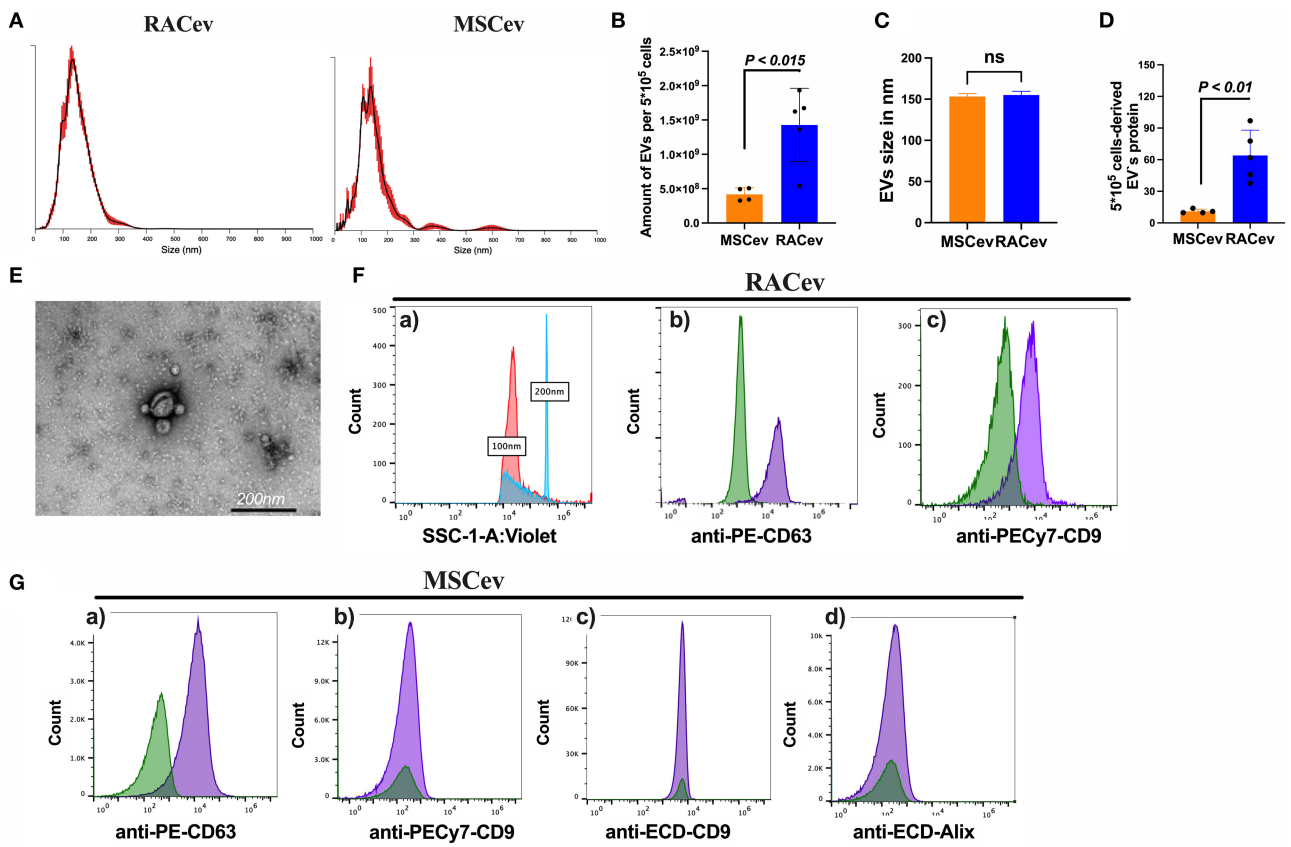

FIGURE 1 | Characterization of extracellular vesicles. **(A–C)** Nano tracking particle analysis of EV characteristics such as size and quantity. **(D)** Representative transmission-electron microscopy figures showing the lipid bilayer structure of EVs. Distinct EV biomarkers expression profiles such as CD9, CD63, and Alix of **(E,F)** RACev and **(G)** MSCev. Statistical significance was determined using Mann-Whitney U test. The results are presented as mean ± SEM (n = 4–7 per group).

(Illumina, Inc., San Diego, CA, USA) in 76-base-pair (bp) single-end reads.

Bioinformatics Analysis of Differentially Expressed miRs

The QIAseq miRNA library kit adopts a unique molecular index (UMI) system, enabling unbiased and accurate quantification of mature miRs. Original FASTQ files generated using NextSeq were uploaded to the Qiagen GeneGlobe Data Analysis Center (https://geneglobe.qiagen.com) and aligned to miRBase v21 (http://www.mirbase.org). All reads assigned to particular miRs were counted, and the associated UMIs were aggregated to count unique molecules. A matrix of the miR UMI counts was subjected to downstream analyses using StrandNGS 3.4, software (Agilent Technologies, Santa Clara, CA). The UMI counts were quantified using the trimmed mean M-value (TMM) method (18). To determine the target genes of differentially expressed miRs, we integrated all the information on PITA miRBase version 18, microRNA.org miRBase version 18, and TargetScan version 6.0. Next, to determine the biological function of the target genes, Gene Ontology (GO) analysis and pathway statistical analysis were performed. Pathway statistical analysis to determine the pathways considering the number of genes in the pathway and the number of target genes was performed on the pathway collection of the Wiki Pathways database (19) using the PathVisio tool (20).

Statistical Analysis

All values are shown as mean ± SEM. Mann-Whitney U and Kruskal Wallis tests were utilized for two and three non-parametric groups, followed by Dunn's multiple comparison tests. Also, one-way-ANNOVA was used for three or more parametric groups, followed by Dunn's or Tukey's multiple comparison tests. For multiple comparisons between groups at different time points, 2-way ANOVA was applied, followed by Tukey's *post-hoc* test. Differentially expressed miRs were determined using a threshold of absolute values of fold change ≥2 and FDR <0.05 (moderated *t*-test followed by Benjamini-Hochberg multiple testing correction). All statistical analyses were performed using GraphPad Prism 9.1 (GraphPad Prism Software Inc., San Diego, CA, USA). Statistical significance was set at $P < 0.05$.

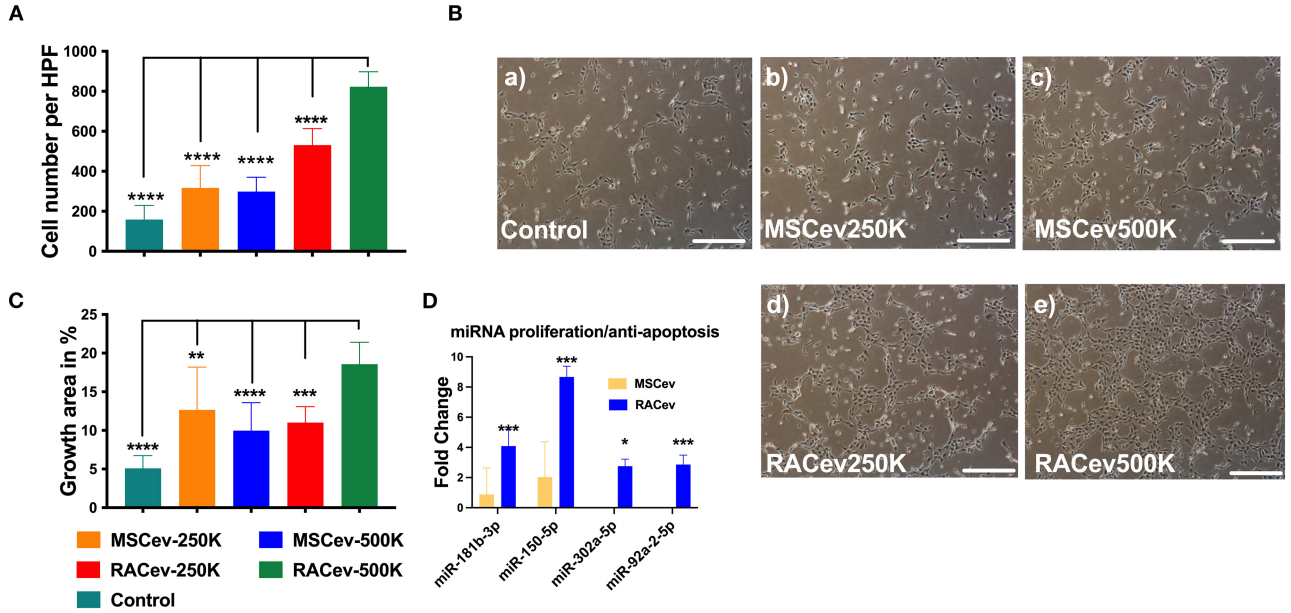

FIGURE 2 | RACev enhanced endothelial cell proliferation in a dose-dependent manner. **(A,B)** 5 *10^5 RACs-derived EVs (500K) increased the cell numbers and **(B,C)** growth area in culture dishes. **(D)** The miRs responsible for proliferation and anti-apoptosis were markedly upregulated in RACev vs. MSCev. * $P < 0.05$; ** $P < 0.01$; *** $P < 0.001$; **** $P < 0.0001$ for RACev-500K vs. other groups. Statistical significance was determined using one way ANOVA followed by Tukey's multiple comparison test. The results are presented as mean ± SEM ($n = 7$–10 per group).

RESULTS

Characterization of EVs

The number and size of EVs derived from RACs and MSCs measured by nanoparticle analyzing machine (**Figures 1A–C**). RACs secrete more EVs (1.62 x 10^9 vs. 4.18 x 10^8, $P < 0.015$) compared to MSCs per 5*10^5 cells (**Figure 1B**). The average diameter of RACev was slightly larger (155 ± 1.7 nm) than MSCev (153.3 ± 2 nm) (**Figure 1C**). Protein content evaluation assay demonstrated that RACev protein level is 6-fold higher than MSCev (11 ± 1 vs. 64 ± 10, $P < 0.01$). Transmission electron microscopy revealed a bi-layered membrane structure (**Figure 1D**), and flow cytometry confirmed the presence of EV-specific markers (CD9, CD63, and Alix) (**Figures 1E,F**). Interestingly, not all classical EV markers are expressed equally; for example, RACev highly expressed CD9, whereas MSCev showed modest expression (**Figure 1G**). Here, we showed that flow cytometry analysis could be utilized as a size evaluation and EV quantification tool using beads of different sizes and appropriate dilutions of EVs (**Figure 1**Fa).

Together, the isolated RACev and MSCev expressed EV-specific markers, and their size range and TEM findings complied with the MISEV 2018 guidelines (21).

RACev Showed Enhanced Proliferative and Anti-apoptotic Effects on HUVECs in a Dose-Dependent Manner

When HUVECs were co-cultured with different concentrations of RAC-derived EV and MSC-derived EV (2.5 * 10^5 and 5 * 10^5), we observed a highly proliferative effect of RACev in a dose-dependent manner compared to MSCev (MSCev-250K vs. RACev-250K, $P < 0.001$ and MSCev-500K vs. RACev-500K, $P < 0.0001$) (**Figures 2A,B**). Of note, MSCev increased proliferation effect and growth area of HUVECs compared to control groups (**Figures 2A–C**). However, growth area of HUVECs was significantly enhanced in the RACev co-culture group compared to that in the MSCev co-culture group (Control vs. RACev-500K, $P < 0.0001$ and MSCev-500K vs. RACev-500K, $P < 0.0001$) (**Figures 2B,C**). Cell cycle analysis confirmed that most of the HUVECs co-cultured with RACev at 250 K and 500 K concentrations entered the S phase and showed increased cell division by up to seven-cell generations (**Supplementary Figure 1**). We then analyzed cell cycle/proliferation-related miR expressional profiles in the RACev vs. MSCev and found that a key miR responsible for anti-apoptotic effects, cell division, and migration was significantly upregulated in RACev (**Figure 2D**). Our *in vitro* results showed that RACev increased the cell division cycle by delivering crucial anti-apoptotic and cell division miRs compared to MSCev.

RACev Transplantation Preserved Heart Function

Based on the previous preclinical data (12) and *in vitro* data, we adjusted the treatment dose to 5 * 10^5 cells derived EVs either RAC or MSC, and injected them repetitively (30 min, day 1, and day 3 after IRI) via tail vein (**Figure 3A**). Echocardiography analysis at 4 weeks showed that the ejection fraction was significantly improved in the RACev transplanted

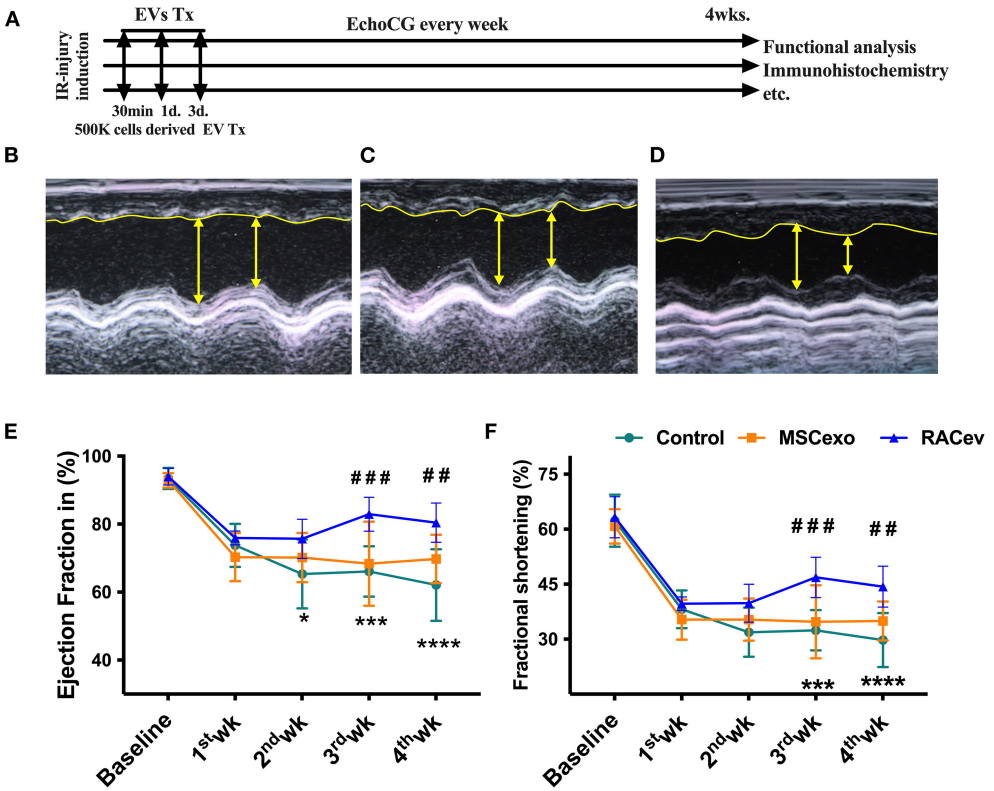

FIGURE 3 | RACev transplantation improved cardiac function. **(A)** Schematic of *in vivo* experiment design. **(B–D)** Representative echocardiographic images of the Control, MSCev, and RACev groups. **(E,F)** The RACev transplanted group showed preserved ejection fraction and fractional shortening at 4 weeks. $^{*}P < 0.05$; $^{***}P < 0.001$; $^{****}P < 0.0001$ vs. the Control group; $^{\#\#}P < 0.01$; $^{\#\#\#}P < 0.001$ vs. the MSCev group. Scale bar = 100 μm Statistical significance was determined using 2-way ANOVA followed by Tukey's multiple comparison post-hoc test. The results are presented as mean ± SEM. (n = 8–10 per group). EchoCG, echocardiography; EV, extracellular vesicles; M-IRI, myocardial ischemic reperfusion injury; Tx, transplantation; 500K is 5 x 10^5 either RACs or MSCs-derived EVs.

group compared to the MSCev and control groups at 4 weeks ($P < 0.006$, RACev vs. MSCev; $P < 0.0001$, RACev vs. Control) (**Figures 3B–E**). The fractional shortening parameter was similarly improved in the RACev group compared to the MSCev and control groups ($P < 0.005$, RACev vs. MSCev; $P < 0.0002$, RACev vs. Control at 4 weeks) (**Figure 3F**). After myocardial IRI, mitral valve insufficiency was observed in most animals in the D-flow mode, and this tendency continued in the MSCev- and saline-treated groups; in contrast, RACev transplantation protected the rats from mitral regurgitation at 4 weeks ($P < 0.03$, RACev vs. MSCev; $P < 0.01$, RACev vs. Control) (**Figures 4A,C**). Consequently, MR caused an end-systolic left ventricle volume increase in the MSCev-treated and Control groups but not in the RACev-treated group (**Figure 4B**). Then, we evaluated the interstitial fibrosis composition at 4 weeks using picrosirius red staining. As shown in **Figures 4D,E**, the highest interstitial fibrotic structure content was detected in the control group. RACev and MSCev-treated groups significantly reduced interstitial myocardial fibrosis compared to control group ($P < 0.006$, RACev vs. Control; $P < 0.03$, MSCev vs. Control). This anti-fibrotic effect of RACev may be coupled with anti-inflammation and anti-fibrotic miR delivery to the ischemic tissue which was beneficially preserved from excessive inflammation and scar formation (**Figures 4F,G**). Interestingly, cardiomyogenesis-related miRs were significantly upregulated in RACev vs. MSCev (**Figure 4H**), suggesting cardiomyogenic properties of RACev. Taken together, repetitive RACev transplantation significantly augmented heart function parameters via reduced interstitial fibrosis accumulation, anti-inflammation, and cardiomyogenesis-related miR delivery.

RACev Increased Capillary Densities

Early angiogenesis initiation is crucial for the regeneration of ischemic injured organs. Representative **Figures 5A,B** show that the microvascular densities of the infarcted myocardium were beneficially enhanced in the RACev transplanted group compared to the MSCev and control groups, indicating the strong angiogenic properties of RACev. Moreover, transcriptome analysis showed that the key pro-angiogenic miRs responsible for angiogenesis, called angiomiRs, were more highly upregulated in RACev than in MSCev (**Figure 5C**).

Evidence of Selective RACev Accumulation at the Site of Injury

We employed an *in vitro* assay to determine the EV internalization time in nucleus-stained (Hoechst) HUVECs.

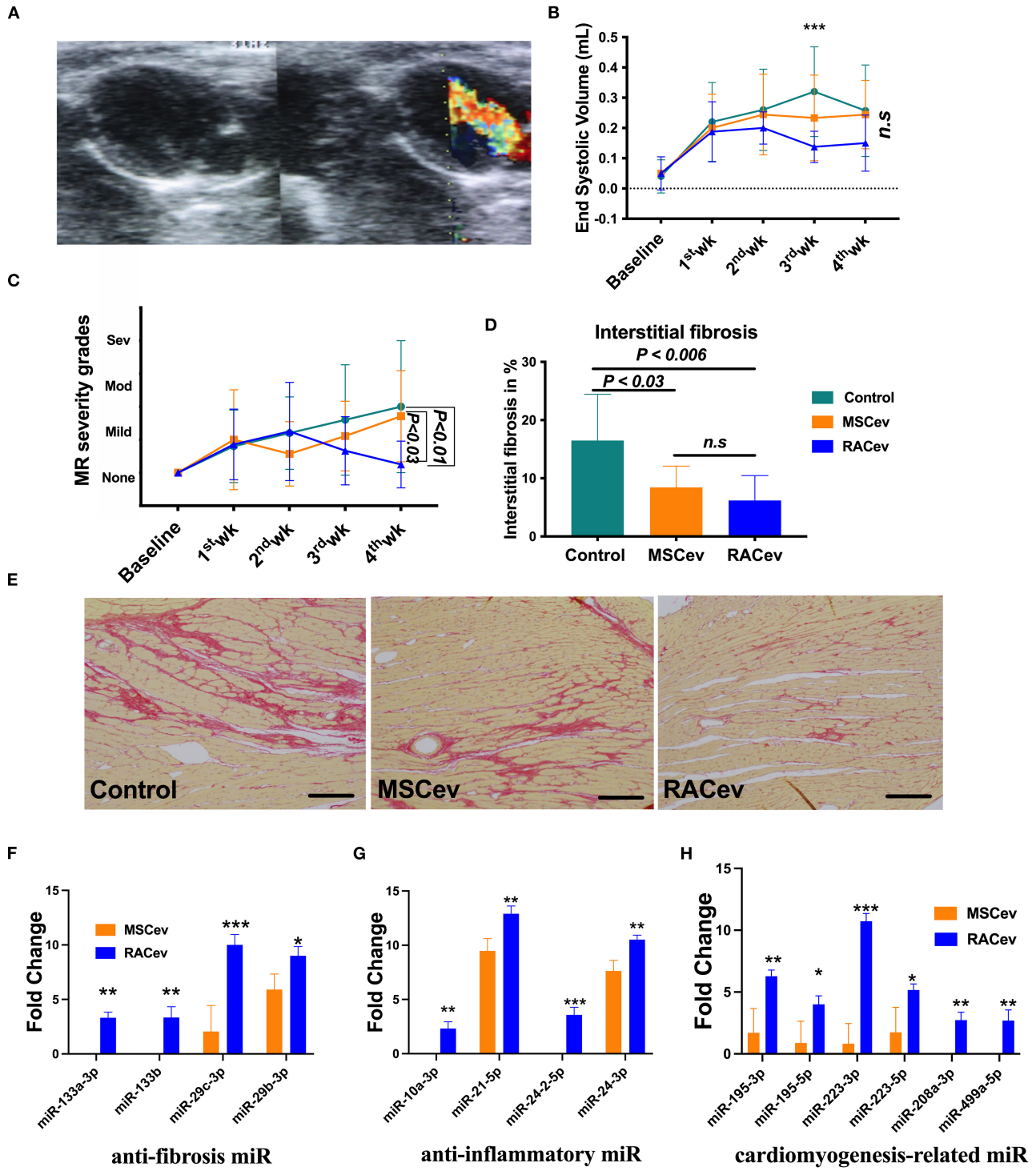

FIGURE 4 | RACev transplantation preserved mitral regurgitation (MR) and interstitial fibrosis. **(A)** Representative mitral regurgitation echocardiographic 2D image. **(B)** At 4 weeks, mitral regurgitation incidences were higher in the Control and MSCev-treated groups than the RACev group. **(C)** Mitral regurgitation caused end-systolic volume increase in the control and MSCev-treated groups but not in the RACev group. **(D, E)** Interstitial fibrosis accumulation was greater in the control group than in the MSCev and RACev groups. **(F)** Anti-fibrosis miRs were significantly upregulated in RACev vs. MSCev. Furthermore, miR-133a-3p and miR-133b are expressed in RACev but not MSCev **(G)** Previously defined anti-inflammation related miRs such as miR10a-3p and miR-24-2-5p were expressed only in RACev group (RACev vs. MSCev). **(H)** Cardiomyogenesis-related miR significantly upregulated in RACev vs. MSCev, and miR-208a-3p and miR499a-5p detected in RACev group but not in MSCev. Scale bar = 100μm $^{*}P < 0.05$; $^{**}P < 0.01$; $^{***}P < 0.001$ vs. the MSCev group. Statistical significance was determined using 2-way ANOVA (for MR and ESV) or one-way ANNOVA (for interstitial fibrosis) followed by Dunn's or Tukey's multiple comparison post-*hoc* tests. The results are presented as mean ± SEM (n = 8–10 per group).

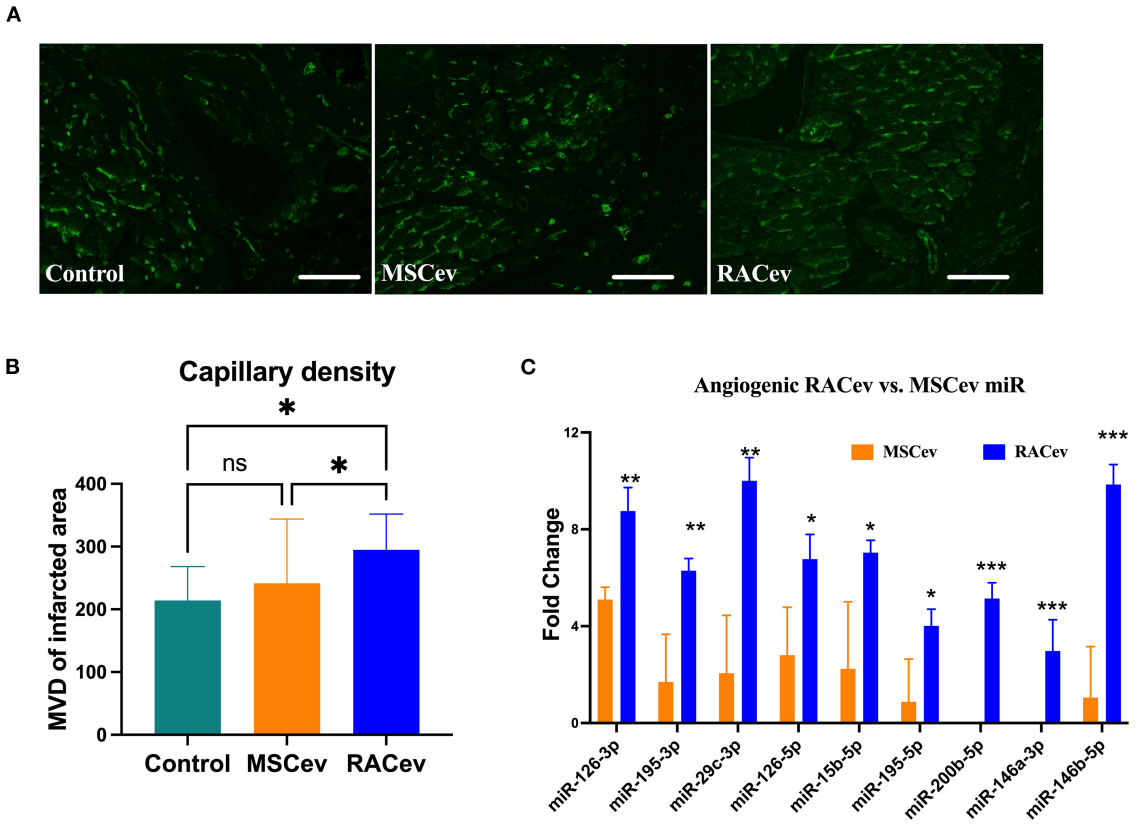

FIGURE 5 | RACev derived angiomiRs enhanced angiogenesis in infarcted tissues. **(A,B)** Microvascular density was enhanced in myocardial infarcted tissue in RACev transplanted group. Cardiac capillaries were stained with FITC conjugated Isolectin B4 (green) **(C)** Mechanistically, enhanced capillary formation in injured myocardium may couple with well-known angiomiRs (miR-126-3p and 5p, miR-195-5p, etc.) delivery by RACev. Scale bar = 50μm. *$P < 0.05$; **$P < 0.01$; ***$P < 0.001$ vs. MSCev group; Statistical significance was determined using Kruskal-Wallis followed by Dunn's multiple comparisons post-*hoc* test. Results are presented as the mean ± SEM (n = 8–10 per group).

This assay result may indicate the EV internalization time in HUVECs and the *in vivo* experiment termination time for EV tracking in IVIS. According to the *in vitro* findings, the optimal time for the observation of EVs in IVIS was between 3–4 h (**Supplementary Figure 2**). In immunohistochemistry analysis, RACev beneficially accumulated into the infarcted myocardium, whereas a few MSCev were selectively infiltrated after systemic injection (**Figures 6A–C**). Furthermore, internalized the transplanted RACev into cardiomyocyte nuclei was higher than MSCev ((**Figure 6C**). IVIS measurement results demonstrated that the average radiance (p/s/cm^{2}sr) was enhanced in the RACev transplanted group compared to the MSCev group ($P < 0.01$, RACev vs. MSCev) (**Figures 6D,E**), indicating the preferential accumulation of RACev to the site of injury (infarcted anterior left ventricle area) as well as confirming the immunohistology findings.

In summary, EV tracking analyses showed that RACev accumulate selectively in ischemia-induced myocardium.

Immunotolerance Effects of RACev

A low immunologic response to allogenic EV transplantation is one of the key factors leading to successful organ regeneration. MSCev have already demonstrated superior immunosuppressive effects even in allogeneic settings. Our previous preclinical experiment showed that RACs mainly comprise M2 macrophages, Bregs, and Tregs, and among these, Tregs have a strong immunotolerance effect (12). In this study we evaluated the critical clinical signs of host immunologic reactions for allogenic EV transplantation at day 4 and day 28. As shown in **Figure 7A**, bodyweight gain and spleen mass were similar in all groups (**Figures 7A,B**). Moreover, we did not observe any skin ulcer/lesion or alopecia, fur texture changes, or diarrhea in either the RACev-or MSCev-treated groups (data not shown). Further, we performed flow cytometry analysis of the peripheral blood (**Figures 7C–F**) and spleen (**Figures 7G–K**) derived CD3+, CD4+, CD8+, Treg, TNK, CD11b/c, and iNK cell numbers which were not elevated and were the same level in all groups. Perhaps transplanted EVs rapidly internalize the damaged tissues (as shown in internalization assay), and peripheral blood immune cells such as antigen-presenting cells may not properly present (or inhibited by miR-142-3p) to the T cells (**Supplementary Figures 3A–D**). This may indicate less immune reactions occurrence after (even xenogeneic) RACev transplantation at the cellular level.

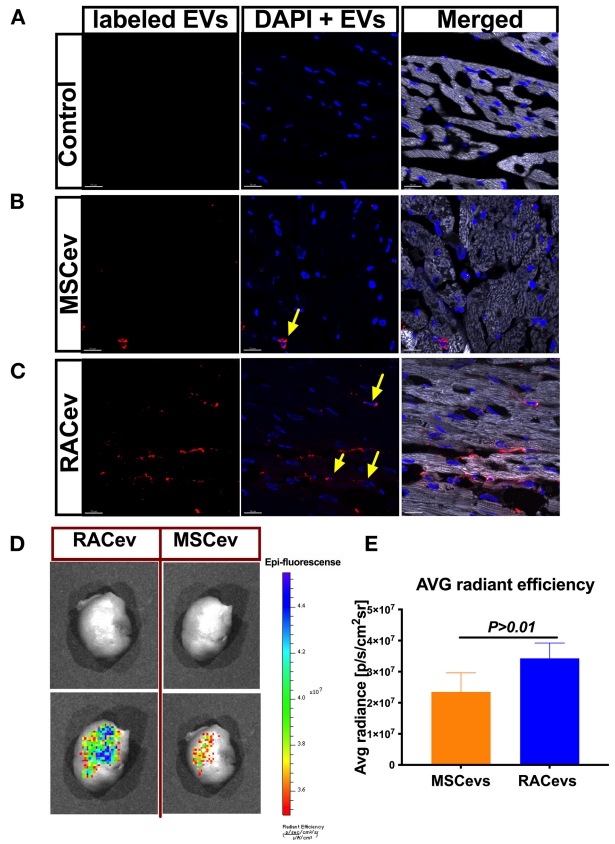

FIGURE 6 | RACev preferentially accumulates to the ischemic myocardium. Representative histological findings of infarcted tissue **(A)** in control groups; **(B)** MSCev showed less infiltration in the ischemic myocardium, whereas **(C)** large amount of RACev accumulated into the infarcted tissue, and the labeled some RACev (red color) were internalized into the cardiomyocyte nuclei (yellow arrows; nuclei stained with Hoechst). **(D,E)** *in vivo* imaging system (IVIS) imaging showed large accumulation of labeled RACev into the infarcted left anterior ventricle. All experiments were repeated twice with the same results. Statistical significance was determined using the Mann-Whitney U test. The results are presented as mean ± SEM ($n = 6$ per group).

DISCUSSION

The therapeutic potential of MSCev for treating ischemic cardiovascular diseases has been well established over the past decade (9). Therefore, in this study, we investigated whether RACev improve the rat myocardial IRI similar to MSCev. In a previous study, Lai et al. transplanted 3.5–1000 μg of proteins derived from MSC exosomes in a mouse or swine model of myocardial ischemia injury, and showed a robust cardioprotective effect along with reduction in the infarct size (9). We first tested the influence of MSCev and RACev on HUVEC proliferation or the cell cycle at different concentrations to determine the optimal dose in an *in vitro* assay. As shown, a high proliferative effect was detected with 5 * 10^5 RACev but not with MSCev; this may be linked with MSCev quality and secretion as particle tracking analysis and protein assay indicated that the number of MSCev and protein level is lower (6-fold) than that of RACev. Our transcriptome results provide further insights into the molecular mechanisms underlying the proliferative and anti-apoptotic activities of RACev as they show that miR-181b-3p, miR-150-5p, and miR-302a-5p are significantly upregulated in RACev but not in MSCev. Regarding these, the miR-181 family is reported to promote the endothelial and cancer cell cycle by targeting *CTDSPL* (22, 23). Another study confirmed that miR-150 significantly promoted the migration and tube formation capability of EPCs (24), whereas miR-92a-2-5p acts as an anti-apoptotic miR in endothelial cell lines (24). Thus, the enhanced migration and proliferative effects of RACev may be coupled with these miRs (24, 25). Of these, miR-92a-2-5p enable preservation of ECs and further enhance cell cycle progression (25).

The therapeutic potential of RACs continues to receive widespread attention (12–14, 26, 27). Therefore, for the first time, we focused on the therapeutic implications of RACs derived EVs as a novel paracrine factor secreted by RACs for ischemic diseases. The current study demonstrated that RACev transplantation enhanced heart function significantly, whereas MSCev had a modest effect. The superior effects of RACs may be related to (1) neovascularization, (2) anti-fibrosis (interstitial) and anti-inflammation, (3) cardioprotection and cardiomyogenesis, and (4) preferential accumulation into the ischemic myocardium. The molecular underpinning of paracrine factor-induced neovascularization, anti-fibrosis, and cardiomyogenesis mainly contributes to the therapeutic benefits of myocardial ischemia. Here, we showed that well known regulators of angiogenesis, angiomiR transcripts such as miR-126-3p, miR-126-5p, miR-195-3p, miR-29c-3p, miR-15b-5p, miR-195-5p, miR-200b-5p, miR-146a-3p, and miR-146b-5p are significantly upregulated in RACev than in MSCev, indicating that RACev cargoes constitute key angiomiRs that promote ischemic tissue recovery as shown experimentally (5, 28–32). In a previous study, we demonstrated that vasculogenic EPC numbers are 30-fold higher among RACs than among peripheral blood mononuclear cells, implicating the origin of angiomiRs (12). Moreover, RACev-shuttled angiomiRs as well as anti-fibrosis miRs, which increased capillary density and reduced interstitial fibrosis in immunohistochemical analysis. The miR-133 family is known to control connective tissue growth factor (CTGF), which is a crucial molecule in the process of interstitial fibrosis regulation in rodents as well as in humans (33). Clinical data indicate that the decrease in miR-133 and miR-29c-3p leads to an increase in *CTGF* levels; miR-29c-3p further contributes to collagen synthesis (33). Interestingly, bioinformatics analysis of differentially expressed miRs showed that RACev highly expressed cardiomyogenesis-related miRs such as miR-195, miR-223, miR-208-3p, and miR-499a compared to MSCev. Dueñas et al. (34) showed that miR-195 and miR-223 selectively enhance cardiomyogenesis via *Smurf1* and *Foxp1* driven process. While miR-208 and miR-499 are involved in the late cardiogenic stages mediating differentiation of cardioblasts to cardiomyocytes (35). Furthermore, previous study findings revealed that systemic RACs transplantation increased cardiomyogenesis by upregulation of early cardiac transcriptional cofactors such as *Nkx2-5* and *Gata-4* (12).

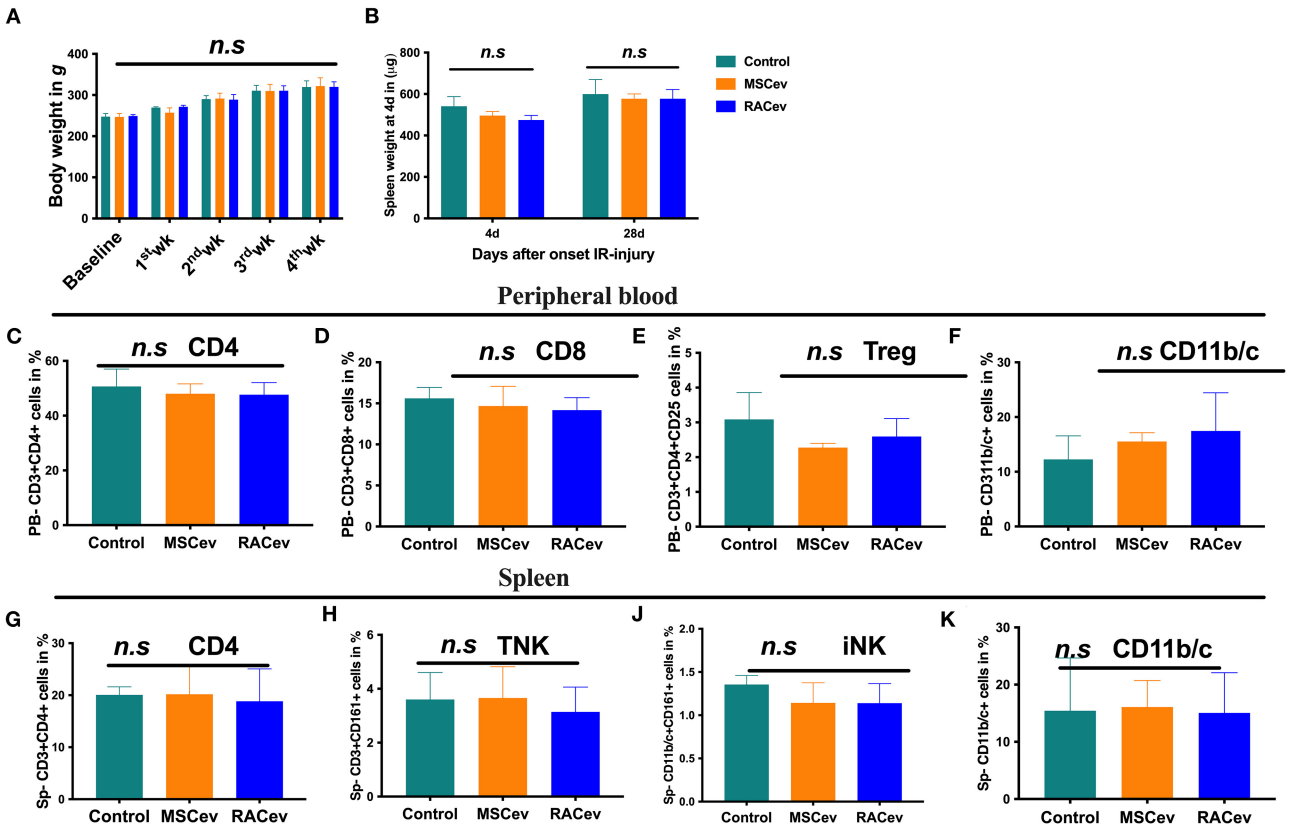

FIGURE 7 | Immunomodulatory effect of RACev. **(A)** The body weights of all three groups were similar across the study period. **(B)** Spleen weight mass at days 4 and 28 days after myocardial ischemia reperfusion injury was not different among the three groups. **(C–F)** Peripheral blood-derived CD4, CD8, Treg, and CD11b/c cells were not elevated, indicating immune tolerance effect of RACev. **(G–K)** Spleen-derived immune reaction or response biomarkers such as CD4, TNK, iNK, and antigen-presenting cells were evaluated and did not change among the three groups. Statistical significance was determined using the One-way ANNOVA followed by Dunn's multiple comparisons *post-hoc* test. The results are presented as mean ± SEM (n = 8–10 per group).

Notably, along with their cardioprotective and immunomodulatory effects, MSCs or MSCev are broadly used in allogenic settings as a recommended therapeutic option for cardiovascular diseases due to their lack of HLA class II, such as HLA-DP, HLA-DM, HLA-DQ, and HLA-DR (36, 37). RACs vastly comprise M2Φ, Treg cells, and regulatory B cells (12); of these, Tregs are crucial in allogenic transplantation in terms of strong anti-inflammatory and immunosuppressive properties. Interestingly, RACev transplanted groups showed neither acute (day 4) nor chronic (day 28) host immune response based on clinical signs such as diarrhea, weight loss, and skin lesions (38). The immunomodulatory and immunosuppressive function of RACev may thus be associated with Treg-derived EV secretion, as Tregs modify the host antigen-presenting cell function via miR-142-3p (2285-fold upregulated in RACev), and EVs may escape T cell recognition as shown previously (**Supplementary Figure 3E**) (39). The miRs have broad functions in immune regulation, for example, miR-10a, miR-21, miR-24 are expressed in immune cells and function as "fine-tuners" for innate and adaptive immune responses (40, 41). In adaptive immunity, they are implicated in the biological processes including pathways involved in the T and B cells central and peripheral tolerance, as well as their function (40). Moreover, flow cytometry findings of PBMCs and spleen cell phenotypes revealed that classical markers of immune reaction such as APC, TNK, iNK, CD8, and CD4/Tregs were similar to the control groups in both the RACev and MSCev groups, indicating the strong immunomodulatory and anti-inflammatory effects of RACev and MSCev miRs.

Emerging evidence highlights that receptor-ligand CXCR4/SDF-1α interaction significantly contributes to the preferential accumulation of EPC-derived EVs into ischemic tissues (42, 43). Mechanistically, RACev may work similarly to the data mentioned above because of their highly selective targeting to the ischemic tissue, as confirmed by IVIS and immunohistology. Moreover, SDF-1α expression in ischemic cardiac tissue is known to be temporarily increased and peaked at 1 to 3 days after ischemic injury and decreased to the background level in the following few days (44–46). Based on this concept, our repetitive EV transplantation timings are suitable and enhance EV uptake by the ischemic myocardium.

Moreover, neither RACev nor MSCev changed the concentration numbers when stored at 4°C for up to 1 week; however, when it exceeded 2 weeks, we observed a reduction in the number of EVs (data not shown). Future studies are thus required to determine the optimal storage temperature and biological activity when EVs are stored for longer period using *in vitro* assays.

The majority of previous MSCev based studies used a considerable number of extracellular vesicles for animal studies and obtained striking results. In this study, the limited quantity of MSCev transplantation may not induce similar results as RACev did. There is a limitation that needs to be acknowledged in this study such as allogenic transplantation setting and it's safety should be analyzed more precisely.

In conclusion, present findings clearly show that repetitive intravenous infusion of RACev is effective and superior compared to MSCev in terms of cardiac function improvement (ejection fraction, LVDS, and mitral regurgitation), strong neovascularization induction by angiomiRs, anti-fibrosis, anti-inflammatory, and selective accumulation in the ischemic myocardium.

DATA AVAILABILITY STATEMENT

The data that support the findings of this study are available from the corresponding author upon reasonable request. The data presented in the study are deposited in the NCBI sequence read archive repository, accession number (SUB10448087).

ETHICS STATEMENT

This study was conducted in accordance with the Declaration of Helsinki and was approved by the Tokai University School of Medicine Clinical Investigation Ethics Committee (IRB no. 14R-126 for human samples). All subjects provided written informed consent prior to participating in the study. The patients/participants provided their written informed consent to participate in this study. The animal study was reviewed and approved by the Tokai University School of Medicine Animal Care and Use Committee approved this study (approval # I-20056), based on the Guide for the Care and Use of Laboratory Animals (National Research Council) guidelines.

AUTHOR CONTRIBUTIONS

AAS: conception and design, collection and/or assembly of data, data analysis and interpretation, manuscript writing, financial support, and final approval of manuscript. AS and YShe: collection and/or assembly of data, data analysis and interpretation. KY: collection and/or assembly of data and data analysis. YShi: collection and/or assembly of data. SK and TA: conception and design, data analysis and interpretation, manuscript writing, financial support, and final approval of manuscript. All authors contributed to the article and approved the submitted version.

FUNDING

This research was supported by JSPS KAKENHI funding (Grant No. 20K17163 to AAS) and Tokai University School of Medicine Research Grant (I-026 to AAS).

ACKNOWLEDGMENTS

We would like to acknowledge following individuals for their expertise and assistance to our study Dr. Takahiro Ochiya and Dr. Nobuyoshi Kosaka (Division of Molecular and Cellular Medicine, National Cancer Center Japan).

SUPPLEMENTARY MATERIAL

The Supplementary Material for this article can be found online at: https://www.frontiersin.org/articles/10.3389/fcvm.2021.754254/full#supplementary-material

Supplementary Figure 1 | RACev enhanced HUVECs proliferation activity in dose-dependently manner. Moreover, cell cycle analysis clearly showed that RACev 250 and 500K treated HUVECs turned into S phase.

Supplementary Figure 2 | Internalization assay was performed to define optimal EVs uptaking time by HUVECs. As shown in representative figures that the highest internalization time of labeled EVs to HUVEC was defined at 3 h. Yellow arrows show the labeled EVs (red color) internalized to cell nuclei (blue color is Hoechst-stained nuclei).

Supplementary Figure 3 | Host immunologic reactions to xenogeneic EV transplantation was evaluated using peripheral blood and spleen derived T cells subsets. Interestingly, miR-142-3p was significantly upregulated in RACev but not in MSCev. Previous study showed that miR-142-3p has immunotolerance effect by inhibiting antigen presenting cells. Statistical significance was determined using the One-way ANNOVA followed by Dunn's multiple comparisons post-*hoc* test. The results are presented as mean ± SEM ($n = 6$ per group).

REFERENCES

1. Van Niel G. d'Angelo G, Raposo G. Shedding light on the cell biology of extracellular vesicles. *Nat Rev Mol Cell Biol.* (2018) 19:213–28. doi: 10.1038/nrm.2017.125
2. Alibhai FJ, Tobin SW, Yeganeh A, Weisel RD, Li RK. Emerging roles of extracellular vesicles in cardiac repair and rejuvenation. *Am J Physiol Heart Circ Physiol.* (2018) 315:H733–44. doi: 10.1152/ajpheart.00100.2018
3. Chistiakov DA, Orekhov AN, Bobryshev YV. Cardiac extracellular vesicles in normal and infarcted heart. *Int J Mol Sci.* (2016) 17:63. doi: 10.3390/ijms17010063
4. Li N, Rochette L, Wu Y, Rosenblatt-Velin N. New insights into the role of exosomes in the heart after myocardial infarction. *J Cardiovasc Transl Res.* (2019) 12:18–27. doi: 10.1007/s12265-018-9831-z
5. Mathiyalagan P, Liang Y, Kim D, Misener S, Thorne T, Kamide CE, et al. Angiogenic mechanisms of human CD34(+) stem cell exosomes in the repair of ischemic hindlimb. *Circ Res.* (2017) 120:1466–76. doi: 10.1161/CIRCRESAHA.116.310557
6. Maring JA, Lodder K, Mol E, Verhage V, Wiesmeijer KC, Dingenouts CK, et al. Cardiac progenitor cell-derived extracellular vesicles reduce infarct size and associate with increased cardiovascular cell proliferation. *J Cardiovasc Transl Res.* (2019) 12:5–17. doi: 10.1007/s12265-018-9842-9

7. Witwer KW, Balkom BWMV, Bruno S, Choo A, Dominici M, Gimona M, et al. Defining mesenchymal stromal cell (MSC)-derived small extracellular vesicles for therapeutic applications. *J Extracell Vesicles.* (2019) 8:1609206. doi: 10.1080/20013078.2019.1609206
8. Sahoo S, Klyachko E, Thorne T, Misener S, Schultz KM, Millay M, et al. Exosomes from human CD34(+) stem cells mediate their proangiogenic paracrine activity. *Circ Res.* (2011) 109:724–8. doi: 10.1161/CIRCRESAHA.111.253286
9. Lai RC, Arslan F, Lee MM,Sze NS,Choo A,Chen TS, et al. Exosome secreted by MSC reduces myocardial ischemia/reperfusion injury. *Stem Cell Res.* (2010) 4:214–22. doi: 10.1016/j.scr.2009.12.003
10. Kore RA, Wang X, Ding Z, Griffin RJ, Tackett AJ, Mehta JL, et al. Exosome-mediated cardioprotection in ischemic mouse heart comparative proteomics of infarct and peri-infarct areas. *Mol Cell Biochem.* (2021) 476:1691–704. doi: 10.1007/s11010-020-04029-6
11. Chen W, Huang Y, Han J, Yu L, Li Y, Lu Z, et al. Immunomodulatory effects of mesenchymal stromal cells-derived exosome. *Immunol Res.* (2016) 64:831–40. doi: 10.1007/s12026-016-8798-6
12. Salybekov AA, Kawaguchi AT, Masuda H, Vorateera K, Okada C, Asahara T. Regeneration-associated cells improve recovery from myocardial infarction through enhanced vasculogenesis, anti-inflammation, and cardiomyogenesis. *PLoS ONE.* (2018) 13:e0203244. doi: 10.1371/journal.pone.0203244
13. Masuda H, Tanaka R, Fujimura S, Ishikawa M, Akimaru H, Shizuno T, et al. Vasculogenic conditioning of peripheral blood mononuclear cells promotes endothelial progenitor cell expansion and phenotype transition of anti-inflammatory macrophage and t lymphocyte to cells with regenerative potential. *J Am Heart Assoc. (*2014) 3:e000743. doi: 10.1161/JAHA.113.000743
14. Salybekov AA, Masuda H, Miyazaki K, Sheng Y, Sato A, Shizuno T, et al. Dipeptidyl dipeptidase-4 inhibitor recovered ischemia through an increase in vasculogenic endothelial progenitor cells and regeneration-associated cells in diet-induced obese mice. *PLoS ONE.* (2019) 14:e0205477. doi: 10.1371/journal.pone.0205477
15. Grange C, Tapparo M, Bruno S, Chatterjee D, Quesenberry PJ, Tetta C, et al. Biodistribution of mesenchymal stem cell-derived extracellular vesicles in a model of acute kidney injury monitored by optical imaging. *Int J Mol Med.* (2014) 33:1055–63. doi: 10.3892/ijmm.2014.1663
16. Kawaguchi AT, Salybekov A, Yamano M, Kitagishi H, Sekine K, Tamaki T. PEGylated carboxyhemoglobin bovine (SANGUINATE((R))) ameliorates myocardial infarction in a rat model. *Artif Organs.* (2018) 42:1174–84. doi: 10.1111/aor.13384
17. Wiklander OP, Nordin JZ, O'Loughlin A, Gustafsson Y, Corso G, Mäger I, et al. Extracellular vesicle in vivo biodistribution is determined by cell source, route of administration and targeting. *J Extracell Vesicles.* (2015) 4:26316. doi: 10.3402/jev.v4.26316
18. Robinson MD, Oshlack A. A scaling normalization method for differential expression analysis of RNA-seq data. *Genome Biol.* (2010) 11:R25. doi: 10.1186/gb-2010-11-3-r25
19. Slenter DN, Kutmon M, Hanspers K, Riutta A, Windsor J, Nunes N, et al. WikiPathways: a multifaceted pathway database bridging metabolomics to other omics research. *Nucleic Acids Res.* (2018) 46:D661–7. doi: 10.1093/nar/gkx1064
20. Kutmon M, van Iersel MP, Bohler A, Kelder T, Nunes N, Pico AR, et al. PathVisio 3: an extendable pathway analysis toolbox. *PLoS Comput Biol.* (2015) 11:e1004085. doi: 10.1371/journal.pcbi.1004085
21. Thery C, Witwer KW, Aikawa E, Alcaraz MJ, Anderson JD, Andriantsitohaina R, et al. Minimal information for studies of extracellular vesicles 2018 (MISEV2018): a position statement of the International Society for Extracellular Vesicles and update of the MISEV2014 guidelines. *J Extracell Vesicles.* (2018) 7:1535750. doi: 10.1080/20013078.2018.1461450
22. Zhang L, He X, Li F, Pan H, Huang X, Wen X, et al. The miR-181 family promotes cell cycle by targeting CTDSPL, a phosphatase-like tumor suppressor in uveal melanoma. *J Exp Clin Cancer Res.* (2018) 37:1–3. doi: 10.1186/s13046-018-0679-5
23. Sun X, Sit A, Feinberg MW. Role of miR-181 family in regulating vascular inflammation and immunity. *Trends Cardiovasc Medicine.* (2014) 24:105–12. doi: 10.1016/j.tcm.2013.09.002
24. Zhang L, Zhou M, Wang Y, Huang W, Qin G, Weintraub N, et al. miR-92a inhibits vascular smooth cell apoptosis: role of the MKK4-JNK pathway. *Apoptosis.* (2014) 19:975–83. doi: 10.1007/s10495-014-0987-y
25. Wang W, Li C, Li W, Hu W, Meng Q, Li Q. miR-150 enhances the motility of the EPCs in vitro and promotes EPCs homing and thrombus resolving in vivo. *Thromb Res.* (2014) 133:590–8. doi: 10.1016/j.thromres.2013.12.038
26. Ohtake T, Kobayashi S, Slavin S, Mochida Y, Ishioka K, Moriya H, et al. Human peripheral blood mononuclear cells incubated in vasculogenic conditioning medium dramatically improve ischemia/reperfusion acute kidney injury in mice. *Cell Transplant.* (2018) 27:520–30. doi: 10.1177/0963689717753186
27. Tanaka R, Ito-Hirano R, Fujimura S, Arita K, Hagiwara H, Mita T, et al. Ex vivo conditioning of peripheral blood mononuclear cells of diabetic patients promotes vasculogenic wound healing. *Stem Cells Transl Med.* (2021) 10:895–909. doi: 10.1002/sctm.20-0309
28. Wang S, Olson EN. AngiomiRs-key regulators of angiogenesis. *Curr Opin Genet Dev.* (2009) 19:205–11. doi: 10.1016/j.gde.2009.04.002
29. Landskroner-Eiger S, Moneke I, Sessa WC. miRNAs as modulators of angiogenesis. *Cold Spring Harb Perspect Med.* (2013) 3:a006643. doi: 10.1101/cshperspect.a006643
30. Salinas-Vera YM, Marchat LA, Gallardo-Rincón D, Ruiz-García E, Astudillo-De La Vega H, Echavarría-Zepeda R, et al. AngiomiRs: microRNAs driving angiogenesis in cancer (Review). *Int J Mol Med.* (2019) 43:657–70. doi: 10.3892/ijmm.2018.4003
31. Urbich C, Kuehbacher A, Dimmeler S. Role of microRNAs in vascular diseases, inflammation, and angiogenesis. *Cardiovasc Res.* (2008) 79:581–8. doi: 10.1093/cvr/cvn156
32. Salybekov A, Kunikeyev A, Kobayashi S, Asahara T. Latest advances in endothelial progenitor cell-derived extracellular vesicles translation to the clinic. *Front. Cardiovasc. Med.* (2021) 8:1184. doi: 10.3389/fcvm.2021.734562
33. Duisters RF, Tijsen AJ, Schroen B, Leenders JJ, Lentink V, van der Made I, et al. miR-133 and miR-30 regulate connective tissue growth factor: implications for a role of microRNAs in myocardial matrix remodeling. *Circ Res.* (2009) 104:170–8. doi: 10.1161/CIRCRESAHA.108.182535
34. Dueñas A, Expósito A, del Mar Muñoz M, de Manuel MJ, Cámara-Morales A, Serrano-Osorio F, et al. MiR-195 enhances cardiomyogenic differentiation of the proepicardium/septum transversum by Smurf1 and Foxp1 modulation. *Sci Rep.* (2020) 10:1–15. doi: 10.1038/s41598-020-66325-x
35. Chistiakov DA, Orekhov AN, Bobryshev YV. Cardiac-specific miRNA in cardiogenesis, heart function, and cardiac pathology (with focus on myocardial infarction). *J Mol Cell Cardiol.* (2016) 94:107–21. doi: 10.1016/j.yjmcc.2016.03.015
36. Hare JM, DiFede DL, Rieger AC, Florea V, Landin AM, El-Khorazaty J, et al. Randomized comparison of allogeneic versus autologous mesenchymal stem cells for nonischemic dilated cardiomyopathy: POSEIDON-DCM trial. *J Am Coll Cardiol.* (2017) 69:526–37.
37. Charles CJ, Li RR, Yeung T, Mazlan SM, Lai RC, de Kleijn DP, et al. Systemic mesenchymal stem cell-derived exosomes reduce myocardial infarct size: characterization with MRI in a porcine model. *Front Cardiovasc Medicine.* (2020) 7:601990. doi: 10.3389/fcvm.2020.601990
38. Naserian S, Leclerc M, Thiolat A, Pilon C, Le Bret C, Belkacemi Y, et al. Simple, reproducible, and efficient clinical grading system for murine models of acute graft-versus-host disease. *Front Immunol.* (2018) 9:10. doi: 10.3389/fimmu.2018.00010
39. Tung SL, Boardman DA, Sen M, Letizia M, Peng Q, Cianci N, et al. Regulatory T cell-derived extracellular vesicles modify dendritic cell function. *Sci Rep.* (2018) 8:1–2. doi: 10.1038/s41598-018-24531-8
40. Tahamtan A, Teymoori-Rad M, Nakstad B, Salimi V. Anti-inflammatory microRNAs and their potential for inflammatory diseases treatment. *Front Immunol.* (2018) 9:1377. doi: 10.3389/fimmu.2018.01377
41. Zheng G, Qiu G, Ge M, Meng J, Zhang G, Wang J, et al. miR-10a in peripheral blood mononuclear cells is a biomarker for sepsis and has anti-inflammatory function. Mediators Inflamm. (2020) 2020:4370983. doi: 10.1155/2020/4370983
42. Viñas JL, Spence M, Gutsol A, Knoll W, Burger D, Zimpelmann J, et al. Receptor-ligand interaction mediates targeting of endothelial colony forming cell-derived exosomes to the kidney after ischemic injury. *Sci Rep.* (2018) 8:16320. doi: 10.1038/s41598-018-34557-7

43. Mayorga ME, Kiedrowski M, McCallinhart P, Forudi F, Ockunzzi J, Weber K, et al. Role of SDF-1: CXCR4 in impaired post-myocardial infarction cardiac repair in diabetes. *Stem cells Transl Med.* (2018) 7:115–24. doi: 10.1002/sctm.17-0172
44. Hu X, Dai S, Wu WJ, Tan W, Zhu X, Mu J, et al. Stromal cell derived factor-1 alpha confers protection against myocardial ischemia/reperfusion injury: role of the cardiac stromal cell derived factor-1 alpha CXCR4 axis. *Circulation.* (2007) 116:654. doi: 10.1161/CIRCULATIONAHA.106.672451
45. Abbott JD, Huang Y, Liu D, Hickey R, Krause DS, Giordano FJ. Stromal cell-derived factor-1alpha plays a critical role in stem cell recruitment to the heart after myocardial infarction but is not sufficient to induce homing in the absence of injury. *Circulation.* (2004) 110:3300–5. doi: 10.1161/01.CIR.0000147780.30124.CF
46. Ceradini DJ, Kulkarni AR, Callaghan MJ, Tepper OM, Bastidas N, Kleinman ME, et al. Progenitor cell trafficking is regulated by hypoxic gradients through HIF-1 induction of SDF-1. *Nat Med.* (2004) 10:858–64. doi: 10.1038/nm1075

Conflict of Interest: The authors declare that the research was conducted in the absence of any commercial or financial relationships that could be construed as a potential conflict of interest.

frontiers in Cardiovascular Medicine

ORIGINAL RESEARCH
published: 28 February 2022
doi: 10.3389/fcvm.2022.813310

Diagnostic and Predictive Values of Circulating Extracellular Vesicle-Carried microRNAs in Ischemic Heart Disease Patients With Type 2 Diabetes Mellitus

Li Zhang[1,2,3†], *Jianchao Zhang*[1,2,3†], *Zhen Qin*[1,2,3], *Na Liu*[4], *Zenglei Zhang*[1,2,3], *Yongzheng Lu*[1,2,3], *Yanyan Xu*[1,2,3], *Jinying Zhang*[1,2,3*] *and Junnan Tang*[1,2,3*]

[1] *Department of Cardiology, The First Affiliated Hospital of Zhengzhou University, Zhengzhou, China,* [2] *Henan Province Key Laboratory of Cardiac Injury and Repair, Zhengzhou, China,* [3] *Henan Province Clinical Research Center for Cardiovascular Diseases, Zhengzhou, China,* [4] *Department of Pediatrics, The First Affiliated Hospital of Zhengzhou University, Zhengzhou, China*

OPEN ACCESS

Edited by:
Ke Huang,
North Carolina State University, United States

Reviewed by:
Kun Wang,
Qingdao University, China
Junjie Xiao,
Shanghai University, China

***Correspondence:**
Junnan Tang
fcctangjn@zzu.edu.cn
Jinying Zhang
jyzhang@zzu.edu.cn

† *These authors have contributed equally to this work*

Specialty section:
This article was submitted to Cardiovascular Biologics and Regenerative Medicine, a section of the journal Frontiers in Cardiovascular Medicine

Received: *11 November 2021*
Accepted: *05 January 2022*
Published: *28 February 2022*

Citation:
Zhang L, Zhang J, Qin Z, Liu N, Zhang Z, Lu Y, Xu Y, Zhang J and Tang J (2022) Diagnostic and Predictive Values of Circulating Extracellular Vesicle-Carried microRNAs in Ischemic Heart Disease Patients With Type 2 Diabetes Mellitus. Front. Cardiovasc. Med. 9:813310. doi: 10.3389/fcvm.2022.813310

Ischemic heart disease patients with diabetes mellitus (IHD-DM) have a higher risk of cardiovascular events than those without DM. Rapid identification of IHD-DM can enable early access to medical treatment and reduce the occurrence of cardiovascular adverse events. In the present study, we identified and examined extracellular vesicle (EV)-carried microRNAs (miRNAs) as the possible diagnostic biomarkers of IHD-DM. Small RNA sequencing was performed to analyze the EV-carried miRNAs spectrum, and differentially expressed miRNAs were further confirmed by quantitative real-time polymerase chain reaction (qRT-PCR). Through small RNA sequencing, we identified 138 differentially expressed EV-carried miRNAs between IHD-DM patients and healthy controls. Furthermore, we identified that five EV-carried miRNAs (miR-15a-3p, miR-18a-5p, miR-133a-3p, miR-155-5p, and miR-210-3p) were significantly down-regulated and one (miR-19a-3p) was significantly up-regulated in the IHD-DM patients compared to healthy controls. The receiver–operating characteristic curve analysis showed that the above six EV-carried miRNAs have excellent diagnostic efficacy of IHD-DM. Our findings indicated that the circulating EV-miRNAs might be promising biomarkers for the convenient and rapid diagnosis of IHD-DM.

Keywords: diagnostic, predictive, extracellular vesicle, ischemic heart disease, type 2 diabetes mellitus

INTRODUCTION

Cardiovascular disease remains an important cause of death both globally and in China, as it accounts for about 40% of the causes of death in the Chinese population (1). Moreover, patients with ischemic heart disease (IHD) are often have diabetes mellitus (DM) as well, a condition referred to as IHD-DM (2). EUROASPIRE IV study (3) showed that about 27% of IHD patients had DM, and among remaining IHD patients with no reported history of DM, screening according to the WHO criteria for fasting plasma glucose (FPG) plus 2-h post-load plasma glucose (2hPG) identifies 45.7% as having a high risk for DM and 27.7% as having newly detected DM. Additionally, clinical data

from China also showed that more than 50% of IHD patients suffer from DM (4). A large number of studies have shown that patients with DM are at higher risk of death than the non-diabetic population (5). Compared with IHD patients without diabetes, the risk of death in IHD patients with diabetes is also significantly increased (6). Furthermore, a recent study suggests that patients with minimal ischemia, once DM is established, have a comparable risk of major cardiovascular adverse events (MACEs) as patients with severe ischemia but not complicated with DM (7). The previous study has revealed that type 2 diabetes mellitus (T2DM) plays a vital role in accelerating the formation and rupture of atherosclerotic plaque, promoting myocardial fibrosis, and reducing cardiac function (8). Thus, establishing a method for the timely, convenient, and rapid diagnosis of IHD-DM and revealing the underlying molecular mechanism of DM promoting the pathological progression of cardiovascular disease will help to alleviate the cardiovascular damage caused by DM (9).

Secreted by a variety of cell types, extracellular vesicles (EVs) contain various proteins and RNA species. EVs play an important role in multiple physiological and pathological processes (10). As key components of EVs cargo, small non-coding RNA, especially microRNAs (miRNAs), are well-known to play a crucial role in the regulation of multiple biological effects including cell proliferation and apoptosis, fibrosis, inflammation, and angiogenesis (11). Moreover, the numbers and contents of EVs vary in different organs and pathological conditions. Thus, EV-carried miRNAs are considered to reflect the physiological and pathological alterations (12). Subsequent studies have also demonstrated that the dysregulation of EV-carried miRNAs could not only reflect the state of the disease but also participate in the pathological activities of the disease (13).

Although a large body of literature has explored the circulating miRNAs signatures in patients with T2DM or IHD (14), few studies have reported the unique expression profiles and signatures of EV-carried miRNAs in IHD-DM patients. Compared to circulating non-EV miRNAs, EV-carried miRNAs appear to be more stable and more sensitive to changes in the state of the disease (15, 16), so it is considered to be a better source for biomarker studies (17). Hence, in the present study, we focused on patients with IHD-DM and observed the changes of the EV-carried miRNAs spectrum to provide a novel biomarker for the diagnosis of IHD-DM.

In the current study, we analyzed the EV-carried miRNAs spectrum from plasma obtained from IHD-DM patients and healthy individuals and identified circulating EV-carried microRNAs (miRNAs) as novel diagnostic biomarkers of IHD-DM.

MATERIALS AND METHODS

The study was approved by the ethics committee of the First Affiliated Hospital of Zhengzhou University and all subjects gave informed consent before participation in the study.

Patients and Sample Collection

This study includes a discovery set ($n = 12$) and a validation set ($n = 40$), involved IHD-DM patients ($n = 32$), and age- and gender-matched healthy volunteers served as controls ($n = 20$). The diagnostic criteria of DM were based on hemoglobin A1c (HbA1c) or FPG or the oral glucose tolerance test (OGTT) (18). IHD was defined by the symptoms and invasive coronary angiography (19). The exclusion criteria included acute myocardial infarction, type 1 diabetes, rheumatic heart disease, severe heart failure, severe heart valve disease, recent (<3 months) major surgical procedures or trauma, serious dysfunction of the liver or kidney, malignant tumor, and infectious disease. Fasting blood samples were collected in ethylenediaminetetraacetic acid tubes from healthy controls and IHD-DM patients after signing informed consent, which was obtained following the declaration of Helsinki. The blood sample was centrifuged at 3,000 rpm for 15 min, and the supernatant containing plasma was collected and stored in a refrigerator at −80°C for further analyses. None of the clinical parameters other than the occurrence of T2DM and HbA1c concentration were significantly different between the two groups.

Isolation of Plasma-Derived EVs

ExoQuick Exosome Precipitation Solution (System Biosciences, Palo Alto, CA, United States) was used to extract EVs from the supernatant containing plasma according to the manufacturer's instructions. In brief, plasma samples were thawed in a water bath at 25°C, then the 1,600 μL supernatant was used to obtain EVs *via* adding 403.2 μL ExoQuick reagent and incubated for 1 h at 4°C. After centrifugation at 4,000 rpm for 30 min and 4,000 rpm for 5 min, the pelleted EVs were resuspended by phosphate buffer solution (PBS), and the EVs solution was stored at −80°C.

miRNA Extraction From EVs

microRNAs were isolated from EVs using the TRIzol method according to the manufacturer's instructions. In brief, we added 800 μL Trizol reagent (Invitrogen, Waltham, MA, United States) to the 1,600 μL buffer containing the purified EVs. After mixing and dissolving for 5 min, we centrifuged the tubes at 12,000 rpm for 10 min to obtain the supernatant and then placed it at 4°C for 10 min. We then added 200 μL chloroform to the supernatant, placed it at 4°C for 10 min, and centrifuged it at 12,000 rpm for 10 min to obtain the supernatant. Then, the same volume of isopropanol and glycogen was added to the supernatant, and the mixture was stored overnight at −20°C. The next day, the supernatant was discarded after centrifugation at 12,000 rpm for 10 min. Finally, we added 1,000 μL of 70% ethanol and the mixture was centrifuged at 12,000 rpm for 10 min. The quantity and quality of the EV-carried miRNA were further analyzed using Nanodrop (Thermo Fisher Scientific, United States). Purified EV-carried miRNAs were used for further RNA sequencing analysis.

Small RNA Library Construction and Sequencing

The EV-carried miRNA library was constructed using TruSeq Small RNA Sample Prep Kits (Illumina, San Diego, CA, United States) according to the manufacturer's instructions. After

obtaining the raw data, the Cutadapt software was used to cut off the connectors at both ends of the reads and retain the reads whose length after pruning was longer than that of 17 nucleotides. The FANse3 ultra-high precision sequence alignment algorithm was used to compare the reads obtained from the sequencing of each sample with the reference sequence of the species (Human mature miRNA, miRBase 22.1).

Immunoblot Analysis of EVs Markers

Extracellular vesicle proteins were quantified using the bicinchoninic acid (BCA) assay. Then, 25 μg of protein was put on 10% gradient SDS-PAGE gels and transferred onto polyvinylidene fluoride. And then the polyvinylidene fluoride was blocked with 5% skimmed milk and subsequently incubated overnight at 4°C with specific primary antibodies such as anti-CD63 antibody (abcam, ab134045), and anti-CD81 antibody (abcam, ab109201). After being washed four times, the polyvinylidene fluoride was incubated with a specific secondary antibody for 1 h, and proteins were detected using the enhanced chemiluminescence method with horseradish peroxidase kit (Thermo Fisher Scientific, Waltham, MA, United States) and visualized by a gel imaging system (AI600, GE Healthcare, United States).

Transmission Electron Microscope

Extracellular vesicles were visualized using a JEOL-1230 transmission electron microscope. In brief, 5 μL of EVs were fixed in 4% paraformaldehyde and deposited onto formvar-carbon on microscopy grids. Then, the grids were washed with 100 μL PBS, followed by 50 μL 1% glutaraldehyde for 5 min, and then eight times with 100 μL ddH_2O each for 2 min. Finally, the grids were stained with uranium oxalate at a pH of 7 for 5 min, and then with methylcellulose for 10 min. After drying the grids, the microscope images were captured at 80 kV.

Nanoparticle Tracking Analysis

We measured the particle size and concentration of EVs were measured using nanoparticle tracking analysis (NTA) with ZetaView PMX 110 (Particle Metrix, Munich, Germany) and corresponding software ZetaView 8.04.02. Isolated EV samples were appropriately diluted using PBS to measure the particle size and concentration. NTA measurement was recorded and analyzed at 11 distinct positions. The ZetaView system was calibrated using 110 nm polystyrene particles. The temperature was maintained around 23°C to 30°C.

Quantitative Real-Time PCR

To validate the data of small RNA sequencing, we performed quantitative real-time PCR (qRT-PCR) analysis of selected miRNAs. Plasma samples from 14 healthy controls and 26 patients with IHD-DM were collected. First, EV-carried miRNAs were reverse transcribed into cDNA by the PrimeScript RT reagent Kit (TaKaRa, Otsu, Shiga, Japan) according to the manufacturer's instructions. Then, synthesized cDNA was used as a template for all the qRT-PCR reactions performed with SYBR Premix Ex Taq (TaKaRa, Otsu, Shiga, Japan). Melting curve analysis was used to confirm the specificity of the amplification reactions. Relative miRNA quantification on the validation set was calculated by the $2^{-\Delta\Delta CT}$ method, that is, the normalized gene expression ($2^{-\Delta CT}$) in the sample A divided by the normalized gene expression ($2^{-\Delta CT}$) in sample B. The ΔCT was equal to the CT values of the target gene minus the CT values of the reference gene. The primers that were used to determine the expression levels of miRNAs are shown in **Supplementary Table 1**.

Data Analysis

After preprocessing and quality control of the RNA-seq files, the miRNA mapping results were normalized using transcripts per kilobase of exon model per million mapped reads (TPMs). MiRNAs with an average read count of more than five TPMs were considered for further analysis. The pairwise differences in miRNA expression levels between the healthy controls group and IHD-DM patients group were examined using the edgeR RNA-seq differential analysis method. To be considered to have a significant concentration change, miRNAs required a fold change >2 [or a $\log_2$ (fold change) > ±1)]with $P < 0.05$. Continuous variables were presented as the mean ± standard deviation, and an Unpaired two-tailed *t*-test (normally distributed data) or Mann–Whitney *U* test (non-normally distributed data) was performed for two-group comparisons. The receiver–operating characteristic (ROC) curve was used to assess the diagnostic efficacy of the EV-carried miRNAs selected for the validation set.

RESULTS

Characterization of Plasma-Derived EVs

Transmission electron microscope analysis revealed the cup-shape morphology of EVs from the healthy controls and IHD-DM patients, and the NTA analysis indicated that plasma-derived EVs from both groups ranged from 50 to 150 nm (**Figures 1A,B**). Immunoblotting exhibited EV markers such as CD63 and CD81 in the plasma-derived EVs (**Figure 1C** and **Supplementary Figure 1**).

Identification of Differentially Expressed EV-Carried miRNAs in Healthy Controls and IHD-DM Patients

The average reads of EVs-miRNAs from healthy controls and IHD-DM patients were 12.58 ± 1.2 and 8.73 ± 1.29 million reads, respectively. Hierarchical clustering showed that the EV-carried miRNA signature distinguished IHD-DM from healthy controls (**Figure 2A**). We found that 138 (6 up-regulated and 132 down-regulated) miRNAs were significantly modulated greater than or equal to two-fold in IHD-DM compared with healthy controls (**Figure 2B**).

Validation of EV-Carried miRNAs in Healthy Controls and IHD-DM Patients

We selected 13 circulating EV-miRNAs with which to further investigate the differential expression between the IHD-DM and healthy controls group via qRT-PCR. It could be found that the levels of miR-15a-3p, miR-18a-5p, miR-133a-3p, miR-155-5p, and miR-210-3p were significantly down-regulated in IHD-DM

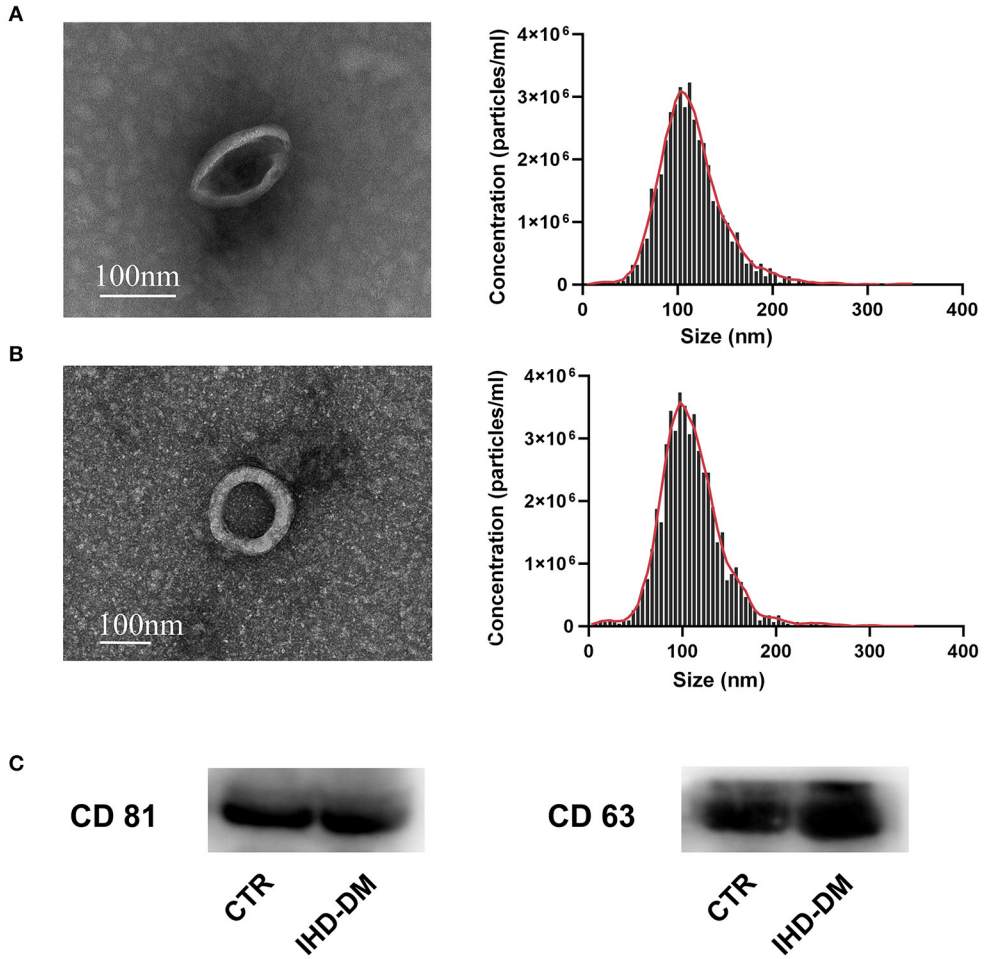

FIGURE 1 | Human sourced plasma-derived EVs were collected and characterized. **(A)** Representative transmission electron microscopy (TEM) images and the nanoparticle tracking analysis (NTA) of plasma-derived EVs from healthy controls. **(B)** Representative TEM and NTA of plasma-derived EVs from IHD-DM patients. **(C)** Representative immunoblot images show enrichment of EV/exosomal markers CD63 and CD81 in plasma-derived EVs. IHD-DM: ischemic heart disease patients with diabetes mellitus; CTR: healthy controls.

patients compared to healthy controls (**Figure 3A**). In contrast, the expression of miR-19a-3p was up-regulated in the IHD-DM patients when compared with those in the healthy individuals (**Figure 3A**). The other seven miRNAs, namely miR-20a-5p, miR-26a-5p, miR-30e-5p, miR-92a-2-5p, miR-181a-5p, miR-181b-5p, and miR-301a-3p, did not have statistically different expressions between the two groups (**Figure 3B**).

EV-Carried miRNAs as Diagnostic Biomarkers for IHD-DM

To assess the specificity and sensitivity of EV-carried miRNAs for the diagnosis of IHD-DM, ROC curve analysis was performed on the validation set. The area under the curve (AUC) of miRNAs was used to quantify the diagnostic efficacy of these miRNAs. The ROC curve analysis results showed that miR-15a-3p (0.874, 95%CI: 0.765-0.982), miR-18a-5p (0.871, 95%CI: 0.760-0.982), miR-19a-3p (0.698, 95%CI: 0.530-0.866), miR-133a-3p (0.745, 95%CI: 0.567-0.922), miR-155-5p (0.901, 95%CI: 0.800-1.000), and miR-210-3p (0.786, 95%CI: 0.647-0.925) were able to discriminate IHD-DM from healthy controls (**Figure 4**).

DISCUSSION

In the present study, we identified 138 differentially expressed EV-carried miRNAs between IHD-DM patients and healthy controls through small RNA sequencing. Selected EV-carried miRNAs (miR-15a-3p, miR-18a-5p, miR-19a-3p, miR-20a-5p, miR-26a-5p, miR-30e-5p, miR-92a-2-5p, miR-133a-3p, miR-155a-5p, miR-181a-5p, miR-181b-5p, miR-210-3p, and miR-301a-3p) were further verified in a larger population through qRT-PCR technology. In comparison to healthy controls, miR-15a-3p, miR-18a-5p, miR-133a-3p, miR-155-5p, and miR-210-3p were down-regulated in IHD-DM patients, whereas miR-19a-3p was up-regulated in the IHD-DM

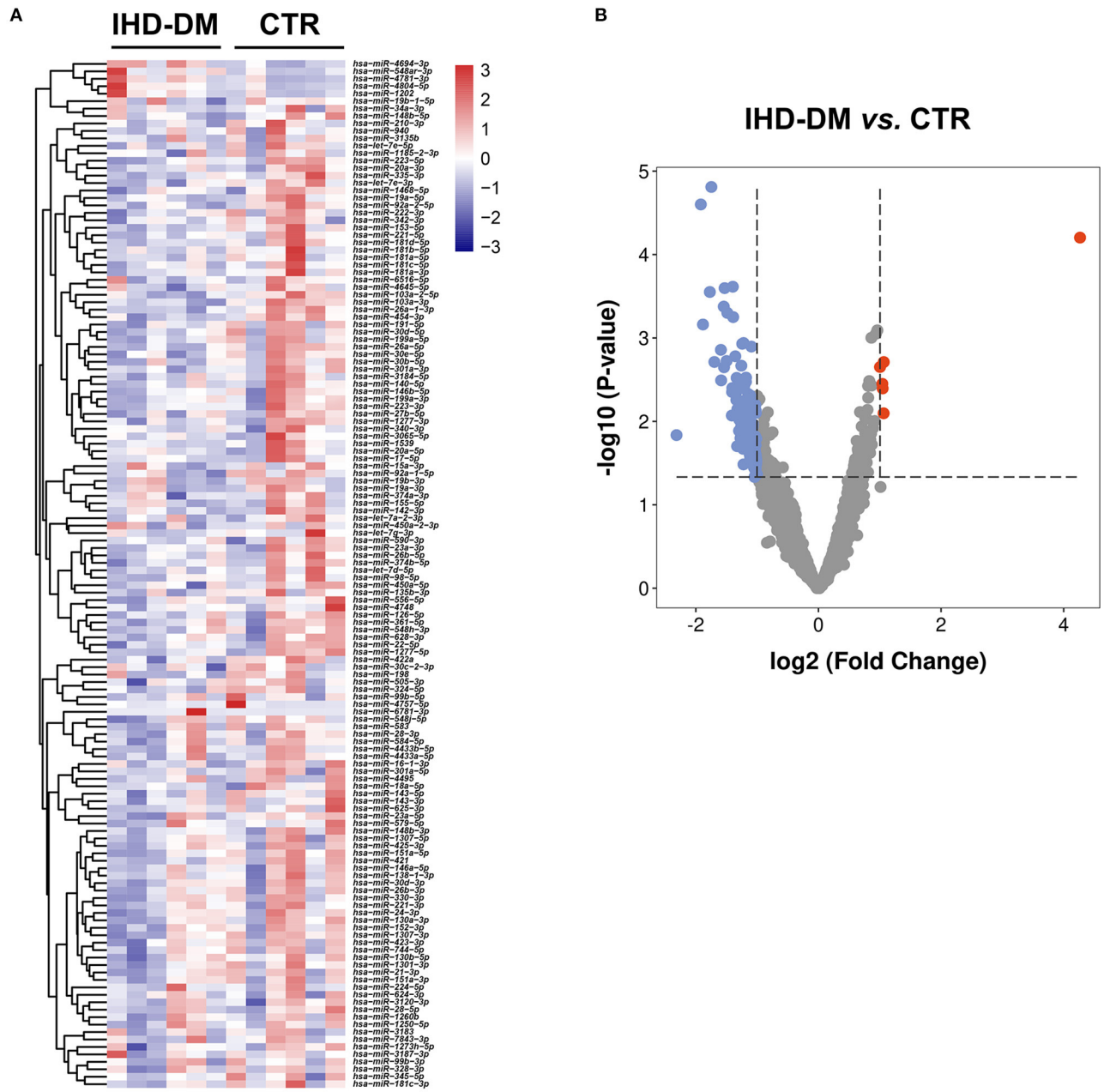

FIGURE 2 | Cluster analysis of differentially expressed EV-carried miRNAs between IHD-DM and healthy controls. **(A)** Heatmap of differentially expressed EV-carried miRNAs between IHD-DM patients and healthy controls. **(B)** Volcano plots of EV-carried miRNAs expression levels in plasma of IHD-DM and healthy controls. *x*- and *y*-axes show estimated expression difference measured in $\log_2$ (fold change) and the significance of the expression difference measured in $-\log_{10}$ (*P*-value), respectively. Vertical lines referred to a two-fold difference in expression between the two groups.

patients (**Figure 3**). Among the numerous differentially expressed EV-carried miRNAs, miR-155-5p, miR-15a-3p, and miR-18a-5p are excellent biomarkers for the diagnosis of IHD-DM with the AUC of 0.901, 0.874, and 0.871, respectively (**Figure 4**).

Previous studies have suggested that multiple mechanisms are involved in the pathological progression of diabetic angiopathy, including hyperglycemia, insulin resistance, hyperlipidemia, inflammation, reactive oxygen species, endothelial dysfunction, hypercoagulability, and vascular calcification (20, 21). Further studies showed that dysregulation of EV-carried miRNAs plays an important role in the process of diabetic heart disease (12). Stepień et al. demonstrated that circulating EVs-carried miRNAs are significantly different between

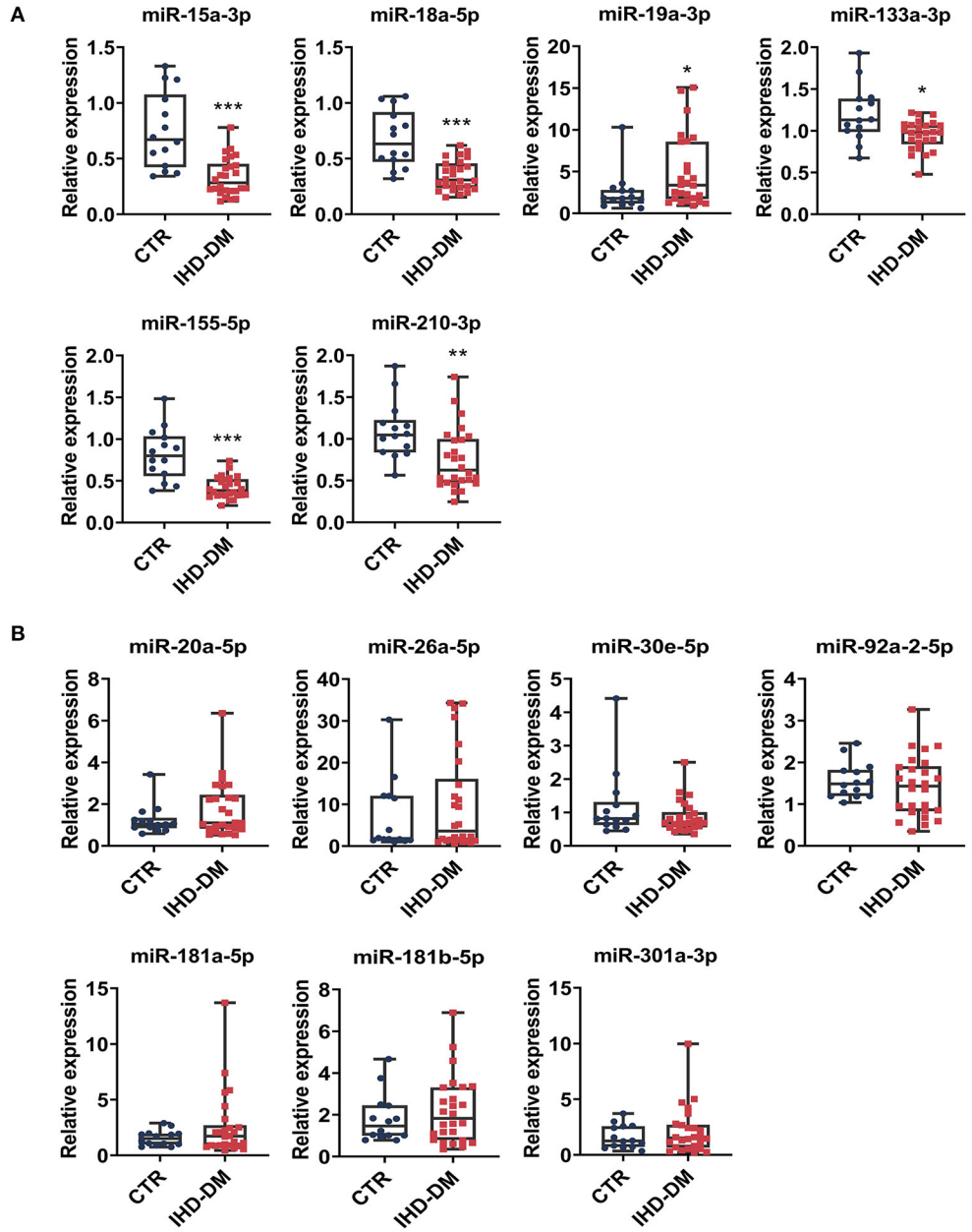

FIGURE 3 | Validation of differentially expressed EV-carried miRNAs between healthy controls and IHD-DM patients. **(A)** EV-carried miRNAs including miR-15a-3p, miR-18a-5p, miR-19a-3p, miR-133a-3p, miR-155-5p, and miR-210-3p are differentially expressed between the IHD-DM patients and healthy controls. **(B)** miRNAs such as miR-20a-5p, miR-26a-5p, miR-30e-5p, miR-92a-2-5p, miR-181a-5p, miR-181b-5p, and miR-301a-3p were not statistically significant between the two groups. $^{*}P < 0.05$, $^{**}P < 0.01$, and $^{***}P < 0.001$ indicates significance compared with the control group.

patients with T2DM and healthy controls, suggesting that dysregulation of EV-carried miRNAs is associated with the occurrence of vascular complications in patients with T2DM (22). Thus, EV-carried miRNAs are considered to reflect the pathophysiological state of the disease (23). In the present study, we screened and identified the differences in EV-carried miRNA cargoes between healthy controls and IHD-DM patients (**Figure 5**).

Accumulating evidence has demonstrated that diabetes-mediated myocardial fibrosis is an important cause of myocardial stiffness and diastolic dysfunction in the diabetic heart (24). Rawal et al. demonstrated that the miR-15 family is involved in fibrotic remodeling of the diabetic heart (25). Furthermore, they found a significant down-regulation of miR-15a and miR-15b in myocardial tissue from diabetic patients complicated with cardiovascular disease (25). Additionally, Geng et al.

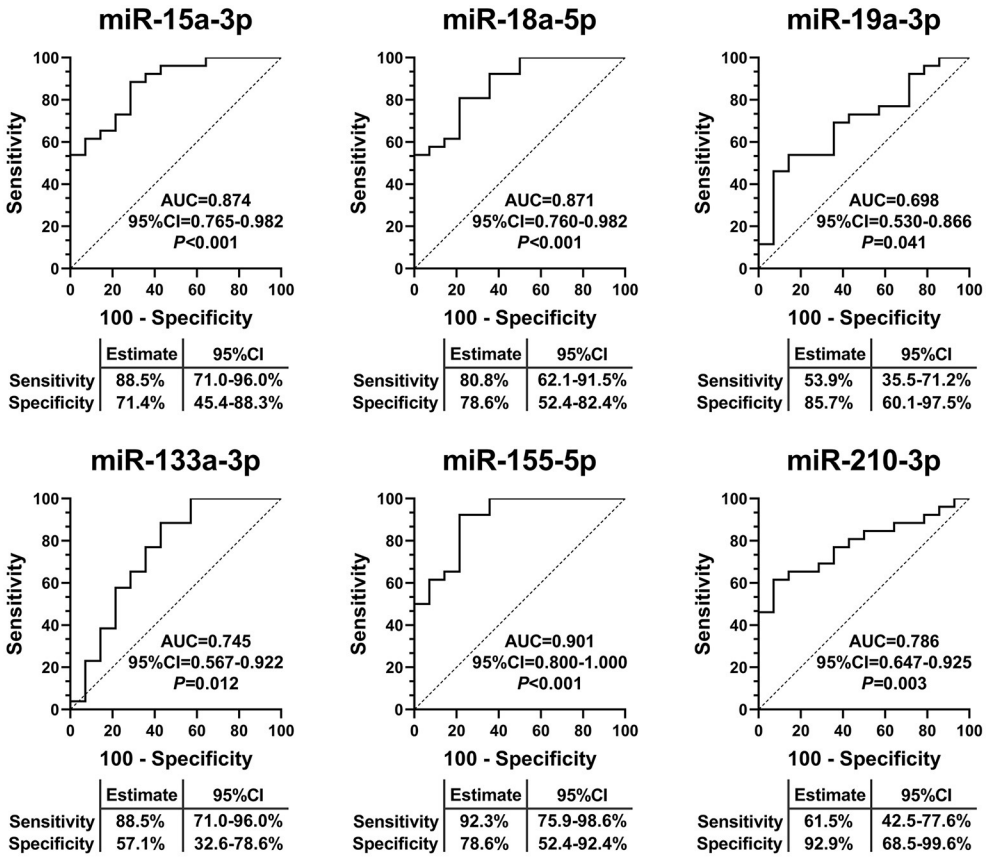

FIGURE 4 | EV-carried miRNAs as useful biomarkers to distinguish IHD-DM from healthy controls. ROC curve analyses displayed EV-carried miR-15a-3p, miR-18a-5p, miR-19a-3p, miR-133a-3p, miR-155-5p, and miR-210-3p as useful biomarkers to discriminate IHD-DM from healthy controls. $P < 0.05$ was considered statistically significant. AUC: area under the curve.

investigated the expression of miR-18a-5p in human aortic valvular endothelial cells and found the overexpression of miR-18a-5p could down-regulate Notch2 expression and subsequently suppress endothelial–mesenchymal transition, to inhibit myocardial fibrosis (26). The results of the present study are in agreement with the above research, showing that EV-carried miR-15a-3p and miR-18a-5p in plasma are significantly down-regulated in IHD-DM patients compared to healthy controls. Interestingly, previous studies showed that miR-19a-3p could significantly improve myocardial fibrosis by inhibiting autophagy-mediated fibrogenesis through targeting TGF-β R II mRNA (27), while Zhu et al. suggested an up-regulation of circulating miR-19a-3p in patients with gestational diabetes mellitus (28). Our current study also found a significant up-regulation of EV-carried miR-19a-3p in IHD-DM patients compared to healthy controls. Therefore, the role of EV-carried miR-19a-3p in diabetic heart disease needs to be further studied.

Diabetes-related vascular inflammation plays an important role in accelerating atherosclerosis formation and plaque rupture, leading to severe acute cardiovascular events (29). Prior studies have demonstrated that a variety of circulating miRNAs such as miR-181b-5p, miR-210-3p, miR-19a, and miR-181a-5p, are involved in vascular inflammation (30–33). Chen et al. suggested that the level of miR-19a is elevated in atherosclerosis-prone ascending aortic wall tissues, which promoted vascular inflammation and foam cell formation by targeting HBP-1 in atherogenesis (32). Qiao et al. demonstrated that miR-210-3p can reduce lipid accumulation and inflammatory response in ox-LDL-induced macrophages by inhibiting the expression of CD36 and NF-κB (33). In the present study, we revealed that the expression of these pro-inflammatory and anti-inflammatory EVs-carried miRNAs were significantly dysregulated, which supports the idea that diabetic status could change the expression of specific inflammatory miRNAs in plasma EVs that is possible to promote systemic or vascular inflammation.

Poor angiogenesis or calcification is also a critical factor worsening the prognosis of diabetic angiopathy. MiR-155-5p is considered to suppress anti-inflammatory signaling in macrophages and participate in the regulation of neovascularization (34, 35). Previous studies on miR-155-5p demonstrated a significant down-regulation in peripheral blood mononuclear cells and whole blood from patients with diabetes (36). Additionally, the expression level of circulating miR-133a-3p is also shown to be significantly down-regulated in patients with diabetes compared with controls (37), which results in the inhibition of human vascular smooth muscle cell proliferation

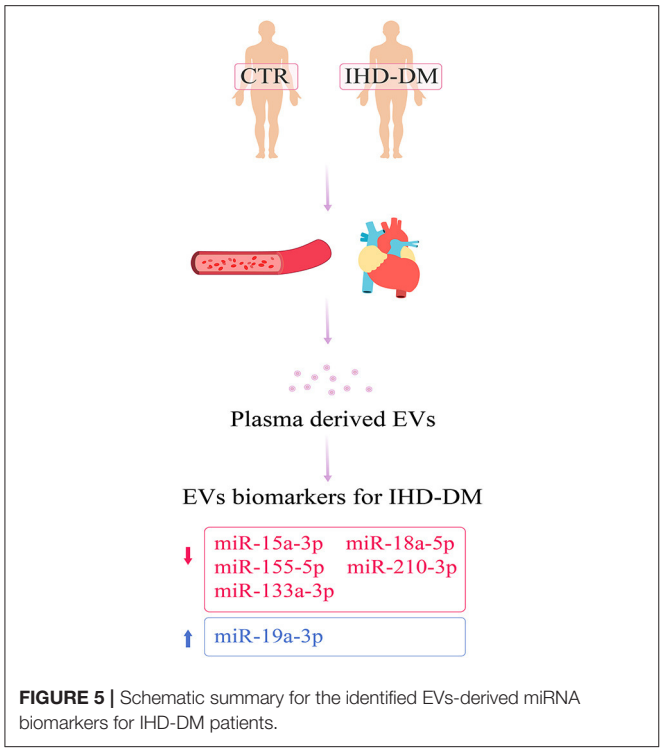

FIGURE 5 | Schematic summary for the identified EVs-derived miRNA biomarkers for IHD-DM patients.

and the induction of cell apoptosis *via* matrix metalloprotein-9 (MMP-9) (38). In the present study, we found that EV-carried miR-155-5p and miR-133a-3p are significantly down-regulated in IHD-DM patients compared to healthy controls.

Moreover, our current work also indicated that there were no significant difference in EV-carried miR-20a-5p, miR-26a-5p, miR-30e-5p, miR-92a-2-5p, miR-181a-5p, miR-181b-5p, or miR-301a-3p in plasma between healthy controls and IHD-DM patients. Concerning miR-181a-5p, previous studies suggested that miR-181a-5p could cooperate with miRNA-181a-3p to restrict vascular inflammation and atherosclerosis, and showed that the level of miR-181a-5p level was significantly reduced in the aorta plaque and plasma (30). However, the expression level of miR-181a-5p in diabetic patients is still debated. Lozano-Bartolomé et al. showed that the expression of miR-181a-5p is reduced in adipose tissue from diabetic subjects (38), whereas other studies showed a significant up-regulation in serum or adipose tissue from diabetic patients (39). In our study, no significant difference in EV-carried miR-181a-5p in plasma was found between healthy controls and IHD-DM patients. Therefore, future research is necessary to further confirm the expression of these EV-carried miRNA in diabetic patients with cardiovascular disease.

There are several limitations to the present study. First, the plasma was collected from patients in a single clinical center, which weakens the external validity required to support widespread changes in practice (40). Hence, a multicenter large sample study should be conducted in the future. Furthermore, we extracted the circulating EVs only through the ExoQuick methods, but not the combination of the ultracentrifugation method and the ExoQuick method. In addition, the present study systematically explored the EV-carried miRNA expression profiles of IHD-DM patients. However, the detailed pathogenesis of these differentially expressed EV-carried miRNA should be explored in future research.

CONCLUSION

The present study systematically reveals the differential expression profile of plasma-derived EV-carried miRNAs through small RNA-sequencing analysis between IHD-DM patients and healthy controls. And these EV-carried miRNAs were further verified in a larger population. Our data suggest that a few of the EVs-carried miRNAs found to be differentially expressed between IHD-DM patients and healthy controls have the potential to be novel circulating EV-carried miRNA biomarkers.

DATA AVAILABILITY STATEMENT

The datasets presented in this study are deposited in the NCBI Sequence Read Archive repository, accession number: PRJNA792080.

ETHICS STATEMENT

The studies involving human participants were reviewed and approved by Ethics Committee of the First Affiliated Hospital of Zhengzhou University. The patients/participants provided their written informed consent to participate in this study.

AUTHOR CONTRIBUTIONS

JT and JinZ: conception and design. LZ, JiaZ, ZQ, NL, and ZZ: analysis and interpretation of data. LZ and JiaZ: drafting the article. YL and YX: critically revising the article. JT, LZ, and JinZ: reviewing submitted version of manuscript. All authors contributed to the article and approved the submitted version.

FUNDING

This work was supported by the National Natural Science Foundation of China (Nos. 81800267, 81870328, U2004203, and 82170281), the Henan Medical Science and Technology Joint Building Program (No. 2018020002), the Henan Thousand Talents Program (No. ZYQR201912131), the Henan Province Youth Talent Promoting Project (No. 2020HYTP051), and the Excellent Youth Science Foundation of Henan Province (No. 202300410362).

ACKNOWLEDGMENTS

We are grateful to BioNovoGene (Suzhou) Co., Ltd. for the help in RNA-seq analysis.

SUPPLEMENTARY MATERIAL

The Supplementary Material for this article can be found online at: https://www.frontiersin.org/articles/10.3389/fcvm.2022.813310/full#supplementary-material

REFERENCES

1. Zhao D, Liu J, Wang M, Zhang X, Zhou M. Epidemiology of cardiovascular disease in China: current features and implications. *Nat Rev Cardiol.* (2019) 16:203–12. doi: 10.1038/s41569-018-0119-4
2. Low Wang CC, Hess CN, Hiatt WR, Goldfine AB. Clinical update: cardiovascular disease in diabetes mellitus: atherosclerotic cardiovascular disease and heart failure in type 2 diabetes mellitus - mechanisms, management, and clinical considerations. *Circulation.* (2016) 133:2459–502. doi: 10.1161/CIRCULATIONAHA.116.022194
3. Gyberg V, De Bacquer D, Kotseva K, De Backer G, Schnell O, Sundvall J, et al. Screening for dysglycaemia in patients with coronary artery disease as reflected by fasting glucose, oral glucose tolerance test, and HbA1c: a report from EUROASPIRE IV–a survey from the European society of cardiology. *Eur Heart J.* (2015) 36:1171–7. doi: 10.1093/eurheartj/ehv008
4. Hu DY, Pan CY, Yu JM, China Heart Survey G. The relationship between coronary artery disease and abnormal glucose regulation in China: the China Heart Survey. *Eur Heart J.* (2006) 27:2573–9. doi: 10.1093/eurheartj/ehl207
5. Rawshani A, Rawshani A, Franzen S, Sattar N, Eliasson B, Svensson AM, et al. Risk factors, mortality, and cardiovascular outcomes in patients with type 2 diabetes. *New Engl J Med.* (2018) 379:633–44. doi: 10.1056/NEJMoa1800256
6. Park DW, Kim YH, Song HG, Ahn JM, Kim WJ, Lee JY, et al. Long-term outcome of stents versus bypass surgery in diabetic and nondiabetic patients with multivessel or left main coronary artery disease: a pooled analysis of 5775 individual patient data. *Circ Cardiovasc Interv.* (2012) 5:467–75. doi: 10.1161/CIRCINTERVENTIONS.112.969915
7. Han D, Rozanski A, Gransar H, Sharir T, Einstein AJ, Fish MB, et al. Myocardial ischemic burden and differences in prognosis among patients with and without diabetes: results from the multicenter international REFINE SPECT registry. *Diabetes Care.* (2020) 43:453–9. doi: 10.2337/dc19-1360
8. Nicholls SJ, Tuzcu EM, Kalidindi S, Wolski K, Moon KW, Sipahi I, et al. Effect of diabetes on progression of coronary atherosclerosis and arterial remodeling: a pooled analysis of 5 intravascular ultrasound trials. *J Am Coll Cardiol.* (2008) 52:255–62. doi: 10.1016/j.jacc.2008.03.051
9. Marble A. Coronary artery disease in the diabetic. *Diabetes.* (1955) 4:290–7. doi: 10.2337/diab.4.4.290
10. De Toro J, Herschlik L, Waldner C, Mongini C. Emerging roles of exosomes in normal and pathological conditions: new insights for diagnosis and therapeutic applications. *Front Immunol.* (2015) 6:203. doi: 10.3389/fimmu.2015.00203
11. Zhang J, Cui X, Guo J, Cao C, Zhang Z, Wang B, et al. Small but significant: Insights and new perspectives of exosomes in cardiovascular disease. *J Cell Mol Med.* (2020) 24:8291–303. doi: 10.1111/jcmm.15492
12. Mori MA, Ludwig RG, Garcia-Martin R, Brandao BB, Kahn CR. Extracellular miRNAs: from biomarkers to mediators of physiology and disease. *Cell Metab.* (2019) 30:656–73. doi: 10.1016/j.cmet.2019.07.011
13. Katayama M, Wiklander OPB, Fritz T, Caidahl K, El-Andaloussi S, Zierath JR, et al. Circulating exosomal miR-20b-5p is elevated in type 2 diabetes and could impair insulin action in human skeletal muscle. *Diabetes.* (2019) 68:515–26. doi: 10.2337/db18-0470
14. Vasu S, Kumano K, Darden CM, Rahman I, Lawrence MC, Naziruddin B. MicroRNA signatures as future biomarkers for diagnosis of diabetes states. *Cells.* (2019) 8:1533. doi: 10.3390/cells8121533
15. Koberle V, Pleli T, Schmithals C, Augusto Alonso E, Haupenthal J, Bonig H, et al. Differential stability of cell-free circulating microRNAs: implications for their utilization as biomarkers. *PLoS ONE.* (2013) 8:e75184. doi: 10.1371/journal.pone.0075184
16. Xie JX, Fan X, Drummond CA, Majumder R, Xie Y, Chen T, et al. MicroRNA profiling in kidney disease: plasma versus plasma-derived exosomes. *Gene.* (2017) 627:1–8. doi: 10.1016/j.gene.2017.06.003
17. Nik Mohamed Kamal N, Shahidan WNS. Non-exosomal and exosomal circulatory microRNAs: which are more valid as biomarkers? *Front Pharmacol.* (2019) 10:1500. doi: 10.3389/fphar.2019.01500
18. Cosentino F, Grant PJ, Aboyans V, Bailey CJ, Ceriello A, Delgado V, et al. 2019 ESC guidelines on diabetes, pre-diabetes, and cardiovascular diseases developed in collaboration with the EASD. *Eur Heart J.* (2020) 41:255–323. doi: 10.1093/eurheartj/ehz486
19. Zeller T, Keller T, Ojeda F, Reichlin T, Twerenbold R, Tzikas S, et al. Assessment of microRNAs in patients with unstable angina pectoris. *Eur Heart J.* (2014) 35:2106–14. doi: 10.1093/eurheartj/ehu151
20. Bornfeldt KE, Tabas I. Insulin resistance, hyperglycemia, and atherosclerosis. *Cell Metab.* (2011) 14:575–85. doi: 10.1016/j.cmet.2011.07.015
21. Bornfeldt KE. 2013 Russell Ross memorial lecture in vascular biology: cellular and molecular mechanisms of diabetes mellitus-accelerated atherosclerosis. *Arterioscler Thromb Vasc Biol.* (2014) 34:705–14. doi: 10.1161/ATVBAHA.113.301928
22. Stepien EL, Durak-Kozica M, Kaminska A, Targosz-Korecka M, Libera M, Tylko G, et al. Circulating ectosomes: determination of angiogenic microRNAs in type 2 diabetes. *Theranostics.* (2018) 8:3874–90. doi: 10.7150/thno.23334
23. He X, Kuang G, Wu Y, Ou C. Emerging roles of exosomal miRNAs in diabetes mellitus. *Clin Transl Med.* (2021) 11:e468. doi: 10.1002/ctm2.468
24. Guido MC, Marques AF, Tavares ER, Tavares de Melo MD, Salemi VMC, Maranhao RC. The effects of diabetes induction on the rat heart: differences in oxidative stress, inflammatory cells, and fibrosis between subendocardial and interstitial myocardial areas. *Oxid Med Cell Longev.* (2017) 2017:5343972. doi: 10.1155/2017/5343972
25. Rawal S, Munasinghe PE, Nagesh PT, Lew JKS, Jones GT, Williams MJA, et al. Down-regulation of miR-15a/b accelerates fibrotic remodelling in the Type 2 diabetic human and mouse heart. *Clin Sci.* (2017) 131:847–63. doi: 10.1042/CS20160916
26. Geng H, Guan J. MiR-18a-5p inhibits endothelial-mesenchymal transition and cardiac fibrosis through the Notch2 pathway. *Biochem Biophys Res Commun.* (2017) 491:329–36. doi: 10.1016/j.bbrc.2017.07.101
27. Zou M, Wang F, Gao R, Wu J, Ou Y, Chen X, et al. Autophagy inhibition of hsa-miR-19a-3p/19b-3p by targeting TGF-beta R II during TGF-beta1-induced fibrogenesis in human cardiac fibroblasts. *Sci Rep.* (2016) 6:24747. doi: 10.1038/srep24747
28. Zhu Y, Tian F, Li H, Zhou Y, Lu J, Ge Q. Profiling maternal plasma microRNA expression in early pregnancy to predict gestational diabetes mellitus. *Int J Gynaecol Obstet.* (2015) 130:49–53. doi: 10.1016/j.ijgo.2015.01.010
29. Dregan A, Charlton J, Chowienczyk P, Gulliford MC. Chronic inflammatory disorders and risk of type 2 diabetes mellitus, coronary heart disease, and stroke: a population-based cohort study. *Circulation.* (2014) 130:837–44. doi: 10.1161/CIRCULATIONAHA.114.009990
30. Su Y, Yuan J, Zhang F, Lei Q, Zhang T, Li K, et al. MicroRNA-181a-5p and microRNA-181a-3p cooperatively restrict vascular inflammation and atherosclerosis. *Cell Death Dis.* (2019) 10:365. doi: 10.1038/s41419-019-1599-9
31. Sun X, Icli B, Wara AK, Belkin N, He S, Kobzik L, et al. MicroRNA-181b regulates NF-kappaB-mediated vascular inflammation. *J Clin Invest.* (2012) 122:1973–90. doi: 10.1172/JCI61495
32. Chen H, Li X, Liu S, Gu L, Zhou X. MircroRNA-19a promotes vascular inflammation and foam cell formation by targeting HBP-1 in atherogenesis. *Sci Rep.* (2017) 7:12089. doi: 10.1038/s41598-017-12167-z
33. Qiao XR, Wang L, Liu M, Tian Y, Chen T. MiR-210-3p attenuates lipid accumulation and inflammation in atherosclerosis by repressing IGF2. *Biosci Biotechnol Biochem.* (2020) 84:321–9. doi: 10.1080/09168451.2019.1685370
34. Fitzsimons S, Oggero S, Bruen R, McCarthy C, Strowitzki MJ, Mahon NG, et al. microRNA-155 is decreased during atherosclerosis regression and is increased in urinary extracellular vesicles during atherosclerosis progression. *Front Immunol.* (2020) 11:576516. doi: 10.3389/fimmu.2020.576516
35. Pankratz F, Bemtgen X, Zeiser R, Leonhardt F, Kreuzaler S, Hilgendorf I, et al. MicroRNA-155 exerts cell-specific antiangiogenic but proarteriogenic effects during adaptive neovascularization. *Circulation.* (2015) 131:1575–89. doi: 10.1161/CIRCULATIONAHA.114.014579
36. Kokkinopoulou I, Maratou E, Mitrou P, Boutati E, Sideris DC, Fragoulis EG, et al. Decreased expression of microRNAs targeting type-2 diabetes susceptibility genes in peripheral blood of patients and predisposed individuals. *Endocrine.* (2019) 66:226–39. doi: 10.1007/s12020-019-02062-0
37. Shi L, Yu C, Tian X, Ma C, Wang L, Xia D, et al. Effect of microRNA-133a-3p/matrix metalloproteinase-9 axis on the growth of atherosclerotic vascular smooth muscle cells. *Exp Ther Med.* (2019) 18:4356–62. doi: 10.3892/etm.2019.8070

38. Lozano-Bartolome J, Llaurado G, Portero-Otin M, Altuna-Coy A, Rojo-Martinez G, Vendrell J, et al. Altered expression of miR-181a-5p and miR-23a-3p is associated with obesity and TNFalpha-induced insulin resistance. *J Clin Endocrinol Metab.* (2018) 103:1447–58. doi: 10.1210/jc.2017-01909
39. He Y, Ding Y, Liang B, Lin J, Kim TK, Yu H, et al. A systematic study of dysregulated microRNA in type 2 diabetes mellitus. *Int J Mol Sci*. (2017) 18:456. doi: 10.3390/ijms18030456
40. Bellomo R, Warrillow SJ, Reade MC. Why we should be wary of single-center trials. *Crit Care Med.* (2009) 37:3114–9. doi: 10.1097/CCM.0b013e3181bc7bd5

Conflict of Interest: The authors declare that the research was conducted in the absence of any commercial or financial relationships that could be construed as a potential conflict of interest.

Publisher's Note: All claims expressed in this article are solely those of the authors and do not necessarily represent those of their affiliated organizations, or those of the publisher, the editors and the reviewers. Any product that may be evaluated in this article, or claim that may be made by its manufacturer, is not guaranteed or endorsed by the publisher.

frontiers | Frontiers in Cardiovascular Medicine

ORIGINAL RESEARCH
published: 18 April 2022
doi: 10.3389/fcvm.2022.864188

Momordica. charantia-Derived Extracellular Vesicles-Like Nanovesicles Protect Cardiomyocytes Against Radiation Injury via Attenuating DNA Damage and Mitochondria Dysfunction

Wen-Wen Cui[1], Cong Ye[1], Kai-Xuan Wang[1], Xu Yang[1,2], Pei-Yan Zhu[1], Kan Hu[2], Ting Lan[1], Lin-Yan Huang[1], Wan Wang[1], Bing Gu[3], Chen Yan[4], Ping Ma[2], Su-Hua Qi[1] and Lan Luo[1]**

[1] Medical Technology School, Xuzhou Medical University, Xuzhou, China, [2] Department of Laboratory Medicine, Affiliated Hospital of Xuzhou Medical University, Xuzhou, China, [3] Department of Laboratory Medicine, Guangdong Provincial People's Hospital, Guangdong Academy of Medical Sciences, Guangzhou, China, [4] Department of Rheumatology, The Second Affiliated Hospital of Nanchang University, Nanchang, China

OPEN ACCESS

Edited by:
Ke Huang,
North Carolina State University,
United States

Reviewed by:
Zhaowei Chen,
Duke University, United States
Tyler A. Allen,
Duke University, United States
Junnan Tang,
First Affiliated Hospital of Zhengzhou University, China

***Correspondence:**
Lan Luo
luolan@xzhmu.edu.cn
Su-Hua Qi
suhuaqi@xzhmu.edu.cn

Specialty section:
This article was submitted to Cardiovascular Biologics and Regenerative Medicine, a section of the journal Frontiers in Cardiovascular Medicine

Received: 28 January 2022
Accepted: 30 March 2022
Published: 18 April 2022

Citation:
Cui W-W, Ye C, Wang K-X, Yang X, Zhu P-Y, Hu K, Lan T, Huang L-Y, Wang W, Gu B, Yan C, Ma P, Qi S-H and Luo L (2022) Momordica. charantia-Derived Extracellular Vesicles-Like Nanovesicles Protect Cardiomyocytes Against Radiation Injury via Attenuating DNA Damage and Mitochondria Dysfunction. Front. Cardiovasc. Med. 9:864188. doi: 10.3389/fcvm.2022.864188

Thoracic radiotherapy patients have higher risks of developing radiation-induced heart disease (RIHD). Ionizing radiation generates excessive reactive oxygens species (ROS) causing oxidative stress, while *Momordica. charantia* and its extract have antioxidant activity. Plant-derived extracellular vesicles (EVs) is emerging as novel therapeutic agent. Therefore, we explored the protective effects of *Momordica. charantia*-derived EVs-like nanovesicles (MCELNs) against RIHD. Using density gradient centrifugation, we successfully isolated MCELNs with similar shape, size, and markers as EVs. Confocal imaging revealed that rat cardiomyocytes H9C2 cells internalized PKH67 labeled MCELNs time-dependently. *In vitro* assay identified that MCELNs promoted cell proliferation, suppressed cell apoptosis, and alleviated the DNA damage in irradiated (16 Gy, X-ray) H9C2 cells. Moreover, elevated mitochondria ROS in irradiated H9C2 cells were scavenged by MCELNs, protecting mitochondria function with re-balanced mitochondria membrane potential. Furthermore, the phosphorylation of ROS-related proteins was recovered with increased ratios of p-AKT/AKT and p-ERK/ERK in MCELNs treated irradiated H9C2 cells. Last, intraperitoneal administration of MCELNs mitigated myocardial injury and fibrosis in a thoracic radiation mice model. Our data demonstrated the potential protective effects of MCELNs against RIHD. The MCELNs shed light on preventive regime development for radiation-related toxicity.

Keywords: *Momordica. charantia*-derived extracellular vesicles-like nanovesicles, radiation-induced heart disease, DNA damage, mitochondria dysfunction, H9C2 cells

INTRODUCTION

With the advances in cancer management, clinicians have seen a remarkable improvement in cancer prognosis. The prolonged overall survival period has driven the recognition of cancer therapy-related adverse effects such as radiation-induced heart disease (RIHD) (1). As an essential modality for thoracic cancer therapy, radiotherapy (RT) eliminates the tumor, and injuries normal

heart cells/tissues. The various heart cell types and structures have differential radiation sensitivity, leading to acute/chronic manifestations, including coronary artery atherosclerosis, valvular disease, pericarditis, conduction defects, and cardiomyopathy (2). Despite the recent development in RT strategy on the control of radiation doses and areas, the risks of RIHD are still unignorable (3). Of late, epidemiological studies have shown that atomic bomb survivors and Mayaka workers exhibited considerable RIHD risks years or decades after receiving low doses of radiation exposures (4, 5). Thus, the underlying mechanism that contributed to the occurrence of RIHD is urgent to comprehensive. Emerging experimental data has shown that radiation generates excessive reactive oxidative species (ROS), causing oxidative stress, epigenetic regulation, mitochondrial dysfunction, and telomere erosion in heart cells/tissues (6). These molecular effects further co-trigger endothelial dysfunction, inflammation, and fibrosis finally in the heart. However, the key determinants that result in the acute and chronic development of RIHD remain largely unidentified (6). Patients with acute RIHD have evident symptoms that are easy to diagnose and receive prompt medications. However, chronic RIHD is asymptomatic at the beginning and difficult to detect, which asks for harmless preventive regimes.

Various types of radioprotective agents, including synthetic chemicals, natural, and phytomedicine, have been discovered (7). Amifostine, the only Food and Drug Administration-approved chemical radioprotector has drawbacks of narrow administration routes and windows, high expenses, and inherent toxicities that minimize its efficacy (8). Recently, natural compounds have gained significant attention owing to their low expense, high accessibility, and less toxicity. It has proved that polyphenols, flavonoids, and various secondary metabolites extracted from different plant parts have radioprotective benefits via their anti-oxidation, DNA repair, anti-inflammation, signaling and apoptotic pathways modulation activities (7). Our group has been focusing on exploring the therapeutic effects of *Momordica. charantia* (*M. charantia*), a fruit of cucurbitaceae plant. We found that *M. charantia* extracts polysaccharides protected against cerebral ischemia/reperfusion injury via suppressing oxidative stress-mediated c-Jun N-terminal Kinase 3 signaling pathway (9). In addition, *M. charantia* polysaccharide promoted neural stem cells proliferation and differentiation via the SIRT1/Beta-catenin axis (10, 11). Considering the ROS scavenging activity of *M. charantia* polysaccharides, we wonder about its radioprotective capacity against RIHD.

Plant-derived extracts have disadvantages of large molecular mass, low solubility, difficulty in crossing physical barriers, and unknown complex composition limit their further applications (12). However, extracellular vesicles (EVs)-like nanovesicles innately derived from the plants could solve all these concerns and are novel candidates for their potential therapeutic benefits evaluation (13). Plant-derived EVs share similarities in size and content (proteins, lipids, DNAs, mRNAs, and microRNAs) of animal derived-EVs, mediating intercellular communications with mammalian cells (14). Chen et al. identified that exosome-like nanoparticles from *Ginger Rhizomes* inhibited NLRP3 inflammasome activation that holds premise for disease settings such as Alzheimer's disease and type 2 diabetes (15). Bruno et al. optimized a method to obtain *Citrus Sinensis*-EVs and found they modulated inflammatory genes and tight junctions in a human model of intestinal epithelium (16).

In this study, we first tried to isolate the *Momordica. charantia*-derived EVs-like nanovesicles (MCELNs) using density gradient centrifugation. We then identified MCELNs according to EVs' characterization criteria. Last, we investigated their protective effects against RIHD *in vitro* and *in vivo*.

MATERIALS AND METHODS

Isolation of MCELNs

Fresh *M. charantia* (Kino Mountain, Xishuangbanna, Yunnan Province, China.) were gently washed with deionized water three times and then milled with the juice extractor. The *M. charantia* juice underwent a series of centrifugations as below. (1) 1,000 × g for 10 min, 3,000 × g for 20 min, 10,000 × g for 40 min at 4°C, the supernatant was kept; (2) 150,000 × g for 90 min at 4°C (Optima XE-90, Beckman Coulter Life Sciences, Indianapolis, U.S.), the pellet was kept; (3) the pellet was suspended with gradient sucrose (8%, 30%, 45%, 60%) and then centrifuged at 150,000 × g for 90 min at 4°C; (4) the band layer around 30–45% was washed with PBS and then centrifuged at 150,000 × g for 90 min at 4°C; (5) the pellet was suspended with PBS and passed through with a 0.22 μm filter (#SLGV004SL, Millipore) for further experiments or stored at −80°C. The BCA assay kit (#23235, Thermo Scientific) was performed to obtain the protein concentration of MCELNs.

Transmission Electron Microscopy

MCELNs suspension (20 μl) was dropped onto Forvar carbon-coated grids (Electron Microscopy Sciences, Hatfield, PA, U.S.) for 3–5 min. Then stain with 2% phosphotungstic acid for 1–2 min at room temperature (RT) and take photos by transmission electron microscopy (FEI, Oregon, U.S.).

Nanoparticle Tracking Analysis (NTA)

We examined the size distribution of MCELNs using a nanoparticle tracking analyzer (ZetaView, Bavaria, Germany). As the manual described, the MCELNs were diluted with PBS and then added to the analytical cell. The data of size distribution was obtained.

Cell Culture and Radiation Exposure

The rat cardiomyocyte cell line (H9C2) was purchased from the National Collection of Authenticated Cell Cultures (Shanghai, China). H9C2 cells were cultured in Dulbecco's modified Eagle's High glucose (DMEM-H, C11995500BT, Gibco) supplemented with 10% fetal bovine serum (FBS, #10091-148, Gibco), 100 U/mL penicillin and 0.1 mg/mL streptomycin (#15140122, Gibco). Cells were maintained in a humidified incubator (37°C, 5% CO_2, Heracell^{TM} 150i, Thermo Scientific).

Before radiation exposure, the culture medium was changed with DMEM-H medium supplemented with 10% exosome-depleted FBS (#EXO-FBS-50A-1, System Biosciences) and MCELNs. The cells were then exposed to 16 Gy X-ray at a dose

rate of 200 cGy/min using X-RAD 225XL Biological Irradiator (Rad Source Technologies, North Branford, CT) as previously reported (17).

Uptake of MCELNs by H9C2 Cells

MCELNs were labeled with the PKH67 Green Fluorescent Cell Linker Kit (#PKH67GL-1KT, Sigma-Aldrich) according to the manufacturer's protocol with minor modifications. In brief, MCELNs (10 μg/mL) diluted in PBS were added to 1 mL Diluent C. In parallel, 4 μl PKH67 dye was added to 1 mL Diluent C and incubated with the MCELNs solution for 4 min. Then, 2 mL 0.5% BSA/PBS was added to bind excess dye. PKH67-labeled MCELNs were washed with PBS and centrifugated at 150,000 × g for 90 min at 4°C. Finally, the pellet was diluted in PBS and went through with a 0.22 μm filter.

H9C2 cells (6.5×10^4 cells/well) were seeded on a confocal dish and incubated with PKH67 labeled MCELNs for 6, 12, and 24 h at 37°C. Then cells were fixed with 4% paraformaldehyde, and the nuclei were stained with DAPI (#2031179, Invitrogen). Then, the images were taken by a confocal microscopy (STELLARIS 5 Confocal Microscope, Leica Microsystems, Illinois, U.S.).

Cell Viability Assay

Cell viability was assessed by the Cell Proliferation Kit I (MTT assay, #11465007001, Roche Life Science). The H9C2 cells (5×10^3 cells/well) were seeded in a 96-well culture plate. Cells were exposed to 0 or 16 Gy X-ray the next day. MCELNs (0, 0.5, 5, 10, and 25 μg/mL) were added to the culture medium before radiation exposure. After 48 h of culture, 10 μl MTT labeling solution was added to each well and incubated at 37°C for 4 h. Then, 100 μl solubilization solution was added to stop the formazan formation. Cells were cultured overnight and the absorbance at 570 nm was measured by an automatic microplate reader (Infinite F50, Tecan, Switzerland). The absorbance value of cells exposed to 0 Gy X-ray was included as a normalization control (%).

Immunofluorescence Staining

The H9C2 cells (6.5×10^4 cells/well) were seeded on the confocal dish. Cells were exposed to 0 or 16 Gy X-ray the next day. MCELNs (0 or 10 μg/mL) were added to the culture medium before radiation exposure. After 48 h of culture, cells were fixed with 4% paraformaldehyde for 15 min at RT. The cells were washed with PBS three times and incubated with 0.5% Triton X-100 for 10 min. Cells were blocked with 5% BSA at RT for 60 min. Then, cells were incubated with rat Ki-67 (#14-5698-82, Invitrogen), rabbit γ-H2A.x (#ab2893, Abcam), and p-ATM (#NB100-306, NOVUS) primary antibody at 4°C overnight, respectively. After washing with PBS three times, cells were incubated with associated fluorescent secondary antibody (#ab150158, Abcam; #A-11001, #A-11008, Thermo scientific) for 60 min at RT. The cells were then washed with PBS three times and stained with DAPI for 10 min. Images were captured by confocal microscopy (STELLARIS 5 Confocal Microscope, Leica Microsystems, Illinois, U.S.). Four fields from each group were selected randomly to calculate the proportion of Ki-67 positive stained cells relative to total cells.

Western Blot Analysis

After indicated treatments, H9C2 cells were homogenized with ice-cold RIPA buffer (#89900, Thermo Scientific) containing 1% phosphatase and protease inhibitors (#78442, Thermo Scientific). Total protein concentration was measured by BCA assay kit (#23225, Thermo Scientific). The proteins were separated on SDS-PAGE gels (7.5%, #1610181, Bio-Rad; 12%, #1610185, Bio-Rad) and transferred to 0.22 μm PVDF membranes (#1620177, Bio-Rad) via Trans-Blot® Turbo™ transfer system (Bio-Rad, California, U.S.). Membranes were blocked with 5% BSA in Tris Buffered Saline with Tween 20 (TBST) for 1 h at RT and then incubated with the primary antibody at 4°C overnight. The primary antibodies included TSG101 (#28283-1-AP, proteintech), CD63 (#25682-1-AP, proteintech), CD9 (#20597-1-AP, proteintech), PCNA (#A0264, ABclonal), Cyclin D1 (#2978, CST), Cyclin B1 (#55004-1-AP, proteintech), cleaved caspase3 (#9664, CST), cleaved PARP (#9548, CST), γ-H2A.x (#ab2893, Abcam), ATM (#NB100-309, NOVUS), p-ATM (#NB100-306, NOVUS), AKT (#60203-2-lg, proteintech), p-AKT (#4060, CST), ERK (#BF8004, affinity), p-ERK (#AF1015, affinity), β-actin (#66009-1-lg, proteintech), α-tubulin (#66031-1-lg, proteintech). After sufficient washing with TBST, membranes were incubated with HRP-conjugated secondary antibodies for 1 h at RT. Blots were visualized using an ECL detection kit (#RPN2135, GE Healthcare Life Sciences) using a ChemiDoc™ Touch imaging system (Bio-Rad, California, U.S.). The density of the band was analyzed by the Image lab software (Bio-Rad, California, U.S.).

Apoptosis Assay

H9C2 cells apoptosis was assessed using PE Annexin V apoptosis detection kit (#559763, BD Biosciences). Cells were exposed to 0 or 16 Gy X-ray the next day. MCELNs (0 or 10 μg/mL) were added to the culture medium before radiation exposure. After 48 h of culture, the cells were harvested with 0.25% trypsin without EDTA (#15090046, Gibco) and washed with PBS three times. Cells (1×10^5 cells) were resuspended in 100 μl of Binding Buffer. Then, 5 μl of Annexin V-PE and 5 μl of 7-AAD were added to the cell suspensions at RT in the dark. After incubation for 15 min, the cells were added with 400 μl ice-cold binding buffer. Cell apoptosis rate was analyzed using a flow cytometer within 1 h (FACS Canto II, Becton Dickinson, New Jersey, U.S.). Q3 and Q2 area represnted the early and late cell apoptosis, respectively. The total cell apoptosis rate was the sum of Q3 and Q2 apoptosis rate.

Measurement of Mitochondria ROS Generation

Mitochondria ROS were detected by MitoSOX kit (#M36008, Invitrogen). H9C2 cells were exposed to 0 or 16 Gy X-ray the next day. MCELNs (0 or 10 μg/mL) were added to the culture medium before radiation exposure. After 48 h of culture, cells were harvested with 0.25% trypsin without EDTA and washed with PBS three times. Then, cell pellets were resuspended with 1 mL

of 5 μM MitoSOX™ reagent working solution and incubated for 10 min at 37°C in the dark. After washing with PBS three times, cells were analyzed using a flow cytometer (FACS Canto II, Becton Dickinson, New Jersey, U.S.).

Measurement of Mitochondrial Membrane Potential (MMP, ΔΨm)

Mitochondrial Membrane Potential Detection Kit (JC-1, #abs50016-100T, absin) was used. H9C2 cells were exposed to 0 or 16 Gy X-ray the next day. MCELNs (0 or 10 μg/mL) were added to the culture medium before radiation exposure. After 48 h of culture, cells were harvested with 0.25% trypsin without EDTA and washed with PBS three times. Then, cells were added with 0.5 mL DMEM and 0.5 mL prepared JC-1 working solution. After incubation for 20 min at 37°C in the dark, cell suspensions were washed with JC-1 staining buffer two times. Then resuspend cell pellets with JC-1 staining buffer and analyzed using flow cytometer (FACS Canto II, Becton Dickinson, New Jersey, U.S.).

Thoracic Mice Irradiation Model

5-6 weeks BALB/c nude mice (GemPharmatech Co., Ltd) weighed about 18–22 g were used in this experiment. This study was approved by the Institutional Animal Care and Use Committee of Xuzhou Medical University (202112A020), and all animal procedures were performed following the institutional and national guidelines.

Animals were randomly divided into three groups ($n = 4$): (1) Control group; (2) IR Group; (3) MCELNs administration post-IR (100 μg/kg every other day for 5 times, intraperitoneal injection). Thoracic radiation exposure was performed in mice at a dose rate of 100 cGy/min, 20 Gy X-ray using X-RAD 225XL Biological Irradiator (Rad Source Technologies, North Branford, CT) as previously reported (18). We covered the other body areas except the chest with lead to shield from the X-ray. The body weight was weighed every two days, and mice were sacrificed 35 days after the initial thoracic radiation exposure. Serum was collected for cardiac injury biomarkers evaluation. Heart weight was measured and then fixed with 4% paraformaldehyde for paraffin sections preparation (4 μm).

Enzyme-Linked Immunosorbent Assay (ELISA)

The mouse serum were used to detect myocardial injury biomarkers with ELISA kits, including CK-MB (#E-EL-M0355c, Elabscience), cTnT (#E-EL-M1801c, Elabscience), and NT-proBNP (#E-EL-M0834c, Elabscience).

Masson Trichrome Staining

The cardiac tissues were sectioned in 4 μm for Masson trichrome staining according to the mannual (#G1006-20ML, Servicebio). The images were observed and scanned using a microscope inspection (Olympus VS120). The fibrosis area were analyzed using Image-J software (1.52n).

Statistical Analysis

All experiments are presented as the mean ± SD. The statistical significance was evaluated by one-way analysis of variance (ANOVA) followed by Turkey's multiple comparisons test among groups (GraphPad Prism 9.3.0). RM two-way ANOVA followed by Turkey's multiple comparisons test was used for significance evaluation of repeat measurement of mice body weight. Differences were considered significant when $P < 0.05$.

RESULTS

Isolation and Characterization of MCELNs

Figure 1A illustrates the flow chart of MCELNs isolation from *M. charantia* (MC). Transmission electron microscopy imaging revealed that MCELNs exhibited a cup-shaped morphology (**Figure 1B**). Using NTA assay, MCELNs had an average diameter of 106.0 nm, similar to animal-derived EVs (**Figure 1C**). Western blot assay showed higher expressions of EVs marker (TSG101, CD63, and CD9) in MCELNs than the supernatant obtained during the isolation process (**Figure 1D**). These data demonstrated the successful isolation of MCELNs characterized as EVs. Next, we labeled MCELNs with fluorescent membrane dyes PKH67 and evaluated the uptake of MCELNs in H9C2 cells at 0, 6, 12, 24 h. Confocal imaging showed that H9C2 cells internalized PKH67-MCELNs in a time-dependent manner (**Figure 1E**).

MCELNs Promote the Proliferation of H9C2 Cells After Radiation Exposure

Firstly, we evaluated whether MCELNs could improve cell proliferation activity in irradiated H9C2 cells. H9C2 cells were previously treated with different doses of MCELNs (0, 0.5, 5, 10, 25 μg/mL) and then exposed to 16 Gy X-ray. After 48 h of culture, the MTT assay identified that MCELNs mitigated radiation-induced decreased cell viability in H9C2 cells dose-dependently (**Figure 2A**). We included 10 μg/mL of MCELNs for further experiments. Cell growth of irradiated or non-irradiated H9C2 cells treated with MCELNs (10 μg/mL) or not after 48 h culture were shown in **Figure 2B**. By the immunofluorescence staining of cell proliferation marker Ki-67, we identified a significantly decreased percentage of Ki-67 positive H9C2 cells after exposure to 16 Gy X-ray (**Figures 2C,D**). However, MCELNs (10 μg/mL) dramatically increased the percentage of Ki-67 positive H9C2 cells (**Figure 2C**). We further investigated the expressions of proliferation marker PCNA (**Figure 2D**) and cell cycle-related proteins, including Cyclin D1 (**Figure 2E**) and Cyclin B1 (**Figure 2F**) in H9C2 cells after indicated radiation exposure and MCELNs treatment. Western blot assay showed that MCELNs (10 μg/mL) recovered the downregulated expressions of PCNA, Cyclin D1, and Cyclin B1 in irradiated H9C2 cells. These data revealed that the MCELNs promoted H9C2 cells proliferation after radiation exposure.

MCELNs Suppress the Apoptosis of H9C2 Cells After Radiation Exposure

We next explored the protective effects of MCELNs on the apoptosis of H9C2 cells against radiation using western blot and Annexin-V flow cytometry assay. MCELNs (10 μg/mL) significantly reduced the expressions of apoptosis proteins cleaved caspase3 and cleaved PARP (**Figures 3A,B**) that were

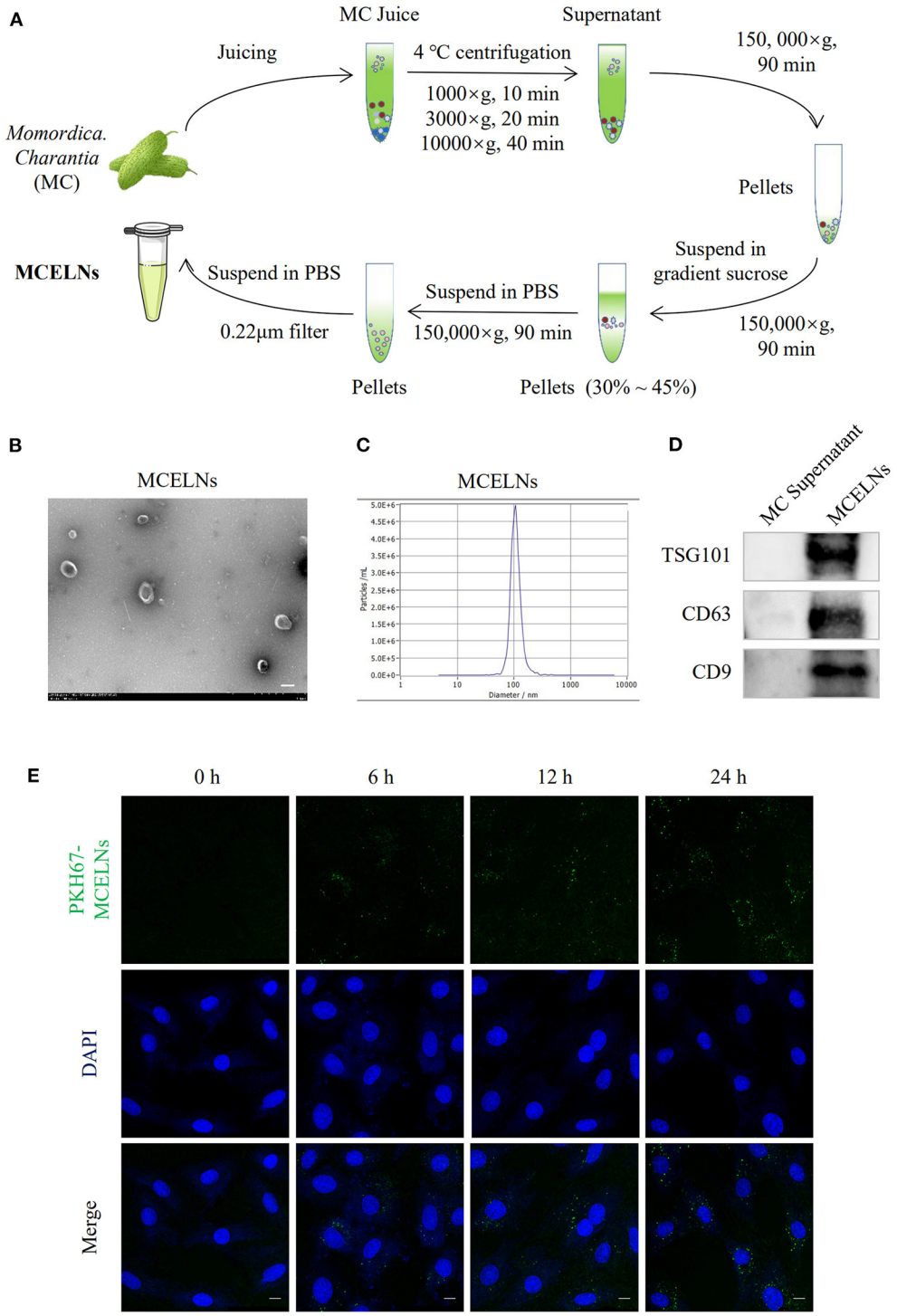

FIGURE 1 | Isolation and characterization of MCELNs. **(A)** Flow sheet on the isolation of MCELNs from *Momordica. charantia* (MC) using gradient density centrifugation. **(B)** Transmission electron microscope image of MCELNs, scale bar: 2 μm. **(C)** NTA analysis exhibited the diameter of MCELNs was around 106.0 nm. **(D)** Western blot analysis of EVs biomarker, including TSG101, CD63, and CD9 in MC supernatant and MCELNs. **(E)** Representative images on the uptake of PKH67-labled MCELNs (green) in H9C2 cells when co-cultured at 0, 6, 12, 24 h. The nucleus were stained with DAPI (blue), scale bar: 10 μm.

elevated in irradiated H9C2 cells. Flow cytometry assay showed that exposure to 16 Gy X-ray significantly enhanced the apoptosis of H9C2 cells, and MCELNs (10 μg/mL) significantly reduced the total apoptosis rate of H9C2 cells, especially the early apoptosis rate (**Figures 3C,D**). These data verified that MCELNs suppressed the apoptosis of H9C2 cells after radiation exposure.

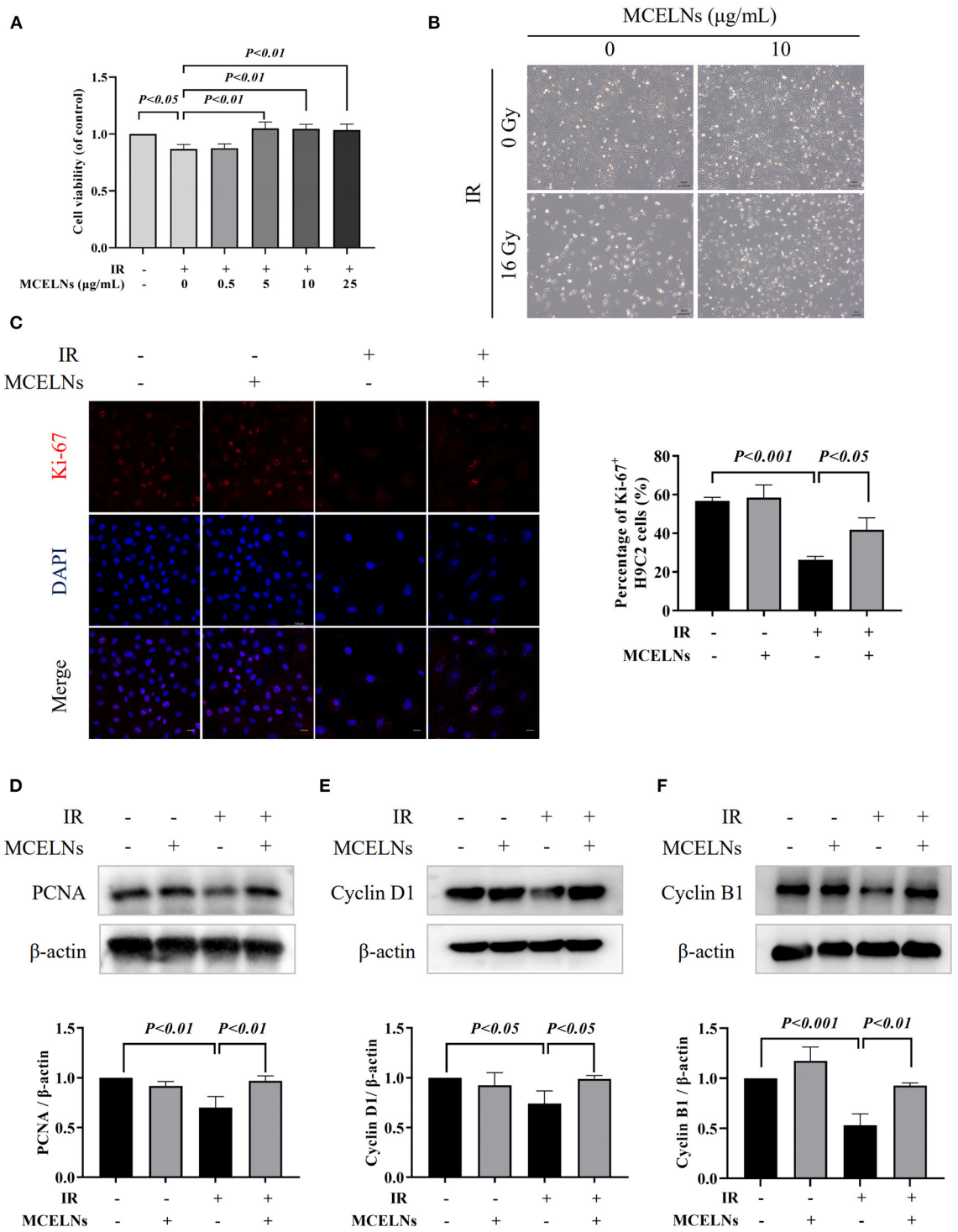

FIGURE 2 | MCELNs enhanced the proliferation of H9C2 cells after radiation exposure. **(A)** H9C2 cells were previously treated with different doses of MCELNs (0, 0.5, 5, 10, 25 μg/mL) and then exposed to 16 Gy X-ray. After 48 h of culture, the cell viability of H9C2 cells was determined using a MTT assay. **(B)** Representative growth images of H9C2 cells after 48 h of culture with indicated treatment, scale bar: 200 μm. **(C)** Immunofluorescence staining (left) and quantitation (right) of Ki-67 (red) positive stained H9C2 cells after 48 h of culture with indicated treatment. The nucleus were stained with DAPI (blue), scale bar: 10 μm. Western blot analysis and quantitation on the expressions of PCNA **(D)**, Cyclin D1 **(E)**, and Cyclin B1 **(F)** in H9C2 cells after 48 h of culture with indicated treatment. IR (–/+): 0/16 Gy X-ray; MCELNs (–/+): 0/10 μg/mL. All data were represented as means ± SD ($n = 3$ independent experiments). The statistical significance was evaluated by one-way ANOVA followed by the Turkey's multiple comparisons test among groups.

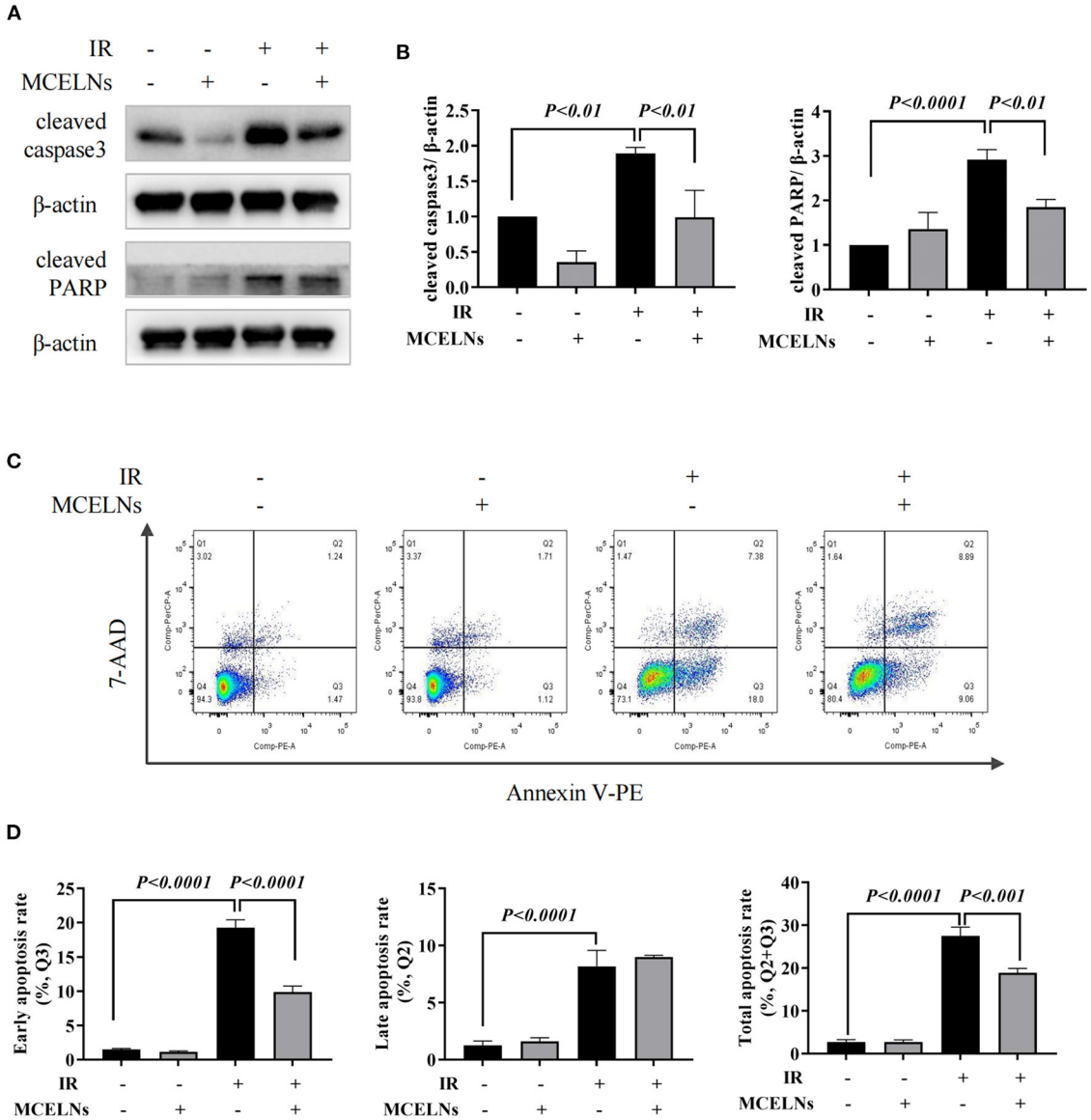

FIGURE 3 | MCELNs inhibited the apoptosis of H9C2 cells after radiation exposure. Western blot images **(A)** and quantitation **(B)** of apoptotic proteins cleaved-caspase3 and cleaved-PARP in H9C2 cells after 48 h of culture with indicated treatment. Annexin V apoptosis Flow detection **(C)** and quantitation **(D)** of the apoptosis rate in H9C2 cells after 48 h of culture with indicated treatment. IR (–/+): 0/16 Gy X-ray; MCELNs (–/+): 0/10 μg/mL. All data were represented as means ± SD ($n = 3$ independent experiments). The statistical significance was evaluated by one-way ANOVA followed by the Turkey's multiple comparisons test among groups.

MCELNs Mitigate the DNA Damage of H9C2 Cells After Radiation Exposure

The direct effect caused by radiation is DNA damage. Here, we tested whether MCELNs could alleviate the DNA damage of H9C2 cells after radiation exposure. Immunofluorescent staining revealed that exposure to 16 Gy X-ray caused a substantial accumulation of DNA damage marker γ-H2A.X foci in the nucleus of H9C2 cells (**Figure 4A**). Western blot assay further confirmed a significantly elevated protein expression of γ-H2A.X in irradiated H9C2 cells (**Figures 4B,C**). MCELNs (10 μg/mL) significantly reduced γ-H2A.X foci formation in the nucleus (**Figure 4A**) and its protein expression (**Figures 4B,C**). The protein kinase ataxia-telangiectasia mutated (ATM) is an apical activator involved in the phosphorylation of the DNA double-strand breaks damage response pathway. After DNA double-strand breaks, ATM was gathered to DNA damage sites and phosphorylated to regulate DNA damage response, especially γ-H2A.X phosphorylation. Immunofluorescent staining showed that MCELNs (10 μg/mL) declined the expressions of p-ATM in the nucleus of irradiated H9C2 cells (**Figure 4D**). Western blot assay further proved these changes (**Figures 4E,F**). Thus,

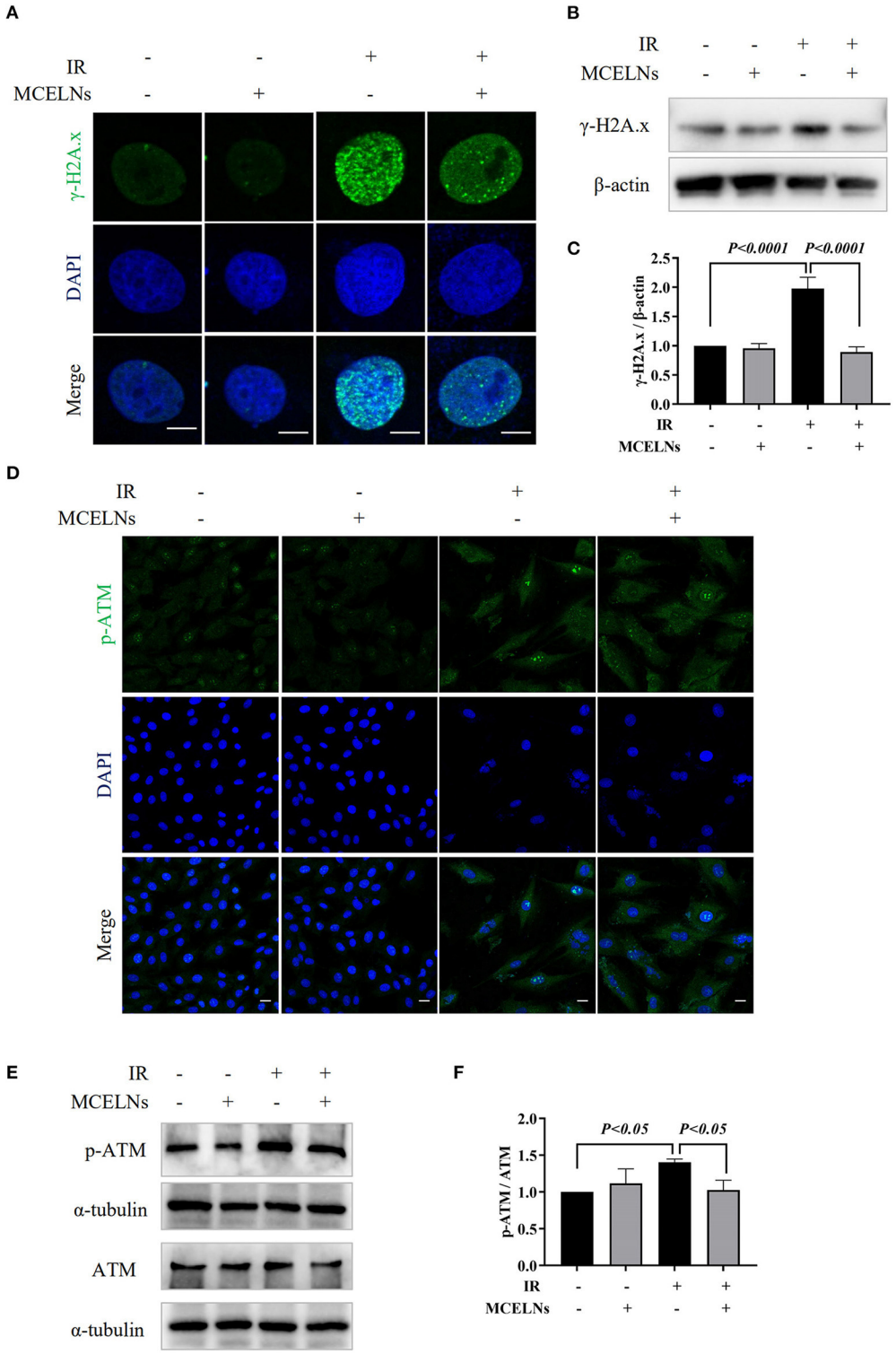

FIGURE 4 | MCELNs decreased the DNA damage of H9C2 cells after radiation. **(A)** Immunofluorescence staining of γ-H2A.X (green) in H9C2 cells after 48 h of culture with indicated treatment. The nucleus were stained with DAPI (blue), scale bar: 10 μm. Western blot images **(B)** and quantitation **(C)** of γ-H2A.X in H9C2 cells after 48 h of culture with indicated treatment. **(D)** Immunofluorescence staining of p-ATM (green) in H9C2 cells after 48 h of culture with indicated treatment. The nucleus were stained with DAPI (blue), scale bar: 10 μm. Western blot images **(E)** and quantitation **(F)** of p-ATM and ATM in H9C2 cells after 48 h of culture with indicated treatment. IR (–/+): 0/16 Gy X-ray; MCELNs (–/+): 0/10 μg/mL. All data were represented as means ± SD ($n = 3$ independent experiments). The statistical significance was evaluated by one-way ANOVA followed by the Turkey's multiple comparisons test among groups.

MCELNs protected the H9C2 cells against DNA damage after radiation exposure.

MCELNs Attenuate the Mitochondrial Dysfunction in H9C2 Cells After Radiation Exposure

Radiation exposure causes cell injury by excessive ROS generation, and mitochondria are the primary source of intracellular ROS. Hence, we tested the mitochondria ROS levels and quality after indicated radiation exposure and MCELNs treatment. Mitochondria ROS staining (**Figure 5A**) and flow cytometry assay (**Figures 5B,C**) demonstrated that exposure to 16 Gy X-ray triggered excessive mitochondria ROS generation in H9C2 cells. MCELNs (10 μg/mL) significantly diminished the mitochondria ROS levels in irradiated H9C2 cells (**Figures 5A–C**). To evaluate the mitochondria quality, we tested the MMP ($\Delta\Psi m$) of H9C2 cells using the JC-1 probe. After radiation exposure, the proportion of JC-1 monomer significantly increased and JC-1 aggregation decreased, indicating reduced MMP (**Figures 5D,E**). MCELNs (10 μg/mL) suppressed radiation-induced JC-1 monomer generation and augmented JC-1 aggregation proportion, thus recovering MMP (**Figures 5D,E**). Last, we evaluated the ROS-related proteins, including p-AKT, AKT, p-ERK, and ERK. MCELNs significantly upregulated the reduction in the ratio of p-AKT/AKT and p-ERK/ERK in irradiated H9C2 cells (**Figures 5F,G**). These data demonstrated that MCELNs could attenuate the mitochondrial dysfunction in H9C2 cells after radiation exposure.

MCELNs Exerted a Cardioprotective Effect in a Thoracic Mice Irradiation Model

To test the radioprotective effect of MCELNs, we generated a thoracic irradiation model (20 Gy X-ray, 100 cGy/min) in BALB/c nude mice by shielding other body areas with lead except for the chest. Mice that received no thoracic radiation exposure were included as a control. Thoracic irradiated mice were then intraperitoneally administrated with MCELNs (100 μg/kg in PBS, IR+MCELNs) or not (PBS, IR) every two days for five times. Mice were sacrificed 35 days after the initial thoracic irradiation (**Figure 6A**). Compared with the control, thoracic irradiated mice exhibited a significantly declined body weight in the first couple of days (**Figure 6B**). The MCELNs administration alleviated the reduction in the body weight of thoracic irradiated mice (**Figure 6B**). However, the heart/body weight ratio was not different among three groups (**Figure 6C**). For monitoring cardiac injury after radiation, we tested the biomarkers of myocardial injury including cTnT, CKMB, and NT-proBNP. The expression levels of cTnT, CKMB and, NT-proBNP were increased in irradiated mice compared with non-irradiated and MCELNs-treated mice, and only CKMB changes showed statistical significance (**Figure 6D**). Moreover, the masson trichrome staining of cardiac tissue sections revealed that the extent of fibrosis in irradiated mice were significantly higher than that of control mice. Meanwhile, MCELNs administration diminished the cardiac fibrosis area in thoracic irradiated mice (**Figure 6E**).

DISCUSSION

In the present study, we isolated MCELNs from *M. charantia* that applied as traditional folk medicine and identified them as EVs. MCELNs enhanced cell proliferation, reduced cell apoptosis, and mitigated the DNA damage in H9C2 cells exposed to 16 Gy X-ray. These effects might be attributed to the free radical scavenging ability of MCELNs, as evidenced by declining ROS levels and restored mitochondria function in irradiated H9C2 cells. In addition, the ratios of ROS-related proteins that p-AKT/AKT and p-ERK/ERK were recovered in irradiated H9C2 cells. Finally, intraperitoneal injection of MCELNs mitigated myocardial injury and fibrosis in a thoracic mice irradiation model.

Plant-derived extracts, including polysaccharides, flavonoids, phenylpropanoids, stilbenoids, vitamin C, and gallic acid, have emerged as novel radioprotectors due to their potent antioxidant activity (19, 20). In addition, EVs represent a novel strategy for mitigating radiation-induced adverse effects (21). Accarie et al. showed that intravenously injection of human mesenchymal stem cells-derived EVs protected the intestinal epithelium's integrity in a mouse model of acute radiation syndrome (22). Lately, the utility of plant-derived EVs in therapeutic drugs has also gained substantial interest (23, 24). Hence, we intended to isolate EVs from *M. charantia* that its extract polysaccharide had neuroprotective effects against cerebral ischemia/reperfusion injury via scavenging excessive free radicals (9) and enhancing neural stem cells proliferation (10) and differentiation (11). Employing desentity gradient centrifugation, we successfully obtained MCELNs with typical sizes, shapes, and markers (TSG101, CD63, and CD9) identified to EVs. The effectiveness of non-cell therapy depends on its uptake by target cells (25). Correspondingly, *in vitro* confocal imaging displayed that H9C2 cells endocytosed membrane fluorescent dye PKH67 labeled-MCELNs time-dependently.

Cardiomyocytes undergo apoptosis after radiation exposure (18, 26). Exposure to 16 Gy X-ray significantly declined the cell viability and induced apoptosis in H9C2 cells, consistent with Dai et al.'s report (17). Co-culturing irradiated H9C2 cells with MCELNs improved cell proliferation, demonstrated by the elevated ratio of Ki-67 positive H9C2 cells and protein expressions of cell proliferation marker PCNA. Moreover, radiation exposure reduced the expression of Cyclin D1 and Cyclin B1, indicating cell cycle arrest in irradiated H9C2 cells. MCELNs improved Cyclin D1 and Cyclin B1 expression, suggesting recovered cell cycle thus improving H9C2 cells proliferation. In addition, MCELNs suppressed the apoptosis in irradaited H9C2 cells, as evidenced by decreased pro-apopototic proteins (cleaved caspase3 and cleaved PARP) and decreased apoptotic cells. These results suggested that MCELNs prevented radiation-induced toxicity in H9C2 cells *in vitro*.

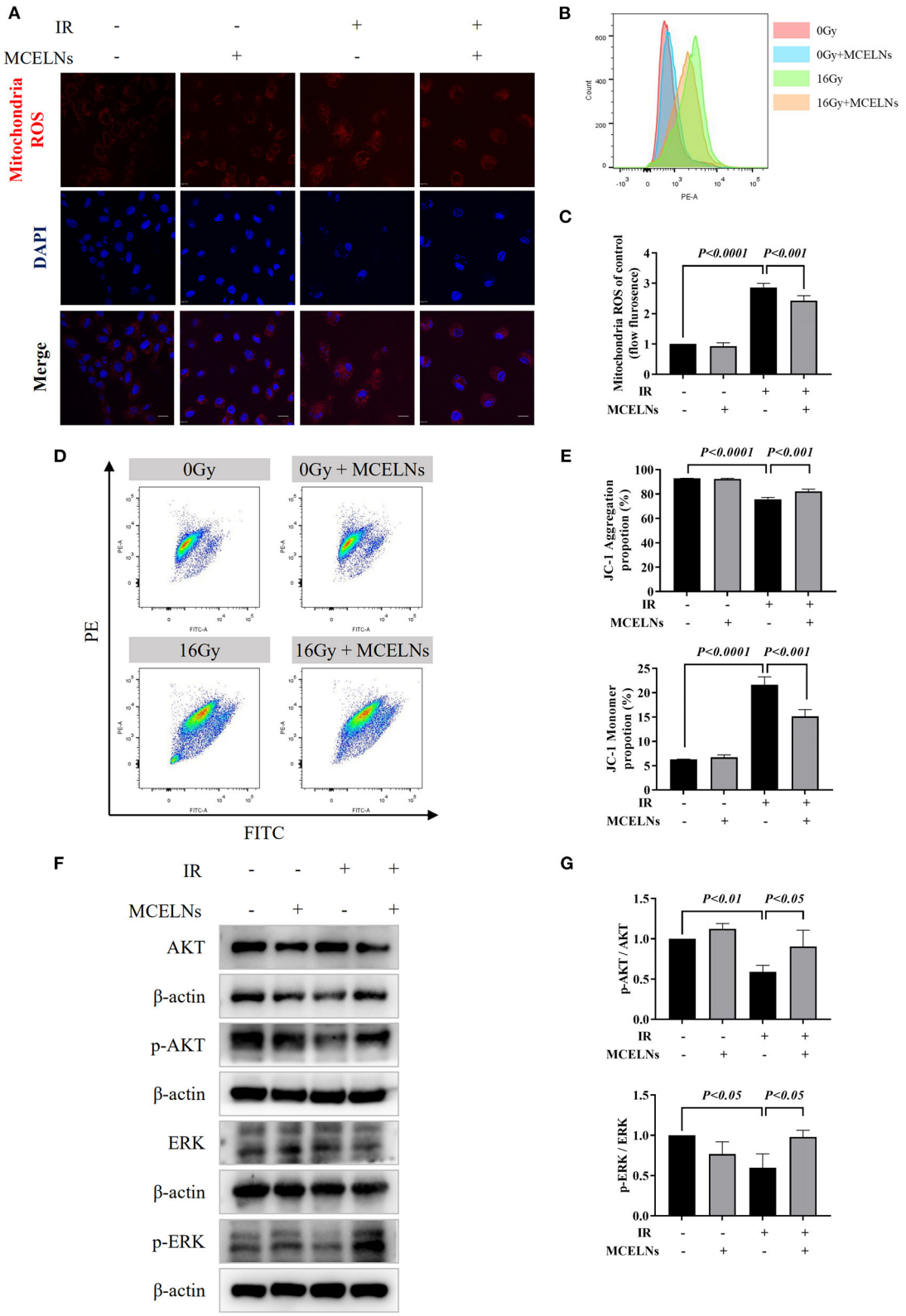

FIGURE 5 | MCELNs ameliorated mitochondrial dysfunction induced cell injury after radiation. **(A)** H9C2 cells after 48 h of culture with indicated treatment were incubated with mitochondria ROS probe (red) for 15 min. Then nucleus were stained with DAPI (blue) for confocal imaging, scale bar: 20 μm. Flow analysis **(B)** and

(Continued)

FIGURE 5 | quantitation **(C)** of mitochondria ROS intensity in H9C2 cells after 48 h of culture with indicated treatment. Flow analysis **(D)** and quantitation **(E)** of mitochondria membrane potential in H9C2 cells after 48 h of culture with indicated treatment that detected by JC-1 probe. Western blot images **(F)** and quantitation **(G)** of AKT, p-AKT, ERK, and p-ERK in H9C2 cells after 48 h of culture with indicated treatment. IR (–/+): 0/16 Gy X-ray; MCELNs (–/+): 0/10 μg/mL. All data were represented as means ± SD ($n = 3$ independent experiments). The statistical significance was evaluated by one-way ANOVA followed by the Turkey's multiple comparisons test among groups.

High doses of radiation cause DNA injury, including base damage, cross-links, single-strand breaks, and double-strand breaks that further alter gene expression, posing genome instability, and cell death (27). Here, we detected the expression of γ-H2A.X, a widely used biomarker of DNA double-strand breaks (28). Radiation exposure significantly upregulated the expression of γ-H2A.X in H9C2 cells, and MCELNs alleviated this damage. Moreover, as the upstream of γ-H2A.X, autophosphorylation of ATM modulates various cellular responses especially initiated DNA double-strand breaks (29). We found that the phosphorylation of ATM significantly increased after radiation exposure. Whereas, MCELNs reversed the abnormal phosphorylated ATM to reduce cardiomyocytes' DNA damage. In all, MCELNs mitigated radiation-induced DNA damage in H9C2 cells.

Mitochondria is a vital organelle in cardiomyocytes that participate in multiple cellular responses. As the primary source of cellular ROS, mitochondria generate appropriate ROS to facilitate cellular immune responses, signal transduction, and apoptosis under normal conditions (30). Radiation disrupts the mitochondria respiratory chain, causing energy metabolism imbalance, generating excessive ROS, initiating cell apoptosis (31). In irradiated H9C2 cells, we observed significantly elevated mitochondria ROS correspondingly. *M. charantia* polysaccharide can clear superoxide, nitric oxide, and peroxynitrite, modulating oxidative stress in neural stem cells (9). Likewise, MCELNs also effectively scavenge radiation-induced excessive mitochondria ROS in H9C2 cells. Standard MMP is the precondition for maintaining mitochondrial oxidative phosphorylation and cellular physiological functions (32). With JC-1 probe staining, we found that MCELNs restored the decreased MMP in irradiated H9C2 cells. Re-balanced mitochondria ROS and MMP may contribute to the protective potentials of MCELNs against RIHD. AKT and ERK signaling pathways have been shown to play vital roles in cell survival and proliferation. And activation of AKT and ERK were associated with cancer radiation resistance. Under stress conditions, excessive ROS generation was reported to reduce the AKT and ERK activation (33). Accordingly, we found significantly reduced p-AKT and p-ERK in irradiated H9C2 cells consistent with Dai et al.'s report (17). MCELNs co-culture recovered the phosphorylation of AKT and ERK. Gu et al. found RhNRG-1β protected the irradiation-induced myocardium injury via activating the ErbB2-ERK-SIRT1 pathway (34). Inhibition of AKT and ERK pathways were also observed in the *in vitro* model of angiotensin II stimulated cardiomyocytes hypetrophy. Ba et al. found allicin activates PI3K/AKT/mTOR and MAPK/ERK/mTOR signaling pathways to inhibit the autophagy process alleviating cardiac hypertrophy (35). Zhang et al. identified FNDC5 mitigates doxorubicin-induced H9C2 cells cardiomyocytes apoptosis via activating AKT (36). Thus, the activation of AKT and ERK signaling pathways might be involved in the protective effects of MCELNs against RIHD. The specific mechanism remains to be further investigated.

Last, we verified the protective effects of MCELNs against RIHD *in vivo*. We generated a mice model of radiation-induced cardiomyopathy by exposing the chest of BALB/c nude mice to 20 Gy X-rays as previously reported (18). In the first couple of days post-IR, the mice's body weight significantly declined, which was mitigated in MCELNs injected mice. However, the body weight of irradiated mice injected with MCELNs or not recovered to the levels comparable to the control mice by the end of observation (35 days post-IR). Due to the unavailability of an electrocardiogram, we failed to assess the cardiac function of mice. Instead, we detected the serum levels of common cardiac injury biomarkers, including cTnT, CKMB, and NT-proBNP. Thoracic RT increased the serum levels of cTnT, CKMB, and NT-proBNP, and MCELNs injection decreased these changes. Moreover, our data showed that CKMB was more sensitive to radiation-induced cardiac injury. Fibrosis is the severe long-term effect of RT that eventually causes cardiac dysfunction and even heart failure (37). We found that MCELNs injection reduced fibrosis in thoracic irradiated mice. Above all, MCELNs may protect cardiac against radiation-induced damage *in vivo*.

There are several limitations in this study. First, cardiomyocytes are the dominant cell type in the heart that we initial investigate the protective effects of MCELNs on them. It would be interesting to investigate whether MCELNs modulate other cardiac cells (endothelial and fibroblast) function in future studies. Second, we just evaluated the uptake of MCELNs by H9C2 cells *in vitro* and did not investigate how the MCELNs were homed to the injured heart. Last but not the least, we did not unravel the role of MCELNs contents (e.g., proteins, microRNAs) in protecting cardiomyocytes from DNA damage and mitochondrial dysfunction.

Collectively, we here successfully isolate EVs-like MCELNs from *M. charantia* and verify their potent cardio-protective effects against radiation *in vitro* and *in vivo*. Plant-derived EVs can access physical barriers, generate less immunogenicity/toxicity, possess inherent cell/tissue targeting capacity, qualifying MCELNs as novel ideal candidates for managing radiation-induced side effects.

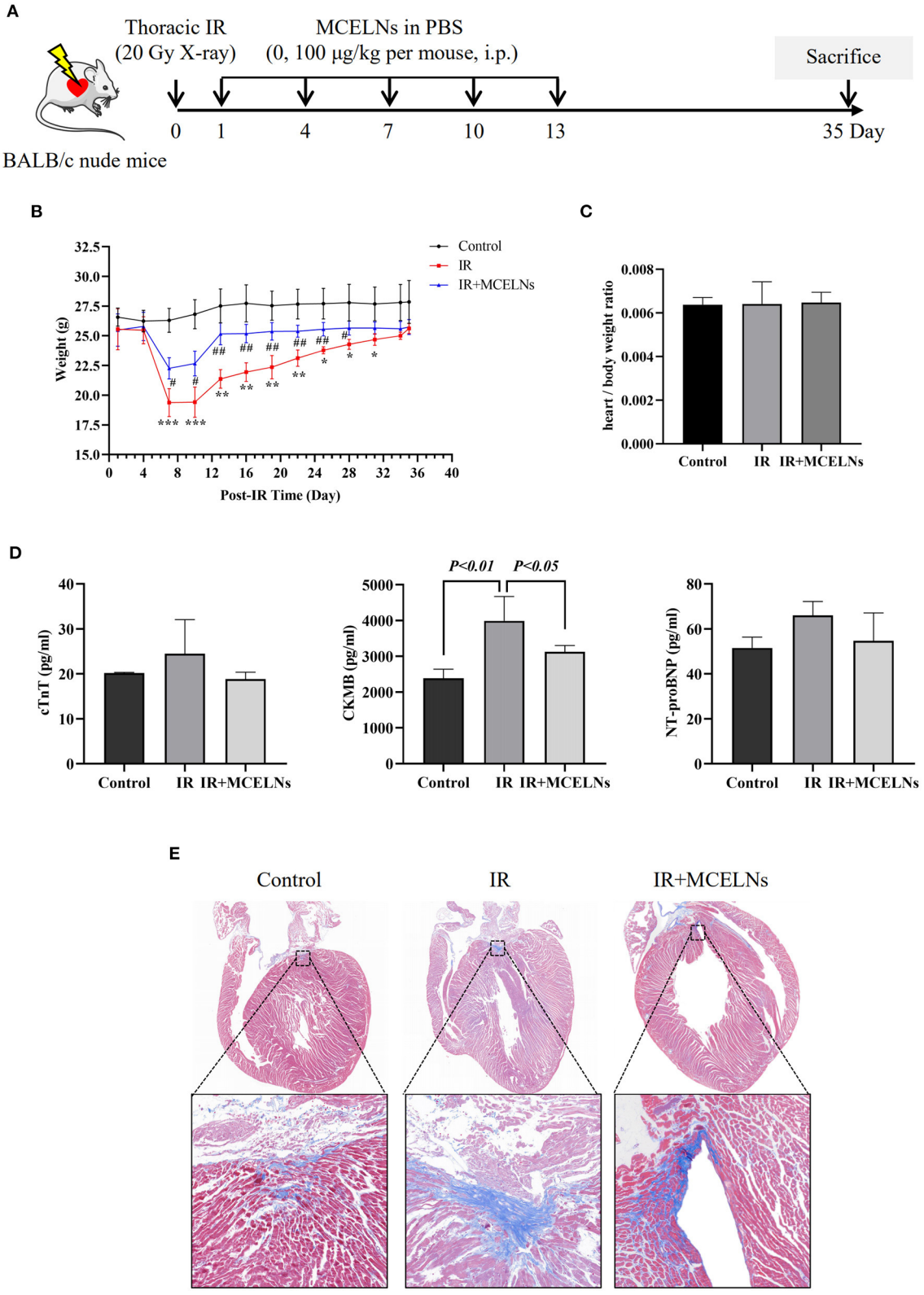

FIGURE 6 | MCELNs exerted *in vivo* protective effect after radiation. **(A)** The generation procedure of thoracic irradiated mice model was illustrated. Briefly, mice were randomly divided into three groups: (1) Control; (2) IR (thoracic irradiation, 20 Gy X-ray, PBS administration post-IR, every other day for 5 times i.p.); (3) IR+MCELNs (thoracic irradiation, 20 Gy X-ray, MCELNs administration post-IR, 100 μg/kg every other day for 5 times, i.p). **(B)** Mice body weight were observed until sacrificed at

(Continued)

FIGURE 6 | day 35. **(C)** The ratio of mice heart weight to body weight were calculated. **(D)** Serum samples were collected to detect the concentrations of cardiac injury marker cTnT, CKMB, and NT-proBNP using ELISA kit. Masson trichrome staining **(E)** were performed to analyze the heart fibrosis area in mice. i.p, intraperitoneal injection. The statistical significance was evaluated by one-way ANOVA followed by the Turkey's multiple comparisons test among groups. RM two-way ANOVA followed by the Turkey's multiple comparisons test was used for significance evaluation of repeat measurement of mice body weight. All data were represented as means ± SD ($n = 4$ independent experiments). $^{*}P < 0.05$, $^{**}P < 0.01$, $^{***}P < 0.001$ vs. Control. $^{\#}P < 0.05$, $^{\#\#}P < 0.01$, vs. IR.

DATA AVAILABILITY STATEMENT

The original contributions presented in the study are included in the article/supplementary material, further inquiries can be directed to the corresponding authors.

ETHICS STATEMENT

The animal study was reviewed and approved by Institutional Animal Care and Use Committee of Xuzhou Medical University.

AUTHOR CONTRIBUTIONS

W-WC: conception and design, collection and/or assembly of data, data analysis and interpretation, and manuscript writing. CYe, K-XW, and XY: collection and/or assembly of data, data analysis, and interpretation. P-YZ and KH: collection and/or assembly of data. TL, L-YH, and W-WC: data analysis and interpretation. BG and CYa: financial support. PM: manuscript editing. S-HQ and LL: conception and design, data analysis and interpretation, manuscript writing, financial support, and final approval of manuscript. All authors contributed to the article and approved the submitted version.

FUNDING

This work was supported by the National Natural Science Foundation of China (Grant Nos. 81802086, 81860425, and 81802063), Scientific Research Project of Jiangsu Provincial Healthy Commission (Grant No. ZDB2020024), Natural Science Foundation of Jiangsu Province (Grant No. BK20211348), the project of Science and Technology Department of Jiangxi Province (Grant No. 20204BCJ23018), the project of Science and Xuzhou Basic Research Project (Grant No. KC21030), the Specialized Research Fund for Senior Personnel Program (Grant No. D2019028), and the Young Science and Technology Innovation Team (Grant No. TD202005) of Xuzhou Medical University.

ACKNOWLEDGMENTS

The experiments in this article were partly performed in Public Experimental Research Center of Xuzhou Medical University, and thanks the teachers for their support and help during the experiments.

REFERENCES

1. Quintero-Martinez JA, Cordova-Madera SN, Villarraga HR. Radiation-induced heart disease. *J Clin Med.* (2021) 11:146. doi: 10.3390/jcm11010146
2. Wang H, Wei J, Zheng Q, Meng L, Xin Y, Yin X, et al. Radiation-induced heart disease: a review of classification, mechanism and prevention. *Int J Biol Sci.* (2019) 15:2128–38. doi: 10.7150/ijbs.35460
3. Mulrooney DA, Hyun G, Ness KK, Ehrhardt MJ, Yasui Y, Duprez D, et al. Major cardiac events for adult survivors of childhood cancer diagnosed between 1970 and 1999: report from the Childhood Cancer Survivor Study cohort. *BMJ.* (2020) 368:l6794. doi: 10.1136/bmj.l6794
4. Shimizu Y, Kodama K, Nishi N, Kasagi F, Suyama A, Soda M, et al. Radiation exposure and circulatory disease risk: Hiroshima and Nagasaki atomic bomb survivor data, 1950-2003. *BMJ.* (2010) 340:b5349. doi: 10.1136/bmj.b5349
5. Azizova TV, Batistatou E, Grigorieva ES, McNamee R, Wakeford R, Liu H, et al. An assessment of radiation-associated risks of mortality from circulatory disease in the cohorts of Mayak and Sellafield nuclear workers. *Radiat Res.* (2018) 189:371–88. doi: 10.1667/RR14468.1
6. Spetz J, Moslehi J, Sarosiek K. Radiation-induced cardiovascular toxicity: mechanisms, prevention, and treatment. *Curr Treat Options Cardiovasc Med.* (2018) 20:31. doi: 10.1007/s11936-018-0627-x
7. Mun GI, Kim S, Choi E, Kim CS, Lee YS. Pharmacology of natural radioprotectors. *Arch Pharm Res.* (2018) 41:1033–50. doi: 10.1007/s12272-018-1083-6
8. Cheki M, Mihandoost E, Shirazi A, Mahmoudzadeh A. Prophylactic role of some plants and phytochemicals against radio-genotoxicity in human lymphocytes. *J Cancer Res Ther.* (2016) 12:1234–42. doi: 10.4103/0973-1482.172131
9. Gong J, Sun F, Li Y, Zhou X, Duan Z, Duan F, et al. Momordica charantia polysaccharides could protect against cerebral ischemia/reperfusion injury through inhibiting oxidative stress mediated c-Jun N-terminal kinase 3 signaling pathway. *Neuropharmacology.* (2015) 91:123–34. doi: 10.1016/j.neuropharm.2014.11.020
10. Ma J, Fan H, Cai H, Hu Z, Zhou X, Li F, et al. Promotion of Momordica Charantia polysaccharides on neural stem cell proliferation by increasing SIRT1 activity after cerebral ischemia/reperfusion in rats. *Brain Res Bull.* (2021) 170:254–63. doi: 10.1016/j.brainresbull.2021.02.016
11. Hu Z, Li F, Zhou X, Zhang F, Huang L, Gu B, et al. Momordica charantia polysaccharides modulate the differentiation of neural stem cells via SIRT1/Beta-catenin axis in cerebral ischemia/reperfusion. *Stem Cell Res Ther.* (2020) 11:485. doi: 10.1186/s13287-020-02000-2
12. Karamanidou T, Tsouknidas A. Plant-derived extracellular vesicles as therapeutic nanocarriers. *Int J Mol Sci.* (2021) 23:191. doi: 10.3390/ijms23010191
13. Urzi O, Raimondo S, Alessandro R. Extracellular vesicles from plants: current knowledge and open questions. *Int J Mol Sci.* (2021) 22:5366. doi: 10.3390/ijms22105366
14. H US, Brotherton D, Inal J. Communication is key: extracellular vesicles as mediators of infection and defence during host-microbe interactions in animals and plants. *FEMS Microbiol Rev.* (2022) 46fuab044. doi: 10.1093/femsre/fuab044
15. Chen X, Zhou Y, Yu J. Exosome-like nanoparticles from ginger rhizomes inhibited NLRP3 inflammasome activation. *Mol Pharm.* (2019) 16:2690–9. doi: 10.1021/acs.molpharmaceut.9b00246
16. Bruno SP, Paolini A, D'Oria V, Sarra A, Sennato S, Bordi F, et al. Extracellular vesicles derived from citrus sinensis modulate inflammatory genes and tight

junctions in a human model of intestinal epithelium. *Front Nutr.* (2021) 8:778998. doi: 10.3389/fnut.2021.778998
17. Dai C, He L, Ma B, Chen T. Facile nanolization strategy for therapeutic ganoderma lucidum spore oil to achieve enhanced protection against radiation-induced heart disease. *Small.* (2019) 15:e1902642. doi: 10.1002/smll.201902642
18. Mezzaroma E, Di X, Graves P, Toldo S, Van Tassell BW, Kannan H, et al. A mouse model of radiation-induced cardiomyopathy. *Int J Cardiol.* (2012) 156:231–3. doi: 10.1016/j.ijcard.2012.01.038
19. Fischer N, Seo EJ, Efferth T. Prevention from radiation damage by natural products. *Phytomedicine.* (2018) 47:192–200. doi: 10.1016/j.phymed.2017.11.005
20. Wang W, Xue C, Mao X. Radioprotective effects and mechanisms of animal, plant and microbial polysaccharides. *Int J Biol Macromol.* (2020) 153:373–84. doi: 10.1016/j.ijbiomac.2020.02.203
21. Nanduri LSY, Duddempudi PK, Yang WL, Tamarat R, Guha C. Extracellular vesicles for the treatment of radiation injuries. *Front Pharmacol.* (2021) 12:662437. doi: 10.3389/fphar.2021.662437
22. Accarie A, l'Homme B, Benadjaoud MA, Lim SK, Guha C, Benderitter M, et al. Extracellular vesicles derived from mesenchymal stromal cells mitigate intestinal toxicity in a mouse model of acute radiation syndrome. *Stem Cell Res Ther.* (2020) 11:371. doi: 10.1186/s13287-020-01887-1
23. Rome S. Biological properties of plant-derived extracellular vesicles. *Food Funct.* (2019) 10:529–38. doi: 10.1039/C8FO02295J
24. Kameli N, Dragojlovic-Kerkache A, Savelkoul P, Stassen FR. Plant-derived extracellular vesicles: current findings, challenges, and future applications. *Membranes.* (2021) 11:411. doi: 10.3390/membranes11060411
25. Dad HA, Gu TW, Zhu AQ, Huang LQ, Peng LH. Plant exosome-like nanovesicles: emerging therapeutics and drug delivery nanoplatforms. *Mol Ther.* (2021) 29:13–31. doi: 10.1016/j.ymthe.2020.11.030
26. Salata C, Ferreira-Machado SC, De Andrade CB, Mencalha AL, Mandarim-De-Lacerda CA, de Almeida CE. Apoptosis induction of cardiomyocytes and subsequent fibrosis after irradiation and neoadjuvant chemotherapy. *Int J Radiat Biol.* (2014) 90:284–90. doi: 10.3109/09553002.2014.887869
27. Nakano T, Xu X, Salem AMH, Shoulkamy MI, Ide H. Radiation-induced DNA-protein cross-links: mechanisms and biological significance. *Free Radic Biol Med.* (2017) 107:136–45. doi: 10.1016/j.freeradbiomed.2016.11.041
28. Kinner A, Wu W, Staudt C, Iliakis G. Gamma-H2AX in recognition and signaling of DNA double-strand breaks in the context of chromatin. *Nucleic Acids Res.* (2008) 36:5678–94. doi: 10.1093/nar/gkn550
29. Guo Z, Kozlov S, Lavin MF, Person MD, Paull TT. ATM activation by oxidative stress. *Science.* (2010) 330:517–21. doi: 10.1126/science.1192912
30. Sies H, Jones DP. Reactive oxygen species (ROS) as pleiotropic physiological signalling agents. *Nat Rev Mol Cell Biol.* (2020) 21:363–83. doi: 10.1038/s41580-020-0230-3
31. Ping Z, Peng Y, Lang H, Xinyong C, Zhiyi Z, Xiaocheng W, et al. Oxidative stress in radiation-induced cardiotoxicity. *Oxid Med Cell Longev.* (2020) 2020:3579143. doi: 10.1155/2020/3579143
32. Yang H, van der Stel W, Lee R, Bauch C, Bevan S, Walker P, et al. Dynamic modeling of mitochondrial membrane potential upon exposure to mitochondrial inhibitors. *Front Pharmacol.* (2021) 12:679407. doi: 10.3389/fphar.2021.679407
33. Zhang J, Wang X, Vikash V, Ye Q, Wu D, Liu Y, et al. ROS and ROS-mediated cellular signaling. *Oxid Med Cell Longev.* (2016) 2016:4350965. doi: 10.1155/2016/4350965
34. Gu A, Jie Y, Sun L, Zhao S, E M, You Q. RhNRG-1beta protects the myocardium against irradiation-induced damage via the ErbB2-ERK-SIRT1 signaling pathway. *PLoS ONE.* (2015) 10:e0137337. doi: 10.1371/journal.pone.0137337
35. Ba L, Gao J, Chen Y, Qi H, Dong C, Pan H, et al. Allicin attenuates pathological cardiac hypertrophy by inhibiting autophagy via activation of PI3K/Akt/mTOR and MAPK/ERK/mTOR signaling pathways. *Phytomedicine.* (2019) 58:152765. doi: 10.1016/j.phymed.2018.11.025
36. Zhang X, Hu C, Kong CY, Song P, Wu HM, Xu SC, et al. FNDC5 alleviates oxidative stress and cardiomyocyte apoptosis in doxorubicin-induced cardiotoxicity via activating AKT. *Cell Death Differ.* (2020) 27:540–55. doi: 10.1038/s41418-019-0372-z
37. Wang B, Wang H, Zhang M, Ji R, Wei J, Xin Y, et al. Radiation-induced myocardial fibrosis: Mechanisms underlying its pathogenesis and therapeutic strategies. *J Cell Mol Med.* (2020) 24:7717–29. doi: 10.1111/jcmm.15479

Conflict of Interest: The authors declare that the research was conducted in the absence of any commercial or financial relationships that could be construed as a potential conflict of interest.

Publisher's Note: All claims expressed in this article are solely those of the authors and do not necessarily represent those of their affiliated organizations, or those of the publisher, the editors and the reviewers. Any product that may be evaluated in this article, or claim that may be made by its manufacturer, is not guaranteed or endorsed by the publisher.

frontiers | Frontiers in Cardiovascular Medicine

TYPE Original Research
PUBLISHED 29 July 2022
DOI 10.3389/fcvm.2022.943068

OPEN ACCESS

EDITED BY
Zhen-Ao Zhao,
Hebei North University, China

REVIEWED BY
Dongtak Jeong,
Hanyang University, South Korea
Guglielmo Saitto,
San Camillo-Forlanini Hospital, Italy

*CORRESPONDENCE
Vincenzo Lionetti
v.lionetti@santannapisa.it

†These authors have contributed equally to this work and share first authorship

SPECIALTY SECTION
This article was submitted to Cardiovascular Biologics and Regenerative Medicine, a section of the journal Frontiers in Cardiovascular Medicine

RECEIVED 13 May 2022
ACCEPTED 04 July 2022
PUBLISHED 29 July 2022

CITATION
Pizzino F, Furini G, Casieri V, Mariani M, Bianchi G, Storti S, Chiappino D, Maffei S, Solinas M, Aquaro GD and Lionetti V (2022) Late plasma exosome microRNA-21-5p depicts magnitude of reverse ventricular remodeling after early surgical repair of primary mitral valve regurgitation. *Front. Cardiovasc. Med.* 9:943068. doi: 10.3389/fcvm.2022.943068

Late plasma exosome microRNA-21-5p depicts magnitude of reverse ventricular remodeling after early surgical repair of primary mitral valve regurgitation

Fausto Pizzino[1,2†], Giulia Furini[1†], Valentina Casieri[1], Massimiliano Mariani[2], Giacomo Bianchi[2], Simona Storti[2], Dante Chiappino[2], Stefano Maffei[2], Marco Solinas[2], Giovanni Donato Aquaro[2] and Vincenzo Lionetti[1,2*]

[1]Unit of Translational Critical Care Medicine, Scuola Superiore Sant'Anna, Pisa, Italy, [2]Fondazione Toscana Gabriele Monasterio, Pisa, Italy

Introduction: Primary mitral valve regurgitation (MR) results from degeneration of mitral valve apparatus. Mechanisms leading to incomplete postoperative left ventricular (LV) reverse remodeling (Rev–Rem) despite timely and successful surgical mitral valve repair (MVR) remain unknown. Plasma exosomes (pEXOs) are smallest nanovesicles exerting early postoperative cardioprotection. We hypothesized that late plasma exosomal microRNAs (miRs) contribute to Rev–Rem during the late postoperative period.

Methods: Primary MR patients (n = 19; age, 45–71 years) underwent cardiac magnetic resonance imaging and blood sampling before (T0) and 6 months after (T1) MVR. The postoperative LV Rev–Rem was assessed in terms of a decrease in LV end-diastolic volume and patients were stratified into high (HiR-REM) and low (LoR-REM) LV Rev–Rem subgroups. Isolated pEXOs were quantified by nanoparticle tracking analysis. Exosomal microRNA (miR)-1, −21–5p, −133a, and −208a levels were measured by RT-qPCR. Anti-hypertrophic effects of pEXOs were tested in HL-1 cardiomyocytes cultured with angiotensin II (AngII, 1 μ M for 48 h).

Results: Surgery zeroed out volume regurgitation in all patients. Although preoperative pEXOs were similar in both groups, pEXO levels increased after MVR in HiR-REM patients (+0.75-fold, p = 0.016), who showed lower cardiac mass index (−11%, p = 0.032). Postoperative exosomal miR-21-5p values of HiR-REM patients were higher than other groups ($p < 0.05$). *In vitro*, T1-pEXOs isolated from LoR-REM patients boosted the AngII-induced cardiomyocyte hypertrophy, but not postoperative exosomes of HiR-REM. This adaptive effect was counteracted by miR-21-5p inhibition.

10.3389/fcvm.2022.943068

Summary/Conclusion: High levels of miR-21-5p-enriched pEXOs during the late postoperative period depict higher LV Rev–Rem after MVR. miR-21-5p-enriched pEXOs may be helpful to predict and to treat incomplete LV Rev–Rem after successful early surgical MVR.

KEYWORDS

exosomes, reverse remodeling, mitral valve (MV) repair, heart surgery, postoperative, miR-21-5p

Introduction

Mitral valve regurgitation (MR) is one of the most common cardiac valve diseases leading to blood regurgitation into the left atrium (LA) and to left ventricular (LV) dilatation, also defined as "LV adverse remodeling," following increased preload up to the onset of heart failure (HF) (1). Primary MR is associated with degeneration of the valve apparatus or with annular dilatation. Even though patients with a severe primary MR remain asymptomatic for a remarkably long period of time with preserved LV function (2–5), an increased risk for cardiovascular morbidity and mortality is described (2, 4, 6). Therefore, early surgical mitral valve repair (MVR) is strongly recommended in experienced surgical center by current guidelines (7) due to the lack of effective pharmacological treatments. Indeed, long-term postoperative survival is worse if surgery is performed after patients become symptomatic and the mitral valve is not successfully repairable.

Most patients with severe primary MR and LV dysfunction undergoing timely MVR (7–9) are at minimal risk of MR recurrence and show progressive reduction of LV volumes defined as "LV reverse remodeling (Rev–Rem)" (10–12). However, a non-negligible number of patients may experience worsened clinical outcome during late postoperative period due to a partial LV Rev–Rem (13–15) after timely and technically successful MVR (16, 17). Early recognition and treatment of these patients remains a desirable goal in hospital setting (4, 18, 19). Indeed, personalization of early-to-late postoperative follow-up and timely escalation of therapy for patients at higher risk for incomplete LV Rev–Rem is expected even when patients with severe MR, preserved LV function, and normal exercise capacity undergo early surgical treatment (7, 9).

Preoperative echocardiography is now commonly used as a method for screening postoperative outcome in terms of long-term survival (20–23), MR recurrence (24), Rev–Rem (12, 25–27) and functional preservation of the left ventricle (13, 14, 28–30). However, the early predictive value of echocardiography is affected by several limitations (31, 32). Conversely, cardiac magnetic resonance imaging (CMRI) is the gold-standard technique in the evaluation of cardiac mass, fibrosis, volumes, dimensions and function (33, 34) and is highly reliable in the characterization of cardiac tissues and in the evaluation of LV remodeling. Yet, its role in depicting the pathogenic events that occur at the molecular level to predict early-to-late LV Rev–Rem after early rescue mitral valve surgery is still undefined (35). Moreover, the perioperative use of CMRI is limited by the low availability of the method, and by the high cost. Despite the availability of present indications for early rescue mitral valve surgery (36) and current non-invasive diagnostic technologies, the quality of surgical outcomes in patients with primary MR remains heterogeneous, and the traditional markers (symptoms, LV phenotype) are poor outcome markers. Therefore, additional reliable and more sensitive indicators of reverse ventricular remodeling during medical management are of paramount importance to start treating adverse myocardial remodeling in the postoperative period even in the absence of cardiac dysfunction and symptoms.

Plasma exosomes (pEXOs) are smallest membrane bound extracellular vesicles (40–150 nm in diameter) released by different cells, which may play a key role in intercellular communication by regulating the magnitude of postoperative LV Rev–Rem. It is conceivable that combining analysis of pEXOs with CMRI parameters may enable more precise and informative assessment of late LV Rev–Rem. Indeed, the previous studies have demonstrated the role of pEXOs in mediating cardioprotection through anti-inflammatory and anti-apoptotic pathways (37, 38) regardless of the type of cardiac surgery (39). Although the investigation on their role in late LV Rev–Rem after surgery is at its infancy, changes of pEXOs profile have been already suggested as non-invasive early indicators of cardiac function in both critically ill (40) and surgical patients (41, 42), even after the heart transplantation (43).

Exosomal microRNA (miR), small non-coding RNA molecule (∼20 nucleotides) regulating gene expression, is effective mediator of the adaptive paracrine responses in cardiomyocytes exposed to different stressors (38, 44). The distinctive microRNAs expression patterns are associated with MR (45) and exosomes are the source of choice for microRNAs in biomarker studies (46, 47). In fact, the exosomal fraction of microRNAs was able to predict the risk of adverse cardiac events in patients with stable coronary artery diseases (48) and

was correlated with postoperative cardiac troponin levels in patients subjected to coronary artery–bypass–graft surgery (38).

The evidences above well support the use of pEXOs and corresponding microRNAs to depict the extent of LV Rev–Rem in our MR patients during the late postoperative period. Since some reports have focused on their predictive value in dogs with MR (49) and in patients undergoing transcatheter valve repair (31), further investigation of their long-lasting cardioprotective role after early surgical valve repair is required.

In this study, we hypothesized that the postoperative change in the levels of pEXOs delivering specific microRNAs may underlie LV Rev–Rem in the primary MR patients after the early surgical MVR. For this purpose, we also used CMRI to better assess the late postoperative changes in cardiac structure and function. Using a gold standard approach, we measured both levels of pEXOs and exosomal microRNAs specifically related to remodeling and heart failure, such as miR-1, miR-133a, and miR208a (50–52), and to cardioprotection, such as miR-21-5p (53). Finally, the anti-remodeling properties of late pEXOs and those of selected exosomal miR were tested in cultured adult murine cardiomyocytes (HL-1) exposed to angiotensin II, an established *in vitro* model of cardiac hypertrophy (54, 55).

Materials and methods

Study design and patients

Our study was approved by Ethics Committee of "G. Monasterio" Foundation (FTGM, Massa, Italy) (EMIGRATE study, approval n°1529) in accord with the principles outlined in the Declaration of Helsinki. We obtained signed informed consent from each patient. Aiming to select patients with higher mitral valve repair probability, the inclusion criteria were as follows: Age (35–75 years); presence of severe primary MR due to prolapse or flail leaflet as assessed by transthoracic echocardiography, sinus rhythm, and clinical indication to surgery. According to clinical guidelines, severe primary MR was diagnosed when at least one of the following parameters was detected by transthoracic echocardiography (56–58): (1) Vena contracta width more than or 7 mm from the parasternal long-axis view, (2) effective regurgitant orifice (ERO) area more than or 0.4 cm^2, as evaluated by proximal isovelocity surface area (PISA) method, and (3) regurgitant volume more than or 60 ml. The patients with echocardiography evidence of leaflet tethering (typical of secondary MR) or calcific degenerative restricted motion of leaflets were excluded. In the case that, during surgery, the surgeon decided to convert intervention to valve replacement, the patients were then excluded from the study. Other exclusion criteria comprehended the following: chronic kidney disease (CKD) defined as glomerular filtration rate less than 50 ml/m^2, the previous cardiac surgery or history of congenital heart disease, the current or past myocardial ischemia/severe coronary artery disease, LV ejection fraction (LVEF) less than 40%, other-than-mitral valve diseases more than mild, and any contraindications to CMRI. The current cardiovascular risk factors, functional capacity according to the New York Heart Association (NYHA) classification (59), presence of CKD, and medications were assessed prior to surgery.

The complete clinical profile of patients is described in **Table 1**. Eight healthy Caucasian volunteers (age, <60 years) with no evidence of cardiac disease were recruited as a control group. Since we detected prevalence of males among our patients (**Table 1**), we enrolled only male volunteers to avoid gender bias.

We performed combined CMRI and blood sampling for pEXO isolation before surgery (baseline) and at 6 months after surgery. The timing of the experimental protocol was in accord with the previous studies (60, 61). Only patients who completed the whole protocol were included in the study.

Mitral valve repair surgery and experimental protocol

All patients underwent same anesthetic protocol and standard hypothermic cardiopulmonary bypass (CPB) procedure. Successful surgical repair of the mitral valve was performed mainly through a minimally invasive endoscopic approach to the mitral valve (39, 62). Briefly, chest access was *via* a small right incision in the third or fourth intercostal space—a periareolar (in males) access or axillary (in females) minithoracotomy was performed. The median sternotomy was the alternative surgical approach when the minimally invasive approach was not possible (**Table 1**). An extracorporeal circulation was established through peripheral femoro–femoral cannulation using surgical cut-down approach. After opening the pericardium, the ascending aorta was gently cross-clamped externally and cold crystalloid cardioplegic solution (Custodiol) was infused in an antegrade fashion. The mitral valve was exposed through opening of the interatrial groove and the atrial lift retractor (USB Medical) was positioned exposing the mitral valve. The repair surgery was carried out according to the usual techniques in accord with the type of mitral pathology. All patients underwent implantation of a prosthetic annulus, and most also underwent the implantation of Gore-Tex prosthetic cords to restore proper posterior leaflet height (**Table 1**). The successful repair was assessed with intraoperative transesophageal echocardiography before suturing the surgical access. Cardiac magnetic resonance imaging and blood collection were performed prior to surgery (T0) and 6-months after surgery (T1) in awaken patients.

10.3389/fcvm.2022.943068

TABLE 1 Clinical features and CMRI parameters of MR patients enrolled in the study.

Clinical picture	
Age (years)	55.2 ± 8.0 (50–69, 57.9%; 70+, 10.5%)
Sex (male)	94,74%
BMI (kg/m^2)	26.1 ± 2.9 (25–30, 57.9%; 30+, 10.5%)
Smoking status (smoker)	15.8%
Hypertension	47.4%
Hypercholesterolemia	31.6%
Peripheral vascular disease	5.3%
Prior stroke/TIA events	0%
Heart failure	0%
Family history of CVD	21.1%
NYHA	I, 36.8%; II, 57.9%; III, 5.3%
CHA_2DS_2-VASc Score	0, 52.6%; 1, 31.6%; 2, 15.8%
Diabetes mellitus	0%
CKD	0%
Pharmacotherapy	
β-Blockers	84.2%
Ace-inhibitors	26.3%
Calcium antagonists	0%
Diuretics	63.2%
Levels in blood	
BNP (ng/L)	39.4 ± 34.4
K (mEq/L)	3.96 ± 0.19
Ca (mg/dl)	8.43 ± 0.32
Mg (mg/dl)	1.78 ± 0.23
MR and surgery	
Type of MR	Flail, 36.8%; Prolapse, 63.2%
Leaflet failure	Anterior, 5.3%; Posterior, 68.4%; Both, 21.1%
Surgical access	Right minithoracotomy, 94.7%; Median sternotomy, 5.3%
Implanted ring	CG Future band, 47.4%; Simulus semi-rigid, 47.4%; Profile 3D, 5.3%
N of neochords implanted	0, 22.2%; 1, 16.7%; 2, 61.1%
Preoperative CMRI	
LVEDVi (ml/m^2)	113.67 ± 25.37
LVESVi (ml/m^2)	42.50 ± 11.77
RVEDVi (ml/m^2)	84.78 ± 15.57
RVESVi (ml/m^2)	34.44 ± 9.00
LV Mass index (g/m^2)	77.44 ± 13.36
LVSV (ml)	142.33 ± 35.93
LVSVi (ml/m^2)	72.36 ± 16.98
RVSV (ml)	100.67 ± 20.93
RVSVi (ml/m^2)	51.15 ± 9.72
LVEF (%)	62.60 ± 5.87
RVEF (%])	59.64 ± 6.56
Heart rate (BPM)	61.00 ± 7.92
Cardiac index (ml/min · m^2)	4180.36 ± 1114.27
LA Area index (cm)	19.37 ± 7.89
RA Area (cm)	14.32 ± 5.71
LA-max volume index (ml/m^2)	77.53 ± 27.15
LAEF (%)	53.44 ± 9.48
LVSV phase contrast (ml)	85 ± 19
Regurgitant volume (ml)	55 ± 31
Regurgitant fraction (%)	37.09 ± 14.00
LGE presence (*n*, %)	44.44%

Clinical features of $N = 19$ patients undergoing MVR surgery were evaluated prior to the surgical procedure; CMRI performed before (T0) the surgical procedure were also analyzed and are shown in the table. Categorical variables are reported as percentage; continuous variables are presented as mean ± SD.

Transthoracic echocardiography

Transthoracic echocardiography was performed with a commercial machine equipped with a 5–1 mHz phased array probe (iE33 system, Phillips Medical Systems, Andover, MA, United States). Left ventricular ejection fraction was evaluated with the modified Simpson Biplane method. The postoperative residual mitral regurgitation was evaluated using a scale from 0 (nil) to 4 (severe), in all patients. All the measurements were performed according to the current standards (63, 64).

Cardiac magnetic resonance imaging

Cardiac magnetic resonance imaging (3.0T scanner, Ingenia, Philips) was used to assess cardiac remodeling and valve function. Briefly, endocardial and epicardial borders of both ventricles and left atrium (LA) were manually delineated at end-diastole (ED) and end-systole (ES) by an experienced operator. For both ventricles, ED and ES volumes (EDV and ESV, respectively) were calculated from a stack of cine balanced steady-state free precession (bSSFP) short-axis images acquired orthogonally to the LV long axis, from mitral valve to apex, without gap between each slice. Left ventricular myocardial mass was calculated by subtracting the total endocardial volume from the total epicardial volume then multiplying for myocardial density (1.06 g/ml). Left ventricular and right ventricular (RV) stroke volumes (LVSV and RVSV, respectively) were calculated as EDV– ESV. The body–surface area indexed values (*i*) were calculated for all parameters (65). To determine global cardiac function, ejection fraction (EF) was calculated as

$$(\mathrm{SV}/\mathrm{EDV}) \times 100$$

for both ventricles.

To assess the positive LV reverse remodeling following surgery, the reduction in LVEDV from T0 to T1 was computed as

$$(\mathrm{LVEDVT1} - \mathrm{LVEDVT0})/\mathrm{LVEDVT1}$$

The patients with a percentage of change lower than the median value were included in the *High LV reverse remodeling group* (HiR-REM) while patients with values above the median value were included in the *Low LV reverse remodeling group* (LoR-REM).

Phase contrast sequences at the level of aorta and pulmonary artery roots were used to obtain a direct quantification of the blood volume pumped out of LV and RV at each systole, respectively (measured stroke volume). For each patient, the velocity of encoding was adapted to be the lower possible level that avoided aliasing noise. Regurgitant volume was obtained by subtracting the anterograde LVSV measured by the analysis of velocity encoded phase contrast images at the aortic root level (66). Briefly, once flow/time curve was generated, the anterograde SV was measured as the area under the curve of positive flow after the subtraction of the area under the retrograde flow in case of aortic regurgitation.

LVSV was also measured in short axis cine bSSFP as

$$\text{LVEDV} - \text{LVESV (66)}$$

and the mitral valve regurgitant volume was measured as

$$\text{LVSV} - \text{anterograde SV (66, 67)}$$

The myocardial fibrosis was assessed by Late Gadolinium Enhancement (LGE) technique (68). Briefly, 10 min after intravenous injection of a gadolinium-based contrast agent [either Omniscan (GE Healthcare, Amersham, United Kingdom) or Magnevist (Schering, Berlin, Germany) at a concentration of 0.1–0.2 mmol/kg], a stack of short axis sections of both ventricles perpendicular to the LV long axis were acquired without gap using a T1-weighted gradient echo inversion recovery sequence. Appropriate Inversion time to null normal myocardium was chosen using a look-locker TI-scout. Slice thickness was set at 8 mm in all scans.

Isolation of plasma exosomes

A 12-ml volume of peripheral venous EDTA-treated blood was collected from MR patients and controls. Plasma was isolated with a 10,000*g* centrifugation for 15 min at 10°C and was stored at –80°C until analysis. pEXOs were isolated and purified from 1-ml plasma using an optimized 2-d ultracentrifugation protocol [adapted from the study discussed in Ref. 39]. Briefly, plasma was diluted with 15 volumes of filtered (0.2-μm pore) phosphate buffer solution (PBS) and centrifuged at 3,000*g* for 15 min at 10°C. Supernatant was filtered (0.2-μm pore) and subjected to the following centrifugation series: 10,000*g* for 15 min at 10°C (discarding pellet), 20,000*g* for 30 min at 10°C (discarding pellet), then 100,000*g* for 5 h at 4°C. The pellet from the ultracentrifugation was re-suspended in 1 ml of PBS and stored at 4°C overnight. The day after, it was vortexed thoroughly and centrifuged at 10,000*g* for 15 min at 10°C. The supernatant obtained was diluted with 15 volumes of filtered PBS, and centrifuged at 20,000*g* for 30 min at 10°C. Eventually, the supernatant was ultracentrifuged at 100,000*g* for 5 h at 4°C. The final exosomal pellet was re-suspended in 100 μl of cold filtered PBS and was stored at –80°C until analysis.

Quantification of plasma exosomes

The particle size and concentration were measured by nanoparticle tracking analysis (NTA) using a NanoSight LM10 NTA instrument with NTA 3.2 software for data acquisition and analysis (Malvern Panalytical). The pEXOs samples were diluted with filtered PBS to match the recommended particle concentration range {20–120 particles/field; $[(1 \times 10^7)$–$(1 \times 10^9)]$ particles/ml}. Three 60-s videos were acquired for each sample maintaining a camera level, 10; and the videos were analyzed at detection threshold, 3. The modal particle size and particles concentration/ml was measured by the software. The pEXOs concentration was inferred from the particle size distribution up to 150-nm size, it was normalized by resuspension volume and expressed relative to the starting plasma volume.

Western blot analysis of plasma exosomes

The analysis of exosomal proteins is used to characterize the profile of pEXOs in hospital setting (39). Isolated pEXOs were suspended in 100 μl RIPA buffer [50-mM Tris, 300-mM NaCl, 5-mM EDTA, 1% (v/v) NP40, 0.1% (w/v) SDS, 0.5% (w/v) di sodium deoxycholate] containing protease inhibitors (Sigma), incubated on ice for 30 min and then sonicated on ice for 5 min to improve homogenization efficiency. The protein concentration was measured using Pierce™ BCA Protein Assay Kit (Thermo Fisher Scientific) as previously described by us (39). Equal amounts of proteins (50 μg) were resolved by 12% SDS polyacrylamide gel and transferred to nitrocellulose membrane (Bio-Rad). Equal loading was controlled by Ponceau staining. The membranes were blocked with 5% (w/v) non-fat milk in TBST [TBS pH 7.4 containing 0.1% (v/v) tween-20] for an hour at room temperature. The primary antibodies were diluted in blocking buffer and membranes incubated overnight at 4°C to detect tetraspanins CD63 (1:1,000, anti-CD63, Santa Cruz Biotechnology) and CD81 (1:1,000, anti-CD81, Santa Cruz Biotechnologies), and tumor susceptibility gene 101 (1:1,000, anti-TSG101, Sigma) common hallmarks of human pEXOs (44, 69). Specific protein bands were detected by chemiluminescence (ECL substrate, Thermo Fisher Scientific) after incubation with a goat horseradish peroxidase-conjugated

antibody toward either rabbit or mouse IgGs (1:3,000 dilution in blocking buffer; Sigma) for 2 h at room temperature. Densitometry analysis of protein bands was performed using ImageJ software (National Institute of Health, United States) as previously showed by us (39).

The quantitative reverse transcription PCR analysis

To quantify microRNA expression on the exosomes, RNA was isolated using miRNeasy mini kit for cells and tissues (Qiagen) following the manufacturer's guidelines with few adaptations. Briefly, the isolated pEXOs were lysed by incubation with 5 volumes QIAzol reagent for 5 min, then 5 μl of 0.33-nM CelMir39 spike-in control (1.65 fmol) and 1 μL of 20 μg/μL molecular grade mussels' glycogen (Sigma) were added to each sample, followed by one volume of chloroform. The samples were vortexed briefly, incubated for 3 min at room temperature and centrifuged at 12,000*g* for 15 min at 4°C. The upper aqueous phase containing the RNA was collected and mixed with 1.5 volumes of 100% (v/v) ethanol. Each sample was transferred into RNeasy® Mini columns (Qiagen). The RNA binding, washed and eluted according to the manufacturer's instructions. Moreover, RNA was eluted in 30 μl of RNAse-free water. Template RNA (7 μl) was reverse transcribed using the miScript II Reverse Transcription (RT) kit (Qiagen) on a 20 μl final volume in line with the manufacturer's instructions. Also, miScript HiSpec Buffer was used in each reaction to selectively target the mature miRNA forms. Before proceeding to quantitative PCR, the cDNA was diluted 12.5 times in nuclease free water. The quantitative PCR was carried out on 5-μl diluted cDNA using the QuantiTect SYBR Green PCR reaction mix (Qiagen) on a 20-μl final reaction volume according to the manufacturer's instructions. Forward primers for each selected miR were inferred from mature miRNA sequences and purchased from Sigma (**Table 2**). The miScript Universal Primer (Qiagen) was utilized as a reverse primer for all reactions. All primers were employed at 500-μM concentration. The reaction was performed on a Rotor-Gene Q real-time PCR cycler (Qiagen) at the following thermocycling conditions: 15 min at 95°C to activate HotStarTaq DNA Polymerase followed by 40 thermo cycles composed of 15 s at 94°C, 30 s at 55°C, and 30 s at 70°C. The relative quantification of miR expression was performed by applying the $2^{-\Delta\Delta Ct}$ comparative method (70). For each patient, CelmiR-39 was employed as the housekeeping gene in the calculation of ΔCt, to normalize miR expression to RNA recovery. For each miRNA analyzed, the average ΔCt of all control patients acted as a calibrator for calculating the ΔΔCt. The resulting $2^{-\Delta\Delta Ct}$ data represent the relative expression of the given miRNA compared to the healthy controls.

To assess mRNA expression on cultured cells, RNA was isolated using PRImeZOL™ reagent (Canvax Reagents SL), following the manufacturer's instructions. Furthermore, RNA was re-suspended into 40 μl of RNAse-free water and quantified by NanoDrop spectrophotometry (Thermo Fisher Scientific); 1 μg of the total RNA was reverse transcribed with the PrimeScript RT kit (Takara) on a 20-μl final volume, following manufacturer's guidelines. The cDNA obtained was diluted 1:10 and analyzed by quantitative PCR using the TB Green® Premix Ex Taq™ reagent (Takara). The following primers, obtained from Sigma, were employed in the analysis at 500-μM concentration: Atrial natriuretic peptide (ANP) 5′-TCGTCTTGGCCTTTTGGCTT-3′ (forward) and 5′-AGGTGGTCTAGCAGGTTCTTGAAA-3′ (reverse); Brain natriuretic peptide (BNP): 5′-CGTTTGGGCTGTAACGCACT-3′ (forward) and 5′-TCACTTCAAAGGTGGTCCCAG-3′ (reverse); Cardiac β-myosin, β-MHC (MYH7) 5′-TCCTGCTGTTTCCTTACTTGCT-3′ (forward) and 5′-GCTGAGCCTTGGATTCTCAAAC-3′ (reverse); Sarcoplasmic/endoplasmic reticulum Ca^{2+}-ATPase 2a (SERCA2a) 5′-CCTTTGCCGCTCATTTTCCAG-3′ (forward) and 5′-GGCTGCACACACTCTTTACC-3′ (reverse); β-Actin 5′-GGCACCACACCTTCTACAATG-3′ (forward) and 5′-GGGGTGTTGAAGGTCTCAAAC-3′ (reverse). All reactions were performed on a Rotor-Gene Q real-time PCR cycler (Qiagen) at the following thermocycling conditions: 30 s at

TABLE 2 Mature miRNA sequences analyzed in this study and related forward primers employed for qPCR. All primers were obtained from Sigma and employed at 500-μM concentration.

	Mature miRNA (Sequence 5′-3′)	Forward primer (5′-3′)
miR-1	hsa-miR-1-3p (UGGAAUGUAAAGAAGUAUGUAU)	TGGAATGTAAAGAAGTATGTAT
miR-21	hsa-miR-21-5p (UAGCUUAUCAGACUGAUGUUGA)	TAGCTTATCAGACTGATGTTGA
miR-133a	hsa-miR-133a-3p (UUUGGUCCCCUUCAACCAGCUG)	TTTGGTCCCCTTCAACCAGCTG
miR-208a	hsa-miR-208a-3p (AUAAGACGAGCAAAAAGCUUGU)	ATAAGACGAGCAAAAAGCTTGT
Cel-miR-39 (Housekeeping spike-in gene)	cel-miR-39-3p (UCACCGGGUGUAAAUCAGCUUG)	TCACCGGGTGTAAATCAGCTTG

95°C followed by 40 cycles of 15 s at 95°C and 30 s at 60°C as suggested by the manufacturer's guidelines. The relative quantification of mRNA expression was performed by applying the $2^{-\Delta\Delta Ct}$ comparative method (68), with β-Actin employed as the housekeeping gene.

Cell culture and experimental protocol

Murine cardiomyocyte cell line HL-1 (a kind gift of W. C. Claycomb, Louisiana State University, New Orleans, LA, United States) was used to evaluate anti-hypertrophic role of human pEXOs. The HL-1 cells were cultured in Claycomb Medium (71) (Sigma) supplemented with 10% (v/v) fetal bovine serum (Sigma), 100-μM norepinephrine, 100 units/ml of penicillin, 100-μg/ml streptomycin, 250-ng/ml Amphotericin B and 2-mM L-Glutamine (Sigma) at 37°C in 5% CO_2. For the experimental purposes, HL-1 cells were seeded at a concentration of 5,000 cells/well on fibronectin pre-coated (1.25-μg/cm^2 human fibronectin, Sigma; 1 h at 37°C) 8-well chamber slides (Milllicell EZ, Millipore) and let adhere for 24 h before the treatment. Cardiomyocytes were then exposed to 1-μM angiotensin II (AngII; Sigma) in complete Claycomb medium for 48 h (54) (antibody-free complete Claycomb medium was employed in case of subsequent miRNA inhibition). T0- or T1-pEXOs (1×10^9 particles/ml) isolated from each group of patients or miRNA inhibitors (30 nM) were added 24 h after the beginning of AngII treatment, and the treatment was maintained for the remaining 24 h. Sterile filtered (0.2-μm pore) PBS vehicle was employed as a negative control.

MiR-21-5p inhibition and plasma exosomes

Furthermore, MiRVANA miRNA miR-21-5p inhibitor and miRVANA miRNA inhibitor negative control #1 were purchased from Thermo Fisher Scientific. To perform direct miR-21-5p inhibition in HL-1 cardiomyocytes, cells were transfected with 30 nM miRNA-21 inhibitor/negative control using Lipofectamine® RNAiMAX Transfection Reagent (3-μl/ml culture medium; Thermo Fisher Scientific) for 24 h, following manufacturer's instruction. All procedures were performed in antibody-free Claycomb medium.

As a different approach, isolated pEXOs were pre-loaded with miR-21 inhibitor then added to HL-1 cells as described above. The protocol for oligonucleotides loading was adapted from Zhang et al. (72). Briefly, 200-pmol miRNA miR-21-5p inhibitor/negative control was combined with pEXOs (5×10^8 particles in PBS), then 30-μl of 1-M $CaCl_2$ were added, and the final volume was adjusted to 300 μl with PBS. The mixture was incubated on ice for 30 min, then heat shocked for 60 s at 42°C and placed again on ice for 5 min. Treated pEXOs were then collected again by differential centrifugation as follows: After a 15-min clear-up step at 10,000*g* at 4°C, exosomes were isolated with a 5-h ultracentrifugation at 100,000*g*, performed at 4°C. The pEXOs collected (approximately 5×10^8 particles) were then re-suspended in 100 uL PBS. The amount of pEXOs obtained with this procedure is sufficient to treat HL-1 cardiomyocytes in one 8-well chamber slide well, in a final volume of 500 μl (1×10^9 particles/ml). All procedures were again performed in antibody-free Claycomb medium.

Measurement of HL-1 size

Actin filaments were stained with phalloidin to define HL-1 cell area (73). Briefly, the cell monolayer was washed twice with PBS for 5 min, fixed with 4% (w/v) paraformaldehyde (PFA) in PBS (Sigma) for 15 min and permeabilized with 0.1% (v/v) TritonX-100 (Sigma) in PBS twice for 2 min, at room temperature; PBS washes (2×5 min) were performed after each step. Cells were incubated with Phalloidin-Atto 550 (1:300; Sigma) in PBS for 1 h at room temperature to stain cytoskeletal F-actin. 4′,6-Diamidino-2-phenylindole dihydrochloride solution (DAPI; 1:1,000, Sigma) was also added to the solution to stain the nuclei. Excess dye was removed by PBS wash (2×5 min) and the slide was mounted with Aqua-Poly/Mount aqueous mounting medium (Polysciences, Inc.). Images were acquired at a fluorescence optical microscope (DM 2500, Leica Microsystems, Germany) (20× magnification). The cell area was measured manually with ImageJ software[1] and expressed as pixels.

Statistical analysis

Continuous clinical variables and CMRI measurements are presented as mean ± SD. Categorical clinical variables are presented as percentages of the total. The pEXOs concentration and miRNA expression are presented as median with interquartile range (IQR). Fisher's exact test was used to reveal differences between the frequencies of categorical variables. Regarding continuous variables, normal distribution was evaluated by the Kolmogorov-Smirnov test. Homoscedasticity was evaluated by the *F*-test of equality of variances (2 groups) or the Brown–Forsythe test (more than 2 groups). Robust Regression and OUTlier removal (ROUT) method was employed to identify outliers (Q = 0.1, FDR < 0.1%), which are reported in the graphs as "×" symbols. Paired Student's *t*-test or the Wilcoxon test were applied to identify significant differences between repeated measurements according to their distribution. Independent samples Student's *t*-test (with or without Welch's correction,

1 https://imagej.nih.gov/ij/

depending on homoscedasticity) or the Mann–Whitney test were employed between two independent groups according to their distribution. One-way ANOVA (or Brown–Forsythe and ANOVA test, depending on homoscedasticity) or the Kruskal–Wallis test, depending on sample distribution, were applied when more than two groups were compared. All statistical tests were performed as two-sided, statistical significance was considered for $p < 0.05$.

Receivers operating characteristic (ROC) curves were constructed with easyROC open source online software (74) using each pEXOs or each corresponding microRNA expression value. The area under the curve (AUC) with 95% CI was calculated for each ROC curve; standard errors and confidence intervals were estimated by applying the DeLong method (75). The Wald test was used to check the null hypothesis that the AUC is equal to 0.5 (i.e., no predictive power).

Results

Characteristics of patients

During a 1-year timeframe (from January 2018 to February 2019), 23 surgical MR patients met inclusion criteria and were enrolled in the study. All the patients underwent to successful MVR. The time of extracorporeal circulation was 134 (114–166) min and the cross-clamp time was 84 (75–101) min; all surgeries were carried out through the initial incision with no need for sternotomy conversion. We had no cases of conversion to replacement during intervention. Four patients were excluded after surgery because one patient died early after the intervention and three patients voluntarily withdrew from the study. Therefore, the final population consisted of 19 patients. As shown in **Table 1**, 19 patients, with average age 55.2 ± 8.0 years, showed average mitral regurgitant volume of 55 ± 32 ml, average regurgitant fraction of 37.09 ± 14.00 % and a high incidence of mitral valve prolapse (63.2%), with predominant involvement of the posterior leaflet (68.4%). Most of the patients were males, 36.8% in NYHA class I, 57.9% in NYHA class II and 5.3% in NYHA class III, and had low atrial fibrillation-associated stroke risk (CHA_2DS_2-VASc Score = 0, 52.6%; **Table 1**). More than 20% patients had history of cardiovascular diseases in their family and 15.8% were smokers (**Table 1**). Hypertension was the main primary comorbidity among the MR patients (47.4%), followed by hypercholesterolemia (31.6%) and peripheral vascular disease (5.3%). No patient had prior ischemic events (**Table 1**). Interestingly, cardiac fibrosis was detected in less than 50% of patients as measured by CMRI (**Table 1**). Most patients underwent MVR through right minithoracotomy (94.7%) and were mainly treated with beta-blockers (84.6%), diuretics (63.2%), and angiotensin-converting enzyme (ACE) inhibitors (26.2%) before surgery (**Table 1**). Postoperative atrial fibrillation occurred in 7 patients (roughly 37%; LoR-REM, $n = 5$; HiR-REM, $n = 2$). No other postoperative complications were observed in the study population. All patients underwent to a transthoracic echocardiography within 1 month after surgery, showing a good postsurgical outcome with nil (grade 0/4; 5/9 LoR-REM; 6/10 HiR-REM) or mild (grade 1/4; 4/9 LoR-REM; 4/10 HiR-REM) residual mitral regurgitation and preserved LV EF (LoR-REM, 58.6 ± 10%; HiR-REM, 59.12 ± 9%).

Perioperative cardiac assessment by cardiac magnetic resonance imaging

Cardiac magnetic resonance imaging was performed before (T0) and 6-months (T1) after surgery to assess cardiac phenotype in all patients (**Figure 1** and **Supplementary Table 1**). Hallmarks of LV Rev–Rem, indeed, were detectable in most patients at 6 months after MVR. In particular, postoperative LV end-diastolic volume index (LVEDVi) was significantly reduced to more than 10% of the pre-surgical value in almost all patients ($p = 1.90 \times 10^{-6}$; **Figure 1** and **Supplementary Table 1**). Similarly, LV end-systolic volume index (LVESVi; $p = 0.0055$), RV end-diastolic volume index (RVEDVi; $p = 1.30 \times 10^{-5}$) and RV end-systolic volume index RVESVi ($p = 0.035$) were lower at T1 compared to T0 (**Figure 1** and **Supplementary Table 1**). The LA area ($p = 7.60 \times 10^{-6}$) and volume ($p = 1.30 \times 10^{-5}$), as well as RA area ($p = 0.001$), were reduced in accord with the previous findings (76) (**Figure 1** and **Supplementary Table 1**). Indexed LV mass was also decreased after surgery ($p = 0.0035$; **Figure 1** and **Supplementary Table 1**). Of note, LV and RV EF were significantly reduced at 6-months after the surgery compared to T0 ($p = 2.80 \times 10^{-7}$ and $p = 0.0215$, respectively), even if its preoperative values were higher than 50% for most patients (**Figure 1** and **Supplementary Table 1**). Similarly, both LV and RV stroke volume indexes at T1 were reduced as compared to preoperative values ($p = 7.26 \times 10^{-7}$ and 3.70×10^{-5}, respectively). Postoperative cardiac index values were also lower than ones at T0 ($p = 7.40 \times 10^{-5}$), which remained within physiological range; while higher resting heart rate was observed after surgery ($p = 0.01$; **Figure 1** and **Supplementary Table 1**).

Role of preoperative cardiac phenotype to predict the extent of left ventricular reverse remodeling after surgery

The extent of the postoperative LV reverse remodeling was assessed for each patient by calculating the percentage change (%Δ) of LVEDVi at T1 compared to T0 using

10.3389/fcvm.2022.943068

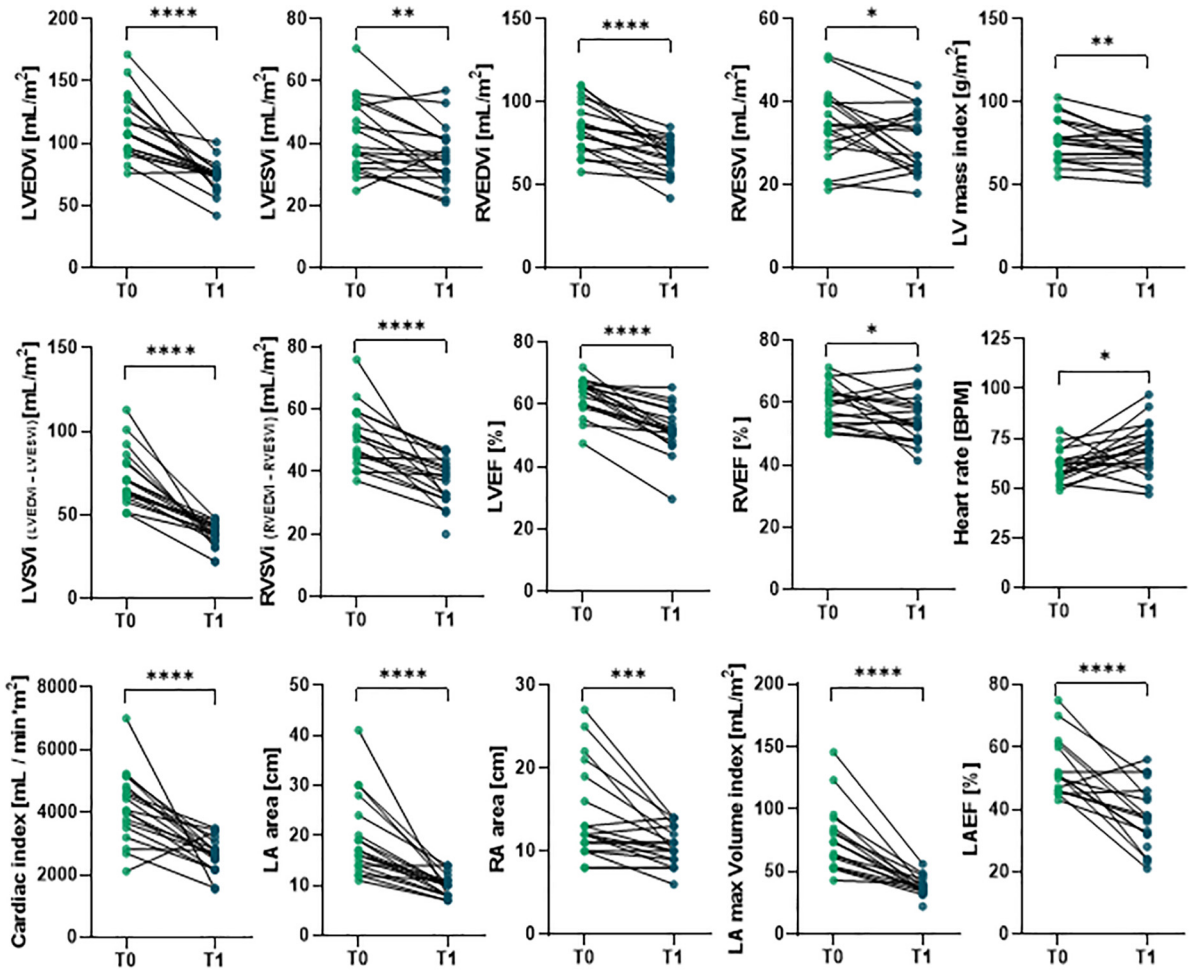

FIGURE 1
Comparison of preoperative and postoperative CMRI results in primary MR patients undergoing MVR surgery. The CMRI was performed on patients undergoing MVR surgery (n = 19) before (T0) and 6 months after (T1) surgery. Individual data are shown for each patient at both time points; statistical comparison between T0 and T1 was performed by paired Student's t-test or the Wilcoxon test depending on data distribution. $^{*}p < 0.05$; $^{**}p < 0.01$; $^{***}p < 0.001$; $^{****}p < 0.0001$.

a cut-off value of −30% (Figure 2). Patients with high degree of LV Rev–Rem showed %Δ LVEDVi values significantly reduced by 44.61 ± 9.94% (HiR-REM group, n = 10); otherwise, patients with low degree of LV Rev–Rem showed %Δ LVEDVi values significantly reduced by 20.23 ± 9.87% (LoR-REM, n = 9; $p = 5.20 \times 10^{-5}$; Figure 2 and Supplementary Table 2). Of note, HiR-REM patients were characterized by preoperative LVEDVi higher than LoR-REM group (p = 0.021; Supplementary Figures 1, 2).

To evaluate the role of preoperative cardiac parameters to predict postoperative LV reverse remodeling, we first compared the clinical and CMRI-derived features at T0 in HiR-REM and LoR-REM groups. We found that both groups have similar clinical profile (Table 3). Moreover, most of HiR-REM patients were in NYHA class I (60%; Table 3).

Second, patients with greater preoperative mitral regurgitant volume (p = 0.011), LVEDVi (p = 0.021), indexed LA volume (p = 0.037), LVSVi (p = 0.0013) and cardiac index (p = 0.007) showed high level of postoperative Rev–Rem (Table 3, Supplementary Figure 1 and Supplementary Table 2). Interestingly, preoperative LVEF was similar in HiR- and LoR-REM patients (Supplementary Figure 1 and Supplementary Table 2).

Finally, the preoperative myocardial fibrosis assessed by CMRI was detectable in patients with primary MR (up to 40%) and even more in patients with mitral leaflets prolapse. Myocardial fibrosis is a hallmark known to be associated to adverse postsurgical outcomes and arrhythmic events (68, 77). In our study, myocardial fibrosis affected 44.4% of patients in the absence of ischemic pattern (Table 1).

10.3389/fcvm.2022.943068

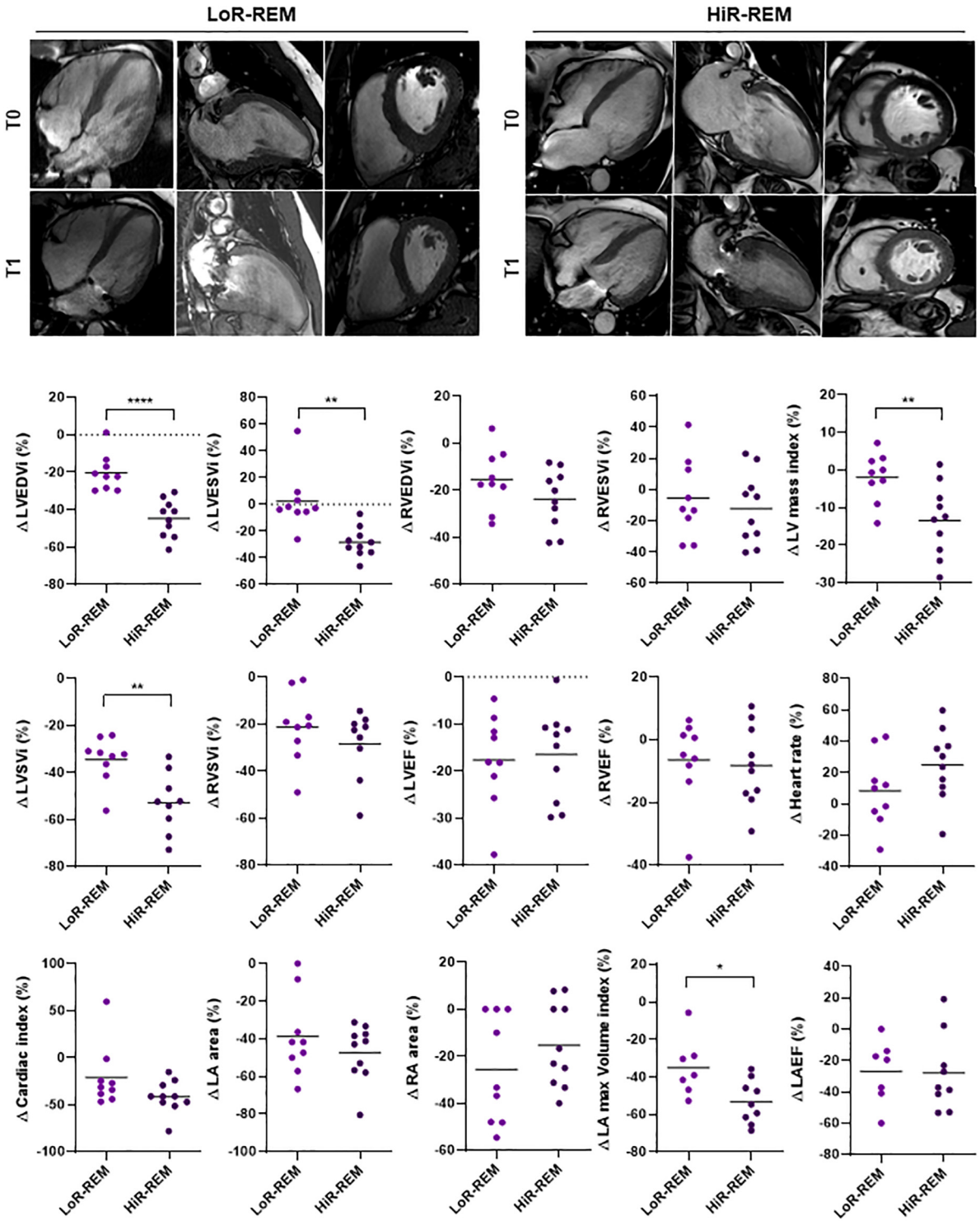

FIGURE 2
Analysis of CMRI parameters change in MR patients with different grade of reverse remodeling after MVR surgery. The CMRI data were collected from patients undergoing MVR surgery (n = 19) before (T0) and 6 months after (T1) surgery. The CMRI acquisitions are shown for a representative Low LV reverse remodeling (LoR-REM) and High LV reverse remodeling patient (HiR-REM). For each CMRI parameter measured, the percentage change between T0 and T1 was computed for each patient as $\%\Delta = (T1 - T0)/T0 \times 100$. The data are compared between LoR-REM and HiR-REM patients. Individual data are shown; horizontal bars represent group average. Statistical significance of the differences was evaluated by independent samples Student's t-test (with or without Welch's correction) or the Mann–Whitney test depending on data distribution. *$p < 0.05$; **$p < 0.01$; ****$p < 0.0001$.

Role of perioperative plasma exosome levels to predict the extent of left ventricular reverse remodeling after surgery

In the current study, we isolated and characterized exosomes from plasma collected before and 6-months after MVR surgery. Plasma was also collected from healthy subjects ($N = 8$, control).

TABLE 3 Analysis of preoperative clinical parameters in MR patients with different grade of reverse remodeling after MVR surgery.

Preclinical picture	LoR-REM	HiR-REM		*p*
Age (years)	54.78 ± 7.81	55.60 ± 9.01	Ns	0.8351
BMI (kg/m^2)	26.51 ± 3.05	25.75 ± 2.94	Ns	0.5884
Smoking status	11.11%	20.00%	Ns	>0.9999
Hypertension	55.56%	40.00%	Ns	0.6563
Hypercholesterolemia	22.22%	40.00%	Ns	0.6285
Peripheral vascular disease	0.00%	10.00%	Ns	>0.9999
Family history of CVD	33.33%	10.00%	Ns	0.3034
NYHA	I, 11.11% II, 77.7% III, 11.11%	I, 60.00% II, 40.00% III, 0.00%	Ns	0.0573 for I
CHA_2DS_2-VASc Score	0, 44.44% 1, 44.44% 2, 11.11%	0, 60.00% 1, 20.00% 2, 20.00%	Ns	0.6563 for 0
β-Blockers	88.89%	80.00%	Ns	>0.9999
Ace-inhibitors	33.33%	20.00%	Ns	0.6285
Diuretics	66.67%	60.00%	Ns	>0.9999
BNP (ng/L)	36.13 ± 26.60	42.63 ± 44.50	Ns	>0.9999
K(mEq/L)	3.90 ± 0.21	4.02 ± 0.18	Ns	0.2706
Ca (mg/dl)	8.28 ± 0.32	8.55 ± 0.31	Ns	0.0953
Mg (mg/dl)	1.70 ± 0.12	1.85 ± 0.29	Ns	0.1563
Type of MR	Flail, 33.33% Prolapse, 66.67%	Flail, 40.00% Prolapse, 60.00%	Ns	>0.9999
Leaflet failure	Anterior, 11.11% Posterior, 66.67% Both, 22.22%	Anterior, 0% Posterior, 77.78% Both, 22.22%	Ns	>0.9999
LVSV phase contrast (ml)	80.22 ± 13.77	90.67 ± 22.82	Ns	0.2570
Regurgitant Volume (mL)	37.56 ± 16.30	73.67 ± 34.00	▲	0.0110
Regurgitant Fraction (%)	30.86 ± 10.38	43.32 ± 14.89	Ns	0.0561
LGE presence (*n*, %)	55.56%	33.33%	Ns	0.6372

Clinical picture of $N = 19$ patients undergoing MVR was evaluated prior to the surgical procedure (T0). Data are compared between LoR-REM and HiR-REM patients. Categorical variables are presented as percentage of the total; continuous variables are presented as mean ± SD. Statistical significance of the differences was evaluated by Fisher's exact test for the categorical variables, while continuous variables were analyzed by independent samples Student's *t*-test (with or without Welch's correction) or the Mann–Whitney test depending on data distribution. The triangle means that it is a statistically significant increase.

Plasma exosomes (pEXOs) were positive for canonical markers CD63, CD81, and TSG101 (**Figures 3A,B**).

All MR patients showed no difference in terms of preoperative pEXOs levels compared to the healthy subjects (median concentration 1.38 × 10^9 particles/ml *vs* 1.08 × 10^9 particles/ml, $p = 0.381$; **Figures 3C,D**). Similarly, no significant change in pEXO levels was observed 6 months after surgery (1.55 × 10^9 particles/ml, $p = 0.932$ *vs* T0; $p = 0.175$ *vs* controls; **Figure 3D**). Conversely, when patients were grouped in terms of postsurgical LV remodeling, HiR-REM patients tended to have higher postoperative pEXOs levels (T1, 1.89 × 10^9 particles/ml) than LoR-REM patients (T1, 1.31 × 10^9 particles/ml, $p = 0.062$) and healthy subjects (1.08 × 10^9 particles/ml, $p = 0.016$; **Figure 4A** and **Supplementary Table 3**). It is conceivable that pEXOs may contribute to late LV reverse remodeling after surgical mitral valve repair.

Therefore, we further assessed the prognostic value of pEXOs and we clustered patients according to the percentage change (%Δ) of pEXOs at T1 compared to T0. In 12 patients, pEXOs levels were significantly higher after surgery (+88% in average; median concentration 1.14 × 10^9 particles/ml *vs* 1.70 × 10^9 particles/ml, $p = 0.015$), while in seven patients the exosomal levels decreased significantly from T0 to T1 (–56% in average; median concentration 2.50 × 10^9 particles/ml *vs.* 1.42 × 10^9 particles/ml, $p = 0.013$; $p = 3.97 \times 10^{-5}$; **Supplementary Figure 2**). Patients with higher postoperative pEXOs levels showed a significant reduction of LV mass index from T0 to T1 in comparison to the group with a reduction of pEXOs after surgery (–11.62% *vs.* –1.75 %, $p = 0.032$; **Supplementary Figure 2** and **Supplementary Table 4**).

Receivers operating characteristic curves were constructed for T0-pEXOs and T1-pEXOs, as well as %Δ pEXO, from HiR- *vs.* LoR-REM (**Figures 5A,E**) to compare their diagnostic value to predict magnitude of LV reverse remodeling after surgical MVR. The AUC for T0-pEXOs was 0.567 (95% CI: 0.29–0.84; $p = 0.635$) and for T1-pEXOs was 0.765 (95% CI: 0.52–1.00; $p = 0.034$), indicating reliable predictive power of the postoperative pEXO levels (**Figure 5A**). Our data suggest that pEXOs levels detected at 6 months after surgery may be reliable enough to depict HiR- and LoR-REM patients.

Relationship between exosomal miR-1, miR-21-5p, and miR-133a and left ventricular reverse remodeling

We further aimed to characterize some miRNAs packaged in postoperative pEXOs. Postoperative (T1) levels of exosomal miR-21-5p were higher in the entire MR population than in healthy controls (∼4-fold, $p = 0.021$), and tended to be higher than preoperative values (T0, ∼2-fold, $p = 0.052$; **Figure 3F**). In contrast, exosomal miR-1 and miR-133a levels did not change after surgery and were similar to healthy controls

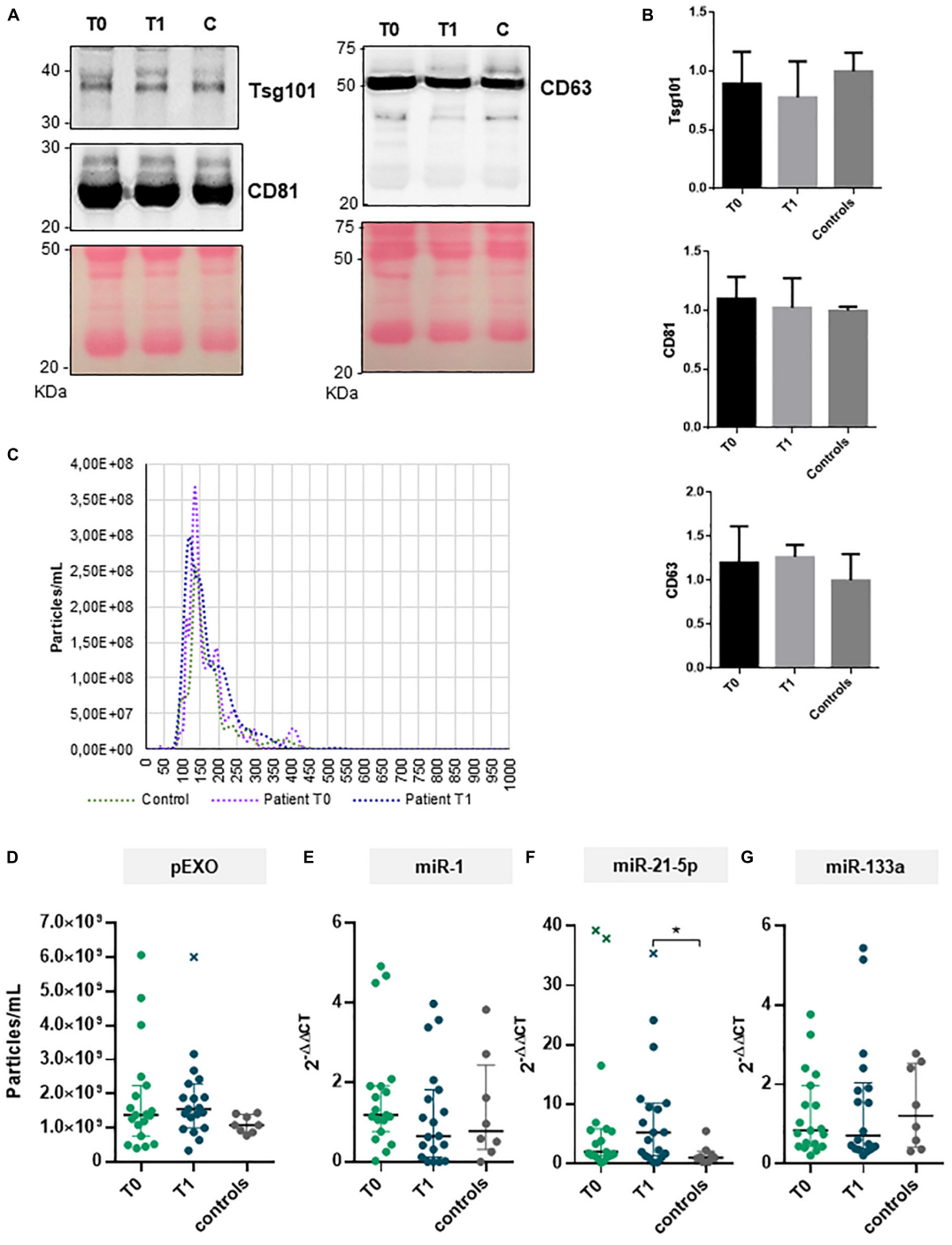

FIGURE 3
pEXOs and exosomal miRNAs in primary MR patients subjected to MVR surgery. The pEXOs were isolated from plasma of MR patients (n = 19) collected before (T0) and 6 months after MVR surgery (T1); pEXOs isolated from healthy controls (n = 8) were used as control. **(A,B)** The exosomal markers TSG101, CD81, and CD3 were assessed on the isolated particles by Western blot as described in the methods. **(A)** One representative experiment is shown. **(B)** Densitometric analysis of each protein target normalized for the corresponding experiment's Ponceau staining shows no difference in marker expression among extracts (N = 3 patients/group). **(C)** Isolated pEXOs were analyzed by NTA as described in the methods; representative size distribution curves are shown. **(D)** The pEXOs concentrations were inferred by the NTA's size distribution curve and shown as particles/ml of starting plasma. **(E–G)** Exosomal miRNA-1 **(E)**, miRNA-21-5p **(F)** and miRNA-133a **(G)** were assessed by qRT-PCR as described in the methods. Individual data, median value and interquartile range are shown in the graphs. Statistical significance of the differences between matching T0 and T1 data was evaluated by paired Student's t-test or the Wilcoxon test depending on data distribution. Statistical differences between patients and controls were evaluated by one-way ANOVA (with or without Brown–Forsythe modification for heteroscedastic groups) or the Kruskal–Wallis test, depending on sample distribution; *$p < 0.05$.

10.3389/fcvm.2022.943068

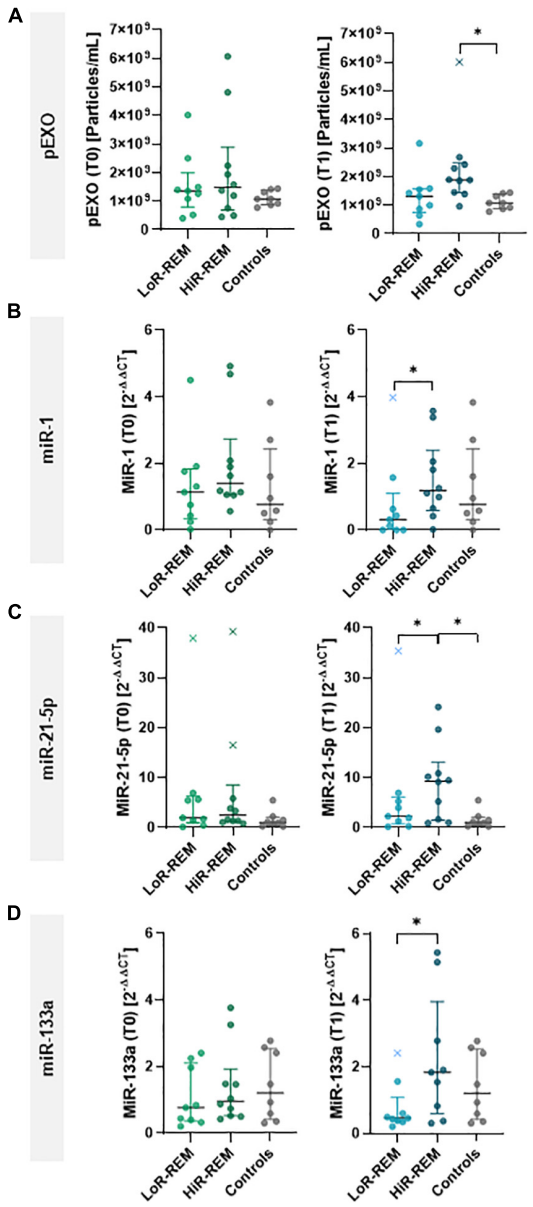

FIGURE 4
Analysis of pEXOs and exosomal miRNA in MR patients with different grade of reverse remodeling after MVR surgery. The pEXOs were isolated from plasma of MR patients (n = 19) collected before (T0) and 6 months after MVR surgery (T1); pEXOs isolated from healthy controls (n = 8) were used as control. **(A)** Isolated pEXOs were quantified by NTA as described in the methods. **(B–D)** Exosomal miRNA-1 **(B)**, miRNA-21-5p **(C)** and miRNA-133a **(D)** were quantified through qRT-PCR. Preoperative (T0) and postoperative (T1) levels were compared between LoR-REM and HiR-REM patients. Individual values are shown in the graphs; bars represent median and interquartile range. Statistical significance of the differences between patients' groups was evaluated by independent samples Student's t-test (with or without Welch's correction) or the Mann–Whitney test depending on data distribution. Statistical differences between patients and controls were evaluated by one-way ANOVA (with or without Brown–Forsythe modification for heteroscedastic groups) or the Kruskal–Wallis test, depending on sample distribution; $^*p < 0.05$.

(Figures 3E,G). Interestingly, miR-208a was not detectable in the isolated pEXOs from the same patients.

Finally, we compared the levels of selected exosomal miRNAs between patients who experienced substantial postoperative reverse remodeling (HiR-REM patients) and patients with minimal reverse remodeling (LoR-REM patients). At T1, exosomal miR-21-5p levels in HiR-REM group were higher than those in the LoR-REM patients (3.1-fold, $p = 0.030$) and healthy subjects (3.1-fold, $p = 0.025$; Figure 4C and Supplementary Table 3). Although the perioperative cargo of exosomal miR-1 and miR-133a was tenfold lower than exosomal miR-21-5p, we found that the T1 levels of miR-1 and miR-133a were reduced in LoR-REM patients compared to HiR-REM by 2.8-fold ($p = 0.018$) and 3.0-fold ($p = 0.046$), respectively (Figures 4B,D and Supplementary Table 3). Interestingly, the levels of exosomal miR-1 and miR-133a were similar in both HiR-REM and control groups (Figures 4B,D and Supplementary Table 3).

As showed in Figures 5B,D,E, receiver operator characteristic (ROC) curves were constructed separately for miR-1, miR-21-5p, and miR-133a levels highlighting significant changes at T1 compared to T0, including %Δ miR-1, miR-21-5p, and miR-133a from HiR- *vs.* LoR-REM groups. The AUC for T1-miR1 was 0.85 (95% CI 0.53–1.00; $p = 0.0002$), for T1-miR-21-5p was 0.763 (95% CI 0.55–1.00; $p = 0.029$) and for T1-miR133a was 0.792 (95 % CI 0.66–1.00; $p = 0.019$) indicating fair predictive power at 6 months after MVR, Therefore, postoperative exosomal miR levels may be reliable enough to depict HiR- and LoR-REM patients.

Anti-remodeling effects of exosomal miR-21-5p

In vitro, we have tested the anti-remodeling effects on murine cardiomyocyte of a single dose of pEXOs isolated from HiR-REM and LoR-REM patients. As showed in Figure 6, the preoperative (T0) and postoperative (T1) pEXOs isolated from LoR-REM patients effectively worsened the AngII-mediated cardiomyocyte enlargement. Conversely, we did not observe similar effect after treatment with T1 pEXOs isolated from HiR-REM. As shown in Supplementary Figure 3, the anti-hypertrophic effect of postoperative HiR-REM plasma exosomes was confirmed by normalization of mRNA levels of ANP, BNP, cardiac β-MHC (MYH7), and SERCA2a during AngII exposure. Consistent with the morphological data, a similar dose of postoperative LoR-REM pEXOs did not counteract the AngII-induced increase in the expression of the above genes.

Because miR-21-5p levels are 10-fold higher than those of other exosomal miRNAs and peak only in pEXOs isolated from HiR-REM patients, we assessed miR-21-5p role during cardiomyocyte response to chronic AngII stimulation. For this purpose, we have performed additional experiments

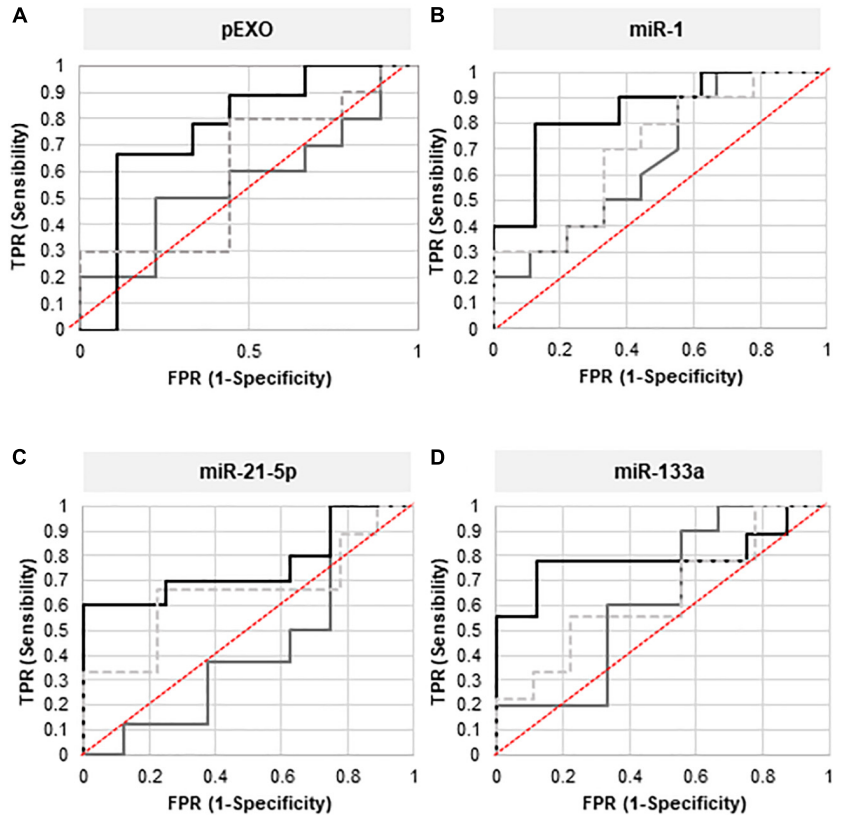

E

		AUC	p-value	CI (95%)
pEXO	T0	0.567	0.635	0.29-0.84
	T1	**0.765**	**0.034**	**0.52-1.00**
	%Δ	0.611	0.430	0.34-0.89
miR-1	T0	0.661	0.224	0.12-0.75
	T1	**0.850**	**0.0002**	**0.53-1.00**
	%Δ	0.700	0.114	0.38-0.93
miR-21-5p	T0	0.438	0.696	0.36-0.91
	T1	**0.763**	**0.029**	**0.55-1.00**
	%Δ	0.654	0.278	0.37-0.91
miR-133a	T0	0.633	0.342	0.40-0.92
	T1	**0.792**	**0.019**	**0.66-1.00**
	%Δ	0.642	0.304	0.45-0.95

FIGURE 5
Diagnostic efficacy of pEXOs levels and exosomal miR-1, miR-21-5p, and miR-133a. The pEXOs were isolated from plasma of MR patients (n = 19) collected before (T0) and 6 months after MVR surgery (T1). **(A)** Isolated pEXOs were quantified by NTA as described in the methods. **(B–D)** Exosomal miRNA-1 **(B)**, miRNA-21-5p **(C)** and miRNA-133a **(D)** were quantified through qRT-PCR as described in the method. Patients were divided into HiR-REM and LoR-REM groups. The diagnostic efficiency of T0, T1, and %Δ levels of pEXOs (particles/uL) **(A)** and of the microRNAs miR-1 **(B)**, miR-21-5p **(C)** and miR-133a **(D)** ($2^{-\Delta\Delta CT}$) in distinguishing patients with Low and High postoperative reverse LV remodeling was evaluated by the receiver operating characteristic (ROC) curve analysis as described in the methods. The AUC quantification and statistical significance (p-value) are reported in the table **(E)**.

by co-treating cardiomyocytes with miR-21-5p inhibitor. As showed in Figure 7A, miR-21-5p inhibitor promotes a slight enlargement of resting cardiomyocytes and further enhances the AngII-mediated hypertrophic response of note, miR-21-5p inhibitor counteracted the anti-hypertrophic effect of T1-pEXOs isolated from HiR-REM in AngII-treated HL1 cadiomyocytes (Figure 7B).

Discussion

In the last decade, plasma exosomes have gained increasing interest as perioperative diagnostic, therapeutic and prognostic factors related to different types of cardiac surgery (38, 39). Yet, their role in the cardiac remodeling during the late postoperative period is unknown and attracts attention. Our study demonstrated that the extent of LV Rev–Rem at 6 months after timely and technically successful MVR surgery is related to a different profile of circulating exosomes.

Importantly, we observed an elevated pEXOs values only in patients with a higher grade of reverse remodeling of the left ventricle characterized by lower values of LVEDVi, LVESVi, and ventricular mass index. Since the release of exosomes can be induced by external factors, we can assume that pre-existing diseases and perioperative factors did not affect late exosomal levels after heart valve surgery. All surgical patients with severe primary MR showed similar preoperative LVEF values and were treated with the same drugs and anesthetics. Indeed, preoperative pEXOs level did not change among patients and were independent of the magnitude of regurgitant volume. Of note, preoperative regurgitation volume was higher in patients who exhibited the greatest postoperative LV Rev–Rem. It is conceivable that with the severity of mitral valve disease, the extent of preoperative regurgitant volume associated with adverse remodeling, co-morbidities, as well as co-medications, did not influence the pEXOs level before surgery. We cannot exclude that late release of exosomes was part of a stress response following exposure to additional,

10.3389/fcvm.2022.943068

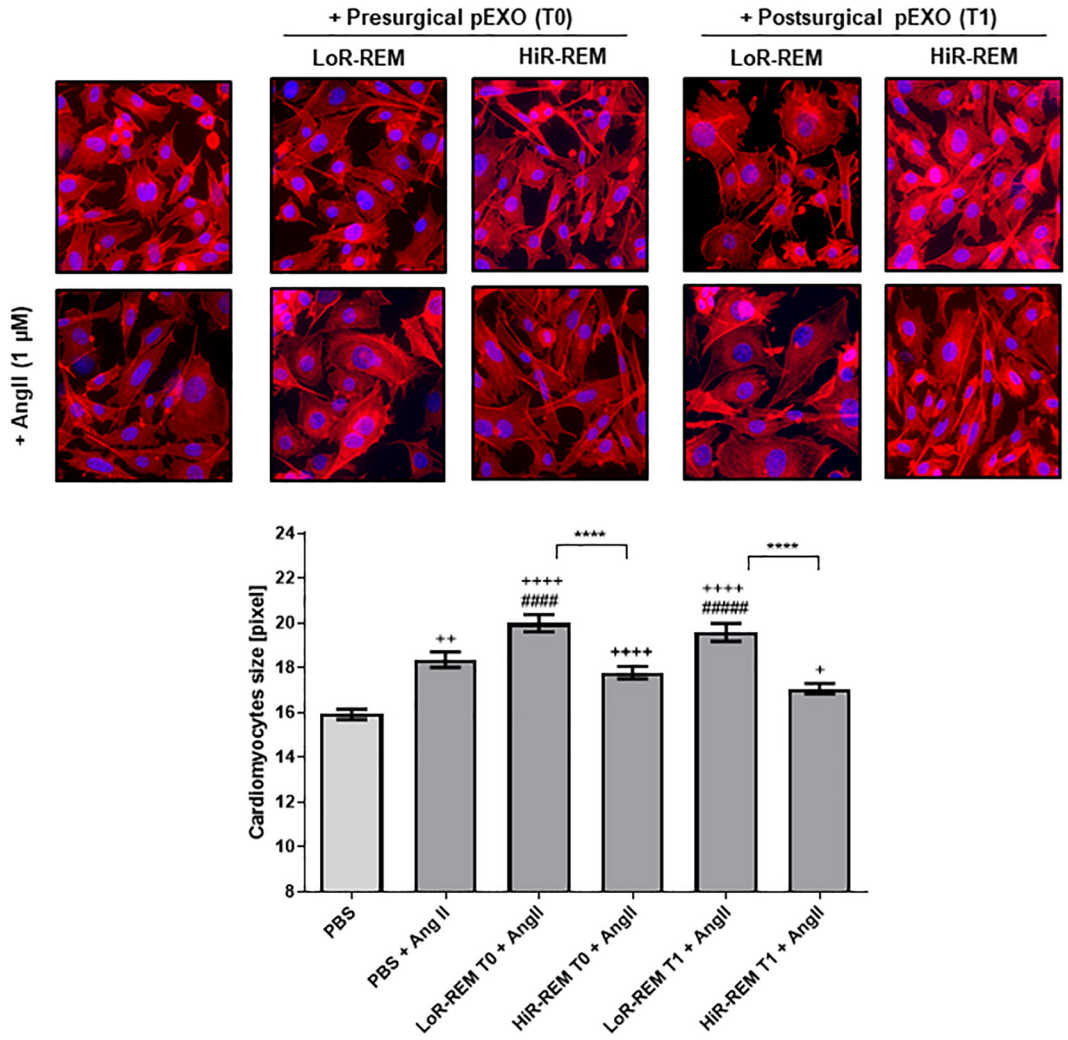

FIGURE 6
Effect of pEXOs from patients with different grade of reverse ventricular remodeling on cardiomyocytes size. The HL-1 cells were seeded at a concentration of 5,000 cells/cm^2 and allowed to adhere for 24 h before treatment. To enlarge cardiomyocyte size, HL-1 cells were treated with ± 1-μM Angiotensin II (AngII, Sigma) in complete Claycomb medium for 48 h. A PBS suspension of pEXOs isolated at T0 or T1 from HiR- or LoR-REM group (N = 4 patients/group) was added to a final concentration of 1 × 10^9 particles/ml, 24 h after the beginning of the treatment, and the treatment was maintained for the remaining 24 h; PBS was employed as a control. The cell monolayer was stained with Phalloidin-Atto 550 as described in the methods. The images were acquired with a fluorescence microscope (Leica; 20× magnification); the cell areas were manually measured with ImageJ software (https://imagej.nih.gov/ij/) and expressed in pixels. Statistical significance of the differences between treatments was evaluated by one-way ANOVA. The symbol "+" represents the significance of the differences against PBS alone (+, $p < 0.05$; ++, $p < 0.01$; ++++, $p < 0.0001$); "#" against PBS + AngII ($^{\#\#\#\#}p < 0.0001$); and "*" between LoR-REM and HiR-REM pEXO treatment in presence of AngII (****$p < 0.0001$).

as yet undefined, intra- and postoperative factors. In our previous study, indeed, we ruled out that anesthesia and minimally invasive on-pump mitral valve surgery lead to an early increase in postoperative pEXOs level in patients without ischemic heart disease (39). Yet, the causal relationship between circulating exosomes and late adverse or reverse ventricular remodeling after surgery is not yet clarified. Understanding the interplay between plasma exosomes levels and different magnitudes of late reverse cardiac remodeling in patients with entirely competent mitral valve after early surgical repair is essential to develop better-tailored interventions of cardioprotection.

Our study suggests that rising postoperative pEXOs level is a reliable indicator of the long-term adaptive response of the heart after mitral valve repair regardless of LV ejection fraction. Indeed, at 6 months after early rescue surgery, among patients with null mitral regurgitation volumes and preserved systolic function, the HiR-REM group showed smaller ventricular volumes and cardiac mass index than the LoR-REM patients. In light of the finding of partial restoration of the left ventricular

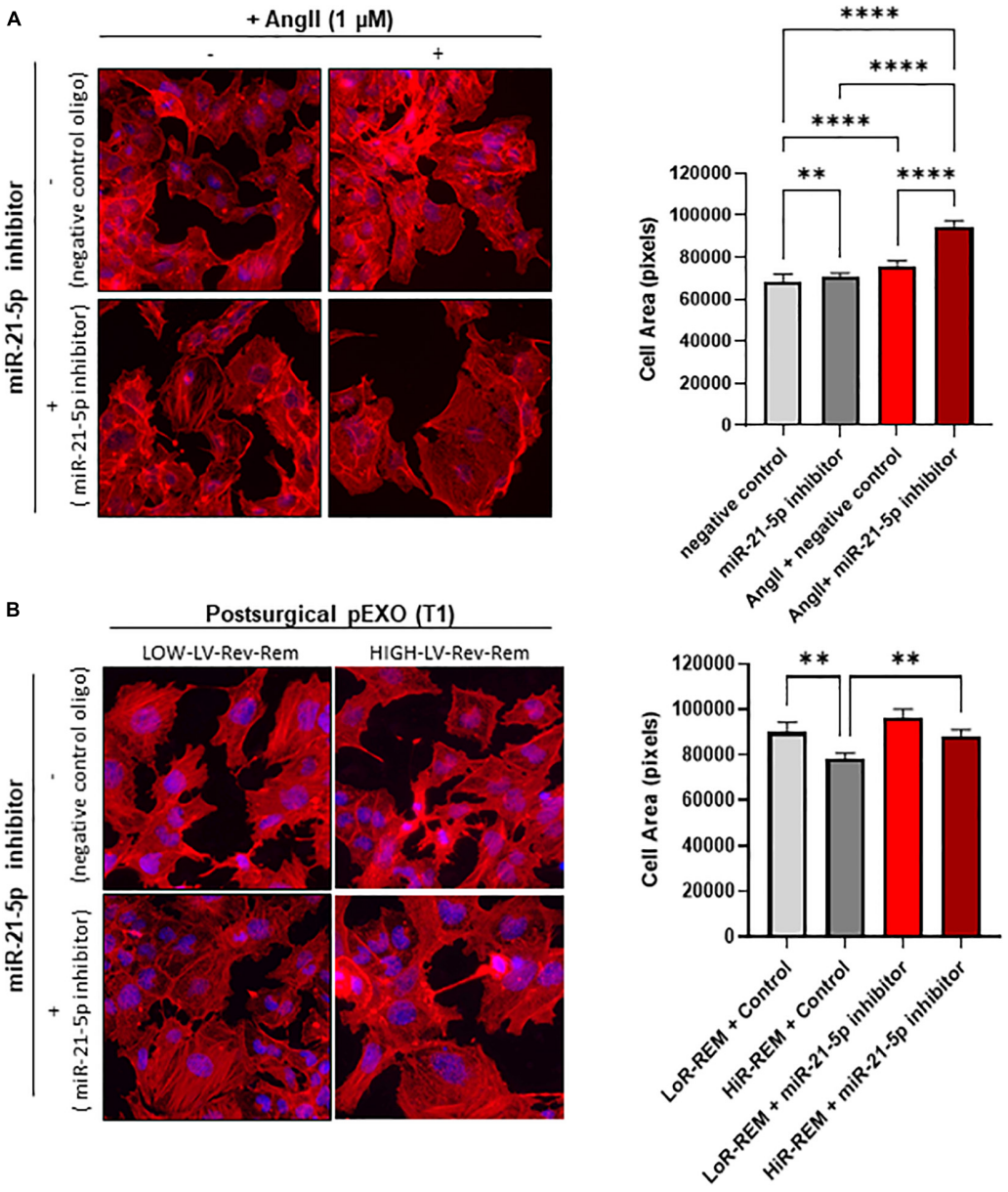

FIGURE 7
Effect of miR-21-5p inhibition on cardiomyocytes size. The HL-1 cells were seeded at a concentration of 5,000 cells/cm^2 and allowed to adhere for 24 h before treatment. **(A)** The HL-1 cells were treated with ± 1-μM angiotensin II (AngII, Sigma) in complete antibody-free Claycomb medium for 48 h. Moreover, 24 h after the beginning of the treatment, 30-nM miRNA-21-5p inhibitor/negative control was added to the cells using Lipofectamine® RNAiMAX Transfection Reagent and transfection was maintained for the following 24 h. **(B)** To stimulate hypertrophy, HL-1 cells were treated with 1-μM angiotensin II (AngII, Sigma) in complete antibody-free Claycomb medium for 48 h. The pEXOs isolated at T1 from LoR-REM or HiR-REM patients were loaded with miRNA-21-5p inhibitor/negative control through a heat shock-mediated protocol, as described in the experimental procedure, then collected by ultracentrifugation. Isolated pEXOs were added at a final concentration of 1 × 10^9 particles/ml 24 h after the beginning of the AngII treatment, and treatment by pEXOs was maintained for the remaining 24 h in the presence of AngII. **(A**,**B)** At the end of each treatment, the cell monolayer was stained with Phalloidin–Atto 550 as described in the methods. The images were acquired with a fluorescence microscope (Leica; 20× magnification); the cell areas were manually measured with ImageJ software (https://imagej.nih.gov/ij/) and expressed in pixels. Statistical significance of the differences between treatments was evaluated by one-way ANOVA. $^{**}p < 0.01$; $^{****}p < 0.0001$.

structure despite full recovery of mitral valve function, we suggest that low postoperative pEXOs level may hinder the maintenance of normal ventricular chamber geometry and mass over time in LoR-REM patients. This finding is clinically relevant because our study population with severe primary chronic MR had adverse tissue remodeling before surgery, as

evidenced by the presence of myocardial fibrosis assessed using CMRI. In fact, adverse remodeling is ongoing even if the ventricle is normocontractile and patients are asymptomatic as demonstrated by the presence of myocardial fibrosis (78).

Even though the *in vivo* kinetics of heterogeneous circulating exosomes is still difficult to investigate, the previous experimental evidence has also ascertained that not all cells release highly cardioprotective exosomes. In this regard, we have demonstrated that higher dose of exosomes released from cardiac progenitor cells provides sustained anti-remodeling effects *in vivo* (44, 79). Although further investigation is needed to define the cellular source and kinetics of pEXOs in our patients, this study is supported by a recent report demonstrating that plasma levels of extracellular vesicles are reduced in patients with more adverse cardiac remodeling (80). However, the mechanisms underlying exosome-based late reverse remodeling remain hitherto unknown.

Exosomes have been proposed as vehicle for miRNA-based intercellular communication (40). To demonstrate how targeting the heart with circulating exosomes may contribute to reverse ventricular remodeling during late postoperative period, we measured exosomal levels of miR-1, –21-5p, and –133a, that were relevant in cardiac remodeling and protection (50–53). First, we compared pre- and postoperative exosomal miRNA levels of our patients to those measured in a cohort of eight healthy volunteers. Although exosomal miR-21-5p copy numbers were ten-fold higher than miR-1 and miR-133a values, miR-21-5p was most abundant in postoperative exosomes of all surgical patients compared to control group (**Figure 3F**). Since exosomes have a very limited capacity to sample the diverse RNA cargo, our findings contribute to better understand the dynamic of exosome-mediated miRNA communication to chronically maintain normal cardiac phenotype after early mitral valve surgery. Because most plasma changes in exosomal miR-21-5p levels are known to occur far from the onset of cardiac injury (81), their longitudinal monitoring may be useful to predict the late favorable LV remodeling as detected by CMRI. Indeed, exosomal miR-21-5p levels in HiR-REM group are higher than in LoR-REM patients and control subjects. Conversely, postoperative exosomal miR-1 and –133a copy numbers in HiR-REM patients were similar to healthy subjects and slightly higher than those of LoR-REM group.

Even if the ROC curve analysis provided evidence about how the T1 values of pEXOs, miR-1, miR-133a and miR-21-5p fairly discriminates between patients with higher or lower reverse ventricular remodeling during late postoperative period (**Figure 5**), only patients with increased levels of T1-pEXOs showed reduced left ventricular mass indexed for body surface area compared with preoperative values (**Supplementary Figure 2**). Our finding is clinically relevant because incomplete regression of the LV mass alone is a hallmark of residual adverse remodeling and limits the ability to recover normal LV systolic function over time after mitral valve repair (26). The causal relationships between incomplete reverse left ventricular remodeling and T1-pEXOs levels, however, need to be further clarified. On this merit, we performed additional experiments *in vitro*. First, we found that T1-pEXOs isolated from LoR-REM patients contribute to further enlarge cardiomyocyte size in response to long-term exposure to AngII, but not T1-pEXOs from HiR-REM group. In line with morphological findings, we found that mRNA levels of ANP, BNP, and cardiac β-MHC (MYH7) established indicators of cardiac hypertrophy (82), do not increase in cardiomyocytes long-term treated with postoperative HiR-REM plasma exosomes during exposure to AngII. In contrast, similar doses of postoperative LoR-REM pEXOs did not inhibit the Ang II-induced fetal hypertrophic gene expression program (83). Of note, we focused on mRNA levels of β-MHC since it is well known that AngII induces both hypertrophy of cultured cardiomyocytes and upregulation of β-MHC levels, without marked effects on α-MHC (84).

Second, we evaluated whether exosomal miR-21-5p, which is highly expressed in T1-pEXOs from HiR-REM patients, plays a key role in counteracting the enhancement of adverse cardiomyocyte remodeling. Our hypothesis was supported by the previous studies showing that downregulation of miR-21-5p reduces the protective effects of extracellular vesicles in limiting cardiomyocyte apoptosis (85) and in preventing cardiac dysfunction (86). However, its direct effect on cardiomyocytes size is still lacking. To this end, our *in vitro* experiments demonstrated that treatment of stressed cardiomyocytes with T1-pEXOs of HiR-REM group in the presence of miR-21-5p inhibitor exacerbated the AngII-induced enlargement of cardiomyocyte size. It is noteworthy that miR-21-5p inhibitor alone was able to worsen the size enlargement of nonexosome-treated cardiomyocytes chronically exposed to AngII. Our results suggest that T1-pEXOs enhanced the autoregulatory feedback mediated by endogenous miR-21-5p to limit AngII-induced remodeling of cardiomyocytes. To further corroborate our experimental findings on exosomal miR-21-5p anti-hypertrophic effects, we investigated changes of SERCA2a gene expression in AngII-stressed cardiomyocytes after treatment with postoperative HiR-REM exosomes, which are rich in miR-21-5p. Indeed, it is well known that SERCA2a expression undergoes significant downregulation after AngII-induced hypertrophy (83), and therefore a reduction in its activity, leading to slower cytosolic Ca^{2+} removal, reduced sarcoplasmic reticulum content and impaired Ca^{2+} transient reduction (87). Moreover, it is already known that exosomal miR-21-5p may increase cardiomyocyte-specific SERCA2a expression in both human engineered cardiac tissue and human pluripotent stem cell-derived cardiomyocyte monolayer, while its mRNA levels are decreased by delivery of exosome-enriched fraction from miR-21-5p inhibitor treated cells (88). In our study, the effect detected after long-term exposure of HL-1 to AngII was a modest yet statistically significant reduction of SERCA2a

transcription with reference to β-actin transcription. Of note, the transcript level of β-actin was found to be unchanged after chronic exposure to AngII. Treating stressed cardiomyocytes with postoperative HiR-REM exosomes significantly increased SERCA2a at normal levels in comparison to T1-pEXOs isolated from LoR-REM patients. Our first results support miR-21-5p-rich plasma exosomes exerting anti-hypertrophic effects by regulating expression of calcium handling genes in accord with the previous study (88).

In conclusion, our data demonstrated that sustained increase in circulating pEXOs levels in the late postoperative period depicts patients with greater extent of reverse ventricular remodeling after MVR since they deliver highest concentration of miR-21-5p, which may play a key role in counteracting worsening of long-term adverse cardiac remodeling by normalizing SERCA2a gene expression in cardiomyocytes. The late postoperative monitoring of miR-21-5p-rich pEXOs level will improve our understanding of long-term adaptive autoregulatory feedback of cardiomyocytes leading to postoperative reverse remodeling. Finally, our findings will be helpful to design a new approach to early predict and treat patients at higher risk of partial reverse remodeling after a successful surgery. Indeed, miR-21-5p-rich exosomes have emerged from our study as a new precision theranostic tool for late postoperative cardioprotection.

Limitations of the study

Some limitations of this study should be considered to promote next investigations. First, the study population consists of a low number of patients. This was in part due to the relatively low number of patients with isolated primary MR who underwent surgery within the timeframe of the study and partly due to the low patient adherence to the experimental protocol, mainly driven by the refusal of the CMRI examination due to claustrophobia. However, the high accuracy and reproducibility of CMRI can partly compensate for the small sample size. In fact, each patient studied with CMRI is equivalent to 10 patients studied with echocardiography, whose measurements are less reliable. Second, our population consists mainly of surgical patients in the early stage of adverse cardiac remodeling induced by primary MR, with mild-to-moderate degrees of LV dilatation. In accord with latest recommendations for acting in elective surgical MVR (36), we cannot ignore that it is difficult to enroll patients with higher degrees of adverse ventricular remodeling. However, the mean preoperative CMRI-derived LVEDVi was 113.67 ± 25 ml/m^2 in our study population, and considering that the upper limit is 95–93 ml/m^2 in middle-aged male subjects, we can affirm that most of our patients had not severe adverse LV remodeling (15/19 subjects showed LVEDVi above the upper limit). Third, our follow-up was limited to 6 months after surgery. Further investigations are required to assess the relationship between miR-21-5p-rich plasma exosome levels and magnitude of reverse ventricular remodeling during longer follow-up after early rescue MVR. Finally, the definition of the cellular source of miR-21-5p-rich plasma exosomes and better understanding of molecular pathways regulated by exosomal miR-21-5p in cardiomyocytes deserve further *ad hoc* investigation *in vivo*.

Data availability statement

The original contributions presented in this study are included in the article/**Supplementary material**, further inquiries can be directed to the corresponding author.

Ethics statement

The studies involving human participants were reviewed and approved by Ethics Committee of "G. Monasterio" Foundation (FTGM, Massa, Italy; EMIGRATE study, approval n°1529). The patients/participants provided their written informed consent to participate in this study.

Author contributions

FP, GF, and VL contributed to the conception and design of the study; GF and VC advised in physiological mechanisms. SS, DC, MS, GB, and SM advised in physiological topics and surgical approach. FP and GF performed the statistical analysis. VL analyzed the results and wrote the first draft of the manuscript. GF, GA, FP, MM, and VL wrote sections of the manuscript. All authors contributed to manuscript revision, read, and approved the submitted version.

Funding

This study was in part supported by institutional funds of Scuola Superiore Sant'Anna (Pisa, Italy) (FP and VL) institutional funds of Fondazione Toscana G. Monasterio (Pisa/Massa, Italy) (DC, GB, GA, MM, MS, SM, SS, and VL), ETHERNA Project (Grant No. 161/16, Fondazione Pisa, Italy) (VL) and the EU Horizon 2020 FETPROACT-01-2018 (NeuHeart) (VL). Funding source had no such involvement in study design, in the collection, analysis, interpretation of data, in the writing of the report, and in the decision to submit the article for publication.

Conflict of interest

The authors declare that the research was conducted in the absence of any commercial or financial relationships that could be construed as a potential conflict of interest.

Publisher's note

All claims expressed in this article are solely those of the authors and do not necessarily represent those of their affiliated organizations, or those of the publisher, the editors and the reviewers. Any product that may be evaluated in this article, or claim that may be made by its manufacturer, is not guaranteed or endorsed by the publisher.

Supplementary material

The Supplementary Material for this article can be found online at: https://www.frontiersin.org/articles/10.3389/fcvm.2022.943068/full#supplementary-material

References

1. Scandura S, Mangiafico S, Giaquinta S. Mitral regurgitation: epidemiology, etiology and physiopathology. In: Tamburino C, Barbanti M, Capodanno D, editors. *Percutaneous Treatment of Left Side Cardiac Valves: A Practical Guide for the Interventional Cardiologist*. Cham: Springer International Publishing (2018). p. 49–61. doi: 10.1007/978-3-319-59620-4_3

2. Otto CM. Timing of surgery in mitral regurgitation. *Heart.* (2003) 89:100–5. doi: 10.1136/heart.89.1.100

3. Maslow AD, Poppas A. Primary mitral valve regurgitation: update and review. *Glob Cardiol Sci Pract.* (2017) 2017:e201703. doi: 10.21542/gcsp.2017.3

4. Enriquez-Sarano M. Timing of mitral valve surgery. *Heart.* (2002) 87:79–85. doi: 10.1136/heart.87.1.79

5. Nishimura RA, Otto CM, Bonow RO, Carabello BA, Erwin JP, Fleisher LA, et al. 2017 AHA/ACC focused update of the 2014 AHA/ACC guideline for the management of patients with valvular heart disease: a report of the American college of cardiology/American heart association task force on clinical practice guidelines. *Circulation.* (2017) 135:e1159–95. doi: 10.1161/CIR.0000000000000503

6. Enriquez-Sarano M, Akins CW, Vahanian A. Mitral regurgitation. *Lancet.* (2009) 373:1382–94. doi: 10.1016/S0140-6736(09)60692-9

7. Vahanian A, Beyersdorf F, Praz F, Milojevic M, Baldus S, Bauersachs J, et al. 2021 ESC/EACTS guidelines for the management of valvular heart disease developed by the task force for the management of valvular heart disease of the European society of cardiology (ESC) and the European association for cardio-thoracic surgery (EACTS). *Eur Heart J.* (2021) 75:524. doi: 10.1016/j.rec.2022.05.006

8. Baumgartner H, Falk V, Bax JJ, De Bonis M, Hamm C, Holm PJ, et al. 2017 ESC/EACTS guidelines for the management of valvular heart disease. *Eur Heart J.* (2017) 38:2739–86. doi: 10.1016/j.rec.2017.12.013

9. Otto CM, Nishimura RA, Bonow RO, Carabello BA, Erwin JP, Gentile F, et al. 2020 ACC/AHA guideline for the management of patients with valvular heart disease: a report of the American college of cardiology/American heart association joint committee on clinical practice guidelines. *Circulation.* (2021) 143:e72–227. doi: 10.1161/CIR.0000000000000923

10. Bax JJ, Braun J, Somer ST, Klautz R, Holman ER, Versteegh MIM, et al. Restrictive annuloplasty and coronary revascularization in ischemic mitral regurgitation results in reverse left ventricular remodeling. *Circulation.* (2004) 110(11 Suppl.):II103–8. doi: 10.1161/01.CIR.0000138196.06772.4e

11. Le Tourneau T, Topilsky Y, Inamo J, Mahoney D, Suri R, Schaff H, et al. Time course of left ventricular remodeling after mitral valve surgery in patients with organic mitral regurgitation: effect of volume overload. *Eur Heart J.* (2013) 34(Suppl. 1):815. doi: 10.1093/eurheartj/eht310.4450

12. Shafii AE, Gillinov AM, Mihaljevic T, Stewart W, Batizy LH, Blackstone EH. Changes in left ventricular morphology and function after mitral valve surgery. *Am J Cardiol.* (2012) 110:403–8.e3. doi: 10.1016/j.amjcard.2012.03.041

13. Quintana E, Suri RM, Thalji NM, Daly RC, Dearani JA, Burkhart HM, et al. Left ventricular dysfunction after mitral valve repair – the fallacy of "normal" preoperative myocardial function. *J Thorac Cardiovasc Surg.* (2014) 148:2752–62. doi: 10.1016/j.jtcvs.2014.07.029

14. Seldrum S, de Meester C, Pierard S, Pasquet A, Lazam S, Boulif J, et al. Assessment of left ventricular reverse remodeling by cardiac MRI in patients undergoing repair surgery for severe aortic or mitral regurgitation. *J Cardiothorac Vasc Anesth.* (2019) 33:1901–11. doi: 10.1053/j.jvca.2018.11.013

15. Vassileva CM, Ghazanfari N, Spertus J, McNeely C, Markwell S, Hazelrigg S. ADULT CARDIAC SURGERY: heart failure readmission after mitral valve repair and replacement: five-year follow-up in the medicare population. *Ann Thorac Surg.* (2014) 98:1544–50. doi: 10.1016/j.athoracsur.2014.07.040

16. De Bonis M, Lapenna E, Verzini A, La Canna G, Grimaldi A, Torracca L, et al. Recurrence of mitral regurgitation parallels the absence of left ventricular reverse remodeling after mitral repair in advanced dilated cardiomyopathy. *Ann Thorac Surg.* (2008) 85:932–9. doi: 10.1016/j.athoracsur.2007.11.021

17. Hung J, Papakostas L, Tahta SA, Hardy BG, Bollen BA, Duran CM, et al. Mechanism of recurrent ischemic mitral regurgitation after annuloplasty: continued LV remodeling as a moving target. *Circulation.* (2004) 110:II85–90. doi: 10.1161/01.CIR.0000138192.65015.45

18. El Sabbagh A, Reddy YNV, Nishimura RA. Mitral valve regurgitation in the contemporary era: insights into diagnosis, management, and future directions. *JACC Cardiovasc Imaging.* (2018) 11:628–43. doi: 10.1016/j.jcmg.2018.01.009

19. De Bonis M, Bolling SF. Mitral valve surgery: wait and see vs. early operation. *Eur Heart J.* (2013) 34:13a–9a. doi: 10.1093/eurheartj/ehs248

20. Enriquez-Sarano M, Tajik AJ, Schaff HV, Orszulak TA, Bailey KR, Frye RL. Echocardiographic prediction of survival after surgical correction of organic mitral regurgitation. *Circulation.* (1994) 90:830–7. doi: 10.1161/01.CIR.90.2.830

21. Reed D, Abbott RD, Smucker ML, Kaul S. Prediction of outcome after mitral valve replacement in patients with symptomatic chronic mitral regurgitation. The importance of left atrial size. *Circulation.* (1991) 84:23–34. doi: 10.1161/01.CIR.84.1.23

22. Enriquez-Sarano M, Avierinos J-F, Messika-Zeitoun D, Detaint D, Capps M, Nkomo V, et al. Quantitative determinants of the outcome of asymptomatic mitral regurgitation. *N Engl J Med.* (2005) 352:875–83. doi: 10.1056/NEJMoa041451

23. Kang DH, Kim JH, Rim JH, Kim MJ, Yun SC, Song JM, et al. Comparison of early surgery versus conventional treatment in asymptomatic severe mitral regurgitation. *Circulation.* (2009) 119:797–804. doi: 10.1161/CIRCULATIONAHA.108.802314

24. Gasser S, von Stumm M, Sinning C, Schaefer U, Reichenspurner H, Girdauskas E. Can we predict failure of mitral valve repair? *J Clin Med.* (2019) 8:526. doi: 10.3390/jcm8040526

25. Athanasopoulos LV, McGurk S, Khalpey Z, Rawn JD, Schmitto JD, Wollersheim LW, et al. Usefulness of preoperative cardiac dimensions to predict success of reverse cardiac remodeling in patients undergoing repair for mitral valve prolapse. *Am J Cardiol.* (2014) 113:1006–10. doi: 10.1016/j.amjcard.2013.12.009

26. Stulak JM, Suri RM, Dearani JA, Burkhart HM, Sundt TM, Enriquez-Sarano M, et al. Does early surgical intervention improve left ventricular mass regression after mitral valve repair for leaflet prolapse? *J Thorac Cardiovasc Surg.* (2011) 141:122–9. doi: 10.1016/j.jtcvs.2010.08.068

27. Song BG, On YK, Jeon E-S, Park JH, Choi J-O, Lee S-C, et al. Ventricular reverse remodeling early after mitral valve repair for severe chronic mitral regurgitation with atrial fibrillation. *Cardiology.* (2009) 114:132–41. doi: 10.1159/000224770

28. Tribouilloy C, Rusinaru D, Szymanski C, Mezghani S, Fournier A, Levy F, et al. Predicting left ventricular dysfunction after valve repair for mitral regurgitation due to leaflet prolapse: additive value of left ventricular end-systolic dimension to ejection fraction. *Eur J Echocardiogr.* (2011) 12:702–10. doi: 10.1093/ejechocard/jer128

29. Suri RM, Schaff HV, Dearani JA, Sundt TM, Daly RC, Mullany CJ, et al. Recovery of left ventricular function after surgical correction of mitral regurgitation caused by leaflet prolapse. *J Thorac Cardiovasc Surg.* (2009) 137:1071–6. doi: 10.1016/j.jtcvs.2008.10.026

30. Suri RM, Schaff HV, Dearani JA, Sundt TM, Daly RC, Mullany CJ, et al. Determinants of early decline in ejection fraction after surgical correction of mitral regurgitation. *J Thorac Cardiovasc Surg.* (2008) 136:442–7. doi: 10.1016/j.jtcvs.2007.10.067

31. Kasner M, Gast M, Galuszka O, Stroux A, Rutschow S, Wang X, et al. Circulating exosomal microRNAs predict functional recovery after MitraClip repair of severe mitral regurgitation. *Int J Cardiol.* (2016) 215:402–5. doi: 10.1016/j.ijcard.2016.04.018

32. de Varennes B, Haichin R. Impact of preoperative left ventricular ejection fraction on postoperative left ventricular remodeling after mitral valve repair for degenerative disease. *J Heart Valve Dis.* (2000) 9:313–8; discussion 318–20.

33. Grothues F, Smith GC, Moon JCC, Bellenger NG, Collins P, Klein HU, et al. Comparison of interstudy reproducibility of cardiovascular magnetic resonance with two-dimensional echocardiography in normal subjects and in patients with heart failure or left ventricular hypertrophy. *Am J Cardiol.* (2002) 90:29–34. doi: 10.1016/S0002-9149(02)02381-0

34. Grothues F, Moon JC, Bellenger NG, Smith GS, Klein HU, Pennell DJ. Interstudy reproducibility of right ventricular volumes, function, and mass with cardiovascular magnetic resonance. *Am Heart J.* (2004) 147:218–23. doi: 10.1016/j.ahj.2003.10.005

35. Mehta NK, Kim J, Siden JY, Rodriguez-Diego S, Alakbarli J, Di Franco A, et al. Utility of cardiac magnetic resonance for evaluation of mitral regurgitation prior to mitral valve surgery. *J Thorac Dis.* (2017) 9(Suppl. 4):S246. doi: 10.21037/jtd.2017.03.54

36. Enriquez-Sarano M, Sundt TM. Early surgery is recommended for mitral regurgitation. *Circulation.* (2010) 121:804–11. doi: 10.1161/CIRCULATIONAHA.109.868083

37. Poon KS, Palanisamy K, Chang SS, Sun KT, Chen KB, Li PC, et al. Plasma exosomal miR-223 expression regulates inflammatory responses during cardiac surgery with cardiopulmonary bypass. *Sci Rep.* (2017) 7:10807. doi: 10.1038/s41598-017-09709-w

38. Emanueli C, Shearn AIU, Laftah A, Fiorentino F, Reeves BC, Beltrami C, et al. Coronary artery-bypass-graft surgery increases the plasma concentration of exosomes carrying a cargo of cardiac microRNAs: an example of exosome trafficking out of the human heart with potential for cardiac biomarker discovery. *PLoS One.* (2016) 11:e0154274. doi: 10.1371/journal.pone.0154274

39. Carrozzo A, Casieri V, Di Silvestre D, Brambilla F, De Nitto E, Sardaro N, et al. Plasma exosomes characterization reveals a perioperative protein signature in older patients undergoing different types of on-pump cardiac surgery. *Geroscience.* (2021) 43:773–89. doi: 10.1007/s11357-020-00223-y

40. Terrasini N, Lionetti V. Exosomes in critical illness. *Crit Care Med.* (2017) 45:1054–60. doi: 10.1097/CCM.0000000000002328

41. Camera M, Brambilla M, Canzano P, Cavallotti L, Parolari A, Tedesco CC, et al. Association of microvesicles with graft patency in patients undergoing CABG surgery. *J Am Coll Cardiol.* (2020) 75:2819–32. doi: 10.1016/j.jacc.2020.03.073

42. Frey UH, Klaassen M, Ochsenfarth C, Murke F, Thielmann M, Kottenberg E, et al. Remote ischaemic preconditioning increases serum extracellular vesicle concentrations with altered micro-RNA signature in CABG patients. *Acta Anaesthesiol Scand.* (2019) 63:483–92. doi: 10.1111/aas.13296

43. Castellani C, Burrello J, Fedrigo M, Burrello A, Bolis S, Di Silvestre D, et al. Circulating extracellular vesicles as non-invasive biomarker of rejection in heart transplant. *J Heart Lung Transplant.* (2020) 39:1136–48. doi: 10.1016/j.healun.2020.06.011

44. Barile L, Lionetti V, Cervio E, Matteucci M, Gherghiceanu M, Popescu LM, et al. Extracellular vesicles fromhuman cardiac progenitor cells inhibit cardiomyocyte apoptosis and improve cardiac function aftermyocardial infarction. *Cardiovasc Res.* (2014) 103:530–41. doi: 10.1093/cvr/cvu167

45. Chen YT, Wang J, Wee ASY, Yong QW, Tay ELW, Woo CC, et al. Differential microRNA expression profile in myxomatous mitral valve prolapse and fibroelastic deficiency valves. *Int J Mol Sci.* (2016) 17:753. doi: 10.3390/ijms17050753

46. Gallo A, Tandon M, Alevizos I, Illei GG. The majority of microRNAs detectable in serum and saliva is concentrated in exosomes. *PLoS One.* (2012) 7:e30679. doi: 10.1371/journal.pone.0030679

47. Nik Mohamed Kamal NNSB, Shahidan WNS. Non-exosomal and exosomal circulatory microRNAs: which are more valid as biomarkers? *Front Pharmacol.* (2020) 10:1500. doi: 10.3389/fphar.2019.01500

48. Jansen F, Yang X, Proebsting S, Hoelscher M, Przybilla D, Baumann K, et al. MicroRNA expression in circulating microvesicles predicts cardiovascular events in patients with coronary artery disease. *J Am Heart Assoc.* (2014) 3:e001249. doi: 10.1161/JAHA.114.001249

49. Yang VK, Loughran KA, Meola DM, Juhr CM, Thane KE, Davis AM, et al. Circulating exosome microRNA associated with heart failure secondary to myxomatous mitral valve disease in a naturally occurring canine model. *J Extracell Vesicles.* (2017) 6:1350088. doi: 10.1080/20013078.2017.1350088

50. Parikh M, Pierce GN. A brief review on the biology and effects of cellular and circulating micrornas on cardiac remodeling after infarction. *Int J Mol Sci.* (2021) 22:4995. doi: 10.3390/ijms22094995

51. Kuwabara Y, Ono K, Horie T, Nishi H, Nagao K, Kinoshita M, et al. Increased microRNA-1 and microRNA-133a levels in serum of patients with cardiovascular disease indicate myocardial damage. *Circ Cardiovasc Genet.* (2011) 4:446–54. doi: 10.1161/CIRCGENETICS.110.958975

52. Moreira-Costa L, Barros AS, Lourenço AP, Leite-Moreira AF, Nogueira-Ferreira R, Thongboonkerd V, et al. Exosome-derived mediators as potential biomarkers for cardiovascular diseases: a network approach. *Proteomes.* (2021) 9:1–29. doi: 10.3390/proteomes9010008

53. Moghaddam AS, Afshari JT, Esmaeili SA, Saburi E, Joneidi Z, Momtazi-Borojeni AA. Cardioprotective microRNAs: lessons from stem cell-derived exosomal microRNAs to treat cardiovascular disease. *Atherosclerosis.* (2019) 285:1–9. doi: 10.1016/j.atherosclerosis.2019.03.016

54. Chen Y, Qiao X, Zhang L, Li X, Liu Q. Apelin-13 regulates angiotensin ii-induced Cx43 downregulation and autophagy *via* the AMPK/mTOR signaling pathway in HL-1 cells. *Physiol Res.* (2020) 69:813–22. doi: 10.33549/physiolres.934488

55. Li M, Qi C, Song R, Xiong C, Zhong X, Song Z, et al. Inhibition of long noncoding RNA SNHG20 improves angiotensin II-induced cardiac fibrosis and hypertrophy by regulating the microRNA 335/ galectin-3 axis. *Mol Cell Biol.* (2021) 41:e0058020. doi: 10.1128/MCB.00580-20

56. Lancellotti P, Tribouilloy C, Hagendorff A, Popescu BA, Edvardsen T, Pierard LA, et al. Recommendations for the echocardiographic assessment of native valvular regurgitation: an executive summary from the European association of cardiovascular imaging. *Eur Heart J Cardiovasc Imaging.* (2013) 14:611–44. doi: 10.1093/ehjci/jet105

57. Tsang W, Lang RM. Degenerative mitral regurgitation. In: *Textbook of Three-Dimensional Echocardiography*, eds L. Badano, R. Lang, and D. Muraru (New York, NY: Springer International Publishing) (2019). p. 127–43. doi: 10.1007/978-3-030-14032-8_9

58. Vahanian A, Baumgartner H, Bax J, Butchart E, Dion R, Filippatos G, et al. Guidelines on the management of valvular heart disease: the task force on the management of valvular heart disease of the European society of cardiology. *Eur Heart J.* (2007) 28:230–68.

59. Criteria Committee of the New York Heart Association. *Nomenclature and Criteria for Diagnosis of Diseases of the Heart and Great Vessels*. 9th ed. (Vol. 253). Boston, MA: Little, Brown & Co (1994). p. 253–6.

60. Liu B, Neil DAH, Bhabra M, Patel R, Barker TA, Nikolaidis N, et al. Reverse myocardial remodeling following valve repair in patients with chronic severe primary degenerative mitral regurgitation. *JACC Cardiovasc Imaging.* (2022) 15:224–36. doi: 10.1016/j.jcmg.2021.07.007

61. Pandis D, Grapsa J, Athanasiou T, Punjabi P, Nihoyannopoulos P. Left ventricular remodeling and mitral valve surgery: prospective study with real-time 3-dimensional echocardiography and speckle tracking. *J Thorac Cardiovasc Surg.* (2011) 142:641–9. doi: 10.1016/j.jtcvs.2010.11.030

62. Glauber M, Karimov JH, Farneti PA, Cerillo AG, Santarelli F, Ferrarini M, et al. Minimally invasive mitral valve surgery *via* right minithoracotomy. *Multimed Man Cardiothorac Surg.* (2009) 2009:mmcts.2008.003350. doi: 10.1510/mmcts.2008.003350

63. Zoghbi WA, Adams D, Bonow RO, Enriquez-Sarano M, Foster E, Grayburn PA, et al. Recommendations for noninvasive evaluation of native valvular regurgitation: a report from the American society of echocardiography developed in collaboration with the society for cardiovascular magnetic resonance. *J Am Soc Echocardiogr.* (2017) 30:303–71.

64. Lang RM, Badano LP, Victor MA, Afilalo J, Armstrong A, Ernande L, et al. Recommendations for cardiac chamber quantification by echocardiography in adults: an update from the American society of echocardiography and the European association of cardiovascular imaging. *J Am Soc Echocardiogr.* (2015) 28:1–39.e14. doi: 10.1016/j.echo.2014.10.003

65. Guenzinger R, Wildhirt SM, Voegele K, Wagner I, Schwaiger M, Bauernschmitt R, et al. Comparison of magnetic resonance imaging and transthoracic echocardiography for the identification of LV mass and volume regression indices 6 months after mitral valve repair. *J Card Surg.* (2008) 23:126–32. doi: 10.1111/j.1540-8191.2007.00558.x

66. Garg P, Swift AJ, Zhong L, Carlhäll CJ, Ebbers T, Westenberg J, et al. Assessment of mitral valve regurgitation by cardiovascular magnetic resonance imaging. *Nat Rev Cardiol.* (2020) 17:298–312. doi: 10.1038/s41569-019-0305-z

67. Kon MWS, Myerson SG, Moat NE, Pennell DJ. Quantification of regurgitant fraction in mitral regurgitation by cardiovascular magnetic resonance: comparison of techniques. *J Heart Valve Dis.* (2004) 13:600–7.

68. Chaikriangkrai K, Lopez-Mattei JC, Lawrie G, Ibrahim H, Quinones MA, Zoghbi W, et al. Prognostic value of delayed enhancement cardiac magnetic resonance imaging in mitral valve repair. *Ann Thorac Surg.* (2014) 98:1557–63. doi: 10.1016/j.athoracsur.2014.06.049

69. Casieri V, Matteucci M, Pasanisi EM, Papa A, Barile L, Fritsche-Danielson R, et al. Ticagrelor enhances release of anti-hypoxic cardiac progenitor cell-derived exosomes through increasing cell proliferation *in vitro*. *Sci Rep.* (2020) 10:1–13. doi: 10.1038/s41598-020-59225-7

70. Livak KJ, Schmittgen TD. Analysis of relative gene expression data using real-time quantitative PCR and the $2-\Delta\Delta CT$ method. *Methods.* (2001) 25:402–8. doi: 10.1006/meth.2001.1262

71. Claycomb WC, Lanson NA, Stallworth BS, Egeland DB, Delcarpio JB, Bahinski A, et al. HL-1 cells: a cardiac muscle cell line that contracts and retains phenotypic characteristics of the adult cardiomyocyte. *Proc Natl Acad Sci U.S.A.* (1998) 95:2979–84. doi: 10.1073/pnas.95.6.2979

72. Zhang D, Lee H, Zhu Z, Minhas JK, Jin Y. Enrichment of selective miRNAs in exosomes and delivery of exosomal miRNAs *in vitro* and *in vivo*. *Am J Physiol Lung Cell Mol Physiol.* (2017) 312:L110–21. doi: 10.1152/ajplung.00423.2016

73. Bloch L, Ndongson-Dongmo B, Kusch A, Dragun D, Heller R, Huber O. Real-time monitoring of hypertrophy in HL-1 cardiomyocytes by impedance measurements reveals different modes of growth. *Cytotechnology.* (2016) 68:1897–907. doi: 10.1007/s10616-016-0001-3

74. Goksuluk D, Korkmaz S, Zararsiz G, Karaagaoglu AE. EasyROC: an interactive web-tool for roc curve analysis using R language environment. *R J.* (2016) 8:213–30. doi: 10.32614/RJ-2016-042

75. DeLong ER, DeLong DM, Clarke-Pearson DL. Comparing the areas under two or more correlated receiver operating characteristic curves: a nonparametric approach. *Biometrics.* (1988) 44:837. doi: 10.2307/2531595

76. Marsan NA, Maffessanti F, Tamborini G, Gripari P, Caiani E, Fusini L, et al. Left atrial reverse remodeling and functional improvement after mitral valve repair in degenerative mitral regurgitation: a real-time 3-dimensional echocardiography study. *Am Heart J.* (2011) 161:314–21. doi: 10.1016/j.ahj.2010.10.029

77. Kitkungvan D, Nabi F, Kim RJ, Bonow RO, Khan MA, Xu J, et al. Myocardial fibrosis in patients with primary mitral regurgitation with and without prolapse. *J Am Coll Cardiol.* (2018) 72:823–34. doi: 10.1016/j.jacc.2018.06.048

78. Liu B, Neil DAH, Premchand M, Bhabra M, Patel R, Barker T, et al. Myocardial fibrosis in asymptomatic and symptomatic chronic severe primary mitral regurgitation and relationship to tissue characterisation and left ventricular function on cardiovascular magnetic resonance. *J Cardiovasc Magn Reson.* (2020) 22:86. doi: 10.1186/s12968-020-00674-4

79. Barile L, Cervio E, Lionetti V, Milano G, Ciullo A, Biemmi V, et al. Cardioprotection by cardiac progenitor cell-secreted exosomes: role of pregnancy-associated plasma protein-A. *Cardiovasc Res.* (2018) 114:992–1005. doi: 10.1093/cvr/cvy055

80. Gąsecka A, Pluta K, Solarska K, Rydz B, Eyileten C, Postula M, et al. Plasma concentrations of extracellular vesicles are decreased in patients with post-infarct cardiac remodelling. *Biology (Basel).* (2021) 10:1–13. doi: 10.3390/biology10020097

81. Danielson KM, Shah R, Yeri A, Liu X, Camacho Garcia F, Silverman M, et al. Plasma circulating extracellular RNAs in left ventricular remodeling post-myocardial infarction. *EBioMedicine.* (2018) 32:172–81. doi: 10.1016/j.ebiom.2018.05.013

82. Chien KR, Knowlton KU, Zhu G, Chien S. Regulation of cardiac gene expression during myocardial growth and hypertrophy: molecular studies of an adaptive physiologic response. *FASEB J.* (1991) 5:3037–64. doi: 10.1096/fasebj.5.15.1835945

83. Vinciguerra M, Santini MP, Claycomb WC, Ladurner AG, Rosenthal N. Local IGF-1 isoform protects cardiomyocytes from hypertrophic and oxidative stresses *via* SirT1 activity. *Aging.* (2009) 2:43–62. doi: 10.18632/aging.100107

84. Shalitin N, Friedman M, Schlesinger H, Barhum Y, Levy MJ, Schaper W, et al. The effect of angiotensin II on myosin heavy chain expression in cultured myocardial cells. *InVitro Cell Dev Biol Anim.* (1996) 32:573–8. doi: 10.1007/BF02722984

85. Gu H, Liu Z, Li Y, Xie Y, Yao J, Zhu Y, et al. Serum-derived extracellular vesicles protect against acute myocardial infarction by regulating miR-21/PDCD4 signaling pathway. *Front Physiol.* (2018) 9:348. doi: 10.3389/fphys.2018.00348

86. Qiao L, Hu S, Liu S, Zhang H, Ma H, Huang K, et al. microRNA-21-5p dysregulation in exosomes derived from heart failure patients impairs regenerative potential. *J Clin Invest.* (2019) 129:2237–50. doi: 10.1172/JCI123135

87. Prasad AM, Ma H, Sumbilla C, Lee DI, Klein MG, Inesi G. Phenylephrine hypertrophy, Ca2+-ATPase (SERCA2), and Ca2+ signaling in neonatal rat cardiac myocytes. *Am J Physiol Cell Physiol.* (2007) 292:C2269–75. doi: 10.1152/ajpcell.00441.2006

88. Mayourian J, Ceholski DK, Gorski PA, Mathiyalagan P, Murphy JF, Salazar SI, et al. Exosomal microRNA-21-5p mediates mesenchymal stem cell paracrine effects on human cardiac tissue contractility. *Circ Res.* (2018) 122:933–44. doi: 10.1161/CIRCRESAHA.118.312420

frontiers | Frontiers in Cardiovascular Medicine

TYPE Original Research
PUBLISHED 17 October 2022
DOI 10.3389/fcvm.2022.922790

OPEN ACCESS

EDITED BY
Zhen-Ao Zhao,
Hebei North University, China

REVIEWED BY
Na Xu,
Cincinnati Children's Hospital Medical Center, United States
Haidong Guo,
Shanghai University of Traditional Chinese Medicine, China

*CORRESPONDENCE
Qing Yao
qingyao@hbust.edu.cn
Meng Zhao
zhaomeng@westlake.edu.cn

†These authors have contributed equally to this work and share first authorship

SPECIALTY SECTION
This article was submitted to Cardiovascular Biologics and Regenerative Medicine, a section of the journal Frontiers in Cardiovascular Medicine

RECEIVED 18 April 2022
ACCEPTED 15 September 2022
PUBLISHED 17 October 2022

CITATION
He Y, Li Q, Feng F, Gao R, Li H, Chu Y, Li S, Wang Y, Mao R, Ji Z, Hua Y, Shen J, Wang Z, Zhao M and Yao Q (2022) Extracellular vesicles produced by human-induced pluripotent stem cell-derived endothelial cells can prevent arterial stenosis in mice via autophagy regulation. *Front. Cardiovasc. Med.* 9:922790. doi: 10.3389/fcvm.2022.922790

Extracellular vesicles produced by human-induced pluripotent stem cell-derived endothelial cells can prevent arterial stenosis in mice via autophagy regulation

Yecheng He[1†], Quanfu Li[3†], Feng Feng[4†], Rupan Gao[5], Huadong Li[6], Yuxin Chu[7], Shaobo Li[8], Yin Wang[8], Ruoying Mao[8], Zhongzhong Ji[8], Yutao Hua[7], Jun Shen[9], Ziao Wang[10], Meng Zhao[8*] and Qing Yao[2*]

[1]Department of Clinical Medicine, Suzhou Vocational Health College, Suzhou, Jiangsu, China, [2]Hubei Key Laboratory of Diabetes and Angiopathy, Medicine Research Institute, Xianning Medical College, Hubei University of Science and Technology, Xianning, Hubei, China, [3]Department of Anesthesiology, Shanghai Pulmonary Hospital, Tongji University School of Medicine, Shanghai, China, [4]Institute of Physical Education, Inner Mongolia Normal University, Hohhot, Inner Mongolia, China, [5]Department of Hematology, Zhongshan Hospital, Shanghai Medical College of Fudan University, Shanghai, China, [6]Department of Cardiovascular Surgery, Union Hospital, Tongji Medical College, Huazhong University of Science and Technology, Wuhan, Hubei, China, [7]Department of Medicine, University of Alabama at Birmingham, Birmingham, AL, United States, [8]School of Life Sciences, Westlake University, Hangzhou, Zhejiang, China, [9]Department of Pharmacy, Suzhou Vocational Health College, Suzhou, Jiangsu, China, [10]School of Life Sciences, Xiamen University, Xiamen, Fujian, China

Intravascular transplantation of human-induced pluripotent stem cells (hiPSCs) demonstrated a significant therapeutic effect in the treatment of restenosis by the paracrine function of extracellular vesicles (EVs). However, the risk of tumorigenicity and poor cell survival limits its clinical applications. In this study, we for the first time applied a highly efficient and robust three-dimensional (3D) protocol for hiPSC differentiation into endothelial cells (ECs) with subsequent isolation of EVs from the derived hiPSC-EC (ECs differentiated from hiPSCs), and validated their therapeutic effect in intimal hyperplasia (IH) models. We found that intravenously (iv) injected EVs could accumulate on the carotid artery endothelium and significantly alleviate the intimal thickening induced by the carotid artery ligation. To elucidate the mechanism of this endothelial protection, we performed miRNA expression profiling and found out that among the most conserved endothelial miRNAs, miR-126 was the most abundant in hiPSC-EC-produced EVs (hiPSC-EC-EV). MiR-126 depletion from hiPSC-EC-EV can hinder its protective effect on human umbilical vein endothelial cells (HUVECs) in an inflammatory process. A variety of functional *in vitro* studies revealed that miR-126 was able to prevent endothelial apoptosis after inflammatory stimulation, as well as promote EC migration and tube formation through autophagy upregulation. The latter was supported by *in vivo* studies demonstrating that treatment with hiPSC-EC-EV can upregulate autophagy in mouse carotid artery ECs,

thereby preventing IH and modulating vascular homeostasis via remodeling of the vascular intima. Our findings suggest a regulatory mechanism for the therapeutic effect on arterial restenosis by autophagy regulation, and provide a potential strategy for clinical treatment of the disease.

KEYWORDS

arterial restenosis, hiPSC-EC, autophagy, extracellular vesicles, miR-126

Introduction

Arterial restenosis represents a major complication in vascular reconstructive procedures, such as balloon angioplasty, bypass grafting, stent angioplasty, and endarterectomy. Stimuli, such as an altered blood flow, mechanical load, and vascular endothelial injury in the postoperative period, followed by recruitment and infiltration of inflammatory cells into the vascular walls and subsequent secretion of cytokines and growth factors lead to the vascular smooth muscle cell (VSMC) proliferation and migration, and result in IH, which further progresses into vascular restenosis (1–4). Therefore, the exploration of effective strategies for IH intervention is necessary to prevent postoperative restenosis.

Recently, stem cell therapy showed great promise for curing restenosis. HiPSCs are generated by reprogramming somatic cells and represent a source of autologous pluripotent stem cells. Since the discovery of induced pluripotent stem cells (iPSCs) in 2006 (5), transplantation of iPSCs and differentiated derivatives thereof emerged as a promising direction in regenerative therapy, owing to the high pluripotency of iPSCs, low immune rejection response to them, and the lack of ethical restrictions associated with their use (5, 6). However, due to some disadvantages of stem cell therapy, such as low cell survival rate, genomic instability, and potential tumorigenicity, as well as a limited targeting efficiency (7, 8), advanced preclinical studies have recognized that paracrine factors generated by transplanted iPSCs, rather than the cells *per se*, confer the major beneficial effects of regeneration on the injured tissues (9, 10).

Among these paracrine molecules, EVs exhibit unique functions and hold great potential in disease diagnosis and therapy. EVs are extracellular membrane vesicles secreted by various cell types (11). EVs contain miRNAs and other components capable of regulating cell proliferation or apoptosis in vascular endothelium and promoting remodeling of the vascular intima. EVs enable cells to modulate molecular mechanisms remotely, i.e., exert molecular effects beyond the intracellular compartments of the effector cell (12–14).

Extracellular vesicles used for vascular healing in previous studies were primarily derived from mesenchymal stem cells (MSCs) or other types of stem cells (15, 16). The impairment of the EC function was believed to be a major regulatory factor in the restenosis mechanism. Although ECs are also likely to generate EVs with therapeutic effects, they are rarely used as an EV source due to the lack of sustainable expandability and quality cell lines. In this study, we employed a 3D differentiation protocol, which can efficiently generate functional ECs from hiPSCs (17). We then isolated EVs from hiPSC-EC and injected them into mice IH models to evaluate their therapeutic effect and identify the disease treatment mechanisms. Compared with MSCs, the major advantages of hiPSCs include that they can be mass-produced and individualized for treatment. Meanwhile, using a microfluidic chip to simulate the circulatory system *in vivo*, we have also demonstrated that hiPSC-EC-EV have better cellular adhesion capacity and therapeutic effect than HUVEC-EV (**Supplementary Figure 1**). Since EC differentiation and hiPSC-EC-EV production using our protocol are remarkably more efficient and robust than those achieved by conventional methods, our results offer a potential strategy for the clinical treatment of vascular restenosis.

Materials and methods

Establishing an animal model for intimal hyperplasia

The C57 mice (cleaning grade) weighing 25–28 g were selected to prepare the arterial injury model. All mice were kept under specific pathogen-free conditions in strict compliance with the facility standards approved by the China Laboratory Animal Management Accreditation Association. The mice were anesthetized by intraperitoneal injection of sodium pentobarbital (40 mg/kg) and placed on the operating table. The animals' neck skin was sterilized with iodine wine and alcohol and then cut off. The subcutaneous tissue and muscle were separated successively, the left common carotid arteries were exposed, and the bifurcation of the internal/external branches was ligated completely with a 5-0 silk suture. At last, the

subcutaneous tissue and skin were sutured layer by layer. All mice were maintained at the Hubei University of Science and Technology.

Cell culture of human-induced pluripotent stem cells

Human iPSCs were obtained from Dr. Pan's laboratory at the Tenth People's Hospital affiliated with Tongji University, where they were generated by reprogramming the human dermal fibroblasts from a 40-year-old volunteer with informed consent. All cell lines were propagated in feeder-free growth conditions. Briefly, cells frozen in a cryopreservation tube were removed from liquid nitrogen and transferred to a 37°C water bath for thawing. Then they were mixed with 2 ml of resurviving medium (mTeSRI + 10 μM Y-276362) (StemCell Technologies, Vancouver, BC, Canada) and centrifuged at 300 g for 5 min. The supernatant was discarded, and the cells were mixed with 2 ml of resurviving medium, transferred onto a Matrigel (Corning)-coated six-well plate, and placed in the incubator for 24 h. On the next day, the medium was replaced with 2 ml of fresh mTeSRI without Y-27632.

Endothelial cell differentiation

The EC differentiation was performed as described previously (17), and the protocol is schematically outlined in **Figure 1A**. Three days before initiating the differentiation procedure, hiPSCs were dissociated into single cells and seeded into a 0.5 ml fibrin scaffold patch in a 24-well plate for 48 h. On day 0, the cell-containing fibrin scaffold was cultured in an EBM2 medium (Lonza) supplemented with B27 minus insulin, activin-A, and bone morphogenetic protein 4 (BMP-4) for 24 h. On day 1, the medium was replaced with an EBM2 medium supplemented with B27 minus insulin, vascular endothelial growth factor (VEGF), erythropoietin (EPO), and transforming growth factor β1 (TGFβ1) for another 4 days (the medium was refreshed on day 3). On day 5, the patch was treated with collagenase IV to release the differentiating cells, and the medium was replaced with EGM2-MV medium (Lonza) supplemented with B27, VEGF, and SB-431542. The medium was replaced every 2 days thereafter. Fluorescence-activated cell sorting (FACS) was performed on day 14 to evaluate the differentiation efficiency by analyzing the CD31 and CD144 expression levels in the differentiated cells. The $CD31^{+}CD144^{+}$-sorted hiPSC-ECs were cultured in an EGM2-MV medium supplemented with B27, VEGF, and SB-431542.

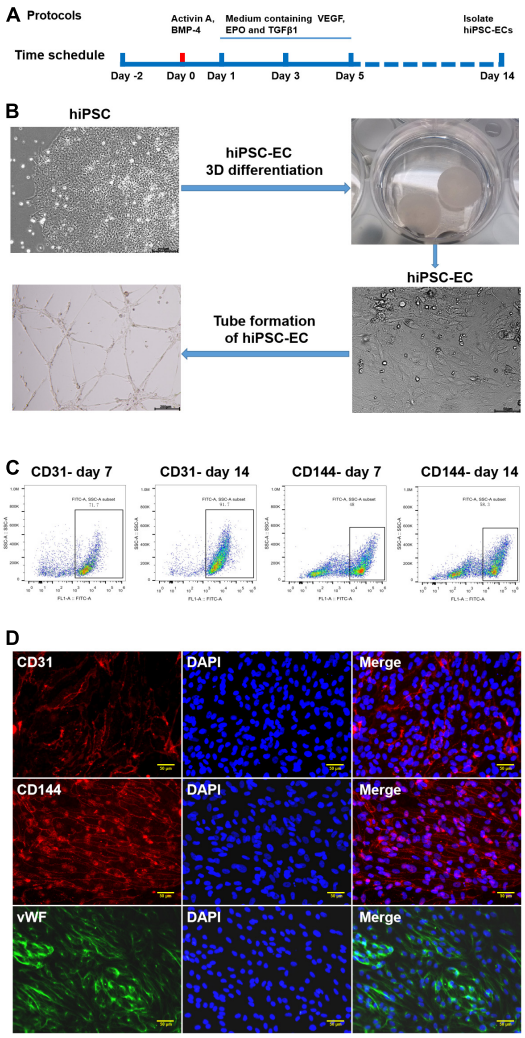

FIGURE 1
Generation and characterization of human-induced pluripotent stem cell-endothelial cells (hiPSC-ECs). **(A)** Schematic representation of the protocol for differentiation of hiPSCs to ECs; **(B)** Differentiation of hiPSC-EC through a 3D protocol; **(C)** Flow cytometry assay for the detection of CD31 and CD144 expression post-hiPSC-EC differentiation; **(D)** Identification of hiPSC-EC by immunofluorescent staining.

Flow cytometry

Flow cytometry was performed as previously described (17). In brief, differentiated hiPSC-ECs were gently dissociated with trypsin (0.05%) and neutralized with the culture medium. After centrifugation and discarding of supernatant, the cells were incubated with FACS buffer (2% FBS in PBS) containing primary PE-conjugated anti-CD31 antibodies or FITC-conjugated anti-CD144 antibodies for 30 min at 4°C. Isotype antibodies were used as control. Then the cells were washed with FACS buffer, resuspended in 0.5 ml of FACS buffer, and analyzed with a FACS instrument (Sony MA900 Cell Sorter).

Extraction and identification of human-induced pluripotent stem cells-endothelial cell-extracellular vesicle

The HiPSC-ECs were cultured to 70% confluency, and the supernatant was collected and centrifuged at 2,000 g for 10 min at 4°C to remove the residual cells and debris followed by another centrifugation at 100,000 g for 1 h at 4°C. Afterward, the EV pellets were resuspended in 50–100 μl of phosphate-buffered saline (PBS). EVs were visualized with a transmission electron microscopy (FEI Tecnai G2 Spirit, ThermoFisher Scientific, Waltham, MA, USA) directly or an inverted fluorescence microscope (Olympus FV3000). The diameter distribution of EVs was determined by NanoSight (Malvern Instruments Inc., Malvern, UK). Some specific protein markers, such as CD9, CD63, and TSG101, were identified by Western blotting analysis.

Transmission electron microscopy

The extracted EVs were first fixed with 2.5% glutaraldehyde and then dropped onto the copper mesh, followed by staining with a 12% phosphor-tungstic acid aqueous solution (pH = 6.5). Afterward, the samples were visualized under the electron microscope, and the target pictures were taken.

Lipophilic dye (PKH) labeling of extracellular vesicles

The resuspended EVs were stained with PKH26 (or PKH67) (Red Fluorescent Cell linker for General Cell Membrane) (Sigma-Aldrich, St. Louis, MO, USA). PKH26 dye was added to 100 μl of diluent C to a final concentration of 8 μM. Then 8 μg of EVs suspended in 20 μl of DPBS was added to 80 μl of diluent C, mixed with the PKH26 solution, and incubated at 37°C for 15 min. Afterward, 10% EV-depleted fetal bovine serum (FBS) diluted in DMEM was added to bind with excess dye, followed by diluting to 1 ml with PBS and centrifuging at 100,000 × g for 1 h at 4°C. The pellet was resuspended in 40 μ l of PBS.

Western blotting analysis

Western blotting was performed as described previously (18). In brief, total protein was extracted from the EVs or cells, and the concentration was determined by a BCA Protein Assay Kit (Beijing Solarbio Science and Technology Co., Ltd., Beijing, China). Total protein obtained from each sample in a lysis buffer was loaded on each lane and run on an SDS-PAGE for 1 h at 100 V, and then transferred onto a polyvinylidene fluoride membrane. The membrane was blocked with 5% milk for 1 h and then incubated with a primary antibody (Table 1) overnight at 4°C. HRP Affini-Pure Goat anti-Rabbit IgG (cat. # ab97051, Abcam) was used as a secondary antibody. Finally, the blots were visualized by enzyme-linked chemiluminescence assay (Beyotime, Shanghai, China) and analyzed by Image J software.

miRNA transfection and depletion of miR-126 on endothelial cell

In the miRNA transfection experiment, HUVECs were seeded in six-well plates first and grown to the confluency of about 70%. Then the cells were transfected with miR-126 mimic (Genepharma, Shanghai, China) and a control mimic (NC) by using Lipofectamine 2000 (Invitrogen, Carlsbad, CA, USA), according to the manufacturer's recommendations. The supernatant was replaced with a complete culture medium after 5 h, and Western blotting was performed to assess the transfection effect after 48 h.

In the miR-126 depletion experiment, the hsa-miR-126/inhibitor and inhibitor negative control oligonucleotides were purchased from GenePharma. Cells in the logarithmic growth phase were trypsinized, counted, and seeded in six-well plates to ensure 50% cell confluence on the next day for transfection. Transfection of cells with oligonucleotides was performed using Lipofectamine^{TM} 2000 Reagent in line with the manufacturer's instructions (Invitrogen, Carlsbad, CA, USA)

TABLE 1 Antibodies summary.

Antibody	Brand	Cat. no.
anti CD9	abcam	ab236630
anti CD63	abcam	ab134045
anti CD31	abcam	ab182981
anti CD144	abcam	ab33168
anti vWF	abcam	ab6994
anti Alix	abcam	ab275377
anti TSG101	abcam	ab133586
anti Bcl-2	abcam	ab182858
anti Ki67	abcam	ab16667
anti α-SMA	abcam	ab7817
anti P-mTOR (Ser2448)	CST	5536T
anti mTOR	CST	2983
anti Bax	CST	2772S
anti β-actin	CST	4970
anti LC3B	CST	2775S
anti P62	CST	39749S

at a final concentration of 100 nM. After transfection with hsa-miR-126/inhibitor in hiPSC-EC cells, EVs were extracted from hiPSC-EC cells.

Scratch test

The HUVECs were seeded in six-well plates and transfected with either a non-coding (NC) control miRNA or miR-126 mimic (300 nM) and cultured to 80–90% confluency. Then a sterile pipette tip was used to inflict a linear scratch injury in the center of the cell monolayer. Then the cells were cultured in a normal medium for another 48 h. The wound was monitored by a phase-contrast microscope (Olympus IX71), and the cell closure was determined by measurements with Image J software.

Tube formation

The HUVECs were treated with either hiPSC-EC-EV or different miRNA mimics for 48 h before performing tube formation assays. Culture plates (24-well) were pre-coated with Matrigel (BD Pharmingen, Piscataway, NJ, USA), and then 5×10^4/well HUVECs were seeded and cultured for 12 h. The proliferation and migration properties of the HUVECs were determined by quantification of the total tubule length in five random view fields per well.

Hematoxylin and eosin staining and immunofluorescent staining

The HiPSC-ECs in chamber slides were treated with miR-126 mimic or control mimic for 48 h. Then the cells were washed with PBS and fixed with 4% paraformaldehyde (PFA) at room temperature for 15 min, and 0.2% Triton X-100 was added to permeabilize the membrane for 10 min. Then cells were blocked with 5% goat serum and incubated with primary antibodies (**Table 1**) overnight at 4°C. On the next day, the cells were incubated with secondary antibodies for 1 h and stained with DAPI (Sigma-Aldrich, St. Louis, MO, USA) for 5 min at room temperature. For mouse artery tissue analysis, excised arteries were fixed in 4% PFA for 1 h, dehydrated in 30% sucrose solution, embedded in OCT, and sliced into 5 μm sections. The sections were then stained with hematoxylin and eosin (H&E). Immunofluorescence analysis was performed as described above. The cells or the tissue sections were visualized by a confocal fluorescence microscope (Olympus FV3000).

Fabrication of the microfluidic chip

The microfluidic chip consists of a PDMS layer and a glass substrate. First, the PDMS layer was fabricated by replica molding on a master by spin-coating SU8-2035 negative photoresist (Microchem Corp., Newton, MA, USA) onto a glass wafer and patterned by photolithography. After the master is prepared, the Sylgard 184 PDMS base and curing agent (Sylgard Silicone Elastomer 184, Dow Corning Corp., Midland, MI, USA) are thoroughly mixed, degassed under vacuum, and poured onto the master. The PDMS layer was incubated in an oven at 80°C for 1 h and peeled off from the master. The inlet and outlet holes are made by punching the PDMS with a razor-sharp punch. After 60 s of oxygen plasma treatment, this piece of PDMS was irreversibly bound to the glass substrate.

Flow experiment in microfluidic chip

The microfluidic channels were pre-coated with 10 μg/mL of MaxGel human extracellular matrix extracts (Sigma-Aldrich, St. Louis, MO, USA) before seeding of cells. After coating, HUVECs (Lonza) were cultured inside the microfluidic channels at a density of 5×10^6 cells/ml to produce a confluent layer. The fresh culture medium was replaced every 6–8 h. Until cell confluence, HUVEC monolayers were inflamed with TNF-α for 12 h. Then, the medium containing 1 μg/ml of PKH67-labeled HUVEC-EV or hiPSC-EC-EV was perfused through the channels for 6 h. The perfusion was performed with a programmable syringe pump connected with a microfluidic device which provides precise control of the flow rate at 20 μl/min. After 6 h, a blank medium without PKH67-labeled EVs was used to perfuse for 0.5 h. The uptake of fluorescently labeled EVs could be visualized under fluorescence microscopy.

Ultrasonic vocalization recording

Mice were anesthetized under 2.5% isoflurane and then placed on a special console (animal handling and physical monitoring platform), and isoflurane concentration was adjusted to the maintenance level of 1.0–1.5%. Mouse ultrasound imaging was performed with the Vevo LAZR photoacoustic micro-ultrasound imaging system (FujiFilm, VisualSonics Inc., Tokyo, Japan). Once the carotid artery was clearly displayed, the probe was adjusted so that the ultrasonic beam was perpendicular to the anterior and posterior walls of the left common carotid artery, and the intima-media of the artery's anterior and posterior walls was displayed. High-resolution anatomic carotid allograft images were generated with the MS550D transducer at 40 MHz.

Statistical analysis

The IBM SPSS 22 software version was used for statistical analysis. An unpaired *t*-test and one-way ANOVA were used to

calculate statistical significance. The results are expressed as a mean ± SD with $P < 0.05$ indicating the statistical significance of the differences.

Results

Generation and identification of human-induced pluripotent stem cell-endothelial cells

Human iPSCs represent an unlimited source of cells for replacing damaged tissues. They can be successfully differentiated into different subtypes of vascular cells, such as ECs (19, 20) and smooth muscle cells (SMCs) (21, 22). In this study, we used an efficient method for differentiating hiPSCs to $CD31^+$ $CD144^+$ ECs as a source of EVs (**Figure 1A**). HiPSCs were embedded in a biodegradable scaffold suspended in a mTeSR stem cell medium for 3 days before culturing in endothelial growth medium EBM2 supplemented with activin A and BMP-4, as well as some other growth factors following differentiation, which gave rise to endothelial-like cells, as demonstrated by a cobblestone morphology and the formation of a robust network of tubular structures upon seeding on Matrigel (**Figure 1B**). The efficiencies of hiPSC-EC differentiation were evaluated at day 7 and day 14 by performing flow cytometry analysis. On day 7, the expression of CD31 and CD144 in the differentiating ECs was 71.7 and 48%, respectively. On day 14, the EC differentiation efficiency increased to 91.7% for CD31 and 58.3% for CD144 (**Figure 1C**). Immunostaining assay further demonstrated that day 14 was the ideal time point for EC isolation when the endothelial-specific genes for CD31, CD144, and vWF proteins exhibited very high expression levels (**Figure 1D**).

Characterization of human-induced pluripotent stem cell-endothelial cell-extracellular vesicle

To validate the harvested hiPSC-EC-EV, the morphology of EVs was first analyzed by TEM. The EVs exhibited a roughly cup-shaped morphology with a diameter of 80–130 nm (**Figure 2A**). The mean diameter was around 125 nm, as determined by NanoSight (**Figures 2C,D**). Aside from the EV shape and size validation, Western blotting revealed the expression of some EV-associated proteins, such as Alix, CD63, and TSG101 (**Figure 2B**), so the EVs were validated as genuine. Furthermore, we observed PKH26 fluorescence in HUVECs at 2 h after incubation with EVs, while the fluorescence intensity became much higher after 12 h (**Figure 2E**). To determine whether the EVs could be taken up by cells or just adhered to the cell surface, we incubated HUVECs with PKH26-labeled hiPSC-EC-EV in the presence of endocytic inhibitor cytochalasin D for 12 h. We could see that the increase of PKH26 fluorescence could be interrupted by endocytic inhibitor cytochalasin D (**Figure 2E**), which demonstrated that over time of incubation, more EVs will be internalized into the cells.

Luminal stenosis in injured carotid arteries is alleviated by treatment with human-induced pluripotent stem cell-endothelial cell-extracellular vesicle

The schematic diagrams illustrating the carotid artery ligation and the process for the hiPSC-EC-EV treatment are depicted in **Figures 3A,B**, respectively. Each group contained 7–9 mice. To evaluate the effect of hiPSC-EC-EV on luminal stenosis, we injected the EVs into the tail vein of mice (10 μg of EVs per injection and injected every 3 days), and the diameter of the carotid arteries in each mouse was analyzed 21 days after the surgery and EV treatment by HE staining and an ultrasound examination (**Figures 3C,D**). Compared with the sham group, the artery ligation induced a substantial increase in the neointimal layer's thickness and the neointima-to-media ratio, although the EV treatment group also showed a higher index but obviously moderate (**Figure 3C**). Meanwhile, ultrasound examination also showed that the luminal diameter in the PBS group was significantly decreased and obviously recovered in the EV treatment group (**Figure 3D**). In addition, to further verify if the injected hiPSC-EC-EVs (green fluorescent PKH67-labeled) were taken up by the ECs located at the inner layer of the ligated carotid artery, PKH67 fluorescence was examined in $CD31^+$ ECs. The immunostaining results showed that PKH67 fluorescence could only be found in the hiPSC-EC-EV treatment group and revealed an uptake of the injected hiPSC-EC-EV by the EC of the carotid artery (**Figure 3E** and **Supplementary Figure 2**). In conclusion, our results suggest a potential treatment effect of hiPSC-EC-EV on arterial stenosis induced by a vascular injury. In other major arterial vascular sites of the IH model, we did not detect the signals of EV (**Supplementary Figure 2**).

Human-induced pluripotent stem cell-endothelial cell-extracellular vesicle could alleviate arterial stenosis by repressing endothelial cell apoptosis

The overproliferation of SMCs and apoptosis of ECs exert important roles in arterial stenosis (1, 2). From the mouse *in vivo* study, we found that the apoptosis of ECs in the carotid artery was downregulated in the hiPSC-EC-EV treatment group compared with the PBS group (**Figure 4B**), but the SMC and

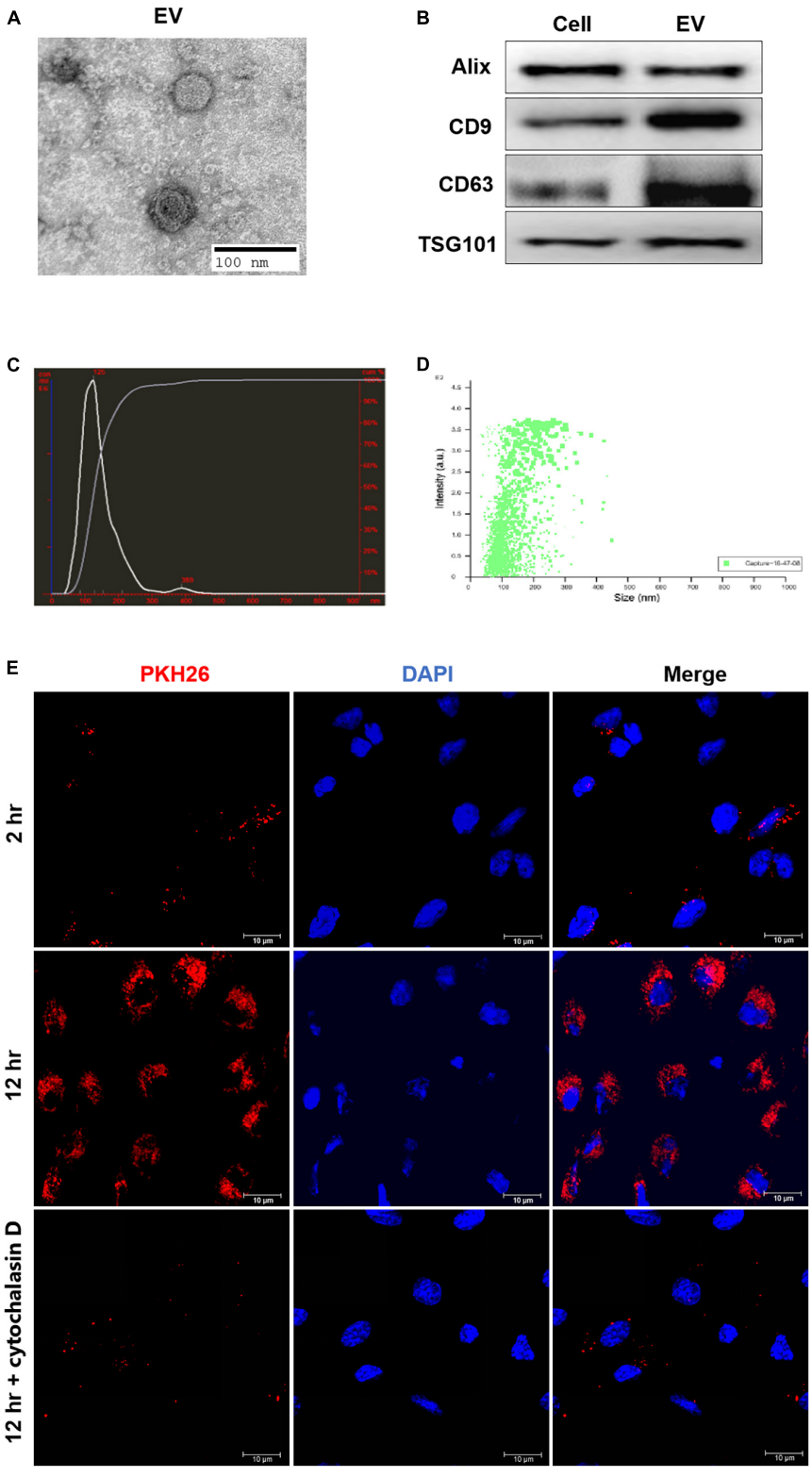

FIGURE 2
Isolation and characterization of human-induced pluripotent stem cell- endothelial cell-extracellular vesicle (hiPSC-EC-EV). **(A)** A representative micrograph of hiPSC-EC-EV visualized by transmission electron microscopy; **(B)** Relative expression levels of Alix, CD9, CD63, and TSG101 proteins in hiPSC-ECs and hiPSC-EC-EV, as revealed by Western blotting; **(C,D)** The hiPSC-EC-EV particle size distribution as measured and analyzed by NanoSight; **(E)** Representative confocal microscopy images of HUVECs exposed for either 2 or 12 h to PKH26-labeled hiPSC-EC-EVs with or without cytochalasin D treatment. The nuclei were counterstained with DAPI.

10.3389/fcvm.2022.922790

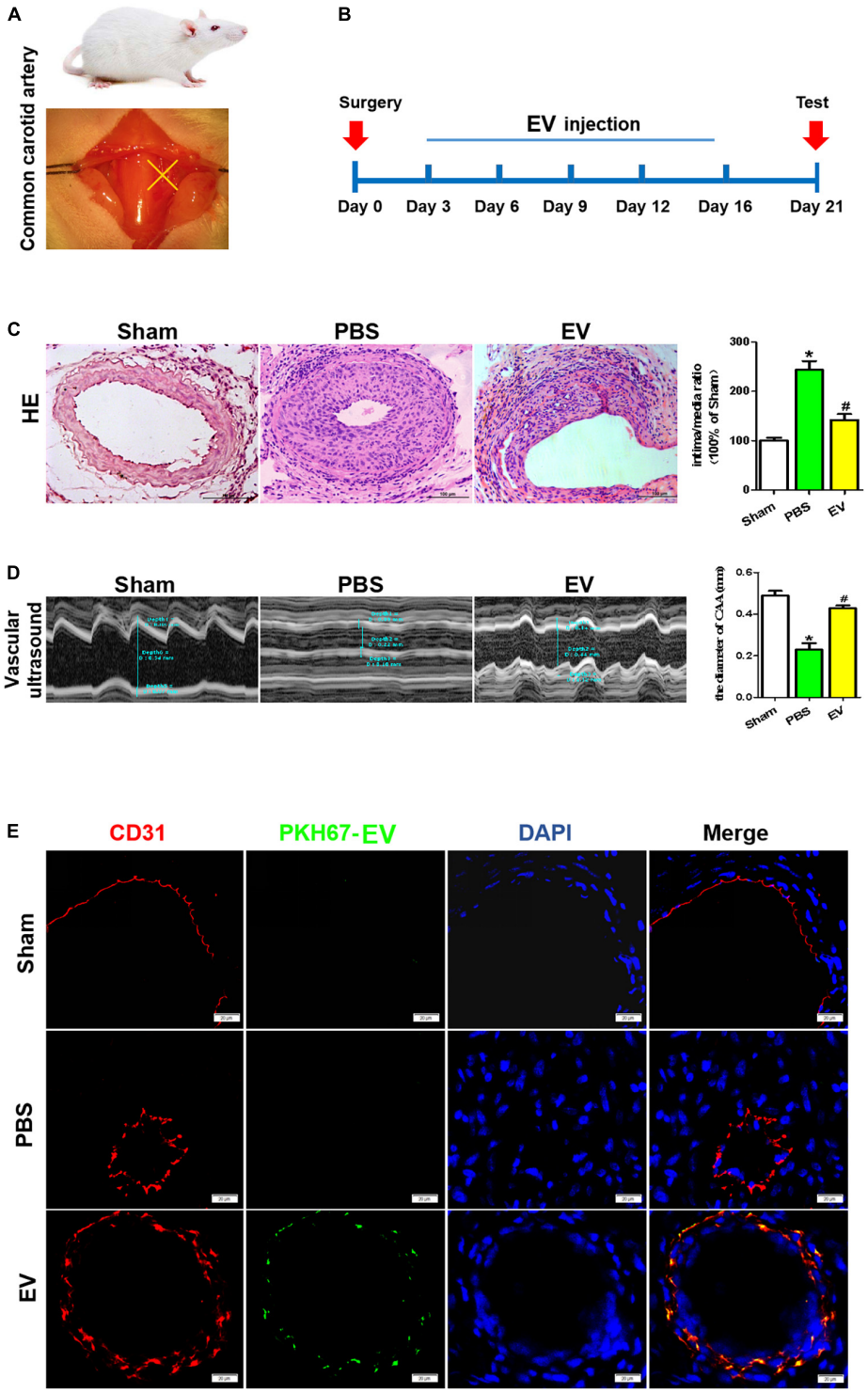

FIGURE 3
Arterial stenosis of carotid artery is reduced by exposure to human-induced pluripotent stem cell- endothelial cell-extracellular vesicle (hiPSC-EC-EV). **(A)** Schematic illustration of the carotid artery ligation procedure in the mouse model. **(B)** Time chart for the *in vivo* treatment of the vascular tissue with hiPSC-EC-EV and its collection for testing. **(C)** Analysis of the neointimal hyperplasia formation in the hiPSC-EC-EV-treated vs untreated mice 21 days after surgery by HE staining, and quantification of the intima-to-media ratio in the blood vessels. Scale bar = 100 μm. **(D)** Representative ultrasound images of the lumen size in the carotid arteries 21 days after the surgery and statistical analysis of the differences. **(E)** Representative images of ECs immunofluorescently stained for CD31 and PKH67 in the carotid arteries 21 days after the surgery. Data represent mean ± SD from three independent experiments (n = 3). Differences between linked groups were evaluated by a two-tailed Student's t-test. $^{*}p < 0.05$ vs. Sham, $^{\#}p < 0.05$ vs. PBS.

EC proliferation showed no difference between the groups (**Figures 4A,C**). At the same time, may be due to the fact that SMCs are located in the middle layer of the arterial lumen wall and receive less blood fluid pressure, there was also no significant difference in the apoptosis of SMCs between the groups (**Figure 4D**). These results indicated that hiPSC-EC-EV might alleviate the arterial stenosis after ligation by repressing EC apoptosis.

The protection effect of human umbilical vein endothelial cells elicited by the human-induced pluripotent stem cell-endothelial cell-extracellular vesicle treatment requires activation of autophagy

To analyze the effect of the hiPSC-EC-EV treatment on the EC function, we detected the tubulation, proliferation, and apoptosis of HUVEC cells *in vitro*. Previous studies established that the inflammatory reaction plays an important role in neointimal hyperplasia (1). To simulate an inflammatory process *in vivo* and evaluate the protecting effect of hiPSC-EC-EV, relevant assays were performed in HUVECs in the presence of 10 ng/ml of TNF-α for 24 h (23). All the *in vitro* tests were repeated at least three times. The results showed that hiPSC-EC-EV could significantly increase the tube length on Matrigel and promoted the proliferation rate of HUVEC (**Figures 5A,B**). Furthermore, we found that the hiPSC-EC-EV treatment could alleviate cell apoptosis relative to the PBS group (**Figure 5C**), suggesting an important role of the hiPSC-EC-EV in endothelial protection. Previous studies have suggested a protective role of autophagy in cardiovascular injury (24). In our study, autophagy-related proteins were analyzed by Western blotting, and found that hiPSC-EC-EV treatment could improve the LC3-II/LC3-I ratio (**Figure 5D**). When autophagy inhibitor 3-MA (10 mM) was added to the cell culture medium following the hiPSC-EC-EV treatment, the enhanced tube formation and cell proliferation capability were interrupted, and the decreased cell apoptosis was also partially reversed, suggesting that the hiPSC-EC-EV-mediated protection is highly related to autophagy pathway, and an autophagy modulation could be used as a strategy to reduce arterial restenosis.

miR-126 contained in human-induced pluripotent stem cell-endothelial cell-extracellular vesicle is a potential therapeutic target

To elucidate the underlying mechanisms of EC protection by hiPSC-EC-EV, some miRNAs commonly expressed by ECs were identified by quantitative PCR (qPCR). We found that the expression level of miR-126 was significantly higher in hiPSC-EC-EV relative to other miRNAs (**Figure 6A**). On the other hand, miR-126 can be more highly enriched in hiPSC-EC-EVs than in hiPSC-ECs (**Figure 6B**). To demonstrate that the protective effects of EVs were at least partially mediated by miR-126, the hsa-miR-126/inhibitor oligonucleotides or NC oligonucleotides were transfected into hiPSC-ECs, and then the EVs in the supernatant were collected at 48 h post-transfection. As compared to NC-oligo EV, miR-126-depleted EV showed a weakened therapeutic effect as indicated by attenuated tubulation and proliferation, as well as enhanced apoptosis in inflammatory cytokine-stimulated HUVECs (**Supplementary Figure 3**).

Furthermore, a series of assays were conducted to verify if miR-126 has a protection effect for HUVEC in inflammatory reactions. As expected, tube formation and scratch-wound tests verified that transfection of HUVECs with miR-126 induced an enhancement of tubulation and migration in contrast to the negative control (NC) miRNA group. Importantly, these improvements could be abolished by treatment with autophagy inhibitor 3-MA (**Figures 6C,D**). On the other hand, miR-126 could also promote the proliferation and inhibit the apoptosis of HUVEC cells *in vitro* (**Figures 6E,F**). In addition, miR-126 was found to enhance the expression of anti-apoptosis protein Bcl-2 and suppress the expression of pro-apoptotic protein Bax, which could be reversed by autophagy inhibitor 3-MA (**Figures 6G,H**).

miR-126 exerts therapeutic effect via autophagy regulation

Some previous studies have reported the effect of miR-126 on autophagy regulation and the role of autophagy in cardiovascular diseases (25, 26). To further verify whether miR-126 exerted its protection effect via an autophagy regulation, Western blotting and immunofluorescence analyses were performed with HUVECs. The immunostaining showed that miR-126 significantly promoted the LC3B expression in HUVECs, while 3-MA suppressed this effect (**Figure 7A**). This was further confirmed by Western blotting, and miR-126 can remarkably increase the LC3-II/LC3-I ratio and suppress the expression of p-mTOR and p62 in HUVECs (**Figures 7B,C**). Taken together, these findings indicate that miR-126 enriched in EV can substantially promote the autophagy function of EC.

To assess the role of hiPSC-EC-EV-induced autophagy in facilitating the injury healing process in the carotid artery, we examined the endothelial autophagy level in murine carotid artery sections by immunofluorescence staining and found that the LC3B levels were consistently higher in the ECs of the hiPSC-EC-EV treatment group when compared

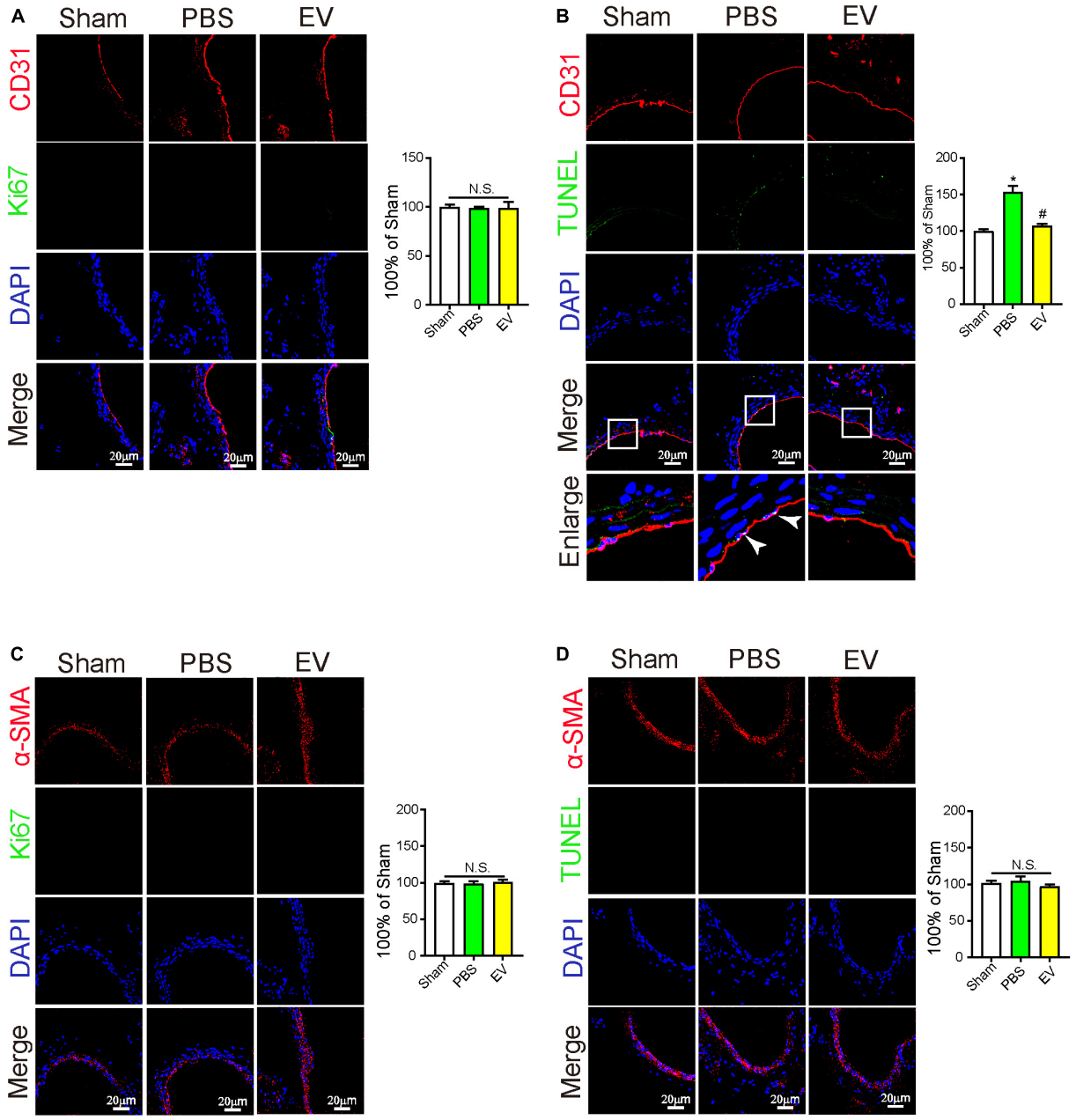

FIGURE 4
The protective effect of human-induced pluripotent stem cell- endothelial cell-extracellular vesicle (hiPSC-EC-EV) on carotid artery through inhibition of EC apoptosis. **(A–D)** Representative immunostaining images stained for CD31 (Red) and Ki67 (Green) in panel **(A)**, stained for CD31 (Red) and TUNEL (Green) in panel **(B)**, stained for α-SMA (Red) and Ki67 (Green) in panel **(C)**, and stained for α-SMA (Red) and TUNEL (Green) in panel **(D)** in the carotid arteries 21 days after the surgery. Data represent mean ± SD from three independent experiments (n = 3). Differences between linked groups were evaluated by two-tailed Student's t-test. *$p < 0.05$ vs. Sham; $^{\#}p < 0.05$ vs. PBS.

with those of the PBS control group (Figure 7D and Supplementary Figure 4A), whereas the P62 expression was weaker (Figure 7E), demonstrating that autophagy was activated in EC by the hiPSC-EC-EV treatment. The mTOR is a master regulator of cellular metabolism, which also plays a crucial role in regulating autophagy. Activation of mTORC1 can lead to autophagy inhibition through the phosphorylation of multiple proteins (27). Our Western blotting analysis results demonstrated that hiPSC-EC-EV could reduce p-mTOR expression in HUVECs *in vitro* (Figure 7B). Here, we also found that a systemic administration of hiPSC-EC-EV into mice could inhibit the mTOR pathway in the EC of the carotid artery

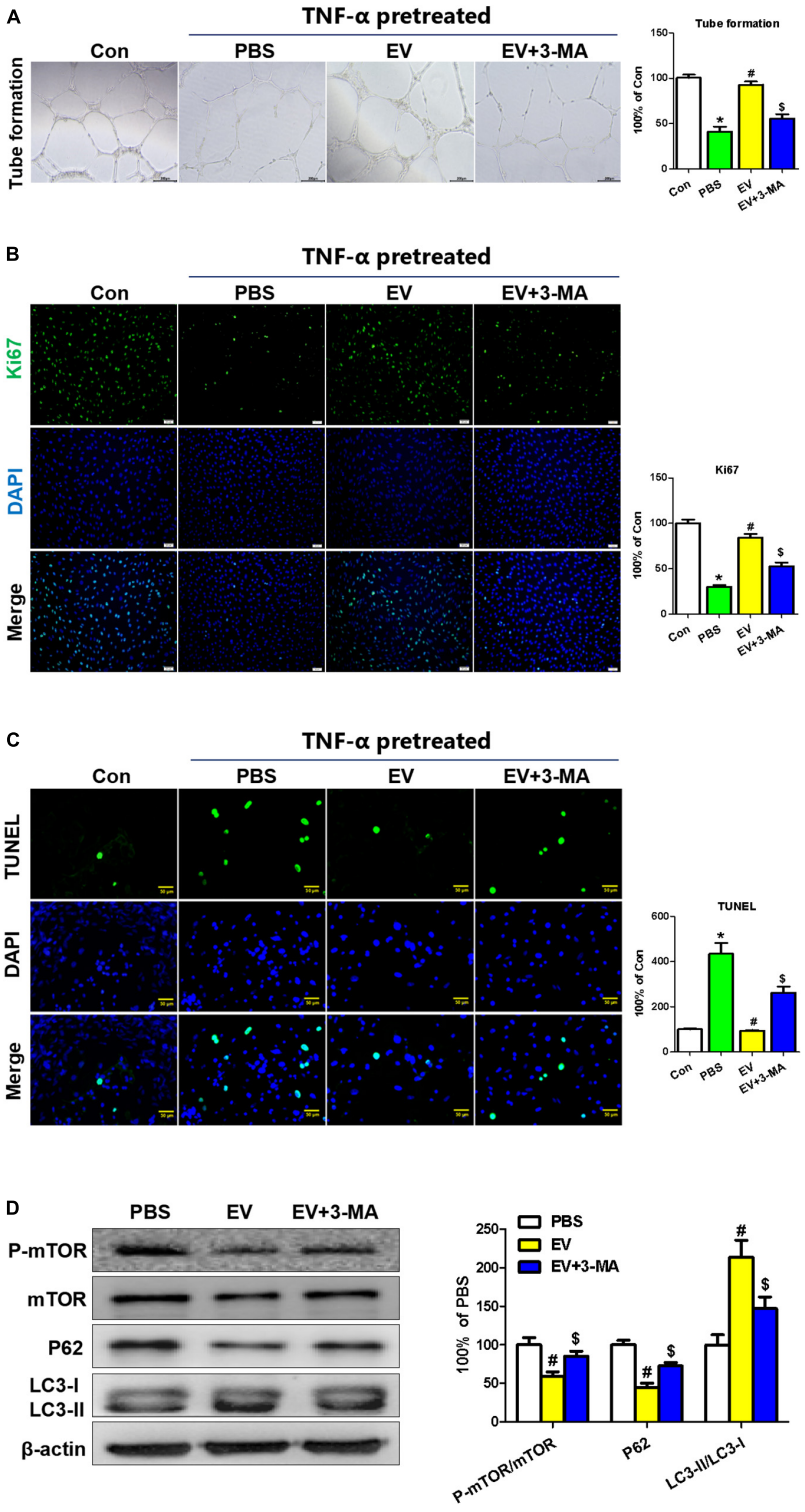

FIGURE 5
The protective effect of human-induced pluripotent stem cell- endothelial cell-extracellular vesicle (hiPSC-EC-EV) on TNF-α-damaged human umbilical vein endothelial cells (HUVECs). **(A)** Representative light microscopy images of the HUVECs in a tube formation assay. **(B)** Ki67 immunostaining and **(C)** TUNEL analysis in the HUVECs treated with or without EV and 3-MA in the presence of TNF-α. **(D)** Western blotting analysis of the autophagy-related protein expression in the HUVECs with different treatments. Data represent mean ± SD from three independent experiments (n = 3). Differences between linked groups were evaluated by a two-tailed Student's t-test. $^{*}p < 0.05$ vs. Con; $^{\#}p < 0.05$ vs. PBS; $^{\$}p < 0.05$ vs. EV.

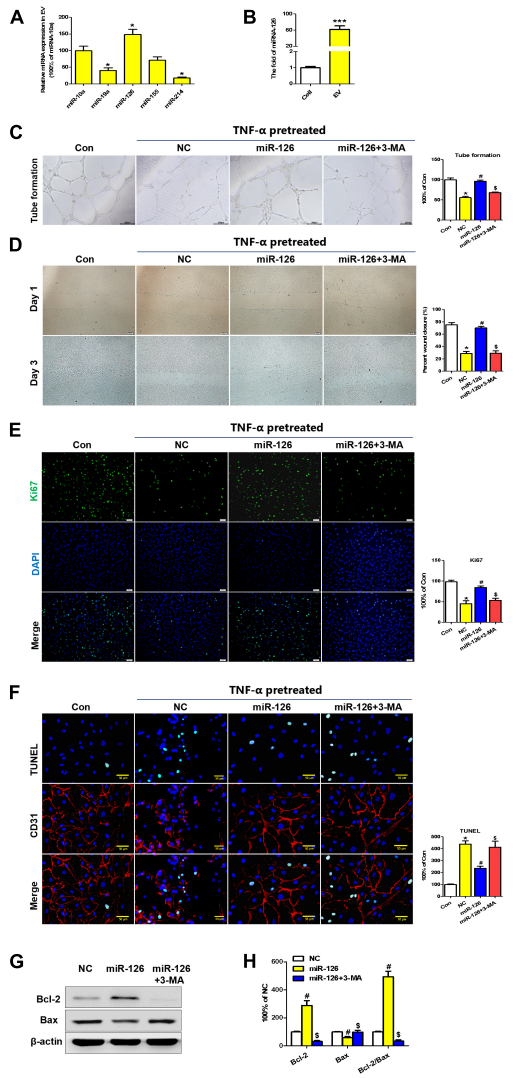

FIGURE 6
Extracellular vesicle (EV)-derived miR-126 promotes human umbilical vein endothelial cell (HUVEC) migration and survival via autophagy regulation. **(A)** The expression profiles of some common EC miRNAs; **(B)** The expression levels of miR-126 in hiPSC-EC and hiPSC-EC-EV; **(C,D)** Light microscopy (bright field) images of the HUVECs in a tube formation **(C)** and a scratch-wound **(D)** assay; **(E)** Ki67 staining (Green) of HUVECs treated with or without miR-126 and 3-MA in the presence of TNF-α; **(F)** TUNEL (Green) and CD31 (Red) staining of HUVECs treated with or without miR-126 and 3-MA in the presence of TNF-α; **(G)** Western blotting analysis of apoptosis-specific proteins in the treated HUVECs; **(H)** Densitometric quantification proteins from the Western blotting image pane in panel **(G)**; Data represent mean ± SD from three independent experiments (n = 3). Differences between linked groups were evaluated by a two-tailed Student's t-test. *$p < 0.05$ vs. Con; $^{\#}p < 0.05$ vs. NC; $^{\$}p < 0.05$ vs. miR-126.

(**Supplementary Figure 4C**), implying its negative regulatory effect on autophagy. Taken together, these results demonstrate an increase in endothelial autophagy levels *in vivo* in response to the hiPSC-EC-EV treatment, which is possibly associated with the downregulation of the mTOR pathway.

Discussion

In the present study, we investigated the protective effect of hiPSC-EC-EV on arterial restenosis conferred by the upregulation of the autophagy function in the arterial ECs. The results confirmed that hiPSC-EC-EV could alleviate ligation-induced arterial restenosis in a mouse model. To elucidate the underlying mechanism, we analyzed the functional role of EV-derived miRNAs and found that among them miR-126 exerted beneficial effects by enhancing proliferation, migration, and tube formation in the injured HUVECs, as well as by inhibiting HUVEC apoptosis via activation of the autophagy signaling pathway (**Figure 8**).

Shear stress, hypoxia, and arterial wall pressure inducing endothelial dysfunction are critical pathological factors observed in artery diseases, such as arterial restenosis (28). Current clinical strategies to reduce arterial restenosis include surgical treatment, drug therapy, cell therapy, etc. However, the therapeutic effects of such treatments are inefficient. Therefore, it is necessary to improve the current treatment approaches or find more effective new strategies.

In the current study, our team utilized an artery ligation technique to model endothelial dysfunction, and it was found that the ligation-treated arteries exhibited increased EC apoptosis. Our results are well consistent with the previous study which demonstrated that shear stress led to EC apoptosis and angiogenic dysfunction (29). MSC and some endothelial progenitor cell-based anti-stenotic therapies have been considered to be ideal interventions for the treatment of arterial restenosis (30–33). It has been demonstrated that MSCs have the ability to repair the shear stress-injured ECs by directly differentiating into functional ECs and secreting a number of angiogenic factors (34). However, cell therapy has many limitations of its own. For example, the low survival rate of transplanted cells and infusion toxicity caused by cell rejection seriously interfere with its therapeutic effect. The use of EVs secreted by stem cells allows avoiding those limitations. EVs are small enough to cross the tissue barrier, and yet allow a reduction in the infusion toxicity and unwanted tissue formation caused by stem cell therapy (35).

In contrast to MSC, hiPSCs have received wider attention with regard to their utility for transplantation therapy because of their self-renewing capability and pluripotency, which have revolutionized the cardiovascular therapy field. Studies have shown that transfer of hiPSC-derived EVs into blood vessels could increase microvessel density and blood perfusion in ischemic limbs *in vivo* (36). Considering the potential tumorigenicity of hiPSC, a better strategy is to differentiate hiPSC into ECs or EPCs and then isolate their EVs to

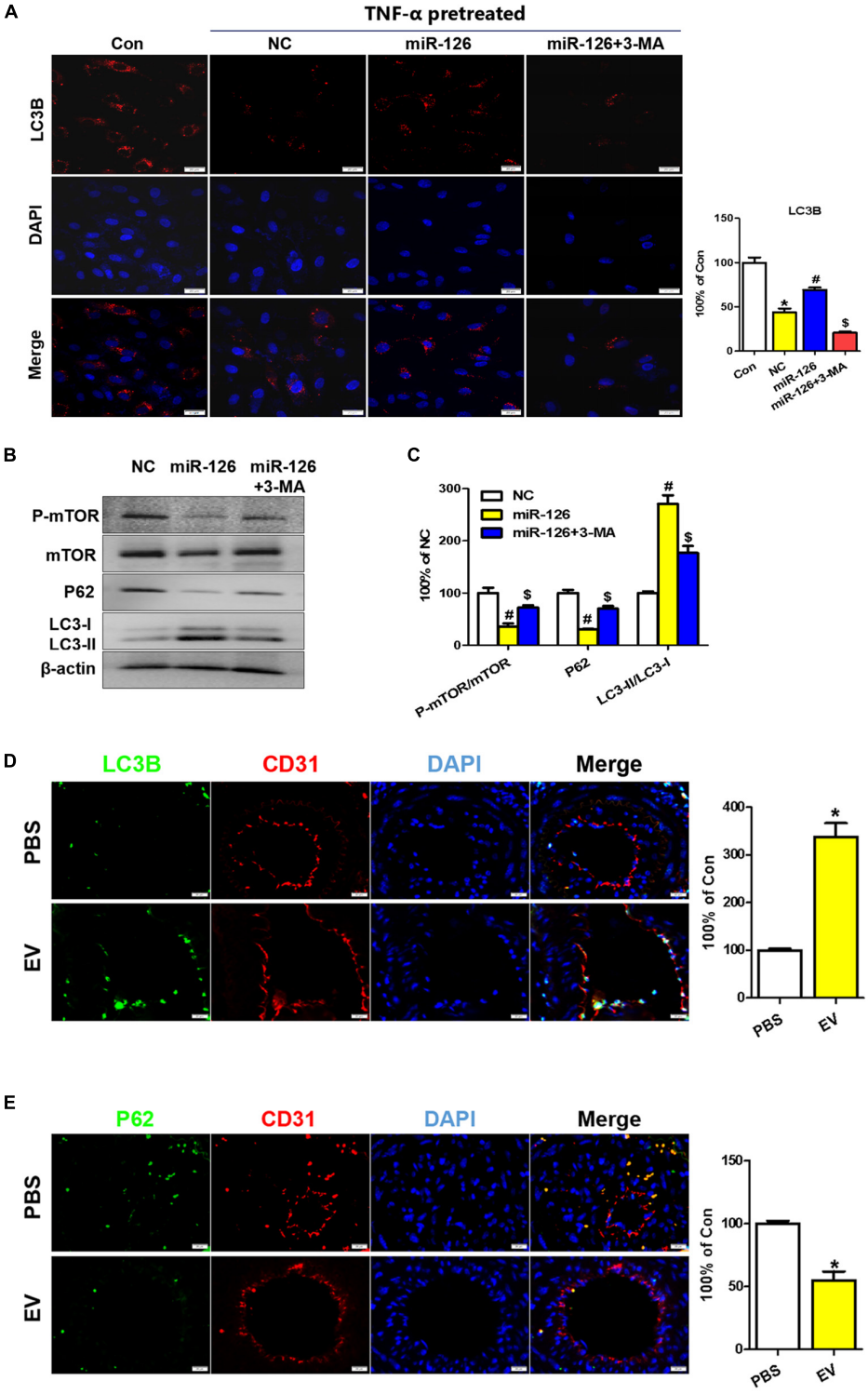

FIGURE 7
Upregulation of autophagy in EC of the carotid artery upon human-induced pluripotent stem cell- endothelial cell-extracellular vesicle (hiPSC-EC-EV) treatment. **(A)** LC3B staining in human umbilical vein endothelial cells (HUVECs) following treatment with or without EV and 3-MA in the presence of TNF-α and quantification of the LC3B-positive signals. **(B)** Western blotting analysis of the p-mTOR, mTOR, P62, and LC3 proteins in the treated and untreated HUVECs. **(C)** Densitometric quantification proteins from the Western blotting image pane in panel **(B)**. $^{*}p < 0.05$ vs. Con; $^{\#}p < 0.05$ vs. NC; $^{\$}p < 0.05$ vs. miR-126. **(D,E)** Immunofluorescence staining of ECs for LC3B **(D)** and P62 **(E)** markers and their quantification (bar charts) in mouse carotid artery sections. Data represent mean ± SD from three independent experiments ($n = 3$). Differences between linked groups were evaluated by a two-tailed Student's *t*-test. $^{*}p < 0.05$ vs. PBS.

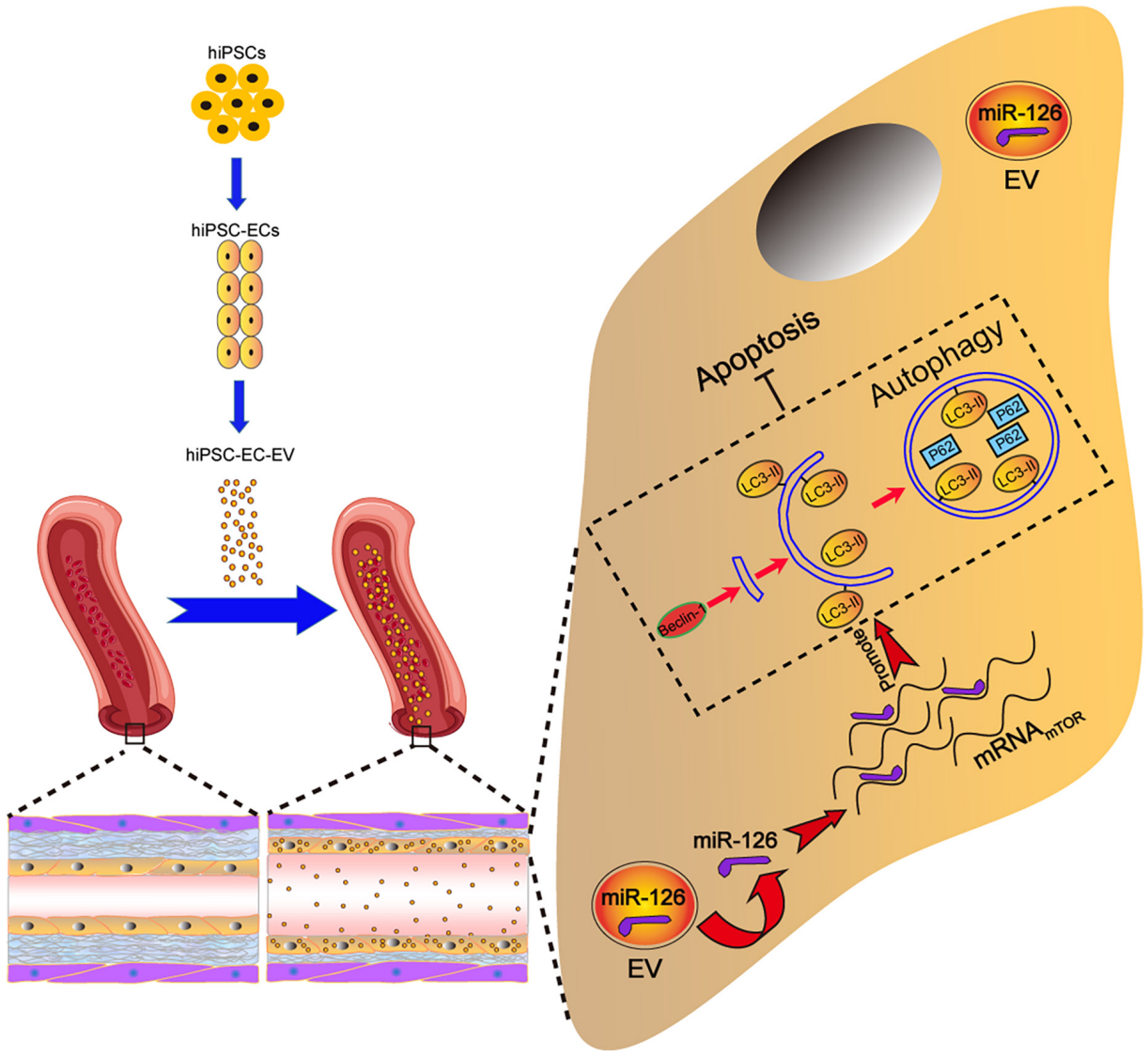

FIGURE 8
Schematic illustration of the tentative mechanism for alleviation of arterial restenosis by hiPSC-EC-EV treatment in mice via the miR-126-mediated autophagy regulation. Intravenously (iv)-injected hiPSC-EC-EV enriched in miR-126 could accumulate on the surface of the carotid artery endothelium, and suppress apoptosis in the ECs via autophagy upregulation.

perform the following treatment. It has also been reported that endothelial progenitor cells (EPCs)-derived EVs can significantly improve the endothelial and vascular repair of intervention-associated vascular injury (37). As compared to primary ECs or EPCs, one key advantage of hiPSC-EC is that it provides a sufficient and individualized resource for EV therapy.

It is known that the endothelial response to injury can be divided into two stages: initial, rapid response and a slower, phenotypic response. The initial or rapid response involves an EC apoptosis and dysfunction. The slower response involves impairment of angiogenesis and vascular remodeling in the artery (38). Our research demonstrated that hiPSC-EC-EV could promote wound healing and tube formation under inflammatory conditions, and significantly reduce EC apoptosis at an early stage, followed by reducing vascular remodeling and arterial restenosis at a later stage.

To validate the effects of hiPSC-EC-EV on shear stress-injured ECs, we co-cultured hiPSC-EC-EV with the HUVECs and found that the inflammation-induced EC dysfunction was significantly alleviated by the hiPSC-EC-EV treatment, as indicated by the upregulation of the EC proliferation, migration, and tube formation capability. It is well known that the migration and tube formation capabilities of ECs contribute to angiogenesis and the artery repair mechanism (39). In

addition, EC apoptosis can lead to the dysfunction of vascular homeostasis and result in arterial restenosis (40).

A series of studies have demonstrated that MSC-EVs are rich in miRNAs, such as miR-126, miR-130a, miR-132, miR-210, and miR-378, and that miRNAs derived from hiPSC-EC-EV exert protective effects on the EC survival and artery function (41, 42). One of the most commonly found in EC miRNAs is miR-126, which exerts beneficial effects on angiogenesis, maintains vascular integrity, and provides atherosclerotic plaque stability (43, 44). In qPCR screening, we found that miR-126 was highly abundant in hiPSC-EC-EV. MiR-126-depleted EV showed a weakened therapeutic effect as indicated by attenuated tubulation and proliferation, as well as enhanced apoptosis in inflammatory cytokine-stimulated HUVECs. To further determine whether miR-126 was responsible for the protective effects observed from hiPSC-EC-EV, we performed a series of experiments to examine the role of miR-126 in regulating EC functions. Scratch and tube formation experiments demonstrated that ECs overexpressing miR-126 exhibited a better survival and an angiogenic potential, as compared to the control group. Additionally, a TUNEL assay-based analysis showed that the number of apoptotic cells in the miR-126 mimic group was significantly reduced, which was further evidenced by the decreased expression of apoptosis marker Bcl-2, indicating the protective role of miR-126 in ECs.

Previous reports have suggested that miR-126 can alleviate EC injury through modulating autophagy (45), which plays a key role in lipid metabolism and has been implicated in the pathogenesis of atherosclerosis (46). The present study showed that miR-126 mimic promotes the accumulation of autophagy marker LC3-II and reduces the expression of P62 protein in TNF-α-treated HUVECs, suggesting that miR-126 restores an impaired autophagic flux under inflammatory conditions. Furthermore, inhibition of the PI3K/Akt/mTOR signaling pathway was reported to upregulate cell autophagy (47). MiR-126 was reported to target PI3K (PI3Kp85b) and inhibit the PI3K/Akt/mTOR pathway, thereby rescuing an impaired autophagy flux (45). Interestingly, in this study, we found a suppression function of mTOR following miR-126 overexpression, which was in agreement with the above report.

Furthermore, overexpression of miR-126, following the inhibition of the autophagy flux by 3-MA, restored protection against the TNF-α-induced HUVEC injury, confirming the role of autophagic flux in the protective effect of miR-126. Immunofluorescence staining of mouse arterial tissues evidenced an elevated expression of autophagy marker LC3B, as well as reduced apoptotic signals in response to the hiPSC-EC-EV treatment of mouse arteries, which argues that hiPSC-EC-EV may alleviate, at least partially, the IH by increasing the autophagy levels in ECs.

In the aggregate, our study revealed that EC-secreted EVs, as natural carriers of miR-126, were capable of preventing an EC injury, highlighting an important regulatory role of autophagic flux in this process and offering a promising new therapeutic strategy for the treatment of arterial restenosis. Considering the feasibility of large-scale production of hiPSC-EC-EV in laboratory settings, our finding has an obvious practical significance for the development of low-cost clinical treatment of arterial restenosis.

Data availability statement

The original contributions presented in the study are included in the article/**Supplementary material**, further inquiries can be directed to the corresponding authors.

Ethics statement

The animal study was reviewed and approved by Ethics Committee of Hubei University of Science and Technology.

Author contributions

QY, MZ, YHe, QL, and FF contributed to design the study. QY, YHe, QL, FF, HL, MZ, and RG analyzed data and prepared the manuscript. QY, YHe, MZ, QL, FF, RG, HL, YC, SL, YW, RM, ZJ, YHu, JS, and ZW contributed to do the experiments. QY and YHe contributed to fund it. All authors contributed to the article and approved the submitted version.

Funding

This work was supported by Hubei Provincial Department of Education guiding project (B2020154); the Diabetes Special Project in Hubei University of Science and Technology (2021TNB04); Overseas Research and Study Project of Excellent Young, Middle-aged Teachers and Principals in Colleges and Universities of Jiangsu Province of 2018; and the Qing Lan Project in Colleges and Universities of Jiangsu Provincial Education Department ([2022]29).

Conflict of interest

The authors declare that the research was conducted in the absence of any commercial or financial relationships that could be construed as a potential conflict of interest.

Publisher's note

All claims expressed in this article are solely those of the authors and do not necessarily represent those of their affiliated

organizations, or those of the publisher, the editors and the reviewers. Any product that may be evaluated in this article, or claim that may be made by its manufacturer, is not guaranteed or endorsed by the publisher.

Supplementary material

The Supplementary Material for this article can be found online at: https://www.frontiersin.org/articles/10.3389/fcvm.2022.922790/full#supplementary-material

SUPPLEMENTARY FIGURE 1
Extracellular vesicle (EV) adhesion study on a microfluidic chip. **(A)** Schematic overview of the microfluidic chip. The microfabricated vessel wall device uses compartmentalized PDMS microchannels to form an organized co-culture of HUVECs, whereby physiological arterial strain and EV adhesion from the liquid flow can be recreated. **(B)** Top, brightfield images of microfluidic chips after seeding with HUVECs. Bottom, immunofluorescent images of the microfluidic chips adhering with PKH67-labeled EVs after 6-h flow; **(C)** Representative images of TUNEL staining for HUVEC in microfluidic chips after TNF-α treatment followed by 6-h-perfusion with medium containing hiPSC-EC-EV or HUVEC-EV.

SUPPLEMENTARY FIGURE 2
Extracellular vesicle (EV) localization in different arteries. Representative images for PKH67-labeled EV (Green) localization in the carotid artery, aorta, and femoral artery 21 days after the surgery.

SUPPLEMENTARY FIGURE 3
miR-126 plays a key role in the protective effect of hiPSC-EC-EV on HUVECs. **(A–C)** Representative images and quantification of **(A)** tube formation assay, **(B)** Ki67 immunofluorescence, and **(C)** TUNEL analysis of the HUVECs treated with normal EV or miR-126-depleted EV. Data represent mean ± SD from three independent experiments (n = 3). Differences between each group were evaluated by a two-tailed Student's t-test. $^{*}p < 0\ 05$ vs. EV.

SUPPLEMENTARY FIGURE 4
The hiPSC-EC-EV treatment could upregulate the endothelial autophagy in carotid artery. **(A–C)** Representative immunofluorescence images for LC3B **(A)**, p-mTOR **(B)**, and mTOR **(C)** in the carotid arteries 21 days after the surgery.

References

1. Zain MA, Jamil RT, Siddiqui WJ. *Neointimal Hyperplasia*. Treasure Island, FL: StatPearls (2022).

2. Park YJ, Min SK, Min SI, Kim SJ, Ha J. Effect of imatinib mesylate and rapamycin on the preformed intimal hyperplasia in rat carotid injury model. *Ann Surg Treat Res*. (2015) 88:152–9. doi: 10.4174/astr.2015.88.3.152

3. Kassem MM, Muqri F, Dacosta M, Bruch D, Gahtan V, Maier KG. Inhibition of heat shock protein 90 attenuates postangioplasty intimal hyperplasia. *Mol Med Rep*. (2020) 21:1959–64. doi: 10.3892/mmr.2020.10994

4. Xu K, Al-Ani MK, Pan X, Chi Q, Dong N, Qiu X. Plant-derived products for treatment of vascular intima hyperplasia selectively inhibit vascular smooth muscle cell functions. *Evid Based Complement Alternat Med*. (2018) 2018:3549312. doi: 10.1155/2018/3549312

5. Takahashi K, Yamanaka S. Induction of pluripotent stem cells from mouse embryonic and adult fibroblast cultures by defined factors. *Cell*. (2006) 126:663–76. doi: 10.1016/j.cell.2006.07.024

6. Mathiyalagan P, Liang Y, Kim D, Misener S, Thorne T, Kamide CE, et al. Angiogenic mechanisms of human CD34(+) stem cell exosomes in the repair of ischemic hindlimb. *Circ Res*. (2017) 120:1466–76. doi: 10.1161/CIRCRESAHA.116.310557

7. Rezabakhsh A, Sokullu E, Rahbarghazi R. Applications, challenges and prospects of mesenchymal stem cell exosomes in regenerative medicine. *Stem Cell Res Ther*. (2021) 12:521. doi: 10.1186/s13287-021-02596-z

8. Gu C, Feng J, Waqas A, Deng Y, Zhang Y, Chen W, et al. Technological advances of 3D scaffold-based stem cell/exosome therapy in tissues and organs. *Front Cell Dev Biol*. (2021) 9:709204. doi: 10.3389/fcell.2021.709204

9. Lu K, Li HY, Yang K, Wu JL, Cai XW, Zhou Y, et al. Exosomes as potential alternatives to stem cell therapy for intervertebral disc degeneration: in-vitro study on exosomes in interaction of nucleus pulposus cells and bone marrow mesenchymal stem cells. *Stem Cell Res Ther*. (2017) 8:108. doi: 10.1186/s13287-017-0563-9

10. Ong SG, Wu JC. Exosomes as potential alternatives to stem cell therapy in mediating cardiac regeneration. *Circ Res*. (2015) 117:7–9. doi: 10.1161/CIRCRESAHA.115.306593

11. Pashova A, Work LM, Nicklin SA. The role of extracellular vesicles in neointima formation post vascular injury. *Cell Signal*. (2020) 76:109783. doi: 10.1016/j.cellsig.2020.109783

12. Hu GW, Li Q, Niu X, Hu B, Liu J, Zhou SM, et al. Exosomes secreted by human-induced pluripotent stem cell-derived mesenchymal stem cells attenuate limb ischemia by promoting angiogenesis in mice. *Stem Cell Res Ther*. (2015) 6:10. doi: 10.1186/scrt546

13. Jung JH, Fu X, Yang PC. Exosomes generated from iPSC-derivatives: new direction for stem cell therapy in human heart diseases. *Circ Res*. (2017) 120:407–17. doi: 10.1161/CIRCRESAHA.116.309307

14. Liu X, Li Q, Niu X, Hu B, Chen S, Song W, et al. Exosomes secreted from human-induced pluripotent stem cell-derived mesenchymal stem cells prevent osteonecrosis of the femoral head by promoting angiogenesis. *Int J Biol Sci*. (2017) 13:232–44. doi: 10.7150/ijbs.16951

15. Hu S, Li Z, Shen D, Zhu D, Huang K, Su T, et al. Exosome-eluting stents for vascular healing after ischaemic injury. *Nat Biomed Eng*. (2021) 5:1174–88. doi: 10.1038/s41551-021-00705-0

16. Cai Y, Liu W, Lian L, Xu Y, Bai X, Xu S, et al. Stroke treatment: Is exosome therapy superior to stem cell therapy? *Biochimie*. (2020) 179:190–204. doi: 10.1016/j.biochi.2020.09.025

17. Zhang S, Dutton JR, Su L, Zhang J, Ye L. The influence of a spatiotemporal 3D environment on endothelial cell differentiation of human induced pluripotent stem cells. *Biomaterials*. (2014) 35:3786–93. doi: 10.1016/j.biomaterials.2014.01.037

18. He Y, Li H, Yao J, Zhong H, Kuang Y, Li X, et al. HO1 knockdown upregulates the expression of VCAM1 to induce neutrophil recruitment during renal ischemiareperfusion injury. *Int J Mol Med*. (2021) 48:185. doi: 10.3892/ijmm.2021.5018

19. Skylar-Scott MA, Huang JY, Lu A, Ng AHM, Duenki T, Liu S, et al. Orthogonally induced differentiation of stem cells for the programmatic patterning of vascularized organoids and bioprinted tissues. *Nat Biomed Eng*. (2022) 6:449–62. doi: 10.1038/s41551-022-00856-8

20. Su L, Kong X, Loo S, Gao Y, Liu B, Su X, et al. Thymosin beta-4 improves endothelial function and reparative potency of diabetic endothelial cells differentiated from patient induced pluripotent stem cells. *Stem Cell Res Ther*. (2022) 13:13. doi: 10.1186/s13287-021-02687-x

21. Vila Cuenca M, Cochrane A, van den Hil FE, de Vries AAF, Lesnik Oberstein SAJ, Mummery CL, et al. Engineered 3D vessel-on-chip using hiPSC-derived endothelial- and vascular smooth muscle cells. *Stem Cell Rep*. (2021) 16:2159–68. doi: 10.1016/j.stemcr.2021.08.003

22. Luo J, Lin Y, Shi X, Li G, Kural MH, Anderson CW, et al. Xenogeneic-free generation of vascular smooth muscle cells from human induced pluripotent stem cells for vascular tissue engineering. *Acta Biomater*. (2021) 119:155–68. doi: 10.1016/j.actbio.2020.10.042

23. Hosseinkhani B, Kuypers S, van den Akker NMS, Molin DGM, Michiels L. Extracellular vesicles work as a functional inflammatory mediator between vascular endothelial cells and immune cells. *Front Immunol*. (2018) 9:1789. doi: 10.3389/fimmu.2018.01789

24. Wang F, He Q, Gao Z, Redington AN. Atg5 knockdown induces age-dependent cardiomyopathy which can be rescued by repeated remote ischemic conditioning. *Basic Res Cardiol*. (2021) 116:47. doi: 10.1007/s00395-021-00888-2

25. Li M, Meng X, Li M. MiR-126 promotes esophageal squamous cell carcinoma via inhibition of apoptosis and autophagy. *Aging*. (2020) 12:12107–18. doi: 10.18632/aging.103379

26. Zhu W, Liu F, Wang L, Yang B, Bai Y, Huang Y, et al. pPolyHb protects myocardial H9C2 cells against ischemia-reperfusion injury by regulating the Pink1-Parkin-mediated mitochondrial autophagy pathway. *Artif Cells Nanomed Biotechnol*. (2019) 47:1248–55. doi: 10.1080/21691401.2019.1594243

27. Ganesan D, Ramaian Santhaseela A, Rajasekaran S, Selvam S, Jayavelu T. Astroglial biotin deprivation under endoplasmic reticulum stress uncouples BCAA-mTORC1 role in lipid synthesis to prolong autophagy inhibition in the aging brain. *J Neurochem*. (2020) 154:562–75. doi: 10.1111/jnc.14979

28. Vanhoutte PM, Shimokawa H, Feletou M, Tang EH. Endothelial dysfunction and vascular disease - a 30th anniversary update. *Acta Physiol*. (2017) 219:22–96. doi: 10.1111/apha.12646

29. Abaci HE, Shen YI, Tan S, Gerecht S. Recapitulating physiological and pathological shear stress and oxygen to model vasculature in health and disease. *Sci Rep*. (2014) 4:4951. doi: 10.1038/srep04951

30. Forte A, Rinaldi B, Sodano L, Berrino L, Rossi F, Finicelli M, et al. Stem cell therapy for arterial restenosis: potential parameters contributing to the success of bone marrow-derived mesenchymal stromal cells. *Cardiovasc Drugs Ther*. (2012) 26:9–21. doi: 10.1007/s10557-011-6359-8

31. Liu Z, Wu C, Zou X, Shen W, Yang J, Zhang X, et al. Exosomes derived from mesenchymal stem cells inhibit neointimal hyperplasia by activating the Erk1/2 signalling pathway in rats. *Stem Cell Res Ther*. (2020) 11:220. doi: 10.1186/s13287-020-01676-w

32. Xu BY, Xiang MX, Wang JA. Endothelial progenitor cells and in-stent restenosis. *Curr Stem Cell Res Ther*. (2015) 10:364–71. doi: 10.2174/1574888x10666150204150430

33. Kou F, Zhu C, Wan H, Xue F, Wang J, Xiang L, et al. Endothelial progenitor cells as the target for cardiovascular disease prediction, personalized prevention, and treatments: progressing beyond the state-of-the-art. *EPMA J*. (2020) 11:629–43. doi: 10.1007/s13167-020-00223-0

34. Bartaula-Brevik S, Pedersen TO, Finne-Wistrand A, Bolstad AI, Mustafa K. Angiogenic and immunomodulatory properties of endothelial and mesenchymal stem cells. *Tissue Eng Part A*. (2016) 22:244–52. doi: 10.1089/ten.TEA.2015.0316

35. Zagrean AM, Hermann DM, Opris I, Zagrean L, Popa-Wagner A. Multicellular crosstalk between exosomes and the neurovascular unit after cerebral ischemia. therapeutic implications. *Front Neurosci*. (2018) 12:811. doi: 10.3389/fnins.2018.00811

36. Ye M, Ni Q, Qi H, Qian X, Chen J, Guo X, et al. Exosomes derived from human induced pluripotent stem cells-endothelia cells promotes postnatal angiogenesis in mice bearing ischemic limbs. *Int J Biol Sci*. (2019) 15:158–68. doi: 10.7150/ijbs.28392

37. Hu H, Jiang C, Li R, Zhao J. Comparison of endothelial cell- and endothelial progenitor cell-derived exosomes in promoting vascular endothelial cell repair. *Int J Clin Exp Pathol*. (2019) 12:2793–800.

38. Sumpio BE, Riley JT, Dardik A. Cells in focus: endothelial cell. *Int J Biochem Cell Biol*. (2002) 34:1508–12. doi: 10.1016/s1357-2725(02)00075-4

39. Nakao-Hayashi J, Ito H, Kanayasu T, Morita I, Murota S. Stimulatory effects of insulin and insulin-like growth factor I on migration and tube formation by vascular endothelial cells. *Atherosclerosis*. (1992) 92:141–9. doi: 10.1016/0021-9150(92)90273-j

40. Isner JM, Kearney M, Bortman S, Passeri J. Apoptosis in human atherosclerosis and restenosis. *Circulation*. (1995) 91:2703–11. doi: 10.1161/01.cir.91.11.2703

41. Goerke SM, Kiefer LS, Stark GB, Simunovic F, Finkenzeller G. miR-126 modulates angiogenic growth parameters of peripheral blood endothelial progenitor cells. *Biol Chem*. (2015) 396:245–52. doi: 10.1515/hsz-2014-0259

42. Chistiakov DA, Orekhov AN, Bobryshev YV. The role of miR-126 in embryonic angiogenesis, adult vascular homeostasis, and vascular repair and its alterations in atherosclerotic disease. *J Mol Cell Cardiol*. (2016) 97:47–55. doi: 10.1016/j.yjmcc.2016.05.007

43. Tang F, Yang TL. MicroRNA-126 alleviates endothelial cells injury in atherosclerosis by restoring autophagic flux via inhibiting of PI3K/Akt/mTOR pathway. *Biochem Biophys Res Commun*. (2018) 495:1482–9. doi: 10.1016/j.bbrc.2017.12.001

44. Miao J, Zang X, Cui X, Zhang J. Autophagy, hyperlipidemia, and atherosclerosis. *Adv Exp Med Biol*. (2020) 1207:237–64. doi: 10.1007/978-981-15-4272-5_18

45. Yang J, Pi C, Wang G. Inhibition of PI3K/Akt/mTOR pathway by apigenin induces apoptosis and autophagy in hepatocellular carcinoma cells. *Biomed Pharmacother*. (2018) 103:699–707. doi: 10.1016/j.biopha.2018.04.072

46. Pan, Q, Wang Y, Lan Q, Wu W, Li Z, Ma X, et al. Exosomes derived from mesenchymal stem cells ameliorate hypoxia/reoxygenation-injured ECs via transferring MicroRNA-126. *Stem Cells Int*. (2019) 2019:2831756. doi: 10.1155/2019/2831756

47. Jansen F, Yang X, Proebsting S, Hoelscher M, Przybilla D, Baumann K, et al. MicroRNA expression in circulating microvesicles predicts cardiovascular events in patients with coronary artery disease. *J Am Heart Assoc*. (2014) 3:e001249. doi: 10.1161/JAHA.114.001249

Frontiers in
Cardiovascular Medicine

Innovations and improvements in cardiovascular treatment and practice

Focuses on research that challenges the status quo of cardiovascular care, or facilitates the translation of advances into new therapies and diagnostic tools.

Discover the latest Research Topics

See more →

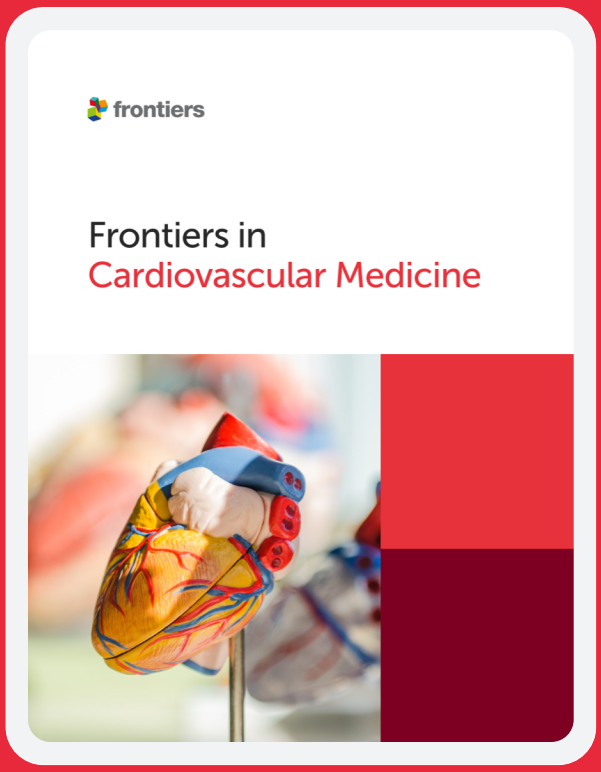

Frontiers

Avenue du Tribunal-Fédéral 34
1005 Lausanne, Switzerland
frontiersin.org

Contact us

+41 (0)21 510 17 00
frontiersin.org/about/contact